MYCOVIRUSES AND RELATED VIRUSES INFECTING FUNGI, LOWER EUKARYOTES, PLANTS AND INSECTS

EDITED BY: Hiromitsu Moriyama, Jiatao Xie, Ioly Kotta-Loizou and Kook-Hyung Kim

PUBLISHED IN: Frontiers in Microbiology

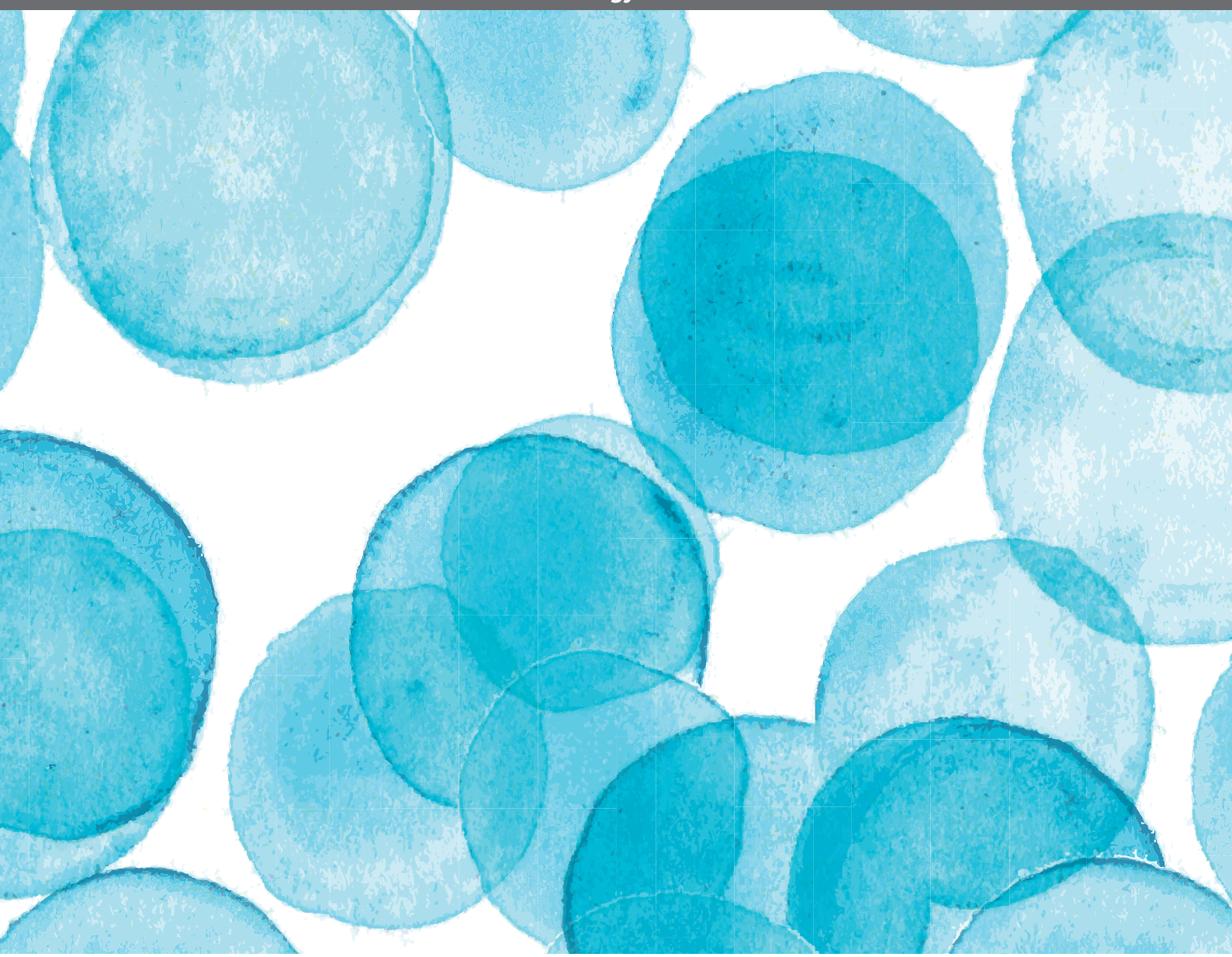

frontiers Research Topics

ISSN 1664-8714
ISBN 978-2-88974-068-0
DOI 10.3389/978-2-88974-068-0

About Frontiers

Frontiers is more than just an open-access publisher of scholarly articles: it is a pioneering approach to the world of academia, radically improving the way scholarly research is managed. The grand vision of Frontiers is a world where all people have an equal opportunity to seek, share and generate knowledge. Frontiers provides immediate and permanent online open access to all its publications, but this alone is not enough to realize our grand goals.

Frontiers Journal Series

The Frontiers Journal Series is a multi-tier and interdisciplinary set of open-access, online journals, promising a paradigm shift from the current review, selection and dissemination processes in academic publishing. All Frontiers journals are driven by researchers for researchers; therefore, they constitute a service to the scholarly community. At the same time, the Frontiers Journal Series operates on a revolutionary invention, the tiered publishing system, initially addressing specific communities of scholars, and gradually climbing up to broader public understanding, thus serving the interests of the lay society, too.

Dedication to Quality

Each Frontiers article is a landmark of the highest quality, thanks to genuinely collaborative interactions between authors and review editors, who include some of the world's best academicians. Research must be certified by peers before entering a stream of knowledge that may eventually reach the public - and shape society; therefore, Frontiers only applies the most rigorous and unbiased reviews.
Frontiers revolutionizes research publishing by freely delivering the most outstanding research, evaluated with no bias from both the academic and social point of view. By applying the most advanced information technologies, Frontiers is catapulting scholarly publishing into a new generation.

What are Frontiers Research Topics?

Frontiers Research Topics are very popular trademarks of the Frontiers Journals Series: they are collections of at least ten articles, all centered on a particular subject. With their unique mix of varied contributions from Original Research to Review Articles, Frontiers Research Topics unify the most influential researchers, the latest key findings and historical advances in a hot research area! Find out more on how to host your own Frontiers Research Topic or contribute to one as an author by contacting the Frontiers Editorial Office: frontiersin.org/about/contact

MYCOVIRUSES AND RELATED VIRUSES INFECTING FUNGI, LOWER EUKARYOTES, PLANTS AND INSECTS

Topic Editors:
Hiromitsu Moriyama, Tokyo University of Agriculture and Technology, Japan
Jiatao Xie, Huazhong Agricultural University, China
Ioly Kotta-Loizou, Imperial College London, United Kingdom
Kook-Hyung Kim, Seoul National University, South Korea

Citation: Moriyama, H., Xie, J., Kotta-Loizou, I., Kim, K.-H., eds. (2022). Mycoviruses and Related Viruses Infecting Fungi, Lower Eukaryotes, Plants and Insects. Lausanne: Frontiers Media SA. doi: 10.3389/978-2-88974-068-0

Table of Contents

frontiers in Microbiology

EDITORIAL
published: 25 November 2021
doi: 10.3389/fmicb.2021.798598

Editorial: Mycoviruses and Related Viruses Infecting Fungi, Lower Eukaryotes, Plants and Insects

Hiromitsu Moriyama[1], *Ioly Kotta-Loizou*[2]*, *Kook-Hyung Kim*[3] and *Jiatao Xie*[4]

[1] Laboratory of Plant Pathology, Graduate School of Agriculture, Tokyo University of Agriculture and Technology, Fuchu, Japan, [2] Department of Life Sciences, Faculty of Natural Sciences, Imperial College London, London, United Kingdom, [3] Department of Agricultural Biotechnology, College of Agriculture and Life Sciences, Plant Genomics and Breeding Institute, Research Institute of Agriculture and Life Sciences, Seoul National University, Seoul, South Korea, [4] State Key Laboratory of Agricultural Microbiology, Huazhong Agricultural University, Wuhan, China

Keywords: mycovirus, RNA virus, virus transmission, virus-host interactions, virus evolution

Editorial on the Research Topic

Mycoviruses and Related Viruses Infecting Fungi, Lower Eukaryotes, Plants and Insects

The Frontiers Research Topic "*Mycoviruses and Related Viruses Infecting Fungi, Lower Eukaryotes, Plants and Insects*" was initiated in the context of *Frontiers in Microbiology* and *Frontiers in Plant Pathology*, covering three sections: (1) Virology, (2) Microbe and Virus Interactions with Plants, and (3) Plant Pathogen Interactions. This reflects the importance of mycovirus-host interplay in phytopathogenic fungi; however, the final article collection is not limited to mycovirus infections in plant pathogens. Our Research Topic accommodates 15 high-quality Original Research manuscripts covering a range of topics, including the discovery and characterization of double-stranded (ds) RNA and single-stranded (ss) RNA viruses, the study of the distribution, transmission, and evolution of viruses in fungal populations, and the effects of viruses on their fungal hosts.

Chrysoviridae, *Hypoviridae*, *Partitiviridae*, and *Reoviridae* are well-studied families that accommodate mycoviruses. Telengech et al. reported the presence of 20 new members of the *Partitiviridae* family in the plant pathogen *Rosellinia necatrix*, causative agent of dematophora root rot. Subsequently, transfection experiments revealed differential RNA accumulation and symptomatology in the natural host, *R. necatrix*, as compared to a heterologous host, the chestnut blight fungus *Cryphonectria parasitica*. Similarly, Yang et al. investigated the effects of Cryphonectria parasitica hypovirus 1 and Mycoreovirus 1, both originally derived from *C. parasitica*, on the heterologous host *Valsa mali*, the causative agent of apple dieback, illustrating potential for biological control applications but also highlighting the complex interactions between the two viruses and the host antiviral RNA silencing machinery. Kashif et al. linked the partial phenotypic recovery of a hypovirulent isolate of the forest pathogen *Heterobasidion*, causative agent of Heterobasidion root rot, infected with a member of *Partitiviridae* with alterations in the virus titer and host gene expression. Owashi et al. investigated the distribution patterns of three different viruses, including members of the families *Partitiviridae* and *Chrysoviridae*, in the rice blast fungus *Magnaporthe oryzae* in Japan.

Polymycoviridae is a newly established family of non-conventionally encapsidated dsRNA viruses. Three novel members of the family were reported: Penicillium janthinellum polymycovirus 1 (PjPmV-1), Beauveria bassiana polymycovirus 3 (BbPmV-3), and Aspergillus fumigatus polymycovirus 1M (AfuPmV-1M). Sato et al. confirmed that the PjPmV-1 proline-alanine-serine rich protein (PASrp), a hallmark of polymycoviruses hypothesized to coat the dsRNA genome, has

OPEN ACCESS

Edited by:
Robert Czajkowski,
University of Gdansk, Poland

Reviewed by:
Massimo Turina,
National Research Council (CNR), Italy

***Correspondence:**
Ioly Kotta-Loizou
i.kotta-loizou13@imperial.ac.uk

Specialty section:
This article was submitted to Virology, a section of the journal Frontiers in Microbiology

Received: 20 October 2021
Accepted: 10 November 2021
Published: 25 November 2021

Citation:
Moriyama H, Kotta-Loizou I, Kim K-H and Xie J (2021) Editorial: Mycoviruses and Related Viruses Infecting Fungi, Lower Eukaryotes, Plants and Insects. Front. Microbiol. 12:798598. doi: 10.3389/fmicb.2021.798598

RNA binding properties and is capable of associating with nucleic acids in a non-sequence specific manner. Filippou et al. illustrated that BbPmV-1 and −3 mediate their effects on the insect pathogen and popular biocontrol agent *Beauveria bassiana* by interfering with host carbon and nitrogen metabolism. Takahashi-Nakaguchi et al. established that AfuPmV-1 causes hypovirulence to the human pathogen *Aspergillus fumigatus* in an immunosuppressed mouse infection model.

Botourmiaviridae is another recently established family, accommodating positive-sense ssRNA viruses. Zhao et al. discovered a new member of the family in the plant pathogen *Fusarium oxysporum*, causative agent of Fusarium wilt. Fusarium oxysporum ourmia-like virus 1 is transmitted horizontally and causes hypovirulence to its host, showing potential for biological control applications.

Fusarium graminearum virus 1 (FgV1) is a positive-sense ssRNA virus related to the proposed family Fusariviridae that results in increased pigmentation, and decreased growth and virulence in the plant pathogen *Fusarium graminearum*, causative agent of Fusarium head blight. Yu and Kim determined the differential effects of FgV1 on its host in the absence of specific fungal transcription factors, providing insights on the molecular mechanisms underpinning the observed phenotypes. In parallel, Heo et al. investigated the evolution of FgV1, taking into account the viral genome sequences, the natural selection pressures acting on the viral proteins and the effects of FgV1 on its host.

In addition to the aforementioned filamentous fungi, yeasts also harbor mycoviruses and the killer yeast system in *Saccharomyces cerevisiae* has been extensively studied. Ramírez et al. reported the presence of a helper virus in the wine yeast *Torulaspora delbrueckii*; the helper virus is a member of the family *Totiviridae*, closely related to those in *S. cerevisiae*, and supports the replication cycle of the dsRNA element responsible for the killer phenotype.

Lichens are stable symbiotic associations between fungi and algae and/or cyanobacteria. Urayama et al. reported the presence of members of the family *Partitiviridae* in lichens.

Oomycetes, despite what their name suggests, are not considered fungi but fungus-like lower eukaryotic organisms. Uchida et al. discovered two positive-sense ssRNA viruses belonging to the family *Endornaviridae* in the plant pathogen *Phytophthora*. Both endornaviruses were shown to affect host hyphal growth, zoosporangium formation and fungicide resistance. Botella et al. reported for the first time the presence of negative-sense ss RNA viruses of the order *Bunyavirales* in marine oomycetes of the genus *Halophytophthora*.

Finally, Fujita et al. discovered *Partitiviridae*-like viruses in the oriental tea trotix moth and pest of tea plants, *Homona magnanima*. These viruses, designated as Osugoroshi viruses, are responsible for the observed phenomenon of late male killing that leads to female-biased sex ratios in *H. magnanima.*

As Associate Editors, we would like to take this opportunity to acknowledge all the contributing authors who chose our Research Topic "*Mycoviruses and Related Viruses Infecting Fungi, Lower Eukaryotes, Plants and Insects*" as a vehicle for sharing their fascinating work on mycoviruses.

AUTHOR CONTRIBUTIONS

IK-L wrote the manuscript. All authors contributed to the article and approved the submitted version.

Conflict of Interest: The authors declare that the research was conducted in the absence of any commercial or financial relationships that could be construed as a potential conflict of interest.

frontiers in Microbiology

ORIGINAL RESEARCH
published: 26 June 2020
doi: 10.3389/fmicb.2020.01064

Diverse Partitiviruses From the Phytopathogenic Fungus, *Rosellinia necatrix*

Paul Telengech[1], *Sakae Hisano*[1], *Cyrus Mugambi*[1], *Kiwamu Hyodo*[1], *Juan Manuel Arjona-López*[1,2], *Carlos José López-Herrera*[2], *Satoko Kanematsu*[3†], *Hideki Kondo*[1] *and Nobuhiro Suzuki*[1*]

[1] *Institute of Plant Science and Resources, Okayama University, Kurashiki, Japan,* [2] *Institute for Sustainable Agriculture, Spanish Research Council, Córdoba, Spain,* [3] *Institute of Fruit Tree Science, National Agriculture and Food Research Organization (NARO), Morioka, Japan*

OPEN ACCESS

Edited by:
Hiromitsu Moriyama, Tokyo University of Agriculture and Technology, Japan

Reviewed by:
Eeva Johanna Vainio, Natural Resources Institute Finland, Finland
K. W. Thilini Chethana, Mae Fah Luang University, Thailand

***Correspondence:**
Nobuhiro Suzuki
nsuzuki@okayama-u.ac.jp

†Present address:
Satoko Kanematsu, NIFTS, NARO, Tsukuba, Japan

Specialty section:
This article was submitted to Virology, a section of the journal Frontiers in Microbiology

Received: *25 March 2020*
Accepted: *29 April 2020*
Published: *26 June 2020*

Citation:
Telengech P, Hisano S, Mugambi C, Hyodo K, Arjona-López JM, López-Herrera CJ, Kanematsu S, Kondo H and Suzuki N (2020) Diverse Partitiviruses From the Phytopathogenic Fungus, Rosellinia necatrix. Front. Microbiol. 11:1064. doi: 10.3389/fmicb.2020.01064

Partitiviruses (dsRNA viruses, family *Partitiviridae*) are ubiquitously detected in plants and fungi. Although previous surveys suggested their omnipresence in the white root rot fungus, *Rosellinia necatrix*, only a few of them have been molecularly and biologically characterized thus far. We report the characterization of a total of 20 partitiviruses from 16 *R. necatrix* strains belonging to 15 new species, for which "*Rosellinia necatrix partitivirus 11–Rosellinia necatrix partitivirus 25*" were proposed, and 5 previously reported species. The newly identified partitiviruses have been taxonomically placed in two genera, *Alphapartitivirus*, and *Betapartitivirus*. Some partitiviruses were transfected into reference strains of the natural host, *R. necatrix*, and an experimental host, *Cryphonectria parasitica,* using purified virions. A comparative analysis of resultant transfectants revealed interesting differences and similarities between the RNA accumulation and symptom induction patterns of *R. necatrix* and *C. parasitica*. Other interesting findings include the identification of a probable reassortment event and a quintuple partitivirus infection of a single fungal strain. These combined results provide a foundation for further studies aimed at elucidating mechanisms that underly the differences observed.

Keywords: partitivirus, dsRNA virus, phytopathogenic fungus, *Rosellinia necatrix*, *Cryphonectria parasitica*, diversity, reassortment, horizontal transfer

INTRODUCTION

Plant pathogenic fungi provide platforms for identifying eukaryotic viruses (Pearson et al., 2009; Xie and Jiang, 2014; Ghabrial et al., 2015; Suzuki, 2017; Hillman et al., 2018). Research performed in previous decades have revealed that the diversity of fungal viruses or mycoviruses is much greater than previously imagined (Yu et al., 2010; Kondo et al., 2013a; Liu et al., 2014; Kanhayuwa et al., 2015; Zhang et al., 2016). Further, studies involving particular fungal-viral systems have provided interesting insights into virus-virus and virus-host interactions (Cho et al., 2013; Jiang et al., 2013; Xie and Jiang, 2014; Hillman et al., 2018). Antagonistic, mutualistic and neutral virus/virus interactions, and beneficial, harmful, or no effects on their hosts have been reported. Among fungal hosts commonly used for the study of viruses is the phytopathogenic ascomycete fungus, *Rosellinia necatrix*, which infects over 400 plant species and causes white root rot in perennial crops worldwide, and particularly in Japan (Pliego et al., 2012; Kondo et al., 2013b). A survey of over 1,000 field isolates showed that ∼20% of field isolates harbor diverse populations of viruses

(Arakawa et al., 2002; Ikeda et al., 2004; Kondo et al., 2013b; Zhang et al., 2014, 2016; Arjona-Lopez et al., 2018). Importantly, the characterization of some viruses has led to the approval of proposals to create new viral families by the International Committee on Taxonomy of Viruses (ICTV) (Chiba et al., 2009; Lin et al., 2012). The majority of viruses detected in *R. necatrix* have been partitiviruses (Yaegashi et al., 2013) (Kanematsu and Sasaki, unpublished results), which was also the case for the fungal forest inhabitant, *Heterobasidion* spp. (Vainio and Hantula, 2016).

Partitiviruses are bisegmented, biparticulate viruses with double-stranded RNA (dsRNA) genomes that range from 3.0 to 4.8 kbp (Nibert et al., 2014; Vainio et al., 2018a). With a few exceptions, RNA-dependent RNA polymerase (RdRP) is encoded within the large segment, while capsid protein (CP) is encoded within the smaller segment. Partitiviruses typically form icosahedral particles that are 30–35 nm in diameter. The near-atomic resolution of ∼5 Å has been achieved for the $T = 1$ capsids of partitiviruses via cryo-electron microscopy (Nibert et al., 2013). Based on phylogenetic relationships and host ranges, partitiviruses are now classified into 5 genera: *Alphapartitivirus*, *Betapartitivirus*, *Gammapartitivirus*, *Deltapartitivirus*, and *Cryspovirus* (Nibert et al., 2014; Vainio et al., 2018a). The first two genera contain members that infect both plant and fungal species, while the genera *Gammapartitivirus* and *Deltapartitivirus* are composed of members that infect exclusively fungal and plant species, respectively. In this regard, it should be noted that fungus-infecting, betapartitivirus-related sequences are detected in various plant genomes, a paleological record of their capacity to infect plant species (viral fossils or endogenous virus elements) and their association with plants several tens of millions of years ago (Liu et al., 2010; Chiba et al., 2011). Cryspoviruses have been isolated from protozoa of the genus *Cryptosporidium* that infect mammals as a parasite. Recently, the novel genera "*Epsilonpartitivirus*" and "*Zetapartitivirus*" have been proposed for some novel viruses or virus-like agents associated with fungi and arthropods (Nerva et al., 2017a; Jiang et al., 2019). Partitiviruses, in most cases, produce symptomless infections. Exceptions include growth-reducing Heterobasidion partitivirus 3 (an alphapartitivirus) (Vainio et al., 2010) and Aspergillus fumigatus partitivirus 1 (a gammapartitivirus) (Bhatti et al., 2011), and hypovirulence-conferring partitiviruses such as *Rhizoctonia solani* partitivirus 2 (an alphapartitivirus, RsPV2) (Zheng et al., 2014), Sclerotinia sclerotiorum partitivirus 1 (a betapartitivirus, SsPV1) (Xiao et al., 2014), Aspergillus flavus partitivirus 1 (a zetapartitivirus) (Jiang et al., 2019) and Heterobasidion partitivirus 13 (an alphapartitivirus) (Vainio et al., 2018b). In other cases, some partitiviruses have been shown to contribute to hypovirulence and/or growth defects induced by other co-infecting fungal dsRNA viruses such as megabirnavirus and chrysovirus (Wang et al., 2014; Sasaki et al., 2016).

Despite the large number of partitiviruses identified thus far (Nibert et al., 2014; Vainio et al., 2018a), only a few including *R. necatrix*-infecting partitiviruses (Rosellinia necatrix partitiviruses: RnPV1, RnPV2, RnPV3, RnPV6, RnPV7, RnPV8, RnPV9, and RnPV10) have been identified (Sasaki et al., 2006, 2007, 2016; Chiba et al., 2013a, 2016; Yaegashi and Kanematsu, 2016; Arjona-Lopez et al., 2018). Biological characterization of fungal viruses has been facilitated by the development of improved virion transfection methods (Hillman et al., 2004). Fungal partitiviruses, unlike plant partitiviruses, can be experimentally introduced into both original and experimental hosts. The method has previously been used to study some partitiviruses including RnPV1, RnPV2, RnPV6, SsPV1, and RsPV2 (Sasaki et al., 2007; Chiba et al., 2013a, 2016; Xiao et al., 2014; Zheng et al., 2014). In this regard, it is important to note that the phytopathogenic ascomycete that causes chestnut blight, *Cryphonectria parasitica*, is a model filamentous host used to explore virus-virus and virus-host interactions. The fungus is an attractive host because it is biologically tractable, genetically manipulatable, and can support many homologous and heterologous fungal viruses (Eusebio-Cope et al., 2015). In addition, a number of biological resources and molecular tools are available for the fungus (Nuss, 2005; Eusebio-Cope et al., 2015; Chiba et al., 2018). Therefore, the use of *C. parasitica* as a viral host has facilitated the study of viral symptom induction via host antiviral RNA silencing to and counter defense of both homologous and heterologous fungal viruses (Faruk et al., 2008; Andika et al., 2017, 2019). Recent advancements made by using this fungus as a model system include the characterization of mechanisms of induction of and susceptibility to mechanisms of antiviral RNA silencing of different fungal viruses (Chiba and Suzuki, 2015; Andika et al., 2017, 2019). It has also been shown that a fungal gammapartitivirus replicates in plant cells (Nerva et al., 2017b).

Here, we report the characterization of a total of 20 partitiviruses belonging to 15 new and 5 previously-identified species placed in the genus *Alphapartitivirus* or *Betapartitivirus*. Some tested partitiviruses differ with respect to viral content in both *R. necatrix* and *C. parasitica*, and symptom induction in the experimental host. This study has enhanced our understanding of the molecular and biological diversity of fungal partitiviruses.

MATERIALS AND METHODS

Fungal and Viral Materials

A total of 16 field isolates of *R. necatrix* listed in **Table 1** were used in the study. Most fungal isolates were collected from Japanese pear or apple trees in Saga, Fukuoka, Hyogo, Nagano, and Gunma Prefectures, Japan, while Rn459 was collected from an avocado tree in Malaga, Spain (Arakawa et al., 2002; Ikeda et al., 2004; Yaegashi et al., 2013; Arjona-Lopez et al., 2018). The Japanese fungal strains had earlier been shown to harbor partiti-like dsRNAs of ∼2.0–2.5 kbp by a conventional dsRNA extraction method (Arakawa et al., 2002; Ikeda et al., 2004; Sasaki and Kanematsu, unpublished data). The partitivirus isolate from the Spanish strain, Rn459, was previously partially sequenced (Arjona-Lopez et al., 2018). The standard strain, W97, of *R. necatrix* has been described in previous reports (Kanematsu et al., 2010; Shimizu et al., 2018). The standard *C. parasitica* strain, EP155, and its *dicer-like 2* (*dcl2*) knockout (KO) mutant strain, Δ*dcl2*, were a generous gift from Dr. Donald L. Nuss (University of Maryland, College Park, MD). The Δ*dcl2* strain

TABLE 1 | List of *Rosellinia necatrix* isolates used.

Isolate[a]	Collection locality	Host plants	Collection year	MCG[b]	Group of NGS	Virus detected[e]	Source
W98	Saga	Japanese pear	1998	80	Pool-3/2	RnPV11	Ikeda et al., 2004
W118	Saga	Japanese pear	1998	86	Pool-3/1	RnPV3, 12, 13	Ikeda et al., 2004
W129	Fukuoka	Japanese pear	1998	88	Pool-2	RnPV25	Ikeda et al., 2004
W442	Hyogo	Unknown	2000	169	Pool-3/1	RnPV18, 19	This study
W558	Saga	Japanese pear	1998	85	Pool-1	RnPV6	Ikeda et al., 2004
W662	Gunma	Apple	2000	301	Pool-1	RnPV23, 24	Ikeda et al., 2004
W744	Saga	Japanese pear	2001	325	Pool-3/2	RnPV1, 14–17	Ikeda et al., 2004
W1030	Nagano	Apple	2009	139	NA[c]	RnPV4	Yaegashi et al., 2013
W1031	Nagano	Apple	2009	139	Pool-4	RnPV3, 4	Yaegashi et al., 2013
W1040	Nagano	Apple	2009	139	Pool-1	RnPV5 (+one)[f]	Yaegashi et al., 2013
W1041	Nagano	Apple	2009	139	NA[c]	RnPV5	Yaegashi et al., 2013
W1050	Nagano	Apple	2009	139	Pool-4	RnPV22	Yaegashi et al., 2013
W1126	Iwate	Lacquer tree	2011	U1	NA[c]	RnPV22	From Dr. M. Tabata
W1134	Kagawa	Lacquer tree	2011	U13	Pool-3/1	RnPV20, 21	From Dr. M. Tabata
W1135	Kagawa	Lacquer tree	2011	U14	NA[c]	RnPV20	From Dr. M. Tabata
Rn459	Malaga	Avocado	2016	unknown	NA[d]	RnPV10	Arjona-Lopez et al., 2018

[a] *All isolates were collected in Japan, except for Rn459 isolated from Spain.*
[b] *Mycelial compatibility group.*
[c] *Not applicable. For these viruses, conventional cDNA libraries were constructed and subjected to Sanger sequencing.*
[d] *Partial genomic sequence was reported by Arjona-Lopez et al. (2018).*
[e] *Viral infection was confirmed by RT-PCR.*
[f] *The partial genome sequence derived from an additional potential novel partitivirus besides RnPV5 was detected in the W1040 strain.*

carries deletion of a key gene used for antiviral RNA silencing, *dcl2* (Segers et al., 2007). All fungal materials were cultured either on potato dextrose agar (PDA, BD Difco Laboratories, Detroit, MI, USA) plates or potato dextrose broth (PDB, BD Difco Laboratories).

Partitivirus Purification, Electron Microscopy, and Transfection

Partitivirus particles were semi-purified following the method described by Chiba et al. (2016). After differential centrifugation, viral fractions were subjected to sucrose/cesium chloride gradient ultracentrifugation. Purified virus preparations were examined by transmission electron microscopic (TEM, H-7650 Hitachi, Tokyo, Japan) observation after EM staining (the EM stainer, an alternative for uranyl acetate, Nissin EM Co., Tokyo, Japan) (Nakakoshi et al., 2011). Virus preparations were loaded on sodium dodecyl sulfate (SDS)—polyacrylamide (10%) gel and electrophoreses, and then stained with Rapid stain CBB kit (Nacalai tesque inc., Kyoto Japan). Semi-purified particle fractions were used to transfect virus-free protoplasts derived from either strain W97 from *R. necatrix*, or EP155 and Δ*dcl2* strains from *C. parasitica.* Transfection of strain W97 was conducted according to the method described by Kanematsu et al. (2010), and transfection of *C. parasitica*-derived strains was performed according to the method described by Salaipeth et al. (2014). After regeneration, partitiviral infection of candidate transfectants were assessed using the one-tube RT-PCR method using PrimeScript™ One Step RT-PCR Kit ver.2 (Takara Bio Inc., Shiga Japan) and toothpicks described by Urayama et al. (2015).

RNA Analyses

Viral genomic dsRNA sequences were determined using two approaches: conventional complimentary DNA (cDNA) library construction using purified viral dsRNA and subsequent Sanger sequencing (Chiba et al., 2016), and next-generation high-throughput sequencing (NGS) of total RNA from fractions obtained from infected mycelia (Shamsi et al., 2019). dsRNA was isolated from mycelia cultured in PDB media for 1 week as previously described (Chiba et al., 2013a). Total RNA, dsRNA or single-stranded RNA (ssRNA) fractions were obtained from *R. necatrix* strains as described by Chiba et al. (2013a).

For RNA-Seq analyses, RNA samples were pooled into four groups: two were comprised of dsRNA samples and were named Pool-1 and -2 (1.2 and 0.9 μg, respectively) and other two, Pool-3 and -4, contained total RNA samples (14.1 and 67.5 μg, respectively) (see **Table 1**). Each RNA pool with/without ribosomal RNA depletion treatment (the Ribo-Zero kit, Illumina, San Diego, CA, USA) was subjected to cDNA library construction (the TruSeq RNA Sample Preparation kit v2, Illumina) and pair-end deep sequencing (100 bp pair-end reads) using the Illumina HiSeq 2500/4000 platforms (Illumina) performed by Macrogen Inc. (Tokyo, Japan). After deep sequencing, adapter-trimmed sequence reads (Pool-1: 28,827,612; Pool-2: 29,248,296, Pool-3: 46,288,894, and Pool-4: 47,084,068 raw reads) were *de novo* assembled using the CLC Genomics Workbench (version 11, CLC Bio-Qiagen, Aarhus, Demark). To verify the virus infection in the fungal strains, we performed RT-PCR using the specific primer sets for each of the partitivirus (**Supplementary Table S1**). Viral genomic sequences were completed by RLM-RACE (RNA

ligase mediated rapid amplification of complementary DNA ends) and gap-filling RT-PCR (Suzuki et al., 2004; Chiba et al., 2009) (**Supplementary Table S1**). Sequences obtained in this study were deposited in EMBL/GenBank/DDBJ databases with accession numbers LC517370–LC517399, as described in **Table 2**.

Bioinformatics

Viral sequences were analyzed with online bioinformatics tools as described by Kondo et al. (2015). After *de novo* assembly, contigs [Pool-1: 23,341 (∼9.9 kb), Pool-2: 23,130 (∼9.8 kb), Pool-3: 10,485 (∼13.2 kb), and Pool-4: 11,016 (∼13.8 kb)] were subjected to local BLAST searches against the viral reference sequence (RefSeq) dataset from the National Center for Biotechnology Information (NCBI). Viral-like sequences were analyzed using Enzyme X v3.3.3[1] or GENETYX-MAC (Genetyx Co., Tokyo, Japan). Database searches of viral sequences were performed using the BLAST (BLASTn and BLASTp) programs available from NCBI. Pairwise amino acid identity was calculated using SDT v1.2 (Muhire et al., 2014).

Phylogenetic reconstruction was carried out using the maximum-likelihood (ML) method as described previously (Kondo et al., 2019). Deduced amino acid sequences from virus RNA sequences were aligned using MAFFT version 7 (Katoh and Standley, 2013) and unreliably aligned regions were eliminated using Gblocks 0.91b (Talavera and Castresana, 2007). ML phylogenetic trees were constructed by PhyML 3.0 (Guindon et al., 2010) using automatic model selection via smart model selection (SMS) (Lefort et al., 2017). Support for branches was examined via bootstrapping with 1,000 repetitions. The phylogenetic trees (mid-point rooted) were visualized and refined using FigTree version 1.3.1 software[2].

RESULTS

dsRNA Profiles of *R. necatrix* Isolates

Field-collected strains of *R. necatrix* have previously been screened for mycoviruses by Japanese research groups (Arakawa et al., 2002; Ikeda et al., 2004; Yaegashi and Kanematsu, 2016). We selected a total of 16 fungal strains harboring ∼1.5–2.5 kbp dsRNAs for the study (**Table 1**). dsRNA profiles of some these strains have been reported previously by Ikeda et al. (2004), Yaegashi et al. (2013), and Arjona-Lopez et al. (2018). Bands were confirmed to be dsRNA following double digestion using RQ1 RNase free DNase I (Promega) and S1 Nuclease (Takara) enzymes (Eusebio-Cope and Suzuki, 2015). dsRNA-enriched or total RNA fractions and their mixed pools (Poo1-1–4) were then subjected to either conventional Sanger sequencing of cDNA clones or NGS analyses, respectively (**Table 2**; see **Figure 1** for the dsRNA profile of Pool-3 from *R. necatrix*-derived strains). It is worth noting that some dsRNA bands of the sequence analysis turned out to be doublets (or more).

[1]https://nucleobytes.com/enzymex/index.html
[2]http://tree.bio.ed.ac.uk/software/

Sequence Analysis

Properties of fully and near-fully sequenced partitiviruses are summarized in **Table 2**. Some partially characterized partitiviruses, i.e., RnPV1, RnPV3, RnPV4, RnPV5, RnPV6, and RnPV10, were previously isolated from *R. necatrix* strains (Sasaki et al., 2005; Chiba et al., 2013b, 2016; Yaegashi et al., 2013; Arjona-Lopez et al., 2018). The partial genomic sequences of RnPV4, RnPV5, and RnPV10, and the complete genomic sequences of RnPV1 and RnPV6 were previously determined. The remainder of the partitivirus isolates for which novel sequence information was obtained in this study were designated Rosellinia necatrix partitivirus 11–25 (RnPV11–RnPV25) (**Table 2**).

NGS and conventional sequencing, followed by subsequent RT-PCR analyses, suggested that tested fungal strains were either singly (W98, W129, W558, W1030, W1041, W1050, W1126, W1135, and Rn459), doubly (W442, W662, W1031, W1040, and W1134), triply (W118) or quintuply (W744) infected by partitiviruses (**Tables 1**, **2**). Partitivirus infection was confirmed by RT-PCR using specific primer sets designed from NGS contigs or sequences by conventional methods (**Table 2** and **Supplementary Table S1**). Particularly, it is noteworthy that W744 was infected by five distinct partitiviruses, RnPV1, RnPV14, RnPV15, RnPV16, and RnPV17, as has also been reported in some other fungal hosts multiply infected by mitoviruses (Hillman et al., 2018). When the nucleotide sequences of these co-infecting viruses were compared, the highest sequence identity is 59% detected between RnPV14 dsRNA1 and RnPV15 dsRNA1 (see **Supplementary Figure S3** for amino acid sequence comparison), which is low enough to avoid possible RNA silencing-mediated inter-virus antagonism. Fifteen novel partitiviruses, including those identified by conventional sequencing methods, from seven fungal strains such as W98 (RnPV11), W118 (RnPV12 and 13), W442 (RnPV18 and 19), W744 (RnPV14–17), W1050/1126 (dsRNA segments with conventional sequencing, RnPV22), W1134 (RnPV20 and 21), and Rn459 (two reported dsRNA contigs for RnPV10, Arjona-Lopez et al., 2018) had two segments that were completely sequenced using the RLM-RACE method (**Table 2**). In addition, the only fully-sequenced coding regions of the three other novel partitiviruses were from the fungal strains W662 (RnPV23 and 24) and W129 (RnPV25) (**Table 2**).

Sequence analysis revealed that each segment encoded one open reading frame (ORF), and BlastP analysis confirmed that the ORF from dsRNA1 (larger dsRNA segments, in general) encoded RdRP, which was closely related to alpha- or betapartitiviruses of the *Partitiviridae* family (**Table 2**, see below). The ORF from dsRNA2 (smaller dsRNA segments, in general) encoded CP, which was also related to other known alpha- or betapartitiviruses. Viral sequences from *R. necatrix* from W744 (RnPV1), W118/1031 (RnPV3), W1030/1031 (RnPV4, dsRNA1 segment determined by conventional sequencing), W1041/1040 (RnPV5) and W558 (RnPV6) strains were 85–100% identical to known *R. necatrix* partitiviruses RnPV1/W8, RnPV3/W1029, RnPV4/W1028 (dsRNA1), RnPV5/W1028 (dsRNA1), and RnPV6/W113, respectively (**Table 2**). For RnPV4 and RnPV5, previously undescribed dsRNA2 segments were newly sequenced

TABLE 2 | Properties of newly discovered partitiviruses from *Rosellinia necatrix*.

Virus name[a]	Original host strain	Contig No.	Total read count	Genus	Segment length[b]	Blastp		Protein size	Symptom[c]		
					dsRNA1/(accession)	Hit with highest score in	Identity	RdRp (aa)	*R.n.*	*C.p.*	
					dsRNA2 (accession)	Blastp	(%)	Cp (aa)		Δ*dcl2*	EP155
RnPV11	W98	4	61129	*Beta-*	2445 (LC517370)	Rosellinia necatrix partitivirus 20	71	757	−∼+	++	+++
		262	26713		2326 (LC517371)	Fusarium poae partitivirus 2	35	652			
RnPV12	W118	148	47804	*Alpha-*	1845 LC517372	Botrytis cinerea partitivirus 2	63	551			
		779	1197		1925 (LC517373)	Erysiphe necator partitivirus 1	38	533			
RnPV13	W118	610	6211	*Alpha-*	1965 (LC517374)*	Rhizoctonia oryzae-sativae partitivirus 1	59	469	−∼+		
		529	4558		1822 (LC517375)	Rhizoctonia oryzae-sativae partitivirus 1	54	488			
RnPV3[f]	W118	317		*Beta-*	2246 (LC010950)	Rosellinia necatrix partitivirus 3	99	709		−	−
		347			2065 (LC010951)	Rosellinia necatrix partitivirus 3	96	613			
RnPV14	W744	118	46844	*Beta-*	2412 (LC517376)	Rosellinia necatrix partitivirus 4	72	743		++	
		750	2477		2427 (LC517377)	Rosellinia necatrix partitivirus 1-W8	47	706			
RnPV15	W744	826	7917	*Beta-*	2517 (LC517378)	Rosellinia necatrix partitivirus 14	59	747			
		2267	3491		2358 (LC517379)	Rosellinia necatrix partitivirus 16	49	663			
RnPV16	W744	509	20228	*Beta-*	2372 (LC517380)	Podosphaera prunicola partitivirus 4	61	730	−∼+	++	+++
		3216	944		2344 (LC517381)	Rosellinia necatrix partitivirus 15	49	662			
RnPV17	W744	671	4185	*Beta-*	2292 (LC517382)	Heterobasidion partitivirus 7	63	725			
		237	8985		2235 (LC517383)	Rhizoctonia solani partitivirus 7	71	670			
RnPV1[f]	W744/	43		*Beta-*	2374 (AB113347)	Rosellinia necatrix partitivirus 1-W8	98	709			
	W1134	82/69			2263 (AB113348)	Rosellinia necatrix partitivirus 1-W8	99/94	686			
RnPV18[d]	W442	110	30695	*Beta-*	2410 (LC517384)	Enteoleuca partitivirus 2	99.7	740		−	−
		874			2337 (LC517385)	Dill cryptic virus 2	43	670			
RnPV19[d]	W442	26	40899	*Alpha-*	2013 (LC517386)	Entoleuca partitivirus 1	99.7	606	−	+	−
		379	5244		1842 (LC517387)	Grosmannia clavigera partitivirus 1	42	520			
RnPV20	W1134	5	186156	*Beta-*	2417 (LC517388)	Rosellinia necatrix partitivirus 11	71	755		+++	+++
		7	55670		2318 (LC517389)	Ceratobasidium partitivirus CP-h	61	643			
RnPV21	W1134	161	49075	*Beta-*	2352 (LC517390)	Podosphaera prunicola partitivirus 4	65	721	−∼+		
		69	3784		2361 (LC517391)	Rosellinia necatrix partitivirus 1-W8	94	686			
RnPV22	W1050/	27		*Alpha-*	2012 (LC517392)	Trichoderma atroviride partitivirus 1	76	613			
	W1126	707			2037 (LC517393)	Trichoderma atroviride partitivirus 1	43	584			
RnPV23	W662	127		*Alpha-*	1831 (LC517394)**	Heterobasidion partitivirus 13	49	571			
		25			1791 (LC517395)**	Heterobasidion partitivirus 13	37	514			
RnPV24	W662	77		*Alpha-*	1946 (LC517396)**	Oyster mushroom isometric virus II	75	598			
		125			1771 (LC517397)**	Medicago sativa alphapartitivirus 1	28	498			
RnPV25	W129	51		*Beta-*	2374 (LC517398)**	Trichoderma citrinoviride partitivirus 1	65	733			
		188			2049 (LC517399)**	Trichoderma citrinoviride partitivirus 1	54	642			
RnPV10	Rn459			*Alpha-*	1896 (LC333736)	Rosellinia necatrix partitivirus 10	100	573			
					1911 (LC333737)	Rosellinia necatrix partitivirus 10	100	539			
RnPV4[e]	W1030/	4		*Alpha-*	2342 (AB698493)	Rosellinia necatrix partitivirus 4	100	744			
	W1031	270			2295 (LC521312)	Sclerotinia sclerotiorum partitivirus 1	48	683			
RnPV5[e]	W1040/	10/522		*Beta-*	2046 (AB698494)	Rosellinia necatrix partitivirus 5	99.7	647			
	W1041	27/62			1906 (LC521313)	Trichoderma atroviride partitivirus 1	44	576			
RnPV6[f]	W558	52		*Beta-*	2499 (LC010952)	Rosellinia necatrix partitivirus 6	100	756	−∼+	+++	+++
		137			2462 (LC010953)	Rosellinia necatrix partitivirus 6	100	729			

[a] *RnPV22 was also detected from the W1126 strain.*

[b] **, 5′-terminal sequence of dsRNA1 is incomplete; **5′- and 3′-terminal sequences of both segments are incomplete. Underlined: RdRp is encoded by the smaller dsRNA segments.*

[c] *R.n., R. necatrix W97 strain; C.p., C. parasitica EP155 or Δdcl2 strain. Growth reduction: –, No; +: Slight; ++, Moderate; +++, Great. See* ***Figure 4*** *and* ***Supplementary Figure S4*** *for colony morphology of virus-infected fungal strains.*

[d,e] *Near-complete or complete dsRNA1 sequences of these viruses from Spanish Entoleuca sp. (d) or R. necatrix (e) have already been deposited in GenBank.*

[f] *Partitiviruses belonging to the same species have previously been reported from different Japanese strains of R. necatrix.*

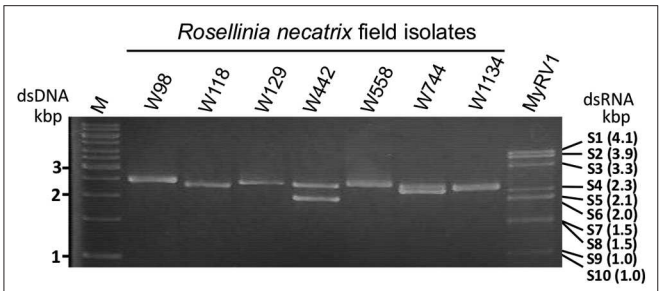

FIGURE 1 | Agarose gel electrophoresis of dsRNA isolated from field isolates of *Rosellinia necatrix*. dsRNA fractions were obtained from fungal isolates as indicated above each lane, and electrophoresed through a 1% agarose gel in 1× TAE (40 mM Tris-acetate−1 mM EDTA, pH 7.8). See **Table 1** for information regarding fungal isolates. A 1-kb DNA ladder (Thermo Fisher Scientific., Inc., Waltham, MA, USA) and MyRV1 genomic dsRNA (Supyani et al., 2007) were used as size markers.

(**Table 2**). Intriguingly, two dsRNA1 sequence for RnPV18 and 19, respectively, from the single W442 strain were 99% identical to two reported partitivirus sequences (Entoleuca partitivirus 2 and 1, EnPV2 and 1), respectively, which were both obtained from a Spanish fungal isolate (E97-14) of *Entoleuca* sp. entirely different from, but sympatric to, *R. necatrix* that infest avocado orchards in Spain (Velasco et al., 2019, 2020) (**Table 2**). Note that the dsRNA2 sequences of EnPV1 and 2 from the GenBank/EMBL/DDBJ databases were unavailable. The 5′-terminus of EnPV1 remains incomplete. Thus, we report the full-length sequence of the genome of RnPV18 and RnPV19, respectively (**Table 2**).

Genome Organization, Protein Sequence Similarities, and Phylogenetic Analysis

All novel partitivirus strains from *R. necatrix* characterized molecularly have been determined to belong to either the genus *Alphapartitivirus* or *Betapartitivirus* (**Table 2**). No gammapartitiviruses, which exclusively infect fungi, were detected within *R. necatrix* as a part of this or previous studies (Sasaki et al., 2005; Chiba et al., 2013a; Yaegashi et al., 2013; Yaegashi and Kanematsu, 2016; Arjona-Lopez et al., 2018). Their sequence characteristics are similar to those of previously reported partitivirus members (Nibert et al., 2014). Namely, the size ranges of their segments, 5′- and 3′-untranslated regions (UTRs), and encoded proteins of these viruses mostly fall within ranges reported previously, whereas a few expand the reported size distributions within alpha- and betapartitiviruses (Nibert et al., 2014). The genome sizes of most reported alphapartitiviruses range from 3.6 to 3.9 kbp (Nibert et al., 2014), but RnPV22 isolate extended the range from 3.6 to 4.0 kbp. Similarly, an expansion of genome segment and coding protein size is also observed for betapartitiviruses RnPV6, RnPV14, and RnPV15. dsRNA1 segments of partitiviruses are usually longer than dsRNA2 segments, but we encountered few exceptions in RnPV12, RnPV14, RnPV21, and RnPV22, which had longer dsRNA2 than dsRNA1 segments (**Table 2**), as also has been reported for RnPV6 (Chiba et al., 2016). As an example, the genome organization, protein component, and virion morphology of a novel *R. necatrix* virus betapartitivirus, RnPV11, isolated from the strain W98, is shown in **Figure 2**. The RnPV11 genomic segments of ∼2.4 and 2.3 kbp were shown to be encased in spherical particles of ∼30 nm in diameter composed of the CP of ∼72 kDa.

Partitiviruses analyzed in this study had terminal sequences similar to those described previously (Nibert et al., 2014; Vainio et al., 2018a). For several partitiviruses from *R. necatrix* isolates, such as RnPV19, RnPV20, and RnPV22, "CAA" repeats were present at the 5′-UTR region, which has been assumed to be a translation enhancer (Jiang and Ghabrial, 2004) (**Supplementary Figure S1**). The 20–30 nucleotides located at the 5′-terminal regions are highly conserved between genome segments, and the 5′-terminal-most nucleotides are considered consensus sequences and are shown in bold in **Supplementary Table S2**. The 5′-terminal G residue is strictly conserved at the terminal end or +1 from the end (**Supplementary Figure S2**). For 3′-termini, the plus strands of the genome segments of some betapartitiviruses, such as RnPV11, RnPV14, and RnPV15, end with interrupted poly(A) tracts, while those of other partitiviruses contain additional nucleotides, which include the di- or tri-nucleotide "UC," "CC," or "CU" that follow interrupted poly(A) tracts (**Supplementary Table S2**).

The BlastP (or BlastN as mentioned above) results are summarized in **Table 2**. The species demarcation criteria set by the ICTV are ≤90% and ≤80% amino acid identities for RdRP and CP, respectively (Vainio et al., 2018a). Of 20 newly sequenced alpha- or betapartitivirus isolates, 15 (including EnPV dsRNA segments) showed much smaller amino acid identities with known partitiviruses, which ranged 28–76% for RdRP or CP, than the above-mentioned species demarcation criteria (**Table 2**). In addition, pairwise comparisons of proteins encoded by new partitiviruses revealed moderate levels of amino acid sequence identity (less than above criteria) among RdRPs and CPs (**Supplementary Figure S3**). These results indicated that the 15 partitiviruses that were newly identified belong to new species, which were named Rosellinia necatrix partitivirus 11 to Rosellinia necatrix partitivirus 25. Notably, the nucleotide sequence identities of dsRNA1 and dsRNA2 of RnPV21/W1134 were most similar to Podosphaera prunicola partitivirus 4 (45%) and RnPV1/W8 or W744 (94%) (**Table 2**), respectively. This strongly suggests that a reassortment event likely occurred between RnPV1 and another partitivirus (see Discussion).

Members of the *Alphapartitivirus* and *Betapartitivirus* genera have been characterized from 14 to 17 species of fungi (ascomycetous and basidiomycetous) and plants (largely dicot plants), respectively (Vainio et al., 2018a). Phylogenetic analysis based on RdRP, encoded by dsRNA1, of the novel 15 *R. necatrix* partitiviruses using selected alpha- and betapartitiviruses that included approved members of both genera revealed that six novel *R. necatrix* partitiviruses clustered with alphapartitiviruses with a bootstrap value of 100 (**Figure 3**). These included RnPV12, RnPV13, RnPV19, RnPV22, RnPV23, and RnPV24.

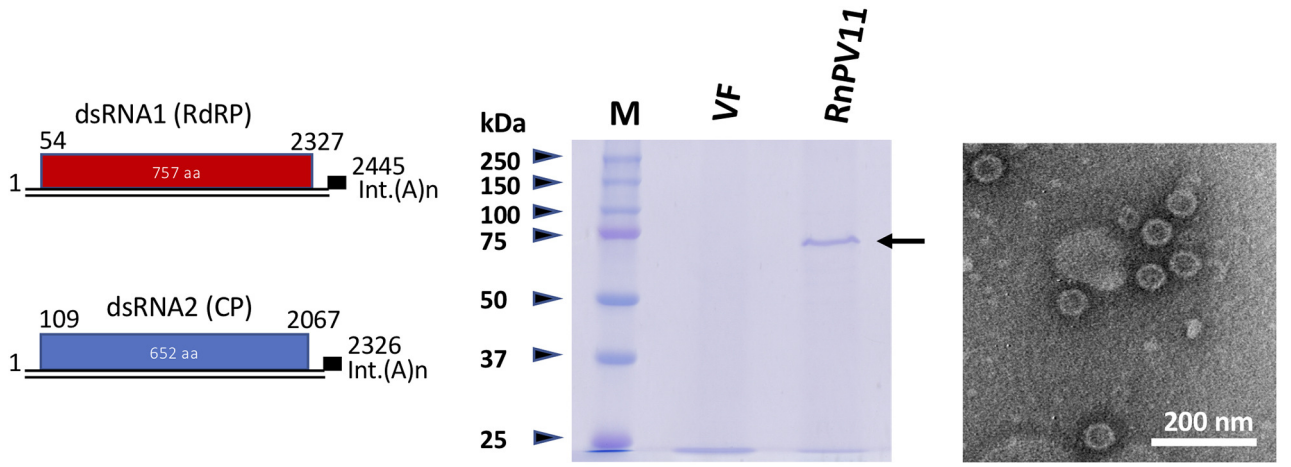

FIGURE 2 | Schematic of the genome organization, particle protein composition, and morphology of a newly discovered partitivirus of *R. necatrix*. **(Left)** Genome organization of a representative betapartitivirus, RnPV11/W98. Sequence information for RnPV11 is summarized in **Table 2**. **(Middle)** SDS-PAGE analysis of purified preparations of RnPV11. Virus particles were purified from the mycelia of the W98 strain (lane RnPV11) and analyzed in 10% polyacrylamide gel electrophoresis. The arrow indicates the migration of RnPV11/W98 CP. A preparation was also obtained in parallel from virus-free W97 (VF). Protein size standards used (lane M, Precision Plus Protein Dual Color Standards) were purchased from Bio-Rad Laboratories, Inc., Hercules, CA, USA. **(Right)** Electron microscopy of RnPV11 virions. A purified virus preparation of RnPV11 was examined using a Hitachi electron microscope model H-7650.

The remaining nine novel *R. necatrix* partitiviruses (RnPV11, RnPV14, RnPV15, RnPV16, RnPV17, RnPV18, RnPV20, RnPV21, and RnPV25) were clustered with betapartitiviruses with bootstrap values of 100. Note that some inter-subgroup relationships within the alphapartitivirus branch were not well supported with high bootstrap values. Notably, most *R. necatrix* partitiviruses were discretely placed within the tree, while some viruses (RnPV4, RnPV6, RnPV14, RnPV15, and RnPV18) were clustered together and nested with a clade of plant betapartitiviruses (namely group 3) (**Figure 3** and **Supplementary Table S4**).

Phenotypic Effects of Novel Partitiviruses on Both Original and Experimental Hosts

The investigation of the biological properties of any virus requires comparing sets of isogenic virus-free and -infected strains. However, when assessing *R. necatrix*-partitivirus interactions, this was difficult because mixed infections occurred frequently and virus curing via hyphal tipping presented difficulties. To this end, we used a virion transfection approach now available for various virus/host combinations.

Of the 15 sequenced, novel partitiviruses of *R. necatrix* identified in this study, 13 (in 5 fungal strains) were tested for their effects on three virus-free strains of two fungal species: the standard strain, W97, of the original host species, *R. necatrix,* and two strains (EP155 wild-type and its Δ*dcl2* KO mutant, an antiviral RNA silencing deficient strain) of the experimental host, *C. parasitica*. Note that many of the fungal strains tested were co-infected by multiple partitiviruses (see **Table 1**). Obtained transfectants are summarized in **Supplementary Table S3**. RnPV11 was singly transfected in W97 (**Table 2**). The five, three and two viruses coinfecting W744, W118, and W1134, respectively, could not be separated via transfection of W97. No significant phenotypic change was observed in W97 transfectants, except W97 co-infected with five viruses (RnPV1 and RnPV14 to RnPV17) originally harbored in W744. Initially, the W97 transfectant infected by the five viruses displayed considerably reduced growth, its mycelia appeared to be deep white in color and were fluffy (**Supplementary Figure S4A**). Subsequent hyphal fusion with virus free W97 led to the presentation of a milder growth defect (**Supplementary Figure S4C**).

Multiple partitiviruses, RnPV18 and RnPV19, coinfecting a single strain W442, segregated and their single infectants could be obtained in *C. parasitica* Δ*dcl2* (**Supplementary Figure S4B**). These Δ*dcl2* transfectants as well as other partitivirus transfectants (RnPV11, RnPV20 and RnPV14–16) (**Supplementary Table S3**) were then anastomosed with RNA silencing-proficient *C. parasitica* EP155 to move the viruses. Even after repeated coculturing, EP155 stably maintained partitiviruses (RnPV11, RnPV20, or RnPV14–16) and their infectants showed reduction in growth rates, pigmentation, and growth of aerial hyphae (**Figure 4**). On the other hand, EP155 strains singly infected by RnPV18 and RnPV19 were either infected asymptomatically or displayed only slightly reduced growth rates in EP155 (**Supplementary Figure S4B**). In Δ*dcl2,* most partitiviruses (RnPV11, RnPV20, RnPV14–16, and probably RnPV19) produced symptomatic infections and induced reduced growth rates and irregular margins (**Figure 4** and **Supplementary Figure S4B**). Similar symptoms have previously been attributed to other partitiviruses from *R. necatrix*, i.e., RnPV2 and RnPV6 (Chiba et al., 2013a, 2016) (**Table 2**).

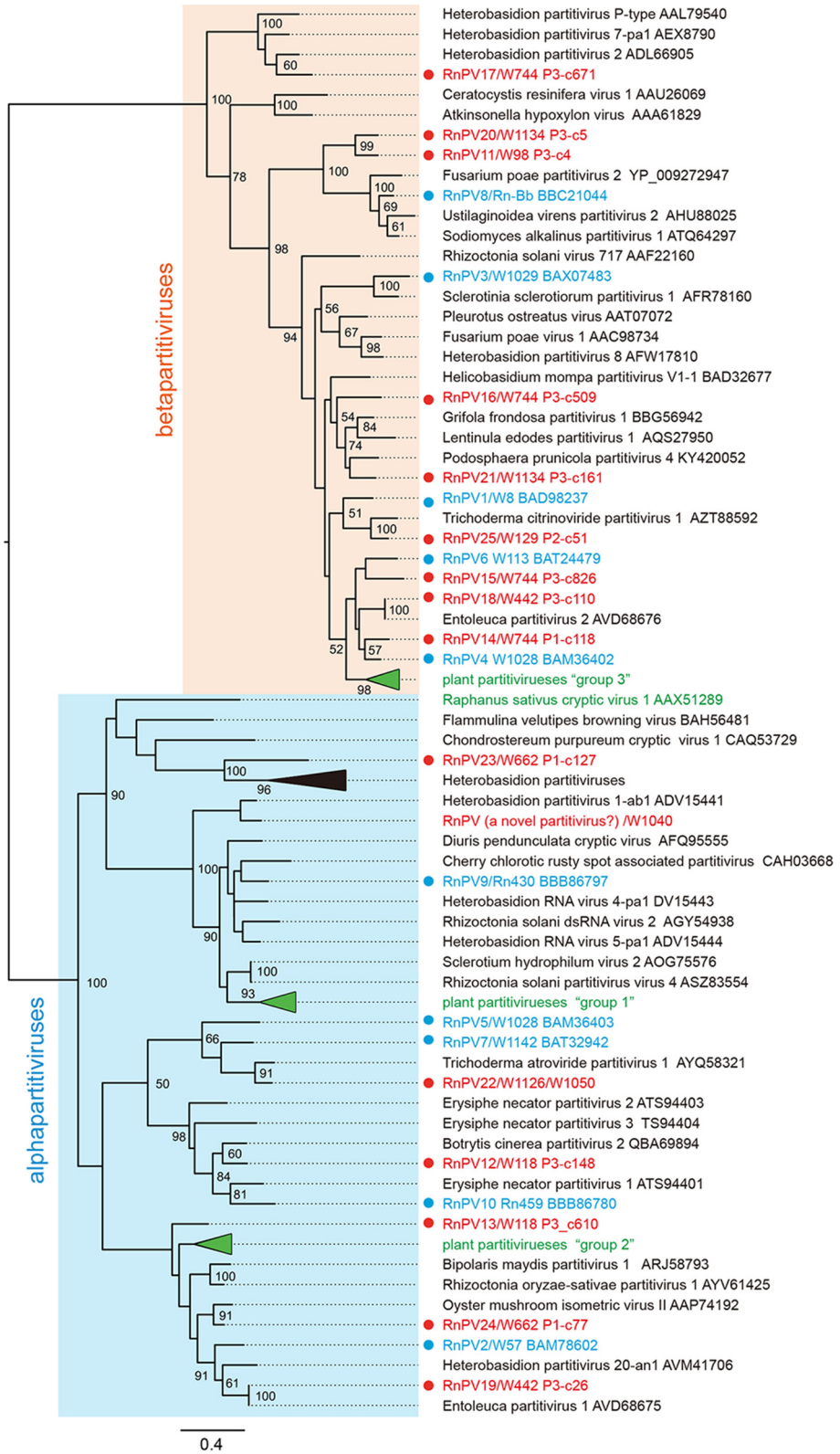

FIGURE 3 | Phylogenetic analysis of novel partitiviruses from field-collected isolates of *R. necatrix*. Maximum likelihood (ML) phylogenetic trees based on amino acid alignments of RdRPs were constructed using PhyML 3.0 with a best fit model RtREV with +G +I +F. Sequences of members of *Alphapartitivirus* and *Betapartitivirus* genera were analyzed together with novel *R. necatrix* partitiviruses. Virus names are followed by GenBank accession numbers. Red and blue circles indicate novel or reported *R. necatrix* partitiviruses, respectively. The numbers at the nodes indicate bootstrap values. The virus names and accession numbers in the collapsed triangles are described in **Supplementary Table S4**.

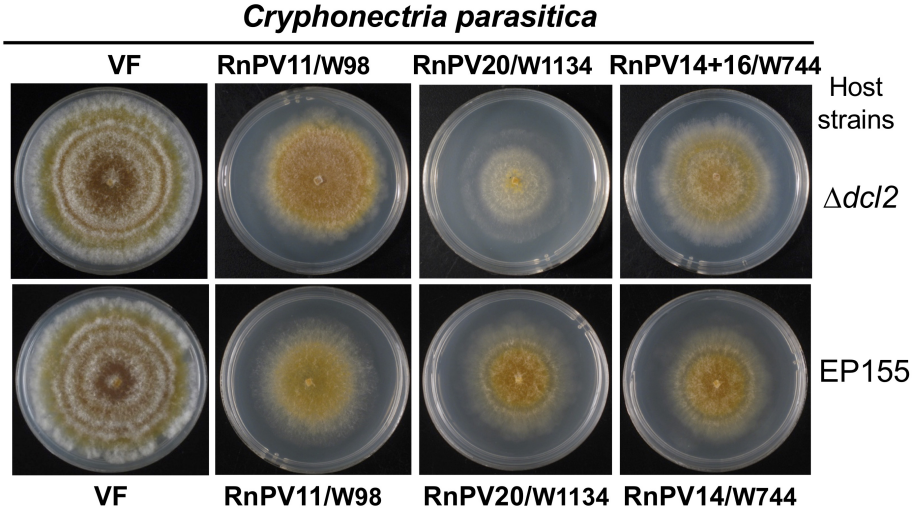

FIGURE 4 | The morphology of *C. parasitica* colonies infected with betapartitiviruses from different *R. necatrix* fungal strains. *C. parasitica* Δ*dcl2* singly infected by RnPV11/W98 or RnPV20/W1134, and doubly infected by RnPV14, and RnPV16 from the W744 strain were grown in PDA for 1 week on a benchtop and photographed. *C. parasitica* EP155 colonies singly infected with the viruses are shown. VF refers to virus free strains.

Different Virus Accumulation Levels in Between Virus Strains and in Between Different Fungal Host Strains

We attempted to compare genomic dsRNA accumulation in the standard *R. necatrix* strain W97. To this end, RnPV6/W558, RnPV10/Rn459, and RnPV11/W98 were selected, because their W97 single transfectants could readily be obtained. For RnPV25/W129, the original filed-collected strain W129 was used. Total RNA fractions were isolated from two biological replicates for each strain, and levels of viral dsRNA accumulation were compared by normalizing to host ribosomal RNAs (**Figure 5**). RnPV11/W98 dsRNA1 and dsRNA2 of 2.4 and 2.3 kbp accumulated in W97 at a level slightly greater than or comparable to, RnPV10/Rn459 (1.9 kbp + 1.9 kbp), or RnPV25/W129 (2.4 kbp + <2.0 kbp). The band intensity of RnPV6/W558 dsRNA (2.5 kbp + 2.5 kbp) was much fainter than those of dsRNA from the other three partitiviruses. Note that dsRNA1 and dsRNA2 of the four tested partitiviruses, except for RnPV25/W129, were completely sequenced and co-migrated in the agarose gel. Considering a second dsRNA band for RnPV25/W129, the size of partially sequenced dsRNA2 appears to be similar to dsRNA1 and have comigrated with it (**Figure 5**). These results suggest variability in partitiviral dsRNA accumulation within the same *R. necatrix* host strain.

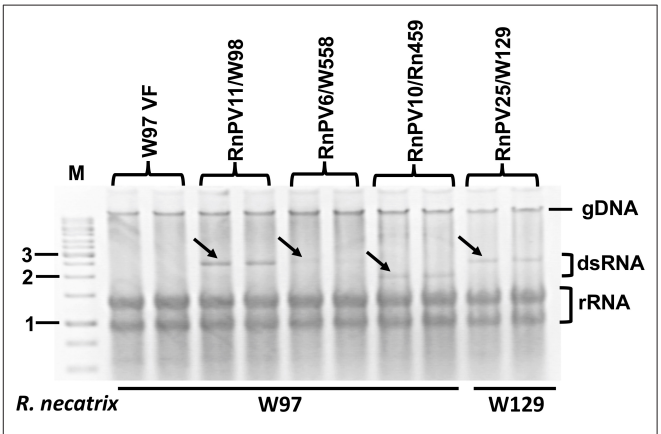

FIGURE 5 | Virus accumulation of four partitivirus strains in *R. necatrix* host strains. One alphapartitivirus (RnPV10) and three betapartitiviruses (RnPV6, RnPV11, and RnPV25) were used for this analysis. Total nucleic acid fractions were isolated from W97 mycelia singly infected by RnPV11/W98, RnPV6/W558, or RnPV10/Rn549, and analyzed via 1.2% agarose gel electrophoresis. These W97 single infectants were obtained by transfection of protoplasts with respective partitivirus virions. For RnPV25/W129, the original host strain W129 was used. Black arrows indicate the migration positions of dsRNA genomic segments of the respective partitiviruses. M refers to the 1-kb DNA ladder. rRNA was used as a loading control. gDNA indicates the migration position of the host genomic DNA.

Generally, partitiviruses from *R. necatrix* accumulate to the greater levels in the original host, rather than the experimental host strain, *C. parasitica* (Chiba et al., 2013a, 2016). Next, we compared the accumulation of a single partitivirus (RnPV11 or RnPV6) in the three host strains, which included the standard *R. necatrix* strain W97, *C. parasitica* EP155 and Δ*dcl2*. Inspection of **Figure 6** clearly shows that RnPV11/W98 and RnPV6/558 accumulated more in the RNA silencing-deficient Δ*dcl2* than in RNA silencing-competent EP155. However, both viruses accumulated more highly in W97 than in wild-type EP155 and Δ*dcl2*. We obtained a similar accumulation profile using three biological replicates (data not shown).

DISCUSSION

In this study, a total of 20 partitiviruses were isolated from 16 field isolates of the white root rot fungus, *R. necatrix*.

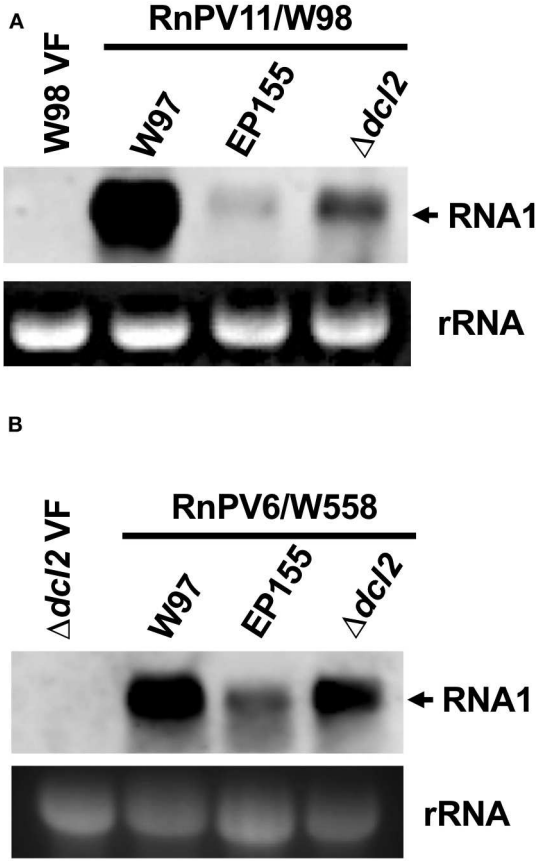

FIGURE 6 | Comparison of virus accumulation in three different fungal strains *R. necatrix* W97 and *C. parasitica* wild-type EP155 and its mutant Δ*dcl2*. A. Equal amounts of total RNA was obtained from three fungal strains each singly infected by RnPV11/W98 **(A)** or RnPV6/W558 **(B)**, and subjected to Northern blotting. The probes used are DIG-labeled PCR fragments specific to RnPV11 dsRNA1 **(A)** and RnPV6 dsRNA1 **(B)**, respectively, that were prepared using specific primer sets, W98-RdRp-F and W98-RdRp-R, and W558-RdRp-F and W558-RdRp-R. See **Supplementary Table S1** for the sequences of the primers used in probe preparation.

The isolates were characterized molecularly and a subset was characterized biologically. Interestingly, 15 (RnPV11 to RnPV25) may belong to new species, Rosellinia necatrix partitivirus 11 to Rosellinia necatrix partitivirus 25, and six other partitiviruses (RnPV1, RnPV3–RnPV6) belong to known or previously proposed partitiviral species. This study has shown that all of the characterized partitiviruses should be placed within the two genera of *Alphapartitivirus* and *Betapartitivirus,* which are members of the family *Partitiviridae*. However, they show great variability with respect to their biological and virological properties. This study also provided a platform for the further exploration of molecular mechanisms that underly differences in viral symptoms and replication patterns.

The 15, completely sequenced, novel *R. necatrix* partitiviruses (6 alphapartitiviruses and 9 betapartitiviruses) provide interesting insights into partitivirus biology. Partitiviruses that infect fungi are currently classified into three genera: *Alphapartitivirus*, *Betapartitivirus*, and *Gammapartitivirus* (Nibert et al., 2014; Vainio et al., 2018a). This and previous studies have revealed the prevalence of alpha- and betapartitiviruses, but not gammapartitiviruses, in *R. necatrix* (Chiba et al., 2013a, 2016; Kondo et al., 2013b; Arjona-Lopez et al., 2018). Our failure to detect gammapartitiviruses in *R. necatrix* is surprising, because gammapartitiviruses have been reported only in ascomycetes thus far (Nibert et al., 2014; Vainio et al., 2018a). Among the other most extensively surveyed fungi for virus hunting are ascomycetous *C. parasitica* (class: Sordariomycetes), and *Sclerotinia sclerotiorum* (class: Leotiomycetes), and basidiomycetous *Heterobasidion* spp. The fact that no gammapartitiviruses have been reported from these fungi (Jiang et al., 2013; Vainio and Hantula, 2016) may suggest that gammapartitiviruses are restricted to specific ascomycetes and/or narrow host ranges, although a gammapartitivirus has been shown to replicate in plant protoplasts (Nerva et al., 2017b). *Alphapartitivirus* and *Betapartitivirus* each include both plant and fungal partitiviruses. It is presumed that those viruses, or their ancestors, may have been transferred between the two kingdoms, which eventually lead to their higher prevalence relative to gammapartitiviruses.

An interesting relation was found between the newly discovered betapartitivirus, RnPV21/W1134, and a previously characterized betapartitivirus, RnPV1/W8 (Sasaki et al., 2005), which was also discovered in the W744 strain in this study. The two segments of RnPV21 possessed the conserved terminal sequences, indicating that they represented the genome of the virus. However, the two viruses shared 56 and 94% amino acid sequence identities for RdRP and CP, respectively. While the highest degree of CP amino acid sequence identify was detected between RnPV1 and RnPV21, the highest degree of RdRP amino acid sequence identity (65%) was observed with an another betapartitivirus (Podosphaera prunicola partitivirus 4) from the sweet cherry powdery mildew fungus. Generally, partitivirus CP genes are less conserved than RdRP (Nibert et al., 2014). These facts strongly suggest that there might have been a reassortment event between two betapartitiviruses. Similar reassortment events have recently been proposed among isolates of different partitiviruses by Petrzik (2019).

Co-infection of the Japanese *R. necatrix* strain, W442, by two novel partitiviruses, RnPV18 (*Betapartitivirus*) and RnPV19 (*Alphapartitivirus*), was detected (**Table 2**). The Japanese fungal strain W442 was isolated in Hyogo Prefecture (**Table 1**). Interestingly, the same combination of partitiviruses (EnPV2 and EnPV1, closely related to RnPV18 and RnPV19, respectively) have been reported from Spanish isolates of *Entoleuca* sp. as well as *R. necatrix* that infested or colonized avocado soil of southern coastal area of Spain (Velasco et al., 2019, 2020). These observations suggest that interspecific horizontal transfer of the two partitiviruses may have occurred between *R. necatrix* and *Entoleuca* sp., as previously suggested or demonstrated for different viruses (Deng et al., 2003; Liu et al., 2003; Yaegashi et al., 2013; Vainio and Hantula, 2016; Khalifa and MacDiarmid, 2019). The coinfection of two fungal hosts by the

same set of two taxonomically different partitiviruses (alpha- and betapartitiviruses) suggests the possibility of mutualistic or commensal interactions between the coinfecting partitiviruses. At present, we cannot rule out the possibility that the two viruses accidentally co-transferred from an originally co-infected fungal strain. Further, these partitiviruses were isolated from geographically distinct locations, Japan and Spain. The fact that RnPV18 and RnPV19, and EnPV2 and EnPV1 were isolated from two different sympatric fungal species suggests that contamination in the laboratory was highly unlikely. It is difficult to determine the origin of the fungus carrying the viruses, which may have been brought together via crop plants and/or host fungi as a result of human activities such as tourism and trade (see below).

Horizontal transfer of fungal viruses between two strains of single fungal species, and also between different fungal species, have been suggested by several research groups (Yaegashi et al., 2013). The same subset of partitiviruses, megabirnaviruses (dsRNA viruses), hypoviruses, and fusagraviruses (ssRNA viruses) were detectable within two different fungal species, *R. necatrix* and *Entoleuca* sp., collected from avocado fields in Andalusia, Spain (Velasco et al., 2018, 2019). Previous viral identification and characterization studies compared genomic sequences of viruses that belonged to the same species, but were isolated from different continents. For example, 95 and 94% amino acid sequence identities were detected between the isolates of positive-sense (a mitovirus, family *Narnaviridae*) and negative-sense (a mymonovirus, family *Mymonavirudae*) ssRNA viruses from *Sclerotinia sclerotiorum* collected from the USA and Australia (Mu et al., 2017). The sequence identities determined in this study were greater than those previously reported. This may suggest that the virus-harboring fungi were imported relatively recently with crop seedlings. In Spain, *R. necatrix* is an endemic soil-borne inhabitant in soils in which previous rainfed susceptible crops such as olive, almond, and grapes were cultivated. Later (1970's) these crops were replaced by high-value avocado irrigated crop (Lopez-Herrera and Zea-Bonilla, 2007), in which soils are highly infested by this pathogen with some colonized by the antagonistic fungi *Entoleuca* sp. (Arjona-Girona and Lopez-Herrera, 2018). EnPV1 and EnPV2 and these have been also detected in a *Fusarium* isolate collected from the same avocado orchards in addition to *Entoleuca* sp. and *R. necatrix* (Velasco et al., 2019, 2020). Presumably, these fungal viruses have been present in these soils for many years and their horizontal transmission between different fungal species inhabiting the same soils is likely to happen. However, it remains unknown which of them has been the initial source of transmission of these fungal viruses to the rest of fungal species or how the viruses have been horizontally transferred.

Of the 16 fungal isolates tested, five produced mixed infections, as exemplified in W744 that was infected with five different betapartitiviruses. There have been reported cases of virus/virus interactions in mixed infections (Hillman et al., 2018). Thus, there is a need to obtain single infectants when assigning two genomic segments to single viruses and characterizing each partitivirus. To this end, we used the transfection approach previously developed for assessing various virus-host combinations (Sasaki et al., 2006; Kanematsu et al., 2010; Chiba et al., 2013a, 2016; Salaipeth et al., 2014). We obtained transfectants either in the *R. necatrix* W97, *C. parasitica* EP155 genetic background, or both W97 and EP155, which were singly infected partitiviruses. For these viruses, we confirmed that the two segments matched that of the genome of specified partitiviruses. For other coinfecting partitiviruses, our conclusions were based on the highly conserved terminal sequences found between segments (**Supplementary Table S2**). Furthermore, this facilitated the comparison of virus titers in EP155 and its Δ*dcl2* disruptant.

Some of the characterized partitiviruses differed from one another with respect to their accumulation levels and degree of symptom induction (**Figures 4–6** and **Table 2**). These characteristics are related to antiviral/counter-defense responses incited by hosts and viruses. Previous studies have revealed that many homologous and heterologous viruses are targeted by antiviral RNA silencing (Segers et al., 2007; Sun et al., 2009; Chiba et al., 2013a,b, 2016; Salaipeth et al., 2014; Chiba and Suzuki, 2015). Many of these viruses induce antiviral RNA silencing via transcriptional up-regulation of the genes including a dicer (*dcl2*) and an argonaute (*agl2*) (Sun et al., 2009; Chiba and Suzuki, 2015). Previous reports showed that a victorivirus (dsRNA virus, family *Totiviridae*), RnVV1, was sensitive to, and targeted by, RNA silencing, but did not induce antiviral RNA silencing (Chiba and Suzuki, 2015). CHV1 is tolerant to RNA silencing and does not induce *dcl2* transcription, which was largely attributed to the activity of the RNA silencing suppressor, p29 (Segers et al., 2007; Chiba and Suzuki, 2015). Andika et al. (2017) developed an antiviral RNA silencing monitoring system through the *dcl2* transcription using a GFP reporter construct driven by the *dcl2* promoter with *C. parasitica* genetic background. Interestingly, partitiviruses isolated from *R. necatrix* showed great variability in induction levels of *dcl2* (Aulia et al., unpublished data). It is known that some partitiviruses tolerate RNA silencing while others are sensitive to silencing (Chiba et al., 2016) (Chiba and Suzuki, unpublished data). This study provided researchers with the materials necessary to obtain insights into mechanisms controlling diversity of host-partitivirus interactions.

DATA AVAILABILITY STATEMENT

The datasets presented in this study can be found in online repositories. The names of the repository/repositories and accession number(s) can be found here: https://www.ddbj.nig.ac.jp/, LC517370-LC517399, LC521312-LC521313 (32 entries).

AUTHOR CONTRIBUTIONS

NS designed the experiments and wrote the manuscript. PT, SH, CM, KH, and JA-L performed the experimental work. SK collected samples. PT, SK, CL-H, HK, and NS analyzed the data. PT and HK were involved in discussion and manuscript revision. All authors have given approval to the final version of the manuscript.

FUNDING

This work was supported in part by Yomogi Inc. (to NS), the Program for the Promotion of Basic and Applied Research for Innovation in Bio-Oriented Industries (to SK and NS), and Grants-in-Aid for Scientific Research (A) and on Innovative Areas from the Japanese Ministry of Education, Culture, Sports, Science, and Technology (MEXT) (17H01463 and 16H06436, 16H06429, and 16K21723 to NS). The funder, Yomogi Inc., was not involved in the study design, collection, analysis, interpretation of data, the writing of this article or the decision to submit it for publication.

ACKNOWLEDGMENTS

The authors sincerely thank Dr. Donald L. Nuss (IBBR, University of Maryland) and Dr. Masanobu Tabata (Forestry & Forest Products Research Institute) for their generous gift of the *C. parasitica* strains EP155, Δ*dcl2*, and Δ*agl2* and some *R. necatrix* field isolates used in this study.

SUPPLEMENTARY MATERIAL

The Supplementary Material for this article can be found online at: https://www.frontiersin.org/articles/10.3389/fmicb.2020.01064/full#supplementary-material

REFERENCES

Andika, I. B., Jamal, A., Kondo, H., and Suzuki, N. (2017). SAGA complex mediates the transcriptional up-regulation of antiviral RNA silencing. *Proc. Natl. Acad. Sci. U.S.A.* 114, E3499–E3506. doi: 10.1073/pnas.1701196114

Andika, I. B., Kondo, H., and Suzuki, N. (2019). Dicer functions transcriptionally and post-transcriptionally in a multilayer antiviral defense. *Proc. Natl. Acad. Sci. U.S.A.* 116, 2274–2281. doi: 10.1073/pnas.1812407116

Arakawa, M., Nakamura, H., Uetake, Y., and Matsumoto, N. (2002). Presence and distribution of double-stranded RNA elements in the white root rot fungus *Rosellinia necatrix*. *Mycoscience* 43, 21–26. doi: 10.1007/s102670200004

Arjona-Girona, I., and Lopez-Herrera, C. J. (2018). Study of a new biocontrol fungal agent for avocado white root rot. *Biol. Control* 117, 6–12. doi: 10.1016/j.biocontrol.2017.08.018

Arjona-Lopez, J. M., Telengech, P., Jamal, A., Hisano, S., Kondo, H., Yelin, M. D., et al. (2018). Novel, diverse RNA viruses from mediterranean isolates of the phytopathogenic fungus, *Rosellinia necatrix*: insights into evolutionary biology of fungal viruses. *Environ. Microbiol.* 20, 1464–1483. doi: 10.1111/1462-2920.14065

Bhatti, M. F., Jamal, A., Petrou, M. A., Cairns, T. C., Bignell, E. M., and Coutts, R. H. (2011). The effects of dsRNA mycoviruses on growth and murine virulence of *Aspergillus fumigatus*. *Fungal. Genet. Biol.* 48, 1071–1075. doi: 10.1016/j.fgb.2011.07.008

Chiba, S., Jamal, A., and Suzuki, N. (2018). First evidence for internal ribosomal entry sites in diverse fungal virus genomes. *MBio* 9:e02350-17. doi: 10.1128/mBio.02350-17

Chiba, S., Kondo, H., Tani, A., Saisho, D., Sakamoto, W., Kanematsu, S., et al. (2011). Widespread endogenization of genome sequences of non-retroviral RNA viruses into plant genomes. *PLoS Pathog.* 7:e1002146. doi: 10.1371/journal.ppat.1002146

Chiba, S., Lin, Y. H., Kondo, H., Kanematsu, S., and Suzuki, N. (2013a). Effects of defective-interfering RNA on symptom induction by, and replication of a novel partitivirus from a phytopathogenic fungus *Rosellinia necatrix*. *J. Virol.* 87, 2330–2341. doi: 10.1128/JVI.02835-12

Chiba, S., Lin, Y. H., Kondo, H., Kanematsu, S., and Suzuki, N. (2013b). A novel victorivirus from a phytopathogenic fungus, *Rosellinia necatrix* is infectious as particles and targeted by RNA silencing. *J. Virol.* 87, 6727–6738. doi: 10.1128/JVI.00557-13

Chiba, S., Lin, Y. H., Kondo, H., Kanematsu, S., and Suzuki, N. (2016). A novel betapartitivirus RnPV6 from *Rosellinia necatrix* tolerates host RNA silencing but is interfered by its defective RNAs. *Virus Res.* 219, 62–72. doi: 10.1016/j.virusres.2015.10.017

Chiba, S., Salaipeth, L., Lin, Y. H., Sasaki, A., Kanematsu, S., and Suzuki, N. (2009). A novel bipartite double-stranded RNA mycovirus from the white root rot fungus *Rosellinia necatrix*: molecular and biological characterization, taxonomic considerations, and potential for biological control. *J. Virol.* 83, 12801–12812. doi: 10.1128/JVI.01830-09

Chiba, S., and Suzuki, N. (2015). Highly activated RNA silencing via strong induction of dicer by one virus can interfere with the replication of an unrelated Virus *Proc. Natl. Acad. Sci. U.S.A.* 112, E4911–E4918. doi: 10.1073/pnas.1509151112

Cho, W. K., Lee, K. M., Yu, J., Son, M., and Kim, K. H. (2013). Insight into mycoviruses infecting fusarium species. *Adv. Virus Res.* 86, 273–288. doi: 10.1016/B978-0-12-394315-6.00010-6

Deng, F., Xu, R., and Boland, G. J. (2003). Hypovirulence-associated double-stranded RNA from Sclerotinia homoeocarpa is conspecific with Ophiostoma novo-ulmi mitovirus 3a-Ld. *Phytopathology* 93, 1407–1414. doi: 10.1094/PHYTO.2003.93.11.1407

Eusebio-Cope, A., Sun, L., Tanaka, T., Chiba, S., Kasahara, S., and Suzuki, N. (2015). The chestnut blight fungus for studies on virus/host and virus/virus interactions: from a natural to a model host. *Virology* 477, 164–175. doi: 10.1016/j.virol.2014.09.024

Eusebio-Cope, A., and Suzuki, N. (2015). Mycoreovirus genome rearrangements associated with RNA silencing deficiency. *Nucl. Acids Res.* 43, 3802–3813. doi: 10.1093/nar/gkv239

Faruk, M. I., Eusebio-Cope, A., and Suzuki, N. (2008). A host factor involved in hypovirus symptom expression in the chestnut blight fungus, *Cryphonectria parasitica*. *J. Virol.* 82, 740–754. doi: 10.1128/JVI.02015-07

Ghabrial, S. A., Caston, J. R., Jiang, D., Nibert, M. L., and Suzuki, N. (2015). 50-plus years of fungal viruses. *Virology* 479–480, 356–368. doi: 10.1016/j.virol.2015.02.034

Guindon, S., Dufayard, J. F., Lefort, V., Anisimova, M., Hordijk, W., and Gascuel, O. (2010). New algorithms and methods to estimate maximum-likelihood phylogenies: assessing the performance of PhyML 3.0. *Syst. Biol.* 59, 307–321. doi: 10.1093/sysbio/syq010

Hillman, B. I., Aulia, A., and Suzuki, N. (2018). Viruses of plant-interacting fungi. *Adv. Virus Res.* 100, 99–116. doi: 10.1016/bs.aivir.2017.10.003

Hillman, B. I., Supyani, S., Kondo, H., and Suzuki, N. (2004). A reovirus of the fungus *Cryphonectria parasitica* that is infectious as particles and related to the coltivirus genus of animal pathogen. *J. Virol.* 78, 892–898. doi: 10.1128/JVI.78.2.892-898.2004

Ikeda, K., Nakamura, H., Arakawa, M., and Matsumoto, N. (2004). Diversity and vertical transmission of double-stranded RNA elements in root rot pathogens of trees, helicobasidium mompa and *Rosellinia necatrix*. *Mycol. Res.* 108, 626–634. doi: 10.1017/S0953756204000061

Jiang, D., Fu, Y., Guoqing, L., and Ghabrial, S. A. (2013). Viruses of the plant pathogenic fungus *Sclerotinia sclerotiorum*. *Adv. Virus Res.* 86, 215–248. doi: 10.1016/B978-0-12-394315-6.00008-8

Jiang, D., and Ghabrial, S. A. (2004). Molecular characterization of *Penicillium chrysogenum* virus: reconsideration of the taxonomy of the genus chrysoVirus *J. Gen. Virol. 85*, 2111–2121. doi: 10.1099/vir.0.79842-0

Jiang, Y., Wang, J., Yang, B., Wang, Q., Zhou, J., and Yu, W. (2019). Molecular characterization of a debilitation-associated partitivirus Infecting the pathogenic fungus aspergillus flavus. *Front. Microbiol.* 10:626. doi: 10.3389/fmicb.2019.00626

Kanematsu, S., Sasaki, A., Onoue, M., Oikawa, Y., and Ito, T. (2010). Extending the fungal host range of a partitivirus and a mycoreovirus from *Rosellinia necatrix* by inoculation of protoplasts with virus particles. *Phytopathology* 100, 922–930. doi: 10.1094/PHYTO-100-9-0922

Kanhayuwa, L., Kotta-Loizou, I., Ozkan, S., Gunning, A. P., and Coutts, R. H. (2015). A novel mycovirus from *Aspergillus fumigatus* contains four unique dsRNAs as its genome and is infectious as dsRNA. *Proc. Natl. Acad. Sci. U.S.A.* 112, 9100–9105. doi: 10.1073/pnas.1419225112

Katoh, K., and Standley, D. M. (2013). MAFFT multiple sequence alignment software version 7: improvements in performance and usability. *Mol. Biol. Evol.* 30, 772–780. doi: 10.1093/molbev/mst010

Khalifa, M. E., and MacDiarmid, R. M. (2019). A novel totivirus naturally occurring in two different fungal genera. *Front. Microbiol.* 10:2318. doi: 10.3389/fmicb.2019.02318

Kondo, H., Chiba, S., Maruyama, K., Andika, I. B., and Suzuki, N. (2019). A novel insect-infecting virga/nege-like virus group and its pervasive endogenization into insect genomes. *Virus Res.* 262, 37–47. doi: 10.1016/j.virusres.2017.11.020

Kondo, H., Chiba, S., Sasaki, A., Kanematsu, S., and Suzuki, N. (2013a). Evidence for negative-strand RNA virus infection in fungi. *Virology* 435, 201–209. doi: 10.1016/j.virol.2012.10.002

Kondo, H., Chiba, S., and Suzuki, N. (2015). Detection and analysis of non-retroviral RNA virus-like elements in plant, fungal, and insect genomes. *Methods Mol. Biol.* 1236, 73–88. doi: 10.1007/978-1-4939-1743-3_7

Kondo, H., Kanematsu, S., and Suzuki, N. (2013b). Viruses of the white root rot fungus, *Rosellinia necatrix*. *Adv. Virus Res.* 86, 177–214. doi: 10.1016/B978-0-12-394315-6.00007-6

Lefort, V., Longueville, J. E., and Gascuel, O. (2017). SMS: smart model selection in PhyML. *Mol. Biol. Evol.* 34, 2422–2424. doi: 10.1093/molbev/msx149

Lin, Y. H., Chiba, S., Tani, A., Kondo, H., Sasaki, A., Kanematsu, S., et al. (2012). A novel quadripartite dsRNA virus isolated from a phytopathogenic filamentous fungus, *Rosellinia necatrix*. *Virology* 426, 42–50. doi: 10.1016/j.virol.2012.01.013

Liu, H., Fu, Y., Jiang, D., Li, G., Xie, J., Cheng, J., et al. (2010). Widespread horizontal gene transfer from double-stranded RNA viruses to eukaryotic nuclear genomes. *J. Virol.* 84, 11876–11887. doi: 10.1128/JVI.00955-10

Liu, L., Xie, J., Cheng, J., Fu, Y., Li, G., Yi, X., et al. (2014). Fungal negative-stranded RNA virus that is related to bornaviruses and nyaviruses. *Proc. Natl. Acad. Sci. U.S.A.* 111, 12205–12210. doi: 10.1073/pnas.1401786111

Liu, Y. C., Linder-Basso, D., Hillman, B. I., Kaneko, S., and Milgroom, M. G. (2003). Evidence for interspecies transmission of viruses in natural populations of filamentous fungi in the genus Cryphonectria. *Mol. Ecol.* 12, 1619–1628. doi: 10.1046/j.1365-294X.2003.01847.x

Lopez-Herrera, C. J., and Zea-Bonilla, T. (2007). Effects of benomyl, carbendazim, fluazinam and thiophanate methyl on white root rot of avocado. *Crop. Protect.* 26, 1186–1192. doi: 10.1016/j.cropro.2006.10.015

Mu, F., Xie, J., Cheng, S., You, M. P., Barbetti, M. J., Jia, J., et al. (2017). Virome characterization of a collection of *S. sclerotiorum* from Australia. *Front. Microbiol.* 8:2540. doi: 10.3389/fmicb.2017.02540

Muhire, B. M., Varsani, A., and Martin, D. P. (2014). SDT: A virus classification tool based on pairwise sequence alignment and identity calculation. *PLoS ONE* 9:e0108277. doi: 10.1371/journal.pone.0108277

Nakakoshi, M., Nishioka, H., and Katayama, E. (2011). New versatile staining reagents for biological transmission electron microscopy that substitute for uranyl acetate. *J. Electron. Microsc.* 60, 401–407. doi: 10.1093/jmicro/dfr084

Nerva, L., Silvestri, A., Ciuffo, M., Palmano, S., Varese, G. C., and Turina, M. (2017a). Transmission of penicillium aurantiogriseum partiti-like virus 1 to a new fungal host (*Cryphonectria parasitica*) confers higher resistance to salinity and reveals adaptive genomic changes. *Environ. Microbiol.* 19, 4480–4492. doi: 10.1111/1462-2920.13894

Nerva, L., Varese, G. C., Falk, B. W., and Turina, M. (2017b). Mycoviruses of an endophytic fungus can replicate in plant cells: evolutionary implications. *Sci. Rep.* 7:1908. doi: 10.1038/s41598-017-02017-3

Nibert, M. L., Ghabrial, S. A., Maiss, E., Lesker, T., Vainio, E. J., Jiang, D., et al. (2014). Taxonomic reorganization of family partitiviridae and other recent progress in partitivirus research. *Virus Res.* 188C, 128–141. doi: 10.1016/j.virusres.2014.04.007

Nibert, M. L., Tang, J., Xie, J., Collier, A. M., Ghabrial, S. A., Baker, T. S., et al. (2013). 3D structures of fungal partitiviruses. *Adv. Virus Res.* 86, 59–85. doi: 10.1016/B978-0-12-394315-6.00003-9

Nuss, D. L. (2005). Hypovirulence: mycoviruses at the fungal-plant interface. *Nat. Rev. Microbiol.* 3, 632–642. doi: 10.1038/nrmicro1206

Pearson, M. N., Beever, R. E., Boine, B., and Arthur, K. (2009). Mycoviruses of filamentous fungi and their relevance to plant pathology. *Mol. Plant. Pathol.* 10, 115–128. doi: 10.1111/j.1364-3703.2008.00503.x

Petrzik, K. (2019). Evolutionary forces at work in partitiviruses. *Virus Genes* 55, 563–573. doi: 10.1007/s11262-019-01680-0

Pliego, C., Lopez-Herrera, C., Ramos, C., and Cazorla, F. M. (2012). Developing tools to unravel the biological secrets of *Rosellinia necatrix*, an emergent threat to woody crops. *Mol. Plant. Pathol* 13, 226–239. doi: 10.1111/j.1364-3703.2011.00753.x

Salaipeth, L., Chiba, S., Eusebio-Cope, A., Kanematsu, S., and Suzuki, N. (2014). Biological properties and expression strategy of *Rosellinia necatrix* megabirnavirus 1 analyzed in an experimental host, *Cryphonectria parasitica*. *J. Gen. Virol.* 95, 740–750. doi: 10.1099/vir.0.058164-0

Sasaki, A., Kanematsu, S., Onoue, M., Oikawa, Y., Nakamura, H., and Yoshida, K. (2007). Artificial infection of *Rosellinia necatrix* with purified viral particles of a member of the genus mycoreovirus reveals its uneven distribution in single colonies. *Phytopathology* 97, 278–286. doi: 10.1094/PHYTO-97-3-0278

Sasaki, A., Kanematsu, S., Onoue, M., Oyama, Y., and Yoshida, K. (2006). Infection of *Rosellinia necatrix* with purified viral particles of a member of Partitiviridae (RnPV1-W8). *Arch. Virol.* 151, 697–707. doi: 10.1007/s00705-005-0662-2

Sasaki, A., Miyanishi, M., Ozaki, K., Onoue, M., and Yoshida, K. (2005). Molecular characterization of a partitivirus from the plant pathogenic ascomycete *Rosellinia necatrix*. *Arch. Virol.* 150, 1069–1083. doi: 10.1007/s00705-005-0494-0

Sasaki, A., Nakamura, H., Suzuki, N., and Kanematsu, S. (2016). Characterization of a new megabirnavirus that confers hypovirulence with the aid of a co-infecting partitivirus to the host fungus, *Rosellinia necatrix*. *Virus Res.* 219, 73–82. doi: 10.1016/j.virusres.2015.12.009

Segers, G. C., Zhang, X., Deng, F., Sun, Q., and Nuss, D. L. (2007). Evidence that RNA silencing functions as an antiviral defense mechanism in fungi. *Proc. Natl. Acad. Sci. U.S.A.* 104, 12902–12906. doi: 10.1073/pnas.0702500104

Shamsi, W., Sato, Y., Jamal, A., Shahi, S., Kondo, H., Suzuki, N., et al. (2019). Molecular and biological characterization of a novel botybirnavirus identified from a Pakistani isolate of alternaria alternata. *Virus Res.* 263, 119–128. doi: 10.1016/j.virusres.2019.01.006

Shimizu, T., Kanematsu, S., and Yaegashi, H. (2018). Draft genome sequence and transcriptional analysis of *Rosellinia necatrix* infected with a virulent mycoVirus *Phytopathology* 108, 1206–1211. doi: 10.1094/PHYTO-11-17-0365-R

Sun, Q., Choi, G. H., and Nuss, D. L. (2009). A single argonaute gene is required for induction of RNA silencing antiviral defense and promotes viral RNA recombination. *Proc. Natl. Acad. Sci. U.S.A.* 106, 17927–17932. doi: 10.1073/pnas.0907552106

Supyani, S., Hillman, B. I., and Suzuki, N. (2007). Baculovirus expression of the 11 mycoreovirus-1 genome segments and identification of the guanylyltransferase-encoding segment. *J. Gen. Virol.* 88, 342–350. doi: 10.1099/vir.0.82318-0

Suzuki, N. (2017). Frontiers in fungal virology. *J. Gen. Plant Pathol.* 83, 419–423. doi: 10.1007/s10327-017-0740-9

Suzuki, N., Supyani, S., Maruyama, K., and Hillman, B. I. (2004). Complete genome sequence of Mycoreovirus-1/Cp9B21, a member of a novel genus within the family reoviridae, isolated from the chestnut blight fungus *Cryphonectria parasitica*. *J. Gen. Virol.* 85, 3437–3448. doi: 10.1099/vir.0.80293-0

Talavera, G., and Castresana, J. (2007). Improvement of phylogenies after removing divergent and ambiguously aligned blocks from protein sequence alignments. *Syst. Biol.* 56, 564–577. doi: 10.1080/10635150701472164

Urayama, S., Katoh, Y., Fukuhara, T., Arie, T., Moriyama, H., and Teraoka, T. (2015). Rapid detection of Magnaporthe oryzae chrysovirus 1-A from fungal colonies on agar plates and lesions of rice blast. *J. Gen. Plant Pathol.* 81, 97–102. doi: 10.1007/s10327-014-0567-6

Vainio, E. J., Chiba, S., Ghabrial, S. A., Maiss, E., Roossinck, M., Sabanadzovic, S., et al. (2018a). ICTV virus taxonomy profile: partitiviridae. *J. Gen. Virol.* 99, 17–18. doi: 10.1099/jgv.0.000985

Vainio, E. J., and Hantula, J. (2016). Taxonomy, biogeography and importance of heterobasidion viruses. *Virus Res.* 219, 2–10. doi: 10.1016/j.virusres.2015.10.014

Vainio, E. J., Jurvansuu, J., Hyder, R., Kashif, M., Piri, T., Tuomivirta, T., et al. (2018b). Heterobasidion partitivirus 13 mediates severe growth debilitation and major alterations in the gene expression of a fungal forest pathogen. *J. Virol.* 92, e01744–e01717. doi: 10.1128/JVI.01744-17

Vainio, E. J., Korhonen, K., Tuomivirta, T. T., and Hantula, J. (2010). A novel putative partitivirus of the saprotrophic fungus Heterobasidion ecrustosum infects pathogenic species of the heterobasidion annosum complex. *Fungal. Biol.* 114, 955–965. doi: 10.1016/j.funbio.2010.09.006

Velasco, L., Arjona-Girona, I., Ariza-Fernandez, M. T., Cretazzo, E., and Lopez-Herrera, C. (2018). A novel hpovirus species from *Xylariaceae* fungi infecting avocado. *Front. Microbiol.* 9:778. doi: 10.3389/fmicb.2018.00778

Velasco, L., Arjona-Girona, I., Cretazzo, E., and Lopez-Herrera, C. (2019). Viromes in *Xylariaceae* fungi infecting avocado in Spain. *Virology* 532, 11–21. doi: 10.1016/j.virol.2019.03.021

Velasco, L., Lopez Herrera, C. J., and Cretazzo, E. (2020). Two novel partitiviruses that accumulate differentially in *Rosellinia necatrix* and *Entoleuca* sp. infecting avocado. *Virus. Res.* 285. doi: 10.1016/j.virusres.2020.198020

Wang, L., Jiang, J., Wang, Y., Hong, N., Zhang, F., Xu, W., et al. (2014). Hypovirulence of the phytopathogenic fungus *Botryosphaeria dothidea*: association with a coinfecting chrysovirus and a partitiVirus *J. Virol.* 88, 7517–7527. doi: 10.1128/JVI.00538-14

Xiao, X., Cheng, J., Tang, J., Fu, Y., Jiang, D., Baker, T. S., et al. (2014). A novel partitivirus that confers hypovirulence on plant pathogenic fungi. *J. Virol.* 88, 10120–10133. doi: 10.1128/JVI.01036-14

Xie, J., and Jiang, D. (2014). New insights into mycoviruses and exploration for the biological control of crop fungal diseases. *Annu. Rev. Phytopathol.* 52, 45–68. doi: 10.1146/annurev-phyto-102313-050222

Yaegashi, H., and Kanematsu, S. (2016). Natural infection of the soil-borne fungus *Rosellinia necatrix* with novel mycoviruses under greenhouse conditions. *Virus Res.* 219, 83–91. doi: 10.1016/j.virusres.2015.11.004

Yaegashi, H., Nakamura, H., Sawahata, T., Sasaki, A., Iwanami, Y., Ito, T., et al. (2013). Appearance of mycovirus-like double-stranded RNAs in the white root rot fungus, *Rosellinia necatrix*, in an apple orchard. *FEMS Microbiol. Ecol.* 83, 49–62. doi: 10.1111/j.1574-6941.2012.01454.x

Yu, X., Li, B., Fu, Y., Jiang, D., Ghabrial, S. A., Li, G., et al. (2010). A geminivirus-related DNA mycovirus that confers hypovirulence to a plant pathogenic fungus. *Proc. Natl. Acad. Sci. U.S.A.* 107, 8387–8392. doi: 10.1073/pnas.0913535107

Zhang, R., Hisano, S., Tani, A., Kondo, H., Kanematsu, S., and Suzuki, N. (2016). A capsidless ssRNA virus hosted by an unrelated dsRNA virus *Nat. Microbiol.* 1:15001. doi: 10.1038/nmicrobiol.2015.1

Zhang, R., Liu, S., Chiba, S., Kondo, H., Kanematsu, S., and Suzuki, N. (2014). A novel single-stranded RNA virus isolated from a phytopathogenic filamentous fungus, *Rosellinia necatrix*, with similarity to hypo-like viruses. *Front. Microbiol.* 5:360. doi: 10.3389/fmicb.2014.00360

Zheng, L., Zhang, M., Chen, Q., Zhu, M., and Zhou, E. (2014). A novel mycovirus closely related to viruses in the genus alphapartitivirus confers hypovirulence in the phytopathogenic fungus *Rhizoctonia solani*. *Virology* 456–457, 220–226. doi: 10.1016/j.virol.2014.03.029

Conflict of Interest: The authors declare that the research was conducted in the absence of any commercial or financial relationships that could be construed as a potential conflict of interest.

The reviewer EV declared a past co-authorship with one of the authors NS.

frontiers in Microbiology

ORIGINAL RESEARCH
published: 15 July 2020
doi: 10.3389/fmicb.2020.01467

Marine Oomycetes of the Genus *Halophytophthora* Harbor Viruses Related to Bunyaviruses

Leticia Botella[1,2], Josef Janoušek[1], Cristiana Maia[3], Marilia Horta Jung[1], Milica Raco[1] and Thomas Jung[1]*

[1] *Phytophthora Research Centre, Department of Forest Protection and Wildlife Management, Faculty of Forestry and Wood Technology, Mendel University in Brno, Brno, Czechia,* [2] *Biotechnological Centre, Faculty of Agriculture, University of South Bohemia, Ceske Budejovice, Czechia,* [3] *Centre for Marine Sciences (CCMAR), University of Algarve, Faro, Portugal*

We investigated the incidence of RNA viruses in a collection of *Halophytophthora* spp. from estuarine ecosystems in southern Portugal. The first approach to detect the presence of viruses was based on the occurrence of dsRNA, typically considered as a viral molecule in plants and fungi. Two dsRNA-banding patterns (~7 and 9 kb) were observed in seven of 73 *Halophytophthora* isolates tested (9.6%). Consequently, two dsRNA-hosting isolates were chosen to perform stranded RNA sequencing for *de novo* virus sequence assembly. A total of eight putative novel virus species with genomic affinities to members of the order *Bunyavirales* were detected and their full-length RdRp gene characterized by RACE. Based on the direct partial amplification of their RdRp gene by RT-PCR multiple viral infections occur in both isolates selected. Likewise, the screening of those viruses in the whole collection of *Halophytophthora* isolates showed that their occurrence is limited to one single *Halophytophthora* species. To our knowledge, this is the first report demonstrating the presence of negative (–) ssRNA viruses in marine oomycetes.

Keywords: dsRNA, (–) ssRNA, RdRp, mycovirus, marine virology, estuaries

OPEN ACCESS

Edited by:
Ioly Kotta-Loizou, Imperial College London, United Kingdom

Reviewed by:
Robert Henry Arnold Coutts, University of Hertfordshire, United Kingdom
Massimo Turina, National Research Council (CNR), Italy

****Correspondence:***
Leticia Botella
qqbotell@mendelu.cz

Specialty section:
This article was submitted to Virology, a section of the journal Frontiers in Microbiology

Received: *04 April 2020*
Accepted: *04 June 2020*
Published: *15 July 2020*

Citation:
Botella L, Janoušek J, Maia C, Jung MH, Raco M and Jung T (2020) Marine Oomycetes of the Genus Halophytophthora Harbor Viruses Related to Bunyaviruses. Front. Microbiol. 11:1467. doi: 10.3389/fmicb.2020.01467

INTRODUCTION

Halophytophthora species are fungal-like oomycetes with similar morphology and life cycles as members from their well-known plant pathogenic sister genus *Phytophthora* (Sullivan et al., 2018). As oomycetes they are distantly related to brown algae and belong to the Kingdom Stramenopila (Heterokonta). In pre-molecular times most marine oomycetes were assigned to the genus *Halophytophthora* but recent phylogenetic studies demonstrated that *Halophytophthora* is polyphyletic. Consequently, numerous *Halophytophthora* species were transferred to several new genera including *Calycofera*, *Phytopythium,* and *Salisapilia* (Marano et al., 2014; Bennett et al., 2017; Jung et al., 2017b; Bennett and Thines, 2019). Currently *Halophytophthora sensu stricto* contains nine described species. Most *Halophytophthora* species live in brackish and salt water habitats and have been traditionally described as saprophytes playing a key role as decomposers mainly in mangrove ecosystems (Newell and Fell, 1992, 1997). However, they may also be pathogenic. Several studies have already illustrated their pathogenicity on the marine eelgrass *Zostera marina* (Govers et al., 2016), which has a key ecological role along shores of North America and Eurasia (Man in 't Veld et al., 2019). *Halophytophthora zostera* was shown to restrict the viability of *Z. marina* seeds

and seedling development (Govers et al., 2016). Knowledge on *Halophytophthora* in temperate ecosystems has been scarce for a long time, hence, the conditions explaining why these decomposers may turn pathogenic are still unknown (Sullivan et al., 2018).

Virus diversity in marine ecosystems appears predominant (Suttle, 2005). With a total estimation of $\sim 10^{30}$ viruses, they have been implicated as the most abundant pathogens in the oceans (Suttle, 2005). Viruses infect all organisms from bacteria to whales but the majority infect bacteria (phages), which control microbial abundance and release dissolved organic matter, influencing global biogeochemical cycles (Wommack and Colwell, 2000; Weinbauer, 2004; Breitbart, 2012). Regarding lower eukaryotes, metagenomic and metatranscriptomic studies are rapidly expanding the knowledge about virus diversity and can detect the presence of a range of DNA or RNA genomes of various architectural type and size (Coy et al., 2018). Viruses with large double-stranded (ds) DNA genomes are typically found in phytoplankton (Weynberg et al., 2017). Single-stranded (ss) DNA viruses have been described in diatom algae (Nagasaki et al., 2005; Coy et al., 2018), corals (Vega Thurber et al., 2008) and stromatolites (Desnues et al., 2008). DsRNA viruses infect photosynthetic flagellates, heterotrophic protists (Desnues et al., 2008) and also fungi. Recently, dsRNA viruses hosted by marine fungi were isolated from the seagrass *Posidonia oceanica* (Nerva et al., 2015) and sea cucumber *Holothuria polii* (Nerva et al., 2019a), and identified a negative (−) ssRNA virus in *Penicillium roseopurpureum.*

The order *Bunyavirales* is comprised of viruses with segmented, linear (−) ssRNA genomes (Abudurexiti et al., 2019). The morphology of Bunyaviruses varies from symmetric icosahedral particles, similar to phleboviruses (Halldorsson et al., 2018), to spherical and pleomorphic particles, similar to orthobunyaviruses (Obijeski et al., 1976) and hantaviruses (Huiskonen et al., 2010). A model bunyavirus genome consists of three RNA segments, the smallest of which (S) may encode nucleocapside proteins (NP) and silencing suppressors (NS) while the medium sized (M) segment usually encodes glycoproteins (Gn and Gc) and movement proteins (Margaria et al., 2014). Finally, the largest segment (L) appears to possess a single open reading frame (ORF), which encodes the RNA dependent RNA polymerase (RdRp). According to the last update from the International Committee on Taxonomy of Viruses (ICTV), there are 12 bunyaviral families, four subfamilies, 46 genera and 287 species registered (Abudurexiti et al., 2019). However, due to more intensive samplings and, in particular, because of the use of *de novo* virus detection with metagenomics sequencing the diversity of bunyaviruses is constantly increasing (Li et al., 2015; Shi et al., 2016). Currently, bunyaviruses have been described in plants, invertebrate and vertebrate hosts and are transmitted by arthropod and mammalian vectors (Abudurexiti et al., 2019). Viruses with genomic similarities to bunyaviruses have also been described from diverse fungal hosts, including the phytopathogenic fungi *Botrytis cinerea* (Botrytis cinerea negative-stranded RNA virus 1, BcNSRV-1) (Donaire et al., 2016) and *Macrophomina phaseolina* (Macrophomina phaseolina negative-stranded RNA virus 1, MpNSRV1) (Marzano et al., 2016). Entoleuca phenui-like virus 1 (EnPLV1) has been identified from an avirulent isolate of *Entoleuca* sp. collected from avocado rhizosphere (Velasco et al., 2019). Coniothyrium diplodiella negative-stranded RNA virus 1 (CdNsRV1), Alternaria tenuissima negative-stranded RNA virus 2 (AtNsRV2) and Cladosporium cladosporioides negative-stranded RNA virus 2 (CcNsRV2), were isolated from the grapevine wood-inhabiting endophytes *Coniothyrium diplodiella*, *Alternaria tenuissima,* and *Cladosporium cladosporioides*, respectively (Nerva et al., 2019b). Likewise, the shiitake mushroom (*Lentinula edodes*) hosts Lentinula edodes negative-stranded virus 2 (LeNSRV2), which is related to phenuiviruses (Lin et al., 2019); a marine fungus, *P. roseopurpureum* hosts Penicillium roseopurpureum negative ssRNA virus 1 (PrNSRV1) (Nerva et al., 2019a) and the oomycete *Pythium polare*, Pythium polare bunya-like RNA virus 1 (PpBRV1) (Sasai et al., 2018). However, no effects of bunyavirus infection on growth or virulence of their fungal or oomycete hosts have been recorded yet.

Knowledge on viruses infecting oomycetes is relatively limited (Sutela et al., 2019). Several viruses have been described in downy mildews (biotrophic plant parasites) including unclassified (+) ssRNA viruses on *Sclerophthora macrospora* with similarities to a Noda-Tombus-like virus (Yokoi et al., 2003) and in *Plasmopara parasitica*, which causes hypovirulence on its host (Grasse et al., 2013; Grasse and Spring, 2017). The genus *Pythium* is comprised of water and soilborne oomycetes causing moderate to significant damages in plant roots (Sutela et al., 2019). Virus-like particles and/or dsRNA have been described in *Pythium irregular* (Gillings et al., 1993). Recently, an unclassified gammapartitivirus was reported in *Pythium nuun* (Shiba et al., 2018), a toti-like virus was also characterized from two strains of *Globisporangium splendens* (formerly *Pythium splendes*) and three virus-like sequences, Pythium polare RNA virus 1 (PpRV1), Pythium polare RNA virus 2 (PpRV2) and PpBRV1 were detected in *Pythium polare* infecting mosses in the Arctic (Sasai et al., 2018). In the genus *Phytophthora* the first virus to be reported in the USA (Hacker et al., 2005) was classified as an alphaendornavirus. It was found in an isolate of the undescribed *Phytophthora* taxon "douglasfir." Later, similar virus strains were detected in *P. ramorum* isolates from several hosts in Europe (Kozlakidis et al., 2010) but no further investigations were performed. *Phytophthora infestans*, the causal agent of potato late blight, also harbors four RNA viruses. Phytophthora infestans RNA virus 1 and 2, (PiRV-1 and PiRV-2, respectively) apparently represent novel virus families (Cai et al., 2009, 2019), Phytophthora infestans RNA virus 3 (PiRV-3) is clustered with the newly proposed family "*Fusagraviridae*" (Cai et al., 2013) and Phytophthora infestans RNA virus 4 (PiRV-4) is an unclassified member of *Narnaviridae* (Cai et al., 2012). Recently, PiRV2, known to be 100% transmittable through asexual spores, was shown to stimulate sporangia production and enhance the virulence of *P. infestans* (Cai et al., 2019). Phytophthora cactorum RNA virus 1 (PcRV1), a toti-like virus, has been newly described in an isolate of *Phytophthora cactorum* collected from a trunk lesion on silver birch in Denmark (Poimala and Vainio, 2020).

Because the genus *Halophytophthora* represents a unique group of marine microorganisms with uncertain roles as

phytopathogens on coastal and estuarine grasses, we wished to expand current research to better understand their behavior by investigating their potential virome. More precisely, our study had two goals: (i) to confirm the presence of viruses in these marine oomycetes by combining traditional and state-of-art technologies, and (ii) to assess their abundance and genetic variability in a collection of *Halophytophthora* isolates from Portugal.

MATERIALS AND METHODS

Oomycete Isolates

All *Halophytophthora* isolates studied were collected from seven localities in southern Portugal (**Table 1**) using an *in situ* baiting technique (Jung et al., 2017a). At each site, 15–20 non-wounded young leaves of three tree species, *Ceratonia siliqua*, *Citrus sinensis* and *Quercus suber*, were placed as baits in a 25 × 30 cm raft, prepared using fly mesh and styrofoam, and the raft put to float in the tidal zone. The rafts were collected after 3 days. Baiting leaves were washed in distilled water and blotted dry on filter paper. Five to ten pieces (approximately 2 × 2 mm) were cut from the margins of each watersoaked or necrotic lesion of each leaf, blotted on filter paper and plated onto selective PARPNH agar (V8-juice agar (V8A) amended with 10 μg/ml pimaricin, 200 μg/ml ampicillin, 10 μg/ml rifampicin, 25 μg/ml pentachloronitrobenzene (PCNB), 50 μg/ml nystatin and 50 μg/ml hymexazol). The *Halophytophthora* isolates are part of the collection of the Phytophthora Research Centre (Mendel University), located in Brno, Czech Republic. The **Supplementary Table S1** provides detailed information and species identification of all *Halophytophthora* isolates, which is currently under investigation. For the different purposes of the present study all isolates were grown for 7–21 days in darkness on V8A media, covered with cellophane (EJA08-100; Gel Company, Inc., CA, United States).

DsRNA Isolation

A total of 73 isolates from Portugal were screened for dsRNA (**Figure 1**), which was purified using a modified version of the protocol of Morris and Dodds (1979). Approximately 2 g of fresh mycelium were transferred to a 50 ml Falcon tube and disrupted by vortexing for 3 min with two stainless steel balls (diameter 10 mm). The rest of the protocol was performed as described by Tuomivirta et al. (2002).

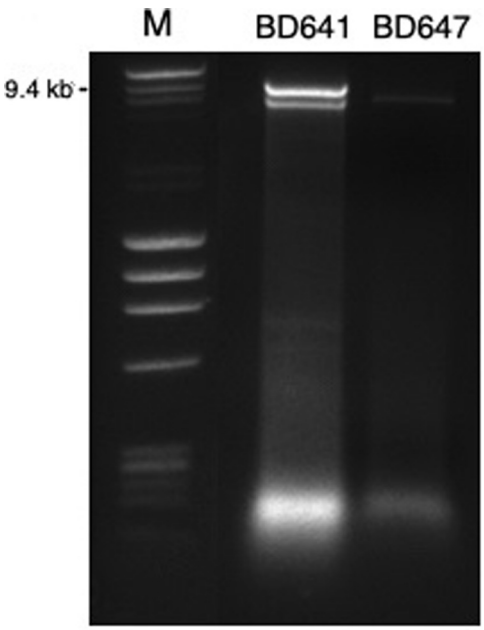

FIGURE 1 | DsRNA profiles found in *Halophytophthora* isolates BD641 (1) and BD647 (2). DsRNA bands were visualized by gel electrophoresis (120 V; 90 min). Analyzed fragments were separated on 1.5% agarose gel prepared with a TBE buffer (106177; Merck KGaA, Germany) and stained by Ethidium Bromide (E1510, Sigma-Aldrich, Germany). Ready-to-use DNA size and mass standard (F-303SD, Thermo Scientific).

Stranded RNA Sequencing of Samples BD641 and BD647

Total RNA was purified from approximately 50 mg of fresh mycelium using SPLIT RNA Extraction Kit (Lexogen, Austria) and treated with DNase I (ThermoFisher Scientific). RNA quantity and quality were checked using respectively a Qubit® 2.0 Fluorometer (Invitrogen) and Tape Station 4200 (Agilent) resulting in a RNA integrity number (RIN) of 10.

TABLE 1 | Relation of isolates per sampling locality and virus detection.

Locality, municipality	N[&]	dsRNA screening[$]	dsRNA patterns	RT-PCR screening[+]	Virus found by RT-PCR*
Ribeira de Odelouca, Silves	14	14	~9 kb	14	None
Rio Séqua, Tavira	9	9	None	9	None
Parque Natural da Ria Formosa, Santa Luzia, Tavira	24	18	~7 and 9 kb	21	HRV1-8
Parque Natural da Ria Formosa, Quelfes, Olhão	6	5	~9 kb	6	None
Ria de Alvor, Alvor, Portimão	8	6	None	8	None
Parque Natural da Ria Formosa, Almancil, Loulé	9	8	~9 kb	8	None
Sapal de Castro Marim /Rio Guadiana, Castro Marim	32	13	None	29	None

*[&]Total number of isolates screened for viruses by both dsRNA isolation and partial amplification of their RdRp by RT-PCR using specific primers for each of them; [$]number of isolates used in the dsRNA screening; [+]number of isolates screened by RT-PCR; *viruses detected by RT-PCR. See **Supplementary Table S1** for the complete information of the isolates, DsRNA and RT-PCR screening.*

Approximately 1 μg of total RNA eluted in RNase-free water was sent to Fasteris SA (Plan-les-Ouates, Switzerland) for RNA library construction and deep sequencing. The library preparation was performed using the Illumina TruSeq® stranded RNA Sample Preparation Kit (Illumina, San Diego, CA, United States). The library was sequenced in pair-end (2x 75 nt) runs on an Illumina NextSeq 500 machine. Prior to the library preparation, Ribo-Zero rRNA Removal Kit (Human/Mouse/Rat) was used successfully. An "in-lane" PhiX control spike was included in each lane of the flow-cell. 93.94% of the reads had a quality value (Q30) $\geq$ 30, i.e., less than 1 error in 1000 bases. The raw data was deposited in the Sequence Read Archive (SRA) with the BioProject ID PRJNA619952 and BioSample ID SAMN14856044.

Bioinformatics Analysis

Adapter trimming was not needed as the adapter sequence was only present in less than 1% of the reads. All reads were compared to the genome sequence of *Phytophthora cinnamomi*[1] with BWA 0.7.5a[2]. Unmapped reads were selected from the mapping files and saved in a fastq format. BAM post-processing was performed with toolbox for manipulation of SAM/BAM files V. 1.1[3] and BEDTOOLS V. 2.21.0[4]. *De novo* assembly was performed with VELVET V1.2.10[5]. As the repeat resolution module of VELVET assumes linearity and uniform coverage distribution, it produces fragmented transcriptome assemblies. To consider the unequal expression levels and alternative splicing breakpoints, the preliminary assemblies produced by VELVET were inputted to OASES 0.2.08[6], which exploits read sequence and pairing information (if available) to produce transcript isoforms. When possible, OASES also detects and reports standard alternative splicing events. The first 1M paired-reads of each library were mapped on each OASES assembly. The alignment was done using the mapping software BWA 0.7.5a and SAMTOOLS 1.1[7]. Reads mapping to several positions on the reference sequence with the same mapping quality were attributed at random to one of the positions with a mapping quality of 0. When an input read had N's in their nucleotide sequence, BWA replaced the Ns with a random nucleotide. *De novo* assembly and validation mapping were done using BWA 0.7.5a. The result of the mapping of the reads on the reference sequences is summarized in **Supplementary Table S2**. The assemblies with a hash of 51 gave the highest representability. The numbers of reads aligning and coverage depth for the final viral sequence were calculated using Geneious Prime® 2020.0.4.

The sequence alignment and blast output post-processing with BLAST ncbi-blast-2.2.26[7]. The contig files were aligned to the NCBI database using a local installation of the BLAST software. The results from the BLASTn, BLASTX and the BLAST search on the viral reference dataset (RefSeq) were compared. The output file was then parsed using in-house (Fasteris) scripts.

Rapid Amplification of cDNA Ends (RACE) and Full-Length Viral Sequences

In order to determine the 5′- and 3′- terminal sequences and lengths of the putative viral genomes the SMARTer® RACE 5′/3′ KIT (Takara Bio USA, Inc.) was used with total RNA extracted as described above using SPLIT RNA Extraction Kit (Lexogen, Austria). The 3′ Poly(A) Tailing of RNA was performed at 37°C for 20 min using yeast Poly(A) Polymerase (MCLAB, San Francisco, CA). Thereafter, approximately 1 μg of total RNA was used for RACE First-strand cDNA synthesis of both 5′- and 3′- termini was performed using specific primers designed for the eight putative viruses in a 5′- and 3′ – orientation (**Supplementary Table S3**) as described by the manufacturer. Then, 5′-RACE and 3′-RACE PCR amplification was performed to generate the corresponding cDNA fragments using SeqAmp DNA Polymerase (Takara Bio USA, Inc.) as described by the manufacturer. Amplicons were extracted and purified from the gel using NucleoSpin® Gel and PCR Clean-Up Kit (Macherey-Nagel GmbH & Co. KG). All amplicons were cloned using In-Fusion HD Cloning Kit and Stellar Competent Cells (Takara Bio USA, Inc.). Recombinant plasmids were extracted with Thermo Scientific GeneJET Plasmid Miniprep Kit and sequenced by GATC Biotech, Germany. Nested PCR was often necessary in order to precisely amplify the virus 3′ termini. Here, the screening forward primers (**Supplementary Table S3**) in combination with the Universal Primer mix (UPM) from the SMARTer® RACE 5′/3′ KIT (Takara Bio USA, Inc.) were used to generate amplicons to act as template for nested PCR. The nested PCR RACE primers and the Short Universal primer provided by the kit were used. To obtain the 3′ end terminal sequence of virus 8 a different primer was designed.

Screening for Virus Incidence by RT-PCR Amplification

Mycelium from individual isolates was collected and homogenized using a bead tube holder devide (740469; Macherey-Nagel; Germany). RNA was isolated and purified using the Monarch Total RNA Miniprep Kit (T2010S; New England Biolabs, MA, United States). Efficient RNA extraction was achieved using the manufacturer's recommended protocol for tough-to-lyse samples. Contaminating host DNA was removed from the extracts using a combination of gDNA removal columns and DNase I treatment. RNA was eluted in 30 μl volumes and stored at −80°C.

cDNA was synthesized using the ProtoScript II First Strand cDNA Synthesis Kit (E6560; New England Biolabs, MA, United States). Here, oligo d(T)23VN was incubated with the RNA at 65°C for 5 min. Next, random primer mix was added together with ProtoScript II Enzyme and Reaction Mix, followed by incubation at 25°C for 5 min, 42°C for 60 min and denatured at 80°C for 5 min.

[1] ftp://ftp.ncbi.nlm.nih.gov/genomes/all/GCA/001/314/365/GCA_001314365.1_MP94-48v2/GCA_001314365.1_MP94-48v2_genomic.fna.gz

[2] http://bio-bwa.sourceforge.net

[3] http://www.htslib.org/

[4] http://code.google.com/p/bedtools/

[5] https://www.ebi.ac.uk/~zerbino/velvet/

[6] https://www.ebi.ac.uk/~zerbino/oases/

[7] http://www.htslib.org/doc/samtools-11.html

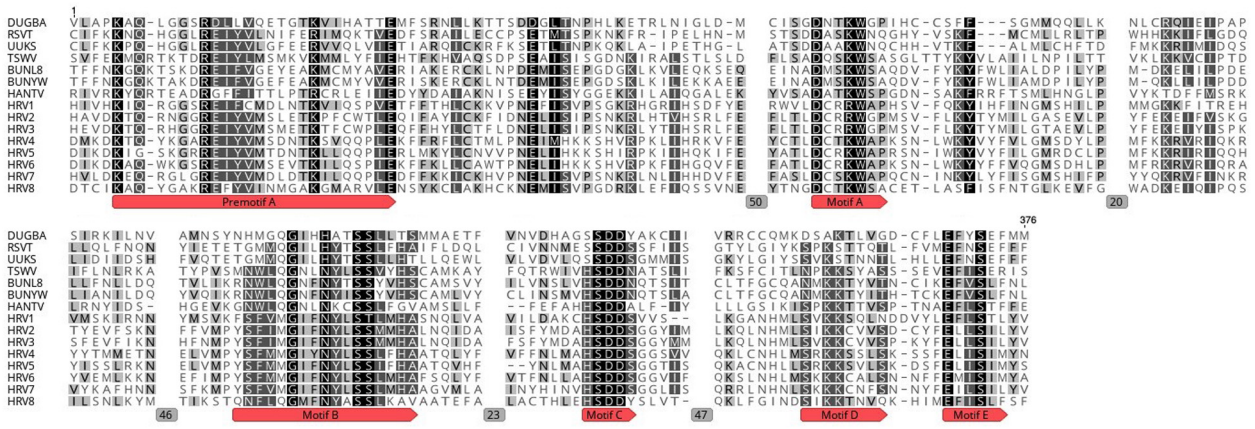

FIGURE 2 | Amino acid alignment showing conserved motifs A to E and premotif A within the RdRp of HRV1-8 and selected bunyaviruses. DUGBA, Dugbe virus (accession number Q66431.1); RSVT, Rice stripe virus (Q85431.1); UUKS, Uukuniemi virus S23 (P33453.1); TSWV, Tomato spotted wilt virus (P28976.1); BUNYW, Bunyawera virus (P20470); BUNL8, La Crosse virus L78 (Q8JPR2.1); HANTV, Hantaan virus 76-118 (P23456.3). Gray boxes with numbers represent the number of positions deleted in the MUSCLE alignment.

Virus incidence in the *Halophytophthora* ssp. isolates was tested using PCR amplification with virus-specific primers (**Supplementary Table S4**). All primers were used to amplify a fragment of the RdRp gene of each virus and were designed by Primer 3 2.3.7 under Geneious Prime® 2020.0.4. Primer sequences, amplicon sizes and annealing temperatures are shown in **Supplementary Table S4**. PCR amplification was performed with 12.5 µl OneTaq Quick-Load 2X Master Mix with Standard Buffer (M0486; New England Biolabs, MA, United States), 0.5 µl of each 10 mM primer, 3 µl of cDNA in a total volume of 25 µl. Cycling conditions were used according to manufacturer's recommendations and the annealing temperature of each primer set was calculated using the on-line tool[8] (v1.9.9 May 30).

Amplicons were visualized and separated by electrophoresis (300 V; 10 min) through 1.5% agarose gels in TBE buffer (106177; Merck KGaA, Germany) and with DNA Stain G (39803; SERVA; Germany). Amplicons of the expected lengths were purified and sequenced in both directions by GATC BioTech (Eurofins; Konstanz, Germany) with the primers used in the initial PCR amplification. All the amplicon sequences were deposited in the GenBank under the accession number MT277331-349. As an internal control for successful PCR amplification from viral RNA templates routine amplification of an actin housekeeping gene (Weiland and Sundsbak, 2000), was performed simultaneously with primers MIDFWACT and MIDREVACT (**Supplementary Table S4**) in all experiments under identical conditions (**Supplementary Figure S1**).

Genetic Variability and Phylogenetic Analysis

Pairwise identities of the nucleotide and amino acid sequences (**Supplementary Tables S5, S6**) were obtained after aligning the eight viral nucleotide and amino acid sequences by MUSCLE (Edgar, 2004) and calculated using Geneious Prime® 2020.0.4. DnaSP v5 (Rozas et al., 2017) was used to estimate genetic diversity parameters for strains of the different *Halophytophthora* viruses.

In order to search for conserved domains within the putative viral proteins the NCBI CD-search tool was used[9] (Lu et al., 2020). Viral protein sequences were aligned by MUSCLE (Edgar, 2004) using Geneious Prime® 2020.0.4 (**Figure 2**).

A maximum likelihood phylogenetic tree was constructed using a rapid bootstrapping algorithm (Stamatakis et al., 2008) in RAxML-HPC v.8 on XSEDE conducted in CIPRES Science Gateway (Miller et al., 2010) (**Figure 3**). Tree search was enabled under the GAMMA model to avoid thorough optimization of the best scoring ML tree at the end of the run. The Jones–Taylor–Thornton (JTT) model was chosen as the substitution model for proteins. Bootstrapping was configurated with the recommended parameters provided by CIPRES Science Gateway. The resulting data were visualized using the software FIGTREE software version 1.4.4[10].

RESULTS

Identification of the Mycoviruses Infecting Selected *Halophytophthora* Isolates

A total of 7 out of 73 *Halophytophthora* isolates (9.6 %) from three different Portuguese localities were found to contain one or two dsRNA segments as illustrated by gel electrophoresis (**Table 1** and **Supplementary Table S1**). Those isolates which contained dsRNA apparently belong to three different previously undescribed *Halophytophthora* species (**Supplementary Table S1**). Isolates BD093 and BD094 (*Halophytophthora* sp. 01) from Ribeira de Odelouca (Silves)

[8]http://tmcalculator.neb.com/

[9]https://www.ncbi.nlm.nih.gov/Structure/cdd/wrpsb.cgi

[10]http://tree.bio.ed.ac.uk/software/figtree/

contained a ∼9 kb-dsRNA segment. Isolates BD641, BD647 and BD654 (*H*. sp. 04*)* from Parque Natural da Ria Formosa (Tavira) contained two different banding patterns with ∼7 and/or ∼9 kb dsRNA bands (**Figure 1**). BD665 (*H*. sp. 03*)* from Parque Natural da Ria Formosa in Olhão and BD685 from Parque Natural da Ria Formosa in Almancil, Loulé, both contained a ∼7 kb segment. Two of these positive isolates, BD641 and BD647, were chosen for stranded RNA sequencing.

One sequencing library was prepared from rRNA-depleted total RNA and generated 3.6×10^{11} 75-nucleotide (nt) paired end (PE) sequence reads (**Supplementary Table S2**). When they were assembled against the genome of *P. cinamomi* as host reference sequence and 1.15×10^{8} PEs mapped. The unmapped 1.12×10^{8} PE reads were selected for the further investigation. The final contig file had 35,621 contigs (including 548 undetermined bases) with an average length of 894 nt and a maximum contig length of 21,602 nt. Assembly of the sequence reads from the final contig file revealed eight potential virus sequences as evidenced by significant E-values and identity percentage of their predicted amino acid sequences (**Table 2**). The contigs representing the eight potential viruses had different read numbers and coverage (**Table 3**), HRV8 had the deepest coverage and HRV2 the least. The eight sequences identified were similar to members of the order *Bunyavirales* hosted by fungal pathogens, including *Botrytis cinerea* (Botrytis cinerea negative-stranded RNA virus 1, BcNSRV-1, YP_009182153), *Macrophomina phaseolina* (Macrophomina phaseolina negative-stranded RNA virus 1, MpNSRV1, ALD89106.2), oomycetes, such as *Pythium polare* (Pythium polare bunya-like RNA virus 1, PpRV1, YP_09551341.1) and arthropod-like insects including *Asellus* sp. (Wuhan insect virus 3, AJG39263.1) and crabs (Beihai sesarmid crab virus 5, APG79283.1) (**Table 2**). According to the convention of the International Committee on Taxonomy of Viruses (ICTV) the eight putative viruses were designated as Halophytophthora RNA virus (HRV) 1–8 (**Table 2**).

[11]http://www.ncbi.nlm.nih.gov/BLAST

Virus Genome Organization

Based on our analyses, only ORFs encoding an RdRp gene were found.

Based on the sequence of the original contigs oligonucleotide primers were designed to amplify and confirm the terminal RdRp sequences of the eight viruses (**Supplementary Table S4**) some of which, including HRV 1, 2, 3, 4, and 5, were complete or nearly complete. The remainder of the viral terminal sequences of HRV6, 7, and 8 were completed by RACE. The eight virus genomes ranged in size from 7.8 up to 9.3 kb (**Table 3**) including a single large ORF encoding an RdRp flanked by 5′ and 3′-untranslated regions (UTRs) (**Figure 4**). The longest genome

TABLE 2 | Identification of *Halophytophthora* viruses' most similar RdRp sequences in the GenBank based on BLASTX search.

Virus name	Acronym	GenBank accession numbers	Most similar virus in GenBank	*E* value	Query cover (%)	Identity (%)
Halophytophthora RNA virus 1	HRV1	MT277350	Beihai sesarmid crab virus 5	0.0	72	32.73
Halophytophthora RNA virus 2	HRV2	MT277351	Botrytis cinerea negative-stranded RNA virus 1	0.0	52	32.40
Halophytophthora RNA virus 3	HRV3	MT277352	Botrytis cinerea negative-stranded RNA virus 1	0.0	54	32.13
Halophytophthora RNA virus 4	HRV4	MT277353	Pythium polare bunya-like RNA virus 1	0.0	82	38.35
Halophytophthora RNA virus 5	HRV5	MT277354	Pythium polare bunya-like RNA virus 1	0.0	84	37.84
Halophytophthora RNA virus 6	HRV6	MT277355	Pythium polare bunya-like RNA virus 1	0.0	86	38.30
Halophytophthora RNA virus 7	HRV7	MT277356	Macrophomina phaseolina negative-stranded RNA virus 1	$7e^{-126}$	68	28.76
Halophytophthora RNA virus 8	HRV8	MT277357	Wuhan Insect virus 3	0.0	60	58.07

TABLE 3 | Parameters of the genome organization of *Halophytophthora* viruses and their initial contigs.

	Initial contig length (nt)	Genome size (nt)	Largest ORF (nt)	Largest ORF (aa)	Function	Read Number	Coverage
Halophytophthora RNA virus 1	9,341	9,340	8,184	2,728	RdRp	630,934	5,066
Halophytophthora RNA virus 2	9,134	9,152	8,361	2,787	RdRp	15,298	126
Halophytophthora RNA virus 3	9,113	9,184	8,985	2,995	RdRp	716,385	5,850
Halophytophthora RNA virus 4	7,794	7,822	7,716	2,572	RdRp	341,627	3,275
Halophytophthora RNA virus 5	7,103	7,735	6,681	2,227	RdRp	376,150	3,647
Halophytophthora RNA virus 6	6,326	7,742	5,796	1,932	RdRp	843,893	8,175
Halophytophthora RNA virus 7	5,644	6,789	6,705	2,235	RdRp	264,248	2,919
Halophytophthora RNA virus 8*	3,299	7,874	7,788	2,596	RdRp	720,641	6,864

**The length of the 3′ end remains unsure.*

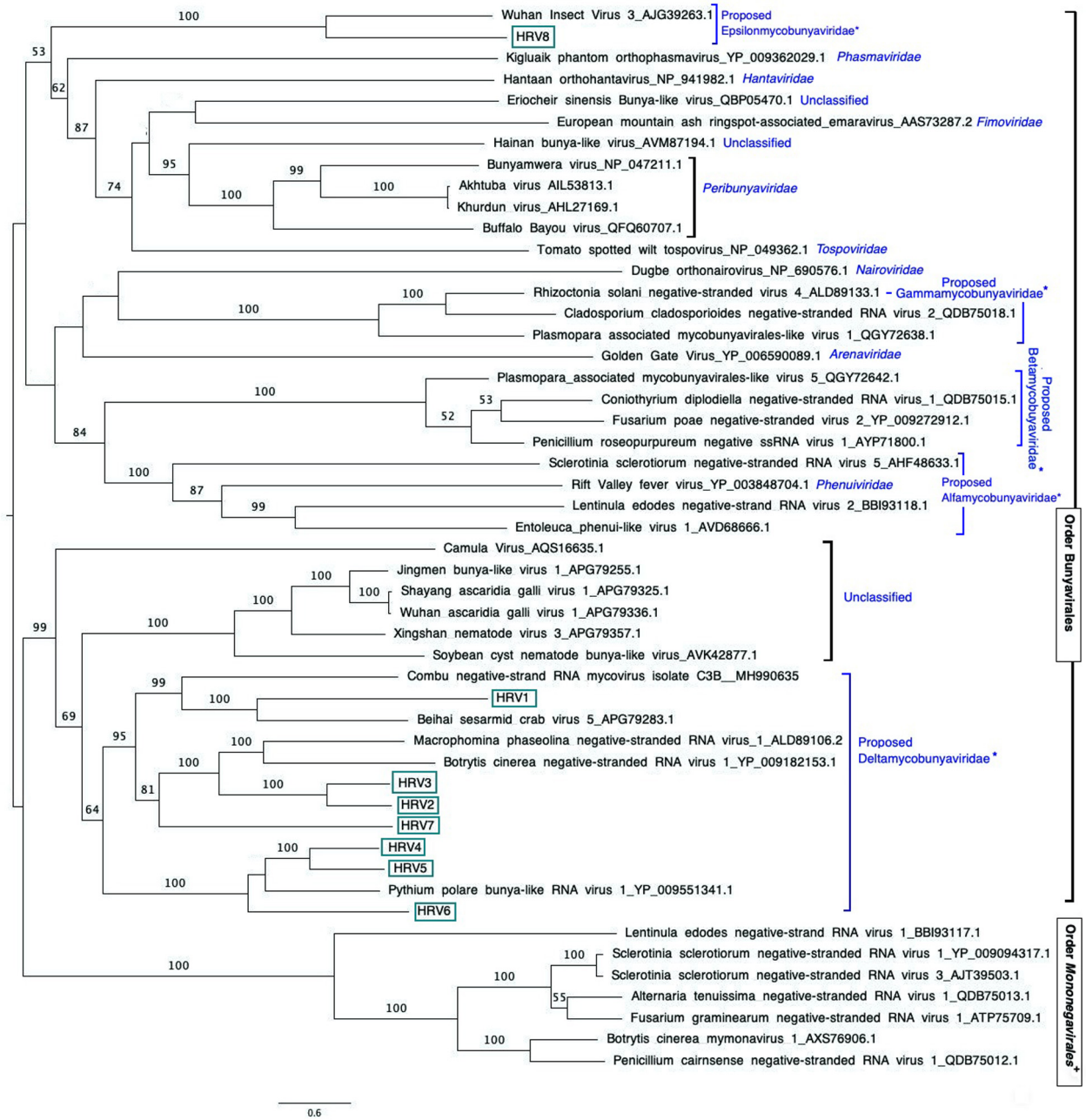

FIGURE 3 | Maximum likelihood tree (RAxML) depicting the phylogenetic relationship of the predicted RdRp of *Halophytophthora* viruses with other complete RdRp belonging to related (–) ssRNA viruses from the orders *Bunyavirales* and *Mononegavirales*. Nodes are labeled with bootstrap support values. Branch lengths are scaled to the expected underlying number of amino acid substitutions per site. Nodes are labeled only with bootstrap percentages ≥ 50%. Tree is rooted in the midpoint. Halophytophthora RNA viruses 1-8 (HRV1-8) are represented by their abbreviation names. Family classification and the corresponding pBLAST accession numbers are shown next to the virus names. *Family names proposed by Nerva et al. (2019b) and family Epsilonmycobunyaviridae, proposed in this study. +These members of the Order *Mononegavirales* are classified within the family *Mymonaviridae.*

corresponds to HRV1 (9,340 bp) and the shortest to HRV6 (6,816 bp) (**Figure 3** and **Table 3**).

Based on the amino acid (aa) sequence analysis of the eight viral ORFs all of them contained conserved regions belonging to pfam04196, Bunyavirus RdRp, which is the solitary member of the superfamily cl20265. Taken in turn, HRV1 has a conserved region ranging from aa 1454–1759 (expect value 1.01 e^{-11}); HRV2 from aa 1036–1394 (*E*-value: 9.37 e^{-13}); HRV3 from aa 1239–1588 (*E*-value: 5.11 e^{-10}); HRV4 from aa 735–1208 (*E*-value: 1.51 e^{-07}); HRV5 from aa 716–1301 (*E*-value: 1.53 e^{-07}); HRV6 from aa 1132- 1421 (*E*-value: 4.89 e^{-06}); HRV7 from aa 1204-1771 (*E*-value: 6.24e^{-10}); HRV8 from aa 894 to 1515

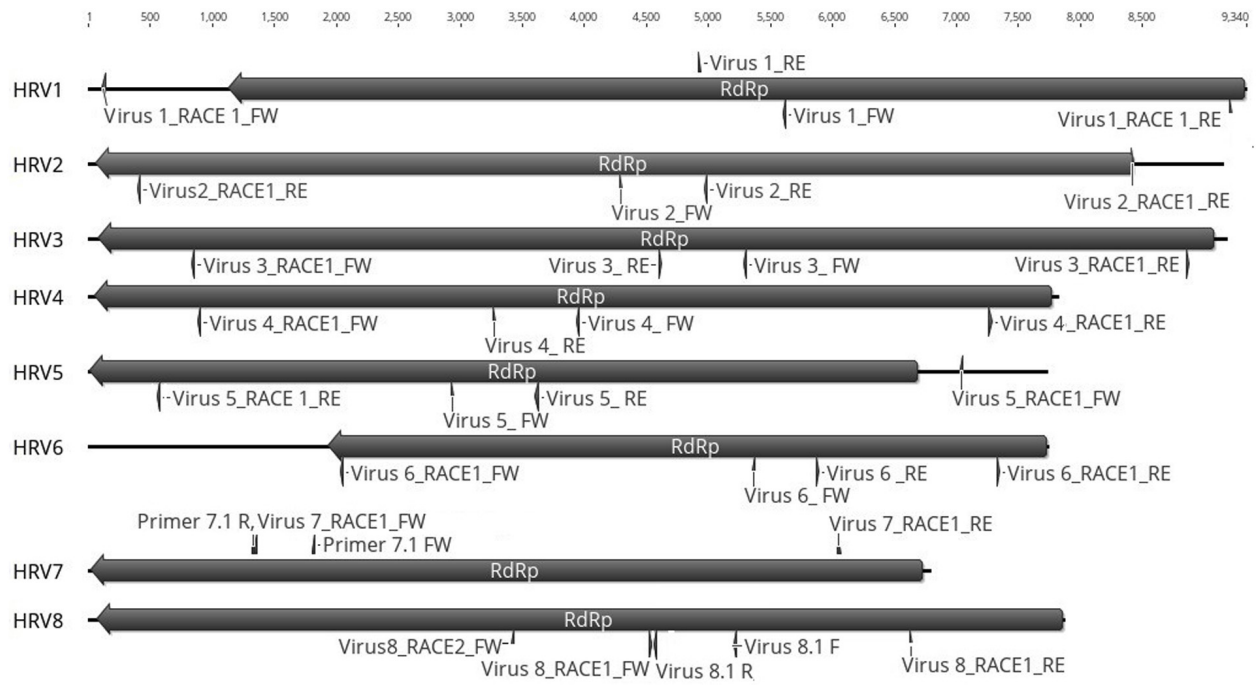

FIGURE 4 | Representation of the RdRp organization of the eight viruses found in *Halophytopthora* spp. Boxes represent the ORFs detected and they are shown in the direction of the original contig, from which primers for RT-PCR screening and RACE were designed. Primer names are indicated next to their position in the nucleotide sequence, primers were designed and named based on the orientation of the original stranded contig, which in the case of HRV3 and 5 it was genomic and in the case of HRV1, 2, 4, 6, 7, and 8, it was antigenomic. Numbers represent the genome length.

(*E*-value: 1.27 e^{-30}) and from aa 615 to 806 (*E*-value: 7.55 e^{-06}). The alignment of the RdRps of HRV1-8 with other viral sequences indicated the presence of the typical conserved motifs in RdRps of bunyaviruses (Kormelink et al., 2011) with certain variability (**Figure 2**): motif A (DxxxWx), where HRV1-3 had an arginine (R) instead of lysine (K) before the tryptophan (W), motif B (XGxxNxxSS), motif C (SDD), motif D (KK) and motif E (ExxSx). Premotif A with the three basic residues inside (K, R and R/K) and, downstream, the glutamic acid (E), were also identified. In addition, the conserved aa triplet TPD, typical of bunyaviruses (Muller et al., 1994), was identified in HRV1-7 (but not in HRV8) in positions 160, 107, 321, 83, 87, 282, and 160, respectively. The doublet RY was strictly conserved in HRV1, 4-8 in positions 894, 754, 757, 970, 1212 and 894, respectively, and partly conserved in HRV2 and 3 (positions 205 and 1019, respectively), which had R (arginine) and N (asparagine) instead of Y (tyrosine).

Phylogenetic Relationships Between the *Halophytophthora* Viruses and Other (−) ssRNA Viruses

An examination of the phylogenetic relationships between the *Halophytophthora* viruses and other (−) ssRNA viruses retrieved from the GenBank shows that they cluster with unclassified viruses with genomic affinities of the order *Bunyavirales* (**Figure 3**). HRV1 to 7 are very closely related to one another and form a cluster with MpNSRV1, BcNSRV-1 and PpRV1. This cluster includes other bunyaviruses described in invertebrate species representing different metazoan phyla including sesarmid crabs (Beihai sesarmid crab virus 5) and nematodes (Soybean cyst nematode bunya-like virus 1, SCN-BLV1). HRV8 differs from HRV1-7 and is grouped in a different cluster with a virus apparently hosted by *Aselus* sp. insects (Wuhan insect virus 3), which are phylogenetically closer to reported members of bunyavirus families including *Tospoviridae*, *Fimoviridae*, *Peribunyaviridae*, *Hantaviridae,* and *Phenuiviridae*. All HRV1-8 appeared distanced from members of the family *Mymonaviridae* in the order *Mononegavirales*.

HRV Occurrence in the *Halophytophthora* Isolate Collection

A total of four out of 95 *Halophytophthora* isolates (4.2%) from one sampling locality (Parque Natural da Ria Formosa, Santa Luzia, Tavira) resulted to host one or more of the eight *Halophytophthora* viruses described in this study. The most abundant was HRV6, which was present in 4 isolates (BD641, BD647, BD650, and BD654); HRV1 and HRV8 in 3 isolates (BD641, BD647, and BD654). HRV7 in isolates BD641 and BD647; HRV3 in isolates BD641 and BD654; HRV5 is in isolates BD647 and BD654, and HRV2 and HRV4 seem to be only present in isolate BD647.

While isolates BD093, BD094, BD665, and BD685 contained dsRNA elements (results not resulted) they were unrelated to the bunyaviral dsRNAs described as determined by RT-PCR (**Supplementary Table S1**). In some cases, e.g., HRV6 in

TABLE 4 | Genetic parameters of the partial RdRp nucleotide sequences of HRV strains.

Species	*N*	Sites	Net sites	S	h	Hd	π	AvNumDif
HRV1	3	708	704	51	3	1.00	0.05	34
HRV2	1	–	–	–	–	–	–	–
HRV3	2	701	700	52	2	1.00	0.07	52
HRV4	1	–	–	–	–	–	–	–
HRV5	2	655	654	80	2	1.00	0.12	80
HRV6	4	523	523	50	4	1.00	0.05	28
HRV7	3	473	473	34	3	1.00	0.05	23
HRV8	3	659	652	65	3	1.00	0.07	44

(–) not assessed; (N) Number of isolates; (Sites) length of the sequence, (Net sites) length of the sequence analyzed; (S) number of segregating sites; (h) number of haplotypes; (π), nucleotide diversity estimated by the average number of differences per site between two sequences; (AvNumDif) average number of differences.

BD650, dsRNA elements were not visualized by gel staining but RT-PCR confirmed the presence of a virus (**Supplementary Table S1**). Isolates BD641 and BD647 contained two and one dsRNA elements, respectively (**Table 1** and **Figure 1**), which have not been correlated with HRV1-8 by RT-PCR using dsRNA as a template.

Genetic Diversity of HRV

At the nucleotide level (**Supplementary Table S5**), the highest pairwise identity between viruses was HRV2 and 3 (57.05%) followed by HRV2 and 3 (39.00%). Conversely, the lowest pairwise identity was between HRV1 and 7 (23.43%). At the amino acid (aa) level (**Supplementary Table S6**), HRV2 and 3 also have the highest pairwise identity (47.48%), followed by HRV5 and 4 (39.91%). And, HRV7 and 8, the lowest (9.00%).

The genetic variability of the partially sequenced RdRp genes of the eight *Halophytophthora* virus strains was also assessed for those viruses that were hosted in more than one isolate (**Table 4**). All of the isolates appear to have very high haplotype diversity with HRV5 possessing the highest nucleotide diversity (0.12) and segregating sites (80). Conversely, HRV7 seems to be the least genetically diverse virus with a low nucleotide diversity (0.05) and the lowest number of segregating sites (34).

DISCUSSION

Traditional dsRNA extraction procedures were used to identify the potential presence of viruses in a collection of *Halophytophthora* spp. isolates from estuarine ecosystems in southern Portugal. Subsequently, stranded RNA sequencing followed by *de novo* contig assembling and comparative BLAST searches were used to identify eight putative novel viral sequences in two dsRNA-hosting isolates (**Figure 1**) belonging to the same *Halophytophthora* species (*H.* sp. 04, **Supplementary Table S1**). Primer-specific RT-PCR and 5′ and 3′ RACE were performed to confirm the presence and complete the sequences of each virus. All eight viral sequences contained elements of RdRp genes and bunyavirus motifs (**Figure 2**). Their eight virus genomes ranged in size from 6.8 to 9.3 kb (**Table 3**). BLAST analysis revealed that the eight viruses were significantly similar in sequence (*ca.* 30% identity; **Table 2**) to a number of unclassified bunya-like viruses isolated from different fungi, oomycetes, insects and crabs (**Table 2**). HRV8 differs from HRV1-7 and appears in a phylogenetic outgroup and is 58.07% similar to Wuhan insect virus 3 which is apparently hosted by *Asellus* sp. in China.

The overall pairwise nucleotide and aa identity of the eight viruses was 30.7 and 16.6%, respectively. HRV2 and 3 appear to one another apparently share identities of 57.05 and 47.80% at the nucleotide and aa levels, respectively. The remainder of the pairwise sequence comparisons (PASC) between the HRV isolates reveal lower identities of 40 and 20% at the nucleotide and aa levels (**Supplementary Tables S5, S6**). Analysis of the RdRp of HRV1-8 illustrate that they differ > 10% between one another and with their most similar matches in the GenBank. Since the primary classification criteria for genus and species used currently are based on pairwise sequence comparisons (PASC) and phylogenetic analyses, the viruses discovered in this investigation may constitute eight novel virus species, designated as Halophytophthora RNA Virus 1-8 (HRV1-8).

Bunyaviruses are enveloped viruses with a genome consisting of three ssRNA segments (called L, M, and S), the S RNA encodes the nucleocapsid protein, the M glycoproteins and the L segments encode the RNA polymerase. Each genome segment is coated by the viral nucleoproteins (NPs) and the polymerase (L protein) to form a functional ribonucleoprotein (RNP) complex, which is necessary for the RNA replication and gene transcription (reviewed in Ferron et al., 2017). However, in our study we have only discovered the L segment. Our result does not categorically rule out the existence of M and S segments but their copy number might be very low compared to the polymerase fragment. The NGS performed in this investigation may not have analyzed sufficient reads to identify smaller HRV genomic components but this is unlikely because it has been established that 100 M reads is sufficient to identify all RNAs of interest and the rRNA depletion worked successfully. A quality check for the presence of rRNAs was performed by mapping the reads on rRNA animal and human databases and <5% of rRNA reads were detected. Similar to HRV1-8 a number of other bunya-like mycoviruses, including BcNSRV-1 (Donaire et al., 2016), MpNSRV1 (Marzano et al., 2016), and PpRV1 (Sasai et al., 2018) apparently only possess an RdRp. However, it is more plausible that the genome description of these viruses (including HRV1-8) is incomplete. The putative NP and other non-structural (Ns) associated proteins are likely not conserved enough to be detected by homology, in contrast to what has been observed in other viruses including PrNSRV1 (Nerva et al., 2019a) and LeNSRV2 (Lin et al., 2019).

The phylogenetic tree shown in **Figure 2**, which includes HRV1-8 and 42 (−) ssRNA viruses, illustrates that HRV1-7 cluster with several unclassified viruses found in a variety of fungal, oomycete, nematode, crab and insect hosts, and a virus detected by NGS approach from the stool of a rhesus monkey (*Macaca mulatta*) (Zhao et al., 2017). More specifically, HRV4-6 are significantly similar in sequence to PpRV1 from the Arctic and Antarctic moss pathogen *Pythium polare* (Sasai

et al., 2018). HRV2, 3, and 7 are closer to BcNSRV-1 from the air-borne fungal pathogen *Botrytis cinerea* (Donaire et al., 2016) and MpNSRV1 from the soil-borne pathogen *Macrophomina phaseolina* (Marzano et al., 2016), and HRV1 is grouped with Combu negative-strand RNA mycovirus isolate C3B from the soil fungus *Mucor irregularis* in Belém, a port municipality in the Brasilian Amazon (accession number MH990635, unpublished), and Beihai sesarmid crab virus 5 detected by NGS from a sesarmid crab mix from Beihai, China. Sesarmid crabs have an important ecological role in mangrove ecosystems because they consume large amounts of leaf litter (Lee, 1998). HRV8 has some sequence similarity with classified bunyaviruses and, particularly, with Wuhan insect virus 3, hosted by an individual of *Asellus* sp. This genus of isopod crustaceans is known to feed primarily on decaying vegetation, microscopic algae and small invertebrates (reviewed in O'Callaghan et al., 2019). Since *Halophytophthora* spp. are the first colonizers of fallen mangrove leaves (Newell and Fell, 1992; Man in 't Veld et al., 2019) and estuarine grasses due to their ability to produce large amounts of chemotactic zoospores (reviewed in Man in 't Veld et al., 2019) they likely share their habitat with insects, nematodes and crustaceans, where they undoubtedly interact. As an example, the class *Oomycota* includes marine holocarpic pathogens of nematodes, algae, crustaceans and molluscs (Thines and Choi, 2016), thus some of the viruses discovered by NGS of invertebrates may have originated from their gut mycoflora and/or parasites. Even though arthropods are thought to be the ancestral hosts of bunyaviruses (Marklewitz et al., 2015) if viruses with similar genomes continue to be discovered in other invertebrates, protists and fungi (Shi et al., 2018) this theory may have to be redefined.

The phylogenetic tree shown in **Figure 2** has similarities with previous phylogenetic studies that group novel bunya-like mycoviruses separated from most of the currently classified bunyavirus families (Donaire et al., 2016; Marzano et al., 2016; Sasai et al., 2018; Nerva et al., 2019b). And, it also supports the proposal of different mycobunyaviral families (Nerva et al., 2019b): family Deltamycobunyaviridae with MpNSRV1, BcNSRV1 also includes PpRV1 and HRV1-7; two other families (proposed alfamycobunyaviridae and betamycobunyaviridae) including myco-phlebo-like viruses (Lin et al., 2019; Velasco et al., 2019; Chiapello et al., 2020) and the family Gammamycobunyaviridae with CcNSRV2, RsNSV4 and Plasmopara associated mycobunyavirales-like RNA Virus 2 (Nerva et al., 2019b; Chiapello et al., 2020). In addition, we propose a fifth family (Epsilonmycobunyaviridae) for HRV8 and Wuhan insect virus 3. As indicated previously (Nerva et al., 2019b), this classification is not formal as it has not been accepted by ICTV but it sheds light on the current knowledge of novel bunya-like mycoviruses.

The genetic variability of the partial RdRp sequences of HRV1-8 showed that they have a relatively low nucleotide but high haplotype diversity since all the strains were different (**Table 4**). In this regard, HRV5 possessed the highest nucleotide variability (0.12). It is well established that bunyavirus replication is error-prone and results in genome modification. Such modifications can accumulate over the time either due either to random genetic drift or as genetic adaptations of the virus to a new environment and/or a new host (Schneider and Roossinck, 2001; Li and Roossinck, 2004; Barr and Fearns, 2010). Novel viral genotypes can be generated through mutation, recombination and reassortment. Viral reassortment seems to be a powerful mechanism underlying the evolution of the *Bunyavirales* order (Coupeau et al., 2019). Briese et al. (2013) pointed out that most bunyaviruses described so far are actually reassortants of existing or extinguished viruses. This process leads to the generation of progeny viruses with novel genomic organizations as a result of gene shuffling between coinfecting closely related bunyaviruses (Coupeau et al., 2019). The same might exist for HRV1-8, which are only hosted by four *Halophytophthora* isolates, BD641, BD647, BD650 and BD654. These isolates belong to the same species (*H.* sp. 04) and were sampled from the same site, Parque Natural da Ria Formosa, Santa Luzia, Tavira, Portugal. As this yet undescribed *Halophytophthora* species has a functional homothallic sexual system it is feasible that the viruses were transferred between isolates during the mating process or by simple contact between vegetative hyphae, resulting in the coinfection of their viruses. Interestingly, HRV1-8 only occur in *H.* sp. 04 despite the presence of at least seven *Halophytophthora* species at the Santa Luzia site. The viruses were not found in isolates of *H.* sp. 04 at the Ria de Alvor, Alvor, Portimão site, suggesting that HRV1-8 might only be transmitted intraspecifically between co-occurring *Halophytophthora* isolates. Little is known about virus transmission in oomycetes. The only studies concerning virus transmission in oomycetes were performed in *P. infestans*, where several viruses are stably maintained (Cai et al., 2019). For instance, individual zoospores show 100% inheritance of PiRV-3 (Cai et al., 2019). In addition, PiRV-2 is readily horizontally transmitted by hyphal anastomosis, and vertically transmitted by asexual reproduction through sporangia (Cai et al., 2019). However, attempts to transfer PiRV-2 into apparently vegetative incompatible *P. infestans* isolates failed. Although several studies have demonstrated that interspecies transmission does occur naturally (Van Diepeningen et al., 1998; Melzer et al., 2002; Vainio et al., 2011), mycovirus transmission typically occurs between strains of the same fungal species. Viruses spread readily through fungal hyphal networks crossing pores contained in compartmenting septa. However, as potential detrimental cytoplasmic elements, their transmission between strains may be restrained by a genetic self/non-self recognition system termed vegetative incompatibility (*vic*), mating type incompatibility or intersterility (Leslie and Zeller, 1996). Oomycetes lack septa and in some cases, as in the genus *Phytophthora*, they are prompted to interspecific hybridizations which play a major role in speciation and species radiations in diverse natural ecosystems (Schardl and Craven, 2003; Jung et al., 2017a). However, viruses might also be recognized as invasive compounds of the cytoplasmatic entities limiting their transfer to another species. While *vic* and mating systems serve as antiviral defense mechanisms at the population level, RNA silencing or RNA interference (RNAi) provides a fungal antiviral defense response at the cellular level (Nuss, 2011). Antiviral RNA silencing has been demonstrated in different types of fungi including the chestnut pathogen

Cryphonectria parasitica (Segers et al., 2007) or the arbuscular mycorrhizal fungus *Gigaspora margarita* (Silvestri et al., 2020) but also in oomycetes (Fahlgren et al., 2013). Since the RNAi machinery targets possible detrimental non-self-nucleic acids, virus-infected host organisms are normally enriched with viral small interfering (si) RNA. For instance, in an analysis of the virus-derived small RNAs following high-throughput sequencing of the *Halophytophthora* isolate BD647 small RNA reads were mapped to HRV6 (unpublished data).

CONCLUSION

A combination of traditional and new technologies has been used to identify and sequence eight bunya-like mycoviruses that coinfect isolates belonging to the same species of *Halophytophthora* from southern Portuguese estuaries. However, any relationships between the different viruses and any effects of the viruses on the phenotype, virulence and host range of their oomycete host remain unknown.

DATA AVAILABILITY STATEMENT

The datasets presented in this study can be found in online repositories. The names of the repository/repositories and accession number(s) can be found at: https://www.ncbi.nlm.nih.gov/bioproject/PRJNA619952.

AUTHOR CONTRIBUTIONS

LB and TJ: original idea. CM, TJ, and MJ: sampling and phylogenetic characterization of *Halophytophthora* isolates. LB, JJ, and MR: methodology. LB: formal analysis, writing—original draft preparation. LB, TJ, and JJ: writing—review and editing.

FUNDING

This research was funded by the Project Phytophthora Research Centre Reg. No. CZ.02.1.01/0.0/0.0/15_003/0000453, co-financed by the European Regional Development Fund.

ACKNOWLEDGMENTS

LB would like to acknowledge Dr. María Ángeles Ayllón from Centro de Biotecnología y Genómica de Plantas (CBGP-UPM-INIA), Universidad Politécnica de Madrid (UPM) (Spain) for her useful suggestions.

SUPPLEMENTARY MATERIAL

The Supplementary Material for this article can be found online at: https://www.frontiersin.org/articles/10.3389/fmicb.2020.01467/full#supplementary-material

TABLE S1 | Complete list of isolates used in the present study, indicating species identification, location, dsRNA pattern and results of the RT-PCR screening title.

TABLE S2 | Mapping results for *P. cinnamomi* as reference sequence.

TABLE S3 | Gene-Specific Primers (GSPs) used in the SMARTer RACE reactions.

TABLE S4 | Specific primers used for the partial amplification of the viral RdRp in order to screen the presence of each virus in all the isolates of the collection.

TABLE S5 | Percentages of pairwise identities between the eight viral full-length nucleotide genome sequences.

REFERENCES

Abudurexiti, A., Adkins, S., Alioto, D., Alkhovsky, S. V., Avšič-Županc, T., Ballinger, M. J., et al. (2019). Taxonomy of the order bunyavirales: update 2019. *Arch. Virol.* 164, 1949–1965.

Barr, J. N., and Fearns, R. (2010). How RNA viruses maintain their genome integrity. *J. Gen. Virol.* 91, 1373–1387. doi: 10.1099/vir.0.020818-20810

Bennett, R. M., de Cock, A. W. A. M., Lévesque, C. A., and Thines, M. (2017). *Calycofera* gen. nov., an estuarine sister taxon to *Phytopythium*. *Peronosporaceae. Mycol. Prog.* 16, 947–954. doi: 10.1007/s11557-017-1326-1329

Bennett, R. M., and Thines, M. (2019). Revisiting salisapiliaceae. *FUSE* 3, 171–184. doi: 10.3114/fuse.2019.03.10

Breitbart, M. (2012). Marine viruses: truth or dare. *Ann. Rev. Mar. Sci.* 4, 425–448. doi: 10.1146/annurev-marine-120709-142805

Briese, T., Calisher, C. H., and Higgs, S. (2013). Viruses of the family *Bunyaviridae* : are all available isolates reassortants? *Virology* 446, 207–216. doi: 10.1016/j.virol.2013.07.030

Cai, G., Fry, W. E., and Hillman, B. I. (2019). PiRV-2 stimulates sporulation in *Phytophthora infestans*. *Virus Res* 271:197674. doi: 10.1016/J.VIRUSRES.2019.197674

Cai, G., Krychiw, J. F., Myers, K., Fry, W. E., and Hillman, B. I. (2013). A new virus from the plant pathogenic oomycete *Phytophthora infestans* with an 8 kb dsRNA genome: the sixth member of a proposed new virus genus. *Virology* 435, 341–349.

Cai, G., Myers, K., Fry, W. E., and Hillman, B. I. (2012). A member of the virus family *Narnaviridae* from the plant pathogenic oomycete *Phytophthora infestans*. *Arch. Virol.* 157, 165–169.

Cai, G., Myers, K., Hillman, B. I., and Fry, W. E. (2009). A novel virus of the late blight pathogen, *Phytophthora infestans* , with two RNA segments and a supergroup 1 RNA-dependent RNA polymerase. *Virology* 392, 52–61. doi: 10.1016/j.virol.2009.06.040

Chiapello, M., Rodríguez-Romero, J., Nerva, L., Forgia, M., Chitarra, W., Ayllón, M. A., et al. (2020). Putative new plant viruses associated with *Plasmopara viticola* -infected grapevine samples. *Ann. Appl. Biol.* 176, 180–191. doi: 10.1111/aab.12563

Coupeau, D., Bayrou, C., Baillieux, P., Marichal, A., Lenaerts, A. C., Caty, C., et al. (2019). Host-dependence of in vitro reassortment dynamics among the sathuperi and shamonda simbuviruses. *Emerg. Microbes Infect.* 8, 381–395. doi: 10.1080/22221751.2019.1586410

Coy, S., Gann, E., Pound, H., Short, S., and Wilhelm, S. (2018). Viruses of eukaryotic algae: diversity, methods for detection, and future directions. *Viruses* 10:487. doi: 10.3390/v10090487

Desnues, C., Rodriguez-Brito, B., Rayhawk, S., Kelley, S., Tran, T., Haynes, M., et al. (2008). Biodiversity and biogeography of phages in modern stromatolites and thrombolites. *Nature* 452, 340–343. doi: 10.1038/nature06735

Donaire, L., Pagán, I., and Ayllón, M. A. (2016). Characterization of Botrytis cinerea negative-stranded RNA virus 1, a new mycovirus related to plant viruses, and a reconstruction of host pattern evolution in negative-sense ssRNA viruses. *Virology* 499, 212–218. doi: 10.1016/J.VIROL.2016.09.017

Edgar, R. C. (2004). MUSCLE: multiple sequence alignment with high accuracy and high throughput. *Nucleic Acids Res.* 32, 1792–1797. doi: 10.1093/nar/gkh340

Fahlgren, N., Bollmann, S. R., Kasschau, K. D., Cuperus, J. T., Press, C. M., Sullivan, C. M., et al. (2013). *Phytophthora* have distinct endogenous small RNA populations that include short interfering and microRNAs. *PLoS One* 8:e77181. doi: 10.1371/journal.pone.0077181

Ferron, F., Weber, F., de la Torre, J. C., and Reguera, J. (2017). Transcription and replication mechanisms of *Bunyaviridae* and *Arenaviridae* L proteins. *Virus Res.* 234, 118–134. doi: 10.1016/j.virusres.2017.01.018

Gillings, M. R., Tesoriero, L. A., and Gunn, L. V. (1993). Detection of double-stranded RNA and virus-like particles in Australian isolates of *Pythium irregulare*. *Plant Pathol.* 42, 6–15. doi: 10.1111/j.1365-3059.1993.tb01466.x

Govers, L. L., Man In 'T Veld, W. A., Meffert, J. P., Bouma, T. J., van Rijswick, P. C. J., Heusinkveld, J. H. T., et al. (2016). Marine *Phytophthora* species can hamper conservation and restoration of vegetated coastal ecosystems. *Proc. R. Soc. B Biol. Sci.* 283:20160812. doi: 10.1098/rspb.2016.0812

Grasse, W., and Spring, O. (2017). ssRNA viruses from biotrophic Oomycetes form a new phylogenetic group between *Nodaviridae* and *Tombusviridae* . *Arch. Virol.* 162, 1319–1324. doi: 10.1007/s00705-017-3243-3242

Grasse, W., Zipper, R., Totska, M., and Spring, O. (2013). *Plasmopara halstedii* virus causes hypovirulence in *Plasmopara halst* edii, the downy mildew pathogen of the sunflower. *Fungal Genet. Biol.* 57, 42–47. doi: 10.1016/j.fgb.2013.05.009

Hacker, C. V., Brasier, C. M., and Buck, K. W. (2005). A double-stranded RNA from a *Phytophthora* species is related to the plant endornaviruses and contains a putative UDP glycosyltransferase gene. *J. Gen. Virol.* 86, 1561–1570. doi: 10.1099/vir.0.80808-80800

Halldorsson, S., Li, S., Li, M., Harlos, K., Bowden, T. A., and Huiskonen, J. T. (2018). Shielding and activation of a viral membrane fusion protein. *Nat. Commun.* 9, 1–9. doi: 10.1038/s41467-017-02789-2782

Huiskonen, J. T., Hepojoki, J., Laurinmaki, P., Vaheri, A., Lankinen, H., Butcher, S. J., et al. (2010). Electron cryotomography of tula hantavirus suggests a unique assembly paradigm for enveloped viruses. *J. Virol.* 84, 4889–4897. doi: 10.1128/jvi.00057-10

Jung, T., Chang, T. T., Bakonyi, J., Seress, D., Pérez-Sierra, A., Yang, X., et al. (2017a). Diversity of *Phytophthora* species in natural ecosystems of Taiwan and association with disease symptoms. *Plant Pathol.* 66, 194–211. doi: 10.1111/ppa.12564

Jung, T., Scanu, B., Bakonyi, J., Seress, D., Kovács, G. M., Durán, A., et al. (2017b). *Nothophytophthora* gen. nov., a new sister genus of *Phytophthora* from natural and semi-natural ecosystems. *Persoonia* 39, 143–174. doi: 10.3767/persoonia.2017.39.07

Kormelink, R., Garcia, M. L., Goodin, M., Sasaya, T., and Haenni, A.-L. (2011). Negative-strand RNA viruses: the plant-infecting counterparts. *Virus Res.* 162, 184–202. doi: 10.1016/j.virusres.2011.09.028

Kozlakidis, Z., Brown, N. A., Jamal, A., Phoon, X., and Coutts, R. H. A. (2010). Incidence of endornaviruses in *Phytophthora* taxon douglasfir and *Phytophthora ramorum* . *Virus Genes* 40, 130–134. doi: 10.1007/s11262-009-0421-427

Lee, S. Y. (1998). Ecological role of grapsid crabs in mangrove ecosystems: a review. *Mar. Freshw. Res.* 49, 335–343. doi: 10.1071/mf97179

Leslie, J. F., and Zeller, K. A. (1996). Heterokaryon incompatibility in fungi—more than just another way to die. *J. Genet.* 75, 415–424. doi: 10.1007/BF02966319

Li, C.-X., Shi, M., Tian, J.-H., Lin, X.-D., Kang, Y.-J., Chen, L.-J., et al. (2015). Unprecedented genomic diversity of RNA viruses in arthropods reveals the ancestry of negative-sense RNA viruses. *Elife* 4:e05378. doi: 10.7554/eLife.05378

Li, H., and Roossinck, M. J. (2004). Genetic bottlenecks reduce population variation in an experimental rna virus population. *Society* 78, 10582–10587. doi: 10.1128/JVI.78.19.10582

Lin, Y.-H., Fujita, M., Chiba, S., Hyodo, K., Andika, I. B., Suzuki, N., et al. (2019). Two novel fungal negative-strand RNA viruses related to mymonaviruses and phenuiviruses in the shiitake mushroom (*Lentinula edodes*). *Virology* 533, 125–136. doi: 10.1016/j.virol.2019.05.008

Lu, S., Wang, J., Chitsaz, F., Derbyshire, M. K., Geer, R. C., Gonzales, N. R., et al. (2020). CDD/SPARCLE: the conserved domain database in 2020. *Nucleic Acids Res.* 48, D265–D268. doi: 10.1093/nar/gkz991

Man in 't Veld, W. A., Rosendahl, K. C. H. M., van Rijswick, P. C. J., Meffert, J. P., Boer, E., Westenberg, M., et al. (2019). Multiple *Halophytophthora* spp. and *Phytophthora* spp. including *P. gemini*, *P. inundata* and *P. chesapea*kensis sp. nov. isolated from the seagrass *Zostera marina* in the Northern hemisphere. *Eur. J. Plant Pathol.* 153, 341–357. doi: 10.1007/s10658-018-1561-1561

Marano, A. V., Jesus, A. L., de Souza, J. I., Leaño, E. M., James, T. Y., Jerônimo, G. H., et al. (2014). A new combination in *Phytopythium*: *P. kandeliae* (*Oomycetes*. *Straminipila*). *Mycosphere* 5, 510–522. doi: 10.5943/mycosphere/5/4/3

Margaria, P., Bosco, L., Vallino, M., Ciuffo, M., Mautino, G. C., Tavella, L., et al. (2014). The NSs Protein of tomato spotted wilt virus is required for persistent infection and transmission by *Frankliniella occidentalis*. *J. Virol.* 88, 5788–5802. doi: 10.1128/jvi.00079-14

Marklewitz, M., Zirkel, F., Kurth, A., Drosten, C., and Junglena, S. (2015). Evolutionary and phenotypic analysis of live virus isolates suggests arthropod origin of a pathogenic RNA virus family. *Proc. Natl. Acad. Sci. U.S.A.* 112, 7536–7541. doi: 10.1073/pnas.1502036112

Marzano, S.-Y. L., Nelson, B. D., Ajayi-Oyetunde, O., Bradley, C. A., Hughes, T. J., Hartman, G. L., et al. (2016). Identification of diverse mycoviruses through metatranscriptomics characterization of the viromes of five major fungal plant pathogens. *J. Virol.* 90, 6846–6863. doi: 10.1128/jvi.00357-316

Melzer, M. S., Ikeda, S. S., and Boland, G. J. (2002). Interspecific Transmission of Double-Stranded RNA and Hypovirulence from Sclerotinia sclerotiorum to S. minor. *Phytopathology* 92, 780–784. doi: 10.1094/PHYTO.2002.92.7.780

Miller, M. A., Pfeiffer, W., and Schwartz, T. (2010). "Creating the CIPRES Science Gateway for inference of large phylogenetic trees," in *2010 Gateway Computing Environments Workshop, GCE 2010*. doi: 10.1109/GCE.2010.5676129

Morris, T. J., and Dodds, J. A. (1979). Isolation and analysis of double-stranded RNA from virus-infected plant and fungal tissue. *Phytopathology* 69, 854. doi: 10.1094/Phyto-69-854

Muller, R., Poch, O., Delarue, M., Bishop, D. H. L., and Bouloy, M. (1994). Rift valley fever virus L segment: correction of the sequence and possible functional role of newly identified regions conserved in RNA-dependent polymerases. *J. Gen. Virol* 75(Pt 6), 1345–1352. doi: 10.1099/0022-1317-75-6-1345

Nagasaki, K., Tomaru, Y., Takao, Y., Nishida, K., Shirai, Y., Suzuki, H., et al. (2005). Previously unknown virus infects marine diatom. *Appl. Environ. Microbiol* 71, 3528–3535. doi: 10.1128/AEM.71.7.3528-3535.2005

Nerva, L., Ciuffo, M., Vallino, M., Margaria, P., Varese, G. C., Gnavi, G., et al. (2015). Multiple approaches for the detection and characterization of viral and plasmid symbionts from a collection of marine fungi. *Virus Res* 219, 22–38. doi: 10.1016/j.virusres.2015.10.028

Nerva, L., Forgia, M., Ciuffo, M., Chitarra, W., Chiapello, M., Vallino, M., et al. (2019a). The mycovirome of a fungal collection from the sea cucumber *Holothuria polii*. *Virus Res.* 273:197737. doi: 10.1016/j.virusres.2019.197737

Nerva, L., Turina, M., Zanzotto, A., Gardiman, M., Gaiotti, F., Gambino, G., et al. (2019b). Isolation, molecular characterization and virome analysis of culturable wood fungal endophytes in esca symptomatic and asymptomatic grapevine plants. *Environ. Microbiol.* 21, 2886–2904. doi: 10.1111/1462-2920.14651

Newell, S. Y., and Fell, J. W. (1992). Distribution and experimental responses to substrate of marine oomycetes (*Halophytophthora* spp.) in mangrove ecosystems. *Mycol. Res.* 96, 851–856. doi: 10.1016/S0953-7562(09)81030-81037

Newell, S. Y., and Fell, J. W. (1997). Competition among mangrove oomycotes, and between oomycotes and other microbes. *Aquat. Microb. Ecol.* 12, 21–28. doi: 10.3354/ame012021

Nuss, D. L. (2011). Mycoviruses. RNA silencing, and viral RNA recombination. *Adv. Virus Res.* 80, 25–48. doi: 10.1016/B978-0-12-385987-7.00002-6

Obijeski, J. F., Bishop, D. H., Murphy, F. A., and Palmer, E. L. (1976). Structural proteins of La Crosse virus. *J. Virol.* 19, 985–997. doi: 10.1128/jvi.19.3.985-997.1976

O'Callaghan, I., Harrison, S., Fitzpatrick, D., and Sullivan, T. (2019). The freshwater isopod *Asellus aquaticus* as a model biomonitor of environmental pollution: a review. *Chemosphere* 235, 498–509. doi: 10.1016/j.chemosphere.2019.06.217

Poimala, A., and Vainio, E. J. (2020). Complete genome sequence of a novel toti - like virus from the plant - pathogenic oomycete *Phytophthora cactorum*. *Arch. Virol.* 165, 1679–1682. doi: 10.1007/s00705-020-04642-4642

Rozas, J., Ferrer-Mata, A., Sanchez-Del Barrio, J. C., Guirao-Rico, S., Librado, P., Ramos-Onsins, S. E., et al. (2017). DnaSP 6: DNA sequence polymorphism analysis of large data sets. *Mol. Biol. Evol.* 34, 3299–3302. doi: 10.1093/molbev/msx248

Sasai, S., Tamura, K., Tojo, M., Herrero, M.-L., Hoshino, T., Ohki, S. T., et al. (2018). A novel non-segmented double-stranded RNA virus from an Arctic isolate of *Pythium polare* . *Virology* 522, 234–243. doi: 10.1016/j.virol.2018.07.012

Schardl, C. L., and Craven, K. D. (2003). Interspecific hybridization in plant-associated fungi and oomycetes: a review. *Mol. Ecol.* 12, 2861–2873. doi: 10.1046/j.1365-294X.2003.01965.x

Schneider, W. L., and Roossinck, M. J. (2001). Genetic diversity in RNA virus quasispecies is controlled by host-virus interactions. *Society* 75, 6566–6571. doi: 10.1128/JVI.75.14.6566

Segers, G. C., Zhang, X., Deng, F., Sun, Q., and Nuss, D. L. (2007). Evidence that RNA silencing functions as an antiviral defense mechanism in fungi. *Proc. Natl. Acad. Sci. U.S.A.* 104, 12902–12906. doi: 10.1073/pnas.0702500104

Shi, M., Lin, X. D., Tian, J. H., Chen, L. J., Chen, X., Li, C. X., et al. (2016). Redefining the invertebrate RNA virosphere. *Nature* 540, 539–543. doi: 10.1038/nature20167

Shi, M., Zhang, Y. Z., and Holmes, E. C. (2018). Meta-transcriptomics and the evolutionary biology of RNA viruses. *Virus Res.* 243, 83–90. doi: 10.1016/j.virusres.2017.10.016

Shiba, K., Hatta, C., Sasai, S., Tojo, M., Ohki, S. T., and Mochizuki, T. (2018). Genome sequence of a novel partitivirus identified from the oomycete *Pythium nunn*. *Arch. Virol.* 163, 2561–2563.

Silvestri, A., Turina, M., Fiorilli, V., Miozzi, L., Venice, F., Bonfante, P., et al. (2020). Different genetic sources contribute to the small RNA Population in the arbuscular mycorrhizal fungus *Gigaspora margarita*. *Front. Microbiol.* 11:395. doi: 10.3389/fmicb.2020.00395

Stamatakis, A., Hoover, P., and Rougemont, J. (2008). A rapid bootstrap algorithm for the RAxML Web Servers. *Syst. Biol.* 57, 758–771. doi: 10.1080/10635150802429642

Sullivan, B. K., Trevathan-Tackett, S. M., Neuhauser, S., and Govers, L. L. (2018). Review: host-pathogen dynamics of seagrass diseases under future global change. *Mar. Pollut. Bull.* 134, 75–88. doi: 10.1016/j.marpolbul.2017.09.030

Sutela, S., Poimala, A., and Vainio, E. J. (2019). Viruses of fungi and oomycetes in the soil environment. *FEMS Microbiol. Ecol.* 95, 1–18. doi: 10.1093/femsec/fiz119

Suttle, C. A. (2005). Viruses in the sea. *Nature* 437, 356–361. doi: 10.1038/nature04160

Thines, M., and Choi, Y. J. (2016). Evolution, diversity, and taxonomy of the *Peronosporaceae*, with focus on the genus *Peronospora*. *Phytopathology* 106, 6–18. doi: 10.1094/PHYTO-05-15-0127-RVW

Tuomivirta, T. T., Uotila, A., and Hantula, J. (2002). Two independent double-stranded RNA patterns occur in the Finnish Gremmeniella abietina var. abietina type A. *For. Pathol.* 32, 197–205. doi: 10.1046/j.1439-0329.2002.00285.x

Vainio, E. J., Hakanpää, J., Dai, Y.-C., Hansen, E., Korhonen, K., and Hantula, J. (2011). Species of Heterobasidion host a diverse pool of partitiviruses with global distribution and interspecies transmission. *Fungal Biol.* 115, 1234–1243. doi: 10.1016/j.funbio.2011.08.008

Van Diepeningen, A. D., Debets, A. J. M., and Hoekstra, R. F. (1998). Intra- and interspecies virus transfer in Aspergilli via protoplast fusion. *Fungal Genet. Biol.* 25, 171–180. doi: 10.1006/fgbi.1998.1096

Vega Thurber, R. L., Barott, K. L., Hall, D., Liu, H., Rodriguez-Mueller, B., Desnues, C., et al. (2008). Metagenomic analysis indicates that stressors induce production of herpes-like viruses in the coral *Porites compressa*. *Proc. Natl. Acad. Sci. U.S.A.* 105, 18413–18418. doi: 10.1073/pnas.0808985105

Velasco, L., Arjona-Girona, I., Cretazzo, E., and López-Herrera, C. (2019). Viromes in Xylariaceae fungi infecting avocado in Spain. *Virology* 532, 11–21. doi: 10.1016/j.virol.2019.03.021

Weiland, J. J., and Sundsbak, J. L. (2000). Differentiation and detection of sugar beet fungal pathogens using pcr amplification of actin coding sequences and its region of the rRNA gene. *Plant Dis.* 84, 475–482. doi: 10.1094/PDIS.2000.84.4.475

Weinbauer, M. G. (2004). Ecology of prokaryotic viruses. *FEMS Microbiol. Rev.* 28, 127–181. doi: 10.1016/j.femsre.2003.08.001

Weynberg, K., Allen, M., and Wilson, W. (2017). Marine prasinoviruses and their tiny plankton hosts: a review. *Viruses* 9:43. doi: 10.3390/v9030043

Wommack, K. E., and Colwell, R. R. (2000). Virioplankton: viruses in aquatic ecosystems. *Microbiol. Mol. Biol. Rev.* 64, 69–114. doi: 10.1128/MMBR.64.1.69-114.2000

Yokoi, T., Yamashita, S., and Hibi, T. (2003). The nucleotide sequence and genome organization of Sclerophthora macrospora virus A. *Virology* 311, 394–399.

Zhao, G., Wu, G., Lim, E. S., Droit, L., Krishnamurthy, S., Barouch, D. H., et al. (2017). VirusSeeker, a computational pipeline for virus discovery and virome composition analysis. *Virology* 503, 21–30. doi: 10.1016/j.virol.2017.01.005

Conflict of Interest: The authors declare that the research was conducted in the absence of any commercial or financial relationships that could be construed as a potential conflict of interest.

frontiers in Microbiology

ORIGINAL RESEARCH
published: 20 October 2020
doi: 10.3389/fmicb.2020.592789

Molecular Characterization of a Novel Polymycovirus From *Penicillium janthinellum* With a Focus on Its Genome-Associated PASrp

*Yukiyo Sato[1], Atif Jamal[2], Hideki Kondo[1] and Nobuhiro Suzuki[1]**

[1] Institute of Plant Science and Resources, Okayama University, Kurashiki, Japan, [2] Crop Diseases Research Institute, National Agricultural Research Centre, Islamabad, Pakistan

OPEN ACCESS

Edited by:
Hiromitsu Moriyama, Tokyo University of Agriculture and Technology, Japan

Reviewed by:
Ioly Kotta-Loizou, Imperial College London, United Kingdom
Wenxing Xu, Huazhong Agricultural University, China

***Correspondence:**
Nobuhiro Suzuki
nsuzuki@okayama-u.ac.jp;
nsuzuki@rib.okayama-u.ac.jp

Specialty section:
This article was submitted to Virology, a section of the journal Frontiers in Microbiology

Received: 08 August 2020
Accepted: 18 September 2020
Published: 20 October 2020

Citation:
Sato Y, Jamal A, Kondo H and Suzuki N (2020) Molecular Characterization of a Novel Polymycovirus From Penicillium janthinellum With a Focus on Its Genome-Associated PASrp. Front. Microbiol. 11:592789. doi: 10.3389/fmicb.2020.592789

The genus *Polymycovirus* of the family *Polymycoviridae* accommodates fungal RNA viruses with different genomic segment numbers (four, five, or eight). It is suggested that four members form no true capsids and one forms filamentous virus particles enclosing double-stranded RNA (dsRNA). In both cases, viral dsRNA is associated with a viral protein termed "proline-alanine-serine-rich protein" (PASrp). These forms are assumed to be the infectious entity. However, the detailed molecular characteristics of PASrps remain unclear. Here, we identified a novel five-segmented polymycovirus, Penicillium janthinellum polymycovirus 1 (PjPmV1), and characterized its purified fraction form in detail. The PjPmV1 had five dsRNA segments associated with PASrp. Density gradient ultracentrifugation of the PASrp-associated PjPmV1 dsRNA revealed its uneven structure and a broad fractionation profile distinct from that of typical encapsidated viruses. Moreover, PjPmV1-PASrp interacted *in vitro* with various nucleic acids in a sequence-non-specific manner. These PjPmV1 features are discussed in view of the diversification of genomic segment numbers of the genus *Polymycovirus*.

Keywords: fungal virus, RNA virus, polymycovirus, *Penicillium janthinellum*, capsidless, multi-segmented, proline-alanine-serine rich protein

INTRODUCTION

Capsidless RNA viruses have been frequently found in fungi, possibly being associated with their persistent life cycle that lacks an extracellular state (Nuss, 2005; Ghabrial et al., 2015). Accumulating evidence suggests that the capsidless lifestyles are diverse, while their details have been revealed for few viruses. The representative capsidless mycoviruses are members of the families *Hypoviridae*, *Endornaviridae*, and *Narnaviridae*, the families of positive-sense, single-stranded RNA [(+)RNA] viruses with non-segmented genome. Instead of capsids, the host membranous vesicles encapsulate their genomic RNAs, and this associations may protect the virus against antiviral defenses in the host fungi (Lakshman et al., 1998; Solorzano et al., 2000; Jacob-Wilk et al., 2006; Hillman and Cai, 2013; Suzuki et al., 2018; Valverde et al., 2019). The members of *Hypoviridae*, *Endornaviridae*, and *Narnaviridae* are phylogenetically distant (Wolf et al., 2018). Other non-segmented fungal RNA viruses that appear to have a potential capsidless

nature, include unclassified viruses called yadokariviruses (Zhang et al., 2016; Hisano et al., 2018), fusariviruses (Kwon et al., 2007; Zhang et al., 2014), and phlegiviruses (Kozlakidis et al., 2009; Magae, 2012). Fusariviruses and phlegiviruses show moderate or low phylogenetic affinity to (+)RNA viruses of the family *Hypoviridae* or to double-stranded RNA (dsRNA) viruses of the family *Megabirnaviridae*, respectively (Petrzik et al., 2016; Suzuki et al., 2018; Sato et al., 2019). Their virus particles cannot be obtained by conventional purification methods (Kozlakidis et al., 2009; Magae, 2012; Zhang et al., 2014), and unstable particle-like forms have been reported for these viruses (Kwon et al., 2007). Thus, how fusariviruses and phlegiviruses protect their genome remains unknown. Unlike the aforementioned capsidless viruses, yadokariviruses (monopartite (+)RNA viruses), which show a distant phylogenetic relationship to some animal (+)RNA viruses such as caliciviruses (the picornavirus-like superfamily), hijack the capsids of other unrelated dsRNA viruses as their potential replication sites and behave like encapsidated dsRNA viruses (Zhang et al., 2016; Hisano et al., 2018).

Recent studies suggest that multi-segmented RNA viruses can also be capsidless, which has been shown for some polymycoviruses (Kanhayuwa et al., 2015; Zhai et al., 2016; Kotta-Loizou and Coutts, 2017; Niu et al., 2018) and one hadakavirus (Sato et al., 2020). Polymycoviruses are a group of mycoviruses belonging to the genus *Polymycovirus* in the family *Polymycoviridae*, which was established in 2020[1]. The genus accommodates six species with relatively characterized viruses and four species with uncharacterized viruses, for which only genomic information is available (top six and lower four, respectively, in **Table 1**). Like yadokariviruses, the type member of polymycovirus is distantly related to caliciviruses (Kanhayuwa et al., 2015). All known polymycoviruses share four conserved genomic segments, called dsRNA1, dsRNA2, dsRNA3, and dsRNA4, which encode P1 (RNA-dependent RNA polymerase, RdRP), P2 (hypothetical protein with unknown function, containing a transmembrane domain and a zinc-finger motif), P3 (putative methyltransferase, MTR), and P4 (a potential genome-associated protein named proline-alanine-serine-rich protein, PASrp), respectively (Kanhayuwa et al., 2015; Zhai et al., 2016; Jia et al., 2017; Kotta-Loizou and Coutts, 2017; Niu et al., 2018; Mahillon et al., 2019; Nerva et al., 2019; and unpublished sequence data deposited in DDBJ/EMBL/GenBank). Several polymycoviruses have additional one to four genomic segments, among which no significant sequence similarities were found (Zhai et al., 2016; Jia et al., 2017; Kotta-Loizou and Coutts, 2017; Mahillon et al., 2019). Hadakavirus is a novel (+)RNA virus that has a close phylogenetic relationship with polymycoviruses (Sato et al., 2020). In contrast to polymycoviruses, the hadakavirus has 11 dsRNA segments as its replicative form, which include three segments cognate with polymycovirus, namely -dsRNA1, -dsRNA2, and -dsRNA3 (Sato et al., 2020). Total genome size considerably varies between polymycoviruses and a hadakavirus due to the expanded genomic segment numbers (**Table 1**). The diversification of the genomic segment number among them may be related to their virus forms.

[1]https://talk.ictvonline.org/taxonomy/

Two viral forms have been proposed for polymycoviruses: a capsidless RNA-protein complex (RNP) form (Kanhayuwa et al., 2015; Zhai et al., 2016; Kotta-Loizou and Coutts, 2017; Niu et al., 2018) and a filamentous encapsidated form (Jia et al., 2017). The dsRNA viruses are generally icosahedral virions. The filamentous polymycovirus, named Colletotrichum camelliae filamentous virus 1 (CcFV1), was identified as the first and the only dsRNA virus with a filamentous virion architecture (Jia et al., 2017). In both capsidless and filamentous polymycoviruses, viral dsRNA was considered to be associated with virally encoded PASrp (Kanhayuwa et al., 2015; Zhai et al., 2016; Jia et al., 2017; Kotta-Loizou and Coutts, 2017; Niu et al., 2018). The capsidless form, suggested as colloidal, was first described for Aspergillus fumigatus tetramycovirus 1 (AfuTmV1), which was observed by atomic force microscopy (AFM) (Kanhayuwa et al., 2015). No typical virus particles have also been observed for Beauveria bassiana polymycovirus 1 (BbPmV1), Botryosphaeria dothidea RNA virus 1 (BdRV1), and Penicillium digitatum polymycovirus 1 (PdPmV1) by AFM or transmission electron microscopy (TEM) (Zhai et al., 2016; Kotta-Loizou and Coutts, 2017; Niu et al., 2018). The PASrp-associated dsRNA form, or even the purified dsRNA form, of some polymycoviruses are infectious when introduced into host fungal protoplasts (Kanhayuwa et al., 2015; Jia et al., 2017; Kotta-Loizou and Coutts, 2017; Niu et al., 2018). Thus, despite its capsidless nature, *Polymycoviridae* has been classified as a dsRNA virus family by the International Committee on Taxonomy of Viruses (ICTV). In contrast to polymycoviruses, the hadakavirus lacks PASrp or its related candidate and is hypothesized to exist as a soluble RNA form, although its alternative strategies for genome protection remain unknown (Sato et al., 2020). It should be noted that proline-alanine-serine (PAS)-rich proteins, phylogenetically unrelated to polymycovirus PASrps, are also encoded in other unclassified RNA viruses with a potentially capsidless nature, including phlegiviruses (Kozlakidis et al., 2009; Kanhayuwa et al., 2015; Kotta-Loizou and Coutts, 2017). Thus, it seems that PAS-rich proteins are required for certain RNA viruses. However, detailed molecular natures of the PASrps or other PAS-rich proteins, as well as the consensus PASrp-associated forms of polymycoviruses and other dsRNA viruses, remain obscure.

In this study, we report the molecular and biological characterization of a novel five-segmented polymycovirus, Penicillium janthinellum polymycovirus 1 (PjPmV1), which is a novel strain of the species *Penicillium digitatum polymycovirus 1* within the genus *Polymycovirus*. To gain further insights into the polymycovirus form, we present the relative buoyant density and sedimentation velocity of PjPmV1 as well as the nucleic acid binding capability of PjPmV1 PASrp.

MATERIALS AND METHODS

Fungal Strains and Growth Conditions

The PjPmV1 was obtained from a fungal strain A58, which was collected in 2017 from a tobacco-potato double cropping

TABLE 1 | Information of the 10 polymycoviruses and a closely related virus, HadV1.

Virus name		Genome information			Accession number for conserved proteins				References
Full	Abbreviation	Total size, kbp or kb	Segment number	Segment size range, kbp or kb	P1 (RdRP)	P2	P3 (MTR)	P4 (PASrp)	
Aspergillus fumigatus tetramycovirus 1	AfuTmV1	7.7	4	1.1–2.4	CDP74618	CDP74619	CDP74620	CDP74621	Kanhayuwa et al., 2015
Beauveria bassiana polymycovirus 1	BbPmV1	8.0	4	1.4–2.4	CUS18595	CUS18596	CUS18597	CUS18598	Kotta-Loizou and Coutts, 2017
Botryosphaeria dothidea RNA virus 1	BdRV1	8.7	5	1.1–2.4	AKE49495	AKE49496	AKE49497	AKE49498	Zhai et al., 2016
Colletotrichum camelliae filamentous virus 1	CcFV1	12.3	8	1.0–2.4	ASV63092	ASV63093	ASV63094	ASV63095	Jia et al., 2017
Fusarium redolens polymycovirus 1	FrPmV1	12.2	8	0.9–2.5	QDH44656	QDH44657	QDH44658	QDH44659	Mahillon et al., 2019
Penicillium digitatum polymycovirus 1	PdPmV1	8.0	4	1.3–2.4	AVZ65983	AVZ65984	AVZ65985	AVZ65986	Niu et al., 2018
Aspergillus spelaeus tetramycovirus 1	AspTmV1	7.8	4	1.2–2.4	AYP71805	AYP71808	AYP71807	AYP71806	Nerva et al., 2019
Cladosporium cladosporioides virus 1	CcV1	8.9	5	0.9–2.4	AII80567	AII80568	AII80569	AII80570	Unpublished
Magnaporthe oryzae polymycovirus 1	MoPmV1	7.9	4	1.3–2.4	QAU09249	QAU09250	QAU09251	QAU09252	Unpublished
Penicillium brevicompactum tetramycovirus 1	PbTmV1	7.8	4	1.2–2.4	AYP71801	AYP71804	AYP71803	AYP71802	Nerva et al., 2019
Hadaka virus 1	HadV1	15.3	11	0.9–2.5	BBU94038	BBU94039	BBU94040	Absent	Sato et al., 2020

soil in Manshera, Pakistan. Fungal species were identified by sequencing the amplified-internal transcribed spacer (ITS) region with the PCR primers (White et al., 1990) listed in **Supplementary Table 1**. Using BLASTN search, the ITS sequence of strain A58 was identical or most similar to that of *Penicillium janthinellum* (an ascomycete) (data not shown). The virus-free isogenic strains, including A58-cf1, were obtained by single conidium isolation from the original strain A58, which is infected by a novel polymycovirus PjPmV1. The presence or absence of PjPmV1 in conidial sub-isolates were initially determined by mycelial direct RT-PCR with PjPmV1-dsRNA1-specific primers (**Supplementary Table 1**) as previously described (Sato et al., 2020). The results were further confirmed by dsRNA extraction and by RT-PCR using total RNA templates. The PjPmV1-cured or PjPmV1-transmitted conidial sub-isolates were named "A58-cf*n*" or "A58-cv*n*," respectively (different number *n* denotes independent sub-isolates).

Fusarium oxysporum chrysovirus 1 (FoCV1) strain A60, an unpublished multi-segmented dsRNA virus related to alphachrysoviruses, was used for virus purification analyses as a typical encapsidated virus. The FoCV1-infected *Fusarium oxysporum* (an ascomycete) strain A60 and its virus-free conidial sub-isolate A60-cf1 were used for this study.

Two virus-free ascomycetous fungi, *Rosellinia necatrix* strain W97 (Sasaki et al., 2007; Shimizu et al., 2018) and *Cryphonectria parasitica* strain EP155 (Crouch et al., 2020), were used for nucleic acid extraction (ribosomal RNA and genomic DNA, respectively) to analyze the interaction with recombinant PjPmV1-PASrp (see the section "Electrophoretic Mobility Shift Assay" in "Materials and Methods").

The above fungal strains were grown on Difco potato dextrose agar (PDA) media (Becton, Dickinson and Co.) on a laboratory bench at room temperature. The fungal colonies were transferred to new plates before they covered the entire plate area. Conidia of *P. janthinellum* were naturally generated on PDA media.

Extraction, Sequencing, and Northern Hybridization of dsRNA

The dsRNA was extracted from 3- or 5-day-old mycelia cultured on cellophane-PDA media and treated with RQ1 DNase (Promega Corp.) and S1 nuclease (Thermo Fisher Scientific, Inc.) as previously described (Sato et al., 2020). The purified dsRNA was separated on 1% (w/v) agarose gel in 0.5 × TBE. For the electrophoretic mobility shift assay (EMSA) described below, TAE was used instead of TBE. The dsRNA extracted from 125 mg (fresh weight) of mycelia (a starting volume) was loaded into a lane in the gel and stained with ethidium bromide (EtBr). The dsRNA band size was estimated based on the migration positions of mycoreovirus 1/S10ss (Sun and Suzuki, 2008). The dsRNA standards were purified from *C. parasitica* infected with the mycoreovirus 1/S10ss and was denoted as "M-dsRNA" in this paper.

The complete genome sequence of PjPmV1 was determined by next-generation sequencing (NGS) and Sanger sequencing. We performed NGS (HiSeq 2500, Illumina, Inc.) as previously

described (Jamal et al., 2019; Shamsi et al., 2019). For NGS, we submitted a mixed dsRNA preparation (called "pool A1") from three fungal strains including *P. janthinellum* strain A58 and *Alternaria alternata* strain A16 (Jamal et al., 2019). The 5'- and 3'-terminal nucleotide sequences were determined by 3' RNA ligase-mediated rapid amplification of cDNA ends (3' RLM-RACE) using dsRNA as templates with the method of Lin et al. (2013). Five to nine 3' RLM-RACE clones for each terminus were analyzed. Primers used for 3' RLM-RACE are listed in **Supplementary Table 1**. The viral sequence obtained by the NGS analysis was further confirmed by resequencing of cloned cDNAs synthesized by a PCR-based method. For RT-PCR in 3' RLM-RACE and resequencing, Moloney murine leukemia virus (M-MLV) reverse transcriptase (Promega Corp.) and KOD -Plus- Neo DNA polymerase (Toyobo Co., Ltd.) were used. Hypothetical open reading frames (ORFs) were predicted by BLASTX[2] and ORFfinder[3]. Conserved protein domains were detected by BLASTP search of the entire database (non-redundant protein sequences, nr) including CDD/SPARCLE (Lu et al., 2020).

Multiple sequence alignment of the 5'- or 3'-terminal nucleotide sequences of each genomic segment was conducted using ClustalW2 in GENETYX-MAC ver. 20.1.0 (GENETYX Corp.).

Northern hybridization of viral RNAs was also performed as previously described (Sato et al., 2020). Digoxigenin (DIG)-11-dUTP-labeled cDNA probes to PjPmV1-dsRNA segments were amplified with primers listed in **Supplementary Table 1**.

RT-PCR With Total RNA Templates

Conidial sub-isolates of *P. janthinellum* A58 was checked by RT-PCR with total RNA templates for the presence of PjPmV1-genomic segments. Total RNA enriched with single-stranded RNA (ssRNA) was extracted from 3-day-old fungal colonies on cellophane-PDA by the method previously described for other fungi (Eusebio-Cope and Suzuki, 2015). Ten nanograms of RNA were subjected to RT-PCR in a 10 μL-reaction mix of PrimeScript One Step RT-PCR Kit Ver.2 (Takara Bio, Inc.). Host β-tubulin (*benA*) used as a control for RT-PCR was detected with the Bt2a and Bt2b primers (Glass and Donaldson, 1995). Used primers are listed in **Supplementary Table 1**.

Phylogenetic Analysis

The phylogenetic relationships of PjPmV1 to 10 reported polymycoviruses (**Table 1**) were analyzed based on predicted amino acid sequences of four conserved proteins. The four proteins of polymycoviruses were described as PmV-P1 (putative RdRP), PmV-P2 (hypothetical protein with unknown function), PmV-P3 (putative MTR), and PmV-P4 (putative PASrp). Each cognate protein of HadV1 was employed as an outgroup, except for PmV-P4 missing from HadV1. The amino acid sequences were retrieved with accession numbers listed in **Table 1**. Multiple sequence alignment was performed by using online MAFFT ver. 7 with default settings (Katoh et al., 2019). Trees were constructed by the maximum likelihood (ML) method with best models in MEGA X with default settings (Kumar et al., 2018). The branch probabilities were analyzed by 500 times bootstrap resampling.

Purification of Virus Particle (VP)-Like Forms

Virus particle (VP) or VP-like form (VPL) fractions of FoCV1 and PjPmV1 were obtained as follows. The crude VPL of PjPmV1 was obtained by two methods: with or without carbon tetrachloride (CCl_4) clarification. In both cases, 5-to-7-day-old fungal colonies cultured on PDA-cellophane were used. Frozen fungal cultures were ground to powder in liquid nitrogen and then mixed with four volumes (v/w) of 0.1 M sodium phosphate (pH 7.0) containing 0.1% (v/v) of β-mercaptoethanol. For the method using CCl_4, mycelial homogenates were clarified with 20% (v/v) of CCl_4 and centrifuged at 2,000 × *g* for 20 min at 4°C. This step was repeated once. A small amount of CCl_4 remained in the supernatants was evaporated in a desiccator by vacuum pumping for 10 min. For the method without CCl_4, cell debris in mycelial homogenates was alternatively removed by centrifugation at 8,000 × *g* for 10 min at 4°C. In both cases, supernatants were ultracentrifuged at 130,000 × *g* for 1.5 h at 4°C in a 70Ti rotor by Optima L-100K (Beckman Coulter, Inc.). Pellets were resuspended in 0.1 volume (against the volume of the crude extract before ultracentrifugation) of 0.05 M sodium phosphate (pH 7.0). Suspensions were centrifuged at 8,000 × *g* for 10 min at 4°C. Supernatants were defined as "crude VP or VPL" and further subjected to cesium chloride (CsCl) or sucrose gradient centrifugation.

For CsCl gradient centrifugation, 2 mL each of 50, 40, 30, 20, and 10% (w/w) CsCl in 0.05 M sodium phosphate (pH 7.0) were overlaid from bottom to top and left overnight at room temperature. Subsequently, 2 mL of crude VP (VPL) suspensions were overlaid on the CsCl gradient and ultracentrifuged at ∼210,000 × *g* for 2 h at 16°C in an SW 41Ti rotor by Optima L-100K (Beckman Coulter, Inc.). For sucrose gradient centrifugation of VP (VPL) extracted with CCl_4, 2 mL each of 50, 40, 30, 20, and 10% (w/v) sucrose in 0.05 M sodium phosphate (pH 7.0) were overlaid and left overnight at 4°C. For sucrose gradient centrifugation of VPL extracted without CCl_4, 5 mL of 72%, 3 mL of 55%, and 2 mL of 10% (w/v) sucrose in 0.05 M sodium phosphate (pH 7.0) were overlaid and left overnight at 4°C. Two milliliter of crude VP (VPL) suspensions were overlaid on the sucrose gradients and ultracentrifuged at ∼210,000 × *g* for 2 h at 4°C in the same swing rotor. After gradient ultracentrifugation, all 1-mL fractions from top to bottom were collected and numbered from #1 to #12. Each fraction containing PjPmV1 dsRNA was mixed together and diluted with three volumes of 0.05 M sodium phosphate (pH 7.0) and ultracentrifuged at 130,000 × *g* for 1.5 h at 4°C in a 70Ti rotor by Optima L-100K (Beckman Coulter, Inc.). Pellets were resuspended in 30 μL of 0.05 M sodium phosphate (pH 7.0) and defined as "pure VPL." Certain amounts of pure VPLs were filtered through a 0.2-μm membrane and used for dsRNA extraction, protein analyses, and transfection.

[2]https://blast.ncbi.nlm.nih.gov/Blast.cgi

[3]https://www.ncbi.nlm.nih.gov/orffinder/

The pure VPLs were negatively stained with a fourfold diluted EM stainer (an alternative for uranyl acetate, Nissin EM Co.) and subsequently observed in a transmission electron microscope (TEM) Hitachi H-7650.

Attempts at Virus Transfection

We tried to transfect pure VPLs and purified dsRNA of PjPmV1 into *P. janthinellum* strain A58-cf1, but the attempt was unsuccessful. Briefly, spheroplasts of A58-cf1 were prepared according to a standard method developed for *C. parasitica* (Churchill et al., 1990). Transfection was performed using a polyethylene glycol (PEG)-mediated method (Hillman et al., 2004), which was applied to a polymycovirus (Kanhayuwa et al., 2015). Subsequently, 100 μL of a suspension containing 1×10^7 cells/mL spheroplasts was mixed with 10 μL of filtered pure VPL containing approximately 0.1 μg/μL of dsRNA. We used VPLs purified by two different ways: one extracted with CCl_4 and separated by CsCl gradient centrifugation and the other one extracted without CCl_4 and separated by sucrose gradient centrifugation. One hundred colonies were transferred from regeneration media to new PDA and screened for PjPmV1-dsRNA1 by mycelial direct RT-PCR. We also tried to transfect *P. janthinellum* spheroplasts (1×10^6 cells) with purified dsRNA preparations (10 μL of approximately 0.5 μg/μL dsRNA) by the same method.

Antibody Preparation and Immunoprecipitation

As antigens for the PjPmV1-PASrp (P4) antibody preparation, the recombinant proteins of PjPmV1-PASrp tagged with glutathione *S*-transferase (GST) at the N-terminal were expressed in *Escherichia coli*. The entire PjPmV1-PASrp ORF was amplified with primers listed in **Supplementary Table 1** and cloned between the *Bam*HI and *Eco*RI sites of the pGEX-4T-3 vector (GE Healthcare, Ltd.) using an In-Fusion HD Cloning Kit (Takara Bio, Inc.). Cloned vectors were once transformed into *E. coli* strain DH5α to screen the proper construct. Plasmids were extracted using the GenElute^{TM} Plasmid Miniprep Kit (Sigma-Aldrich Co. LLC). The correct plasmid was transformed into *E. coli* strain BL21 (DE3) (New England Biolabs, Inc.) to purify the recombinant protein.

Recombinant protein (GST-PjPmV1-PASrp) was purified according to the manufacturer's instruction (GE Healthcare, Ltd.). Briefly, expression of the recombinant protein gene in *E. coli* was induced with 0.6 mM isopropyl β-D-thiogalactopyranoside (IPTG) by shaking for 3 h at 37°C. Cultures were collected by centrifugation and resuspended into phosphate-buffered saline (PBS, pH 7.3). Resuspended cells were sonicated on ice and stirred with 1% (v/v) Triton X-100 at room temperature for 30 min. The solubilized proteins were purified with Glutathione Sepharose 4B (GE Healthcare, Ltd.) and GST-tag was not excised. These affinity-purified proteins were termed "native antigens." Part of the affinity-purified proteins was separated by SDS−polyacrylamide gel electrophoresis (PAGE). A protein band of GST-PjPmV1-PASrp was excised and eluted by Model 422 Electro-Eluter (Bio-Rad Laboratories, Inc.). These proteins eluted after SDS−PAGE were called "denatured antigens." The quality of the native and denatured antigens was checked by SDS−PAGE (**Supplementary Figure 1**). Antibody preparation was performed by Eurofins Genomics K.K. One milliliter of native and denatured antigens (more than 1 mg/mL concentration) was alternately injected into a New Zealand white rabbit five times at a 2-week interval.

Immunoprecipitation with anti-GST-PjPmV1-PASrp antibodies was performed as previously described (Zhang et al., 2016).

SDS−PAGE and Western Blotting

Proteins extracted from mycelia or potential VP fractions (VPLs) were subjected to SDS−PAGE and western blotting. For extraction of mycelial proteins, frozen mycelia (5-day-old culture on PDA-cellophane) were ground in liquid nitrogen and suspended in four volumes (v/w) of PBS (pH 7.3). These mycelial extracts or pure VPLs (see above) were mixed with equal volumes of 2 × Laemmli sample buffer containing 12% (v/v) β -mercaptoethanol and denatured for 5 min at 100°C. The denatured proteins (10 μL for mycelial proteins and 2 μL for pure VPLs) were loaded in 10% (w/v) or 12% (w/v) polyacrylamide gel, and SDS−PAGE was performed according to a standard protocol (Sambrook and Russell, 2001). Total proteins were stained with Coomassie Brilliant Blue (CBB) R-250 using the Rapid Stain CBB Kit (Nacalai tesque, Inc.). Protein size was estimated with Precision Plus Protein Dual Color Standards (Bio-Rad Laboratories, Inc.) and denoted as "M-protein" in this paper.

Proteins on SDS−PAGE gels were transferred to a polyvinylidene difluoride (PVDF) membrane (Immobilon-P, Merck Millipore) in 10 mM *N*-cyclohexyl-3-aminopropanesulfonic acid (CAPS, pH 11.0) and 10% methanol. The membranes were first incubated with anti-GST-PjPmV1-PASrp antibody, followed by anti-rabbit IgG conjugated with alkaline phosphatase (formerly Kirkegaard & Perry Laboratories, Inc.) and nitro blue tetrazolium (NBT)-5-bromo-4-chloro-3-indolyl-phosphate (BCIP) solution, according to a standard protocol (Sambrook and Russell, 2001).

Electrophoretic Mobility Shift Assay (EMSA)

The binding specificity of PjPmV1-PASrp with nucleic acids was analyzed by an electrophoretic mobility shift assay (EMSA). For this, GST-PjPmV1-PASrp and free GST (produced from pGEX-4T-3 empty vector) were purified by the method described above (see the section "Antibody Preparation and Immunoprecipitation") with slight modifications. Briefly, glutathione sepharose beads were stringently washed prior to the elution steps. The beads were first washed three times in PBS (pH 7.3), as described in the normal protocol, and then four times with PBS containing 1 M NaCl, followed by three times with PBS. Approximately 1 mg/mL of GST-PjPmV1-PASrp and 4 mg/mL of GST were yielded in a maximum concentration. The protein concentration was estimated by standards of bovine serum albumin (BSA) on SDS−PAGE stained with CBB. The GST-PjPmV1-PASrp in part was heat-denatured for 5 min at

100°C. Purified proteins were incubated with 0.5−1.0 μg of dsRNA, ssRNA, or double-stranded DNA (dsDNA) in 50 mM Tris−HCl (pH 7.6), 150 mM NaCl, and 2.5 mM $CaCl_2$ for 30 min at 30°C in a 10-μL mixture. The reaction solution (10 μL) was electrophoresed on 1.0% (w/v) agarose gel in 0.5 × TAE and stained with EtBr.

Nucleic acids used for EMSA were prepared as follows. PjPmV1-dsRNA was purified from mycelia of *P. janthinellum* strain A58 as described above, and FoCV1-dsRNA was purified from mycelia of *F. oxysporum* strain A60 by the same method. For the preparation of PjPmV1-RNA3 transcripts, a plasmid containing full-length cDNA to PjPmV1-dsRNA3 was prepared. Briefly, linear pGEM-T Easy vector (Promega Corp.) and PjPmV1-dsRNA3 were amplified with primers listed in **Supplementary Table 1** and recombined with the In-Fusion HD Cloning Kit (Takara Bio, Inc.). The resulting plasmid was linearized by *Pst*I and used as a template for *in vitro* transcription by T7 RNA polymerase (Promega Corp.) according to the manufacturer's instruction. Total RNA containing ribosomal RNA was extracted from *R. necatrix* strain W97 as previously described (Chiba et al., 2013). An expression cassette of hygromycin resistance gene (hygromycin B phosphotransferase, *HygR*) was amplified by PCR with primers listed in **Supplementary Table 1**, using pCPXHY3 (Guo et al., 2009) as a template. Genomic DNA was extracted from *C. parasitica* strain EP155 with phenol-chloroform-SDS followed by RNase A treatment.

RESULTS

Molecular Characterization of PjPmV1

A novel five-segmented polymycovirus, named Penicillium janthinellum polymycovirus 1 (PjPmV1), was discovered from one of fungal strains collected in Pakistan as previously described (Jamal et al., 2019; Shamsi et al., 2019; Sato et al., 2020). The host fungal strain A58 was identified as *Penicillium* species *P. janthinellum* based on the ITS sequence (see Materials and Methods). Five PjPmV1 dsRNA segments ranging approximately from 1.3 to 2.4 kbp, which was comparable to a size range of known polymycoviruses (**Table 1**), were accumulated in the strain A58 (**Figure 1A**). The complete genome sequence of the five dsRNA segments was obtained by NGS and Sanger sequencing (**Figure 1B**). The nucleotide sequences of the PjPmV1 genomic segments were deposited in EMBL/Genbank/DDBJ (accession numbers: LC571078-LC571082). These segments were numbered in decreasing order of the nucleotide length (**Figure 1B**, dsRNA1–5). Northern hybridization with segment-specific cDNA probes detected corresponding major single bands (**Figure 1A**). The BLASTX search revealed that the four genomic segments (dsRNA1, dsRNA2, dsRNA3, and dsRNA5) each encode proteins with 75–83% in amino acid identity to the counterparts of PdPmV1, a member of the genus *Polymycovirus* (**Table 2**). The PdPmV1 was isolated from a phytopathogenic *Penicillium* species, *P. digitatum,* and was reported to have a four-segmented dsRNA genome (Niu et al., 2018). The PjPmV1 dsRNA1, dsRNA2, dsRNA3, and dsRNA5 putatively encode proteins homologous to polymyco-P1 (RdRP), -P2 (hypothetical protein), -P3 (MTR), and -P4 (PASrp), respectively. The putative PjPmV1 RdRP contains "GDNQ" as the catalytic core residues which is common to known polymycoviruses and a hadakavirus as well as mononegaviruses (non-segmented, negative-stranded RNA viruses) (Kanhayuwa et al., 2015; Sato et al., 2020). The putative PjPmV1 PASrp contains 27% of PAS residues (data not shown), which is comparable to PASrps of other polymycoviruses containing 24–32% of PAS (Sato et al., 2020). The PjPmV1 dsRNA4 possesses an ORF (P5) encoding 365 amino acids (**Figure 1B**), which showed no significant similarity to any sequences by BLASTX and BLASTN search (**Table 2** and data not shown).

The terminal nucleotide sequences of the five dsRNA segments of PjPmV1 were highly conserved (**Figure 1C**). The 5'-termini on the positive-sense strand of all dsRNA segments started with the 21-nt identical sequence (**Figure 1C**). The 3'-termini on positive sense of PjPmV1 dsRNA1, dsRNA2, dsRNA4, and dsRNA5 commonly stopped with three to eight "Us" (**Figure 1C** and **Supplementary Figure 2A**). By contrast, the 3'-terminus of PjPmV1 dsRNA3 stopped with five or six "Cs" (**Figure 1C** and **Supplementary Figure 2A**). The numbers of "U" (three to eight) or "C" (five or six) repeats varied among RACE clones (**Supplementary Figure 2A**). **Figure 1** shows the majority sequence. The 19-nt of 5'-terminal nucleotide sequences are also common among all the genomic segments of PjPmV1 and PdPmV1 (**Supplementary Figure 2B**). By contrast, the 3'-terminal nucleotide sequences of PjPmV1 are distinct from that of PdPmV1, while those are conserved, to some extent, in each virus (**Supplementary Figure 2C**).

Phylogenetic Analysis of PjPmV1

The phylogenetic relationships of PjPmV1 with 10 members of the genus *Polymycovirus* (**Table 1**) were analyzed based on the amino acid sequence of four conserved proteins using the ML method (**Figure 2**). The cognate proteins of a hadakavirus (HadV1) (**Table 1**) were employed as an outgroup except in the analysis of P4 (PASrp), which is absent in HadV1. When trees of different proteins were compared, their topology was largely similar, with a few minor differences in branching (**Figures 2A–D**). The PjPmV1 was most closely related to PdPmV1 in all the trees (**Figures 2A–D**), in accordance with the result of the BLASTX search (**Table 2**). The five-segmented polymycoviruses, namely PjPmV1, BdRV1, and CcV1, were placed to distinct branches (**Figures 2A–D**). The PjPmV1 and BdRV1 were distantly placed from eight-segmented polymycoviruses including CcFV1, the one with filamentous capsids (**Figures 2A–D**). Neither sequence similarity nor phylogenetic relationship was observed in their fifth to eighth segments (dsRNA5-dsRNA8), which are not conserved in the polymycoviruses (**Supplementary Table 2**). Thus, it seems that frequent gain or loss of

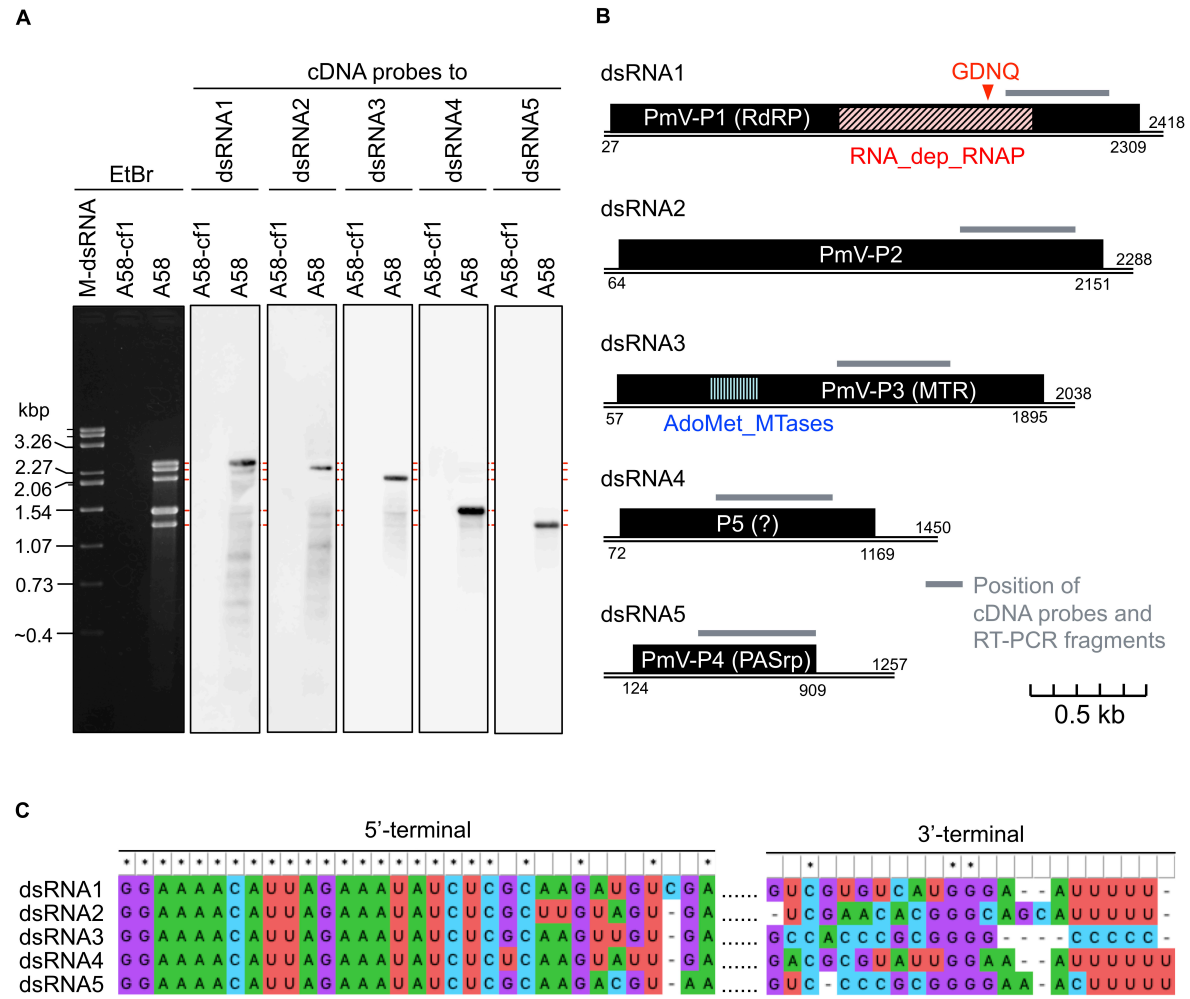

FIGURE 1 | Genome organization of a novel polymycovirus PjPmV1. **(A)** Electrophoretic profile and northern hybridization of the viral dsRNA segments. *Penicillium janthinellum* A58 is the original strain infected with PjPmV1; A58-cf1 is a virus-free isogenic sub-isolate obtained from a single conidium of A58 (see **Figure 3**). Here and after "M-dsRNA" indicates the viral dsRNA (genomic segments of mycoreovirus 1/S10ss) as a molecular size maker. **(B)** Scheme of PjPmV1 genome organization. Black boxes indicate hypothetical open reading frames (ORFs). PmV-P1 (RdRP), -P2 (hypothetical protein), -P3 (MTR) and -P4 (PASrp) indicate ORFs encoding proteins homologous to polymyco-P1 (RNA-dependent RNA polymerase), -P2 (hypothetical protein with unknown function), -P3 (methyltransferase), or -P4 (proline-alanine-serine rich protein), respectively. RNA_dep_RNAP (RNA-dependent RNA polymerase domain, cd01699) and AdoMet_MTases (S-adenosylmethionine-dependent methyltransferases domain, cd02440) indicate positions of conserved protein domains hit in the CDD/SPARCLE database. An ORF shown on dsRNA4 is the hypothetical longest ORF predicted by ORFfinder. Gray bars indicate the position of cDNA probes (**Figure 1A**) and RT-PCR amplifications (**Figure 3A** and **Supplementary Figure 3**). **(C)** Comparison of 5'- and 3'-terminal nucleotide sequences among the five dsRNA segments. 5'- or 3'-terminal sequences were separately subjected to multiple sequence alignment. For analyses of the 5'-terminal, full sequences of each segment were aligned, and the 5'-terminal part is shown. For analyses of 3'-terminal, sequences of 3'-untranslated regions of each segment were aligned. The results were visualized in MEGA X.

specific genomic segments may spontaneously occur among polymycoviruses.

Vertical Transmission of PjPmV1 to Conidia and Effects of PjPmV1 Infection on Host Fungal Growth

To analyze vertical transmission of PjPmV1 to conidia, we screened conidial sub-isolates of the original fungal strain A58 of *P. janthinellum*. We initially checked the presence or absence of PjPmV1 in 46 conidial sub-isolates based on the detection of the RdRP-encoding segment (PjPmV1-dsRNA1) by mycelial direct RT-PCR (data not shown). As a result, we obtained eight PjPmV1-free sub-isolates [PjPmV1(-), designated as A58-cf*n*] and remining PjPmV1-transmitted sub-isolates [PjPmV1(+), designated as A58-cv*n*]. No dsRNA bands were detectable in the eight PjPmV1(-) sub-isolates A58-cf1 to A58-cf8 (**Figure 3A**, top left panel). The RT-PCR detection of PjPmV1-dsRNA1 using total RNA preparations further confirmed that PjPmV1 was eliminated from all the PjPmV1(-) sub-isolates (**Figure 3A**, middle left panel). By contrast, all the PjPmV1 dsRNA segments were transmitted to the eight PjPmV1(+) sub-isolates A58-cv1 to

TABLE 2 | Summary of BLAST search with the PjPmV1 genomic segments.

Query	Hit[a]	Domain or motif (BLASTP search)	Top hit			
			Description	Query cover (%)	Identity (%)	*E*-value	Accession
dsRNA1	Yes	RNA_dep_RNAP (cd01699)	RNA-dependent RNA polymerase [Penicillium digitatum polymycoviruses 1]	94	75.30	0.0	YP_009551548.1
dsRNA2	Yes	None	hypothetical protein [Penicillium digitatum polymycoviruses 1]	91	78.42	0.0	YP_009551551.1
dsRNA3	Yes	AdoMet_MTases (cd02440)	methyltransferase [Penicillium digitatum polymycoviruses 1]	90	75.65	0.0	YP_009551549.1
dsRNA4	No	None	–	–	–	–	–
dsRNA5	Yes	None	hypothetical protein [Penicillium digitatum polymycoviruses 1]	62	82.76	1e−140	YP_009551550.1

[a]*Presence or absence of hits by BLASTX search of the database "nr, Non-redundant protein sequences".*

A58-cv8, which were randomly selected from the 38 PjPmV1(+) sub-isolates (**Figure 3A** and **Supplementary Figure 3**). In several PjPmV1(+) conidial sub-isolates and the original strain A58, defective or satellite-like dsRNAs of various sizes occasionally appeared (indicated by an asterisk in **Figure 3A**). The presence of these defective species appeared to be associated with the ratio among PjPmV1 dsRNA segments, typically resulting in the decrease of relative dsRNA5 accumulation and the increase of dsRNA4 accumulation (**Figure 3B**).

We compared fungal growth between PjPmV1(-) and PjPmV1(+) sub-isolates on PDA media under laboratory conditions. As a result, no obvious growth change was observed depending on the presence or absence of PjPmV1 (**Figure 3B** and **Supplementary Figure 4**). Pigmentation accompanied with conidiation seemed different in some sub-cultures, but it was not correlated with the presence or absence of PjPmV1 (**Supplementary Figures 4A,B**). Average colony area tended to be slightly higher in PjPmV1(-) sub-isolates than in PjPmV1(+) sub-isolates, but the difference was neither statistically significant nor reproducible (**Supplementary Figures 4C,D**).

CsCl and Sucrose Gradient Centrifugation of a Particle-Like Form of PjPmV1

We have previously revealed that PjPmV1 dsRNA in mycelial homogenates is resistant to RNase A treatment (Sato et al., 2020), suggesting a protective form of the viral genomic dsRNA. Thus, we tried to analyze the physical nature of the protected dsRNA, assumed to be a potential virus particle-like form (VPL) (a capsidless RNP or filamentous particle). Our previous results suggest that this form can be extracted by an organic solvent (CCl_4) and precipitated by ultracentrifugation (Sato et al., 2020). Thus, the VPL was first extracted with CCl_4 and concentrated by ultracentrifugation. In parallel, we subjected FoCV1, an alphachrysovirus that makes rigid spherical capsids enclosing genomic dsRNA. The crude virus fractions of each virus were subjected to CsCl or sucrose density gradient centrifugation for 2 h (**Figure 4**). As a result of CsCl gradient centrifugation, PjPmV1 dsRNA was detected in much broader fractions than FoCV1-dsRNA (**Figures 4A–C**). That is, PjPmV1 dsRNA was detected in the fractions #4-#8 (1.15−1.35 g/cm^3, and slightly in the fraction #3), while FoCV1 dsRNA was mainly detected in the fraction #7 (1.30 g/cm^3, and slightly in the fractions #3 and #8) (**Figures 4A–C**). Interestingly, band intensity of PjPmV1 dsRNA3 peaked in the fraction #7, while intensity of the other segments peaked in the fraction #6 (**Figures 4B,C**). The broader fractionation of PjPmV1 was also observed by sucrose density gradient centrifugation (**Figures 4D,E**). In sucrose density gradient centrifugation, PjPmV1 dsRNA was detected in the fractions #5-#12 (1.08–1.20 g/cm^3, and slightly in the fraction #3 and #4), while FoCV1 dsRNA was mainly detected in the fractions #8-#10 (1.14–1.18 g/cm^3, and slightly in the other fractions) (**Figures 4D,E**). These results imply that potential PjPmV1 particle-like forms have uneven forms with various buoyant densities and sedimentation velocities.

To confirm that the above gradient centrifugation profiles were not caused by CCl_4, we subsequently used crude VPLs obtained without CCl_4. In gradient centrifugation, PjPmV1-dsRNA was also detected in the broad fractions (1.13–1.33 g/cm^3 in the CsCl gradient and 1.09–1.23 g/cm^3 in the sucrose gradient) (**Supplementary Figures 5A-D**). Thus, uneven PjPmV1 forms seemed to naturally occur in infected cells rather than being generated by CCl_4.

Components of a Particle-Like Form of PjPmV1

To examine components of the potential PjPmV1 particle-like forms, we concentrated the fractions containing PjPmV1 dsRNA (fractions #3-#8 in **Figure 4B**) by further ultracentrifugation. The resuspended fraction, called "pure VPL," retained all the dsRNA segments of PjPmV1 (**Figure 5A**). Detection of total proteins by SDS−PAGE revealed that the pure VPL from A58, but not from A58-cf1, contained a specific major band between 25 and 37 kDa, comparable to the expected molecular size of PjPmV1-PASrp (27.7 kDa) (**Figure 5B**). Immunological detection of PjPmV1 PASrp with polyclonal antibodies further confirmed that the major specific band corresponded to PASrp (**Figure 5C**). In contrast to A58, no signals were immunologically detected in mycelial proteins and pure VPL fractions from PjPmV1-free A58-cf1 (**Figure 5C**). In immunoprecipitation, PjPmV1-dsRNA was specifically co-purified with PjPmV1 PASrp antibody (**Figure 5D**). These results suggest that like other

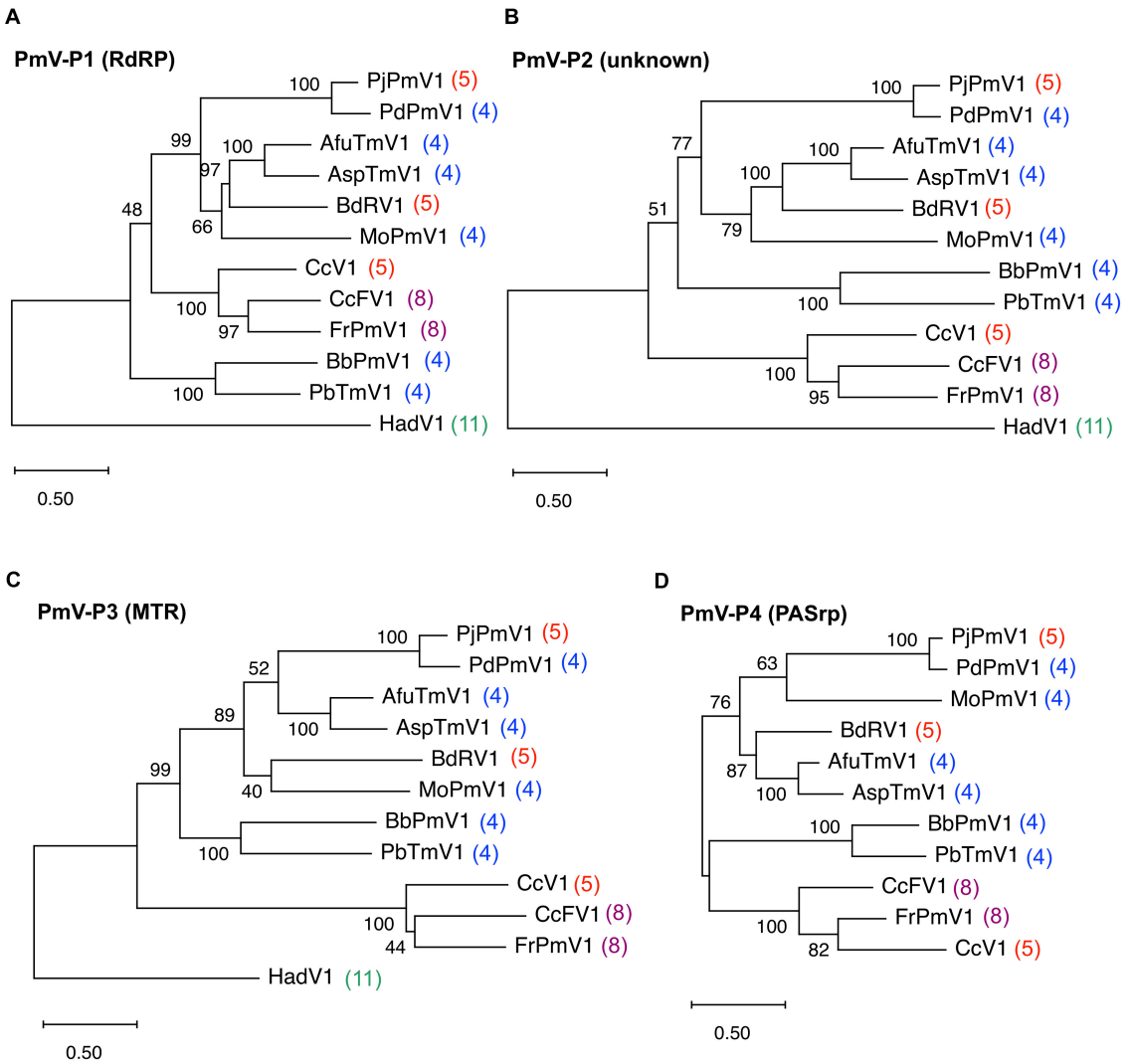

FIGURE 2 | Maximum likelihood (ML) phylogenetic trees of PjPmV1 and other polymycoviruses. Trees were constructed based on amino acid sequence alignment of polymycovirus (PmV)-P1 **(A)**, -P2 **(B)**, -P3 **(C)**, or -P4 **(D)**. Analysis involved the members of 10 species in the family *Polymycoviridae* and one hadakavirus (an unassigned ssRNA virus) as an outgroup. For analysis of polymycovirus P4, no outgroup was employed. Abbreviations of virus names and accession numbers for each protein are listed in **Table 1**. Numbers behind the virus names indicate genomic segment numbers of each virus. The trees were constructed via the ML method with best fit models, namely LG + G + I + F for panels **(A–C)** and WAG + G + I for panel **(D)** in MEGA X. Scale bar and branch length indicate numbers of amino acid substitutions per site. Values next to the branches indicate a bootstrap probability in 500 iterations.

previously characterized polymycoviruses, PjPmV1 dsRNA was also associated with PASrp, which was the major component of the potential particle-like forms. However, we failed to detect any PjPmV1 particles with filamentous or icosahedral structure in any VPL preparations under TEM observation (data not shown), suggesting that PASrp-associated PjPmV1 dsRNA forms a capsidless RNP structure, as previously proposed.

We tried to transfect PjPmV1 using its pure VPL preparations, but this was unsuccessful. For the transfection, we used pure VPLs obtained by two ways: one extracted with CCl_4 and separated by a CsCl gradient (**Figures 4A–C, 5A–C**) and the other extracted without CCl_4 and separated by sucrose gradient centrifugation (**Supplementary Figures 5C–E**). The latter preparation was obtained by the mildest class of purification way. Approximately 100 colonies from each transfection tested negative. The attempts to transfect with purified dsRNA of PjPmV1 were also unsuccessful.

Non-specific Interactions of PjPmV1-PASrp With Nucleic Acids

While co-purification of polymyco-PASrps with their genomic dsRNA has previously been demonstrated, the binding properties of PASrps-nucleic acids have not been investigated. Thus, we examined whether PjPmV1-PASrp can interact with other nucleic acids besides its dsRNA genome by EMSA (an assay

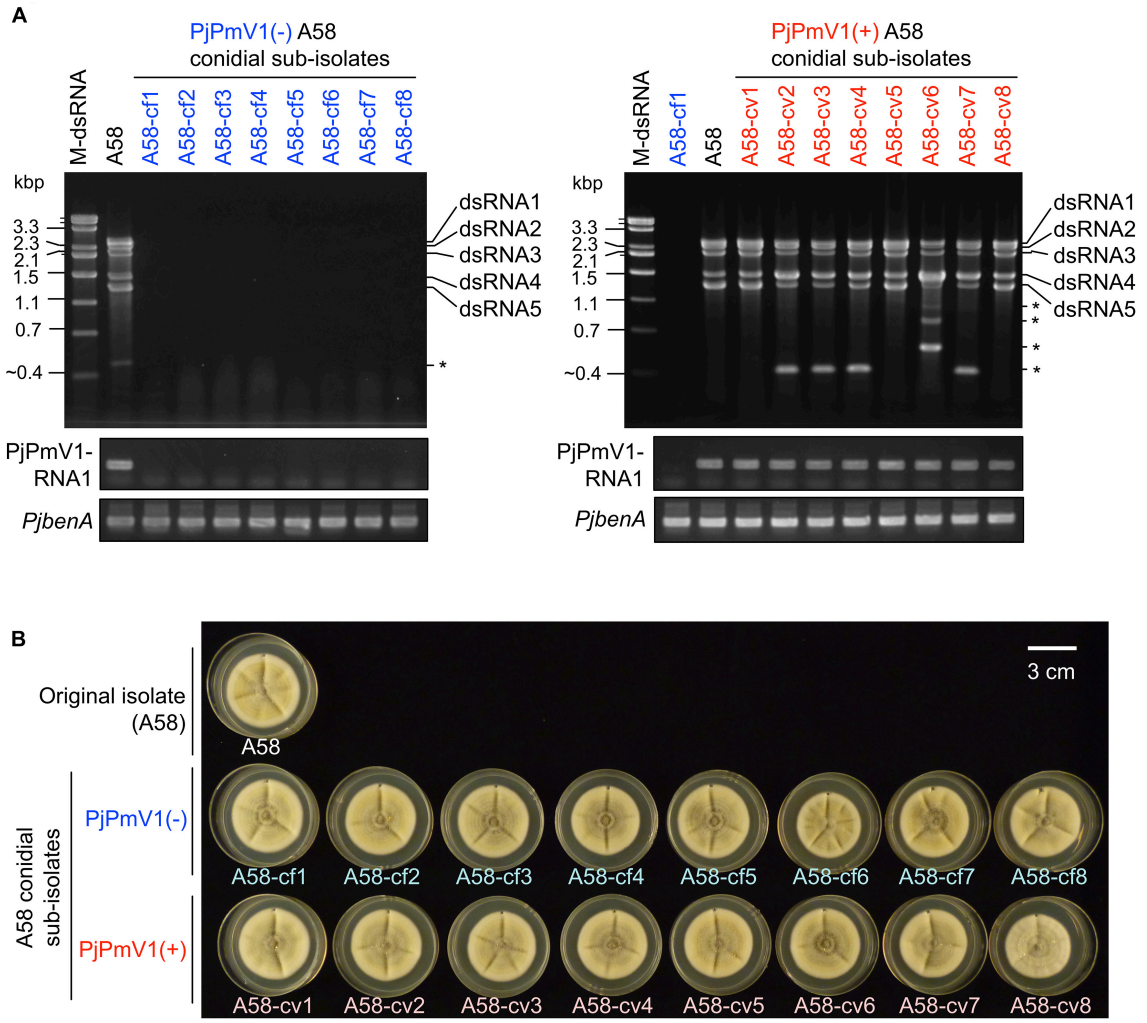

FIGURE 3 | Vertical transmission of PjPmV1 to conidia. Eight independent sub-isolates were randomly selected from each PjPmV1-free [PjPmV1(–)] or PjPmV1-transmitted [PjPmV1(+)] population in conidial sub-isolates of *P. janthinellum* A58. **(A)** Detection of PjPmV1-derived RNAs in the eight PjPmV1(–) or PjPmV1(+) sub-isolates (left or right panels, respectively). The top panels show electrophoretic profiles of dsRNA-enriched fractions, while the middle and lower panels show RT-PCR products. Asterisks (*) indicate the position of putative defective or satellite-like dsRNAs. "M-dsRNA" indicates the molecular size of mycoreoviral dsRNAs. By RT-PCR, messenger RNAs of the RdRP-encoding dsRNA1 segment of PjPmV1 (PjPmV1-RNA1) were detected. Host β-tubulin (*benA*) gene was detected as a control for RT-PCR reaction. **(B)** Picture of fungal colonies (7-day-old) of *P. janthinellum* A58 sub-isolates cultured on PDA plates.

with gel electrophoretic mobility shift). We used various amounts (0.01–1 μg) of the recombinant GST-PjPmV1-PASrps including heat-denatured (boiled) ones and 4 μg of free-GST as a control (**Figure 6A**). The GST-PjPmV1-PASrp was more insoluble and yielded lower amounts than GST in *E. coli* (**Figure 6A**). These recombinant proteins were incubated with various dsRNA (viral dsRNA from PjPmV1 or FoCV1, **Figure 6B**), ssRNA (*in vitro* transcript of PjPmV1-RNA3 or ribosomal RNA from *R. necatrix*, **Figure 6C**), and dsDNA (PCR amplicon of hygromycin resistance gene from a plasmid vector or genomic DNA from *C. parasitica*, **Figure 6D**). The electrophoretic mobility of all nucleic acids became retarded by pre-incubation with GST-PjPmV1-PASrp in a dose-dependent manner (**Figures 6B–D**). Some of the dsRNA, but not ssRNA and dsDNA, incubated with native GST-PjPmV1-PASrp stayed in the wells on the gel (**Figure 6B**), suggesting stronger interaction of PASrp with dsRNA than with ssRNA or dsDNA. Simultaneously, no mobility shift was observed in samples pre-incubated with boiled GST-PjPmV1-PASrp or with excessive amounts of GST (**Figures 6B–D**).

Taken together, PjPmV1-PASrp of native conformation can interact with dsRNA, ssRNA, and dsDNA in a sequence-non-specific manner.

DISCUSSION

While polymycoviruses, a relatively newly established group, are classified as a dsRNA virus, they represent an evolutionary link between ssRNA and dsRNA viruses (Kanhayuwa et al., 2015;

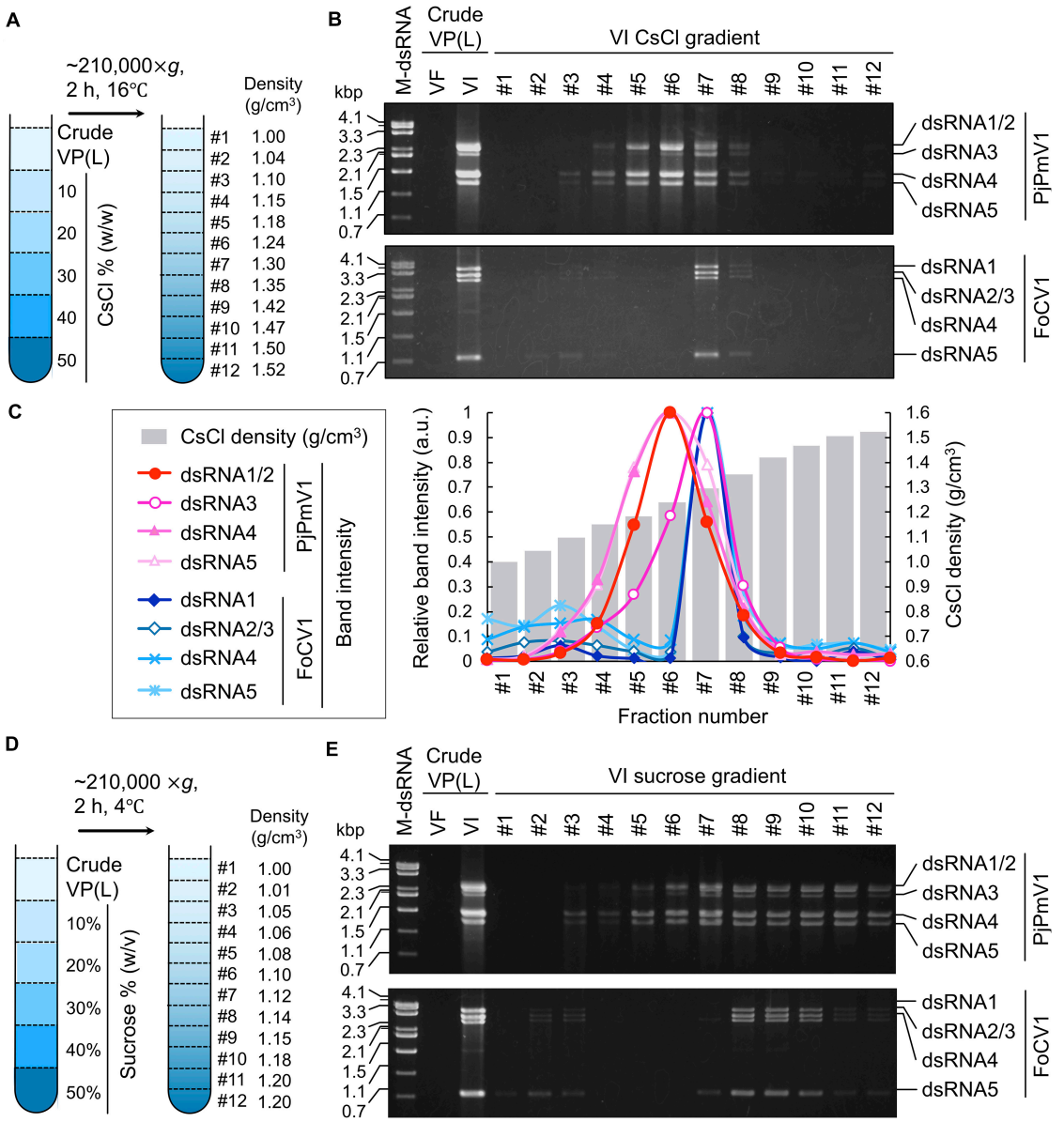

FIGURE 4 | CsCl or sucrose density gradient centrifugation of PjPmV1 particle-like forms. **(A)** Scheme of the CsCl density gradient centrifugation. **(B)** Electrophoretic profile of viral dsRNA in the separated fractions after CsCl gradient centrifugation. **(C)** Digitalization of relative band intensity of panel **(B)** by Image J (https://imagej.nih.gov/ij/). Relative band intensity of every dsRNA segment is shown as a relative value against the peak value of each segment. **(D)** Scheme of sucrose density gradient centrifugation. **(E)** Electrophoretic profile of viral dsRNA in the separated fractions after sucrose density gradient centrifugation. A Pakistani *Fusarium oxysporum* strain A60 infected by FoCV1 (an alphachrysovirus) was used as the reference of a typical encapsidated dsRNA virus. In panels **(B,E)**, "VF" and "VI" indicate virus-free or virus-infected fungal strains, respectively. In the analysis of PjPmV1 (top panel), "VI" or "VF" indicate *P. janthinellum* A58 or its conidial sub-isolate A58-cf1, respectively. In the analysis of FoCV1 (bottom panel), "VI" or "VF" indicate *F. oxysporum* A60 or its conidial sub-isolate A60-cf1, respectively. "M-dsRNA" indicates molecular size of dsRNA.

Sato et al., 2020). Here, we revealed the genome organization and detailed molecular characteristics of PjPmV1, which is the first polymycovirus isolated from *P. janthinellum* (**Table 1**). The PjPmV1 has a five-segmented dsRNA genome which consists of four conserved polymycoviral segments and one unique segment, showing no similarity to any known sequences (**Figure 1** and **Table 2**). The PjPmV1 is most closely related to PdPmV1, a four-segmented polymycovirus from *P. digitatum*, rather than other five-segmented polymycoviruses (**Figure 2**). The five dsRNA segments share highly conserved terminal sequences (**Figure 1C**) and were transmitted to conidia in an all-or-none fashion (**Figure 3A**), which supports that all the five dsRNA species (dsRNA1-dsRNA5) were derived from PjPmV1.

The PjPmV1 dsRNA was associated with PASrp *in vivo* (**Figure 5**), similar to other polymycoviruses (Kanhayuwa et al., 2015; Zhai et al., 2016; Kotta-Loizou and Coutts, 2017; Niu

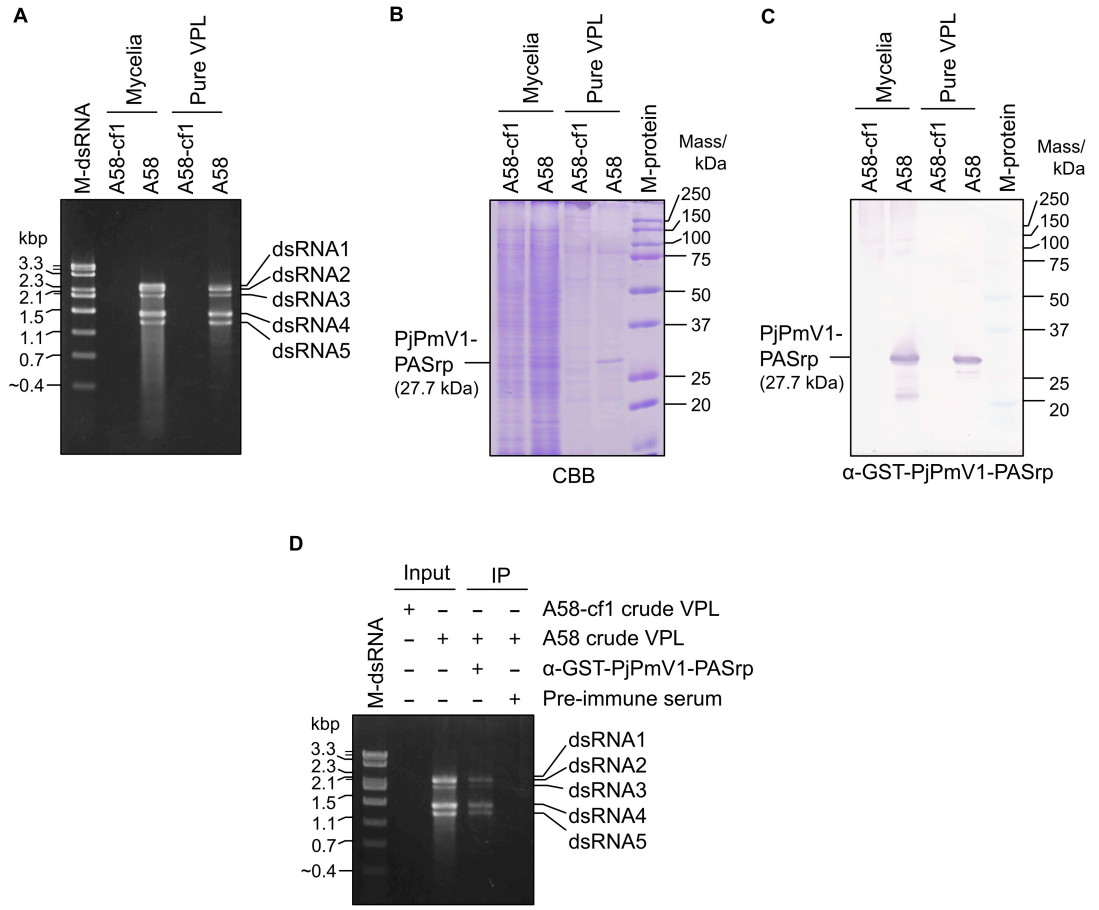

FIGURE 5 | Components of a potential particle-like form of PjPmV1. **(A)** DsRNA extracted from mycelia or pure VPL (virus particle-like form) fraction. "Pure VPL" means resuspended pellets obtained by ultracentrifugation of the CsCl gradient fractions #3–#8 in **Figures 4A–C**. "M-dsRNA" indicates the molecular size of mycoviral dsRNA segments. **(B)** Detection of total proteins from mycelia or pure VPL on SDS–PAGE gel stained with CBB. **(C)** Detection of PjPmV1-PASrp (P4) in the total protein fractions from mycelia or pure VPL preparation using polyclonal antibody (α-GST-PjPmV1-PASrp) by western blotting. In panels **(B,C)**, proteins were separated on 12% (w/v) polyacrylamide gel. "M-protein" indicates the molecular size of proteins. **(D)** Immunoprecipitation of PjPmV1 particle-like forms in the crude VPL fraction with α-GST-PjPmV1-PASrp antibody. Electrophoretic profiles of dsRNA in input and immunoprecipitated (IP) fractions were shown. Pre-immune serum was used as control for IP.

et al., 2018). The PASrp-associated PjPmV1 dsRNA showed a broader range of buoyant density and sedimentation velocity than icosahedral virions of a chryovirus (a multi-segmented dsRNA virus) (**Figure 4** and **Supplementary Figure 5**). The TEM observation of the purified PjPmV1 fractions revealed that the PASrp-associated dsRNA may not form filamentous or icosahedral structures (data not shown). Thus, PjPmV1-genomic dsRNA seems to exist as a non-rigid or unstable nucleoprotein form rather than as encapsidated form. This broader range of buoyant density and sedimentation velocity appears not to result from differently sized genomic segments, because of no great variation in segment ratios in different fractions (**Figures 4B,E**). The separate existence of the PASrp-associated dsRNA segments is suggested by the observation that the accumulation ratio of each dsRNA segment was unequal depending on sub-cultures. For example, dsRNA4 sometimes accumulated more than dsRNA5 (**Figure 1**) and *vice versa* (**Figure 3A**). These characteristics of the PASrp-associated forms might have contributed to the frequent gain or loss of specific genomic segments of polymycoviruses. The PjPmV1-PASrps interacted with various nucleic acids in a sequence-non-specific manner *in vitro* (**Figure 6**). The phosphoprotein of rhabdovirus, a member of the order *Mononegavirales*, has also non-specific nucleic acid-binding capability, and the rhabdovirus nucleoprotein serves as a chaperon to facilitate its specific binding with the viral genomic RNA (Masters and Banerjee, 1988; Mavrakis et al., 2006). There must be a mechanism by which PASrps is associated specifically with polymycovirus genomic dsRNA segments in cellular environments rich in diverse nucleic acids.

So far, we failed to transfect PjPmV1 in both PASrp-associated and purified dsRNA (PASrp-free) forms despite repeated attempts (data not shown), likely due to technical difficulty. Jia et al. reported that CcFV1 was also not infectious as a PASrp-associated form (filamentous particles), although it was infectious as purified PASrp-free dsRNA at low efficiency

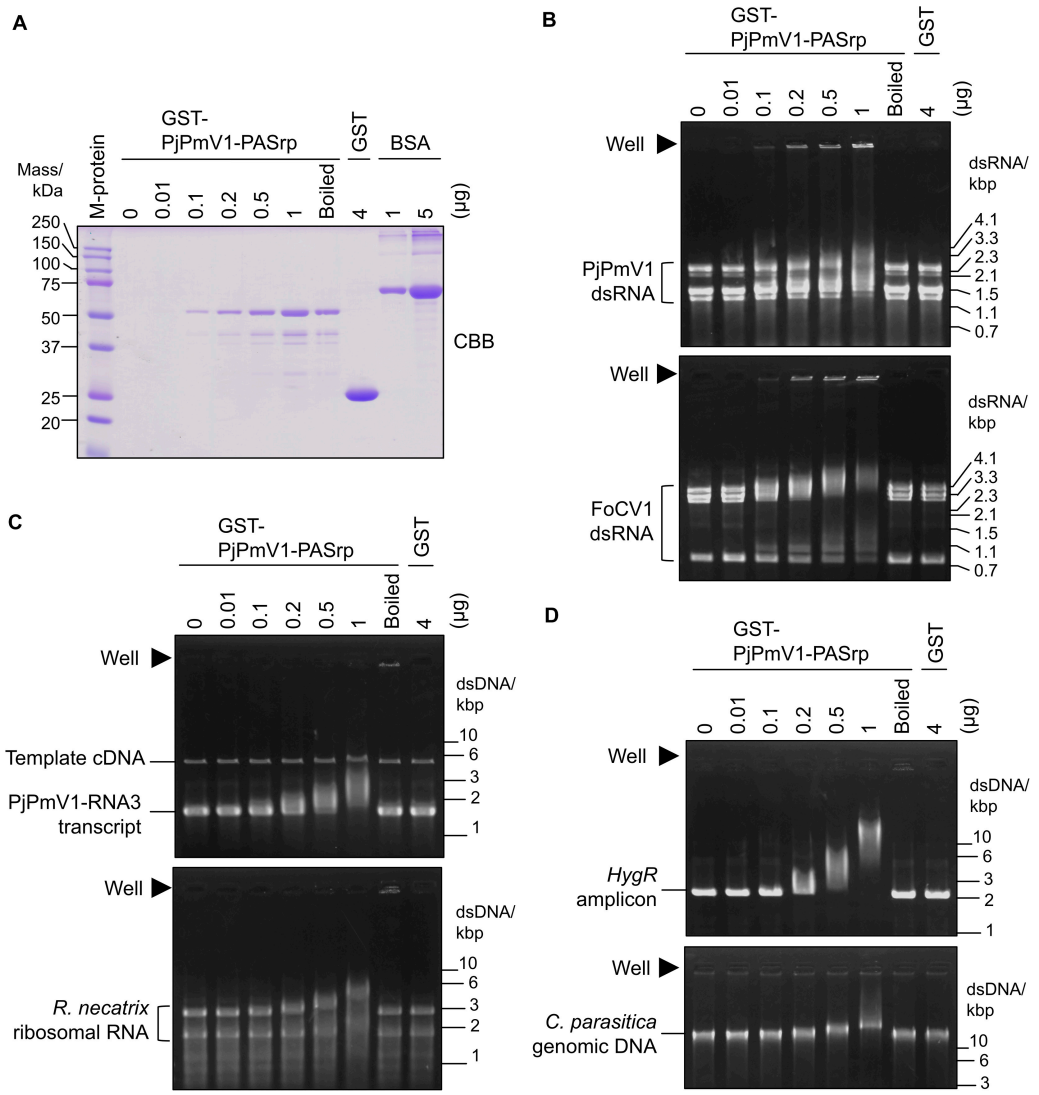

FIGURE 6 | Nucleic acid interactions of PjPmV1-PASrp. Electrophoretic mobility shift assay (EMSA) of PjPmV1-PASrp was conducted with various nucleic acids. Various amounts of GST-PjPmV1-PASrp [0.01–1 μg (0.19–19 pmol) per lane] and a constant amount of GST [4 μg (0.15 nmol) per lane] were used. "Boiled" indicates heat-denatured GST-PjPmV1-PASrp (1 μg/μL of the protein was boiled and 1 μL per lane was used for each experiment). **(A)** CBB staining of purified recombinant proteins (GST-PjPmV1-PASrp and free-GST) and bovine serum albumin (BSA) in SDS–PAGE. BSA was used to estimate the amount of recombinant proteins. Proteins were separated on 12% (w/v) polyacrylamide gel. "M-protein" indicates size marker proteins with their respective molecular weight (kDa). **(B)** Interactions of PASrp with viral dsRNAs. PjPmV1 dsRNA from *P. janthinellum* A58 [upper panel, 1 μg (∼0.16 pmol) per lane], and FoCV1 dsRNA from *F. oxysporum* A60 [lower panel, 1 μg (∼0.12 pmol) per lane] were used. Here approximate total moles were calculated on the assumption that each dsRNA segment was accumulated at equal moles. **(C)** Interaction of PASrp with viral or non-viral ssRNAs. PjPmV1-RNA3 *in vitro* transcripts with its template cDNA [upper panel, 1 μg (1.5 pmol) per lane] and the total RNA extracted from *Rosellinia necatrix* (lower panel, 1 μg per lane) were used. **(D)** Interaction of PASrp with dsDNA. PCR amplicon of hygromycin resistance gene [*HygR* amplicon, upper panel, 0.5 μg (0.38 pmol) per lane] and genomic DNA extracted from *Cryphonectria parasitica* [lower panel, 0.5 μg (0.018 fmol) per lane] were used. In panel **(B)**, the size marker of dsRNA (from mycoreovirus 1/S10ss) was loaded in a lane of the same gels (not shown). In panels **(C,D)**, the size marker of dsDNA [GeneRuler 1 kb DNA ladder (Thermo Fischer Scientific, Inc.)] was loaded in a lane of the same gels (not shown). In panels **(B–D)**, filled triangles indicate position of wells.

(approximately 2%) (Jia et al., 2017). Niu et al. also suggested that purified PASrp-free dsRNA of PdPmV1 was infectious at low efficiency (approximately 2–3%) (Niu et al., 2018), although they did not describe the transfection efficiency of the PASrp-associated form. Thus, the role of the PASrp-associated form of polymycoviral dsRNA in infection remains unclear. We showed, however, that PjPmV1 dsRNA associated with PASrp was tolerant to a ribonuclease (Sato et al., 2020), and its PASrp associated form was stable under organic solvent (CCl_4) treatment (**Figures 4**, **5**). Thus, an assumed role of PASrp is to protect the genomic RNA, as in the case of viral capsids.

According to the proposal for the genus *Polymycovirus* in the ICTV, species differentiation should be based on host fungus, identity of RdRP (≤70% in amino acid sequence),

size and number of dsRNA segments, and presence of true capsid. The amino acid sequence of RdRP of PjPmV1 was 75% identical to that of PdPmV1 (**Table 2**), slightly higher than the species criteria. The genomic segments of both viruses share an identical 19-bp nucleotide sequence at 5'-terminal (**Supplementary Figure 2B**). On the other hand, both viruses have apparently different nucleotide sequences at the 3'-terminal (**Supplementary Figure 2C**). Furthermore, PjPmV1 has a five-segmented genome (**Figure 1B**), while PdPmV1 has only a four-segmented genome. The PdPmV1 was alternatively co-infected with a narna-like virus of 1702 nt (Niu et al., 2018), a similar size to the PjPmV1-specific segment (PjPmV1-dsRNA4, 1450-bp). Typical virus particles were neither observed for PdPmV1 (Niu et al., 2018) nor for PjPmV1 (data not shown); PjPmV1 and PdPmV1 were commonly isolated from fungi of same genus, *Penicillium*, but these hosts belong to two different species, *P. janthinellum* and *P. digitatum*, respectively. Taken together, PjPmV1 can be regarded as a strain distinct from PdPmV1, both of which belong to the same species, *Penicillium digitatum polymycovirus 1*.

Host phenotypic alterations are noted for a few polymycoviruses. For example, PdPmV1 along with a co-infecting narna-like virus increase fungicide susceptibility of *P. digitatum* and decreases virulence of the host to citrus fruits (Niu et al., 2018). However, it remains to be determined whether PdPmV1 or the narna-like virus is the major contributor to the phenotypic change. AfuTmV1 and CcFV1 were shown to confer mild hypovirulence in their fungal hosts (Kanhayuwa et al., 2015; Jia et al., 2017). Another previous study showed BdRV1 to induce hypovirulence in its phytopathogenic host *Botryosphaeria dothidea* (Zhai et al., 2016). In our case, PjPmV1 had no obvious effect on host growth under normal conditions, based on the macroscopic observation of conidial sub-isolates (**Figure 3C** and **Supplementary Figure 4**). However, we could not efficiently investigate the effects of PjPmV1 on the host because we failed to re-inoculate PjPmV1. In addition to the transfection failure, we could not inoculate PjPmV1 via hyphal anastomosis (data not shown). Further studies are therefore needed to identify infectious entities and inoculation ways of PjPmV1.

DATA AVAILABILITY STATEMENT

The datasets presented in this study can be found in online repositories. The names of the repository/repositories and accession number(s) can be found in the article/**Supplementary Material**.

AUTHOR CONTRIBUTIONS

NS and YS designed the experiments and wrote the manuscript. YS, AJ, and HK performed the experimental work. All authors analyzed the data and have given approval to the final version of the manuscript.

FUNDING

This work was supported in part by Grants-in-Aid for JSPS (Japan Society for the Promotion of Science) Fellows (19J00261 to YS), and for Scientific Research (A) (17H01463 to NS) and on Innovative Areas from the Japanese Ministry of Education, Culture, Sports, Science, and Technology (MEXT) (16H06436, 16H06429, and 16K21723 to NS and HK). YS was a JSPS fellow. The funder, Yomogi Inc., was not involved in the study design, collection, analysis, and interpretation of data, the writing of this article or the decision to submit it for publication.

ACKNOWLEDGMENTS

The authors are grateful to Dr. Donald L. Nuss (IBBR, University of Maryland) for his generous gift of fungal strains.

SUPPLEMENTARY MATERIAL

The Supplementary Material for this article can be found online at: https://www.frontiersin.org/articles/10.3389/fmicb.2020.592789/full#supplementary-material

REFERENCES

Chiba, S., Lin, Y. H., Kondo, H., Kanematsu, S., and Suzuki, N. (2013). Effects of defective-interfering RNA on symptom induction by, and replication of a novel partitivirus from a phytopathogenic fungus *Rosellinia necatrix*. *J. Virol.* 87, 2330–2341. doi: 10.1128/JVI.02835-2812

Churchill, A. C. L., Ciuffetti, L. M., Hansen, D. R., Vanetten, H. D., and Van Alfen, N. K. (1990). Transformation of the fungal pathogen *Cryphonectria parasitica* with a variety of heterologous plasmids. *Curr. Genet* 17, 25–31. doi: 10.1007/BF00313245

Crouch, J. A., Dawe, A., Aerts, A., Barry, K., Churchill, A. C. L., Grimwood, J., et al. (2020). Genome sequence of the chestnut blight fungus *Cryphonectria parasitica* EP155: a fundamental resource for an archetypical invasive plant pathogen. *Phytopathology* 110, 1180–1188.

Eusebio-Cope, A., and Suzuki, N. (2015). Mycoreovirus genome rearrangements associated with RNA silencing deficiency. *Nucleic Acids Res.* 43, 3802–3813. doi: 10.1093/nar/gkv239

Ghabrial, S. A., Caston, J. R., Jiang, D., Nibert, M. L., and Suzuki, N. (2015). 50-plus years of fungal viruses. *Virology* 479-480, 356–368. doi: 10.1016/j.virol.2015.02.034

Glass, N. L., and Donaldson, G. C. (1995). Development of primer sets designed for use with the PCR to amplify conserved genes from filamentous ascomycetes. *Appl. Environ. Microbiol.* 61, 1323–1330. doi: 10.1128/Aem.61.4.1323-1330.1995

Guo, L. H., Sun, L., Chiba, S., Araki, H., and Suzuki, N. (2009). Coupled termination/reinitiation for translation of the downstream open reading frame B of the prototypic hypovirus CHV1-EP713. *Nucleic Acids Res.* 37, 3645–3659. doi: 10.1093/nar/gkp224

Hillman, B. I., and Cai, G. (2013). The family *Narnaviridae*: simplest of RNA viruses. *Adv. Virus Res.* 86, 149–176. doi: 10.1016/B978-0-12-394315-6.00006-4

Hillman, B. I., Supyani, S., Kondo, H., and Suzuki, N. (2004). A reovirus of the fungus *Cryphonectria parasitica* that is infectious as particles and related to the *Coltivirus* genus of animal pathogens. *J. Virol.* 78, 892–898. doi: 10.1128/jvi.78.2.892-898.2004

Hisano, S., Zhang, R., Faruk, M. I., Kondo, H., and Suzuki, N. (2018). A neo-virus lifestyle exhibited by a (+)ssRNA virus hosted in an unrelated dsRNA virus: taxonomic and evolutionary considerations. *Virus Res.* 244, 75–83. doi: 10.1016/j.virusres.2017.11.006

Jacob-Wilk, D., Turina, M., and Van Alfen, N. K. (2006). Mycovirus cryphonectria hypovirus 1 elements cofractionate with trans-Golgi network membranes of the fungal host *Cryphonectria parasitica*. *J. Virol.* 80, 6588–6596. doi: 10.1128/JVI.02519-2515

Jamal, A., Sato, Y., Shahi, S., Shamsi, W., Kondo, H., and Suzuki, N. (2019). Novel victorivirus from a Pakistani isolate of *Alternaria alternata* lacking a yypical translational stop/restart sequence signature. *Viruses* 11:577. doi: 10.3390/v11060577

Jia, H., Dong, K., Zhou, L., Wang, G., Hong, N., Jiang, D., et al. (2017). A dsRNA virus with filamentous viral particles. *Nat. Commun.* 8:168. doi: 10.1038/s41467-017-00237-239

Kanhayuwa, L., Kotta-Loizou, I., Ozkan, S., Gunning, A. P., and Coutts, R. H. (2015). A novel mycovirus from *Aspergillus fumigatus* contains four unique dsRNAs as its genome and is infectious as dsRNA. *Proc. Natl. Acad. Sci. U.S.A.* 112, 9100–9105. doi: 10.1073/pnas.1419225112

Katoh, K., Rozewicki, J., and Yamada, K. D. (2019). MAFFT online service: multiple sequence alignment, interactive sequence choice and visualization. *Brief Bioinform.* 20, 1160–1166. doi: 10.1093/bib/bbx108

Kotta-Loizou, I., and Coutts, R. H. A. (2017). Studies on the virome of the entomopathogenic fungus *Beauveria bassiana* reveal novel dsRNA elements and mild hypervirulence. *PLoS Pathogens* 13:e1006183. doi: 10.1371/journal.ppat.1006183

Kozlakidis, Z., Hacker, C. V., Bradley, D., Jamal, A., Phoon, X., Webber, J., et al. (2009). Molecular characterisation of two novel double-stranded RNA elements from *Phlebiopsis gigantea*. *Virus Genes* 39, 132–136. doi: 10.1007/s11262-009-0364-z

Kumar, S., Stecher, G., Li, M., Knyaz, C., and Tamura, K. (2018). MEGA X: molecular evolutionary genetics analysis across computing platforms. *Mol .Biol. Evol.* 35, 1547–1549. doi: 10.1093/molbev/msy096

Kwon, S. J., Lim, W. S., Park, S. H., Park, M. R., and Kim, K. H. (2007). Molecular characterization of a dsRNA mycovirus, Fusarium graminearum virus-DK21, which is phylogenetically related to hypoviruses but has a genome organization and gene expression strategy resembling those of plant potex-like viruses. *Mol. Cells* 23, 304–315.

Lakshman, D. K., Jian, J. H., and Tavantzis, S. M. (1998). A double-stranded RNA element from a hypovirulent strain of *Rhizoctonia solani* occurs in DNA form and is genetically related to the pentafunctional AROM protein of the shikimate pathway. *Proc. Natl. Acad. Sci. U.S.A.* 95, 6425–6429. doi: 10.1073/pnas.95.11.6425

Lin, Y. H., Hisano, S., Yaegashi, H., Kanematsu, S., and Suzuki, N. (2013). A second quadrivirus strain from the phytopathogenic filamentous fungus *Rosellinia necatrix*. *Arch. Virol.* 158, 1093–1098. doi: 10.1007/s00705-012-1580-1588

Lu, S., Wang, J., Chitsaz, F., Derbyshire, M. K., Geer, R. C., Gonzales, N. R., et al. (2020). CDD/SPARCLE: the conserved domain database in 2020. *Nucleic Acids Res.* 48, D265–D268. doi: 10.1093/nar/gkz991

Magae, Y. (2012). Molecular characterization of a novel mycovirus in the cultivated mushroom. *Lentinula edodes*. *Virol. J.* 9, 60. doi: 10.1186/1743-422X-9-60

Mahillon, M., Decroes, A., Lienard, C., Bragard, C., and Legreve, A. (2019). Full genome sequence of a new polymycovirus infecting *Fusarium redolens*. *Arch. Virol.* 164, 2215–2219. doi: 10.1007/s00705-019-04301-1

Masters, P. S., and Banerjee, A. K. (1988). Complex formation with vesicular stomatitis virus phosphoprotein NS prevents binding of nucleocapsid protein N to nonspecific RNA. *J. Virol.* 62, 2658–2664. doi: 10.1128/JVI.62.8.2658-2664.1988

Mavrakis, M., Mehouas, S., Real, E., Iseni, F., Blondel, D., Tordo, N., et al. (2006). Rabies virus chaperone: identification of the phosphoprotein peptide that keeps nucleoprotein soluble and free from non-specific RNA. *Virology* 349, 422–429. doi: 10.1016/j.virol.2006.01.030

Nerva, L., Forgia, M., Ciuffo, M., Chitarra, W., Chiapello, M., Vallino, M., et al. (2019). The mycovirome of a fungal collection from the sea cucumber Holothuria polii. *Virus Res.* 273:197737. doi: 10.1016/j.virusres.2019.197737

Niu, Y., Yuan, Y., Mao, J., Yang, Z., Cao, Q., Zhang, T., et al. (2018). Characterization of two novel mycoviruses from *Penicillium digitatum* and the related fungicide resistance analysis. *Sci. Rep.* 8:5513. doi: 10.1038/s41598-018-23807-3

Nuss, D. L. (2005). Hypovirulence: mycoviruses at the fungal-plant interface. *Nat. Rev. Microbiol.* 3, 632–642. doi: 10.1038/nrmicro1206

Petrzik, K., Sarkisova, T., Stary, J., Koloniuk, I., Hrabakova, L., and Kubesova, O. (2016). Molecular characterization of a new monopartite dsRNA mycovirus from mycorrhizal *Thelephora terrestris* (Ehrh.) and its detection in soil oribatid mites (*Acari*: *Oribatida*). *Virology* 489, 12–19. doi: 10.1016/j.virol.2015.11.009

Sambrook, J., and Russell, D. W. (2001). *Molecular Cloning: A Laboratory Manual*, 3rd Edn. Cold Spring Harbor, N.Y: Cold Spring Harbor Laboratory.

Sasaki, A., Kanematsu, S., Onoue, M., Oikawa, Y., Nakamura, H., and Yoshida, K. (2007). Artificial infection of *Rosellinia necatrix* with purified viral particles of a member of the genus *Mycoreovirus* reveals its uneven distribution in single colonies. *Phytopathology* 97, 278–286. doi: 10.1094/PHYTO-97-3-0278

Sato, Y., Miyazaki, N., Kanematsu, S., Xie, J., Ghabrial, S. A., Hillman, B. I., et al. (2019). ICTV Virus Taxonomy Profile: *Megabirnaviridae*. *J. Gen. Virol.* 100, 1269–1270. doi: 10.1099/jgv.0.001297

Sato, Y., Shamsi, W., Jamal, A., Bhatti, M. F., Kondo, H., and Suzuki, N. (2020). Hadaka virus 1: a capsidless eleven-segmented positive-sense single-stranded RNA virus from a phytopathogenic fungus, *Fusarium oxysporum*. *mBio* 11:e00450-20. doi: 10.1128/mBio.00450-20

Shamsi, W., Sato, Y., Jamal, A., Shahi, S., Kondo, H., Suzuki, N., et al. (2019). Molecular and biological characterization of a novel botybirnavirus identified from a Pakistani isolate of *Alternaria alternata*. *Virus Res.* 263, 119–128. doi: 10.1016/j.virusres.2019.01.006

Shimizu, T., Kanematsu, S., and Yaegashi, H. (2018). Draft genome sequence and transcriptional analysis of *Rosellinia necatrix* infected with a virulent mycovirus. *Phytopathology* 108, 1206–1211. doi: 10.1094/PHYTO-11-17-0365-R

Solorzano, A., Rodriguez-Cousino, N., Esteban, R., and Fujimura, T. (2000). Persistent yeast single-stranded RNA viruses exist in vivo as genomic RNA center dot RNA polymerase complexes in 1 : 1 stoichiometry. *J. Biol. Chem.* 275, 26428–26435. doi: 10.1074/jbc.M002281200

Sun, L., and Suzuki, N. (2008). Intragenic rearrangements of a mycoreovirus induced by the multifunctional protein p29 encoded by the prototypic hypovirus CHV1-EP713. *RNA* 14, 2557–2571. doi: 10.1261/rna.1125408

Suzuki, N., Ghabrial, S. A., Kim, K. H., Pearson, M., Marzano, S. L., Yaegashi, H., et al. (2018). ICTV Virus Taxonomy Profile: *Hypoviridae*. *J. Gen. Virol.* 99, 615–616. doi: 10.1099/jgv.0.001055

Valverde, R. A., Khalifa, M. E., Okada, R., Fukuhara, T., Sabanadzovic, S., and Ictv Report, C. (2019). ICTV Virus Taxonomy Profile: *Endornaviridae*. *J. Gen. Virol.* 100, 1204–1205. doi: 10.1099/jgv.0.001277

White, J., Bruns, T. D., Lee, S., and Taylor, J. (1990). "Amplification and direct sequencing of fungal ribosomal RNA genes for phylogenetics," in *PCR Protocols: A Guide to Methods and Applications* M. A. Innis, D. H. Gelfand, J J. Sninsky, T J. White, (New York, NY: Academic Press)315–322.

Wolf, Y. I., Kazlauskas, D., Iranzo, J., Lucia-Sanz, A., Kuhn, J. H., Krupovic, M., et al. (2018). Origins and evolution of the global RNA virome. *mBio* 9:e02329-18. doi: 10.1128/mBio.02329-18

Zhai, L., Xiang, J., Zhang, M., Fu, M., Yang, Z., Hong, N., et al. (2016). Characterization of a novel double-stranded RNA mycovirus conferring hypovirulence from the phytopathogenic fungus *Botryosphaeria dothidea*. *Virology* 493, 75–85. doi: 10.1016/j.virol.2016.03.012

Zhang, R., Hisano, S., Tani, A., Kondo, H., Kanematsu, S., and Suzuki, N. (2016). A capsidless ssRNA virus hosted by an unrelated dsRNA virus. *Nat. Microbiol.* 1:15001.

Zhang, R., Liu, S., Chiba, S., Kondo, H., Kanematsu, S., and Suzuki, N. (2014). A novel single-stranded RNA virus isolated from a phytopathogenic filamentous fungus, *Rosellinia necatrix*, with similarity to hypo-like viruses. *Front. Microbiol.* 5:360. doi: 10.3389/fmicb.2014.00360

Conflict of Interest: The authors declare that the research was conducted in the absence of any commercial or financial relationships that could be construed as a potential conflict of interest.

frontiers in Microbiology

ORIGINAL RESEARCH
published: 21 October 2020
doi: 10.3389/fmicb.2020.561344

Diverged and Active Partitiviruses in Lichen

Syun-ichi Urayama[1,2,3], Nobutaka Doi[4], Fumie Kondo[5], Yuto Chiba[2], Yoshihiro Takaki[5], Miho Hirai[5], Yasutaka Minegishi[4], Daisuke Hagiwara[2,3] and Takuro Nunoura[1]*

[1] Research Center for Bioscience and Nanoscience (CeBN), Japan Agency for Marine-Earth Science and Technology (JAMSTEC), Yokosuka, Japan, [2] Laboratory of Fungal Interaction and Molecular Biology (Donated by IFO), Department of Life and Environmental Sciences, University of Tsukuba, Tsukuba, Japan, [3] Microbiology Research Center for Sustainability (MiCS), University of Tsukuba, Tsukuba, Japan, [4] Nippon Gene Co., Ltd., Toyama, Japan, [5] Super-cutting-edge Grand and Advanced Research (SUGAR) Program, JAMSTEC, Yokosuka, Japan

The lichen is a microbial consortium that mainly consists of fungi and either algae (Viridiplantae) or cyanobacteria. This structure also contains other bacteria, fungi, and viruses. However, RNA virus diversity associated with lichens is still unknown. Here, we analyzed RNA virus diversity in a lichen dominated by fungi and algae using dsRNA-seq technology and revealed that partitiviruses were dominant and active in the microbial consortium. The *Partitiviridae* sequences found in this study were classified into two genera, which have both plant- and fungi-infecting partitiviruses. This observation suggests that the lichen provides an opportunity for horizontal transfer of these partitiviruses among microbes that form the lichen consortium.

Keywords: RNA virus, lichen, dsRNA, partitivirus, viral metagenome

OPEN ACCESS

Edited by:
Kook-Hyung Kim,
Seoul National University,
South Korea

Reviewed by:
Martin Grube,
University of Graz, Austria
Matthew Nelsen,
Field Museum of Natural History,
United States

****Correspondence:***
Syun-ichi Urayama
urayama.shunichi.gn@u.tsukuba.ac.jp

Specialty section:
This article was submitted to Virology, a section of the journal Frontiers in Microbiology

Received: *12 May 2020*
Accepted: *24 September 2020*
Published: *21 October 2020*

Citation:
Urayama S, Doi N, Kondo F, Chiba Y, Takaki Y, Hirai M, Minegishi Y, Hagiwara D and Nunoura T (2020) Diverged and Active Partitiviruses in Lichen. Front. Microbiol. 11:561344. doi: 10.3389/fmicb.2020.561344

INTRODUCTION

The lichen is a symbiotic microbial consortium that is mainly composed of a fungus (mycobiont) and photosynthetic partner (photobiont), either green algae (Viridiplantae) or cyanobacteria, or both, that harbor chlorophyll. The phototrophic partner feeds organic compounds to the fungus. In contrast, the fungus protects minute photosynthetic cells from environmental stresses, such as drought and nutrient deficiencies, and provides a suitable environment for photosynthesis and gas exchange (White and Torres, 2009). In general, these organisms form delicate structures and stratification of the lichen thallus with other microorganisms including endophytic fungi, other algae, and bacteria. For example, a typical foliose lichen thallus reveals four zones of interlaced fungal filaments (Moore et al., 2020). The uppermost zone, called the cortex, is formed by densely interwoven hyphae forming an outer protective tissue layer. The algal cells occur in a zone beneath the cortex embedded in a dense hyphal tissue. The third zone, called the medulla, is formed by loosely interwoven fungal hyphae without algal cells. The lower surface of the thallus is called the lower cortex and may consist of densely packed fungal hyphae. It is noteworthy that an endosymbiotic interaction was recently reported; green algal cells can enter fungal cells under certain conditions (Du et al., 2019). Given that pathogenic and mutualistic biotrophic interactions between plants and fungi are common on Earth (Kohler et al., 2015), the plant– and green algae–fungal interaction has a long history (Remy et al., 1994; Honegger et al., 2013; Lutzoni et al., 2018; Nelsen et al., 2020).

RNA viruses associated with lichen have been reported. Partial sequences of Cytorhabdovirus (family *Rhabdoviridae*) and Apple mosaic virus (family *Bromoviridae*) were detected by RT-PCR from lichens (Petrzik et al., 2013). In addition, *Chrysothrix chrysovirus 1* (family *Chrysoviridae*) and *Lepraria chrysovirus 1* (family *Chrysoviridae*) were identified from *Chrysothrix chlorina* and *Lepraria incana* lichens, respectively, and the former was observed in accompanying endolichenic fungus in the lichen by *in situ* hybridization (Petrzik et al., 2019). Although these studies revealed the presence of RNA viruses in lichens, the RNA viral community in lichens is still unknown. In this study, we identified viruses related to the family *Partitiviridae*. *Partitiviridae* are bisegmented dsRNA viruses that infect plants, fungi, or protozoa. Five viral genera (*Alphapartitivirus*, *Betapartitivirus*, *Gammapartitivirus*, *Deltapartitivirus*, and *Cryspovirus*) have been established in this family. Among them, host of *Gammapartitivirus* and *Deltapartitivirus* are identified as fungi and plant, respectively, and some of the species in *Alphapartitivirus* and *Betapartitivirus* infect fungi or plant (Nibert et al., 2014).

The metagenomic approach is a powerful tool to understand RNA virus diversity (Shi et al., 2016, 2018). To date, several methods to construct (meta)genomic sequencing libraries from RNA viral genomes have been established and applied to environmental samples (Culley et al., 2006; Roossinck et al., 2010; Steward et al., 2013; Urayama et al., 2016, 2018b; Decker et al., 2019). Among them, fragmented and primer ligated dsRNA sequencing (FLDS) has remarkable advantages in construction of complete viral genomes (Urayama et al., 2018a; Fukasawa et al., 2020; Kadoya et al., 2020). In this study, we applied dsRNA-seq and ssRNA-seq techniques to elucidate RNA virus diversity associated with a lichen.

MATERIALS AND METHODS

Sample Collection

Lichen on sand mud in Toiya-machi, Toyama (36.7007°N and 137.2475°E) was sampled in February 2019 (**Figure 1**). Sample was stored at −80°C until further analysis. A voucher for this lichen was not preserved due to stored sample quality.

FIGURE 1 | The lichen community from which samples were taken in this study.

Extraction and Purification of dsRNA and ssRNA

The lichen sample was disrupted in liquid nitrogen in a mortar. For dsRNA extraction and purification, the ISOVIRUS (Nippon Gene, Tokyo, Japan) kit was used. In brief, total RNA was extracted in the extraction buffer, and dsRNA was purified with cellulose resin and eluted by nuclease-free water after DNase I treatment according to the manufacturer's protocol. To obtain total RNA, the TRIzol Plus RNA Purification Kit (Invitrogen, Carlsbad, CA, United States) was used according to the manufacturer's protocol. Total RNA was treated with DNase I (Invitrogen) and further purified using the RNA Clean and Concentrator-5 Kit (Zymo Research, Orange, CA, United States).

cDNA Synthesis and Sequencing Library Construction

In this study, we applied FLDS to obtain RNA viral sequences. dsRNA, which is a molecular marker of RNA virus infection, is used as a template for cDNA synthesis because cellular long dsRNA is a replicative intermediate of ssRNA virus as well as genome of dsRNA virus. Simultaneously, full-length cDNA is synthesized by applying template-switching activity of the reverse transcriptase with an oligonucleotide primer against adapter-ligated dsRNA fragments, which enabled us to obtain complete genome sequences of non-retro RNA viruses.

Sequencing libraries were constructed as described previously (Urayama et al., 2016, 2018b). dsRNA was converted to cDNA using the FLDS method. In brief, DNase I and S1 nuclease-treated dsRNA was fragmented and ligated to a DNA adapter. With an oligonucleotide primer against the adapter sequence, cDNA was synthesized by using the SMARTer RACE 5′/3′ Kit (Takara Bio, Kusatsu, Japan). ssRNA was applied to the SMARTer Universal Low Input RNA Kit (Takara Bio) for cDNA synthesis.

Illumina sequence libraries were constructed from the double-stranded cDNAs. Double-stranded cDNAs were fragmented using Covaris S220 (settings: run time 55 s, peak power 175.0 W, duty factor 5.0% and 200 cycles/burst), and fragmented cDNAs were applied to KAPA Hyper Prep Kit Illumina platforms (Kapa Biosystems, Woburn, MA, United States). The quality and quantity of the Illumina libraries were evaluated using the KAPA library quantification kit (Kapa Biosystems) and applied to the Illumina MiSeq platform (Illumina, San Diego, CA, United States) according to the manufacturer's protocol (600-cycle kit to perform 300-bp paired-end sequencing).

Data Processing

Raw sequencing reads for dsRNA-seq were processed as described previously (Urayama et al., 2018b). rRNA reads in trimmed reads were identified by SortMeRNA (Kopylova et al., 2012) and removed. Potential genome segments were extracted from contigs, and putative RNA virus genomes were reconstructed (Urayama et al., 2020). RNA viral genes in potential genome segments and contigs were identified based on sequence similarity to known RNA viral proteins in the NCBI non-redundant (nr) database using BLASTX (Camacho et al., 2009) with an *e*-value $\leq 1 \times 10^{-5}$. Sequences that matched a known RNA-dependent RNA polymerase (RdRp) gene by BLASTX with an *e*-value $\leq 1 \times 10^{-5}$ were collected from RNA virus contigs and segments. In addition, a conserved domain database (CDD) search was also used. Nucleotide sequences encoding the RdRp gene were clustered at 90% identity using VSEARCH (Rognes et al., 2016).

Raw sequencing reads from ssRNA-seq were processed as described previously (Urayama et al., 2018b). Small subunit (SSU) rRNA sequences were mapped using phyloFlash (Gruber-Vodicka et al., 2019) with the option-skip_spades and -id 98. For detailed identification of major organisms, we also used EMIRGE (Miller et al., 2011) and BLASTN (Camacho et al., 2009) programs.

Phylogenetic Analyses

Amino acid sequences of putative RdRp genes obtained in this study and their relatives in the NCBI nr database were aligned by using MUSCLE (Edgar, 2004) in MEGA6 (Tamura et al., 2013). To exclude ambiguous amino acid positions, the alignment was trimmed by trimAl (option: −gt 1) (Capella-Gutiérrez et al., 2009). Phylogenetic trees were constructed using RAxML (Stamatakis, 2014). The number of bootstrap replicates was 1000. The model of amino acid substitution was selected by Aminosan (Tanabe, 2011), as judged by the Akaike information criterion (Sugiura, 1978). MEGA6 was used to illustrate the resulting phylogeny.

Accession Numbers

Sequences obtained in this study are available in the GenBank database repository (accession nos. DDBJ: BLWB01000001–BLWB01000058 and LC533392–LC533410) and Short Read Archive database (accession no. DDBJ: DRA009807).

RESULTS

Diversity of Cellular rRNAs in Lichen

To reveal the composition of active microorganisms in the lichen sample, total ssRNA-seq reads were mapped on SSU rRNA sequences in the Silva database (SILVA SSU version 138) (Quast et al., 2012) using phyloFlash (Gruber-Vodicka et al., 2019), and their relative abundances were determined (**Figure 2**). The most abundant rRNA phylotype (43%) belonged to Lecanoromycetes (Fungi), the largest class of lichenized fungi (Miadlikowska et al., 2006), and the second abundant class was lichen-forming algae Trebouxiophyceae (Viridiplantae) (Muggia et al., 2018) that consisted of two phylotypes (17% total). These results were consistent with our morphological observation that the collected sample was a lichen. In addition to these two dominant classes, rRNA sequences from other fungi and moss were also detected (**Figure 2**). Classification of sequencing reads obtained by total RNA-seq is shown in **Table 1**.

Reconstruction of RNA Virus Genomes

Following the *de novo* assembly and reconstruction of the full-length genome segments, a total of 65 RdRp-encoding operational taxonomic units (OTUs) (>1.5 kb,

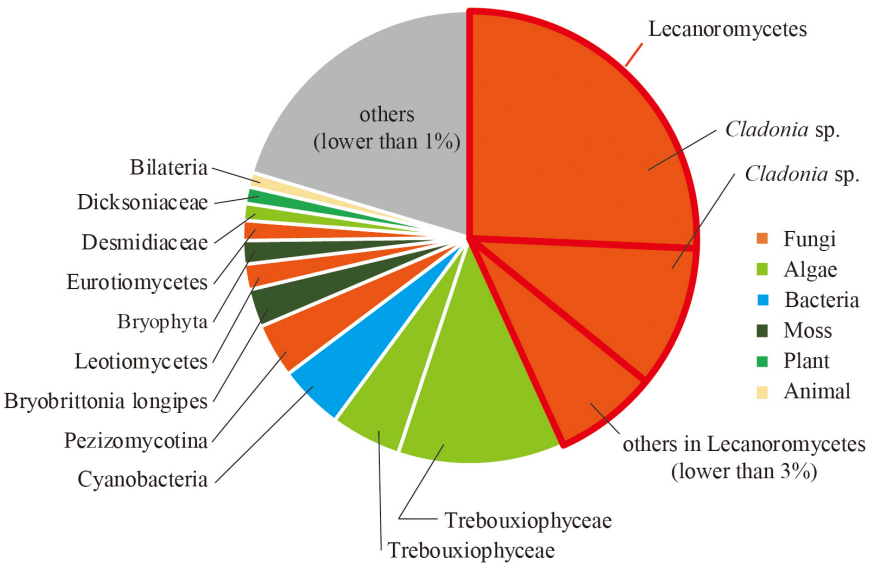

FIGURE 2 | Relative abundance of sequence reads mapped on SSU rRNA sequences classified by using phyloFlash.

TABLE 1 | Classification of sequencing reads obtained by FLDS and total RNA-seq.

	dsRNA		ssRNA	
	Number of reads	Reads (%)	Number of reads	Reads (%)
Trimmed	3,955,680	100.0	1,139,888	100.0
rRNA	158,014	4.0	1,069,362	93.8
Major RNA viruses	3,340,351	84.4	2,107	0.2
Others	457,315	11.6	68,419	6.0

<90% identity between these sequences) were identified from the dsRNA-seq library (**Supplementary Table 1** and described below) using BLASTX against the NCBI nr database and CDD search program. Notably, only one sequence encoding RdRp (>1.5 kb) was identified from the ssRNA-seq library, which was from Lichen partiti-like RNA virus 1 (LpaRV1) (described below). Taxonomic lineages of BLASTX top hit sequences (*e*-values ranging from 2×10^{-30} to 0) suggested that 17 of 65 OTUs were related to *Partitiviridae*. In addition, viruses related to seven dsRNA virus families (*Amalgaviridae*, *Botybirnaviridae, Chrysoviridae*, *Endornaviridae*, *Megabirnaviridae*, *Picobirnaviridae*, and *Totiviridae*), three ssRNA virus families (*Gammaflexviridae*, *Hypoviridae*, and *Narnaviridae*), and one unclassified RNA virus family (*Polymycoviridae*) were also identified (**Figure 3**).

Among the 65 OTUs, seven full-length genome segments, whose both ends were determined to be termini based on read mapping information (Urayama et al., 2018b), showed relatively high average read coverage (>1000×) (**Figure 4A**) and occupied 94% average read coverage of RdRp-encoding OTUs in the dsRNA-seq library. In the ssRNA-seq library, the seven segments also occupied 87% average read coverage of RdRp-encoding OTUs (**Figure 4A**). Therefore, the viruses that harbored the seven dominant RdRp sequences were defined as the dominant RNA viral population in the lichen sample, and further analyses were focused on these viruses. Classification of sequencing reads obtained by FLDS is shown in **Table 1**.

The putative complete genome sets encoding these seven dominant RdRp sequences were reconstructed (**Figure 4B** and **Supplementary Table 2**). Terminal sequences of genome segments are shared among segments in a single virus genome in some RNA viral lineages (Hutchinson et al., 2010). Thus, we reconstructed putative genome sets based on the terminal sequences of the full-length genome segments obtained by the dsRNA-seq FLDS method. As a result, 84% of the trimmed dsRNA reads (**Table 1**; **Supplementary Table 2**) were mapped to theses major RNA viral genomes. Based on the taxonomical classification of the top hit RNA viruses in BLASTX search using entire genome segments as query sequences, these viruses were named as LpaRV1–6 and Lichen RNA virus 1 (LRV1). However, we could not distinguish the genome sets of LpaRV3–6 because the genome segments encoding their RdRps share terminal sequences. Notably, LRV1 genome sequences were not found among ssRNA reads, although LpaRV1–6 were also detected (**Figure 4A**).

LpaRVs and LRV1

LpaRV1–6 genomes consist of two to four genome segments encoding RdRp, coat protein (CP), and additional unknown proteins. The genome structures of LpaRV1–6 resemble those of partitiviruses, which are known to have a bisegmented genome encoding RdRp and CP in each segment (Nibert et al., 2014). Phylogenetic analysis of the RdRp sequences also suggested that LpaRV1–6 are members of the family *Partitiviridae* (**Figure 5**). To date, five genera and unidentified clades are classified into *Partitiviridae* (Nibert et al., 2014). The phylogenetic analysis of RdRp suggested that five LpaRVs (1, 2, 4, 5, and 6) are members of genus *Alphapartitivirus* and LpaRV3 belongs to genus *Betapartitivirus*. Both genera harbor viruses that infect either plants or fungi (**Figure 5**; Nibert et al., 2014). It is noteworthy that LpaRV1 and LRV1

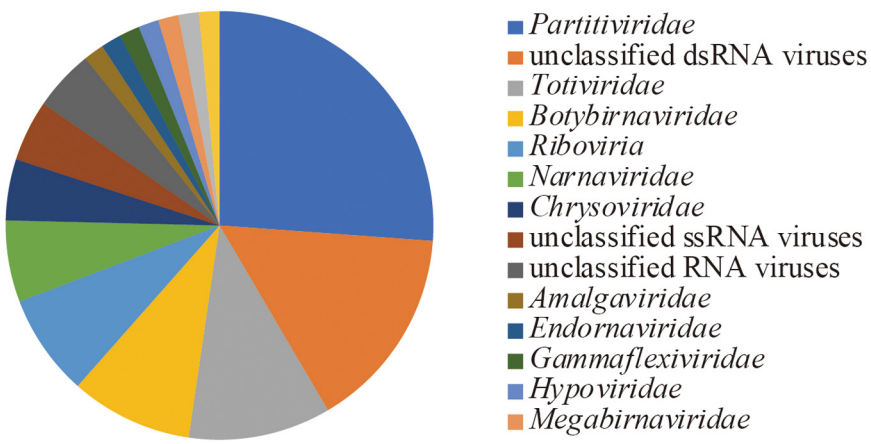

FIGURE 3 | Richness of OTUs based on the taxonomic lineage of top hit sequences in BLASTX.

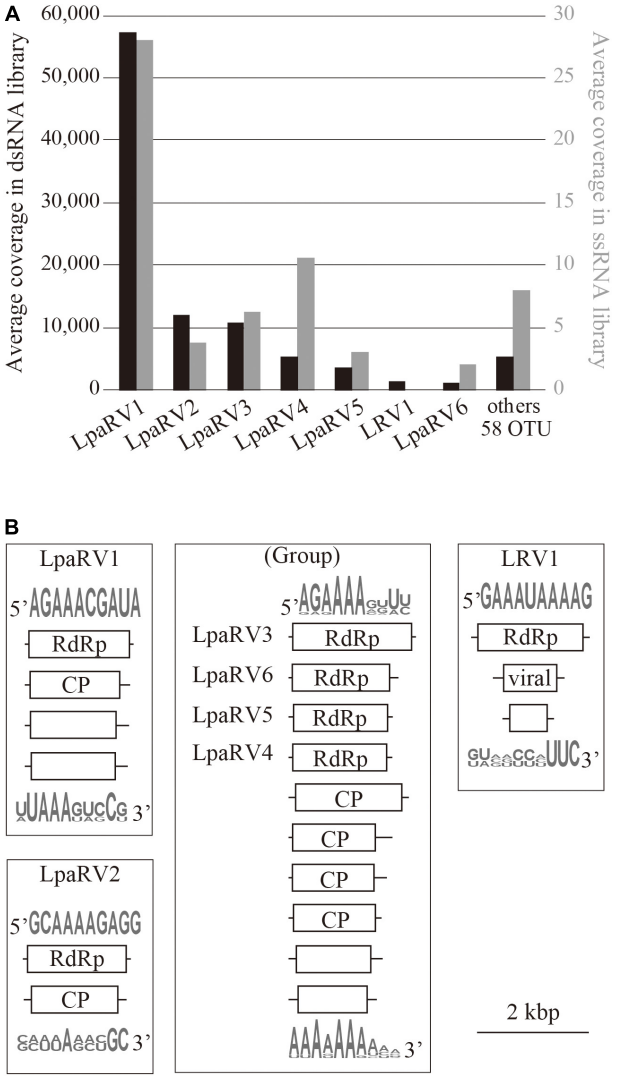

FIGURE 4 | Overview of major RNA viruses identified in the lichen sample. **(A)** Average coverage of major RdRp-encoding segments in dsRNA-seq (left axis, black bar) and ssRNA-seq (right axis, gray bar) libraries. **(B)** Organization of reconstructed major RNA viral genomes. Domains identified by CDD search are shown in open reading frames (box). Sequence logos represent sequence similarities for the 5′ or 3′ terminal region of the predicted genome segments.

located within a clade of fungus-infecting clade. Because our sample included a lot of other organisms (**Figure 2**), it was difficult to pinpoint the host organism, but our phylogenetic data suggested that these two viruses are infecting the fungi.

The published top hit sequence of LRV1 in the BLASTX search was Fusarium graminearum virus 4 (FgV4), which was shown to be closely related to *Partitiviridae* but not classified into the family (Yu et al., 2009). The phylogenetic analysis of partitiviruses and related viruses in this study revealed that LRV1 and FgV4 form a clade with two uncharacterized putative fungal RNA viruses, but the phylogenetic relationship among *Partitiviridae*, *Picobirnaviridae* (outgroup), and the LRV1-FgV4 cluster was not clarified. Therefore, we could not provide family-level classification of LRV1 as in the case of FgV4.

DISCUSSION

In this study, all dominant and putatively active RNA viruses were classified into the family *Partitiviridae* or its relative group. Among non-retro RNA viruses, only *Partitiviridae* and *Endornaviridae* harbor the genera including plant and fungal viruses. Although a single partitivirus that can infect both plant and fungal hosts has never been reported, recent studies revealed that a few viruses belonging to another RNA virus family can infect both plant and fungal hosts. For instance, cucumber mosaic virus, a positive-sense ssRNA virus belonging to the genus *Cucumovirus* in the family *Bromoviridae*, was discovered to infect both plants and fungi (Andika et al., 2017). Genome replication of a few plant viruses in *Tombusviridae* and *Bromoviridae* in a fungus (Panavas and Nagy, 2003; Panavas et al., 2005; Inaba and Nagy, 2018) and vice versa (Nerva et al., 2017) under experimental conditions was also reported. These observations suggested that the partitiviruses found in the lichen in this study might have the ability to replicate in both plants and fungi constituting symbiotic consortium of the lichen. To confirm this hypothesis, we need to conduct laboratory experiments to detect viral replication in algae cells after the infection of virus particles isolated from fungi.

It has been suggested that horizontal virus transfer among diverse hosts is one of the important driving forces of RNA virus evolution (Dolja and Koonin, 2017). In addition, Dr. Roossinck indicated that "a majority of virus families with members that infect fungi have counterparts that infect plants, and in some cases the phylogenetic analyses of these virus families indicate transmission between the plant and fungal kingdoms" (Roossinck, 2018). The strong interaction between land plants and fungi found in the symbiotic consortium of the lichen may provide an opportunity for horizontal virus transfer. In this point of view, in other fungal symbioses such as mycorrhizal fungi and their host plants, and endophytic fungi and their host plants, a similar horizontal virus transmission may occur between the symbionts. Although we could not delineate the host of each virus using our metagenomic approach, the phylogenetic information of RNA viruses associated with the lichen suggested that multiple viruses infect across higher taxonomic range between plants and fungi and impact fungi–Viridiplantae (including land plant and green algae) interaction.

Fragmented and primer ligated dsRNA sequencing provides novel insights into the RNA viromes associated with lichen. Microbial consortium of lichen would be a model system to understand virus–host coevolution. Comparison with the RNA viromes associated with the related lichens with different algae may also reveal more information about the specificity and diversity of RNA viruses and host organisms. We are also

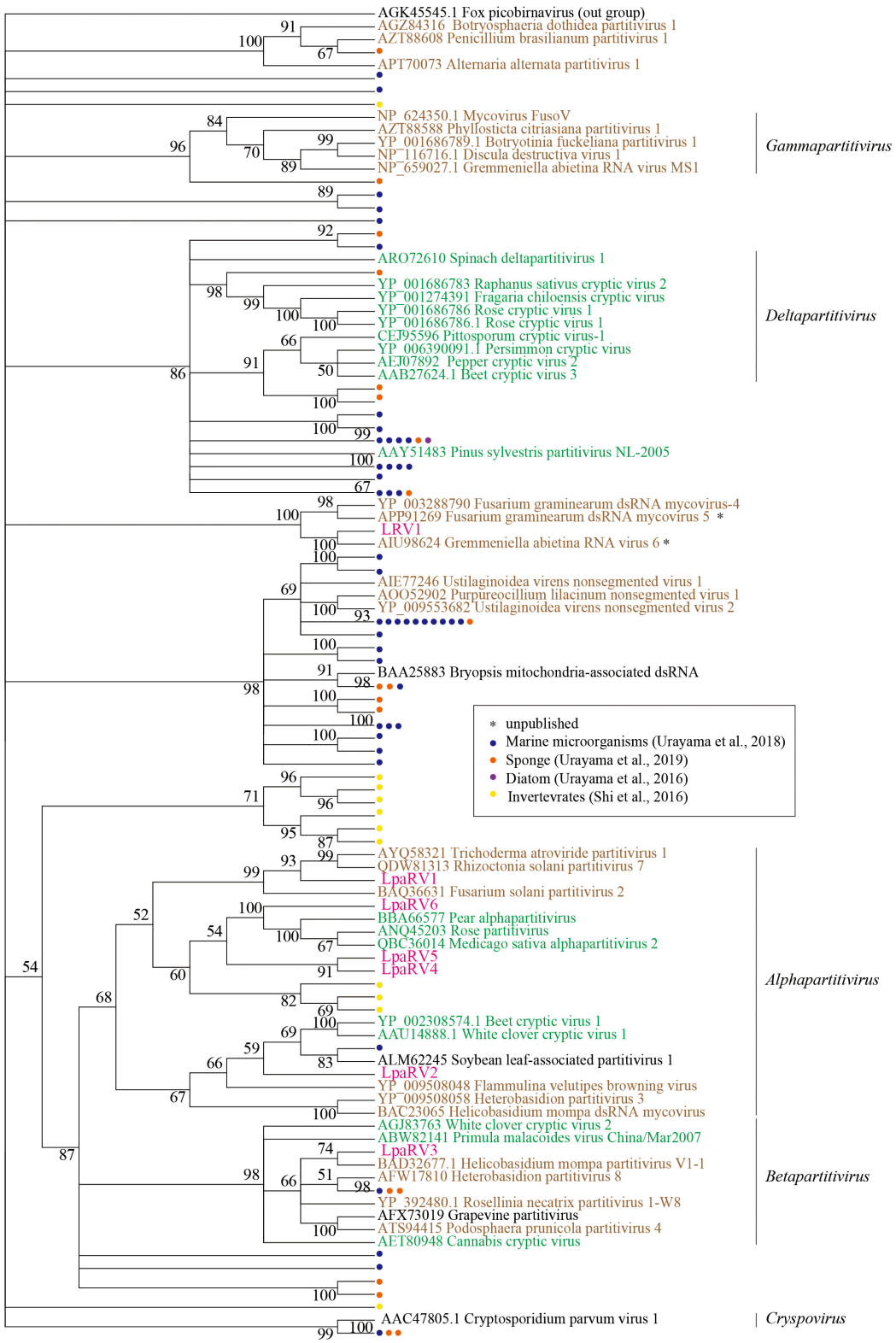

FIGURE 5 | Maximum-likelihood tree of RdRp domains from representative members of the family *Partitiviridae* and related sequences (including LpaRV1–6 and LRV1) based on amino acid residues. Numbers indicate the percentage bootstrap support from 1000 RAxML bootstrap replicates. We used RAxML with the RTREV+I+G+F model. Colors of virus names indicate the classification of the host organism: green, plant; brown, fungi; black, others or unclear. Pink color represents the newly derived sequences from the lichen. All weakly supported clades (i.e., those with bootstrap support <50%) were collapsed.

interested in the impacts of those RNA viruses on the delicate structure formation of the lichen thallus and on the symbiotic relationship between fungi and algae.

DATA AVAILABILITY STATEMENT

Sequences obtained in this study are available in the GenBank database repository (accession nos. DDBJ: BLWB01000001–BLWB01000058, LC533392–LC533410) and Short Read Archive database (accession no. DDBJ: DRA009807).

AUTHOR CONTRIBUTIONS

SU, TN, ND, and YM designed the research. FK and MH performed the research. ND and YM collected samples. YT, YC, and SU analyzed the data. All the authors listed wrote the manuscript. All authors contributed to the article and approved the submitted version.

FUNDING

This research was supported in part by a Grant-in-Aid for Scientific Research (Nos. 18H05368 and 20H05579) from the Ministry of Education, Culture, Sports, Science, and Technology (MEXT) of Japan and Grants-in-Aid for Scientific Research on Innovative Areas from MEXT of Japan (Nos. 16H06429, 16K21723, and 16H06437).

SUPPLEMENTARY MATERIAL

The Supplementary Material for this article can be found online at: https://www.frontiersin.org/articles/10.3389/fmicb.2020.561344/full#supplementary-material

Supplementary Table 1 | A list of RdRp-encoding OTUs except for major RNA viruses.

Supplementary Table 2 | Putative complete genomes of RNA viruses obtained from a lichen.

REFERENCES

Andika, I. B., Wei, S., Cao, C., Salaipeth, L., Kondo, H., and Sun, L. (2017). Phytopathogenic fungus hosts a plant virus: a naturally occurring cross-kingdom viral infection. *Proc. Natl. Acad. Sci. U.S.A.* 114, 12267–12272. doi: 10.1073/pnas.1714916114

Camacho, C., Coulouris, G., Avagyan, V., Ma, N., Papadopoulos, J., Bealer, K., et al. (2009). BLAST+: architecture and applications. *BMC Bioinformatics* 10:421. doi: 10.1186/1471-2105-10-421

Capella-Gutiérrez, S., Silla-Martínez, J. M., and Gabaldón, T. (2009). trimAl: a tool for automated alignment trimming in large-scale phylogenetic analyses. *Bioinformatics* 25, 1972–1973. doi: 10.1093/bioinformatics/btp348

Culley, A. I., Lang, A. S., and Suttle, C. A. (2006). Metagenomic analysis of coastal RNA virus communities. *Science* 312, 1795–1798. doi: 10.1126/science.1127404

Decker, C. J., Steiner, H. R., Hoon-Hanks, L. L., Morrison, J. H., Haist, K. C., Stabell, A. C., et al. (2019). dsRNA-Seq: identification of Viral Infection by Purifying and Sequencing dsRNA. *Viruses* 11:943. doi: 10.3390/v11100943

Dolja, V. V., and Koonin, E. V. (2017). Metagenomics reshapes the concepts of RNA virus evolution by revealing extensive horizontal virus transfer. *Virus Res.* 244, 36–52. doi: 10.1016/j.virusres.2017.10.020

Du, Z. Y., Zienkiewicz, K., Vande Pol, N., Ostrom, N. E., Benning, C., and Bonito, G. M. (2019). Algal-fungal symbiosis leads to photosynthetic mycelium. *eLife* 8:e47815.

Edgar, R. C. (2004). MUSCLE: multiple sequence alignment with high accuracy and high throughput. *Nucleic Acids Res.* 32, 1792–1797. doi: 10.1093/nar/gkh340

Fukasawa, F., Hirai, M., Takaki, Y., Shimane, Y., Thomas, C. E., Urayama, S., et al. (2020). A new polycipivirus identified in *Colobopsis shohki*. *Arch. Virol.* 165, 761–763. doi: 10.1007/s00705-019-04510-8

Gruber-Vodicka, H. R., Seah, B. K., and Pruesse, E. (2019). phyloFlash—Rapid SSU rRNA profiling and targeted assembly from metagenomes. *bioRxiv [Preprint]* doi: 10.1101/521922

Honegger, R., Edwards, D., and Axe, L. (2013). The earliest records of internally stratified cyanobacterial and algal lichens from the Lower Devonian of the Welsh Borderland. *New Phytol.* 197, 264–275. doi: 10.1111/nph.12009

Hutchinson, E. C., von Kirchbach, J. C., Gog, J. R., and Digard, P. (2010). Genome packaging in influenza A virus. *J. Gen. Virol.* 91, 313–328. doi: 10.1099/vir.0.017608-0

Inaba, J.-I., and Nagy, P. D. (2018). Tombusvirus RNA replication depends on the TOR pathway in yeast and plants. *Virology* 519, 207–222. doi: 10.1016/j.virol.2018.04.010

Kadoya, S.-S., Urayama, S.-I., Nunoura, T., Hirai, M., Takaki, Y., Kitajima, M., et al. (2020). Bottleneck size-dependent changes in the genetic diversity and specific growth rate of a rotavirus a strain. *J. Virol.* 94, e02083-19.

Kohler, A., Kuo, A., Nagy, L. G., Morin, E., Barry, K. W., Buscot, F., et al. (2015). Convergent losses of decay mechanisms and rapid turnover of symbiosis genes in mycorrhizal mutualists. *Nat. Genet.* 47:410. doi: 10.1038/ng.3223

Kopylova, E., Noé, L., and Touzet, H. (2012). SortMeRNA: fast and accurate filtering of ribosomal RNAs in metatranscriptomic data. *Bioinformatics* 28, 3211–3217. doi: 10.1093/bioinformatics/bts611

Lutzoni, F., Nowak, M. D., Alfaro, M. E., Reeb, V., Miadlikowska, J., Krug, M., et al. (2018). Contemporaneous radiations of fungi and plants linked to symbiosis. *Nat. Commun.* 9:5451.

Miadlikowska, J., Kauff, F., Hofstetter, V., Fraker, E., Grube, M., Hafellner, J., et al. (2006). New insights into classification and evolution of the Lecanoromycetes (Pezizomycotina, Ascomycota) from phylogenetic analyses of three ribosomal RNA-and two protein-coding genes. *Mycologia* 98, 1088–1103. doi: 10.3852/mycologia.98.6.1088

Miller, C. S., Baker, B. J., Thomas, B. C., Singer, S. W., and Banfield, J. F. (2011). EMIRGE: reconstruction of full-length ribosomal genes from microbial community short read sequencing data. *Genome Biol.* 12, R44.

Moore, D., Robson, G. D., and Trinci, A. P. (2020). *21st Century Guidebook to Fungi*. Cambridge: Cambridge University Press.

Muggia, L., Leavitt, S., and Barreno, E. (2018). The hidden diversity of lichenised Trebouxiophyceae (Chlorophyta). *Phycologia* 57, 503–524. doi: 10.2216/17-134.1

Nelsen, M. P., Lücking, R., Boyce, C. K., Lumbsch, H. T., and Ree, R. H. (2020). No support for the emergence of lichens prior to the evolution of vascular plants. *Geobiology* 18, 3–13. doi: 10.1111/gbi.12369

Nerva, L., Varese, G., Falk, B., and Turina, M. (2017). Mycoviruses of an endophytic fungus can replicate in plant cells: evolutionary implications. *Sci. Rep.* 7:1908.

Nibert, M. L., Ghabrial, S. A., Maiss, E., Lesker, T., Vainio, E. J., Jiang, D., et al. (2014). Taxonomic reorganization of family Partitiviridae and other recent progress in partitivirus research. *Virus Res.* 188, 128–141. doi: 10.1016/j.virusres.2014.04.007

Panavas, T., and Nagy, P. D. (2003). Yeast as a model host to study replication and recombination of defective interfering RNA of Tomato bushy stunt virus. *Virology* 314, 315–325. doi: 10.1016/s0042-6822(03)00436-7

Panavas, T., Serviene, E., Brasher, J., and Nagy, P. D. (2005). Yeast genome-wide screen reveals dissimilar sets of host genes affecting replication of RNA

viruses. *Proc. Natl. Acad. Sci. U.S.A.* 102, 7326–7331. doi: 10.1073/pnas.0502604102

Petrzik, K., Koloniuk, I., Sehadova, H., and Sarkisova, T. (2019). Chrysoviruses Inhabited Symbiotic Fungi of Lichens. *Viruses* 11,

Petrzik, K., Vondrák, J., Barták, M., Peksa, O., and Kubešová, O. (2013). Lichens—a new source or yet unknown host of herbaceous plant viruses? *Eur. J. Plant Pathol.* 138, 549–559. doi: 10.1007/s10658-013-0246-z

Quast, C., Pruesse, E., Yilmaz, P., Gerken, J., Schweer, T., Yarza, P., et al. (2012). The SILVA ribosomal RNA gene database project: improved data processing and web-based tools. *Nucleic Acids Res.* 41, D590–D596.

Remy, W., Taylor, T. N., Hass, H., and Kerp, H. (1994). Four hundred-million-year-old vesicular arbuscular mycorrhizae. *Proc. Natl. Acad. Sci. U.S.A.* 91, 11841–11843. doi: 10.1073/pnas.91.25.11841

Rognes, T., Flouri, T., Nichols, B., Quince, C., and Mahé, F. (2016). VSEARCH: a versatile open source tool for metagenomics. *PeerJ* 4:e2584. doi: 10.7717/peerj.2584

Roossinck, M. J. (2018). Evolutionary and ecological links between plant and fungal viruses. *New Phytol.* 221, 86–92. doi: 10.1111/nph.15364

Roossinck, M. J., Saha, P., Wiley, G. B., Quan, J., White, J. D., Lai, H., et al. (2010). Ecogenomics: using massively parallel pyrosequencing to understand virus ecology. *Mol. Ecol.* 19(Suppl. 1), 81–88. doi: 10.1111/j.1365-294x.2009.04470.x

Shi, M., Lin, X. D., Chen, X., Tian, J. H., Chen, L. J., Li, K., et al. (2018). The evolutionary history of vertebrate RNA viruses. *Nature* 556, 197–202. doi: 10.1038/s41586-018-0012-7

Shi, M., Lin, X. D., Tian, J. H., Chen, L. J., Chen, X., Li, C. X., et al. (2016). Redefining the invertebrate RNA virosphere. *Nature* 540, 539–543. doi: 10.1038/nature20167

Stamatakis, A. (2014). RAxML version 8: a tool for phylogenetic analysis and post-analysis of large phylogenies. *Bioinformatics* 30, 1312–1313. doi: 10.1093/bioinformatics/btu033

Steward, G. F., Culley, A. I., Mueller, J. A., Wood-Charlson, E. M., Belcaid, M., and Poisson, G. (2013). Are we missing half of the viruses in the ocean? *ISME J.* 7, 672–679. doi: 10.1038/ismej.2012.121

Sugiura, N. (1978). Further analysts of the data by akaike's information criterion and the finite corrections. *Commun. Stat. Theor. Methods* 7, 13–26. doi: 10.1080/03610927808827599

Tamura, K., Stecher, G., Peterson, D., Filipski, A., and Kumar, S. (2013). MEGA6: molecular evolutionary genetics analysis version 6.0. *Mol. Biol. Evol.* 30, 2725–2729. doi: 10.1093/molbev/mst197

Tanabe, A. S. (2011). Kakusan4 and Aminosan: two programs for comparing nonpartitioned, proportional and separate models for combined molecular phylogenetic analyses of multilocus sequence data. *Mol. Ecol. Resour.* 11, 914–921. doi: 10.1111/j.1755-0998.2011.03021.x

Urayama, S., Takaki, Y., Hagiwara, D., and Nunoura, T. (2020). dsRNA-seq Reveals Novel RNA Virus and Virus-Like Putative Complete Genome Sequences from Hymeniacidon sp. Sponge. *Microbes Environ.* 35, ME19132.

Urayama, S., Takaki, Y., and Nunoura, T. (2016). FLDS: a Comprehensive dsRNA Sequencing Method for Intracellular RNA Virus Surveillance. *Microbes Environ.* 31, 33–40. doi: 10.1264/jsme2.me15171

Urayama, S., Takaki, Y., Nunoura, T., and Miyamoto, N. (2018a). Complete Genome Sequence of a Novel RNA Virus Identified from a Deep-Sea Animal. *Osedax japonicus*. *Microbes Environ.* 33, 446–449. doi: 10.1264/jsme2.me18089

Urayama, S., Takaki, Y., Nishi, S., Yoshida-Takashima, Y., Deguchi, S., Takai, K., et al. (2018b). Unveiling the RNA virosphere associated with marine microorganisms. *Mol. Ecol. Resour.* 18, 1444–1455. doi: 10.1111/1755-0998.12936

White, J. F. Jr., and Torres, M. S. (2009). *Defensive Mutualism in Microbial Symbiosis*. Boca Raton, FL: CRC Press.

Yu, J., Kwon, S. J., Lee, K. M., Son, M., and Kim, K. H. (2009). Complete nucleotide sequence of double-stranded RNA viruses from Fusarium graminearum strain DK3. *Arch. Virol.* 154, 1855–1858. doi: 10.1007/s00705-009-0507-5

Conflict of Interest: This research is a joint project funded by Nippon Gene Co., Ltd. In this research, we used ISOVIRUS, a product sold by Nippon Gene Co., Ltd. YM and ND are employed by Nippon Gene Co., Ltd.

The remaining authors declare that the research was conducted in the absence of any commercial or financial relationships that could be construed as a potential conflict of interest.

frontiers in Microbiology

ORIGINAL RESEARCH
published: 28 October 2020
doi: 10.3389/fmicb.2020.593784

Population Structure of Double-Stranded RNA Mycoviruses That Infect the Rice Blast Fungus *Magnaporthe oryzae* in Japan

*Yuta Owashi[1,2], Mitsuhiro Aihara[1], Hiromitsu Moriyama[1], Tsutomu Arie[1], Tohru Teraoka[1] and Ken Komatsu[1]**

[1]Laboratory of Plant Pathology, Graduate School of Agriculture, Tokyo University of Agriculture and Technology (TUAT), Fuchu, Japan, [2]Western Region Agricultural Research Center, National Agriculture and Food Research Organization, Fukuyama, Japan

Various viruses infect *Magnaporthe oryzae* (syn. *Pyricularia oryzae*), which is a well-studied fungus that causes rice blast disease. Most research has focused on the discovery of new viruses and the hypovirulence-associated traits conferred by them. Therefore, the diversity and prevalence of viruses in wild fungal populations have not been explored. We conducted a comprehensive screening of *M. oryzae* mycoviruses from various regions in Japan using double-stranded RNA (dsRNA) electrophoresis and RT-PCR assays. We detected three mycoviruses, Magnaporthe oryzae virus 2 (MoV2), Magnaporthe oryzae chrysovirus 1 (MoCV1), and Magnaporthe oryzae partitivirus 1 (MoPV1), among 127 of the 194 *M. oryzae* strains screened. The most prevalent virus was MoPV1 (58.8%), which often co-infected in a single fungal strain together with MoV2 or MoCV1. MoV2 and MoCV1 were found in 22.7 and 10.8% of strains, respectively, and they were usually distributed in different regions so that mixed-infection with these two mycoviruses was extremely rare. The predominance of MoPV1 in *M. oryzae* is supported by significant negative values from neutrality tests, which indicate that the population size of MoPV1 tends to increase. Population genetic analyses revealed high nucleotide diversity and the presence of phylogenetically diverse subpopulations among the MoV2 isolates. This was not the case for MoPV1. Furthermore, studies of a virus-cured *M. oryzae* strain revealed that MoV2 does not cause any abnormalities or symptoms in its host. However, a leaf sheath inoculation assay showed that its presence slightly increased the speed of mycelial growth, compared with virus-free mycelia. These results demonstrate that *M. oryzae* in Japan harbors diverse dsRNA mycovirus communities with wide variations in their population structures among different viruses.

Keywords: rice blast, mycovirus, *Pyricularia oryzae* (formerly *Magnaporthe oryzae*), Magnaporthe oryzae virus 2, Magnaporthe oryzae partitivirus 1, Magnaporthe oryzae chrysovirus 1, victorivirus, screening

OPEN ACCESS

Edited by:
Nobuhiro Suzuki, Okayama University, Japan

Reviewed by:
Massimo Turina, National Research Council (CNR), Italy
Tomofumi Mochizuki, Osaka Prefecture University, Japan

***Correspondence:**
Ken Komatsu
akomatsu@cc.tuat.ac.jp

Specialty section:
This article was submitted to Virology, a section of the journal Frontiers in Microbiology

Received: *11 August 2020*
Accepted: *28 September 2020*
Published: *28 October 2020*

Citation:
Owashi Y, Aihara M, Moriyama H, Arie T, Teraoka T and Komatsu K (2020) Population Structure of Double-Stranded RNA Mycoviruses That Infect the Rice Blast Fungus Magnaporthe oryzae in Japan. Front. Microbiol. 11:593784. doi: 10.3389/fmicb.2020.593784

INTRODUCTION

Fungal viruses (mycoviruses) are widespread in a variety of fungal species. Since their first discovery in cultivated mushrooms (Hollings, 1962), many mycoviruses have been found in numerous fungal species. They are classified into three groups based on the compositions of their genomes: linear double-stranded RNA (dsRNA), linear positive- and negative-sense single-stranded RNA (ssRNA), and circular single-stranded DNA (ssDNA). Among these, mycoviruses

with dsRNA genomes represent the majority, and they are classified into seven families: *Totiviridae* (a non-segmented genome of 4.6–7.0 kbp), *Amalgaviridae* (a non-segmented genome about 3.1–3.5 kbp), *Partitiviridae* (bisegmented genomes of 1.3–2.5 kbp), *Megabirnaviridae* (bisegmented genomes of 7.2–8.9 kbp), *Chrysoviridae* (3–7 segments of 2.4–3.6 kbp), *Quadriviridae* (four segments of 3.7–4.9 kbp), and *Reoviridae* (11–12 segments of 0.7–4.1 kbp; Ghabrial and Suzuki, 2009; Nibert et al., 2014; Ghabrial et al., 2015; Depierreux et al., 2016; Zhai et al., 2018).

One of the most widely used techniques for the detection of mycoviruses is extraction and gel electrophoresis of dsRNA elements (Morris and Dodds, 1979; Herrero et al., 2012; Okada et al., 2015). This technique is a relatively cheap and has an advantage of detecting most abundant mycoviruses including those having ssRNA or DNA genome, except for the viruses which may not accumulate abundant dsRNA as their replication intermediate during infection (Nerva et al., 2016). The numbers and sizes of dsRNA elements vary among dsRNA mycovirus species. Multiple dsRNA elements found in one fungal strain may be derived from multipartite viral genomes, mixed infections, or even from defective products of the viral RNA (Chiba et al., 2013b; Jiang et al., 2015). Mycoviruses generally have no extracellular phase; they are transmitted in a host-dependent, intracellular manner, such as through cell division, sporogenesis, or hyphal anastomosis (Ghabrial et al., 2015). Due to this exclusively intracellular lifestyle, it is likely that polymorphic dsRNA profiles and mycovirus phylogenic diversity are associated with specific geographical areas and host strains (Arakawa et al., 2002; Voth et al., 2006). However, this is not always the case (Schoebel et al., 2018; Wang et al., 2020).

Most mycoviruses infections cause no obvious symptoms in their fungal hosts. This could be explained by "the ancient infection hypothesis," reflecting the long period of coevolution between fungal hosts and mycoviruses, and driving viruses into nonvirulence (Pearson et al., 2009). One good example is Rosellinia necatrix partitivirus 2, whose infection induces phenotypic alterations in an artificial host *Cryphonectria parasitica* but not in its natural host *R. necatrix* (Chiba et al., 2013b). In contrast, mycoviruses that attenuate virulence of their hosts are unusual. However, as exemplified by Cryphonectria hypovirus 1, viruses that induce so-called hypovirulence in their hosts can be used as biological control agents against plant pathogenic fungi (Milgroom and Cortesi, 2004; Rigling and Prospero, 2018). Other mycoviruses establish a relationship that is beneficial to the host fungus, even though they sometimes impair host fungal growth. For example, an *Alternaria alternata* strain with a high titer of Alternaria alternata chrysovirus 1 exhibits enhanced pathogenicity toward Japanese pear, and this is called hypervirulence (Okada et al., 2018). In many cases, it is difficult to comprehensively understand the complex interactions between mycoviruses and their hosts, because the effects of mycovirus infection might differ depending on environmental conditions and/or the plant cultivars that are infected (Aihara et al., 2018).

Magnaporthe oryzae (syn. *Pyricularia oryzae*) is an important fungus that is the causal agent of rice blast disease, and a number of mycoviruses have been reported to infect it. Among these are dsRNA viruses including Magnaporthe oryzae virus 1, 2, and 3 (MoV1, MoV2, and MoV3), which belong to the genus *Victorivirus* of the family *Totiviridae* (Yokoi et al., 2007; Maejima et al., 2008; Tang et al., 2015), Magnaporthe oryzae partitivirus 1 (MoPV1) in the family *Partitiviridae* (Du et al., 2016), and several isolates of Magnaporthe oryzae chrysovirus 1 (MoCV1-A, -B, -C, and -D) in the family *Chrysoviridae* (Urayama et al., 2010, 2012, 2014; Tang et al., 2015; Higashiura et al., 2019). In addition, some ssRNA viruses have been reported in this host: Magnaporthe oryzae virus A (MoVA) in the family *Tombusviridae* (Ai et al., 2016), Magnaporthe oryzae ourmia-like virus 1 and 4 and Pyricularia oryzae ourmia-like virus 1 to 3 (MOLV1, MOLV4, and PoOLV1–3), which are closely related to the ourmia-like viruses (Illana et al., 2017; Li et al., 2019; Ohkita et al., 2019), and Magnaporthe oryzae narnavirus 1 (MoNV1) in the family *Narnaviridae* (Lin et al., 2020). To date, these *M. oryzae* mycoviruses have been detected mainly in Asian countries, including China (MoV3, MoCV1-C, MoPV1, MoVA, MoLV4, and MoNV1), Japan (MoV1, MoV2, and MoCV1-D), and Vietnam (MoCV1-A and MoCV1-B). Among these mycoviruses, the MoCV1 isolates have been studied the most because they induce hypovirulence-associated traits in *M. oryzae*, including impaired mycelial growth and abnormalities in cell morphology (Urayama et al., 2010). MoLV4 was reported to be asymptomatic in its host (Li et al., 2019). However, most of these mycoviruses have not been studied to determine the symptoms they cause in their fungal host. Furthermore, their population structures in the natural environment have not been investigated.

In this study, we surveyed the mycovirus infections in Japanese *M. oryzae* strains, and analyzed their population structures. Screening of 194 *M. oryzae* strains in Japan for viruses by dsRNA electrophoresis and sequencing analyses revealed that the three mycoviruses MoV2 (a victorivirus), MoCV1 (a chrysovirus), and MoPV1 (a partitivirus) were present in the Japanese strains of *M. oryzae*, and their infection rates were quite variable depending on the regions, where the strains were found. Furthermore, this study examined whether MoV2 infection can affect the host phenotype. As a result, the elimination of a MoV2 isolate from its host strain revealed that MoV2 does not cause any abnormalities or symptoms in its host, but slightly promotes hyphal growth in infected plants.

MATERIALS AND METHODS

Strains of *M. oryzae* and Culture Conditions

A total of 194 strains of *M. oryzae* were obtained from symptomatic rice leaves in various regions of Japan, including the Kyushu region (in southern Japan), the Hokuriku region (a coastal region in north-western Japan), and others. All strains were grown on potato dextrose agar (PDA) medium for 1 week, then mycelial plugs were incubated in YG broth [0.5% (w/v) yeast extract and 2% glucose] with shaking (65 r/min) for up to 2 weeks at 25°C. These mycelia were stored at −80°C until use.

Purification and Detection of dsRNAs

Total nucleic acids were extracted, and dsRNA was subsequently purified using the micro-spin column method (Okada et al., 2015)

with Cellulose D (Advantec, Japan). Fungal mycelium (approximately 0.1 g dry weight) was pulverized with 500 µl extraction buffer [2× STE (100 mM NaCl; 10 mM Tris-HCl, pH 8.0; 1 mM EDTA, pH 8.0) containing 0.1% (v/v) ß-mercaptoethanol and 1% (w/v) SDS], and then 500 µl phenol-chloroform-isoamyl alcohol (25:24:1) was added. The mixture was vortexed, centrifuged at 15,000 rpm for 5 min, and the supernatant was collected. The supernatant was mixed with ethanol (final concentration 16%) and loaded onto a spin column and centrifuged. After washing the column with 400 µl of wash buffer [1× STE containing 16% (v/v) ethanol; 15,000 rpm for 50 s, three times], the dsRNA solution was eluted with 350 µl of elution buffer (1× STE; 15,000 rpm for 1 min). The dsRNAs were concentrated by ethanol precipitation and dissolved in 20 µl nuclease-free water. The purified dsRNA solution (10 µl) was electrophoresed in a 1.0% (w/v) agarose gel (17 V, 18 h) and visualized by ethidium bromide staining to determine the sizes and numbers of dsRNA segments.

Reverse Transcription (RT)-PCR and Direct Sequencing

One-step RT-PCR was carried out using purified dsRNA as the template. Virus-specific primer sets were designed based on the RNA-dependent RNA polymerase (RdRp) coding regions of MoCV1, MoPV1, MoV1, MoV2, and MoV3 (**Supplementary Table S1**). SuperScript™ III Reverse Transcriptase (Thermo Fisher Scientific, Witham, MA, United States) was used according to the manufacturer's protocol, with a final reaction volume of 10 µl. Reactions were performed as follows: reverse transcription at 55°C for 20 min and 60°C for 10 min, followed by 94°C for 2 min, then 35 cycles of 94°C for 15 s, 55°C for 30 s, and 68°C for 45 s, then 68°C for 5 min. The amplified fragments were directly sequenced using the same primer sets in an ABI Prism 3130xl Genetic Analyzer (Thermo Fisher Scientific, Witham, MA, United States).

Complete Genome Sequencing of the MoV2 Isolates

The dsRNAs extracted from *M. oryzae* strains from the Kyushu region, NHH12P-1, MZ4-12-2, and MZ13-12-1, were used as templates for cDNA synthesis using the PrimeScript™ first-strand cDNA Synthesis Kit (Takara Bio, Kusatsu, Japan) with MoV2-specific primers (**Supplementary Table S1**). Three overlapping PCR products were amplified using the KOD FX Neo polymerase (Toyobo, Osaka, Japan) with the primer sets Hind-T7-MoV2F/MoV2-2697R, MoV2-2657F/MoV2-detect R 4052–4073, and MoV2-detect F 3703–3725/Bam-MoV2R-re (**Supplementary Table S1**). The amplified PCR products were treated with 10× A-attachment mix (Toyobo, Osaka, Japan) and ligated into the pGEM T-Easy vector (Promega, Madison, United States), which was then used to transformation Hit-DH5α cells (RBC Bioscience, Taipei, Taiwan). Plasmid DNA was purified using the Wizard Plus SV Minipreps DNA Purification System (Promega, Madison, United States). Sequencing was conducted using both the universal primers (M13-M3 and M13-RV) and designed sequencing primers (**Supplementary Table S1**). The 5′- and 3′-terminal sequences of each dsRNA segment were determined using the SMARTer® RACE cDNA Amplification Kit (Clontech Laboratories, Inc., Mountain View, United States).

Phylogenetic and Population Genetic Analyses

Total 35 isolates of MoV2 in Japan (29 isolates from the Kyushu region and six isolates from other regions) and 24 isolates of MoPV1 (23 isolates from the Kyushu region in Japan and an isolate from China) were used for phylogenetic and population genetic analyses. A partial RdRp-coding region of MoV2 (371 bp), which includes the conserved RdRp motifs characteristic of RdRps of the members of the family *Totiviridae* (Bruenn, 1993; Yokoi et al., 2007), as well as that of MoPV1 (466 bp), were analyzed. Total 32 isolates of MoV2 in Japan (29 isolates from the Kyushu region and 3 isolates from other regions) were also used for phylogenetic and population genetic analyses for 394 bp of partial coat protein (CP) coding domain. Nucleotide sequences were aligned using Clustal W (Thompson et al., 1994). Phylogenetic trees based on the nucleotide sequences were constructed by the Maximum Likelihood method using the MEGA 7.0 software (Kumar et al., 2016). Kimura's two parameter model, assessed by the best-fit method, was applied for the calculation. Genetic parameters and neutrality tests were determined and carried out using DnaSP version 6.11 (Rozas et al., 2017). The rates of nonsynonymous (d_N) and synonymous (d_S) substitutions were estimated using the Pamilo-Bianchi-Li method, implemented in the MEGA 7.0 software.

Fungal Growth and Inoculation Assays

Two *M. oryzae* strains: Ken 60-19, in which MoV2 was originally detected (Maejima et al., 2008), and the virus-cured strain Ken 60-19-VC, which was produced by single-spore isolation, were used for biological assays and pathogenicity tests. Morphologies and growth rates were assessed by culturing mycelial plugs (5 mm diameter) on PDA medium for 10 days at 25°C. The growth rate data were analyzed using a paired *t*-test with the software R version 3.4.1 (R Core Team, 2017). For microscopic observations of aerial mycelia, mycelial plugs were cultured in YG liquid medium at 25°C with shaking (65 r/min) for 1 week. The observations were performed using a light microscope with differential interference contrast optics (Olympus DP80).

Inoculation tests were conducted using seedlings of the rice variety Lijiangxintuanheigu (LTH). The seedlings were planted in plastic pots and were grown in a greenhouse. To induce conidiation, fungal strains were grown on solid oatmeal agar medium for 2 weeks at 25°C, and then aerial hyphae were removed and cultured under black light blue lamps for 3 days. The conidia were brushed off into distilled water.

For spray inoculations, conidia were suspended in distilled water containing 0.1% (v/v) Tween 20 to a final density of 1×10^5 conidia/ml. The conidial suspension was sprayed on 3-week-old rice seedlings at a rate of 1 ml/individual. After 24 h of incubation in a humid box (24°C in the dark), the seedlings were placed in a growth chamber for 6 days at 25°C, and the disease was scored according to Hayashi et al. (2009).

For leaf sheath inoculations, 4-week-old leaf sheaths were cut into 4 cm segments, and the inner spaces were filled up with a 5×10^5 conidia/ml suspension. After 48 h of incubation in a humid box (24°C in the dark), the sheath segments were trimmed to remove the sides and to expose the epidermal layer above the midvein. Lower midvein tissues were then sliced and observed using an Olympus CX41 microscope. Hyphal growth inside plants was scored with four grades as described by Namai et al. (1996): 1, no branched hyphae; 2, branched in a cell; 3, progression to other cells; and 4, filling more than two cells. The data for mycelial development were analyzed using the Wilcoxon rank-sum test with the R software.

RESULTS

Detection of dsRNA Mycoviruses Infecting *M. oryzae* in Japan

In order to identify dsRNA mycoviruses infecting Japanese *M. oryzae* strains, we purified dsRNA from fungal mycelia and performed electrophoresis. Among 194 strains, we found three types of dsRNA elements: a single band at about 5.2 kb, multiple bands ranging from 2.5 to 3.5 kb, and double bands at about 1.5 and 1.8 kb (**Figure 1A**). Based on the sizes and numbers of dsRNA elements in known *M. oryzae* mycoviruses, these three types of dsRNA elements represented the genome segments of MoV1/2/3, MoCV1, and MoPV1, respectively (Yokoi et al., 2007; Maejima et al., 2008; Urayama et al., 2010; Tang et al., 2015; Du et al., 2016).

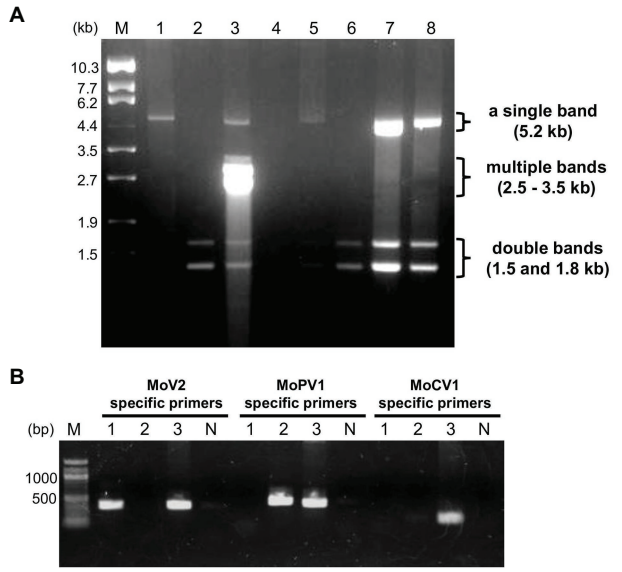

FIGURE 1 | Detection of double-stranded RNA (dsRNA) mycoviruses infecting *Magnaporthe oryzae* by dsRNA electrophoresis and RT-PCR. **(A)** An example of an electrophoretic profile of dsRNAs from *M. oryzae* strains in Japan (lane 1, MZ19-12-2; lane 2, KMK12P-5; lane 3, APU10-199A; lane 4, MZ3-12-2; lane 5, MZ12-12-2; lane 6, MZ10-12-1; lane 7, NHH12P-1; and lane 8, KIO12P-11). Lane M, DNA size markers (λDNA digested with *Eco*T14 I). **(B)** Specific detection of three mycoviruses by RT-PCR. Lane numbers 1–3 correspond to the same *M. oryzae* strains as in **(A)**. Lane N, negative control with no DNA; lane M, 100 bp DNA ladder (New England BioLabs: N3231).

We used virus-specific RT-PCR and partial sequencing to confirm the identities of the three dsRNA mycoviruses (**Figure 1B**). Among the *M. oryzae* strains tested (35 strains from Kyushu and other regions), all those carrying dsRNA elements of about 5.2 kb produced amplification products when tested with the MoV2-specific primers. No amplification products were obtained when the same set of strains were tested with MoV1- and MoV3-specific primers (data not shown). Direct sequencing of these amplified products showed that they exhibited over 91.9% nucleotide identity with the first reported MoV2 isolate (from strain Ken 60-19, Japan: GenBank Accession no. AB300379). They exhibited less than 54.3 and 64.4% identities, respectively, with the previously reported MoV1 (from strain TH 65-105, Japan: GenBank Accession no. AB176964) and MoV3 (from strain QSP5, China: GenBank Accession no. KP893140). Similarly, the strains with multiple bands ranging from 2.8 to 3.5 kb (two of the 35 tested strains) produced amplification products when tested with the MoCV1-specific primers, and those with double bands at about 1.5 and 1.8 kb (23 of the tested strains) produced amplification products when tested with the MoPV1-specific primers. Sequencing of these amplification products showed that they exhibited higher than 85.4 and 96.8% identities, respectively, with the previously obtained sequences of MoCV1 (from strain S-0412-II 1a, Vietnam: GenBank Accession no. AB560761) and MoPV1 (from strain NJ20, China: GenBank Accession no. KX119172). We concluded that *M. oryzae* strains collected in Japan could be infected with one or more of the three dsRNA mycoviruses MoV2, MoCV1, and MoPV1.

Prevalence of dsRNA Mycoviruses in *M. oryzae* in Japan

We next performed a comprehensive investigation of the dsRNA mycoviruses in 194 Japanese *M. oryzae* strains. These included 100 strains from the Kyushu region (in southern Japan), 88 strains from the Hokuriku region (a coastal region in north-western Japan), and six strains from other regions. We found that that 127 of the 194 strains were infected with one or more of the three dsRNA mycoviruses (**Figure 2** and **Supplementary Table S2**). All three mycoviruses were detected in strains from the Hokuriku region: 3/88 strains had MoV2, 17/88 strains had MoCV1, and 44/88 strains had MoPV1. Likewise, among strains from the Kyushu region, we detected MoV2 in 35/100 strains, MoCV1 in 2/100 strains, and MoPV1 in 65/100 strains. Among the six strains from other regions, all six had MoV2, two had MoCV1, and one had MoPV1. Some *M. oryzae* strains were co-infected with multiple mycoviruses. MoPV1 was often present with MoV2 and/or MoCV1; however, co-infections of MoV2 and MoCV1 were rare, and observed in only two cases (**Figure 2**).

Phylogenetic Analysis of MoV2 and MoPV1

We performed phylogenetic analyses to examine the intraspecies population structures of MoV2 and MoPV1, which were the two major viruses found in our screening. For MoV2, the analysis was performed using partial nucleotide sequences (371 bp) from

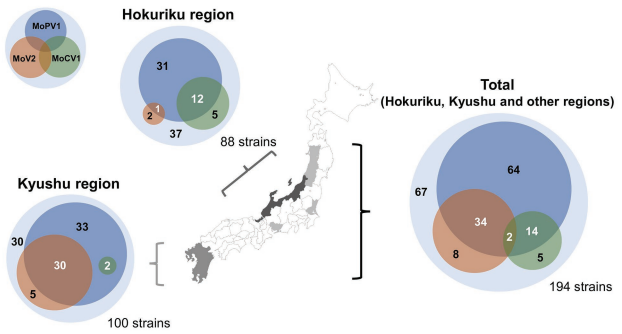

FIGURE 2 | Frequencies of Magnaporthe oryzae virus 2 (MoV2), Magnaporthe oryzae partitivirus 1 (MoPV1), and Magnaporthe oryzae chrysovirus 1 (MoCV1) detected in *M. oryzae* from each area of Japan. Each inner circle indicates the number of *M. oryzae* strains infected with MoV2 (orange), MoPV1 (blue), and/or MoCV1 (green). Overlapping circles indicate multiple infections. The outer circles indicate the numbers of *M. oryzae* strains that had none of these mycoviruses.

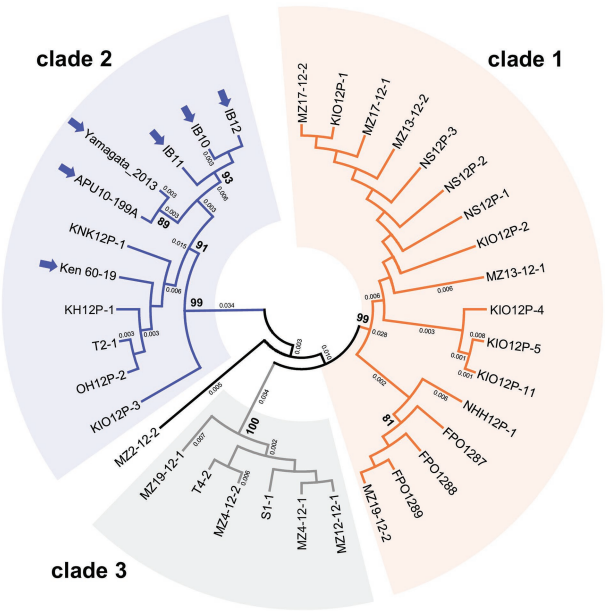

FIGURE 3 | An unrooted phylogenetic tree, inferred by the Maximum Likelihood method based on the Kimura 2-parameter model (Kimura, 1980), was constructed using partial nucleotide sequences (371 bp) of the RNA-dependent RNA polymerase (RdRp) coding domain in 35 MoV2 isolates from Japan. Numbers at nodes represent bootstrap values calculated from 1,000 replicates, and smaller numbers indicate genetic distances. Bootstrap values less than 70% are not shown. Each MoV2 isolate is indicated by the name of its host *M. oryzae* strain. MoV2 isolates from other regions (see **Supplementary Table S2**) are indicated by arrows.

the RdRp coding domain. Among the 35 MoV2 isolates examined, there were three tentative clades with high bootstrap support (**Figure 3**). MoV2 isolates from the Kyusyu region were present in all three clades. On the other hand, all MoV2 isolates from other regions (shown by arrows in **Figure 3**) belonged to "clade 2," along with some isolates from the Kyushu region. Almost the same result was shown in partial nucleotide sequences (394 bp) from the CP coding domain (**Supplementary Figure S1**). The phylogenetic tree revealed no clear clustering patterns based on geographic region or co-infection status within the Kyushu population (**Supplementary Figure S2**). However, some clustering based on geographical location was visible among the MoV2 isolates from other regions. The MoV2 isolates from two *M. oryzae* strains, APU10-199A, and Yamagata 2013 (both from northern Japan), and from three other *M. oryzae* strains, IB10, IB11, and IB12 (from the middle of the northeastern area of Japan), formed distinct subclades within "clade 2" (**Figure 3**).

For the phylogenetic analysis of the MoPV1 isolates, we used 466 bp partial nucleotide sequences of the RdRp coding domain. Among the 24 isolates tested, there were no well-supported clusters (**Supplementary Figure S3**). The MoPV1 isolate (GenBank Accession no. KX119172) in the Chinese *M. oryzae* strain NJ20 was slightly separated from the Japanese isolates, although they all showed high sequence identities, with greater than 96.8% identity at the nucleotide level and greater than 97.4% identity at the amino acid level.

Population Genetic Parameters and Neutrality Tests of MoV2 and MoPV1

The population genetic parameters for the two viruses based from partial sequence sets showed that the MoV2 isolates were more genetically variable than the MoPV1 isolates (**Table 1**). For example, the nucleotide diversity (π) and haplotype diversity (Hd) of RdRp coding domain among the MoV2 isolates (π = 0.04486, Hd = 0.928) were considerably higher than those of MoPV1 (π = 0.00397, Hd = 0.605). High nucleotide diversity and haplotype diversity were also shown in CP coding domain among the MoV2 isolates (π = 0.03837, Hd = 0.954). The d_N/d_S ratios were less than 1 for both MoV2 and MoPV1 (**Table 1**), suggesting that both viruses underwent purifying selection. The similar nucleotide diversity and low d_N/d_S ratios were calculated from full length of MoV2 sequences (**Supplementary Table S3**).

Demographic forces on the MoV2 and MoPV1 populations were estimated using *D* statistics of Tajima (1989) and *D* and *F* statistics of Fu and Li (1993) (**Table 2**). These tests gave positive but not significant values for the MoV2 population and significantly negative values for the MoPV1 population. Positive values with these statistics indicate the occurrence of balancing selection, suggesting a decrease in population size, and negative values indicate a low frequency of polymorphisms and the occurrence of purifying selection, suggesting an increase in population size. The significantly negative values for the MoPV1 population suggest that their population size tends to increase.

Sequence Properties of Three MoV2 Isolates

To examine whether the genome structures of the MoV2 isolates detected in this study are similar to those of the previously reported MoV2 isolates from *M. oryzae* strains Ken 60-19 (Maejima et al., 2008) and APU10-199A (Higashiura et al., 2019), we sequenced the entire MoV2 genomes from the *M. oryzae*

TABLE 1 | Population genetic parameters for the partial RdRp and coat protein (CP) sequences of MoV2 and MoPV1.

Virus	Gene	*n*	Net sites	*S*	*h*	π	Hd	d_N	d_S	d_N/d_S
MoV2	RdRp	35	366	47	19	0.04486	0.928	0.0054	0.1703	0.0317
MoV2	CP	32	394	47	20	0.03837	0.954	0	0.1354	0
MoPV1	RdRp	24	466	16	7	0.00397	0.605	0.0009	0.0118	0.0763

n, number of isolates examined; Net sites, length of sequence (excluding sites with gaps and missing data); S, number of polymorphic sites; h, number of haplotypes; π, nucleotide diversity; Hd, haplotype diversity; d_N, nonsynonymous rate; d_S, synonymous rate.

TABLE 2 | Neutrality test for partial RdRp and CP sequences of MoV2 and MoPV1.

Virus	Gene	*n*[a]	Net sites[b]	Tajima's *D*	Fu and Li's *D*	Fu and Li's *F*
MoV2	RdRp	35	366	1.58983 ns	0.43511 ns	0.97952 ns
MoV2	CP	32	394	1.08626 ns	−0.14516 ns	0.31312 ns
MoPV1	RdRp	24	466	−2.02511*	−2.94973*	−3.11718*

[a]*Number of isolates.*
[b]*Length of sequence (excluding sites with gaps and missing data).*
**p < 0.05.*

TABLE 3 | Pairwise comparisons of complete nucleotide sequences between three tested MoV2 isolates and two reference isolates.

MoV2 tested isolate[a]	MoV2 reference isolates[a]	Identity (%)
NHH12P-1	Ken 60-19	94.0
	APU10-199A	93.9
MZ4-12-2	Ken 60-19	94.6
	APU10-199A	94.5
MZ13-12-1	Ken 60-19	93.9
	APU10-199A	93.8

[a]*The names are those of the host M. oryzae strains.*

strains NHH12P-1, MZ4-12-2, and MZ13-12-1, which all came from the Kyushu region. The complete sequences consisted of 5,194 or 5,197 nucleotides and contained two open reading frames (ORFs). BLAST searches[1] revealed significant identities (>93.8%) between each of the three new MoV2 isolates and the isolates from Ken 60-19 and APU10-199A (**Table 3**). All the MoV2 isolates have the same lengths of 5′-untranslated region (275 nt) and 3′-untranslated region (63 nt). In all isolates, ORF1 has 2,367 nt, encoding a 788 aa coat protein. ORF2 encodes the RdRp; in the isolates from NHH12P-1 and MZ4-12-2, this gene consists of 2,493 nt encoding a protein of 830 aa, and in the isolate from MZ13-12-1, the gene has 2,496 nt, encoding a protein of 831 aa (**Supplementary Table S4**). In all three new isolates of MoV2, the termination codon of ORF1 overlaps the initiation codon of ORF2 in the tetranucleotide AUGA. This is also the case for the isolate from Ken 60-19, but in the isolate from APU10-199A, the ORFs overlap in an octonucleotide sequence, AUGAUUGA.

A Comparison Between MoV2 Infected and Cured *M. oryzae* Strains

Even though MoV2 is widely distributed in Japan, its effects on the host had not been examined. To investigate the effects of MoV2 infection on host virulence, we evaluated the biological characteristics of the *M. oryzae* strain Ken 60-19, which is solely infected with MoV2, and Ken 60-19-VC, which is an MoV2-cured variant of Ken 60-19 (**Supplementary Figure S4**). Mycelial growth rates on PDA medium were not significantly different between Ken 60-19 and Ken 60-19-VC (**Figure 4A**), and there were no obvious differences in pigmentation or morphology of the aerial mycelia (**Supplementary Figures S5A**,**B**). Similar lesions were observed after spray-inoculation tests, with 100% of the lesions in plants infected by Ken 60-19 being scored as susceptible, and 94.9% of those in plants infected by Ken 60-19-VC being scored as susceptible (**Figure 4B**). However, the results of the leaf sheath inoculation tests demonstrated that the disease index scores were significantly different between plants infected with Ken 60-19 and those infected with Ken 60-19-VC (**Figure 4C**). In the Ken 60-19-infected plants, mycelial development inside the plant cells tended to be faster than in the plants infected with Ken 60-19-VC.

[1]https://blast.ncbi.nlm.nih.gov/Blast.cgi

DISCUSSION

In previous studies, three dsRNA viruses, MoV1, MoV2, and MoCV1, were found in *M. oryzae* strains from Japan (Yokoi et al., 2007; Maejima et al., 2008; Higashiura et al., 2019). In this study, we performed a comprehensive screening of dsRNA mycoviruses from *M. oryzae* for the first time, and detected MoV2 and MoCV1, but not MoV1, in *M. oryzae* in Japan. MoV1 and MoV2 were among the earliest mycoviruses to be identified in Japan, and were first reported almost half a century ago (Yamashita et al., 1971). It is possible that the MoV1 was not detected in this study because of its low prevalence and/or its localized distribution. The rates of infection with mycoviruses vary widely among species and regions, ranging from a few percent to over 90%. For example, Botrytis cinerea mymonavirus 1 (BcMyV1) was detected in only 0.8% of the tested *B. cinerea* strains in China (Hao et al., 2018). Schoebel et al. (2017) also reported a low prevalence (1.1%) of Hymenoscyphus fraxineus mitovirus 1 (HfMV1) infection in *H. fraxineus* in Japan, whereas its prevalence was much higher in Europe (78.7%), especially in Lithuania (92.9%). We mainly screened *M. oryzae* strains from the Kyushu and Hokuriku regions in Japan, and more extensive screening may

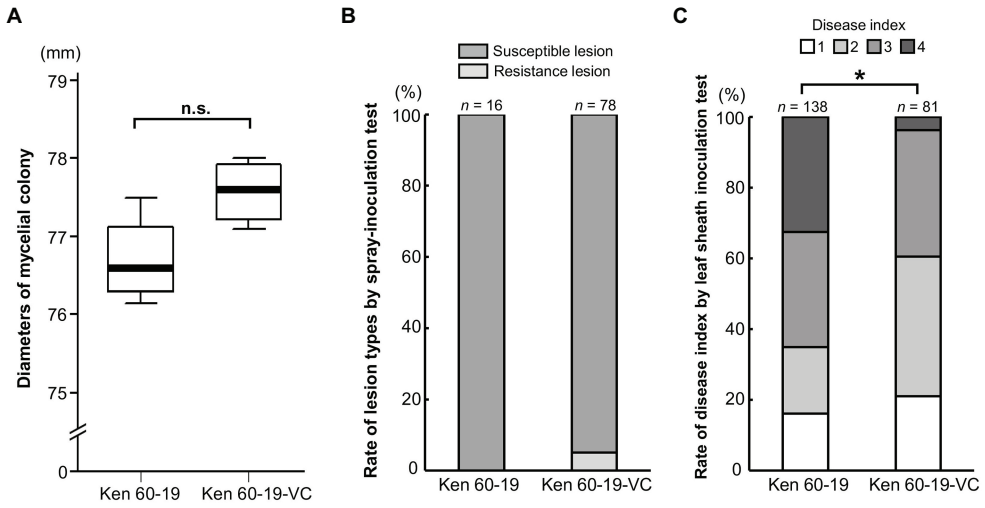

FIGURE 4 | Comparison of the MoV2-infected *M. oryzae* strain Ken 60-19 and its corresponding virus-cured strain Ken 60-19-VC. **(A)** Diameters of mycelial colonies grown on potato dextrose agar (PDA) medium at 25°C for 10 days ($n = 4$). No significant differences were observed by the paired *t*-test ($p = 0.0527$). **(B)** Percentages of rice blast lesion types on the rice cultivar Lijiangxintuanheigu (LTH) after a spray-inoculation test, at 7 days post inoculation. **(C)** Percentage of each disease index score in LTH after a leaf sheath inoculation test, at 48 h post inoculation. Significant differences were found based on the Wilcoxon rank sum test ($^*p = 0.0234$).

result in the re-detection of MoV1. It is also possible that the MoV1 population has diminished over the past half-century. There have been few studies of the long-term population dynamics of mycoviruses; however, some studies have suggested that their populations do change over time (Vainio et al., 2013; Bryner et al., 2014). Thus, the mycovirus population sizes in Japanese *M. oryzae* may have changed since MoV1 was first detected.

In addition to MoV2 and MoCV1, which have been reported from Japan previously, we also detected MoPV1 for the first time in Japan. The partial RdRp sequences showed over 96.8% identity with the reference sequence of a Chinese isolate (Du et al., 2016). Since the MoCV1 isolates has been found worldwide, including in Vietnam (MoCV1-A, -B; Urayama et al., 2010, 2014), China (MoCV1-C; Tang et al., 2015) and Japan (MoCV1-D; Higashiura et al., 2019), further investigations might lead to the detection of MoPV1 in other countries. In our electrophoresis analysis, we also found unclassified dsRNAs patterns other than those of MoV2, MoCV1, and MoPV1 (unpublished data). It is thus possible that we might discover new dsRNA mycoviruses from *M. oryzae* in Japan, by conducting next-generation sequencing analysis (e.g., Komatsu et al., 2016).

Among the 194 strains of *M. oryzae* tested in the present study, 127 strains (65.5%) were infected with MoV2, MoCV1, and/or MoPV1. The most prevalent of these three mycoviruses was MoPV1 (58.8%), followed by MoV2 (22.7%), and the least prevalent was MoCV1 (10.8%). These differences may be mainly explained by the different rates of vertical transmission with each mycovirus, because they have no extracellular phase and are transmitted only *via* host-dependent intracellular mechanisms (Ghabrial et al., 2015). A recent study revealed that the transmission rate of MoCV1-A *via* secondary conidia, whose production is induced by black light blue lamps after harvesting primary conidia, in the host strain S-0412-II 1a is about 80% (Aihara et al., 2018). Similar, less efficient transmission through conidia was reported for MoCV1-D in the *M. oryzae* strain APU10-199A (Higashiura et al., 2019). In contrast to MoCV1, MoV2 and MoPV1 are generally stably maintained in conidia, as revealed by single-spore isolation of the strain APU10-199A, which was co-infected with MoCV1, MoV2, and MoPV1 (Higashiura et al., 2019). MoCV1 may have reduced opportunities for vertical transmission, because infection with MoCV1 can severely decrease the production of conidia by the host fungus. In fact, a MoCV1-B-infected *M. oryzae* strain is unable to form conidia (Urayama et al., 2014). However, we cannot exclude the possibility that factors other than vertical transmission rates influence the prevalence of each mycovirus species. Indeed, although MoCV1 was the least prevalent among the three mycoviruses we examined, it was detected more frequently than MoV2 in the Hokuriku region (**Figure 2**). Aihara et al. (2018) suggested that MoCV1 could increase the fitness of its host *M. oryzae*, especially in specific rice lines containing a particular *R* gene, based on their finding that MoCV1 converted the host fungus from avirulent to virulent in the specific rice line. We could not carry out pathogenicity tests of the fungal strains screened in this study with different rice varieties. However, the improved fitness of the *M. oryzae* strain Ken 60-19 when infected with MoV2 suggests that this effect of MoV2 could contribute to its differing spatial distribution between the Kyushu and the Hokuriku regions.

We observed relatively high nucleotide and haplotype diversities in MoV2 compared with MoPV1 (**Table 1**). Based on the analysis of nonsynonymous and synonymous

substitution rates (**Table 1** and **Supplementary Table S3**), this high genetic diversity appeared to be mainly shaped by purifying selection, which has often been detected in genes of other mycoviruses (e.g., Botella et al., 2012; Schoebel et al., 2017). Moreover, although the MoV2 isolates from the Kyusyu region can be separated into three clades in the phylogenetic tree (**Figure 3**), we did not find any correlations related to the spatial distribution of MoV2 within the Kyushu region because the distribution areas of each clade were overlapped, and different clades of MoV2 were sometimes detected from same location (**Supplementary Figure S2**). Higashiura et al. (2019) reported that MoV2 is rarely transmitted horizontally *via* hyphal fusion, in contrast to their extremely high vertical transmission rates through conidia. These results suggested that the MoV2 isolates in each clade evolved independently of those in the other clades and were distributed throughout the Kyushu region as their host *M. oryzae* has spread (Voth et al., 2006; Bryner et al., 2012). Therefore, the distribution of MoV2 is likely driven by the virulence-dependent distribution of its host, which changes depending on which rice cultivars, possessing different resistance genes, are grown. Considering that the combination of *M. oryzae* races and rice cultivars determines the distribution of MoV2, its patterns of diversity could be formed independently of geographical barriers. This hypothesis can also explain the difference in prevalence of MoV2 between the Kyushu and Hokuriku regions, because the composition of *M. oryzae* races differs between these regions (Kawasaki-Tanaka et al., 2016). On the other hand, we found that the phylogenetic relationships among some MoV2 isolates were closely correlated with their spatial distributions. Therefore, we cannot rule out the possibility that neutral mutations have been fixed randomly in some MoV2 populations. For example, the MoV2 isolates from the APU10-199A and Yamagata 2013 strains, both from the northern part of Japan, and those from IB10, IB11, and IB12 from the middle northeastern part of Japan formed two distinct subclades within clade 2. Moreover, all the MoV2 isolates other than those from the Kyushu region belong to the same clade. This might indicate some geographical clustering of the MoV2 populations on a large scale. However, our sample sizes other than from the Kyushu region were not large enough to confirm this assumption. Further experiments with more extensive screening combined with genetic analyses of both MoV2 and its host would shed further light on the population structure and evolutionary history of MoV2 in Japan.

The extremely low genetic diversity among the MoPV1 isolates implies that their population emerged recently, or that they have been subjected to strong bottlenecks. Furthermore, the detection of MoPV1 in two countries (China and Japan), its high prevalence in Japan, and its frequent co-infection with other mycoviruses (**Figure 2**) suggest that its population size is increasing. This notion is supported by the significant negative values in the neutrality test (**Table 2**).

We determined the complete nucleotide sequences of three MoV2 isolates from the Kyushu region and found that they all had two ORFs overlapping within the tetranucleotide AUGA (**Supplementary Table S4**). This pattern is conserved in many other victoriviruses (Ghabrial and Nibert, 2009; Li et al., 2011), and is present in the MoV2 isolate from Ken 60-19 (Maejima et al., 2008) but not in the isolate from APU10-199A (Higashiura et al., 2019). In the isolate from APU10-199A, the two ORFs overlap within the octonucleotide AUGAUUGA. Although the overlapping of two ORFs in an octonucleotide sequence is observed in some other victoriviruses (e.g., Park et al., 2005), to our knowledge, this is the first example of two overlapping patterns in one species in the genus *Victorivirus*. Despite the difference in overlapping lengths, the complete nucleotide sequences of the three MoV2 isolates determined in this study were all highly similar (ranging in identity from 93.8 to 94.6%) to those of the MoV2 isolates from both Ken 60-19 and APU10-199A (**Table 3**). All five isolates use the opal codon (UGA) as the stop codon in their overlapped sequences. Future research will address the relationships between the types of overlapping sequences and the phylogeny within each mycovirus species.

Almost all victoriviruses infect their natural hosts without any apparent symptoms; examples include Rosellinia necatrix victorivirus 1 and Alternaria alternata victorivirus 1 (Chiba et al., 2013a; Jamal et al., 2019). Exceptions include Helminthosporium victoriae virus 190S, which induces disease symptoms in its natural host *H. victoriae* (Xie et al., 2016). As with most other victoriviruses studied thus far, MoV2 infection did not induce any obvious symptoms in its *M. oryzae* host, nor did it significantly change the fungal pathogenicity in rice plants (**Figures 4A,B** and **Supplementary Figures S5A**,**B**). Interestingly, however, our leaf sheath inoculation test showed that the MoV2-infected *M. oryzae* tended to show increased mycelial growth within rice cells, as compared with the MoV2-cured fungus (**Figure 4C**). The *M. oryzae* strains TH 65-105 and Ken 60-19, in which MoV1 and MoV2 were originally detected, produced larger amounts of the phytotoxic secondary metabolite pyriculol than other tested strains (Sato, 1978). Moreover, high concentrations of pyriculol have been shown to cause increased mycelial growth of *M. oryzae* (Namai et al., 1996). Although the causal relationship between MoV2 infection and increased pyriculol production is unknown, it is possible that the larger amount of pyriculol due to MoV2 infection in Ken 60-19 lead to its faster mycelial growth compared with its MoV2-cured variant.

DATA AVAILABILITY STATEMENT

The datasets presented in this study can be found in online repositories. The names of the repository/repositories and accession number(s) can be found at https://www.ddbj.nig.ac.jp/, LC573905-LC573960 and LC586101-LC586127.

AUTHOR CONTRIBUTIONS

TT collected the materials and designed the study. YO and MA performed the experiments with academic and technical

assistance from TA. HM contributed to the DNA extractions and the virus-cured assays. YO and KK analyzed the data and wrote the first draft of the manuscript. All authors critically reviewed the manuscript and approved the final submission.

FUNDING

This work was supported by a Grant-in-Aid for Challenging Exploratory Research from the Japan Society for the Promotion of Science (26660033).

ACKNOWLEDGMENTS

The authors would like to express our gratitude to Dr. Kazuyuki Hirayae and Dr. Mami Takahashi, National Agriculture and Food Research Organization, for providing the *M. oryzae* strains from the Kyushu and Hokuriku regions, respectively.

SUPPLEMENTARY MATERIAL

The Supplementary Material for this article can be found online at: https://www.frontiersin.org/articles/10.3389/fmicb.2020.593784/full#supplementary-material

REFERENCES

Ai, Y. -P., Zhong, J., Chen, C. -Y., Zhu, H. -J., and Gao, B. -D. (2016). A novel single-stranded RNA virus isolated from the rice-pathogenic fungus *Magnaporthe oryzae* with similarity to members of the family *Tombusviridae*. *Arch. Virol.* 161, 725–729. doi: 10.1007/s00705-015-2683-9

Aihara, M., Urayama, S., Le, M. T., Katoh, Y., Higashiura, T., Fukuhara, T., et al. (2018). Infection by *Magnaporthe oryzae* chrysovirus 1 strain A triggers reduced virulence and pathogenic race conversion of it host fungus, *Magnaporthe oryzae*. *J. Gen. Plant Pathol.* 84, 92–103. doi: 10.1007/s10327-018-0766-7

Arakawa, M., Nakamura, H., Uetake, Y., and Matsumoto, N. (2002). Presence and distribution of double-stranded RNA elements in the white root rot fungus *Rosellinia necatrix*. *Mycoscience* 43, 21–26. doi: 10.1007/s102670200004

Botella, L., Tuomivirta, T. T., Vervuurt, S., Diez, J. J., and Hantula, J. (2012). Occurrence of two different species of mitoviruses in the European race of *Gremmeniella abietina* var. *abietina*, both hosted by the genetically unique Spanish population. *Fungal Biol.* 116, 872–882. doi: 10.1016/j.funbio.2012.05.004

Bruenn, J. A. (1993). A closely related group of RNA-dependent RNA polymerases from double-stranded RNA viruses. *Nucleic Acids Res.* 21, 5667–5669. doi: 10.1093/nar/21.24.5667

Bryner, S. F., Prospero, S., and Rigling, D. (2014). Dynamics of *Cryphonectria hypovirus* infection in chestnut blight cankers. *Phytopathology* 104, 918–925. doi: 10.1094/PHYTO-03-13-0069-R

Bryner, S. F., Rigling, D., and Brunner, P. C. (2012). Invasion history and demographic pattern of *Cryphonectria hypovirus 1* across European populations of the chestnut blight fungus. *Ecol. Evol.* 2, 3227–3241. doi: 10.1002/ece3.429

Chiba, S., Lin, Y. -H., Kondo, H., Kanematsu, S., and Suzuki, N. (2013a). A novel victorivirus from a phytopathogenic fungus, *Rosellinia necatrix*, is infectious as particles and targeted by RNA silencing. *J. Virol.* 87, 6727–6738. doi: 10.1128/JVI.00557-13

Chiba, S., Lin, Y. -H., Kondo, H., Kanematsu, S., and Suzuki, N. (2013b). Effects of defective interfering RNA on symptom induction by, and replication of, a Novel Partitivirus from a Phytopathogenic fungus, *Rosellinia necatrix*. *J. Virol.* 87, 2330–2341. doi: 10.1128/JVI.02835-12

Depierreux, D., Vong, M., and Nibert, M. L. (2016). Nucleotide sequence of *Zygosaccharomyces bailii* virus Z: evidence for +1 programmed ribosomal frameshifting and for assignment to family *Amalgaviridae*. *Virus Res.* 217, 115–124. doi: 10.1016/j.virusres.2016.02.008

Du, Y., He, X., Zhou, X., Fang, S., and Deng, Q. (2016). Complete nucleotide sequence of *Magnaporthe oryzae* partitivirus 1. *Arch. Virol.* 161, 3295–3298. doi: 10.1007/s00705-016-3025-2

Fu, Y. -X., and Li, W. -H. (1993). Statistical tests of neutrality of mutations. *Genetics* 133, 693–709

Ghabrial, S. A., Castón, J. R., Jiang, D., Nibert, M. L., and Suzuki, N. (2015). 50-plus years of fungal viruses. *Virology* 479–480, 356–368. doi: 10.1016/j.virol.2015.02.034

Ghabrial, S. A., and Nibert, M. L. (2009). *Victorivirus*, a new genus of fungal viruses in the family *Totiviridae*. *Arch. Virol.* 154, 373–379. doi: 10.1007/s00705-008-0272-x

Ghabrial, S. A., and Suzuki, N. (2009). Viruses of plant pathogenic fungi. *Annu. Rev. Phytopathol.* 47, 353–384. doi: 10.1146/annurev-phyto-080508-081932

Hao, F., Wu, M., and Li, G. (2018). Molecular characterization and geographic distribution of a mymonavirus in the population of *Botrytis cinerea*. *Viruses* 10:432. doi: 10.3390/v10080432

Hayashi, N., Kobayashi, N., Cruz, C. M. V., and Fukuta, Y. (2009). Protocols for the sampling of diseased specimens and evaluation of blast disease in rice. *JIRCAS Working Rep.* 63, 17–33.

Herrero, N., Dueñas, E., Quesada-Moraga, E., and Zabalgogeazcoa, I. (2012). Prevalence and diversity of viruses in the entomopathogenic fungus *Beauveria bassiana*. *Appl. Environ. Microbiol.* 78, 8523–8530. doi: 10.1128/AEM.01954-12

Higashiura, T., Katoh, Y., Urayama, S., Hayashi, O., Aihara, M., Fukuhara, T., et al. (2019). *Magnaporthe oryzae* chrysovirus 1 strain D confers growth inhibition to the host fungus and exhibits multiform viral structural proteins. *Virology* 535, 241–254. doi: 10.1016/j.virol.2019.07.014

Hollings, M. (1962). Viruses associated with a die-back disease of cultivated mushroom. *Nature* 196, 962–965. doi: 10.1038/196962a0

Illana, A., Marconi, M., Rodríguez-Romero, J., Xu, P., Dalmay, T., Wilkinson, M. D., et al. (2017). Molecular characterization of a novel ssRNA ourmia-like virus from the rice blast fungus *Magnaporthe oryzae*. *Arch. Virol.* 162, 891–895. doi: 10.1007/s00705-016-3144-9

Jamal, A., Sato, Y., Shahi, S., Shamsi, W., Kondo, H., and Suzuki, N. (2019). Novel victorivirus from a Pakistani isolate of *Alternaria alternata* lacking a typical translational stop/restart sequence signature. *Viruses* 11:577. doi: 10.3390/v11060577

Jiang, Y., Zhang, T., Luo, C., Jiang, D., Li, G., Li, Q., et al. (2015). Prevalence and diversity of mycoviruses infecting the plant pathogen Ustilaginoidea virens. *Virus Res.* 195, 47–56. doi: 10.1016/j.virusres.2014.08.022

Kawasaki-Tanaka, A., Hayashi, N., Yanagihara, S., and Fukuta, Y. (2016). Diversity and distribution of rice blast (*Pyricularia oryzae* Cavara) races in Japan. *Plant Dis.* 100, 816–823. doi: 10.1094/PDIS-04-15-0442-RE

Kimura, F. (1980). A simple method for estimating evolutionary rates of base substitutions through comparative studies of nucleotide sequences. *J. Mol. Evol.* 16, 111–120. doi: 10.1007/BF01731581

Komatsu, K., Katayama, Y., Omatsu, T., Mizutani, T., Fukuhara, T., Kodama, M., et al. (2016). Genome sequence of a novel victorivirus identified in the phytopathogenic fungus *Alternaria arborescens*. *Arch. Virol.* 161, 1701–1704. doi: 10.1007/s00705-016-2796-9

Kumar, S., Stecher, G., and Tamura, K. (2016). MEGA7: molecular evolutionary genetics analysis version 7.0 for bigger datasets. *Mol. Biol. Evol.* 33, 1870–1874. doi: 10.1093/molbev/msw054

Li, H., Havens, W. M., Nibert, M. L., and Ghabrial, S. A. (2011). RNA sequence determinants of a coupled termination-reinitiation strategy for downstream open reading frame translation in *Helminthosporium victoriae* virus 190S and other Victoriviruses (family *Totiviridae*). *J. Virol.* 85, 7343–7352. doi: 10.1128/JVI.00364-11

Li, C. X., Zhu, J. Z., Gao, B. D., Zhu, H. J., Zhou, Q., and Zhong, J. (2019). Characterization of a novel ourmia-like mycovirus infecting *Magnaporthe oryzae* and implications for viral diversity and evolution. *Viruses* 11:223. doi: 10.3390/v11030223

Lin, Y., Zhou, J., Zhou, X., Shuai, S., Zhou, R., An, H., et al. (2020). A novel narnavirus from the plant-pathogenic fungus *Magnaporthe oryzae*. *Arch. Virol.* 165, 1235–1240. doi: 10.1007/s00705-020-04586-7

Maejima, K., Himeno, M., Komatsu, K., Kakizawa, S., Yamaji, Y., Hamamoto, H., et al. (2008). Complete nucleotide sequence of a new double-stranded RNA virus from the rice blast fungus, *Magnaporthe oryzae*. *Arch. Virol.* 153, 389–391. doi: 10.1007/s00705-007-1101-3

Milgroom, M. G., and Cortesi, P. (2004). Biological control of chestnut blight with hypovirulence: a critical analysis. *Annu. Rev. Phytopathol.* 42, 311–338. doi: 10.1146/annurev.phyto.42.040803.140325

Morris, T. J., and Dodds, J. A. (1979). Isolation and analysis of double-stranded RNA from virus-infected plant and fungal tissue. *Phytopathology* 69, 854–858. doi: 10.1094/Phyto-69-854

Namai, T., Nukina, M., and Togashi, J. (1996). Effects of two toxins and derivative of one toxin produced by rice blast fungus on its infection to inner epidermal tissue of rice leaf sheath. *Ann. Phytopathol. Soc. Jpn.* 62, 114–118. doi: 10.3186/jjphytopath.62.114

Nerva, L., Ciuffo, M., Vallino, M., Margaria, P., Varese, G. C., Gnavi, G., et al. (2016). Multiple approaches for the detection and characterization of viral and plasmid symbionts from a collection of marine fungi. *Virus Res.* 219, 22–38. doi: 10.1016/j.virusres.2015.10.028

Nibert, M. L., Ghabrial, S. A., Maiss, E., Lesker, T., Vainio, E., Jiang, D., et al. (2014). Taxonomic reorganization of family *Partitiviridae* and other recent progress in partitivirus research. *Virus Res.* 188, 128–141. doi: 10.1016/j.virusres.2014.04.007

Ohkita, S., Lee, Y., Nguyen, Q., Ikeda, K., Suzuki, N., and Nakayashiki, H. (2019). Three ourmia-like viruses and their associated RNAs in *Pyricularia oryzae*. *Virology* 534, 25–35. doi: 10.1016/j.virol.2019.05.015

Okada, R., Ichinose, S., Takeshita, K., Urayama, S., Fukuhara, T., Komatsu, K., et al. (2018). Molecular characterization of a novel mycovirus in *Alternaria alternata* manifesting two-sided effects: down-regulation of host growth and up-regulation of host plant pathogenicity. *Virology* 519, 23–32. doi: 10.1016/j.virol.2018.03.027

Okada, R., Kiyota, E., Moriyama, H., Fukuhara, T., and Natsuaki, T. (2015). A simple and rapid method to purify viral dsRNA from plant and fungal tissue. *J. Gen. Plant Pathol.* 81, 103–107. doi: 10.1007/s10327-014-0575-6

Park, Y., James, D., and Punja, Z. K. (2005). Co-infection by two distinct totivirus-like double-stranded RNA elements in *Chalara elegans* (*Thielaviopsis basicola*). *Virus Res.* 109, 71–85. doi: 10.1016/j.virusres.2004.10.011

Pearson, M. N., Beever, R. E., Boine, B., and Arthur, K. (2009). Mycoviruses of filamentous fungi and their relevance to plant pathology. *Mol. Plant Pathol.* 10, 115–128. doi: 10.1111/j.1364-3703.2008.00503.x

R Core Team (2017). R: a language and environment for statistical computing. R Foundation for Statistical Computing, Vienna, Austria. Available at: https://www.R-project.org/ (Accessed June 22, 2020).

Rigling, D., and Prospero, S. (2018). *Cryphonectria parasitica*, the causal agent of chestnut blight: invasion history, population biology and disease control. *Mol. Plant Pathol.* 19, 7–20. doi: 10.1111/mpp.12542

Rozas, J., Ferrer-Mata, A., Sánchez-DelBarrio, J. C., Guirao-Rico, S., Librado, P., Ramos-Onsins, S. E., et al. (2017). DnaSP 6: DNA sequence polymorphism analysis of large data sets. *Mol. Biol. Evol.* 34, 3299–3302. doi: 10.1093/molbev/msx248

Sato, Z. (1978). "Studies on production of pyriculol by rice blast fungus, *Pyricularia oryzae*" in *Proceedings of the Association for Plant Protection of Hokuriku* 26, 86–88 (in Japanese).

Schoebel, C. N., Botella, L., Lygis, V., and Rigling, D. (2017). Population genetic analysis of a parasitic mycovirus to infer the invasion history of its fungal host. *Mol. Ecol.* 26, 2482–2497. doi: 10.1111/mec.14048

Schoebel, C. N., Prospero, S., Gross, A., and Rigling, D. (2018). Detection of a conspecific mycovirus in two closely related native and introduced fungal hosts and evidence for interspecific virus transmission. *Viruses* 10:628. doi: 10.3390/v10110628

Tajima, F. (1989). Statistical method for testing the neutral mutation hypothesis by DNA polymorphism. *Genetics* 123, 585–595.

Tang, L., Hu, Y., Liu, L., Wu, S., Xie, J., Cheng, J., et al. (2015). Genomic organization of a novel victorivirus from the rice blast fungus *Magnaporthe oryzae*. *Arch. Virol.* 160, 2907–2910. doi: 10.1007/s00705-015-2562-4

Thompson, J. D., Higgins, D. G., and Gibson, T. J. (1994). CLUSTAL W: improving the sensitivity of progressive multiple sequence alignment through sequence weighting, position-specific gap penalties and weight matrix choice. *Nucleic Acids Res.* 22, 4673–4680. doi: 10.1093/nar/22.22.4673

Urayama, S., Kato, S., Suzuki, Y., Aoki, N., Le, M. T., Arie, T., et al. (2010). Mycoviruses related to chrysovirus affect vegetative growth in the rice blast fungus *Magnaporthe oryzae*. *J. Gen. Virol.* 91, 3085–3094. doi: 10.1099/vir.0.025411-0

Urayama, S., Ohta, T., Onozuka, N., Sakoda, H., Fukuhara, T., Arie, T., et al. (2012). Characterization of *Magnaporthe oryzae* chrysovirus 1 structural proteins and their expression in *Saccharomyces cerevisiae*. *J. Virol.* 86, 8287–8295. doi: 10.1128/JVI.00871-12

Urayama, S., Sakoda, H., Takai, R., Katoh, Y., Le, T. M., Fukuhara, T., et al. (2014). A dsRNA mycovirus, *Magnaporthe oryzae* chrysovirus 1-B, suppresses vegetative growth and development of the rice blast fungus. *Virology* 448, 265–273. doi: 10.1016/j.virol.2013.10.022

Vainio, E. J., Piri, T., and Hantula, J. (2013). Virus community dynamics in the conifer pathogenic fungus *Heterobasidion parviporum* following an artificial introduction of a partitivirus. *Microb. Ecol.* 65, 28–38. doi: 10.1007/s00248-012-0118-7

Voth, P. D., Mairura, L., Lockhart, B. E., and May, G. (2006). Phylogeography of *Ustilago maydis virus H1* in the USA and Mexico. *J. Gen. Virol.* 87, 3433–3441. doi: 10.1099/vir.0.82149-0

Wang, Q., Mu, F., Xie, J., Cheng, J., Fu, Y., and Jiang, D. (2020). A single ssRNA segment encoding RdRp is sufficient for replication, infection, and transmission of ourmia-like virus in fungi. *Front. Microbiol.* 11:379. doi: 10.3389/fmicb.2020.00379

Xie, J., Havens, W. M., Lin, Y. H., Suzuki, N., and Ghabrial, S. A. (2016). The victorivirus Helminthosporium victoriae virus 190S is the primary cause of disease/hypovirulence in its natural host and a heterologous host. *Virus Res.* 213, 238–245. doi: 10.1016/j.virusres.2015.12.011

Yamashita, S., Doi, Y., and Yora, K. (1971). A polyhedral virus found in rice blast fungus, *Pyricularia oryzae* cavara. *Ann. Phytopathol. Soc. Jpn.* 37, 356–359. doi: 10.3186/jjphytopath.37.356

Yokoi, T., Yamashita, T., and Hibi, T. (2007). The nucleotide sequence and genome organization of *Magnaporthe oryzae* virus 1. *Arch. Virol.* 152, 2265–2269. doi: 10.1007/s00705-007-1045-7

Zhai, L. F., Zhang, M. X., Hong, N., Xiao, F., Fu, M., Xiang, J., et al. (2018). Identification and characterization of a novel hepta-segmented dsRNA virus from the phytopathogenic fungus *Colletotrichum fructicola*. *Front. Microbiol.* 9:754. doi: 10.3389/fmicb.2018.00754

Conflict of Interest: The authors declare that the research was conducted in the absence of any commercial or financial relationships that could be construed as a potential conflict of interest.

frontiers in Microbiology

ORIGINAL RESEARCH
published: 12 November 2020
doi: 10.3389/fmicb.2020.600775

The Signatures of Natural Selection and Molecular Evolution in Fusarium graminearum Virus 1

*Jeong-In Heo[1], Jisuk Yu[2], Hoseong Choi[3] and Kook-Hyung Kim[1,2,3]**

[1] Department of Agricultural Biotechnology, College of Agriculture and Life Sciences, Seoul National University, Seoul, South Korea, [2] Plant Genomics and Breeding Institute, Seoul National University, Seoul, South Korea, [3] Research Institute of Agriculture and Life Sciences, Seoul National University, Seoul, South Korea

Fusarium graminearum virus 1 (FgV1) is a positive-sense ssRNA virus that confers hypovirulence in its fungal host, *Fusarium graminearum*. Like most mycoviruses, FgV1 exists in fungal cells, lacks an extracellular life cycle, and is therefore transmitted during sporulation or hyphal anastomosis. To understand FgV1 evolution and/or adaptation, we conducted mutation accumulation (MA) experiments by serial passage of FgV1 alone or with FgV2, 3, or 4 in *F. graminearum*. We expected that the effects of positive selection would be highly limited because of repeated bottleneck events. To determine whether selection on the virus was positive, negative, or neutral, we assessed both the phenotypic traits of the host fungus and the RNA sequences of FgV1. We inferred that there was positive selection on beneficial mutations in FgV1 based on the ratio of non-synonymous to synonymous substitutions (d_N/d_S), on the ratio of radical to conservation amino acid replacements (p_{NR}/p_{NC}), and by changes in the predicted protein structures. In support of this inference, we found evidence of positive selection only in the open reading frame 4 (ORF4) protein of DK21/FgV1 (MA line 1); mutations at amino acids 163A and 289H in the ORF4 of MA line 1 affected the entire structure of the protein predicted to be under positive selection. We also found, however, that deleterious mutations were a major driving force in viral evolution during serial passages. Linear relationships between changes in viral fitness and the number of mutations in each MA line demonstrated that some deleterious mutations resulted in fitness decline. Several mutations in MA line 1 were not shared with any of the other four MA lines (PH-1/FgV1, PH-1/FgV1 + 2, PH-1/FgV1 + 3, and PH-1/FgV1 + 4). This suggests that evolutionary pathways of the virus could differ with respect to hosts and also with respect to co-infecting viruses. The data also suggested that the differences among MA lines might also be explained by mutational robustness and other unidentified factors. Additional research is needed to clarify the effects of virus co-infection on the adaptation or evolution of FgV1 to its environments.

Keywords: FgV1, positive selection, deleterious mutation, viral fitness, serial passage

OPEN ACCESS

Edited by:
Nobuhiro Suzuki,
Okayama University, Japan

Reviewed by:
Ken Komatsu,
Tokyo University of Agriculture and Technology, Japan
Huiquan Liu,
Northwest A&F University, China

***Correspondence:**
Kook-Hyung Kim
kookkim@snu.ac.kr

Specialty section:
This article was submitted to Virology, a section of the journal Frontiers in Microbiology

Received: *31 August 2020*
Accepted: *27 October 2020*
Published: *12 November 2020*

Citation:
Heo J-I, Yu J, Choi H and Kim K-H (2020) The Signatures of Natural Selection and Molecular Evolution in Fusarium graminearum Virus 1. Front. Microbiol. 11:600775. doi: 10.3389/fmicb.2020.600775

INTRODUCTION

Because they have small genomes and high mutation rates, RNA viruses usually form populations with high genetic variation. Such viral populations, which are known as quasispecies, maintain the balance between the continuous generation of mutations and the natural selection that acts on the mutants in relation to their fitness (Domingo and Holland, 1997). Researchers have therefore tried to understand the various evolutionary processes that shape the structure and fitness of viral populations. In this regard, mutation accumulation (MA) experiments have been conducted with several host–virus systems to determine the effects of spontaneous mutations on viral fitness (Elena et al., 2006). When viruses undergo consecutive transmission within their hosts, the effects of mutations arise in different ways depending on the size of the population (Domingo and Holland, 1997). If large population sizes are maintained, deleterious mutations are purged by natural selection, and beneficial mutations steadily increase in frequency over time to increase fitness. However, if a population experiences increased genetic drift under repeated bottleneck events during transmission, i.e., plaque-to-plaque transfer, fitness gradually decreases with the accumulation of deleterious mutations; this process is termed Muller's ratchet (Domingo and Holland, 1997; McCrone and Lauring, 2018).

Muller's ratchet has been widely studied via MA experiments for many RNA viruses that infect bacteria, animals, and plants (Elena et al., 2006). A study of bacteriophage φ6, for which this phenomenon was first demonstrated, revealed that the fitness of the virus was reduced by an average of 22% after 40 bottleneck passages as the result of plaque-to-plaque transfers (Chao, 1990). Similarly, the animal pathogens vesicular stomatitis virus, foot and mouth disease virus, and human immunodeficiency virus type 1 showed 38%, 35%, and 82% fitness loss after 20, 30, and 15 bottleneck passages, respectively (Duarte et al., 1992; Escarmís et al., 1996; Yuste et al., 1999). Among plant RNA viruses, tobacco etch virus experienced a 5% decline in fitness per passage for up to 11 passages (De la Iglesia and Elena, 2007). Although a few lineages experienced an increase in fitness, fitness decline has been the dominant phenomenon in various MA experiments with RNA viruses. Such sensitivity of RNA viruses to deleterious mutations (caused by their highly unstable replication systems along with the compactness of their genomes and the overlapping functions of their non-redundant genes) suggests that the fitness of RNA viruses will be dominated by purifying selection of deleterious mutations.

To date, four RNA mycoviruses (Fusarium graminearum virus 1–4, hereafter referred to as FgV1–4) of the plant-pathogenic fungus *Fusarium graminearum* have been discovered in South Korea (Chu et al., 2002, 2004; Cho et al., 2013). FgV1–4 were assigned to four families (Kwon et al., 2007; Yu et al., 2009, 2011; Li et al., 2019). We previously adapted FgV1–4 to the laboratory host, *F. graminearum* strain PH-1, in order to investigate the effects of virus infection on the biological characteristics and transcriptional alterations of the fungus (Lee et al., 2014). FgV1 and 2 cause hypovirulence, while FgV3 and 4 cause asymptomatic infection in their fungal host (Cho et al., 2013; Lee et al., 2014). Host transcriptome analysis revealed that phenotypic differences in PH-1were not always correlated with differential gene expression caused by FgV1–4 infections (Lee et al., 2014). Moreover, recent studies demonstrated that the transcriptional response of host RNA interference (RNAi)-related genes to infection by FgV1, FgV2, or FgV3 differed depending on which virus infected the host, and that FgV1 can interfere with the induction of RNAi-related genes to counteract host antiviral defense responses (Yu et al., 2018, 2020). However, researchers have yet to determine how these viruses adapt to their host and continuously maintain their own characteristics.

FgV1–4 were originally isolated from different host strains, i.e., FgV1 was isolated from *F. graminearum* strain DK21 (*F. boothii*; lineage 3), FgV2 from strain 98-8-60 (*F. asiaticum*; lineage 6), and FgV3 and FgV4 from strain DK3 (*F. graminearum sensu stricto*; lineage 7) (Lee et al., 2014). In addition, two viruses that share high sequence similarity with FgV1 or FgV2 have been recently isolated in China (hereafter referred to as FgV1-ch and FgV-ch9, respectively) (Zhang et al., 2020). Considering that the original host strains of FgV1–4 belong to different lineages in the *Fusarium graminearum* species complex (FGSG), a complex that includes eight and several additional phylogenetic lineages that cause Fusarium head blight (FHB), the potential of adaptive evolution in FgVs can be inferred (Amarasinghe et al., 2019). In this regard, the following question should be answered: Which evolutionary processes dominate FgV1 populations and consequently shape the structure and fitness of the populations?

Here, we conducted MA experiments to detect and quantify natural selection on FgV1 at the molecular level. We also introduced FgV2, FgV3, or FgV4 into FgV1-infected hosts to observe the effects of passages on FgV1 and to understand the changes in viral fitness caused by interactions between co-infecting viruses.

MATERIALS AND METHODS

Virus Infections and Fungal Cultures

All fungal host strains used in this study (**Table 1**; Lee et al., 2014) were stored in 25% (v/v) glycerol at −80°C and were reactivated on potato dextrose agar (PDA; Difco) plates. Fungal hosts infected with two viruses (PH-1/FgV1 + FgV2, 3, or 4) were obtained through hyphal anastomosis on PDA agar medium. Mycelial plugs taken from the interface region between two isolates infected respectively with FgV1 and FgV2, 3, or

TABLE 1 | MA lines subjected to serial passage.

MA line	Host strain	Virus infection	Generations selected for RNA-Seq
1	DK21	FgV1 (Single infection)	1st, 5th, 10th, and 15th
2	PH-1	FgV1 (Single infection)	1st, 5th, 10th, and 15th
3	PH-1	FgV1 and FgV2 (Multiple infection)	2nd, 6th, 11th, and 12th
4	PH-1	FgV1 and FgV3 (Multiple infection)	2nd, 6th, 11th, and 16th
5	PH-1	FgV1 and FgV4 (Multiple infection)	2nd, 6th, 11th, and 12th

4 (PH-1/FgV1 and PH-1/FgV2, 3, or 4) were subcultured on PDA medium. In case of FgV1 and 2, infection of each isolate grown from the mycelial plugs was confirmed by dsRNA profiles on 0.8% agarose gel after S1 nuclease and DNase I treatment, while in case of FgV3 and 4, infection was confirmed by a semi-quantitative RT-PCR. Fungal colonies were subcultured on complete medium (CM) agar plates and were incubated at 25°C. After infection by FgV1 was confirmed based on phenotype, each subculture was cultured in 50 ml of liquid CM at 25°C on an orbital shaker (150 rpm) for 5 days. Mycelia were harvested by filtration through Whatman 3MM filter paper, and were then washed with distilled water, pressed between paper towels to remove the excess water, and stored at −80°C (Lee et al., 2014). Stored mycelia were used for further experiments.

Total RNA Extraction, dsRNA Isolation, and Reverse Transcription-Polymerase Chain Reaction (RT-PCR)

Total RNA was extracted with RNAiso Plus (Takara Bio Inc.) according to the manufacturer's instructions with slight modifications, and was treated with DNase I (Takara Bio Inc.) to eliminate genomic DNA. RNA was precipitated by ethanol with 3M NaOAc and was suspended in DEPC-treated water and then examined by agarose gel (0.8%) electrophoresis. Due to low viral titers in FgV3 or FgV4 infected fungal strains, we performed RT-PCR with virus specific primer to determine existence of virus. To detect FgV3 and 4 infections, cDNAs were synthesized from 5 μg of RNA with GoScript reverse transcriptase (Promega) followed by PCR reactions with virus-specific primer sets for FgV3 and 4 (**Supplementary Table S1**). PCR reactions used synthesized cDNAs to detect the viruses and were performed with the following conditions for FgV3: one step at 94°C for 3 min; followed by 30 cycles at 94°C for 20 s, 58°C for 30 s, and 72°C for 30 s; and a final step at 72°C for 10 min. In the case of FgV4, the PCR conditions included one step at 94°C for 3 min; followed by 35 cycles at 94°C for 25 s, 58°C for 40 s, and 72°C for 30 s; and a final one step at 72°C for 10 min. Amplified PCR products were analyzed by 1.2% agarose gel electrophoresis. To detect FgV1 and 2, generally have high viral titers in fungal strains, dsRNAs were isolated from total RNA through S1 nuclease and DNase I treatment and were analyzed by 0.8% agarose gel electrophoresis.

Serial Passages in Fungal Hosts

Experimental evolution of FgV1 was promoted by consecutive vertical transmissions in two hosts, *F. graminearum* strains DK21 and PH-1. Vertical transmission of viruses was conducted by serial passaging in the FgV1-host (without or with other viruses, as indicated in **Table 1**), which included the following steps: (1) conidiation of the host in carboxymethyl cellulose (CMC) liquid medium; (2) isolation of single conidia infected by virus(es) in different MA lines (**Table 1**); and (3) confirmation of virus infection in each single isolate. In brief, mycelial blocks were placed in CMC and incubated at 25°C and 150 rpm for 5 days. In the next step, diluted conidial suspensions containing approximately 100 conidia per mL were spread on CM agar plates, and the plates were incubated at 25°C for at least 24 h until the conidia germinated. After single conidia were transferred to CM agar plates, infection of FgV1 was first confirmed by the phenotype of the fungal colony produced by each conidium. Each colony was placed in liquid CM to obtain mycelia for total RNA extraction. Co-infection by FgV1 and 2 was confirmed by dsRNA profiles on 0.8% agarose gel after S1 nuclease and DNase I treatment. Co-infection by FgV1 and 3 and by FgV1 and 4 was confirmed by a semi-quantitative RT-PCR. Among isolates for which single infections (MA lines 1 and 2) or multiple infections (lines 3, 4, and 5) were confirmed, three isolates were randomly chosen per line and placed on CMC to obtain conidia of the next generation.

Extraction of Total RNA and RNA-Sequencing Analysis

For RNA-sequencing, fungal isolates were grown, harvested, and stored as described in the previous section. Three single conidial isolates, where single or co-infection was confirmed by the aforementioned methods, were randomly chosen from each generation of each line (three biological replicates), and used for RNA-sequencing. After each isolate was cultured three times and harvested separately, total RNA was extracted from each of the three replicate cultures (three technical replicates), mixed to constitute one total RNA sample of one isolate, and used for RNA-Sequencing. Total RNAs were extracted from ground mycelia using the easy-spin^{TM} Total RNA Extraction Kit (iNtRON Biotechnology) according to the manufacturer's instructions. Extracted total RNAs were treated with DNase I (Takara Bio Inc.) to eliminate genomic DNA. Pair-end mRNA libraries were generated using the TruSeq^{TM} Stranded mRNA kit and were sequenced using Illumina NovaSeq6000 platforms at Macrogen (Seoul, South Korea).

Analysis of SNPs of FgV1 Using Transcriptome Data

SNP analysis for FgV1 was conducted as previously described (Jo et al., 2018). In the current study, we mapped the raw sequence reads for each transcriptome to the complete sequence of FgV1 (NC_006937.2) using the BWA program. The SAM files obtained by BWA mapping were converted to BAM files using SAMtools (Li et al., 2009). With the mpileup function of SAMtools, we generated VCF files from the sorted BAM files. Finally, we applied BCFtools to identify the SNPs.

Statistical Analyses

Sequences of each open reading frame (ORF) containing SNPs were aligned using MUSCLE software[1] (Okonechnikov et al., 2012), and phylogenetic trees were reconstructed with the neighbor-joining method implemented with Unipro UGENE software[2] (Okonechnikov et al., 2012). With the multiple sequence alignments obtained as described above, the site-specific models (Nielsen and Krogh, 1998) that allow the

[1]http://ugene.net/

[2]http://ugene.net/

d_N/d_S (hereafter referred to as ω) ratio to vary among sites but not among lineages were implemented by CodeML in the PAML (Phylogenetic Analysis by Maximum Likelihood) package of programs (Yang, 1997). After observed data were fit under models M1 (nearly neutral model), M2 (positive selection model), M7 (beta), and M8 (beta and omega > 1), the goodness-of-fit of each model was determined by calculation of log-likelihoods. Based on log-likelihoods, M1 with two classes of codons (ω = 0 for conserved sites and ω = 1 for neutral sites) was compared to M2 with an additional class of codons with ω estimated from the data allowed to be greater than 1. Likewise, M7 with ω ratios under a beta distribution was compared to M8 with an additional class of codons with ω allowed to be greater than 1 (Swanson and Aquadro, 2002). Statistically significant evidence of positive selection was inferred by a likelihood ratio test (LRT) that compared twice the log-likelihood difference (2ΔlnL) between two models which is assumed to be under the χ^2 distribution with df = 2 (Wang et al., 2014). The null hypothesis was that a simpler model with no consideration of positive selection, i.e., M1 or M2, best fit the observed data. If the null hypothesis was rejected by LRTs, we concluded that M2 or M8 fit the observed data significantly better than M1 or M7; this would indicate that there was positive selection among compared sequences.

To calculate *pNR/pNC* ratios, all possible amino acid replacements were classified according to two widely used criteria, i.e., charge and polarity. The ratio of the number of radical amino acid replacements per radical non-synonymous site, the proportion of radical non-synonymous substitutions (*pNR*) and the number of conservative amino acid replacement changes per conservative non-synonymous site, and the proportion of conservative non-synonymous substitutions (*pNC*) were calculated with the HON-NEW program[3], which uses a modification of the previous method (Hughes et al., 1990) by taking the transition bias into account.

In a second method to assess positive selection, we examined the overall tendency in the type of amino acid replacements caused by non-synonymous mutations. Such a tendency is determined by the *pNR/pNC* ratio, i.e., the ratio of the number of radical amino acid replacements per radical non-synonymous site (the proportion of radical non-synonymous substitutions; *pNR*) to the number of conservative amino acid replacement changes per conservative non-synonymous site (the proportion of conservative non-synonymous substitutions; *pNC*). When *pNR* = *pNC*, we can infer that amino acid replacements take place at random with respect to the property of amino acids and that there is no selection under neutral evolution. When *pNR* < *pNC*, the replacements conserve the property under purifying selection. However, when *pNR* > *pNC*, the replacements promote radical changes in the property under positive selection (Swanson and Aquadro, 2002).

Prediction of Protein Structures

The structures of proteins from sequences with different combinations of mutations found in each replicate were predicted using the I-TASSER Server[4] and were compared to the wild type and to one another using the PyMOL program[5].

RESULTS

Changes in Biological Traits During Passages

As shown in **Table 1**, passaging was conducted with isolates infected with a single virus (MA lines 1 and 2) or with two viruses (MA lines 3, 4, and 5) for at least 12 generations to observe the effect of spontaneous mutations. Passaging of MA lines 3 (PH-1/FgV1 + 2) and 5 (PH-1/FgV1 + 4) was conducted for 12 generations (the co-infection by two viruses was not maintained after the 12th generation), and replicates from the 2nd, 6th, 11th, and 12th generations were selected. Because of the hypovirulence conferred by FgV1 on both host strains, the phenotypes of the host fungi in the 1st generation of the MA lines 3, 4, and 5 were indistinguishable from each other (**Figure 1A**). Throughout serial passaging up to the 15th, 12th, or 16th generation (for lines 3, 5, and 4, respectively), the phenotypes of both host strains singly infected with FgV1 (MA lines 1 and 2) were generally maintained with a slight decrease in mycelial growth and with slight variation between replicates in each generation (**Figures 1B,C**). PH-1 strain infected with FgV1 + FgV2, 3, or 4 (MA lines 3, 4, and 5) exhibited a few differences relative to the other MA lines. In the case of MA line 3 (PH-1/FgV1 + 2) (**Figure 1D**), variation among replicates of the same generation were greater than for other MA lines. Observation of dsRNA accumulation among biological replicates in the same generation of MA line 3 showed variation of dsRNA accumulation (**Supplementary Figure S1**). Also, colony morphologies of virus-infected isolates in MA line 3 exhibited unstable and irregular growth in the 11th and 12th generations (**Figure 1D**). While the phenotype was more regular at earlier and later generation for MA line 5 (PH-1/FgV1 + 4) than for the singly infected line (**Figures 1C,F**), some isolates in MA line 4 (PH-1/FgV1 + 3) began to exhibit faster mycelial growth in the 7th generation (**Figure 1E**) than those infected with FgV1. The biggest differences in the phenotype of fast-growing isolates compared to that of virus-free isolates included scarce aerial mycelia and increased pigmentation. From the 11th generation of MA line 4, all the conidia spread on agar media grew into fast-growing isolates, and their changed phenotype was maintained until the last generation (**Figure 1E**).

FgV1 had a vertical transmission rate of 100% except for MA line 3 (PH-1/FgV1 + 2), for which the FgV1 vertical transmission rate decreased to 71% in the 11th generation and to 75% in the 12th generation (**Table 2**). However, there was no clear trend in the changes in vertical transmission rates for any of three other co-infected lines, but fluctuations in the transmission rate were substantial for FgV3 in co-infected MA line 4 (**Table 2**). Because the accumulation of FgV4 in co-infected MA line 5 was low according to semi-quantitative RT-PCR, FgV4 was not

[3]http://igem.temple.edu/labs/nei/

[4]http://zhanglab.ccmb.med.umich.edu/I-TASSER/

[5]https://pymol.org/2/

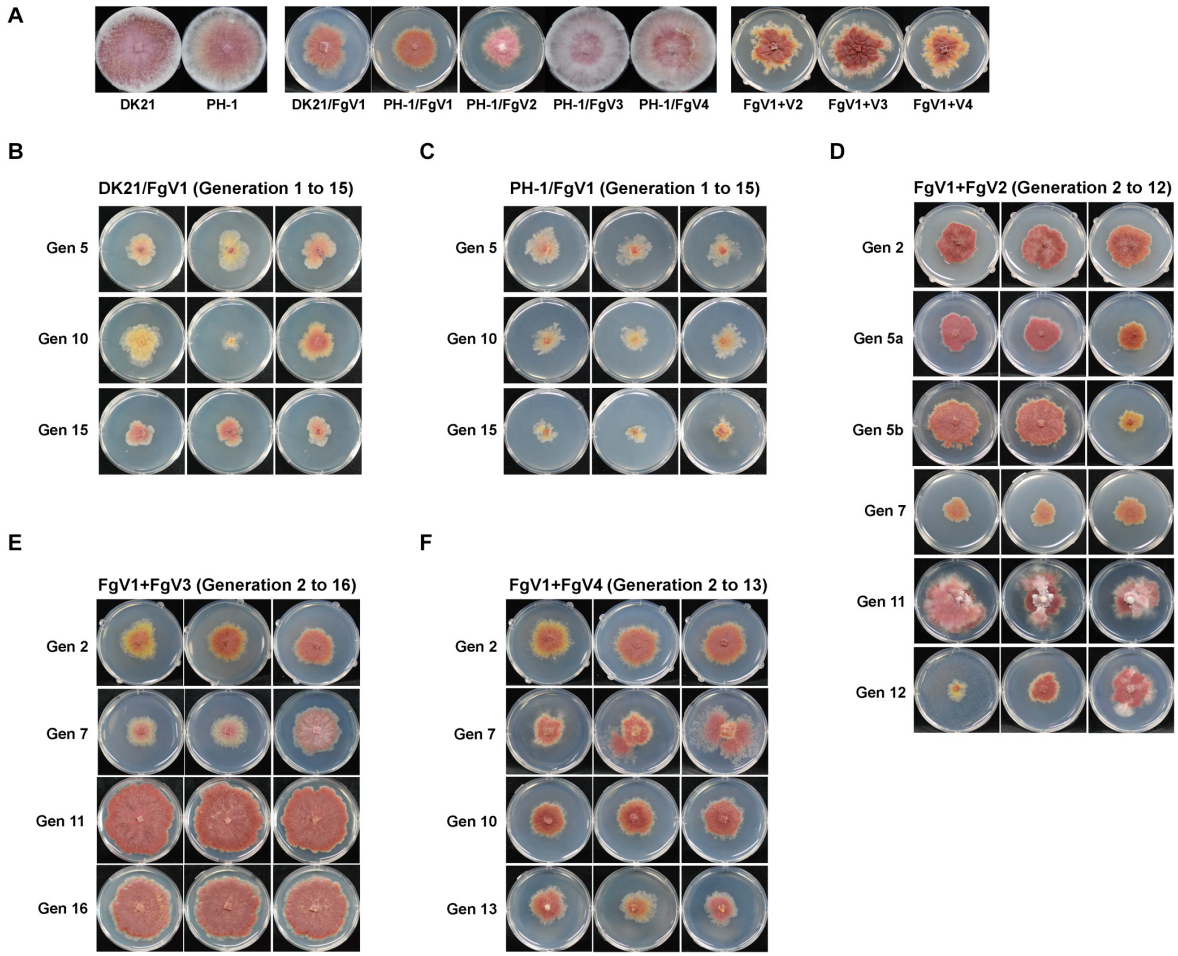

FIGURE 1 | Colony morphologies throughout passaging. **(A)** Colony morphology of virus-free and virus-infected fungal strains used for single conidia isolation in this study. Cultures were photographed after 5 days on CM. DK21/FgV1 (**B**; MA line 1), PH-1/FgV1 (**C**; MA line 2), PH-1/FgV1 + 2 (**D**; MA line 3), PH-1/FgV1 + 3 (**E**; MA line 4), and PH-1/FgV1 + 4 (**F**; MA line 5). **(B,C)** Gen 5, 10, and 15 indicate the 5th, 10th, and 15th generations, respectively. **(D)** Gen 5a shows morphologies of isolates infected with FgV1 + 2 in the 5th generation of MA line 3, while 5b shows the morphologies of isolates infected singly with FgV1, i.e., with no FgV2 transmitted from the previous generation. For Gen 12 of those isolates originally infected with FgV1 + 2, the two cultures on the left were infected only with FgV1, while the culture on the right was infected with both FgV1 and FgV2. **(B–F)** All cultures in were photographed 4 days after transfer of single conidia, except cultures of Gen 7 **(E)** were photographed 2 days after transfer to show their fast growth.

considered to have been transmitted to the last (13th) generation of MA line 5 (PH-1/FgV1 + 4) in the first replicate, which included 12 conidia (**Supplementary Figure S2**).

RNA-Sequencing

As noted earlier, we conducted passaging up to the 12th or 15th generation on each MA line, and three replicates from each of the indicated generations were subjected to RNA-Sequencing. The percentage of the total viral reads obtained from all generations of MA lines was higher for FgV1 than for the other viral strains (**Supplementary Table S2**). Observation of higher accumulation level of FgV1 viral dsRNA compared to that of other FgVs in fungal host could support high proportion of viral reads in MA lines (**Supplementary Figure S3**). All of the transcriptomic data have been deposited in NCBI data base (Accession: PRJNA656941, **Supplementary Table S3**).

Overview of Single-Nucleotide Polymorphisms

We first focused on the patterns of SNPs in the whole genome of FgV1 that differed with the host strains. We could not find a specific insertion/deletion polymorphism that occurred all of the MA lines. We did find synonymous and non-synonymous mutations unique to individual strains among virus(es)-infected PH-1 strains and several shared polymorphisms consistent with the provenance of each strain. In the overall distribution of synonymous and non-synonymous SNPs, FgV1 genomes with non-synonymous substitutions were more abundant than FgV1 genomes with synonymous substitutions in most generations of MA lines 1, 2, and 4 (**Figure 2**). MA line 3 had nearly equal non-synonymous and synonymous substitution rates along the entire genome of FgV1 except in the 5th generation. Proportions of non-synonymous vs. synonymous nucleotide substitutions were

TABLE 2 | Vertical transmission efficiency of FgV1–4.

Host strain	DK21	PH-1	PH-1					
Virus infection	FgV1	FgV1	FgV1 + FgV2		FgV1 + FgV3		FgV1 + FgV4	
MA line	1	2	3		4		5	
Generation[a]	FgV1	FgV1	FgV1	FgV2	FgV1	FgV3	FgV1	FgV4
1 (2)	1.00	1.00	1.00	0.96	1.00	0.83	1.00	0.96
5 (6)	1.00	1.00	1.00	0.96	1.00	0.75	1.00	0.71
10 (11)	1.00	1.00	0.71	0.86	1.00	0.83	1.00	0.58
15 (12 or 16)	1.00	1.00	0.75	1.00	1.00	0.21	1.00	0.46

[a]*Each value indicates the vertical transmission rate of each virus from the previous to the next generation. Generation numbers 1, 5, 10, and 15 apply to MA line 1 and 2, while generation numbers in parenthesis (2, 6, 11, 12, or 16) apply to MA line 3, 4, and 5.*

more variable in MA line 5 than in the other lines. We observed only one polymorphism located in the 5' UTR region (this was detected in the 1st generation of MA line 4), while the 3' UTR region seemed highly conserved in all of the MA lines. There were several mutations in MA line 1 (DK21/FgV1) that were not shared with any of the other four MA lines (PH-1/FgV1, PH-1/FgV1 + 2, PH-1/FgV1 + 3, and PH-1/FgV1 + 4), suggesting that evolutionary pathways of the virus could differ depending on the host. For the functional domains in each protein, there were a few mutations in RNA-dependent RNA polymerase (RdRp) and helicase domains, which are generally considered to be important for the survival of RNA viruses (Ranji and Boris-Lawrie, 2010; Choi, 2012).

Inference of Positive Selection Based on d_N/d_S and LRTs

Because the function of each domain and each ORF in FgV1 has not been clearly identified, we attempted to understand the patterns of spontaneous mutations based on statistical methods including d_N/d_S ratios, *pNR/pNC* ratios, and a series of likelihood-ratio tests (LRTs) (Yang, 1998). The models that assume that d_N/d_S ratios vary among sites were used to estimate d_N/d_S ratios and to detect evidence of positive selection on each codon (Nielsen and Krogh, 1998).

To predict genomic regions under positive selection, we calculated d_N/d_S and *pNR/pNC* ratios based on SNPs in each MA line. The altered sequences of each generation of each MA line used for the calculation of d_N/d_S and *pNR/pNC* ratios incorporated all of the substitutions from each of three replicates. ORF3 was excluded in this analysis because its low frequency of substitutions is insufficient for analysis by the PAML program. First, the d_N/d_S ratios for each MA line and each ORF were calculated using CodeML (Yang, 1997) and were used to infer overall selective pressures on each protein. Based on the assumption that d_N/d_S ratios < 1, $= 1$, and > 1 indicate negative selection, neutral evolution, and positive selection, respectively, there was no clear sign of positive selection in any ORF of any line. Next, positive selection on individual codons within each ORF was inferred by comparing two pairs of models based on LRTs using log-likelihood values for each model. M1 (nearly neutral model) was compared with M2 (positive selection model) and M7 (beta) was compared with M8 (beta & omega > 1) (**Table 3**). We performed a LRT at significance level $\alpha = 0.05$ to test the null hypothesis that a simpler model with no consideration of positive selection, i.e., M1 or M7, best fits the observed data. If the LRT statistic is greater than the critical value (5.991 for $P > 0.05$, df = 2), we rejected the null hypothesis and concluded that M2 or M8 fit the observed data significantly better than M1 or M7. As the null hypothesis was rejected only in case of ORF4 of MA line 1 (DK21/FgV1) with the LRT statistics of 6.00 (M1 vs. M2) and 6.01 (M7 vs. M8), respectively, we concluded that the signature of positive selection was found only in the ORF4 of MA line 1. Therefore, determination of the best-fitting models in each ORF and each MA line indicated the signature of positive selection only in the ORF4 of DK21/FgV1.

Identification of Positively Selected Sites

To localize specific amino acid sites in ORF4 involved in positive selection during serial passage of DK21/FgV1, we applied the

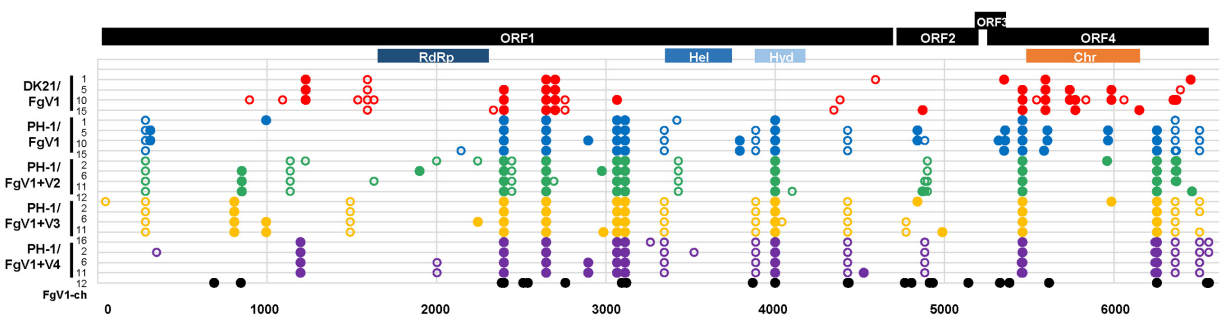

FIGURE 2 | Overview of single-nucleotide polymorphisms. Closed and open circles, respectively, indicate non-synonymous and synonymous SNPs identified by statistical analyses. All SNPs found in each consensus sequence of FgV1 obtained from raw sequence data of the three biological replicates in each generation of each MA line were incorporated and shown together in each row. RdRp, RNA-dependent RNA polymerase-like family; Hel, DEAD-like helicases superfamily; Hyd, P-loop containing nucleoside triphosphate hydrolases; Chr, chromosome segregation protein (provisional), based on the NCBI database. [In case of FgV1-ch (Accession: MT024571.1), only non-synonymous substitutions identified by the sequence alignment of FgV-ch and the reference sequence of FgV1 in the NCBI database are shown].

TABLE 3 | d_N/d_S and determination of best-fitting models based on LRT.

Region[a]	Number of amino acids	MA line	LRT statistic (−2ΔlnL)		Best-fitting model based on LRT		d_N/d_S under best-fitting model	
			M1 vs. M2	M7 vs. M8				
ORF1	1550	1	6E-06	−0.05	M1	M7	0.23	0.23
		2	4.38	4.47	M1	M7	0.52	0.60
		3	-6E-06	0.00	M1	M7	0.39	0.39
		4	3.46	3.47	M1	M7	0.57	0.60
		5	0.00	8E-06	M1	M7	0.52	0.52
ORF2	154	1-5	3.11	3.13	M1	M7	0.27	0.30
ORF4	429	1	2.11	2.11	M1	M7	1.00	1.00
		2	6.00	6.01	M2	M8	0.68	0.68
		3	1.39	−1.39	M1	M7	0.71	0.70
		4	0.00	0.00	M1	M7	0.96	0.96
		5	0.01	−0.01	M1	M7	0.59	0.58

[a] *−2ΔlnL = the negative of twice the log-likelihood difference between the two models; M1 = model 1, etc.*

Bayes empirical Bayes (BEB) method in CodeML[6] (Yang et al., 2005). In the ORF4 of MA line 1 (DK21/FgV1) where positive selection was inferred based on LRTs, the sites predicted to be selected for under M2 and M8 and estimates of parameters for each model are shown in **Table 4**. In addition, we calculated the allele frequency at each SNP site by calculating the mapped reads with substitution out of total mapped reads at a given site in each sample (**Supplementary Table S4**). The sites at ORF4 of MA line 1 that were predicted to be under positive selection with the highest posterior probabilities were those with amino acid replacements at 163A (P = 0.808 and 0.899 under M2 and M8, respectively) and 289H (P = 0.806 and 0.897, respectively), which were not shared in any of the other four MA lines. The replacements at 163A and 289H (nucleotide positions 5772 and 6150, respectively) in the ORF4 sequence brought critical changes in the entire protein structure in the 15th generation of MA line 1, while the structure predicted from the ORF4 sequence of the 10th generation of MA line 1 which only included the replacement at 163A showed no difference in the predicted structure compared that from the wild type. In line with this, the frequency (%) of a mutation at nucleotide position 5772 increased from 0.03449 in the 10th generation to 0.05133 in the 15th generation, along with the emergence of a mutation at nucleotide position 6150 in the 15th generation. The changes in the protein structure caused by replacements at 163A and 289H will further be investigated in the next section to build evidence of positive selection.

Inference of Natural Selection Based on the Properties of Amino Acid Replacements

We selected the two most widely used properties to classify amino acids, charge and polarity. After determining the criteria for classification, we calculated p_{NR}/p_{NC} for ORF1 and ORF4 of each MA line using the methods of Hughes et al. (1990) with the complete genome sequence of Fusarium graminearum virus 1, according to the NCBI database (Accession: NC_006937.2) which was used as a reference. With respect to charge changes, we found that no ORF in any of the five MA lines had a p_{NR} greater than pNC. With respect to polarity, however, pNR came close to or even exceeded p_{NC} in the ORF4 of some generations in all MA lines except MA line 4 (PH-1/V1 + 3) (**Table 5**). Therefore, natural selection seems to favor polarity changes while conserving the overall charge of amino acids. This result suggests that there was a signature of positive selection in ORF4 with respect to polarity, which had more frequent mutations than ORF1.

[6]http://abacus.gene.ucl.ac.uk/software/paml.html

TABLE 4 | Positively selected sites in ORF4 inferred based on CodeML.

Region	Best-fitting model	Parameter estimates under each model	Positively selected sites[a]
ORF4	M2	p0 = 0.94507, p1 = 0.00000, p2 = 0.05493 ω0 = 0.00000, (ω1 = 1.00000), ω2 = 12.3767	**163A (0.808), 289H (0.806)**
	M8	p0 = 0.94506, p = 0.00500, q = 2.86802 (p1 = 0.05494) ω = 12.36550	59V (0.570), 104K (0.554), 152A (0.564), **163A (0.899)**, 234E (0.554), **289H (0.897)**, 356E (0.561), 362A (0.558), 390N (0.549)

[a] *Numbers in parenthesis indicate probabilities of predicting each site to be under positive selection. The sites with a probability > 0.8 are in boldface.*

Comparison of Predicted Protein Structures

Protein structures for ORFs 1, 2, 3, and 4 with 18, 4, 3, and 17 amino acid substitution mutations, respectively, were compared. Each amino acid replacement was assigned to one of three groups based on the degree of change in protein structure (**Table 6**). For ORF1, all of the replacements caused minor changes in the protein structure and caused no changes in the ligand or enzyme-binding sites. For ORF2, although some replacements (41G→S, 41G→V) resulted in changes to the entire structure of the protein, the replacements were found in only one of three replicates in a generation, which may represent a low possibility of fixation in the population. For ORF3, only three replacements were found, and these did not result in any change in the secondary structure of the protein. For ORF4, replacements in four amino acid sites including 163A and 289H, which were predicted to be under positive selection, seemed to cause changes in the entire protein structure. When there were replacements at 163A and 289H in the ORF4 of MA line 1, the alpha helix structures covering about half of the protein at the N-terminal part were modified into coil structures (**Figure 3**, panel A for the wild type and panel B for imposed). This modification generated a new active site for enzyme binding (340Y) and slight alterations in ligand binding sites, which seems to indicate the addition of a function to the protein with the original functions maintained.

TABLE 5 | p_{NR}/p_{NC} ratio with respect to charge and polarity.

Property		Charge						Polarity					
Region		ORF1 (n = 1550)			ORF4 (n = 429)			ORF1 (n = 1550)			ORF4 (n = 429)		
Line	Gen	*r*	*c*	*r/c*	*r*	*c*	*r/c*	*r*	*c*	*r/c*	*r*	*c*	*r/c*
1	1	0.001	0.001	0.901	0.002	0.004	0.631	0.000	0.001	0.000	0.000	0.005	0.000
	5	0.001	0.001	0.601	0.002	0.005	0.422	0.000	0.002	0.000	0.003	0.005	0.600
	10	0.001	0.002	0.450	0.007	0.009	0.772	0.000	0.002	0.000	0.011	0.006	1.833
	15	0.001	0.001	0.601	0.002	0.005	0.425	0.000	0.002	0.000	0.003	0.005	0.600
2	1	0.000	0.003	0.000	0.000	0.002	0.000	0.001	0.002	0.500	0.000	0.002	0.000
	5	0.000	0.003	0.000	0.002	0.007	0.317	0.001	0.002	0.500	0.003	0.006	0.500
	10	0.001	0.003	0.257	0.002	0.009	0.254	0.001	0.003	0.333	0.006	0.006	1.000
	15	0.001	0.002	0.360	0.002	0.004	0.636	0.001	0.002	0.500	0.003	0.003	1.000
3	2	0.000	0.002	0.000	0.000	0.007	0.000	0.000	0.002	0.000	0.006	0.003	2.000
	6	0.001	0.003	0.258	0.000	0.005	0.000	0.001	0.003	0.333	0.003	0.003	1.000
	11	0.000	0.003	0.000	0.000	0.005	0.000	0.000	0.003	0.000	0.003	0.003	1.000
	12	0.000	0.003	0.000	0.000	0.005	0.000	0.000	0.003	0.000	0.003	0.003	1.000
4	2	0.001	0.002	0.328	0.002	0.004	0.631	0.000	0.003	0.000	0.000	0.005	0.000
	6	0.001	0.002	0.328	0.000	0.004	0.000	0.000	0.003	0.000	0.000	0.005	0.000
	11	0.001	0.003	0.241	0.000	0.004	0.000	0.001	0.003	0.333	0.000	0.005	0.000
	16	0.001	0.003	0.240	0.000	0.004	0.000	0.001	0.003	0.333	0.000	0.005	0.000
5	2	0.000	0.003	0.000	0.000	0.004	0.000	0.000	0.003	0.000	0.000	0.003	0.000
	6	0.000	0.003	0.000	0.000	0.004	0.000	0.000	0.003	0.000	0.000	0.003	0.000
	11	0.000	0.003	0.000	0.002	0.004	0.628	0.000	0.003	0.000	0.003	0.003	1.000
	12	0.000	0.004	0.000	0.002	0.004	0.628	0.000	0.004	0.000	0.003	0.003	1.000

Line: MA line; Gen: generation; n: number of amino acids; r: p_{NR}; c: p_{NC}.

TABLE 6 | Properties of amino-acid replacements based on changes in protein structures.

Region	Region and degree of change[a]								
	ORF1			ORF2			ORF4		
Degree[a]	1	2	3	1	2	3	1	2	3
Sites	251E→G 266V→A 314G→A 382T→S 392H→N 731P→S 782N→S 883M→L 948A→V 978S→P 1020L→F 1246A→D 1316V→I	616D→A 865A→V 975A→T 1005I→V 1490I→M	None	None	31L→S 80E→G	41G→S 41G→V	24F→L 57A→D 59V→L 101D→V 104K→R 152A→S 234E→K 362A→T 390N→D	108T→A 227D→G 323E→D 356E→V	12P→S 163A→T 225I→T 289H→Y

[a] *Degree of change: Amino acid replacements cause (1) no change in the structure of the protein; (2) a transition between the alpha helix and coil, which does not change the entire structure of a protein; or (3) changes in the entire structure of a protein.*

Also for ORF4, there were replacements at 12P in MA line 2 and at 225I in MA line 3 that resulted in changes to the entire structure of the protein (**Figure 3**, panels C and D). Unlike the replacements found in MA line 1, however, these replacements caused critical omissions in ligand binding sites and did not add new active sites. In addition, these replacements were not found in subsequent generations in each line, which might indicate that they had negative effects on the fitness of the virus and were therefore purged by purifying selection.

According to the NCBI database, ORF4 protein of FgV1 had the highest sequence similarity (27.2%) with a bacterial SMC-like (structural maintenance of chromosomes) domain (GenBank conserved domain TIGR02168) and with homologous proteins of other putative fusariviruses (Hrabáková et al., 2017),

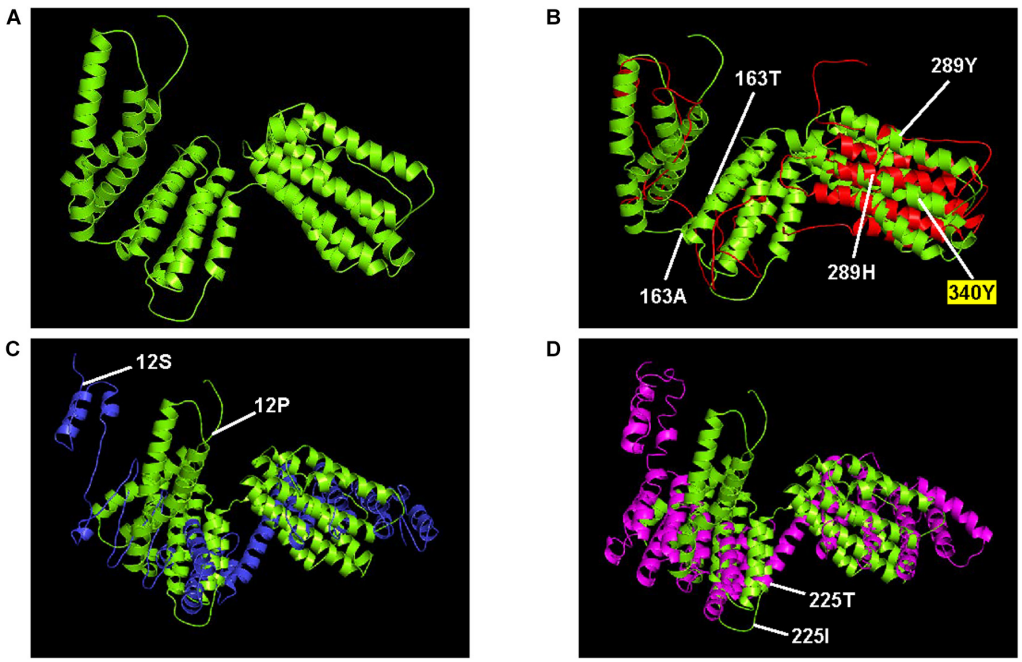

FIGURE 3 | ORF4 protein structures that were substantially changed during serial passage. The protein structure predicted from **(A)** the wild type (lime) are aligned with the structures predicted from **(B)** 15th generation of MA line 1 (red), **(C)** the 10th generation of MA line 2 (blue), and **(D)** the 2nd generation of MA line 3 (magenta). Also indicated are amino acid replacements predicted to change the entire structure of the protein (163, 289, 12, and 225), and the new active site for enzyme binding (340).

including ORF2 of Penicillium roqueforti ssRNA mycovirus 1 which showed the highest amino acid sequence identity (27.15%). As the SMC domain has been detected in similar positions on ORF2 (ORF4 in the case of FgV1) protein in most fusariviruses, the significance and function of this domain can be inferred from the function of the bacterial SMC domain, which, in prokaryotes, is proposed to be involved in the repair of DNA double-strand breaks (DSBs) and the maintenance of genome integrity (Pellegrino et al., 2012).

Relationship Between Viral Fitness and the Number of Mutations

Taking into account the selective pressures predicted based on d_N/d_S ratios and also the inferred presence of positively selected sites, we assumed that most of the mutations were neutral or deleterious. Based on this assumption, we expected that the fitness of FgV1 would gradually decline during passages. The fitness of the virus was estimated using two methods, i.e., real-time qRT-PCR, and the enumeration of viral RNA reads.

Figure 4 shows the fitness of FgV1 in each of four generations of the five MA lines. The results obtained by two methods did not exactly correspond to one another, but a similar pattern was found among some MA lines. In MA lines 1, 2, and 5, the fitness declined at least up to the 10th generation despite a sudden increase in the 15th generation of MA line 5 based on real-time qRT-PCR (**Figure 4A**) and in the MA line 2 based on the number of viral reads (**Figure 4B**). To determine whether the decline was related to the accumulation of deleterious mutations, the relationship between the fitness and the number of total or non-synonymous mutations was analyzed. First, we determined whether there was a linear relationship between the fitness and the number of total mutations; a negative linear relationship between the two fitness variables and the number of mutations was found only in MA line 2 (PH-1/FgV1) (**Figure 5**). When the number of non-synonymous mutations were used instead of total mutations, we obtained the same result but with slightly higher R^2 values (0.628 and 0.924). Next, we conducted correlation analyses to quantify the strength of the negative linear relationship, which confirmed the negative correlation between the fitness and the number of total mutations (correlation coefficient, $r = -0.78$ and -0.93, respectively, for the above two methods) and non-synonymous mutations ($r = -0.76$ and -0.96, respectively). Overall, the results suggest that although the total number of mutations may help explain the decline in viral fitness in MA line 2 (PH-1/FgV1), factors other than the total number of mutations appear to explain the decline in FgV1 fitness for MA lines 1 and 5.

DISCUSSION

This work represents a first study of fitness changes of a mycovirus caused by the accumulation of spontaneous mutations. When FgV1 was unaffected by other co-infecting viruses, we found that changes in FgV1 fitness during serial passage were dominated by neutral or deleterious mutations. This result is in agreement with previous findings from many

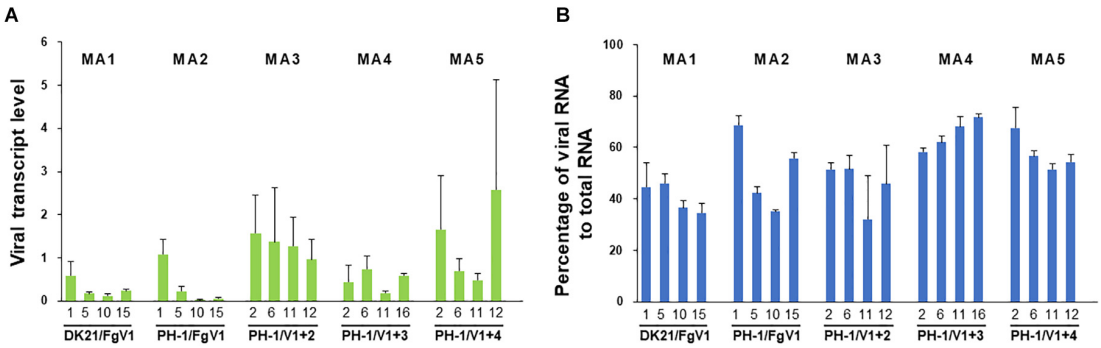

FIGURE 4 | Fitness of FgV1 estimated by **(A)** real-time PCR and **(B)** numbers of mapped viral reads. Numbers below each lane indicate the generations of each MA line.

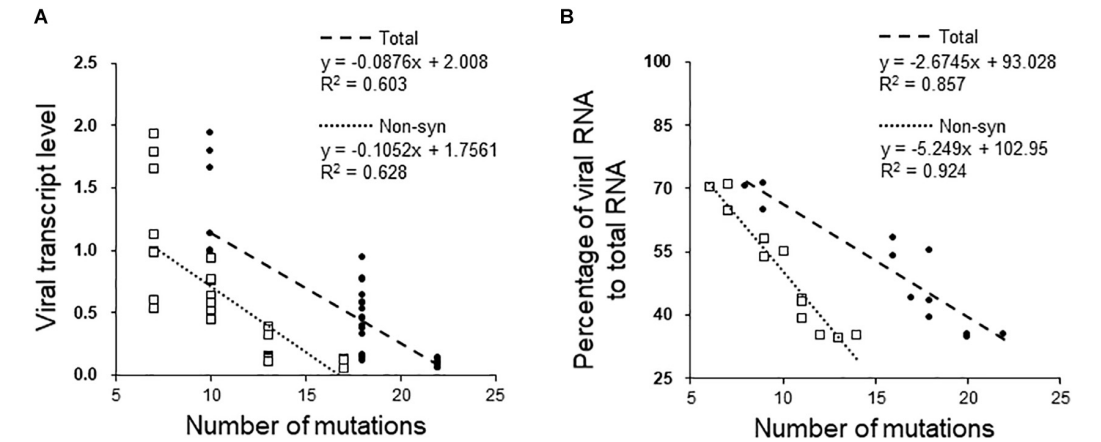

FIGURE 5 | Effects of mutations acquired by passaging on viral fitness in the MA2 line. Relationship between the fitness of FgV1 estimated by **(A)** real-time qRT-PCR and by **(B)** counting the number of mapped reads, and the number of total and non-synonymous mutations. Dotted and dashed lines indicate the linear regression between the fitness and the number of total (•) and non-synonymous (□) mutations, respectively.

other RNA viruses including bacteriophage φ6, VSV, FMDV, and HIV-1 (Chao, 1990; Duarte et al., 1992; Escarmís et al., 1996; Yuste et al., 1999). Despite biological differences among the virus-host systems, observed decreases in viral fitness seem to support the operation of Muller's ratchet under repeated bottleneck passages. We did also find evidence of positive selection on a few sites within the ORF4 of FgV1 as indicated by maximum-likelihood methods and predicted protein structures. Interestingly, several mutations in MA line 1 (DK21/FgV1) were not shared in any of the other four MA lines, including mutations at nucleotide positions 5772 and 6150 (with average mutation frequency percentage of 0.05133 and 0.04979, respectively, in three biological replicates of the 15th generation) which bring amino acid replacements at 163A→T and 289H→Y of ORF4 which were predicted to be under positive selection. This implies the possibility of different cellular mechanisms or immune responses of DK21 (*F. boothii*; lineage 3) and PH-1 (*F. graminearum*, lineage 7) against pathogens, which can be inferred, for instance, from the significantly high self-fertility of the strains of lineage 7 (Lee et al., 2012). Similarly, in the previous study on VSV under Muller's ratchet, bottleneck passages on a new host cells led to more regular and severe fitness losses than passages on the cells to which the virus strain used in the study had been well adapted for years (Duarte et al., 1992). In the present study, we found that a negative linear relationship between the fitness of FgV1 and the number of mutations was found only in PH-1, between two strains (DK21 and PH-1) infected singly with FgV1 and free from other co-infecting viruses. Assuming that FgV1 had been well adapted to its natural host, DK21, we can expect that negative effects of deleterious mutations which cause fitness losses will stand out in the natural host rather than in the laboratory host. Despite the high mutation rates of RNA viruses which contribute to their remarkable ability to adapt to fluctuating environments, this study and the previous studies found the great possibility of fitness decrease during repeated bottleneck events as a consequence of Muller's ratchet.

Factors Affecting Evolution—Mutational Robustness

One factor that might affect the evolution of a virus is its ability to deal with accumulated deleterious mutations, which account

for a large proportion of mutations in a small population with severe bottlenecks. Such an ability, which is termed mutational robustness, is defined as constancy of phenotype in the face of mutational perturbation and is critical for the adaptation of viruses to changing environments. In an MA experiment using the RNA virus phage φ6, researchers determined that variance in fitness was significantly lower for lines that evolved under lower levels of co-infection only in the short term (Montville et al., 2005). In the long term, however, a defective virus can buffer the negative effects of mutations through frequent genetic complementation at a high level of co-infection, which eventually enables defective viruses to propagate and thus decreases mutational robustness (Lauring et al., 2013). In this regard, the decreased robustness of viruses which obtained high levels of accumulated mutations under high levels of co-infection might explain the large variation in viral loads and host phenotypes among replicates in the 11th and 12th generations of PH-1/FgV1 + 2 (**Figures 2**, **5** and **Supplementary Figure S3**). This seems more convincing if one considers that the levels of viral RNA accumulation in the host fungi were higher for FgV1 and 2 than for FgV3 and FgV4.

Factors Affecting Evolution—Interaction Between Viruses

Within-host interactions between plant viruses have been widely studied. When two or more viruses infect the same host at the same time or within short intervals, the fitness of each virus depends not only on its own ability to adapt to the environment, but also on the activity of the other co-infecting virus(es). Unrelated viruses generally interact with each other in a synergistic manner, resulting in higher accumulations of the viruses and more severe symptoms in their hosts (Syller and Grupa, 2016). A synergistic interaction between mycoviruses has also been observed in a pathosystem involving *Sclerotinia sclerotiorum* and a hypovirulence-associated mycoreovirus, Sclerotinia sclerotiorum mycoreovirus 4 (SsMYRV4). In the latter case, SsMYRV4 suppressed non-self-recognition of its host by suppressing G-protein signaling pathways and thereby facilitated horizontal transmission of heterologous viruses between two fungal host strains that were otherwise vegetatively incompatible (Wu et al., 2017). Antagonistic interactions between co-infecting viruses, however, also occur and involve cross-protection and mutual exclusion (Syller and Grupa, 2016). Mutual exclusion has been frequently found in human parasites. With dengue virus, for example, virus titers and virus transmission were lower with infections by multiple virus strains than with infections by single virus strains (Pepin et al., 2008). The effects of interactions between FgV1 and the other co-infecting virus were not rigorously determined in the current study. Isolates of MA line 3 (PH-1/FgV1 + 2) showed unstable phenotypes and decreased vertical transmission of FgV1. In case of MA line 4 and 5 (PH-1/FgV1 + 3 and 1 + 4), however, the transmission of FgV1 was maintained, while the transmission of FgV3 and FgV4 decreased with fluctuations between generations. As demonstrated in the previous study on HIV-1, one of several mechanisms which may accelerate fitness losses induced by bottleneck passages is the level of virus titers. Titers from HIV-1 plaques, which were relatively lower than those from φ6, VSV and FMDV, seems to have further reduced the possibility of competition and compensatory mutations among quasispecies and resulted in relatively large fitness losses (Yuste et al., 1999; De la Iglesia and Elena, 2007). Besides, repeated transfers of large virus populations, represented by high level of virus titers, increased the fitness of the populations (Clarke et al., 1993). Since the numbers of viral genomes of FgV1 do not distinctly vary among MA lines 3, 4 and 5 in our pathosystem, we can expect that the ability of FgV1 to adapt to the environment would be influenced by other factors related to interactions between viruses, rather than the aforementioned possibility of competition, etc. When it comes to interactions between viruses, our previous study revealed that the dsRNA accumulation of FgV2 or FgV3 was higher in fungal transformed mutants expressing FgV1−encoded ORF2 than wild-type strains, because FgV1-encoded pORF2 was able to inhibit the host's antiviral RNA silencing responses by suppressing the transcription of FgDICER2 and FgAGO1 (Yu et al., 2020). Therefore, we expected that FgV1 might help accumulation or maintenance of co-infecting viruses, as shown by the synergistic effect of Cryphonectria hypovirus 1 (CHV1) on a co-infecting dsRNA virus, mycoreovirus 1 (MyRV1), represented by increased accumulation and vertical transmission of MyRV1 (Sun et al., 2006). The effect of interactions between FgV1 and the other co-infecting virus or the reason for aforementioned changes in the phenotype of MA line 4 has not been rigorously determined in the current study. However, tendency in dsRNA accumulation among biological replicates in the same generation of MA line 3 may support our assumption that there is an antagonistic, rather than synergistic, interaction between FgV1 and FgV2 (**Supplementary Figure S1**). In case of MA line 4 and 5, there was no evidence of beneficial effects of FgV1 on the vertical transmission or accumulation of its counterpart. On the contrary, especially in case of FgV4, its accumulation was often below the significant detection level in RT-PCR, which was not the case of isolates infected singly with FgV4 (**Supplementary Figure S2**), despite average vertical transmission ratio of around 60% during passaging of MA line 5 (data not shown). However, there is a possibility that FgV1-infected fungal host does not provide a favorable condition for FgV3 and FgV4 despite the host's antiviral activities inhibited by FgV1. Because we focused on the adaption and fitness of FgV1 in this study, further investigations are needed to clarify the effects of interactions between FgV1–4.

Effects of Host Species on the Evolution of Viruses

One concept widely used to evaluate evolutionary processes in a population is the distribution of fitness effects (DFE), which explains the proportion of new mutations that are advantageous, neutral, and deleterious and whether and how those effects alter the total fitness of the population. The shape of the DFE curve varies depending on species, population size, and other factors (Eyre-Walker et al., 2006). In a study of tobacco etch virus infecting eight susceptible host species, the characteristics

of the fitness effects of mutations differed between the natural host (along with its close relative) and the alternative hosts (Lalić et al., 2011). DFE therefore indicates the likelihood that a pathogen can cross the species barrier and successfully infect a new host (Lalić et al., 2011). The results of the current study suggest that the evolutionary trajectories of FgV?/FgV1–4? may differ among the lineages of FGSG. Both of the *F. graminearum* strains used in this study, DK21 (*F. boothii*; lineage 3) and PH-1 (*F. graminearum sensu stricto*; lineage 7), not only belong to the three most closely related lineages of FGSG, i.e., *F. graminearum*, *F. boothii*, and *F. asiaticum*, but also to the four lineages found to date in South Korea, i.e., *F. graminearum* (representing 75% of all isolates), *F. boothii* (12%), *F. asiaticum* (12%), and *F. meridionale* (1%) (Lee et al., 2012). In terms of their origin relative to plant hosts, however, *F. graminearum* mostly infects maize and is thought to have been introduced from the United States, while *F. boothii* seems to have originated from local populations infecting rice (Lee et al., 2012). It follows that despite the close phylogenetic relationship between PH-1 and DK21, their difference in host preference may be related to their differences in supporting spontaneous mutations of FgV1 and may also help explain why FgV1 has adapted so well to the laboratory environment.

A new asymptomatic strain FgV1-ch was recently isolated and characterized in China (Zhang et al., 2020). Interestingly, FgV1-ch did not show strong virulence to the host (PH-1), despite slight differences in the colony morphology, mycelial growth rate, and the production of conidia between FgV1-ch-infected and virus-free strains of PH-1 (Zhang et al., 2020). Regarding its sequence, FgV1-ch showed 95.91% nucleotide identities (6350/6621) with the reference sequence of FgV1 (Accession number; NC_006937.2) in the NCBI database, with 26 amino acid replacements (**Figure 2**). We found significant variation between the numbers of synonymous and non-synonymous substitutions in FgV1-ch as well as differences in the numbers of substitutions between FgV1-ch and the MA lines in the current study. With respect to the number of substitutions, one study with RNA and DNA viruses found a decline in the ratio of transitions to transversions (Ts/Tv) over time (Duchêne et al., 2015); the authors suggested that the decline could be caused by an underestimation of the Ts/Tv ratio due to the nature of RNA viruses, which rapidly attain mutational saturation. Likewise, variable genes might attain saturation more rapidly and thus display a stronger decline in Ts/Tv than conserved genes (Duchêne et al., 2015). In this context, the lower Ts/Tv ratio in ORF1 (6.9) than in ORF4 (11.0) along with the relatively higher concentration of substitutions in ORF1 (212 substitutions of 4653 nt) than in ORF4 (36 of 1290 nt) in FgV1-ch (Zhang et al., 2020) might reflect a rapid mutational saturation in ORF1 in the course of the evolution of the asymptomatic strain FgV1-ch in a different strain of the host fungus.

In a previous study, FgV1 was artificially transmitted via protoplast fusion to filamentous fungi of two different genera, *Cryphonectria parasitica* and *Fusarium oxysporum*, and was found to maintain its ability to induce hypovirulence in those species (Lee et al., 2014). Whether FgV1 can adapt to the more stringent environments in non-host species is an important question generated by the current study. Further comparisons of the genetic variation of FgV1 in non-hosts and natural hosts and of the modifications in the gene expression of those FgV1-infected hosts are needed to increase our understanding of factors affecting viral pathogenicity and evolution.

DATA AVAILABILITY STATEMENT

The datasets generated for this study can be found in the online repositories. The virus and virus-like sequences derived from this study can be found in GenBank under the accession number PRJNA656941.

AUTHOR CONTRIBUTIONS

J-IH and K-HK designed the experiments, analyzed the data, and wrote the manuscript. J-IH, JY, and HC performed the experimental work. All authors contributed to the article and approved the submitted version.

FUNDING

This work was supported in part by grants from the Korea Institute of Planning and Evaluation for Technology in Food, Agriculture and Forestry (120080-05-1-HD030), the Ministry of Agriculture, Food and Rural Affairs and the National Research Foundation (NRF-2020R1C1C1011779) funded by the Ministry of Education, Science, and Technology, South Korea. J-IH and HC were supported by research fellowships from the Brain Korea 21 Plus Project.

SUPPLEMENTARY MATERIAL

The Supplementary Material for this article can be found online at: https://www.frontiersin.org/articles/10.3389/fmicb.2020.600775/full#supplementary-material

REFERENCES

Amarasinghe, C., Sharanowski, B., and Fernando, W. (2019). Molecular phylogenetic relationships, trichothecene chemotype diversity and aggressiveness of strains in a global collection of *Fusarium graminearum* species. *Toxins* 11:263. doi: 10.3390/toxins11050263

Chao, L. (1990). Fitness of RNA virus decreased by Muller's ratchet. *Nature* 348, 454–455. doi: 10.1038/348454a0

Cho, W. K., Lee, K.-M., Yu, J., Son, M., and Kim, K.-H. (2013). Insight into mycoviruses infecting Fusarium species. *Adv. Virus Res.* 86, 273–288. doi: 10.1016/b978-0-12-394315-6.00010-6

Choi, K. H. (2012). Viral polymerases. *Viral Mol. Mach.* 726, 267–304.

Chu, Y.-M., Jeon, J.-J., Yea, S.-J., Kim, Y.-H., Yun, S.-H., Lee, Y.-W., et al. (2002). Double-stranded RNA mycovirus from *Fusarium graminearum*. *Appl. Environ. Microbiol.* 68, 2529–2534. doi: 10.1128/aem.68.5.2529-2534.2002

Chu, Y.-M., Lim, W.-S., Yea, S.-J., Cho, J.-D., Lee, Y.-W., and Kim, K.-H. (2004). Complexity of dsRNA mycovirus isolated from *Fusarium graminearum*. *Virus Genes* 28, 135–143. doi: 10.1023/b:viru.0000012270.67302.35

Clarke, D. K., Duarte, E. A., Moya, A., Elena, S. F., Domingo, E., and Holland, J. (1993). Genetic bottlenecks and population passages cause profound fitness differences in RNA viruses. *J. Virol.* 67, 222–228. doi: 10.1128/jvi.67.1.222-228.1993

De la Iglesia, F., and Elena, S. F. (2007). Fitness declines in Tobacco etch virus upon serial bottleneck transfers. *J. Virol.* 81, 4941–4947. doi: 10.1128/jvi.02528-06

Domingo, E., and Holland, J. (1997). RNA virus mutations and fitness for survival. *Annu. Rev. Microbiol.* 51, 151–178. doi: 10.1146/annurev.micro.51.1.151

Duarte, E., Clarke, D., Moya, A., Domingo, E., and Holland, J. (1992). Rapid fitness losses in mammalian RNA virus clones due to Muller's ratchet. *Proc. Natl. Acad. Sci. U.S.A.* 89, 6015–6019. doi: 10.1073/pnas.89.13.6015

Duchêne, S., Ho, S. Y., and Holmes, E. C. (2015). Declining transition/transversion ratios through time reveal limitations to the accuracy of nucleotide substitution models. *BMC Evol. Biol.* 15:36. doi: 10.1186/s12862-015-0312-6

Elena, S. F., Carrasco, P., Daròs, J. A., and Sanjuán, R. (2006). Mechanisms of genetic robustness in RNA viruses. *EMBO Rep.* 7, 168–173. doi: 10.1038/sj.embor.7400636

Escarmís, C., Dávila, M., Charpentier, N., Bracho, A., Moya, A., and Domingo, E. (1996). Genetic lesions associated with Muller's ratchet in an RNA virus. *J. Mol. Biol.* 264, 255–267. doi: 10.1006/jmbi.1996.0639

Eyre-Walker, A., Woolfit, M., and Phelps, T. (2006). The distribution of fitness effects of new deleterious amino acid mutations in humans. *Genetics* 173, 891–900. doi: 10.1534/genetics.106.057570

Hrabáková, L., Grum-Grzhimaylo, A. A., Koloniuk, I., Debets, A. J. M., Sarkisova, T., and Petrzik, K. (2017). The alkalophilic fungus *Sodiomyces alkalinus* hosts beta- and gammapartitiviruses together with a new fusarivirus. *PLoS One* 12:e0187799. doi: 10.1371/journal.pone.0187799

Hughes, A. L., Ota, T., and Nei, M. (1990). Positive Darwinian selection promotes charge profile diversity in the antigen-binding cleft of class I major-histocompatibility-complex molecules. *Mol. Biol. Evol.* 7, 515–524.

Jo, Y., Lian, S., Chu, H., Cho, J. K., Yoo, S.-H., Choi, H., et al. (2018). Peach RNA viromes in six different peach cultivars. *Sci. Rep.* 8:1844. doi: 10.1038/s41598-018-20256-w

Kwon, S.-J., Lim, W.-S., Park, S.-H., Park, M.-R., and Kim, K.-H. (2007). Molecular characterization of a dsRNA mycovirus, *Fusarium graminearum* virus-DK21, which is phylogenetically related to hypoviruses but has a genome organization and gene expression strategy resembling those of plant potex-like viruses. *Mol. Cells* 23, 304–315.

Lalić, J., Cuevas, J. M., and Elena, S. F. (2011). Effect of host species on the distribution of mutational fitness effects for an RNA virus. *PLoS Genet.* 7:e1002378. doi: 10.1371/journal.pgen.1002378

Lauring, A. S., Frydman, J., and Andino, R. (2013). The role of mutational robustness in RNA virus evolution. *Nat. Rev. Microbiol.* 11, 327–336. doi: 10.1038/nrmicro3003

Lee, J., Kim, H., Jeon, J.-J., Kim, H.-S., Zeller, K. A., Carter, L. L., et al. (2012). Population structure of and mycotoxin production by *Fusarium graminearum* from maize in South Korea. *Appl. Environ. Microbiol.* 78, 2161–2167. doi: 10.1128/aem.07043-11

Lee, K.-M., Cho, W. K., Yu, J., Son, M., Choi, H., Min, K., et al. (2014). A comparison of transcriptional patterns and mycological phenotypes following infection of *Fusarium graminearum* by four mycoviruses. *PLoS One* 9:e100989. doi: 10.1371/journal.pone.0100989

Li, H., Handsaker, B., Wysoker, A., Fennell, T., Ruan, J., Homer, N., et al. (2009). The sequence alignment/map format and SAMtools. *Bioinformatics* 25, 2078–2079. doi: 10.1093/bioinformatics/btp352

Li, P., Bhattacharjee, P., Wang, S., Zhang, L., Ahmed, I., and Guo, L. (2019). Mycoviruses in *Fusarium* species: an updating review. *Front. Cell. Infect. Microbiol.* 9:257. doi: 10.3389/fcimb.2019.00257

McCrone, J. T., and Lauring, A. S. (2018). Genetic bottlenecks in intraspecies virus transmission. *Curr. Opin. Virol.* 28, 20–25. doi: 10.1016/j.coviro.2017.10.008

Montville, R., Froissart, R., Remold, S. K., Tenaillon, O., and Turner, P. E. (2005). Evolution of mutational robustness in an RNA virus. *PLoS Biol.* 3:e381. doi: 10.1371/journal.pbio.0030381

Nielsen, H., and Krogh, A. (1998). Prediction(of)signal peptides and signal anchors by a hidden Markov model. *Ismb* 6, 122–130.

Okonechnikov, K., Golosova, O., Fursov, M., and Team, U. (2012). Unipro UGENE: a unified bioinformatics toolkit. *Bioinformatics* 28, 1166–1167. doi: 10.1093/bioinformatics/bts091

Pellegrino, S., Radzimanowski, J., de Sanctis, D., Boeri, E. E., McSweeney, S., and Timmins, J. (2012). Structural and functional characterization of an SMC-like protein RecN: new insights into double-strand break repair. *Structure* 20, 2076–2089. doi: 10.1016/j.str.2012.09.010

Pepin, K. M., Lambeth, K., and Hanley, K. A. (2008). Asymmetric competitive suppression between strains of dengue virus. *BMC Microbiol.* 8:28. doi: 10.1186/1471-2180-8-28

Ranji, A., and Boris-Lawrie, K. (2010). RNA helicases: emerging roles in viral replication and the host innate response. *RNA Biol.* 7, 775–787. doi: 10.4161/rna.7.6.14249

Sun, L., Nuss, D. L., and Suzuki, N. (2006). Synergism between a mycoreovirus and a hypovirus mediated by the papain-like protease p29 of the prototypic hypovirus CHV1-EP713. *J. Gen. Virol.* 87, 3703–3714. doi: 10.1099/vir.0.82213-0

Swanson, W. J., and Aquadro, C. F. (2002). Positive Darwinian selection promotes heterogeneity among members of the antifreeze protein multigene family. *J. Mol. Evol.* 54, 403–410. doi: 10.1007/s00239-001-0030-0

Syller, J., and Grupa, A. (2016). Antagonistic within-host interactions between plant viruses: molecular basis and impact on viral and host fitness. *Mol. Plant Pathol.* 17, 769–782. doi: 10.1111/mpp.12322

Wang, Z., Zhong, M., Fu, M., Dou, T., and Bian, Z. (2014). Evidence of positive selection at signal peptide region of interferon gamma. *Biosci. Biotechnol. Biochem.* 78, 588–592. doi: 10.1080/09168451.2014.896732

Wu, S., Cheng, J., Fu, Y., Chen, T., Jiang, D., Ghabrial, S. A., et al. (2017). Virus-mediated suppression of host non-self recognition facilitates horizontal transmission of heterologous viruses. *PLoS Pathog.* 13:e1006234. doi: 10.1371/journal.ppat.1006234

Yang, Z. (1997). PAML: a program package for phylogenetic analysis by maximum likelihood. *Comput. Appl. Biosci.* 13, 555–556. doi: 10.1093/bioinformatics/13.5.555

Yang, Z. (1998). Likelihood ratio tests for detecting positive selection and application to primate lysozyme evolution. *Mol. Biol. Evol.* 15, 568–573. doi: 10.1093/oxfordjournals.molbev.a025957

Yang, Z., Wong, W. S., and Nielsen, R. (2005). Bayes empirical Bayes inference of amino acid sites under positive selection. *Mol. Biol. Evol.* 22, 1107–1118. doi: 10.1093/molbev/msi097

Yu, J., Kwon, S.-J., Lee, K.-M., Son, M., and Kim, K.-H. (2009). Complete nucleotide sequence of double-stranded RNA viruses from *Fusarium graminearum* strain DK3. *Arch. Virol.* 154:1855. doi: 10.1007/s00705-009-0507-5

Yu, J., Lee, K.-M., Son, M., and Kim, K.-H. (2011). Molecular characterization of *Fusarium graminearum* virus 2 isolated from *Fusarium graminearum* strain 98-8-60. *Plant Pathol. J.* 27, 285–290. doi: 10.5423/ppj.2011.27.3.285

Yu, J., Park, J. Y., Heo, J. I., and Kim, K. H. (2020). The ORF2 protein of *Fusarium graminearum* virus 1 suppresses the transcription of FgDICER2 and FgAGO1 to limit host antiviral defences. *Mol. Plant Pathol.* 21, 230–243. doi: 10.1111/mpp.12895

Yu, J., Lee, K.-M., Cho, W. K., Park, J. Y., and Kim, K.-H. (2018). Differential contribution of RNA interference components in response to distinct *Fusarium*

graminearum virus infections. *J. Virol.* 92:e01756-17. doi: 10.1128/JVI.01756-17

Yuste, E., Sánchez-Palomino, S., Casado, C., Domingo, E., and López-Galíndez, C. (1999). Drastic fitness loss in human immunodeficiency virus type 1 upon serial bottleneck events. *J. Virol.* 73, 2745–2751. doi: 10.1128/jvi.73.4.2745-2751.1999

Zhang, L., Chen, X., Bhattacharjee, P., Shi, Y., Guo, L., and Wang, S. (2020). Molecular characterization of a novel strain of *Fusarium graminearum* Virus 1 infecting *Fusarium graminearum*. *Viruses* 12:357. doi: 10.3390/v12030357

Conflict of Interest: The authors declare that the research was conducted in the absence of any commercial or financial relationships that could be construed as a potential conflict of interest.

frontiers in Microbiology

ORIGINAL RESEARCH
published: 23 November 2020
doi: 10.3389/fmicb.2020.593846

Genome Organization of a New Double-Stranded RNA LA Helper Virus From Wine *Torulaspora delbrueckii* Killer Yeast as Compared With Its *Saccharomyces* Counterparts

Manuel Ramírez, Rocío Velázquez, Matilde Maqueda and Alberto Martínez*

Departamento de Ciencias Biomédicas (Área de Microbiología), Facultad de Ciencias, Universidad de Extremadura, Badajoz, Spain

OPEN ACCESS

Edited by:
Ioly Kotta-Loizou,
Imperial College London,
United Kingdom

Reviewed by:
Elena Servienė,
Nature Research Centre, Lithuania
Roy Walker,
Macquarie University, Australia

***Correspondence:**
Manuel Ramírez
mramirez@unex.es

Specialty section:
This article was submitted to Virology, a section of the journal Frontiers in Microbiology

Received: *11 August 2020*
Accepted: *02 November 2020*
Published: *23 November 2020*

Citation:
Ramírez M, Velázquez R, Maqueda M and Martínez A (2020) Genome Organization of a New Double-Stranded RNA LA Helper Virus From Wine Torulaspora delbrueckii Killer Yeast as Compared With Its Saccharomyces Counterparts. Front. Microbiol. 11:593846. doi: 10.3389/fmicb.2020.593846

Wine killer yeasts such as killer strains of *Torulaspora delbrueckii* and *Saccharomyces cerevisiae* contain helper large-size (4.6 kb) dsRNA viruses (V-LA) required for the stable maintenance and replication of killer medium-size dsRNA viruses (V-M) which bear the genes that encode for the killer toxin. The genome of the new V-LA dsRNA from the *T. delbrueckii* Kbarr1 killer yeast (TdV-LAbarr1) was characterized by high-throughput sequencing (HTS). The canonical genome of TdV-LAbarr1 shares a high sequence identity and similar genome organization with its *Saccharomyces* counterparts. It contains all the known conserved motifs predicted to be necessary for virus translation, packaging, and replication. Similarly, the Gag-Pol amino-acid sequence of this virus contains all the features required for cap-snatching and RNA polymerase activity, as well as the expected regional variables previously found in other LA viruses. Sequence comparison showed that two main clusters (99.2–100% and 96.3–98.8% identity) include most LA viruses from *Saccharomyces*, with TdV-LAbarr1 being the most distant from all these viruses (61.5–62.5% identity). Viral co-evolution and cross transmission between different yeast species are discussed based on this sequence comparison. Additional 5′ and 3′ sequences were found in the TdV-LAbarr1 genome as well as in some newly sequenced V-LA genomes from *S. cerevisiae*. A stretch involving the 5′ extra sequence of TdV-LAbarr1 is identical to a homologous stretch close to the 5′ end of the canonical sequence of the same virus (self-identity). Our modeling suggests that these stretches can form single-strand stem loops, whose unpaired nucleotides could anneal to create an intramolecular kissing complex. Similar stem loops are also found in the 3′ extra sequence of the same virus as well as in the extra sequences of some LA viruses from *S. cerevisiae*. A possible origin of these extra sequences as well as their function in obviating ssRNA degradation and allowing RNA transcription and replication are discussed.

Keywords: yeast, *Torulaspora*, killer, virus, dsRNA LA genome, high-throughput sequencing, sequence comparison

INTRODUCTION

Most killer yeasts secret a killer toxin encoded by the positive strand of medium-size (about 2 kb) dsRNA of M viruses. Different types of M viruses have been described, each one encoding a specific killer toxin (Schmitt and Tipper, 1995; Rodríguez-Cousiño et al., 2011; Ramírez et al., 2017; Vepštaitė-Monstavičė et al., 2018). Each killer yeast contains only one type of M virus together with a large-size (about 4.6 kb) helper dsRNA virus (V-LA) that is required to maintain stability of the former and for its replication. V-LA provides the capsids and polymerase required to separately encapsidate, transcribe, and replicate both the LA and M dsRNAs. The M dsRNA contains some stem loops that mimic LA dsRNA signals required for packaging and replication (reviewed by Schmitt and Breinig, 2006). Two proteins are encoded in the V-LA genome—the coat protein (Gag), and a fusion protein translated by a -1 ribosomal frameshifting mechanism (Gag-Pol) that contains the polymerase activities required for virus propagation (Icho and Wickner, 1989; Dinman and Wickner, 1992; Fujimura et al., 1992; Park et al., 1996). Viral RNA packaging and replication require some *cis* signals located in the 3′-terminal regions of the positive strands (Wickner et al., 1995; Rodríguez-Cousiño et al., 2011). It has been proposed that the signal for transcription initiation of the mRNA (positive strand) is located in the first 25 nucleotides of the 5′ end of the same strand, involving the terminal 5′-GAAAAA motif itself (Thiele and Leibowitz, 1982; Thiele et al., 1982; Fujimura et al., 1990; Rodríguez-Cousiño et al., 2011), which is 3′-CTTTTT in the negative-strand template.

Based on the sequence identity and type of the accompanying M virus, several V-LA isotypes found in yeast species included in the *Saccharomyces sensu stricto*: *S. cerevisiae*, *S. paradoxus*, *S. kudriavzevii*, and *S. uvarum* (**Table 2**). These viruses share 73–93% identity in viral genome nucleotide sequences and 87–99% identity in amino-acid Gag-Pol sequences. The identity among viruses from *S. paradoxus* strains seems to depend on their geographical location. Although sequences of *S. paradoxus* LA viruses are found to be more homogeneous than their *S. cerevisiae* counterparts, two separate clusters have been proposed for the former: one including SpV-LA66, SpV-LA28, and SpV-LA21, and the other containing the remaining LA viruses from *S. paradoxus*. The data available does not allow any cluster to be defined for *S. cerevisiae* LA viruses. Despite this, all the *Saccharomyces* LA viruses investigated thus far conserve the essential features found in the first *S. cerevisiae* LA virus to be described (ScV-LA1-original), such as the frameshift region and encapsidation signal (Rodríguez-Cousiño et al., 2017; Vepštaitė-Monstavičė et al., 2018).

Based on the association of some V-LA isotypes with specific M viruses in the same type of killer yeast, it has been suggested that each viral pair co-evolved with each other in their natural environment (Rodríguez-Cousiño et al., 2013). This suggestion is reinforced with the finding that neither ScV-LA nor ScV-LAlus show helper activity for M2, while the specific presence of ScV-LA2 is required for M2 maintenance in the same genetic background (Rodríguez-Cousiño and Esteban, 2017). However, ScV-LAlus helper activity for M2 has being found by other authors in another *S. cerevisiae* strain (Lukša et al., 2017). Sequence identity variations among these virus isotypes seem to depend on the geographical location of the host, it has also been suggested that V-LA cross-species transmission occurs between different yeast species living in the same habitat (Rodríguez-Cousiño et al., 2017).

The yeasts included in the *Saccharomyces sensu stricto* taxon (*S. cerevisiae*, *S. uvarum*, *S. paradoxus*, *S. mikatae*, *S. kudriavzevii*, *S. arboricola*, and *S. eubayanus*) have very similar genomes and a close phylogenetic relationship. Among them, *S. paradoxus* is considered to be the closest relative to *S. cerevisiae* (Kurtzman and Robnett, 2003; Scannell et al., 2011). Therefore, in the wild, hybridization can be expected among these yeast species. Indeed, natural hybrids have been found between *S. cerevisiae* and *S. eubayanus*, *S. uvarum* and *S. eubayanus*, and between *S. cerevisiae* and *S. kudriavzevii* (Hittinger, 2013). Most species of the *sensu stricto* taxon are frequently associated with human activities such as bread baking and alcoholic fermentations. These circumstances may favor horizontal cross-species transmission of killer viruses by yeast mating. Even some species that seem to live in different natural habitats, such as *S. cerevisiae* (mainly involved in food fermentation processes) and *S. paradoxus* [mainly present in the wild, associated with oak trees or the surrounding soil (Liti et al., 2009)], can mate in close-to-wild laboratory conditions and transfer killer viruses from one to another (Rodríguez-Cousiño et al., 2017). As these viruses are cytoplasmically inherited and spread horizontally by cell-cell mating or heterokaryon formation (Wickner, 1991), the presence of a specific virus isotype in different yeast species indicates that these yeasts may be able to mate in the wild.

The phylogenetic relationship between *Torulaspora* and *Saccharomyces* is not as close as that among the yeasts of the *sensu stricto* group. However, *T. delbrueckii* is quite similar to *S. cerevisiae* in the sense that both are among the best fermentative yeasts for biotechnological applications, and can share the same habitat in several ecosystems such as the spontaneous fermentations of bread dough, beer, wine, and different fruits (Kurtzman and Robnett, 2003; Kurtzman, 2011a,b). *T. delbrueckii* is probably the most used non-*Saccharomyces* yeast in winemaking. Killer Kbarr1 *T. delbrueckii* kills all known *S. cerevisiae* killer strains and other non-*Saccharomyces* yeasts. The Kbarr1 phenotype is encoded with the M virus (TdV-Mbarr1) that depends on an LA virus (TdV-LAbarr1) for its maintenance and replication. The TdV-Mbarr1 dsRNA sequence organization is quite similar to that of the *S. cerevisiae* killer M dsRNAs: a 5′-end coding region followed by an internal A-rich sequence and a 3′-end non-coding region. All these viruses also share *cis* acting signals at their 5′ and 3′ termini of the RNA positive strand for transcription and replication, respectively. However, they do not share a relevant overall sequence identity with either the full nucleotide sequence of dsRNA or their toxin amino-acid sequences (Ramírez et al., 2015, 2017).

The objective of this study was to determine the genome organization of the *T. delbrueckii* killer Kbarr1 strain LA virus as well as of other LA viruses from various *S. cerevisiae*

killer strains isolated from the same geographical region. We addressed the following issues: (i) purification, sequencing, and characterization of TdV-LAbarr1, (ii) purification, sequencing, and characterization of several ScV-LA viruses from different types of *S. cerevisiae* killer strains, and (iii) analysis of the TdV-LAbarr1 genome organization and its Gag-Pol ORF as compared with the dsRNAs of other LA viruses. We discuss the evolutionary relationship between these yeast viruses, as well as the possible secondary structure and function of the 5′- and 3′-extra sequences found in the newly sequenced genomes.

MATERIALS AND METHODS

Yeast Strains and Media

Torulaspora delbrueckii killer Kbarr1 yeast is a prototrophic strain isolated from the spontaneous fermentation of grapes from vines located in the Albarregas river valley in Spain (Ramírez et al., 2015). The industrial use of these Kbarr1 yeasts is under patent application. The *S. cerevisiae* killer strains EX231, EX1125, EX229, EX436, and EX1160 are also isolated from wine spontaneous fermentations in the Ribera del Guadiana region, which includes the Albarregas river valley, in Extremadura (southwestern Spain). We chose these strains because they present different mtDNA RFLP profiles and contain different isotypes of M dsRNA (Maqueda et al., 2010, 2012; Ramírez et al., 2017). All these yeasts are also prototrophic strains. The killer phenotype and the presence of viral dsRNA (L and M) in these yeasts have been analyzed previously (Rodríguez-Cousiño et al., 2011; Ramírez et al., 2015, 2017). The genomes of LA, LBC, and Mlus4 dsRNAs from EX229 have been analyzed by traditional techniques of cloning and sequencing (Rodríguez-Cousiño et al., 2011, 2013; Rodríguez-Cousiño and Esteban, 2017), and those of Mbarr1, M1-1, M2-4, Mlus1, Mlus4, and MlusA (from EX1180, EX231, EX1125, EX436, EX229, and EX1160, respectively) by HTS techniques (Ramírez et al., 2017). **Table 1** summarizes the yeasts used in this study.

Standard culture media were used for yeast growth (Guthrie and Fink, 1991). The YEPD contained 1% yeast extract, 2% peptone, and 2% glucose. The corresponding solid medium also contained 2% agar.

Purification of dsRNA From LA Viruses

Samples containing total nucleic acids from killer yeast strains were obtained as described previously (Maqueda et al., 2010; Ramírez et al., 2015). Briefly, yeasts were placed in 10 mM Tris-HCl (pH 7.5) buffer containing 0.1 M NaCl, 10 mM EDTA, and 0.2% SDS. An equal volume of phenol (pH 8.0) was then added, and the mixtures incubated at room temperature for 30 min with shaking. Samples were centrifuged, and nucleic acids recovered in the aqueous phase were precipitated with isopropanol, washed with 70% ethanol, dried, and dissolved in TE buffer pH 8.0. The L and M dsRNAs were obtained from each yeast strain by CF-11 cellulose chromatography (Toh-e et al., 1978). After 1% agarose gel electrophoresis of each sample, the slower-moving dsRNA band (4.6 kb) was cut out of the gel and purified with RNaid Kit (MP Biomedicals, LLC, Illkrich, France). This procedure was repeated for each yeast strain to obtain at least 20 μg of each purified dsRNA.

Preparation of cDNA Libraries From Purified V-L dsRNA and DNA Sequencing

The cDNA library preparation and high-throughput sequencing (HTS) were done at the Unidad de Genómica Cantoblanco (Fundación Parque Científico de Madrid, Spain) as has previously been described (Ramírez et al., 2017). Briefly, libraries from TdV-Lbarr1 (4.6 kb dsRNA purified band) were prepared with the "TruSeq RNA Sample Preparation kit" (Illumina) using 200 ng of purified dsRNA as input. The protocol was started at the fragmentation step, skipping the RNA purification step as the viral dsRNA had previously been purified. To facilitate the dsRNA denaturation, 15% DMSO was added to the Illumina fragment-prime solution before incubation at 94°C for 8 min. The first strand of cDNA was synthesized using random primers (dTVN and dABN oligonucleotides from Isogen Life Science, De Meern, The Netherlands) and SuperScriptIII retrotranscriptase. Then, the second cDNA strand synthesis, end repair, 3′-end adenylation, and ligation of the TruSeq adaptors were done (Illumina). These adaptor oligonucleotides include signals for further amplification and sequencing, and also short sequences referred to as indices which allow multiplexing in the sequencing run. An enrichment procedure based on PCR was then performed to amplify the library, ensuring that all the molecules in the library included the desired adaptors at both ends. The final libraries were denatured prior to seeding on a flow cell, and sequenced on a MiSeq instrument using 2 × 80 – 2 × 150 sequencing runs.

dsRNA Sequence Assembly

The cDNA sequences obtained were analyzed and assembled by the firm Biotechvana (Technological Park of Valencia, Spain) basically as has previously been described (Ramírez et al., 2017). As a modification of this method, first, SOAP deNOVO2 (Luo et al., 2012) was used to obtain a *de novo* assembly based on two Illumina libraries for each virus, trying multiple assembly attempts with scaffolding and insert size of 200 and varying the Kmer value, with 47 found to be the most effective. This K47 assembly comprised several contigs and scaffolds. Contigs of size shorter than 300 nucleotides were removed from the contig file, while the remaining contigs were used as input to the NR database of the NCBI via the BLASTX search protocol (Altschul et al., 1997) implemented in the GPRO 1.1 software (Futami et al., 2011). Highly significant similarity was found between several contigs/scaffolds and some known viral RNA sequences (LA, LBC, and others) or host transcripts. Supposed contaminating sequences non-homologous to previously known LA genomes were filtered from the assembly. Each virus was sequenced at least three times using independent samples and different dates during a period of several years. Full coverage of the canonical genome sequence was obtained at least twice for

TABLE 1 | Yeasts used in this study.

Strain	Genotype (relevant phenotype)	Origin, date, grape variety, geographical location in Extremadura (Spain)
Td EX1180	*wt* LAbarr1 LBCbarr1 Mbarr1 [Kbarr1$^+$]	Wine, 2006, Cayetana, Albarregas (Mérida)
Sc EX231	*MAT a/α HO/HO* LA1 LBC M1-1 [K1$^+$]	Wine, 2003, Macabeo, Guadajira
Sc EX1125	*MAT a/α HO/HO* LA2 LBC M2-4 [K2$^+$]	Wine, 2005, Moscatel, La Albuera
Sc EX436	*MAT a/α HO/HO* LAlus1 Mlus1 [Klus$^+$]	Wine, 2003, Tempranillo, Guadajira
Sc EX229	*MAT a/α HO/HO cyhS/cyhS* LAlus4 LBC Mlus4 [Klus$^+$]	Wine, 2003, Macabeo, Guadajira
Sc EX1160	*MAT a/α HO/HO* LAlusA LBC MlusA MlusB MlusC [Klus$^+$]	Wine, 2005, Moscatel, La Albuera

Sc, Saccharomyces cerevisiae; Td, Torulaspora delbrueckii.

each virus, and 100% identity was found between all sequences obtained from the same yeast strain. Coverage of the 5′ and 3′ extra sequences was 100% in at least two replicates from each virus. These extra 5′ and 3′ sequences were the same for each biological replicate. Only these full coverage sequences were considered for comparison of viral genomes from different yeasts.

Miscellaneous

The sequence identity and phylogenetic relationship (phylogram) among LA genomes were obtained by the ClustalW(2.1) program for comparing nucleotide sequences (Thompson et al., 1994), and the MUSCLE(3.8) program for comparing amino-acid sequences (Madeira et al., 2019). The MFOLD program[1] was used to predict the folding and hybridization of ssRNA (Zuker et al., 1999), and the FORNA program[2] to visualize the RNA secondary structure (Kerpedjiev et al., 2015). The parameters used in MFOLD were: folding temperature fixed at 37°C; ionic conditions, 1 M NaCl, no divalent ions; percent suboptimality number, 5; upper bound on the number of computed foldings, 50; maximum interior/bulge loop size, 30; maximum asymmetry of an interior/bulge loop, 30; maximum distance between paired bases, no limit.

Nucleotide Sequence Accession Numbers

The cDNA nucleotide sequence and amino-acid sequence of the Gag-Pol protein of newly sequenced (HTS) LA viruses appear in NCBI/GenBank under the following accession numbers: TdV-LAbarr1, (MW174763); ScV-LA1 from strain EX231, (MW174760); ScV-LA2 from EX1125, (MW174759); ScV-LAlus1 from EX436, (MW174761); and ScV-LAlusA from EX1160 (MW174762). These ScV-LA viruses are those described previously (Rodríguez-Cousiño et al., 2011; Ramírez et al., 2017) but *de novo* sequenced by HTS techniques for this study. The previously described ScV-L-A-lus from EX229 (Rodríguez-Cousiño et al., 2013) is here named ScV-LAlus4 because it comes from a killer Klus-4 type strain, and was *de novo* sequenced by HTS (accession number: MW174758). The genome sequences of other LA viruses used in this study are described in **Table 2**.

[1]http://unafold.rna.albany.edu/?q=mfold/RNA-Folding-Form

[2]http://rna.tbi.univie.ac.at/forna/

RESULTS

Analysis of the dsRNA and Gag-Pol Sequences From TdV-LAbarr1

Two different sequences were obtained from the L band (4.6 kb) cDNA present in the Kbarr1 strain—one shows above 60% nucleotide identity with the ScV-LA-original genome (that we named TdV-LAbarr1), and the other shows above 56% nucleotide identity with the ScV-LBC genome (TdV-LBCbarr1). The full sequence obtained for TdV-LAbarr1 cDNA is of 4,622 nucleotides, which is very close to the size estimated by agarose-gel electrophoresis. Most of this sequence (4,591 nt central stretch) shows 62% nucleotide identity with previously known ScV-LA-original and ScV-LAlus4 (**Supplementary Figures S1**, **S3**), while these two ScV-LA genomes share a greater identity of 74% (Rodríguez-Cousiño et al., 2013). This central stretch is therefore considered to be the canonical sequence of the TdV-LAbarr1 genome, and sequences upstream (14 nt) and downstream (17 nt) as 5′- and 3′-extra sequences, respectively (**Figure 1**). The TdV-LAbarr1 genome organization is quite similar to that of ScV-LA-original and ScV-LAlus4, with the three viral RNAs containing two ORFs. Based on the sequence homology, the first TdV-LAbarr1 sequence ORF (from nt 61 to 2,093) can be assigned as being the coat (Gag) protein of the virion, and the second ORF (from nt 2,376 to 4,567) as the viral RNA-dependent RNA polymerase (RdRp). This polymerase is probably expressed as a Gag-Pol fusion protein together with Gag ORF by a -1 ribosomal frameshift at the conserved frameshifting site located upstream of the Gag ORF stop codon (from nt 1,983 to 1,988) (**Figure 1** and **Supplementary Figure S1**). These ORF assignments are also based on the amino-acid sequence homology of the Gag-Pol fusion protein of TdV-LAbarr1 to those of ScV-LA-original and ScV-LAlus4 (see below). Nonetheless, these three LA genomes have one or two putative in-frame translation re-initiation start codons downstream of the Gag-ORF stop codon and upstream of the Pol domain (indicated in boldface in **Figure 1** and **Supplementary Figure S1**).

Furthermore, as described previously for ScV-LA-original and ScV-LAlus4 (Rodríguez-Cousiño et al., 2013), there are three regions in the TdV-LAbarr1 genome that are highly conserved: (i) the stem-loop region known to be involved in frameshifting (nt 1,969 to nt 2,004) adjacent to the slippery site 1983GGGUUUA1989 in TdV-LAbarr1, (ii) a 24 nt stem-loop region responsible for binding to and packaging of the

TABLE 2 | Previously known sequence of yeast LA viruses used in this study.

Virus	Accession number	Reference/comment
ScV-LA1-original	J04692.1	Icho and Wickner, 1989. Previously known as ScV-LA. Renamed in this study to distinguish it from other LA-virus from different K1 killer yeasts
ScV-L-A-lus	JN819511.1	Rodríguez-Cousiño et al., 2013
ScV-LA2-8F13	KC677754.1	Rodríguez-Cousiño and Esteban, 2017
SpV-LA28	KU845301.2	Konovalovas et al., 2016. Formerly assigned to S. cerevisiae but recently re-assigned to *S. paradoxus* (Vepštaitė-Monstavičė et al., 2018)
SpV-LA21	KY489962.1	Rodríguez-Cousiño et al., 2017
SpV-LA45	KY489963.1	Rodríguez-Cousiño et al., 2017
SpV-LA74	KY489964.1	Rodríguez-Cousiño et al., 2017
SpV-LA4650	KY489965.1	Rodríguez-Cousiño et al., 2017
SpV-LA1939	KY489966.1	Rodríguez-Cousiño et al., 2017
SpV-LA1143	KY489967.1	Rodríguez-Cousiño et al., 2017
SpV-LA62	KY489968.1	Rodríguez-Cousiño et al., 2017
SpV-LA66	MH784501.1	Vepštaitė-Monstavičė et al., 2018
SkV-LA1082	KY489970.1	Rodríguez-Cousiño et al., 2017
SkV-LAFM1183	KX601068.1	Rowley et al., 2016
SuV-LA10560	KY489969.1	Rodríguez-Cousiño et al., 2017

Sc, S. cerevisiae; Sp., S. paradoxus; Sk, S. kudriavzevii; Su, S. uvarum.

LA (+) strand (nt 4,205 to nt 4,228 in TdV-LAbarr1), and (iii) a 15-nt stem-loop region responsible for RNA replication (nt 4,587–4,601 in TdV-LAbarr1) (**Figure 1**). This indicates the importance of these regions in the translation, packaging, and replication steps of these viruses. Only three nucleotide changes are found in the packaging stem loop of TdV-LAbarr1 with respect to ScV-LA-original or ScV-LAlus4 (C4180A, T4189C, and A4195G), and these changes even slightly decrease the free energy of the structure from ΔG = -16 kJ/mol in ScV-LA-original to ΔG = -18 kJ/mol in TdV-LAbarr1. The frameshifting stem loop of TdV-LAbarr1 is also highly conserved with respect to those of ScV-LA-original and ScV-LAlus4. Only three nucleotide changes are found (C1977T and G1997T with respect to ScV-LA-original and ScV-LAlus4, and T1991A with respect to ScV-LA-original or C1991A with respect to ScV-LAlus4), which slightly increase the free energy of the structure from ΔG = -64 kJ/mol in ScV-LA-original to ΔG = -59 kJ/mol in TdV-LAbarr1. Some other nucleotide changes are also found in the replication stem-loop sequence of TdV-LAbarr1 with respect to ScV-LA-original (G4565A, A4566T, A4567T, T4569A, and C4571T) and ScV-LAlus4 (G4562T, T4565A, T4569A, and C4571T). These changes do not alter the putative stem-loop structure, although they increase the free energy of the structure from ΔG = -21 kJ/mol in ScV-LA-original to ΔG = -14 kJ/mol in TdV-LAbarr1. Nonetheless, it has previously been described that the nucleotide sequence of the loop (here conserved) is important but that of the stem is not (Esteban et al., 1989; Rodríguez-Cousiño et al., 2013).

Despite the aforementioned similarities, TdV-LAbarr1 differs from the ScV-LA-original and ScV-LAlus4 genomes in that it contains: (i) 14 extra nucleotides at the 5′ end, (ii) 17 extra nucleotides at the 3′ end, (iii) a 17-nucleotide non-homologous stretch close to the 5′ end, and (iv) it does not have the conserved 5′GAAAAA motif present in ScV-LA-original and ScV-LAlus4 (**Figure 1** and **Supplementary Figure S1**). Although no experimental evidence has been reported, it has been suggested that this conserved motif is related to the supposed *cis* signals required for transcription, similarly to other 5′ AU-rich regions in dsRNA viruses that facilitate the "melting" of the molecule and the access of the RNA polymerase to the template strand for conservative transcription (Rodríguez-Cousiño et al., 2013). In this sense, the 5′ UTR (untranslated terminal region) of the three LA viruses contains an AU-rich 15-nucleotide stretch (100% AU for ScV-LA-original, 93.3% for ScV-LAlus4, and 100% for TdV-LAbarr1) that may be responsible for facilitating this melting. The putative Gag-Pol amino-acid sequence of TdV-LAbarr1 shows 62 and 63% identity with that of ScV-LA1-original and ScV-LAlus4, respectively, while those of ScV-LA1-original and ScV-LAlus4 share a greater identity of 87% (Rodríguez-Cousiño et al., 2013; **Figure 2** and **Supplementary Figure S2**). The identity shared by these three Gag-Pol proteins is good enough to expect similar spatial organization and polymerase functional behavior for all these LA viruses. The Gag His154 residue (His153 in TdV-LAbarr1) required for the cap-snatching mechanism (transferring cap groups from other yeast mRNAs to the nascent mRNA of LA virus when extruded from the virion; Fujimura and Esteban, 2011) in *S. cerevisiae* viruses and the four crucial residues for 5′cap recognition (Tyr-150, Asp-152, Tyr-452, and Tyr-538 Fujimura and Esteban, 2013) are present in the Gag protein of the three viruses. Moreover, the central third of the Pol sequence, which is highly conserved among the RdRps (underlined in **Figure 2** and **Supplementary Figure S2**), shares 82% identity with that of ScV-LA1-original, and the four conserved motifs in this region (A, B, C, and D; Bruenn, 2003) are 100% identical in the three Pol proteins. Other parts of Gag and Pol are also highly conserved. Worthy of mention among the poorly conserved regions are a 19-amino-acid variable region located downstream of H154/153, and the

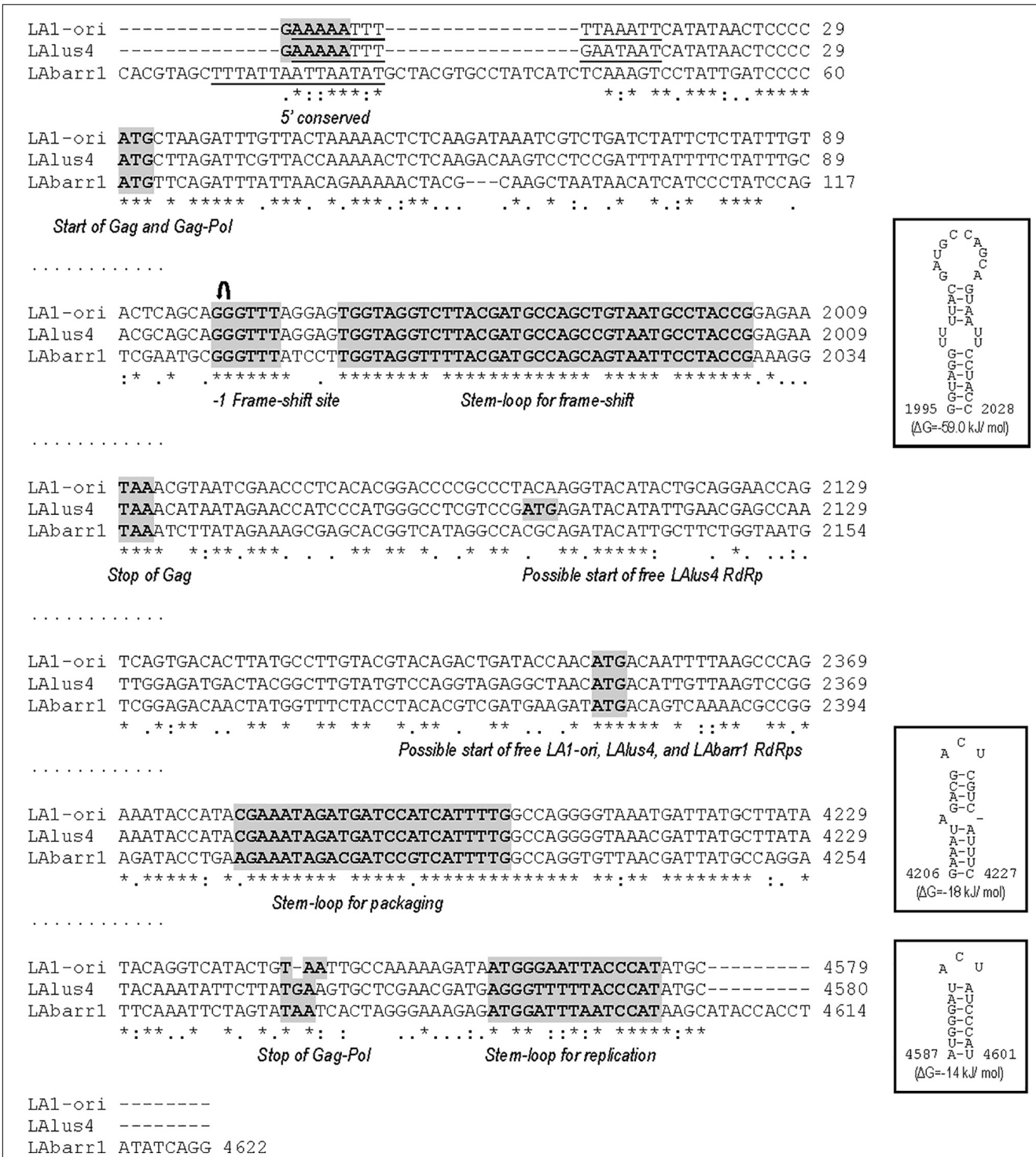

FIGURE 1 | Partial multiple sequence alignment between ScV-LA-original, ScV-LAlus4, and TdV-LAbarr1 (+) strand nucleotide sequences (cDNA). The full sequence alignment is presented in **Supplementary Figure S1**. 5′GAAAAA conserved motif (5′ conserved), translation initiation (start of Gag and Gag-Pol, or internal ATG in Pol ORF of ScV-LA-original, ScV-LAlus4, and TdV-LAbarr1) and termination (stop of Gag or Gag-Pol) codons, ribosome frameshifting site (−1 frameshift site), frameshifting associated sequence (stem loop for frameshift), packaging signal (stem loop for packaging), and replication signal (stem loop for replication) are indicated and gray shaded in the nucleotide sequence. An AU-rich 15-nucleotide stretch located in the 5′ untranslated terminal region is underlined. ⋂, ribosomal frameshift. Asterisks (*), colons (:), and dots (.) indicate identical nucleotide positions, transitions, and transversions, respectively. The secondary structures of the putative *cis* signals for frameshifting, packaging, and replication of TdV-LAbarr1 are displayed at the right of the sequence panel.

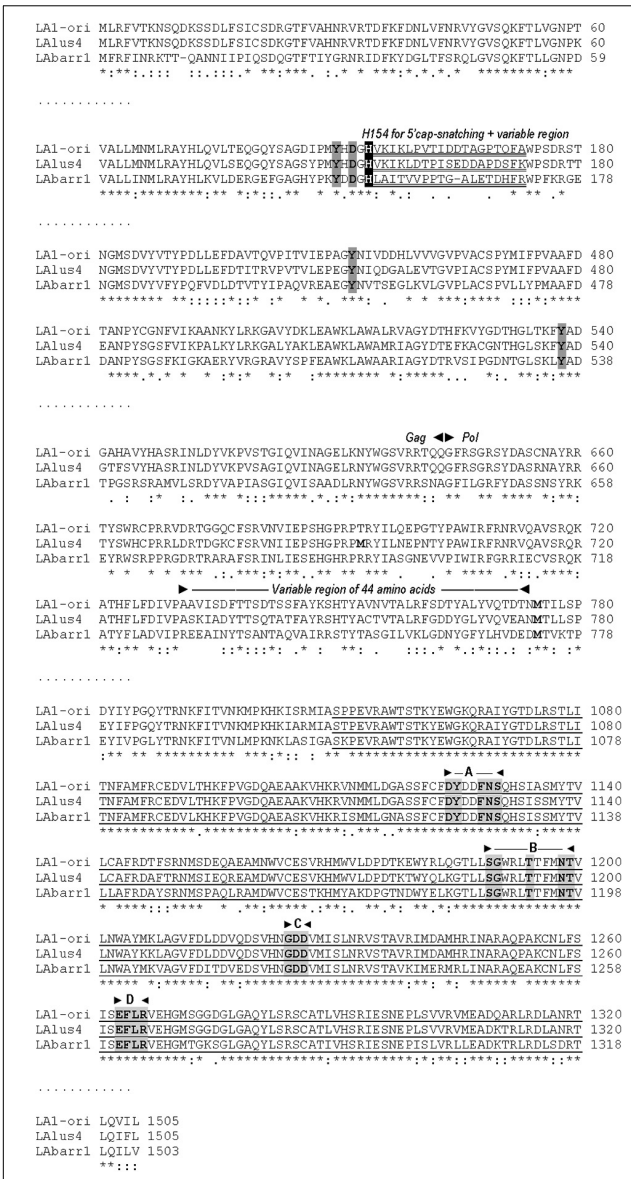

FIGURE 2 | Comparison between partial amino-acid sequences of Gag-Pol encoded by ScV-LA-original, ScV-LAlus4, and TdV-LAbarr1 dsRNA genomes. The full sequence alignment is presented in **Supplementary Figure S2**. The separation between Gag and Pol is indicated (Gag◄►Pol). The H154 residue required for 5′cap-snatching is black shaded. The stretch of variable amino-acid sequence located downstream from H154 is double underlined. The four crucial residues for cap recognition (Tyr-150, Asp-152, Tyr-452, and Tyr-538) are gray shaded. A variable region of 44 amino acids in the N-terminal region of Pol is indicated above the sequence. The highly conserved central third of Pol is underlined, and the four consensus motifs (A–D) conserved in RNA-dependent RNA polymerases from totiviruses are indicated above the sequence, and the conserved amino acids for each motif are gray shaded. Methionines (M) in the N-terminal region of Pol are in boldface. Asterisks (*) indicate identical amino acids; colons (:) and single dots (.) indicate conserved and semi-conserved amino acids, respectively.

44-amino-acid variable region located in the N-terminal third of Pol (amino acids 729A to 772D in ScV-LA-original Gag-Pol) in which only eight amino acids are identical (**Figure 2**), both of which stretches have previously been described as variable regions (Rodríguez-Cousiño et al., 2013).

Comparison of TdV-LAbarr1 With LA Viruses From *Saccharomyces* Yeasts

The dsRNA and Gag-Pol sequences of TdV-LAbarr1 were compared with their counterparts from *Saccharomyces* yeasts to analyze their phylogeny. The sequences of *S. cerevisiae* ScV-LA1-original (Icho and Wickner, 1989), ScV-LAlus4 (Rodríguez-Cousiño et al., 2013), ScV-LA2-8F13 (Rodríguez-Cousiño and Esteban, 2017), and SpV-LA28 (Konovalovas et al., 2016) were already known, as also were the sequences of *S. paradoxus* SpV-LA21, SpV-LA45, SpV-LA74, SpV-LA4650, SpV-LA1939, SpV-LA1143, and SpV-LA62 (Rodríguez-Cousiño et al., 2017), *S. paradoxus* SpV-LA66 (Vepštaitė-Monstavičė et al., 2018), *S. kudriavzevii* SkV-LA1082 (Rodríguez-Cousiño et al., 2017) and SkV-LAFM1183 (Rowley et al., 2016), and *S. uvarum* SuV-LA10560 (Rodríguez-Cousiño et al., 2017). The viruses ScV-LA1 from strain EX231, ScV-LA2 from EX1125, ScV-LAlus1 from EX436, and ScV-LAlusA from EX1160 have been described previously (Rodríguez-Cousiño et al., 2011; Ramírez et al., 2017), and their genomes were *de novo* sequenced by HTS techniques for this study. ScV-LAlus4 from EX229, previously named ScV-L-A-lus (Rodríguez-Cousiño et al., 2013), was also de novo sequenced as a control to assess the accuracy of our HTS procedure. Only two nucleotide changes were found in the nucleotide sequence of ScV-LAlus4 with respect to ScV-L-A-lus: G2434A and A3645T. As nucleotides of ScV-LAlus4 (HTS) in these two positions coincided best with the rest of the *S. cerevisiae* LA viruses, this sequence was the one used for further analyses.

The percentage of identity among the different viruses was always greater for Gag-Pol amino-acid sequences than for genomic nucleotide sequences (**Figure 3** and **Supplementary Figure S3**), similar to earlier findings for *Saccharomyces* LA viruses (Rodríguez-Cousiño et al., 2017; Vepštaitė-Monstavičė et al., 2018). Two main clusters were found to include most LA virus sequences: a *S. cerevisiae* cluster that grouped the viruses of all the wine yeasts isolated from the Region of Extremadura (99.2–100% identity of Gag-Pol), and a *S. paradoxus* cluster that grouped most viruses of this yeast species (except for SpV-LA-45) and SuV-LA10560 of *S. uvarum* (96.3–98.8% identity) (**Figure 3** and **Supplementary Figure S3**).

Viruses SpV-LA45 of *S. paradoxus* and SkV-LAFM1183 of *S. kudriavzevii* were closer to the *S. paradoxus* than the *S. cerevisiae* cluster (90–95% and 89–90% identity of Gag-Pol, respectively), and both viruses show 91% identity in their Gag-Pol amino-acid sequence. The virus ScV-LA2-8F13 of *S. cerevisiae* was closer to the *S. cerevisiae* than the *S. paradoxus* cluster (92–93% and 89–90% identity, respectively). The viruses SkV-LA1082 of *S. kudriavzevii* and ScV-LA1-original of *S. cerevisiae* were equally distant from both main clusters (85 and 87% identity, respectively), and both viruses show 85% identity in their Gag-Pol amino-acid sequence. Finally, the virus TdV-LAbarr1 of *T. delbrueckii* (isolated from Ribera del Guadiana, Extremadura, Spain) was the most distant from the rest of the viruses (62–63% identity)

A

Percent identity matrix for V-LA Gag-Pol amino-acid sequences

TdV-LAbarr1	100	62	62	62	63	63	62	63	63	62	62	62	62	62	62	62	62	62	62	62
SkV-LA1082	62	100	85	85	85	85	85	85	85	85	85	85	85	85	85	85	85	85	85	85
ScV-LA1-original	62	85	100	87	87	87	87	87	87	88	87	87	87	87	87	87	87	87	87	87
ScV-LA2-8F13	62	85	87	100	92	92	92	93	93	89	90	89	89	89	89	89	89	89	89	90
ScV-LA1-EX231	63	85	87	92	100	100	99	99	99	89	90	90	90	90	90	90	90	90	90	90
ScV-LAlus-EX1160	63	85	87	92	100	100	99	99	99	89	90	90	90	90	90	90	90	90	90	90
ScV-LA2-EX1125	62	85	87	92	99	99	100	99	99	89	90	90	90	90	90	90	90	90	90	90
ScV-LAlus4-EX229	63	85	87	93	99	99	99	100	99	89	90	90	90	90	90	90	90	90	90	90
ScV-LAlus1-EX436	63	85	87	93	99	99	99	99	100	89	90	90	90	90	90	90	90	90	90	90
SpV-LA45	62	85	88	89	90	89	89	89	89	100	91	91	90	91	91	90	91	90	91	90
SkV-LAFM1183	62	85	87	90	90	90	90	90	90	91	100	95	94	94	94	94	95	94	94	94
SpV-LA62	62	85	87	89	90	90	90	90	90	91	95	100	98	98	98	98	98	97	97	97
SpV-LA1143	62	85	87	89	90	90	90	90	90	90	94	98	100	98	98	98	98	96	97	97
SpV-LA4650	62	85	87	89	90	90	90	90	90	91	94	98	98	100	98	99	99	97	97	97
SuV-LA10560	62	85	87	89	90	90	90	90	90	91	94	98	98	98	100	99	99	96	97	97
SpV-LA74	62	85	87	89	90	90	90	90	90	90	94	98	98	99	99	100	99	97	97	97
SpV-LA1939	62	85	87	89	90	90	90	90	90	91	95	98	98	99	99	99	100	97	97	97
SpV-LA66	62	85	87	89	90	90	90	90	90	90	94	97	96	97	96	97	97	100	98	98
SpV-LA28	62	85	87	89	90	90	90	90	90	91	94	97	97	97	97	97	97	98	100	98
SpV-LA21	62	85	87	90	90	90	90	90	90	90	94	97	97	97	97	97	97	98	98	100

B

Phylogram

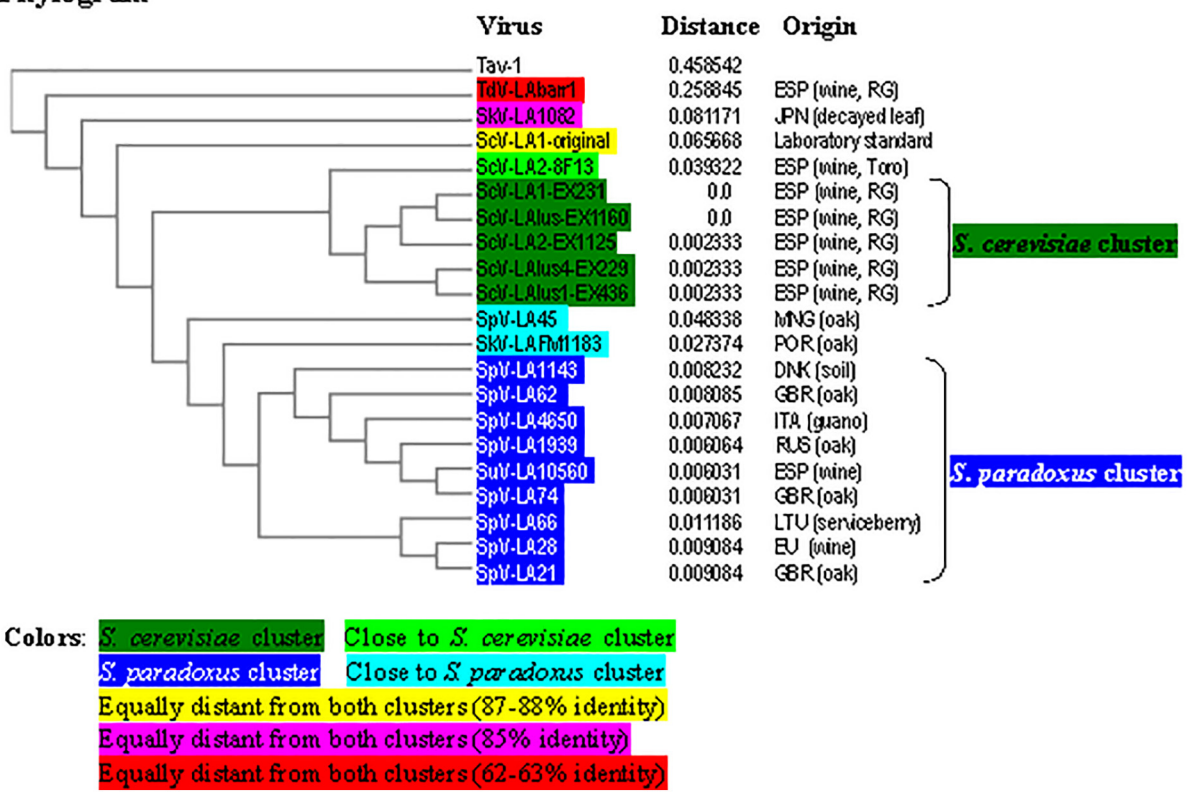

FIGURE 3 | Phylogenetic relationship of yeast LA viruses. **(A)** Percentage identity matrix between the complete amino acid sequences of the Gag-Pol proteins of LA viruses. Each identity value is rounded to the nearest whole number. **(B)** Phylogram with evolutionary distances (given by the MUSCLE program) and geographical location at which each killer yeast strain was isolated. RG, Ribera del Guadiana. Country codes are in accordance with the International Organization for Standardization ISO 3166-2. Viruses included in each of the two main clusters, as well as their identity values, are shaded in dark-green or dark-blue. The relative identity with these clusters of the rest of the viruses is indicated by shading in other colors.

(**Figure 3**). Similar results were found for cluster formation and virus association when comparing separately the amino-acid sequence of Gag and the highly conserved RdRp-domain of Pol. However, the percentage identity between RdRp domains was greater than with comparisons using full Gag-Pol sequences (compare **Figure 3A** and **Supplementary Figure S4**). On the contrary, the percentage identity between Gag domains was less than with comparisons using full Gag-Pol sequences, and ScV-LA1-original was then slightly closer to the *S. cerevisiae* (80–81%) than to the *S. paradoxus* cluster (74–78%) (compare **Figure 3A** and **Supplementary Figure S5**). The greatest change was found for TdV-LAbarr1. The TdV-LAbarr1 Gag sequence was approximately 18% lower in identity (from 62–63% to 44–47%), while the TdV-LAbarr1 RdRp domain sequence was approximately 22% higher (from 62–63% to 82–85%), in both cases with respect to the rest of the viruses (compare **Figure 3A** and **Supplementary Figures S4**, **S5**). Thus, Gag amino-acid sequence comparison seems to be the most efficacious procedure for grouping all the viruses from each yeast species. As was to be expected, identity between most viruses decreased when comparing the variable hydrophobic 44-amino-acid stretch located in the N-terminal region of Pol. The exception was among viruses of the *S. cerevisiae* cluster that increased up to 100% identity in all cases (compare **Figure 3A** and **Supplementary Figure S6**). The results were similar in comparing the variable 19-amino-acid stretch located downstream of H153/154 of Gag (compare **Figure 3A** and **Supplementary Figure S7**). This was not found, however, for viruses of the *S. paradoxus* cluster in which the identity values for these variable stretches decreased, probably because these yeast strains were isolated from geographical locations that were insufficiently close.

Analysis of the 5′- and 3′-Extra Sequences Found in TdV-LAbarr1 and Some ScV-LA Genomes

The complete sequences obtained for the TdV-LAbarr1 and the five ScV-LA viruses from Ribera del Guadiana were longer than the former's estimated canonical sequence or the latter's previously known sequences (**Table 3**). Extra nucleotides were found on both sides of the canonical sequence—the 5′ and 3′ ends. For sequence descriptions in this section, nucleotides are numbered from the 5′GAAAAA conserved motif in ScV-LA viruses, which is generally accepted as the 5′-end in most *S. cerevisiae* viral L canonical genomes (Fujimura and Wickner, 1989). The homologous motif 5′AATTAA is considered for TdV-LAbarr1. The 5′-terminal G or A is denoted as number 1. Extra nucleotides found upstream from 5′GAAAAA or 5′AATTAA motif are numbered with a negative symbol starting at (−)1 from the first nucleotide upstream from 5′G or 5′A. Similarly, extra nucleotides found downstream from the previously considered 3′-end of ScV-LA genomes (CCATATGC3′, or CCAAATGC3′ in ScV-LAlus1 from the EX436 strain) and now considered for TdV-LAbarr1 (CCATAAGC3′) are numbered with a positive symbol starting at (+)1 from the first nucleotide located downstream from C3′ (**Figures 4**, **5**).

No relevant identity was found between the extra 5′ or 3′ sequences of the different LA viruses, or between these two extra sequences of each virus. However, 100% local identity was found among some stretches in the 5′-extra sequence of some *S. cerevisiae* LA genomes: 13 nt [5′-GACAAGTCCTCCG-3′] [G(−)7 to G(−)19] in ScV-LA1-EX231 and ScV-LAlus1-EX436, and 22 nt [5′-CTCTGACAAAGGTACTTTTGTT-3′] in ScV-LA2-EX1125 [C(−)57 to T(−)36] and ScV-LAlusA-EX1160 [C(−)47 to T(−)25] (**Figure 5A**).

A 51 nt stretch of TdV-LAbarr1, part in the 5′-extra sequence (14 nt) and part in the 5′-end (37 nt) [C(−)14 to A37], showed 100% identity with a homologous stretch located near the 5′-end in the canonical sequence of the same virus [C401 to A451] (viral self-identity). This stretch is almost a palindromic sequence, and about half of this sequence (5′-CACGTAGCTTTATTAATTAATATGCTACGTG-3′) can form a stem loop (ΔG = -50 kJ/mol), a loop that contains the first four nucleotides of the canonical sequence (5′-AATT) as unpaired. These nucleotides are complementary to the unpaired nucleotides in the stem loop of the homologous stretch located downstream in the RNA sequence (5′-AAUU/3′-UUAA), and it is possible that a kissing complex could be formed by four-base-pair annealing (**Figure 4A**). A similar palindromic sequence (44 nt), with the 5′GAAAAATTT conserved motif included at about the middle of the stretch, capable of forming a stem loop (ΔG = -71 kJ/mol) was also found in ScV-LA2-EX1125. Additionally, a stretch in the 5′-extra sequence that has 100% identity with a homologous stretch located close to the 5′GAAAAA conserved motif in the canonical sequence was also found in the same ScV-LA2-EX1125 virus (viral self-identity). This conserved motif was similar to that also found in the rest of the ScV-LA viruses except for ScV-LAlus4-EX229. However, ScV-LAlus4-EX229 showed two stem loops in the 5′-extra sequence. Another stem loop, close to the 5′GAAAAATTT conserved motif in the canonical sequence, was also found in all ScV-LA viruses (**Figure 5A**). Nevertheless, no probable kissing-loop interactions were found near the 5′-end of *S. cerevisiae* viruses. Other interesting sequences were also found in ScV-LA1-EX231, ScV-LAlus4-EX229, and ScV-LAlus1-EX436: 118 nt of 100% identity with a chromosome II sequence of *S. cerevisiae,* 178 nt of 100% identity with *S. cerevisiae* 18S rRNA, and 213 nt of 93% identity with *S. cerevisiae* 26S rRNA, respectively (**Table 3** and **Figure 5A**).

With respect to 3′-extra sequences, a 16 nt stretch [T(+)2 to G(+)17] of TdV-LAbarr1 showed 100% identity with a homologous stretch located close to 3′-extra in the canonical sequence of the same virus [T4457 to G4472], and part of each can form a stem loop (ΔG = -2.5 kJ/mol). The unpaired nucleotides of these homologous RNA loops are complementary to each other (5′-AUAU/3′-UAUA). Therefore, similarly to the case for the 5′-end of the same virus, intramolecular kissing-loop interaction is possible through four-base-pair annealing (**Figure 4B**). A similar situation was found in ScV-LA1-EX231, whose 3′-extra sequence contains a 44 nt stretch [G4579 to C(+)42] of 100% identity with a homologous stretch located close to the 3′-end of the canonical sequence of the same virus [G4457 to C4500], which can also

TABLE 3 | Characteristics of dsRNA LA-virus genomes sequenced by HTS.

Virus	Previous sequenced length (bp)/yeast strain	Newly analyzed yeast strain	Killer phenotype/M dsRNA isotype	Sequenced length in (bp) /canonical	5′-extra sequence (bp)/% identity to, size (position)	3′-extra sequence (bp)/% identity to, size (position)	Stem-loop involving 5′-extra sequence (position) (Δ G)	Stem-loop involving 3′-extra sequence (position) (Δ G)
LAbarr1	Unknown/*Td* EX1180	*Td* EX1180	Kbarr1/Mbarr1	4622/4591	14/100% self-identity to (+) strand, 51 nt [C(−)14–A37] to 51 nt [C401 to A451]	17/100% self-identity to (+) strand, 16 nt [T(+)2–G(+)17] to 16 nt [T4457–G4472]	[C(−)14 to G(+)17] (−50)	[C(+)7 to G(+)17] (−2.5)
LA1-original	4579/*Sc* RE59	*Sc* EX231	K1/M1-1	4874/4580	252/100% *Sc* chromosome II, 118 nt, [C(+)252–A(+)65]; and 100% self-identity to (+) strand, 58 nt [T(−)63–A(−)6] to 58 nt [T16 to A73]	42/100% self-identity to (+) strand, 44 nt [G4579–C(+)42] to 44 nt [G4457–C4500]	[A(−)16 to T(−)3] (−12)	[G4579 to C(+)30] (−24)
LA2	4580/*Sc* 8F13	*Sc* EX1125	K2/M2–4	4696/4580	58/100% self-identity to (+) strand, 23 nt [G(−)58–T (−)36] to 23 nt [G88–T110]. Same as in LAlusEX1160	58/no identity found	[G(−)53 to U(−)36] (−15). Same as in LA-lus EX1160	[A(+)8 to U(+)28] (−6.3)
LAlus4	4580/*Sc* S3920 = EX229	*Sc* EX436	Klus/Mlus1	5052/4617	232/93% identity to *Sc* 26S (−) rRNA, 213 nt [C(−)232 to T(−)20]	203/261 nt are 100% to *Sc* 26S (+) rRNA, [C4560 to T(+)203]	[C(−)28 to G(−)1] (−29)	[C(+)3 to G(+)21] (−20)
		Sc EX229	Klus/Mlus4	4776/4580	187/100% identity to *Sc* 18S (+) rRNA, 178 nt [G(−)187–G10]	9/no identity found	[C(−)74 to G(−)52] (−31), and [C(−)41 to G(−)10] (−16)	[A4577 to U(+)8] (−18)
		Sc EX1160	Klus/MlusA	4648/4580	46/100% self-identity to (+) strand, 44 nt [C(−)46–G(−)3] to 44 nt [C89–G132]. Same as in LA2-EX1125	22/no identity found	[G(−)42 to U(−)25] (−15). Same as in LA2-EX1125	[C(+)2 to G(+)22] (−20)

ΔG was obtained for the ssRNA(+) with the program MFOLD. ΔG is in kJ/mol. Sc, Saccharomyces cerevisiae; Td, Torulaspora delbrueckii; the cDNA sequence was considered for nucleotide position.

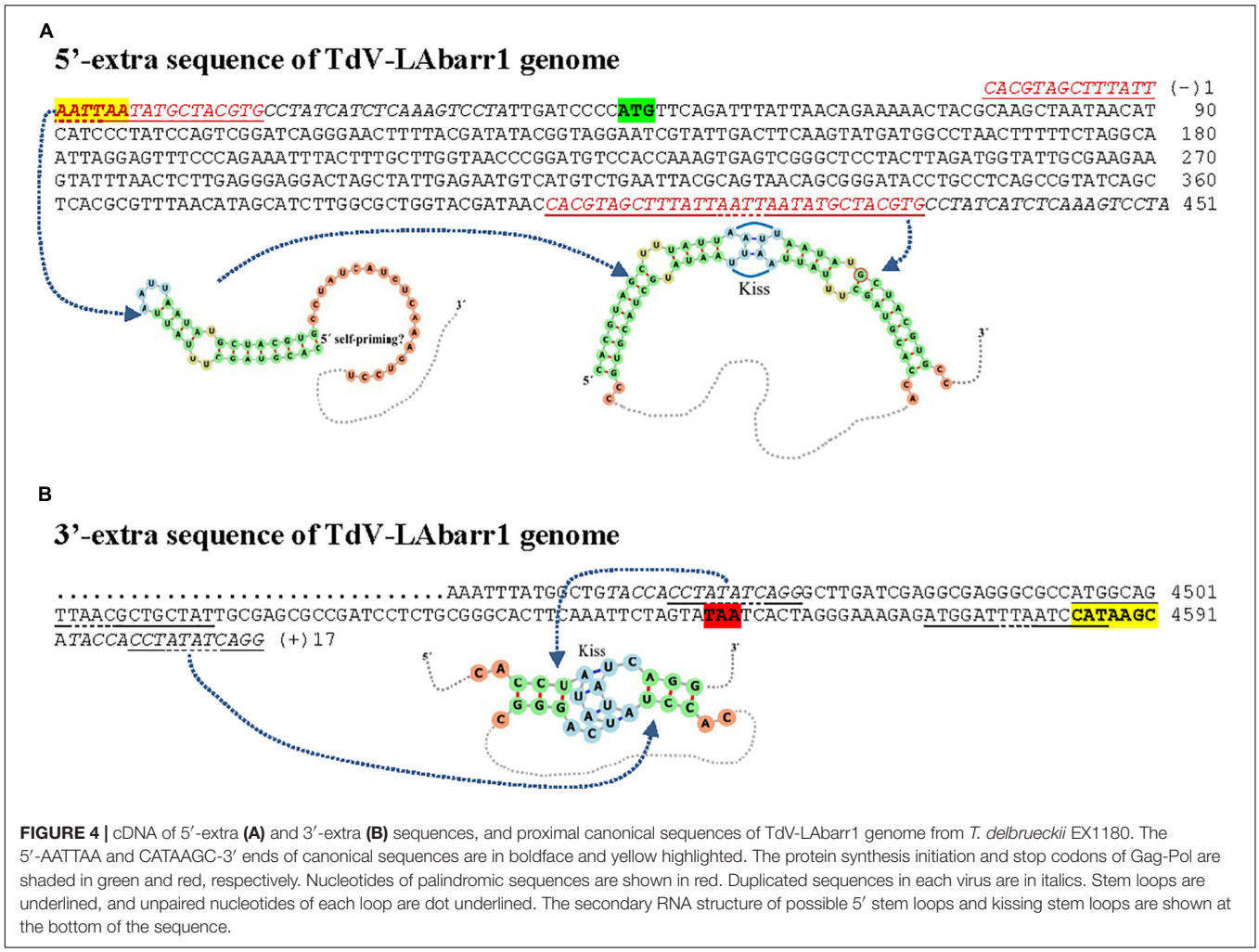

FIGURE 4 | cDNA of 5′-extra **(A)** and 3′-extra **(B)** sequences, and proximal canonical sequences of TdV-LAbarr1 genome from *T. delbrueckii* EX1180. The 5′-AATTAA and CATAAGC-3′ ends of canonical sequences are in boldface and yellow highlighted. The protein synthesis initiation and stop codons of Gag-Pol are shaded in green and red, respectively. Nucleotides of palindromic sequences are shown in red. Duplicated sequences in each virus are in italics. Stem loops are underlined, and unpaired nucleotides of each loop are dot underlined. The secondary RNA structure of possible 5′ stem loops and kissing stem loops are shown at the bottom of the sequence.

form a stem loop (ΔG = -24 kJ/mol) with unpaired nucleotides compatible with a kissing RNA interaction (5′-AAUU/3′-UUAA). No stretch with viral self-identity was found in 3′-extra sequences of ScV-LA2-EX1125, ScV-LAlus1-EX436, ScV-LAlus4-EX229, or ScV-LAlusA-EX1160, but a possible stem loop was found in every case, and one or two stem loops were also found close to the 3′-end of the canonical sequence of each virus (**Figure 5B**). No kissing-loop interaction was detected, however, for any of these four viruses. Further additional sequences were also found in ScV-LAlus1-EX436, 261 nt [C4560 to T(+)203] with 100% identity with *S. cerevisiae* 26S rRNA (**Table 3** and **Figure 5B**), which could also be involved in kissing-like interactions. This sequence stretch belongs to a part of the 26S-rRNA different from that found in the 5′-extra sequence of the same virus.

DISCUSSION

Analysis of the TdV-LAbarr1

The average nucleotide similarity of TdV-LAbarr1 with ScV-LA1-original and ScV-LAlus4 was high, but not as high as that found between both *S. cerevisiae* viruses. This was to be expected given that they come from different yeast species with different ecological niches—*S. cerevisiae* is rarely isolated from natural environments (Kurtzman, 2011a), while *T. delbrueckii* in widely distributed in nature (Kurtzman, 2011b)—and no external infection capability has yet been described for these viruses. However, the TdV-LAbarr1 genome organization is quite similar to that of ScV-LA-original and ScV-LAlus4. It contains the same two Gag and Pol ORFs and shares 87.5–100% identity in some regions considered important for the virus replication cycle, such as the frameshifting region that facilitates the fusion of Gag and Pol or the virus packaging signal. Nevertheless, the few nucleotide changes we found in the frameshifting region may affect the frameshift efficiency, and hence the ratio between Gag and Gag-Pol (Dinman and Wickner, 1992). With respect to the 5′ and 3′ untranslated terminal regions, where important *cis* signals for transcription and replication are located, the degree of sequence conservation observed was less than that of the translated region—only 67% conservation in the 3′-end replication stem-loop sequence and absence of the conserved 5′GAAAAA motif in TdV-LAbarr1. Despite this, as has previously been argued (Rodríguez-Cousiño et al., 2013), it is likely that the secondary or tertiary structure of the 3′-end replication stem loop is the

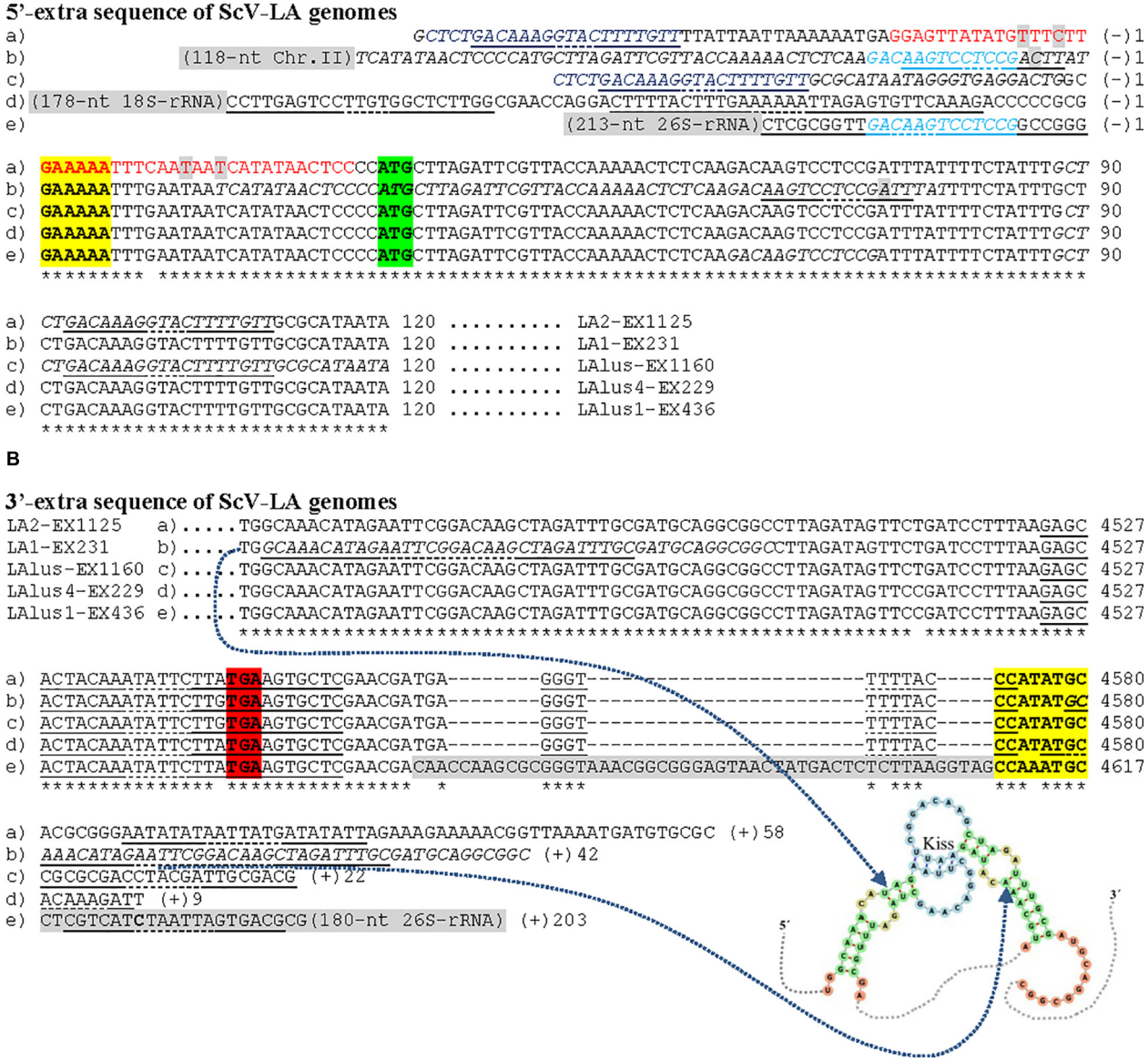

FIGURE 5 | Nucleotide sequence (cDNA) alignment of 5′- **(A)** and 3′-extra **(B)** sequences, and proximal canonical sequences of ScV-LA genomes from *S. cerevisiae* strains isolated from Ribera del Guadiana: (a) LA2-EX1125; (b) LA1-EX231; (c) LAlusA-EX1160; (d) LAlus4-NGS; (e) LAlus1-EX436. Asterisks (*) indicate identical nucleotides. The 5′-GAAAAA and CCA(T/A)TGC-3′ ends of canonical sequences are in boldface and yellow highlighted. The protein synthesis initiation and stop codons of Gag-Pol are shaded in green and red, respectively. Sequence stretches that are homologous in two different virus genomes are light-blue or dark-blue shaded. The 5′-extra sequences that are homologous to rRNA or chromosome II sequences of *S. cerevisiae* are light- gray shaded. Nucleotides of palindromic sequences are shown in red. Duplicated sequences in each virus are in italics. Stem loops are underlined, and unpaired nucleotides of each loop are dot underlined. The possible kissing stem-loop secondary RNA structure in ScV-LA1-EX231 is shown at the bottom of the sequence.

feature required for LA virus replication instead of the sequence itself. Similarly, despite the absence of the 5′GAAAAA motif in TdV-LAbarr1, it does contain an AU-rich 15-nucleotide stretch (100% AU for ScV-LA-original and TdV-LAbarr1) that could be responsible for facilitating the melting of the molecule and the access of the RNA polymerase to the template strand for the conservative transcription (Rodríguez-Cousiño et al., 2013). Additionally, 14 extra nucleotides at the 5′ end, 17 extra nucleotides at the 3′ end, and a 17-nucleotide non-homologous stretch close to the 5′ end account for the rest of the relevant differences of TdV-LAbarr1 with ScV-LA-original and ScV-LAlus4. As the ends of these dsRNA genomes are usually harder to sequence accurately than the rest of the molecule, the finding of these extra sequences suggests that they might have been missed in previously published ScV-LA-original and ScV-LAlus4 genomes that were sequenced using traditional cDNA

sub-cloning approaches (Urayama et al., 2018, 2020). Such a missing sequence might be the reason for the failure up to now of LA launching experiments between different yeast strains (Valle and Wickner, 1993).

In agreement with the nucleotide sequence, the amino-acid sequence identity of TdV-LAbarr1 Gag-Pol with that of ScV-LA-original and ScV-LAlus4, while high, is lower than that between ScV-LA-original and ScV-LAlus4. Once again, however, the relevant features previously described for the ScV-LA-original Gag and Pol proteins (Rodríguez-Cousiño et al., 2013) are conserved in TdV-LAbarr1. In particular, these are as follows: a similar central part of Gag, probably reflecting structural constraints of Gag to interact with another Gag subunit and form the asymmetric Gag dimer present in the icosahedral LA virion; the 100% identity of the His154 residue (His153 in TdV-LAbarr1) required for cap-snatching and the four crucial residues for cap recognition (Blanc et al., 1994; Tang et al., 2005); and the four conserved motifs in the central domain of the RdRps (Ribas and Wickner, 1992; Bruenn, 2003). Even two non-homologous regions that can be considered as relevant Gag-Pol features, which should not require a high degree of conservation among the different Gag-Pol fusion proteins, are also present. These are the 19-amino-acid variable stretch located downstream from the aforementioned His-153 (likely to be facing the outer surface of the virion and probably not structurally important), and the hydrophobic 44-amino-acid variable stretch located in the N-terminal region of Pol (likely to be separating the Gag and Pol domains in the fusion protein) (Rodríguez-Cousiño et al., 2013). All these features, similar to those already found in *S. cerevisiae,* point to TdV-LAbarr1 being a typical LA virus sharing a lower sequence identity than ScV-LA-original and ScV-LAlus4 because it belongs to a different yeast genus.

Phylogenetic Relationship of TdV-LAbarr1 and LA Viruses From *Saccharomyces* Yeasts

The phylogenetic relationship we found for *Saccharomyces* LA viruses is similar to that reported previously (Vepštaitė-Monstavičė et al., 2018), showing two main clusters, one including mainly *S. cerevisiae* viruses, and another including most *S. paradoxus* viruses. An alternative proposal is of two clades for LA viruses included in the *S. paradoxus* cluster: an LA-28 type, including SpV-LA-66, SpV-LA-21, and SpV-LA-28, and the rest of the *S. paradoxus* viruses (Rodríguez-Cousiño et al., 2017; Vepštaitė-Monstavičė et al., 2018). However, contrary to what has previously been described (Vepštaitė-Monstavičė et al., 2018), LA viruses from *S. cerevisiae* seem to be more homogeneous than those from *S. paradoxus*. This may just be a reflection of the geographical closeness of the locations at which the *S. cerevisiae* strains were collected from which the new LA viruses included in our study were isolated. Further analysis of new killer yeasts isolated from different, well documented, geographical locations (close and distant) is needed to clarify this issue.

Comparing the amino acid sequence of Gag proteins represents an interesting approach to study the co-evolution of each LA virus with each yeast species. Indeed, we found that this approach was clearly the best method to group all yeast strains of the same species, at least in the case of *S. cerevisiae*. Surprisingly, two stretches of the Gag-Pol sequences previously known as poorly conserved (Rodríguez-Cousiño et al., 2013) were those most conserved among the *S. cerevisiae* viruses isolated from the same geographical region (spontaneous wine fermentation, Ribera del Guadiana, Spain), regardless of which type of M killer virus was supported by these helper LA viruses in each case. However, the opposite was found when comparing the same sequence stretches of the viruses included in the *S. cerevisiae* cluster with the rest of the viruses. The corresponding identity percentage was the lowest found even when the viruses belonged to the same yeast species isolated at only 300 km distance (K2 *S. cerevisiae* 8F13 from Toro and *S. cerevisiae*-cluster yeasts from Ribera del Guadiana, both in Spain), to different yeast species isolated in the same area (Kbarr1 *T. delbrueckii* EX1180 and *S. cerevisiae*-cluster yeasts, all from Ribera del Guadiana, Spain), or to different yeast species isolated at only 120 km distance (*S. kudriavzevii* FM1183 from Castelo de Vide, Portugal and *S. cerevisiae*-cluster yeasts from Ribera del Guadiana, Spain). In particular therefore, if 100% identity is found in these two variable sequence stretches of Gag-Pol, those LA viruses may be considered to come from the same yeast species isolated from the same geographical area, no matter which type of M killer virus coincides with the LA virus in the same yeast strain. Therefore, these LA-virus variable sequences could be a good genetic marker of the unknown geographical origin of a given yeast killer strain.

Contrary to a previous suggestion (Rodríguez-Cousiño and Esteban, 2017; Rodríguez-Cousiño et al., 2017), there seems to occur no specific association of each toxin-producing M with its helper virus as a result of viral co-evolution. Therefore, as dsRNA nucleotide and Gag-Pol amino-acid sequence identity of ScV-LA viruses depends mostly on the geographical location at which the *S. cerevisiae* strains were isolated, viral cross transmission between yeast strains of the same species living in the same habitat is to be expected. The lowest identity among ScV-LA viruses was found between different yeast species, even if they came from the same geographical location, as was the case for *T. delbrueckii* EX1180 and the *S. cerevisiae*-cluster strains. Therefore, contrary to what has previously been suggested for some yeast species of the *Saccharomyces sensu stricto* taxon (Rodríguez-Cousiño et al., 2017), cross-species LA virus transmission between *S. cerevisiae* and *T. delbrueckii* seems improbable. Unfortunately, we have no LA virus sequences from different *Saccharomyces* species isolated from the same location or locations that are very close geographically in order to analyze in depth whether cross-species transmission of LA viruses between yeasts of the *Saccharomyces sensu stricto* group actually occurs.

Our finding that the sequence identity of ScV-LA viruses from *S. kudriavzevii* and *S. uvarum* with some *S. paradoxus* viruses is greater than that between some *S. paradoxus* strains themselves indicates possible cross-species transmission among

closely related yeasts (such as those of the *Saccharomyces sensu stricto* taxon) when they coincide in the same habitat, as has previously been suggested (Rodríguez-Cousiño et al., 2017).

As mentioned above, an associated co-evolution of specific LA virus variants with the corresponding specific type of M virus has been suggested based on a possible role of each killer toxin selecting the LA variants that best support each specific toxin-encoding M virus. This is a plausible hypothesis to explain why LAlus4 is specifically associated with Mlus4 virus (Rodríguez-Cousiño et al., 2013) and that LA2 is required for specific M2 maintenance, whereas neither LA nor LAlus4 show helper activity for M2 with the same genetic background (Rodríguez-Cousiño and Esteban, 2017). Our results, however, do not support this hypothesis because the same ScV-LAlus virus found in all strains of the *S. cerevisiae* cluster, whose Gag-Pol amino-acid sequence varied only by 0–1.5%, supports various M virus types (M1 in EX231, M2 in EX1125, and Mlus in EX229, EX436, and EX1160). These results indicate that there was no associated co-evolution of specific LA with specific M viruses at all. It seems that an M virus can infect new yeasts and be stably maintained inside the cell as long as a given LA virus provides it with the required helper activity.

TdV-LAbarr1 is the most distant from the rest of the viruses (62–63% identity), even from those viruses from *S. cerevisiae* strains isolated in the same location. Therefore, the co-evolution can be hypothesized of a specific LA virus with its specific host and habitat. The sequence identity percentage of TdV-LAbarr1 with its *Saccharomyces* counterparts was less when comparing only Gag sequences, but greater when comparing only the RdRp domain sequences. This indicates that LA viruses may have evolved to adapt their capsid's functioning to better ensure replication in different yeast species and habitats. On the contrary, as features of the RNA polymerase are strongly conserved, no great changes in this enzyme would be required for these viruses to replicate in unrelated yeast species.

Features of 5′- and 3′-Extra Sequences Found in LA Genomes

The extra sequences we found are probably only part of the actual extra sequences that might be present in each virus, and we cannot be sure whether they are present in the dsRNA within the completed virion or just part of an RNA intermediary of the virus. Similar results have been reported for yeast M viruses sequenced using HTS techniques (Ramírez et al., 2017). In that case, however, no viral self-identity was found between the extra and canonical sequences of the same virus, ribosomal RNA sequences were only found in the 3′-extra sequences, and sequences from other organisms (such as *S. cerevisiae* LBC-2 virus, wine grape, *Saccharomycopsis fibuligera*, and melon) were also found in the 5′-extra sequences. It was suggested in that work that ScV-M RNA could somehow promiscuously covalently join other host viral or cellular RNAs, as has also been suggested for poliovirus RNA (Gmyl et al., 2003) and plant viruses (Sztuba-Soliñska et al., 2011). In this way, M viruses could stay integrated in cellular RNA as rRNA, similarly to the case of retroviruses and retrotransposons in chromosomal DNA, protecting themselves from disappearance under potential stressing conditions as long as the receptor RNA remains in the cell.

Our new results do not contradict that hypothesis, but do suggest new possibilities to explain the existence of extra sequences beyond the canonical ends of LA viruses. The presence of identical stretches in the 5′-extra sequences of some LA genomes (LA2-EX1125 and LAlusA-EX1160, or LA1-EX231 and LAlus1-EX436) suggests that at least part of these extra sequences may have a common origin. Given that viral self-identity is frequently found between some stretches of extra and canonical sequences, the presence of extra sequences may be a collateral result of some imprecise molecular mechanism involved in the viral replication cycle—cap-snatching, for example (Fujimura and Esteban, 2011). This circumstance may favor LA RNA recombination with other RNA and which may fulfill some still unknown structural feature. As mentioned above, this possibility could provide these viruses with a strategy to protect themselves from disappearance under strongly stressing conditions, as long as they stay bound to a less vulnerable host RNA molecule. This phenomenon could be similar to the endogenization of certain ant genome RNA viruses (Flynn and Moreau, 2019), but, in yeasts, employing a different strategy that may involve rRNA instead of nuclear chromosomes. Alternatively, the formation of double-strand stem loops at the ends of these virus genomes may protect the intermediary ssRNA from degradation by single-strand exonucleases, or also provide a free 3′-end in the ssRNA to be used by primer-dependent RNA-dependent RNA polymerases for double-stranded RNA synthesis. These double-strand stem loops might even have both functions at the same time. Moreover, the formation of kissing stem loops may help maintain part of the viral genome temporarily unpaired so as to facilitate the accessibility of polymerase to an (−)ssRNA template for mRNA transcription.

Intramolecular interaction between extra sequences and proximal canonical sequences (such as the possible kissing stem loops found in TdV-LAbarr1 and ScV-LA1-EX231) may play an as yet unknown role in the biology of these viruses (Lim and Brown, 2018). Beyond these intramolecular interactions, the presence of terminal rRNA sequences in 5′- and 3′-extra sequences of yeast viruses could be involved in intermolecular interactions related to some biological process of these viruses. Indeed, rRNA-containing mRNAs have been found extensively in mammal cells. Among these, short rRNA sequences seem to function as *cis*-regulatory elements in translational efficiency, and large portions or even almost entire sequences of rRNA may have functional significance for some neurodegenerative diseases (Mauro and Edelman, 1997; Kong et al., 2008; Pánek et al., 2013). Moreover, as the portions of rRNA found in yeast viruses are different and do not share homology, sequence stretches in the same or different viruses such as LA and M could interact in a similar way to how they interact in the ribosome, maybe even involving ribosomal proteins as has been suggested for rRNA-like sequences and rRNA interaction for *cis*-regulation events

(Mauro and Edelman, 1997). This also raises the possibility of a ribonucleoprotein being created that may resemble the yeast ribosome and contain the virus genome. This ribosome-like complex may also be a strategy of these viruses to ensure that they remain in the yeast cell, or it may be related to some other, still unknown, biological function.

CONCLUSION

The killer dsRNA virus system of *T. delbrueckii* Kbarr1 yeast seems very similar to that previously described for *S. cerevisiae*. The autonomous LA viruses from the two yeast species show high nucleotide sequence identity, especially in the most relevant functional motifs, which indicates that they are phylogenetically related. LA virus transmission among yeasts of the same species living in the same geographical location seems to be feasible, but not cross-species transmission among phylogenetically distant yeasts such as *T. delbrueckii* and *S. cerevisiae*. Co-evolution of LA and M viruses does not seem likely, although co-evolution of LA virus with a given yeast species may occur in a specific location or habitat. Extra sequences located up- and down-stream from the viral canonical genome may form interesting RNA secondary structures, which could be involved in virus maintenance by avoiding ssRNA degradation and facilitating dsRNA synthesis.

DATA AVAILABILITY STATEMENT

The datasets generated for this study can be found in the online repositories. The names of the repository/repositories and accession number(s) can be found in the article/ **Supplementary Material**.

AUTHOR CONTRIBUTIONS

MR conceived the project, analyzed the data, and wrote and edited the manuscript. MR, RV, AM, and MM designed and performed the experiments. All authors contributed to the article and approved the submitted version.

FUNDING

This study was funded with the Grants GR18117 from the Extremadura Regional Government (Consejería de Economía, Ciencia y Agenda Digital) and AGL2017-87635-R from the Spanish Ministry of Education and Science, and the European Regional Development Fund (ERDF - European Union). RV gratefully acknowledges the support of a studentship from the Extremadura Regional Government.

ACKNOWLEDGMENTS

We thank the Unidad de Genómica Cantoblanco (Fundación Parque Científico de Madrid, Spain) for setting up the protocols for library preparation and sequencing of viral dsRNA, and the firm Biotechvana S.L. (Technological Park of Valencia, Spain) for setting up the dsRNA sequence assembly strategy.

SUPPLEMENTARY MATERIAL

The Supplementary Material for this article can be found online at: https://www.frontiersin.org/articles/10.3389/fmicb.2020.593846/full#supplementary-material

REFERENCES

Altschul, S. F., Madden, T. L., Schäffer, A. A., Zhang, J., Zhang, Z., Miller, W., et al. (1997). Gapped BLAST and PSI-BLAST: a new generation of protein database search programs. *Nucleic Acids Res.* 25, 3389–3402. doi: 10.1093/nar/25.17.3389

Blanc, A., Ribas, J. C., Wickner, R. B., and Sonenberg, N. (1994). His-154 is involved in the linkage of the *Saccharomyces cerevisiae* L-A double-stranded RNA virus Gag protein to the cap structure of mRNAs and is essential for M1 satellite virus expression. *Mol. Cell. Biol.* 14, 2664–2674. doi: 10.1128/mcb.14.4.2664

Bruenn, J. A. (2003). A structural and primary sequence comparison of the viral RNA-dependent RNA polymerases. *Nucleic Acids Res.* 31, 1821–1829. doi: 10.1093/nar/gkg277

Dinman, J. D., and Wickner, R. B. (1992). Ribosomal frameshifting efficiency and gag/gag-pol ratio are critical for yeast M1 double-stranded RNA virus propagation. *J. Virol.* 66, 3669–3676. doi: 10.1128/jvi.66.6.3669-3676.1992

Esteban, R., Fujimura, T., and Wickner, R. B. (1989). Internal and terminal cis-acting sites are necessary for *in vitro* replication of the L-A double-stranded RNA virus of yeast. *Embo J.* 8, 947–954. doi: 10.1002/j.1460-2075.1989.tb03456.x

Flynn, P. J., and Moreau, C. S. (2019). Assessing the diversity of endogenous viruses throughout ant genomes. *Front. Microbiol.* 10:1139. doi: 10.3389/fmicb.2019.01139

Fujimura, T., and Esteban, R. (2011). Cap-snatching mechanism in yeast L-A double-stranded RNA virus. *Proc. Natl. Acad. Sci. U.S.A.* 108, 17667–17671. doi: 10.1073/pnas.1111900108

Fujimura, T., and Esteban, R. (2013). Cap snatching in yeast L-BC double-stranded RNA totivirus. *J. Biol. Chem.* 288, 23716–23724. doi: 10.1074/jbc.M113.490953

Fujimura, T., Esteban, R., Esteban, L. M., and Wickner, R. B. (1990). Portable encapsidation signal of the L-A double-stranded-RNA virus of *Saccharomyces cerevisiae*. *Cell* 62, 819–828. doi: 10.1016/0092-8674(90)90125-x

Fujimura, T., Ribas, J. C., Makhov, A. M., and Wickner, R. B. (1992). Pol of gag-pol fusion protein required for encapsidation of viral RNA of yeast L-A virus. *Nature* 359, 746–749. doi: 10.1038/359746a0

Fujimura, T., and Wickner, R. B. (1989). Reconstitution of template-dependent *in vitro* transcriptase activity of a yeast double-stranded RNA virus. *J. Biol. Chem.* 264, 10872–10877.

Futami, R., Muñoz-Pomer, L., Dominguez-Escriba, L., Covelli, L., Bernet, G. P., and Sempere, J. M. (2011). GPRO The professional tool for annotation, management and functional analysis of omic databases. *Biotechvana Bioinform. SOFT* 3:2011.

Gmyl, A. P., Korshenko, S. A., Belousov, E. V., Khitrina, E. V., and Agol, V. I. (2003). Non-replicative homologous RNA recombination: promiscuous joining of RNA pieces? *RNA* 9, 1221–1231. doi: 10.1261/rna.5111803

Guthrie, C., and Fink, G. R. (1991). Guide to yeast genetics and molecular biology. *Methods Enzymol.* 194, 3–57.

Hittinger, C. T. (2013). *Saccharomyces* diversity and evolution: a budding model genus. *Trends Genet.* 29, 309–317. doi: 10.1016/j.tig.2013.01.002

Icho, T., and Wickner, R. B. (1989). The double-stranded RNA genome of yeast virus L-A encodes its own putative RNA polymerase by fusing two open reading frames. *J. Biol. Chem.* 264, 6716–6723.

Kerpedjiev, P., Hammer, S., and Hofacker, I. L. (2015). Forna (force-directed RNA): simple and effective online RNA secondary structure diagrams. *Bioinformatics* 31, 3377–3379. doi: 10.1093/bioinformatics/btv372

Kong, Q., Stockinger, M. P., Chang, Y., Tashiro, H., and Lin, C. L. (2008). The presence of rRNA sequences in polyadenylated RNA and its potential functions. *Biotechnol. J.* 3, 1041–1046. doi: 10.1002/biot.200800122

Konovalovas, A., Serviené, E., and Serva, S. (2016). Genome sequence of *Saccharomyces cerevisiae* double-stranded RNA Virus L-A-28. *Genome Announc.* 4:e00549-16. doi: 10.1128/genomeA.00549-16

Kurtzman, C. P. (2011a). "*Saccharomyces* Meyen ex Reess (1870)," in *The Yeasts: A Taxonomic Study*, 5th Edn, eds C. P. Kurtzman, J. W. Fell, and T. Boekhout (London: Elsevier), 733–763. doi: 10.1016/b978-0-444-52149-1.00061-6

Kurtzman, C. P. (2011b). "*Torulaspora* Lindner (1904)," in *The Yeasts: A Taxonomic Study*, 5th Edn, eds C. P. Kurtzman, J. W. Fell, and T. Boekhout (London: Elsevier), 867–874.

Kurtzman, C. P., and Robnett, C. J. (2003). Phylogenetic relationships among yeasts of the '*Saccharomyces complex*' determined from multigene sequence analyses. *FEMS Yeast Res.* 3, 417–432. doi: 10.1016/s1567-1356(03)00012-6

Lim, C. S., and Brown, C. M. (2018). Know your enemy: successful bioinformatic approaches to predict functional RNA structures in viral RNAs. *Front. Microbiol.* 8:2582. doi: 10.3389/fmicb.2017.02582

Liti, G., Carter, D. M., Moses, A. M., Warringer, J., Parts, L., James, S. A., et al. (2009). Population genomics of domestic and wild yeasts. *Nature* 458, 337–341. doi: 10.1038/nature07743

Lukša, J., Ravoitytė, B., Konovalovas, A., Aitmanaitė, L., Butenko, A., Yurchenko, V., et al. (2017). Different metabolic pathways are involved in response of *Saccharomyces cerevisiae* to L-A and M Viruses. *Toxins* 9:233. doi: 10.3390/toxins9080233

Luo, R., Liu, B., Xie, Y., Li, Z., Huang, W., Yuan, J., et al. (2012). SOAPdenovo2: an empirically improved memory-efficient short-read *de novo* assembler. *Gigascience* 1, 18–24. doi: 10.1186/2047-217X-1-18

Madeira, F., Park, Y. M., Lee, J., Buso, N., Gur, T., Madhusoodanan, N., et al. (2019). The EMBL-EBI search and sequence analysis tools APIs in 2019. *Nucleic Acids Res.* 47, W636–W641. doi: 10.1093/nar/gkz268

Maqueda, M., Zamora, E., Álvarez, M. L., and Ramírez, M. (2012). Characterization, ecological distribution, and population dynamics of *Saccharomyces* "sensu stricto" killer yeasts in the spontaneous grape-must fermentations of south-western Spain. *Appl. Environ. Microbiol.* 78, 735–743. doi: 10.1128/aem.06518-11

Maqueda, M., Zamora, E., Rodríguez-Cousiño, N., and Ramírez, M. (2010). Wine yeast molecular typing using a simplified method for simultaneously extracting mtDNA, nuclear DNA and virus dsRNA. *Food Microbiol.* 27, 205–209. doi: 10.1016/j.fm.2009.10.004

Mauro, V. P., and Edelman, G. M. (1997). rRNA-like sequences occur in diverse primary transcripts: implications for the control of gene expression. *Proc. Natl. Acad. Sci. U.S.A.* 94, 422–427. doi: 10.1073/pnas.94.2.422

Pánek, J., Kolár, M., Vohradský, J., and Shivaya Valášek, L. (2013). An evolutionary conserved pattern of 18S rRNA sequence complementarity to mRNA 5′ UTRs and its implications for eukaryotic gene translation regulation. *Nucleic Acids Res.* 41, 7625–7634. doi: 10.1093/nar/gkt548

Park, C. M., Lopinski, J. D., Masuda, J., Tzeng, T. H., and Bruen, J. A. (1996). A second double-stranded RNA virus from yeast. *Virology* 216, 451–454. doi: 10.1006/viro.1996.0083

Ramírez, M., Velázquez, R., López-Pineiro, A., Naranjo, B., Roig, F., and Llorens, C. (2017). New Insights into the genome organization of yeast killer viruses based on "atypical" killer strains characterized by high-throughput sequencing. *Toxins* 9:292. doi: 10.3390/toxins9090292

Ramírez, M., Velázquez, R., Maqueda, M., López-Piñeiro, A., and Ribas, J. C. (2015). A new wine *Torulaspora delbrueckii* killer strain with broad antifungal activity and its toxin-encoding double-stranded RNA virus. *Front. Microbiol.* 6:983. doi: 10.3389/fmicb.2015.00983

Ribas, J. C., and Wickner, R. B. (1992). RNA-dependent RNA polymerase consensus sequence of the L-A double-stranded RNA virus: definition of essential domains. *Proc. Natl. Acad. Sci. U.S.A.* 89, 2185–2189. doi: 10.1073/pnas.89.6.2185

Rodríguez-Cousiño, N., and Esteban, R. (2017). Relationships and evolution of double-stranded RNA Totiviruses of yeasts inferred from analysis of L-A-2 and L-BC variants in wine yeast strain populations. *Appl. Environ. Microbiol.* 83:e02991-16. doi: 10.1128/aem.02991-16

Rodríguez-Cousiño, N., Gómez, P., and Esteban, R. (2013). L-A-lus, a new variant of the L-A Totivirus found in wine yeasts with Klus killer toxin-encoding Mlus double-stranded RNA: possible role of killer toxin-encoding satellite RNAs in the evolution of their helper viruses. *Appl. Environ. Microbiol.* 79, 4661–4674. doi: 10.1128/aem.00500-13

Rodríguez-Cousiño, N., Gómez, P., and Esteban, R. (2017). Variation and distribution of L-A helper Totiviruses in *Saccharomyces sensu stricto* yeasts producing different killer toxins. *Toxins* 9:313. doi: 10.3390/toxins9100313

Rodríguez-Cousiño, N., Maqueda, M., Ambrona, J., Zamora, E., Esteban, E., and Ramírez, M. (2011). A new wine *Saccharomyces cerevisiae* double-stranded RNA virus encoded killer toxin (Klus) with broad antifungal activity is evolutionarily related to a chromosomal host gene. *Appl. Environ. Microbiol.* 77, 1822–1832. doi: 10.1128/aem.02501-10

Rowley, P. A., Ho, B., Bushong, S., Johnson, A., and Sawyer, S. L. (2016). XRN1 is a species-specific virus restriction factor in yeasts. *PLoS Pathog.* 12:e1005890. doi: 10.1371/journal.ppat.1005890

Scannell, D. R., Zill, O. A., Rokas, A., Payen, C., Dunham, M. J., Eisen, M. B., et al. (2011). The awesome power of yeast evolutionary genetics: new genome sequences and strain resources for the *Saccharomyces sensu* stricto genus. *G3* 1, 11–25. doi: 10.1534/g3.111.000273

Schmitt, M. J., and Breinig, F. (2006). Yeast viral killer toxins: lethality and self-protection. *Nat. Rev. Microbiol.* 4, 212–221. doi: 10.1038/nrmicro1347

Schmitt, M. J., and Tipper, D. J. (1995). Sequence of the M28 dsRNA: preprotoxin is processed to an α/β heterodimeric protein. *Virology* 213, 341–351. doi: 10.1006/viro.1995.0007

Sztuba-Solińska, J., Urbanowicz, A., Figlerowicz, M., and Bujarski, J. J. (2011). RNA-RNA recombination in plant virus replication and evolution. *Annu. Rev. Phytopathol.* 49, 415–443. doi: 10.1146/annurev-phyto-072910-095351

Tang, J., Naitow, H., Gardner, N. A., Kolesar, A., Tang, L., Wickner, R. B., et al. (2005). The structural basis of recognition and removal of cellular mRNA 7-methyl G 'caps' by a viral capsid protein: a unique viral response to hose defense. *J. Mol. Recogn.* 18, 158–168. doi: 10.1002/jmr.724

Thiele, D. J., and Leibowitz, M. J. (1982). Structural and functional analysis of separated strands of killer double-stranded RNA of yeast. *Nucleic Acids Res.* 10, 6903–6918. doi: 10.1093/nar/10.21.6903

Thiele, D. J., Wang, R. W., and Leibowitz, M. J. (1982). Separation and sequence of the 3′ termini of M double-stranded RNA from killer yeast. *Nucleic Acids Res.* 10, 1661–1678.

Thompson, J. D., Higgins, D. G., and Gibson, T. J. (1994). CLUSTAL W: improving the sensitivity of progressive multiple sequence alignment through sequence weighting, position-specific gap penalties and weight matrix choice. *Nucleic Acids Res.* 22, 4673–4680. doi: 10.1093/nar/22.22.4673

Toh-e, A., Guerry, P., and Wickner, R. B. (1978). Chromosomal superkiller mutants of *Saccharomyces cerevisiae*. *J. Bacteriol.* 136, 1002–1007. doi: 10.1128/jb.136.3.1002-1007.1978

Urayama, S. I., Takaki, Y., Hagiwara, D., and Nunoura, T. (2020). dsRNA-seq reveals novel RNA virus and virus-like putative complete genome sequences from *Hymeniacidon sp. sponge*. *Microbes Environ.* 35:ME19132. doi: 10.1264/jsme2.ME19132

Urayama, S. I., Takaki, Y., Nishi, S., Yoshida-Takashima, Y., Deguchi, S., Takai, K., et al. (2018). Unveiling the RNA virosphere associated with marine microorganisms. *Mol. Ecol. Resourc.* 18, 1444–1455. doi: 10.1111/1755-0998.12936

Valle, R. P. C., and Wickner, R. B. (1993). Elimination of L-A double-stranded RNA virus of *Saccharomyces cerevisiae* by expression of gag and gag-pol from an L-A cDNA clone. *J. Virol.* 67, 2764–2771. doi: 10.1128/jvi.67.5.2764-2771.1993

Vepštaitė-Monstavičė, I., Lukša, J., Konovalovas, A., Ežerskytė, D., Stanevičienė, R., Strazdaitė-Žielienė, Ž, et al. (2018). *Saccharomyces paradoxus* K66 killer system evidences expanded assortment of helper and satellite viruses. *Viruses* 10:564. doi: 10.3390/v10100564

Wickner, R. B. (1991). "Yeast RNA virology: the killer systems," in *The Molecular and Cellular Biology of the Yeast Saccharomyces: Genome Dynamics,*

Protein Synthesis, and Energetics, eds J. R. Broach, J. R. Pringle, and E. W. Jones (Cold Spring Harbor, NY: Cold Spring Harbor Laboratory Press), 263–296.

Wickner, R. B., Bussey, H., Fujimura, T., and Esteban, R. (1995). "Viral RNA and the killer phenomenon of *Saccharomyces*," in *The Mycota. vol.II. Genetics and Biotechnology*, ed. U. Kück (Berlin: Springer Verlag), 211–226. doi: 10.1007/978-3-662-10364-7_13

Zuker, M., Mathews, D. H., Turner, D. H., Barciszewski, J., and Clark, B. F. C. (1999). "Algorithms and thermodynamics for RNA secondary structure prediction: A practical guide," in *RNA Biochemistry and Biotechnology*, eds J. Barciszewski and B. F. C. Clark (Boston: Kluwer Academic Publishers).

Conflict of Interest: The authors declare that the research was conducted in the absence of any commercial or financial relationships that could be construed as a potential conflict of interest.

frontiers in Microbiology

ORIGINAL RESEARCH
published: 09 December 2020
doi: 10.3389/fmicb.2020.569869

A Novel Ourmia-Like Mycovirus Confers Hypovirulence-Associated Traits on *Fusarium oxysporum*

*Ying Zhao[1], Yuanyan Zhang[1], Xinru Wan[1], Yuanyuan She[1], Min Li[1], Huijun Xi[1], Jiatao Xie[2] and Caiyi Wen[1]**

[1] College of Plant Protection, Henan Agricultural University, Zhengzhou, China, [2] State Key Laboratory of Agricultural Microbiology, Huazhong Agricultural University, Wuhan, China

Fusarium wilt caused by *Fusarium oxysporum* f. sp. *momordicae* (*FoM*) is an important fungal disease that affects the production of bitter gourd. Hypovirulence-associated mycoviruses have great potential and application prospects for controlling the fungal disease. In this study, a novel ourmia-like virus, named *Fusarium oxysporum* ourmia-like virus 1 (FoOuLV1), was isolated from *FoM* strain HuN8. The viral genomic RNA is 2,712 nucleotides (nt) in length and contains an open reading frame (ORF) encoding a putative RNA-dependent RNA polymerase (RdRp) using either standard or mitochondrial codes. In strain HuN8, there was also a FoOuLV1-associated RNA segment with 1,173 nt in length with no sequence homology. Phylogenetic analysis showed that FoOuLV1 is a member of the genus *Magoulivirus* of the family *Botourmiaviridae*. FoOuLV1 was found to be associated with hypovirulence in *FoM*. Moreover, FoOuLV1 and its hypovirulence trait can be transmitted horizontally to other *FoM* strains and also to other formae speciale strains of *F. oxysporum*. In addition, FoOuLV1 showed significant biological control effect against the bitter gourd Fusarium wilt. To our knowledge, this study reveals the first description of a hypovirulence-associated ourmia-like mycovirus, which has the potential to the biological control of Fusarium wilt.

Keywords: ***Fusarium oxysporum*, ourmia-like virus, hypovirulence, mycovirus, transfection**

OPEN ACCESS

Edited by:
Akio Adachi,
Kansai Medical University, Japan

Reviewed by:
Jeesun Chun,
Jeonbuk National University, South Korea
David Turra,
Università degli Studi di Napoli Federico II, Italy

****Correspondence:***
Caiyi Wen
wencaiyi@henau.edu.cn

Specialty section:
This article was submitted to Virology, a section of the journal Frontiers in Microbiology

Received: *05 June 2020*
Accepted: *12 November 2020*
Published: *09 December 2020*

Citation:
Zhao Y, Zhang Y, Wan X, She Y, Li M, Xi H, Xie J and Wen C (2020) A Novel Ourmia-Like Mycovirus Confers Hypovirulence-Associated Traits on Fusarium oxysporum. Front. Microbiol. 11:569869. doi: 10.3389/fmicb.2020.569869

INTRODUCTION

Mycoviruses are widespread in all major filamentous fungi, yeasts, and oomycetes (Xie and Jiang, 2014; Ghabrial et al., 2015). According to a recent study, more than 300 mycoviral sequences have been logged in the National Center for Biotechnology Information (NCBI) database (Zhou et al., 2020), which are grouped into at least 19 families by the International Committee on Taxonomy of Viruses (ICTV). Most mycoviruses have double-stranded RNA (dsRNA); however, some mycoviruses have positive single-stranded RNA (+ssRNA), and a few mycoviruses have single-stranded DNA (ssDNA) or negative single-stranded RNA (−ssRNA; Ghabrial and Suzuki, 2009; Xie and Jiang, 2014; Ghabrial et al., 2015). The ssRNA mycoviruses are grouped into seven families: *Alphaflexiviridae*, *Barnaviridae*, *Botourmiaviridae*, *Gammaflexiviridae*, *Hypoviridae*, *Mymonaviridae*, and *Narnaviridae* (Amarasinghe et al., 2018). There are also unclassified mycoviruses (Li H. et al., 2019).

Ourmiavirus is a genus of viruses isolated from various plants. The genome of *Ourmiavirus* contains three linear + ssRNAs, each encoding a single protein: RNA-dependent RNA polymerase (RdRp), movement protein (MP), or capsid protein (CP; Lisa et al., 1988; Turina et al., 2017). The *Ourmiavirus* has a unique bacilliform virion structure (Avgelis et al., 1989). Viruses in the family *Narnaviridae* have a 2.5- to 3.0-kb genome that encodes only an RdRp with no capsid; they have been widely discovered in fungi, oomycetes, invertebrates, and plants (Cai et al., 2012; Bruenn et al., 2015; Shi et al., 2016). Recently, many mycoviruses containing only one RNA segment encoding RdRp have been identified to be phylogenetically related to *Ourmiavirus* genus (Xu et al., 2015; Shi et al., 2016; Amarasinghe et al., 2018; Zheng et al., 2019; Li C.X. et al., 2019). Therefore, the ICTV created a new family (*Botourmiaviridae*) to incorporate these ourmia-like viruses (Turina et al., 2017; Wang et al., 2020). *Botourmiaviridae* comprising five genera: *Magoulivirus*, *Ourmiavirus*, *Botoulivirus*, *Scleroulivirus*, and *Penoulivirus* (Zhou et al., 2020). Whether these ourmia-like mycoviruses have other RNA segments remains unknown (Wang et al., 2020).

The mycoviruses infection usually causes no associated symptoms and sometimes even has beneficial effects on their fungal hosts (Zheng et al., 2019). Some mycoviruses in plant pathogenic fungi can reduce the ability of their fungal hosts to cause disease in plants. This property, named hypovirulence, has explored for biological control of crop fungal diseases. (Nuss, 2005; Xie and Jiang, 2014). Cryphonectria hypovirus 1 (CHV1) and Sclerotiorum sclerotiorum hypovirulence-associated DNA virus 1 (SsHADV-1) have been successfully used to control diseases caused by *Cryphonectria parasitica* and *Sclerotiorum sclerotiorum* (Anagnostakis, 1982; Yu et al., 2013). Besides these examples, many hypovirulence-associated mycoviruses, belonging to various genera, have been identified from diverse plant pathogenic fungi, such as Hubei sclerotinia RNA virus 1 (HuSRV1), Botryosphaeria dothidea botourmiavirus 1 (BdBOV-1), Alternaria alternata hypovirus 1 (AaHV1), and Rhizoctonia solani endornavirus 1 (RsEV1), etc. (Xie et al., 2011; Azhar et al., 2019; Zheng et al., 2019; Li H. et al., 2019). However, to our knowledge, no hypovirulence-associated ourmia-like mycovirus has been reported so far.

Fusarium is widely distributed in soil, associated with plants worldwide. It includes many important plant pathogenic fungi (Li P. et al., 2019). Many mycoviruses have been reported in different species of *Fusarium* genus, and a few of them have hypovirulent effects on their hosts, including: Fusarium graminearum virus 1 (FgV1), Fusarium graminearum virus-ch9 (FgV-ch9), Fusarium graminearum hypovirus 2 (FgHV2), and so on (Kwon et al., 2007; Darissa et al., 2012; Li et al., 2015). *F. oxysporum* is an important plant pathogenic fungus and causes vascular wilt in a wide variety of agricultural crop species. *F. oxysporum* is classified into different host-specific forms (formae speciales) based on the types of host plants (Di Pietro et al., 2003). Although a number of mycoviruses have been identified in the genus *Fusarium*, only three mycoviruses have been reported in *F. oxysporum*. *Fusarium oxysporum* chrysovirus 1 (FoCV1) was found in *F. oxysporum* f. sp. *melonis* and assigned to the family *Chrysoviridae*, but its complete genomic sequence has not been determined (Sharzei et al., 2007). *Fusarium oxysporum* f. sp. dianthi mycovirus 1 (FodV1), a new member of the family *Chrysoviridae*, has been isolated from *F. oxysporum* f. sp. *dianthi* and exerts a hypovirulent effect (Lemus-Minor et al., 2015). In addition, *Fusarium oxysporum* f. sp. dianthi mitovirus 1 (FodMV1) has been identified from *F. oxysporum* f. sp. *dianthi*, but it has no hypovirulence trait (Torres-Trenas and Pérez-Artés, 2020).

In this study, we identified and characterized a novel hypovirulence-inducing ourmia-like mycovirus from *F. oxysporum* f. sp. *momordicae* named *Fusarium oxysporum* ourmia-like virus 1 (FoOuLV1) and verified its hypovirulence trait and its horizontal transmission ability. In addition, we evaluated the biocontrol potential of FoOuLV1 by the pot and field experiments.

MATERIALS AND METHODS

Fungal Isolates and Plant Materials

Fusarium oxysporum f. sp. *momordicae* strains HuN8 and SD-1 were isolated from bitter gourd, showing symptoms of Fusarium wilt disease in Hunan and Shandong Province, China, in 2017. *F. oxysporum* f. sp. *cucumerinum* (*FoC*) strain HK3 was kindly gifted by Dr. Xuehong Wu (China Agricultural University, Beijing, China). The strains were cultured on potato dextrose agar (PDA) medium at 28°C. Fungal DNA was isolated using standard phenol-chloroform extraction and ethanol precipitation, then used for polymerase chain reaction (PCR) amplification with universal primers (ITS1 and ITS4) and specific primers (fp7318 and fp7335) to perform formae speciales identification of *F. oxysporum* (van Dam et al., 2018). Bitter gourd seeds were purchased from Fujian Agricultural Science Agricultural Seed Development Co. Ltd. All primers used in this manuscript are listed in **Supplementary Table 1**.

RNA Extraction and RT-PCR Detection

The extraction of ssRNA and dsRNA was performed following the procedure described previously (Xie et al., 2006). Strains grew for 4–5 days on cellophane membranes of the PDA medium. Fresh mycelia (1–2 *g*) were harvested to isolate dsRNA. 2 × GPS (glycine 15.0 g/L, Na_2HPO_4 14.2 g/L, NaCl 35.1 g/L, and pH = 9.6) 400 μl, phenol (pH 8.0) 400 μl, chloroform-isoamyl alcohol (24:1) 400 μl, and 10% SDS 92 μl were added to a sterile centrifuge tube each 0.2 *g* sample and were shaken for 10 min at room temperature, then centrifuged at 12,000 revolutions per minute (rpm) for 10 min. The supernatant was transferred to another clean centrifuge tube and mixed with 114 μl anhydrous ethanol for every 600 μl of the supernatant. Then 0.04 *g* cellulose powder CF-11 (Sigma–Aldrich, St. Louis, MO, United States) was added. The supernatant was shaken for 30 min in an ice bath. After centrifugation at 12,000 rpm for 1 min, the supernatant was discarded, 600 μl of eluent buffer [10 × STE (0.5 M Tris; 1 M NaCl, 10 mM EDTA, and pH = 7.0) 10 ml, 95% ethanol 17 ml, DEPC-H_2O 73 ml] was added to elute for two to three times. After centrifugation at 12,000 rpm for 2 min, the supernatant was discarded and added with 600 μl

1 × STE, mixed and shaken for 5 min, and centrifuged at 12,000 rpm for 5 min. Then the supernatant was transferred to a new centrifuge tube, and the same volume isopropyl alcohol, with acryl carrier nucleic acid co-precipitator (item No. RP2001, ®Bioteke Corporation, Beijing, China) were added to improve the yield of dsRNA. After centrifugation at 12,000 rpm at 4°C for 25 min, the precipitation was washed with 75% ethanol, dried at 37°C for 10 min, and dissolved in 25 μl DEPC-H_2O. The dsRNA was treated with RNase-free DNase I (0.6 U/μl) and S1 nuclease (3 U/μl). The segments were electrophoresed on a 1% agarose gel, stained with ethidium bromide, and visualized with gel documentation and image analysis system (InGenius LhR, Syngene, United Kingdom).

To extract total RNA, strains were grown on the cellophane membrane overlying a PDA plate for 4–5 days, and 100–200 mg fresh mycelia were harvested and ground to powder in liquid nitrogen. Total RNA was prepared using an RNA reagent (Newbio Industry, Wuhan, China), according to the manufacturer's instructions.

For RT-PCR detection, first-strand cDNAs were synthesized using TransScript One-Step gDNA Removal and cDNA Synthesis SuperMix (®TransGen Biotech, Beijing, China) according to the manufacturer's instructions. Then the PCR amplification was carried out using the specific primers (FV-L-S and FV-L-A for L-segment; FV-S-S and FV-S-A for S-segment). All primers are listed in **Supplementary Table 1**.

cDNA Cloning and Sequencing

The cDNA library was constructed using TransScript One-Step gDNA Removal and cDNA Synthesis SuperMix (TransGen Biotech) according to the manufacturer's instructions.

To obtain initial sequence clones, a random primer (RACE3RT) was used for RT-PCR amplification. The PCR products were cloned into a pMD18-T vector (Takara, Dalian, China) for Sanger sequencing, with the internal gaps between the initial sequences filled by RT-PCR. The terminal sequence cloning was performed according to the method previously described (Potgieter et al., 2009). All primers used for cDNA cloning and sequencing are listed in **Supplementary Table 1**.

Sequence and Phylogenetic Analysis

Open reading frames (ORFs) and conserved domains were predicted using ORF finder and CD-search on the website of NCBI[1] and motifs scan website[2]. Multiple sequence alignments were performed, and the phylogenetic tree was constructed using MEGA7 software (Kumar et al., 2016). Potential secondary structures were predicted by Mfold version 2.3 (Zuker, 2003).

Viral Transmission Assay

Hyphal fusion was conducted to investigate viral horizontal transmission between *Fusarium oxysporum* f. sp. *momordicae* (*FoM*) strains and *FoC* strains, following the procedure described previously (Li H. et al., 2019). The SD-1Hyg^R and HK3 Hyg^R strains which obtained hygromycin resistance by agrobacterium-mediated transformation from the strains SD-1 and HK3. The agrobacterium-mediated transformation was following the procedure described previously (Mullins et al., 2001). The agrobacterium (EHA105) and the plasmid (pTFCM) were kindly gifted by Dr. Daohong Jiang (Huazhong Agricultural University, Wuhan, China), which were described previously (Li et al., 2005). The biological phenotype of strains SD-1Hyg^R and HK3 Hyg^R were the same as the strains SD-1 and HK3.

A schematic diagram of the co-culturing performed using the viral transmission assay is shown in **Supplementary Figure 1**. Strains HuN8, SD-1HygR, and HK3Hyg^R were grown for 4–5 days on PDA medium. Then, mycelia blocks of strains HuN8 and the SD-1Hyg^R (or HK3Hyg^R) were inoculated on the same PDA plate, growing for 4–5 days until the colony of HuN8 and the SD-1HygR (or HK3HygR) covered each other. Mycelia blocks of the common colony were transferred to new PDA plates with hygromycin (50 mg/ml), growing for 2–3 days. The mycelia could grow on the hygromycin-resistant PDA plates and became the derivative strains. The viral transmission was evaluated based on dsRNA extraction or RT-PCR detection.

Virulence Assay of *in vitro* Inoculation and Pot and Field Experiments

The virulence of *FoM* strains was assessed by *in vitro* inoculation and the pot and field experiments on bitter gourd plants. For *in vitro* experiment, young leaves and petioles of bitter gourd were inoculated with *FoM* strains, moisturized for 4–5 days, observed, and photographed. The leaves inoculated with nothing were used as control. Four leaves were used for a group in each experiment, and all the experiments were repeated three times.

For the pot experiment, bitter gourd seedlings with two or three leaves grown in sterile soil were inoculated with 10 ml of *F. oxysporum* spore (10^7 ml^{-1}) suspension into the root, cultivated in the growth chamber, observed, and photographed. The plants inoculated with water were used as control. Four plants were used for a group in each experiment, and all the experiments were repeated three times.

The virulence assay of *FoC* strains was similar with the *FoM* strains. Cucumber seedlings with two leaves grown in sterile soil were inoculated with 10 ml of *F. oxysporum* spores (10^7 ml^{-1}) suspension, cultivated, observed, and photographed. Plants inoculated with water were used as control. Four plants were used for a group in each experiment, and all the experiments were repeated three times.

The field experiment was conducted from 21 May 2019 to 16 July 2019 in two fields where Fusarium wilt had been present for many years in Yuanyang, Henan Province, China. The bitter gourd seedlings (about 30 seedlings for each group in each field) were planted according to the experimental design (a schematic representation of the experiment distribution is shown in **Supplementary Figure 2**). In the treatment group, 10 ml of spores (10^7 ml^{-1}) of the SD-V strains were inoculated into the area surrounding the roots on 21 May 2019; at the same time, the control group was instead inoculated with water. The

[1]http://www.ncbi.nlm.nih.gov

[2]http://www.genome.jp/tools/motif/

disease incidence, severity, and index were assessed twice, on 25 June and on 16 July. Disease incidence was defined as the percentage of infected plants, and disease severity was rated on a scale of 0–9 as follows: level 0, no symptoms; level 1, <30% of leaves showing leaf veins with yellowing; level 3, 30–70% of leaves showing leaf veins with yellowing; level 5, leaf veins on the whole plant are yellowed, but the growth and development of the plant are not affected; level 7, the whole plant is yellowed and wilted, and the vascular bundle has turned brown and stopped growing and developing; and level 9, the plant is dead. The different levels of symptoms are shown in **Supplementary Figure 3**.

RESULTS

Viruses in *F. oxysporum* f. sp. *momordicae* Strain HuN8

Total RNA was extracted from the *FoM* strain to perform NGS. The assembled sequences were used for homology searches against the NCBI virus amino acid sequence database using BLASTX. Eight contigs could be assembled into one long contig from the database. The long contig was similar to the sequence of Magnaporthe oryzae ourmia-like virus (SBQ28480.1), thus was named FoOuLV1.

Based on the RT-PCR analysis, we found that FoOuLV1 was harbored in *FoM* strain HuN8, which was isolated from the stem of a diseased bitter gourd plant collected in Hunan Province, China. Strain HuN8 displayed a similar colony morphology to strain SD-1 (virus free) on PDA medium (**Figure 1A**) and induced slight leaf yellowing, while the virus-free strain SD-1 induced obvious leaf yellowing (**Figure 1B**). The dsRNA was extracted from strain HuN8 and treated with DNase I to digest the genomic DNA. We found that two segments, the L-segment and the S-segment, were harbored in strain HuN8 (**Figure 1C**).

Molecular Characterization of FoOuLV1

The full-length sequence of the L-segment (GenBank Accession No. MT551010) in FoOuLV1 was 2,712 nt with a GC content of 55.5%. The genome contained only one large ORF that initiated at position 56 and terminated at position 2,612 based on the universal or mitochondrial genetic codes, potentially encoding 701 amino acid residues with a calculated molecular mass of 78.9 kDa from an AUG triplet to a UAG triplet (**Figure 2A**). Using the Mfold RNA structure software, the complex secondary structures of the L-segment of FoOuLV1

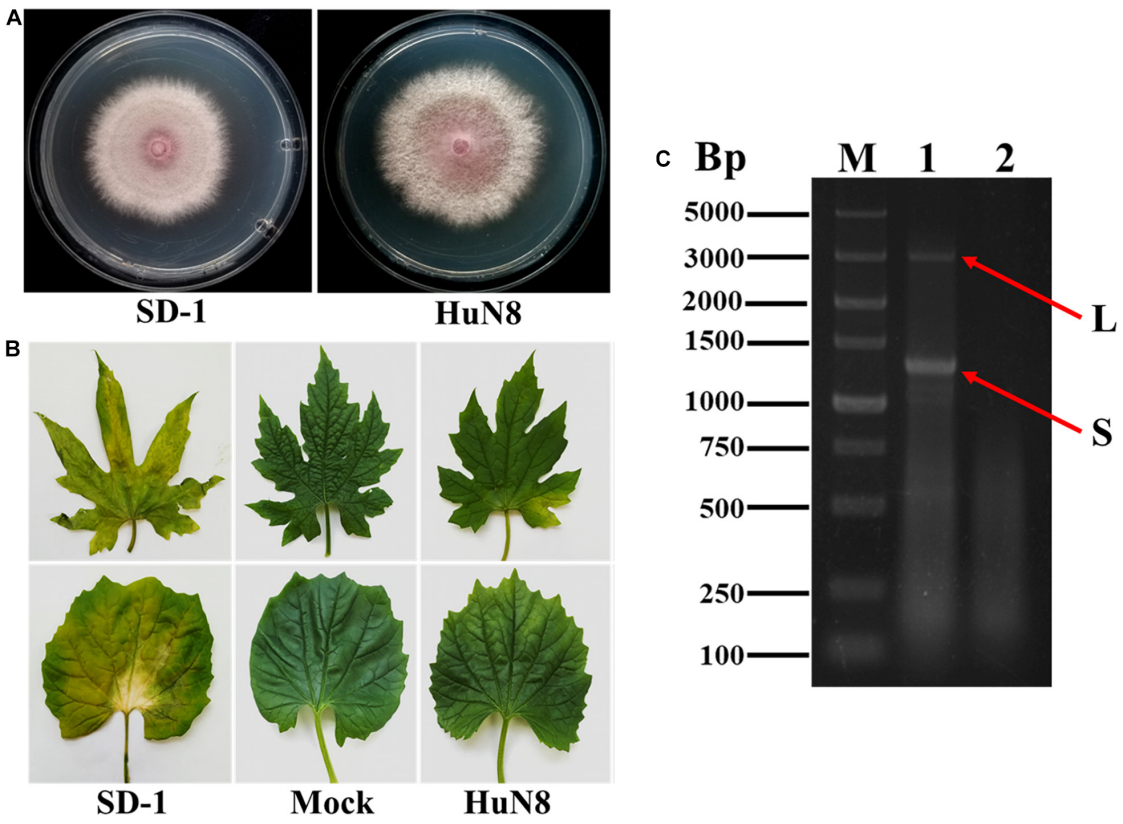

FIGURE 1 | The biological characteristics and dsRNA pattern of *Fusarium oxysporum* f. sp. *momordicae* strain HuN8. **(A)** Colony morphology of strain HuN8 and virulent strain SD-1 (cultured on PDA for 2 days at 28°C). **(B)** Pathogenicity of strain HuN8 and SD-1 on the detached bitter gourd leaves (72 h post-inoculation at 28°C). Mock, blank control. **(C)** Agarose gel electrophoretic analysis of the dsRNA extracted from strain HuN8. The dsRNA was treated with DNase I. M, molecular weight marker; 1, dsRNA extracted from strain HuN8; and 2, dsRNA extracted from strain SD-1.

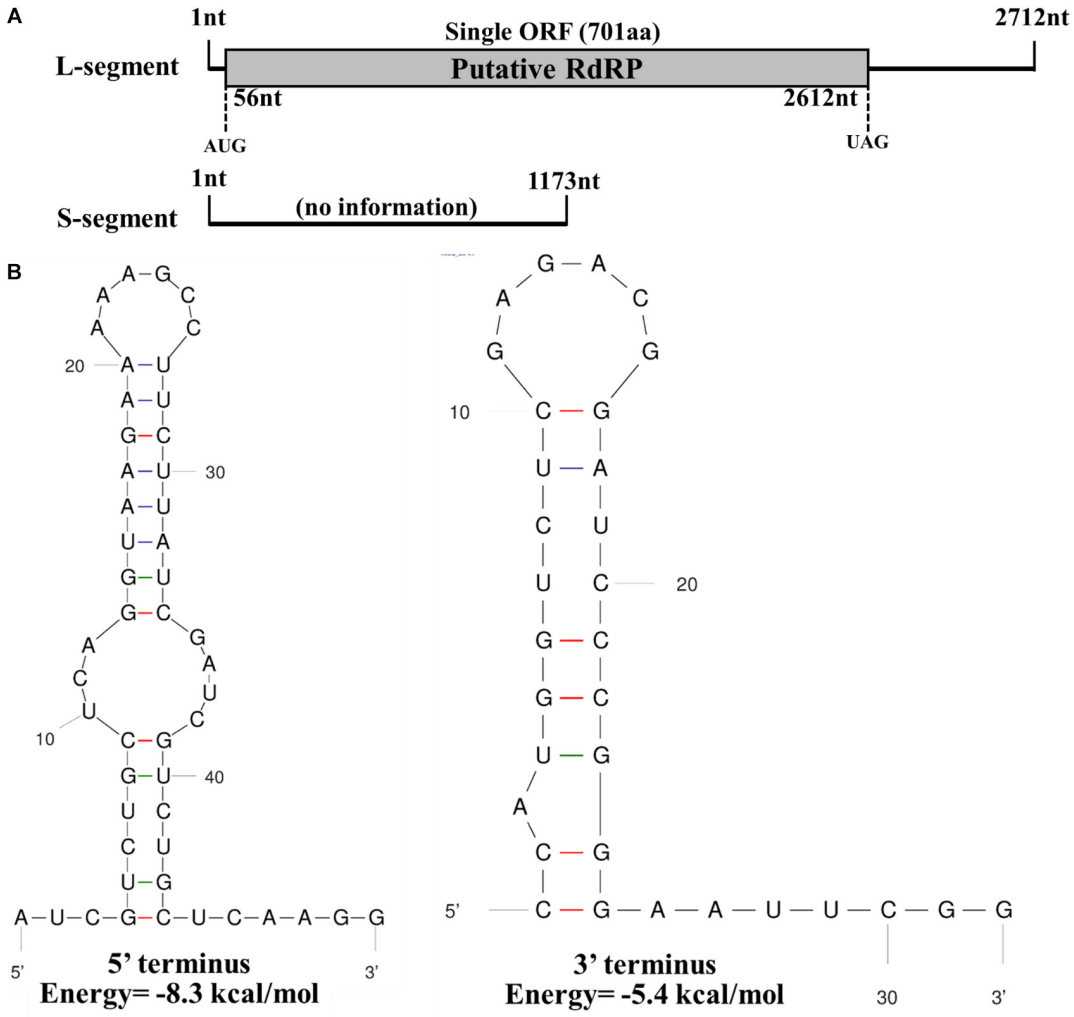

FIGURE 2 | Genomic organization and terminal structure of *Fusarium oxysporum* ourmia-like virus 1 (FoOuLV1). **(A)** Schematic representation of the putative genomic organization of FoOuLV1. The open reading frame (ORF) shown as a gray box (56–2,162 nt) was putatively encoding the RNA-dependent-RNA polymerase (RdRp) domain. **(B)** Potential secondary structures of the 5′- (left) and 3′-termini (right) of the L fragment of FoOuLV1.

were predicted. The results indicated that the first 50 nt at the 5′ terminus were folded into two stable stem–loop structures, while the last 32 nt at the 3′ terminus formed a stable stem–loop structure (**Figure 2B**). Stem–loop structures are typical features of members of *Narnaviridae* (including mitovirus) and *Ourmiavirus*.

Using the homology search on BLASTP, the ORF encoded a protein with one conserved domain, which was closely related to RdRps of Penicillium citrinum ourmia-like virus 1, Cladosporium cladosporioides ourmia-like virus 2, and Phaeoacremonium minimum ourmia-like virus 2 (**Table 1**). Furthermore, a conserved domain database (CDD) search and multiple protein alignment suggested that the predicted RdRp domain contained seven conserved motifs (**Figure 3**).

The full-length sequence of the S-segment (GenBank Accession No. MT551011) associated with FoOuLV1 was composed of 1,173 nt with a GC content of 43.8%, and the segment contained no ORFs (**Figure 2A**). There was no significant similar information from NCBI database using BLASTX.

Phylogenetic Analysis of FoOuLV1

To examine the phylogenetic relationship between FoOuLV1 and other mycoviruses, the phylogenetic tree was constructed using a maximum likelihood method based on the RdRp amino acid sequences of FoOuLV1 and other related viruses from *Narnaviridae* (including *Narnarvirus*, *Chrysovirus*, *Tetramycovirus*, and *Mitovirus*) and *Botourmiaviridae* (including *Penoulivirus*, *Botoulivirus*, *Scleroulivirus*, *Magoulivirus*, and *Ourmiavirus*). The results indicated that FoOuLV1 was closely related to the genus *Magoulivirus* and clustered with viruses such as Cladosporium cladosporioides ourmia-like virus, Phaeoacremonium minimum ourmia-like virus 2, and Magnaporthe oryzae ourmia-like virus. Thus, FoOuLV1 was

TABLE 1 | Identifications of the RdRp of FoOuLV1 and those of ourmia-like mycoviruses.

Taxon	Virus name	Accession	Query cover (%)	Identity (%)	*E* value
Magoulivirus	*Penicillium citrinum* ourmia-like virus 1	AYP71797.1	66	38.87	3.00E–83
	Cladosporium cladosporioides ourmia-like virus 2	QDB75008.1	77	35.93	8.00E–81
	Phaeoacremonium minimum ourmia-like virus 2	QDB75007.1	77	35.55	2.00E–77
Scleroulivirus	Soybean leaf-associated ourmiavirus 1	YP009666497.1	44	33.02	3.00E–34
	Sclerotinia sclerotiorum ourmia-like virus 1	ALD89138.1	43	32.15	3.00E–33
	Pyricularia oryzae ourmia-like virus 3	BBF90578.1	41	34.85	3.00E–31
Botoulivirus	*Sclerotinia sclerotiorum* ourmia-like virus 2	ALD89139.1	33	29.67	9.00E–22
	Epicoccum nigrum ourmia-like virus 1	QDB75003.1	28	31.73	2.00E–28
	Entoleuca ourmia-like virus 1	AVD68674.2	32	30.92	2.00E–24
Penoulivirus	*Penicillium sumatrense* ourmia-like virus 1	QDB75000.1	39	29.74	2.00E–21
	Sclerotinia sclerotiorum ourmia-like virus 4	QHG11400.1	40	27.70	4.00E–16
	Aspergillus neoniger ourmia-like virus 1	AZT88620.1	30	31.36	2.00E–16
Ourmiavirus	Epirus cherry virus	ACF16357.1	42	26.22	8.00E–20
	Ourmia melon virus	YP002019757.1	22	33.90	5.00E–21
	Cassava virus C	YP003104770.1	22	32.00%	4.00E–16

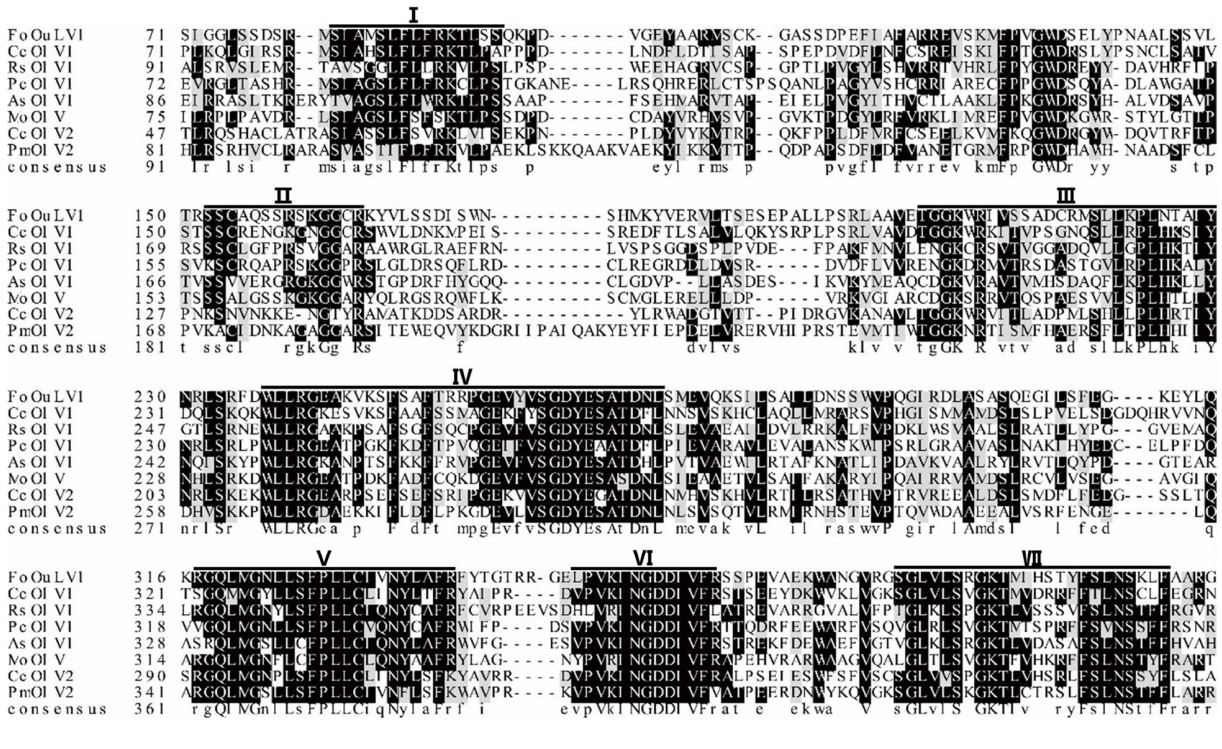

FIGURE 3 | Multiple alignment of the amino acid sequences of RNA-dependent RNA polymerase (RdRp) proteins encoded by FoOuLV1 and other selected ourmia-like viruses. Horizontal lines above the alignment indicate seven motifs (Roman numerals I to VII). Abbreviations: CcOLV1, *Cladosporium cladosporioides* ourmia-like virus 1; RsOLV1, *Rhizoctonia solani* ourmia-like virus 1; PcOLV1, *Penicillium citrinum* ourmia-like virus 1; AsOLV1, *Acremonium sclerotigenum* ourmia-like virus 1; MoOLV, Magnaporthe oryzae ourmia-like virus; CcOLV2, *Cladosporium cladosporioides* ourmia-like virus 1; and PmOLV2, *Phaeoacremonium minimum* ourmia-like virus 2.

determined to be a new member of *Magoulivirus* within the family *Botourmiaviridae* (**Figure 4**).

Influence of FoOuLV1 to the Virulence of *FoM*

Pathogenicity detection of FoOuLV1-containing strain HuN8 and virus-free strain SD-1 on the detached bitter gourd leaves showed that FoOuLV1 reduced the virulence of the *FoM* strain as described above (**Figure 1B**). Fusarium wilt caused by *F. oxysporum* is a systemic infection disease characterized by a typical symptom of whole plant wilting. In order to further determine whether the presence of FoOuLV1 reduced the virulence of *FoM* strain in terms of infecting living bitter gourd plants, the *FoM* strains HuN8 and SD-1 were inoculated

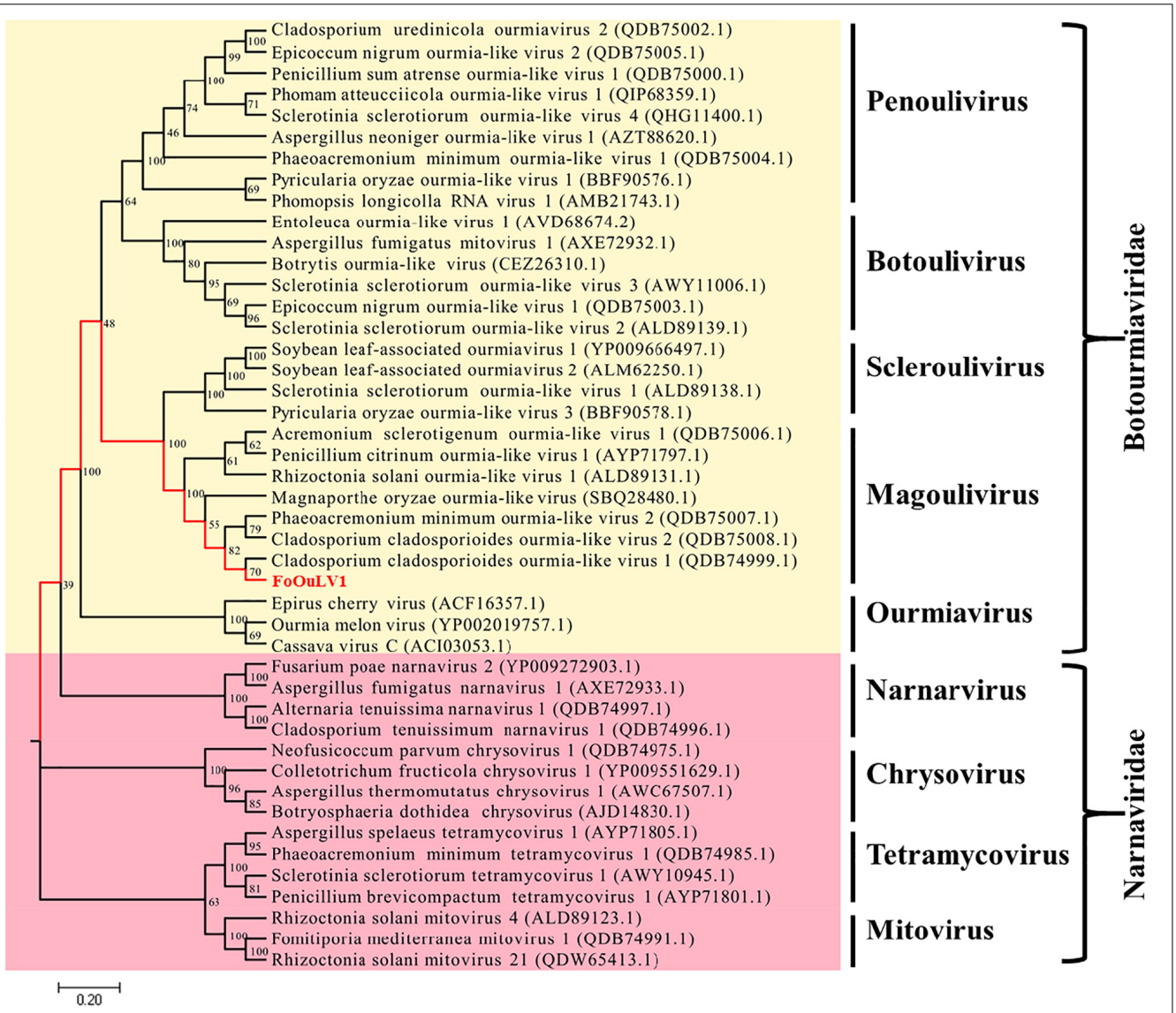

FIGURE 4 | Maximum likelihood phylogenetic tree based on the RdRps of FoOuLV1 and other related viruses. The phylogenetic analysis was generated using the MEGA7 software with 1,000 bootstrap replicates. The scale bar represents a genetic distance of 0.2.

onto bitter gourd seedlings at the stage of two or three leaves. Pathogenicity data were investigated before, during, and after the presentation of typical wilt symptoms.

At the early stage (15 dpi), the basal leaves of bitter gourd inoculated with SD-1 strain showed the symptoms of vein fading and yellowing on leaves, while the leaves of bitter gourd inoculated with HuN8 strain showed no symptoms (**Figures 5A,D**). At the middle stage (19 dpi), most of the leaves of bitter gourd inoculated with SD-1 strain had shown the typical symptoms of Fusarium wilt (leaf vein fading and yellowing), while those leaves inoculated with HuN8 strain still showed no symptoms (**Figures 5B,E**). At the later stage (23 dpi), the whole bitter gourd plant inoculated with SD-1 strain exhibited dryness and wilting, while the bitter gourd inoculated with HuN8 strain remained no symptoms during the entire observation period (**Figures 5C,F**).

Horizontal Transmission of FoOuLV1 Among FoM Strains

The dual-culture technique was used to determine whether the hypovirulence traits and RNA elements of FoOuLV1 could be transmitted horizontally. The results indicated that the L- and S-elements were both successfully transmitted from the hypovirulent strain HuN8 to the mycovirus-free strain SD-1Hyg^R, yielding the derivative strain SD-V. The colony morphology of strain SD-V was similar to that of the strain SD-1 (**Figure 6A**). The presence of L- and S-segments was confirmed in strain SD-V by dsRNA extraction

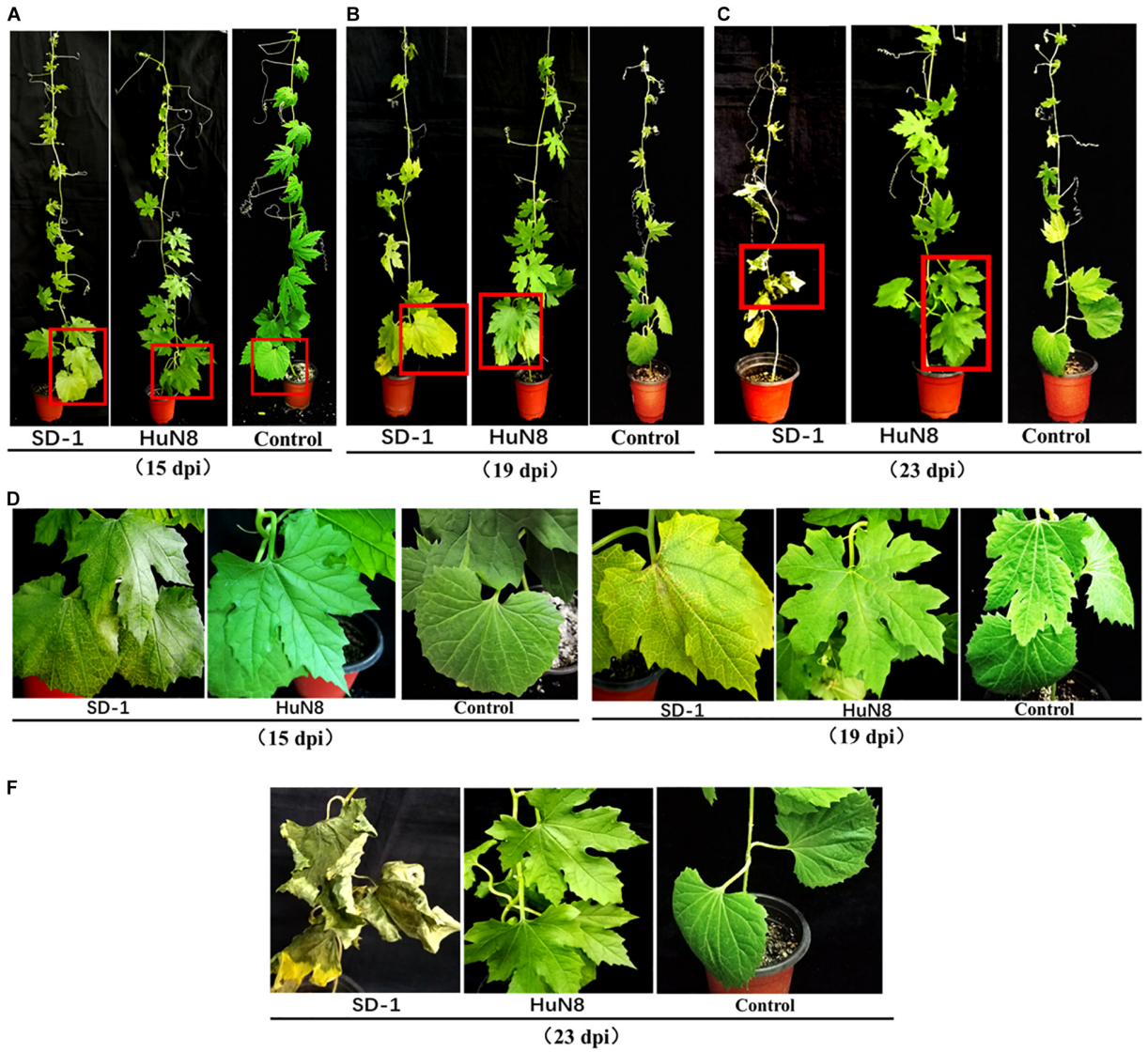

FIGURE 5 | Pathogenicity detection of strains HuN8 and SD-1 in living bitter gourd seedlings. **(A–C)** Symptoms at the early (15 dpi), middle (19 dpi), and later (23 dpi) stages. **(D–F)** The enlarged images of the red boxes in **(A–C)**, respectively.

(**Supplementary Figure 4A**) and RT-PCR with specific primers (**Figure 6B**). The hypovirulence traits were also successfully transmitted, as indicated by the pathogenicity detection results: the whole bitter gourd plants inoculated with strain SD-1 exhibited dryness and wilting, while plants inoculated with strain SD-V showed no symptoms, appearing in the same way as the strain HuN8 (**Figure 6C**).

Horizontal Transmission of FoOuLV1 Between Different Special Form Strains of *F. oxysporum*

The specialization of *F. oxysporum* is closely related to its pathogenicity. In order to determine whether the hypovirulent traits could be transmitted from *FoM* strain to *FoC* strain, dual culture was performed. The results showed the L- and S-segments were successfully transmitted from *FoM* strain HuN8 to virus-free *FoC* strain HK3Hyg^R, yielding the derivative strains HK3-V-1 and HK3-V-2. The L- and S-segments were detected by dsRNA extraction (**Supplementary Figure 4B**) and RT-PCR (**Figure 7A**). The hypovirulent traits were also successfully transmitted: whole cucumber plants inoculated with the strain HK3 exhibited dryness and wilting, while plants inoculated with strains HK3-V-1 and HK3-V-2 showed no symptoms (**Figure 7B**).

Biological Control Effects of FoOuLV1 Against Fusarium Wilt in Bitter Gourd

To verify the biological control effect of FoOuLV1 against Fusarium wilt in bitter gourd plants, field experiment was

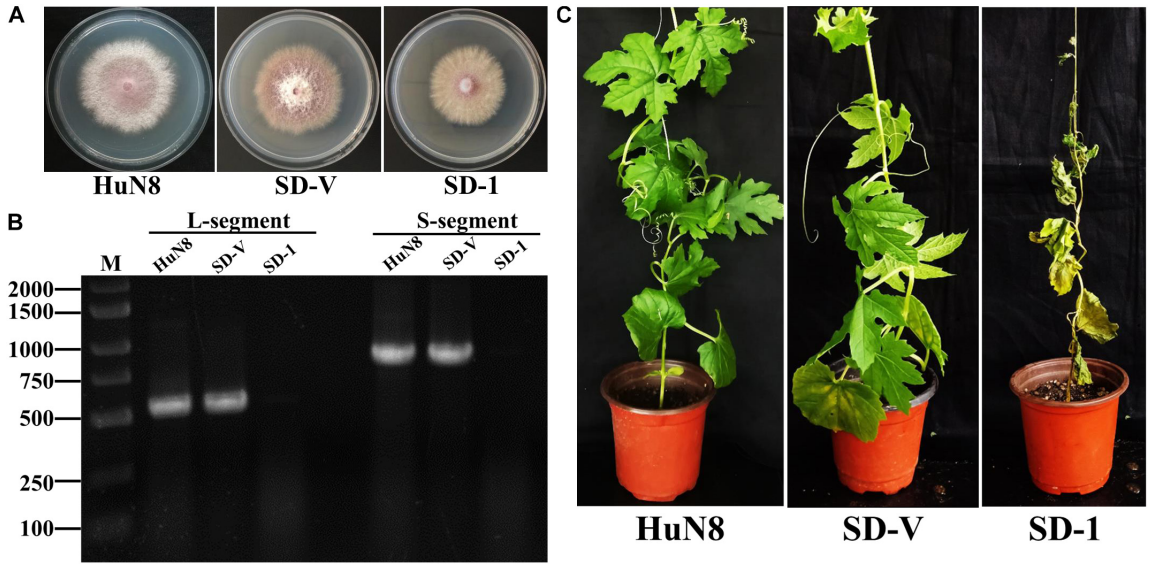

FIGURE 6 | FoOuLV1 infectivity and pathogenicity in *FoM* strains. **(A)** Colony morphology of the HuN8 strain, the virulent strain SD-1, and the derivative strain SD-V (cultured on PDA for 2 days at 28°C). **(B)** Detection of the L- and S-segments by RT-PCR. M, DNA marker. **(C)** Pathogenicity detection in a living bitter gourd seedling.

conducted from 21 May to 16 July 2019 in two fields. The results are shown in **Table 2**. According to the first results obtained from Field 1 on 25th June, the disease incidence of bitter gourd Fusarium wilt in the control group was 29.03% and the disease index was 18.28. In contrast, in the mycovirus FoOuLV1-treated group, the disease incidence was only 7.69%, the disease index was only 3.42, and the control effect reached 81.29%. A similar result was observed in Field 2, where the control effect reached 78.92%. The second results collected on 16th July showed a similar control effect (79.76% in Field 1 and 88.10% in Field 2; **Table 1**).

DISCUSSION

Genomic Differences Between FoOuLV1 and Other Ourmia-Like Viruses

Recently, an increasing number of ourmia-like viruses have been reported in diverse fungi, including two ourmia-like viruses from *Magnaporthe oryzae* (Illana et al., 2017; Li C.X. et al., 2019), three ourmia viruses from *Pyricularia oryzae* (Ohkita et al., 2019), two ourmia viruses from *Sclerotinia sclerotiorum* (Marzano et al., 2016; Wang et al., 2020), and other ourmia viruses from *Botrytis* (Donaire et al., 2016), *Phomopsis longicolla* (Hrabáková et al., 2017), and *Phoma matteucciicola* (Zhou et al., 2020). All of them are phylogenetically related to those in the newly established family *Botourmiaviridae*, which currently comprised five genera, according to current taxonomic information from ICTV and research report. Members of the genus *Ourmiavirus* are found only in plant-infecting viruses and usually harbor three RNA segments encoding RdRp, MP, and CP protein. Viruses in the genera *Botoulivirus*, *Penoulivirus*, and *Magoulivirus* are only isolated from fungi, while *Scleroulivirus* viruses are isolated from both fungi and plants. The mycoviruses in these four genera contain only one RNA segment encoding RdRp (Crivelli et al., 2011; Wang et al., 2020).

In this study, we described a novel ourmia-like mycovirus FoOuLV1, which is identified in *F. oxysporum* for the first time and a new member of the genus *Magoulivirus* within the family *Botourmiaviridae*. The genome of FoOuLV1 only has one ORF encoding RdRp in the L-segment similar to the other ourmia-like mycoviruses (Guo et al., 2019; Wang et al., 2020; Zhou et al., 2020). In addition, it contains a shorter segment named S-segment, which has no blast information. In this regard, the FoOuLV1 is significantly different from other ourmia-like mycoviruses.

The FoOuLV1 Is Unique Compared With Other Ourmia-Like Mycoviruses

Some mycoviruses in pathogenic fungi can cause a decline in the pathogenicity of the host fungi. This is known as mycovirus-mediated hypovirulence and has attracted research attention, owing to its importance in controlling fungal diseases (Nuss, 2005; Suzuki et al., 2018). To date, many families of mycoviruses have been identified as being associated with fungal hypovirulence, including the following: *Hypoviridae* (e.g., CHV1), *Megabirnaviridae* [e.g., Rosellinia necatrix megabirnavirus 1 (RnMBV1)], *Reoviridae* [e.g., Rosellinia necatrix mycoreovirus 3 (RnMYRV-3)], and *Narnaviridae* [e.g., Sclerotinia sclerotiorum mitovirus 1 (SsMV1)] (Hillman et al., 1990; Kanematsu et al., 2004; Sasaki et al., 2007; Chiba et al., 2009; Xu et al., 2015). In addition, some unclassified hypoviruses (such as

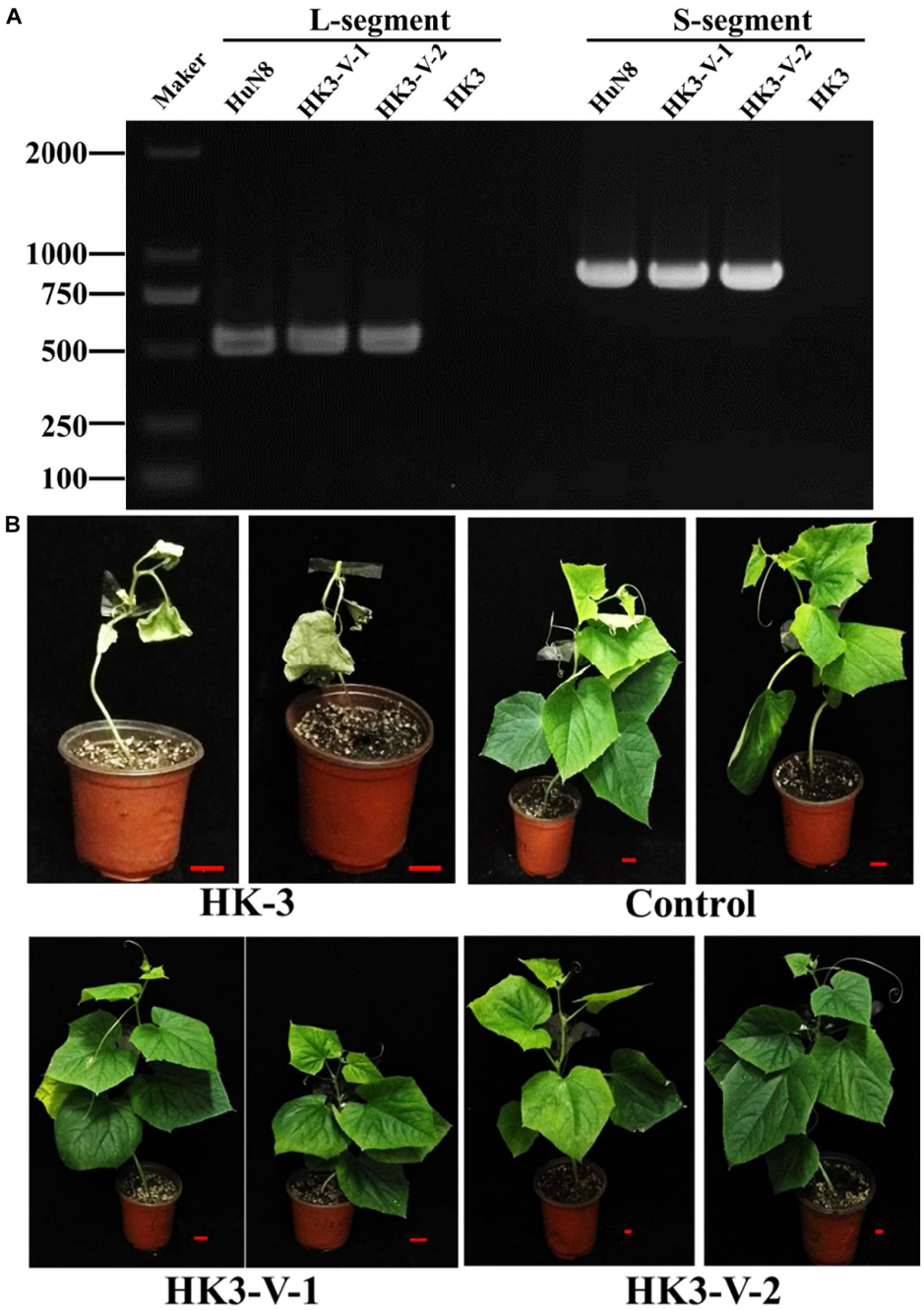

FIGURE 7 | FoOuLV1 infectivity and pathogenicity in FoC strains. **(A)** Detection of L- and S-segments by RT-PCR. **(B)** Pathogenicity detection in living cucumber seedlings. HuN8 is the FoM strain (with FoOuLV1), HK3 is the mycovirus-free FoC strain, HK3-V-1, and HK3-V-2 are the FoC derivative strains obtained from the dual-culture technique with strains HuN8 and HK3.

SsHADV-1 and Sclerotinia sclerotiorum hypovirus 1) have been recognized as inducing hypovirulence (Yu et al., 2010; Xie et al., 2011).

A large number of ourmia-like viruses have been reported in diverse fungi, but none of them exhibit hypovirulence. As reported in this study, FoOuLV1 is the first ourmia-like mycovirus to be reported that exhibits hypovirulence. The S-segment associated with FoOuLV1 is unique among ourmia-like mycoviruses. A previous study showed that SsHV1 and its satellite-like RNA were able to co-infect the hypovirulent strain SZ-150, with the satellite-like RNA in conferring hypovirulence on *S. sclerotiorum* (Xie et al., 2011). Therefore, S-segment associated with FoOuLV1 may play an important role in its hypovirulence.

TABLE 2 | Control effects of FoOuLV1 against *Fusarium* wilt in bitter gourd in field.

	Numbers of each level									
	Level 0	Level 1	Level 3	Level 5	Level 7	Level 9	Total number	Disease incidence (%)	Disease index	Control effect (%)
Field 1										
First statistics (June 25)										
Control	22	3	0	0	3	3	31	29.03	18.28	81.29
SD-V	24	0	1	1	0	0	26	7.69	3.42	
Second statistics (July 16)										
Control	11	5	3	1	6	5	31	64.52	37.99	79.76
SD-V	22	1	1	1	0	1	26	15.38	7.69	
Field 2										
First statistics (June 25)										
Control	31	0	2	3	1	0	37	16.22	8.4	78.92
SD-V	23	1	1	0	0	0	25	8.00	1.77	
Second statistics (July 16)										
Control	20	2	3	6	4	2	37	45.95	26.13	88.10
SD-V	22	1	2	0	0	0	25	12.00	3.11	

Note: The disease incidence $= \frac{\text{The total numbers of level 1 to level 9}}{\text{Total numbersof level 0 to level 9}} \times 100\%$.

The disease index $= \frac{\text{Sum (the value of each level} \times \text{the numbers on this level) from level 0 to level 9)}}{\text{Total numbers} \times \text{the value of the highest level}}$.

The control effect $= \frac{\text{The disease index of Control} - \text{the disease index of SD} - \text{V}}{\text{The disease index of Control}} \times 100\ \%$.

The Transmission of FoOuLV1 Is Important for *F. oxysporum*

Mycoviruses are generally transmitted by hyphal anastomosis and during sporogenesis, with the hyphal anastomosis occurring naturally between individuals belonging to the same or closely related vegetative compatibility groups (Lee et al., 2014). Furthermore, transmission via protoplast fusion has been reported in many mycoviruses (van Diepeningen et al., 1998; Kanematsu et al., 2010). The efficient transmission observed among isolates under natural conditions is considered to be an important condition for the successful application of mycoviruses to the control of plant fungal disease.

Fusarium wilt caused by *F. oxysporum* affects a large number of economically important crops. The pathogenic species contain a diversity of host-plant–specific forms (Torres-Trenas and Pérez-Artés, 2020), with different formae speciales potentially existing together in the soil concurrently. The hypovirulent traits of FoOuLV1 reported here can be transmitted horizontally from *FoM* strains to virus-free *FoM* strains and to *FoC* strains. This indicates that FoOuLV1 could be potentially used to control Fusarium wilt in various crops.

Potential Use of FoOuLV1

A large number of hypovirulent mycoviruses have been identified in previous studies, and some have been explored as potential biocontrol agents against fungal diseases. CHV1 has successfully been used to control chestnut blight in Europe (Anagnostakis, 1982), while SsHADV1 was used to control the disease caused by *S. sclerotiorum* (Yu et al., 2013). Except for these two mycoviruses, attempts to control diseases in field using mycoviruses are rare.

Many mycoviruses have been identified from the genus *Fusarium* (Cho et al., 2013); but, to our knowledge, only three mycoviruses have been identified in *F. oxysporum* (FoCV1, FodV1, and FodMV1). Furthermore, among these, only FodV1 induces hypovirulence (Sharzei et al., 2007; Lemus-Minor et al., 2015; Torres-Trenas and Pérez-Artés, 2020). In this study, FoOuLV1 was not only able to induce hypovirulence in *F. oxysporum* but also exhibited significant biological control effects against bitter gourd Fusarium wilt in the pot and field experiments. This suggests that FoOuLV1 has a potential to be used in the future.

CONCLUSION

In this study, we characterized a novel mycovirus (FoOuLV1) related to members of the *Magoulivirus* genera from a phytopathogenic fungus, *F. oxysporum* f. sp. *momordicae*. Although some ourmia-like mycoviruses have been identified in diverse fungi, this is the first report of a mycovirus in *F. oxysporum* f. sp. *momordicae* and the first report of an ourmia-like mycovirus in *F. oxysporum*. Furthermore, FoOuLV1 is the first ourmia-like mycovirus harboring an associated RNA segment and possessing a hypovirulence-inducing trait. Therefore, this virus provides a valuable experimental system to study the interaction of ourmia-like mycovirus and its fungal host. In addition, FoOuLV1 is also a potential biocontrol agent that could be further studied to control Fusarium wilt.

DATA AVAILABILITY STATEMENT

The sequence file of FoOuLV1 is available from the NCBI, GenBank Accession Nos. MT551010 and MT551011.

AUTHOR CONTRIBUTIONS

YiZ designed the research. YuZ, YS, ML, XW, HX, and YiZ performed the experimental work. YiZ, JX, and CW analyzed the data and wrote the manuscript. All authors contributed to the article and approved the submitted version.

FUNDING

This work was financially supported by the National Natural Science Foundation of China (31901934) and the Special Fund for Agro-scientific Research in the Public Interest (201503110).

ACKNOWLEDGMENTS

We express our deep gratitude to Dr. Jinlu Wu (National University of Singapore), Dr. Yanping Fu (Huazhong Agricultural University), and Yan Shi (Henan Agricultural University) for providing advice and guidance and to Dr. Xuehong Wu for providing research materials.

SUPPLEMENTARY MATERIAL

The Supplementary Material for this article can be found online at: https://www.frontiersin.org/articles/10.3389/fmicb.2020.569869/full#supplementary-material

REFERENCES

Amarasinghe, G. K., Aréchiga Ceballos, N. G., Banyard, A. C., Basler, C. F., Bavari, S., Bennett, A. J., et al. (2018). Taxonomy of the order Mononegavirales: update 2018. *Arch. Virol.* 163, 2283–2294. doi: 10.1007/s00705-018-3814-x

Anagnostakis, S. L. (1982). Biological control of chestnut blight. *Science* 215, 466–471. doi: 10.1126/science.215.4532.466

Avgelis, A., Barba, M., and Rumbos, I. (1989). Epirus cherry virus, an unusual virus isolated from cherry with rasp—leaf symptoms in Greece. *J. Phytopathol.* 126, 51–58. doi: 10.1111/j.1439-0434.1989.tb01089.x

Azhar, A., Mu, F., Huang, H., Cheng, J., Fu, Y., Hamid, M. R., et al. (2019). A novel RNA virus related to *Sobemoviruses* confers hypovirulence on the phytopathogenic fungus *Sclerotinia sclerotiorum*. *Viruses* 11:759. doi: 10.3390/v11080759

Bruenn, J. A., Warner, B. E., and Yerramsetty, P. (2015). Widespread *Mitovirus* sequences in plant genomes. *PeerJ* 3:e876. doi: 10.7717/peerj.876

Cai, G., Myers, K., Fry, W. E., and Hillman, B. I. (2012). A member of the virus family *Narnaviridae* from the plant pathogenic oomycete *Phytophthora infestans*. *Arch. Virol.* 157, 165–169. doi: 10.1007/s00705-011-1126-5

Chiba, S., Salaipeth, L., Lin, Y.-H., Sasaki, A., Kanematsu, S., and Suzuki, N. (2009). A novel bipartite double-stranded RNA mycovirus from the white root rot fungus *Rosellinia necatrix*: molecular and biological characterization, taxonomic considerations, and potential for biological control. *J. Virol.* 83, 12801–12812. doi: 10.1128/jvi.01830-09

Cho, W. K., Lee, K. M., Yu, J., Son, M., and Kim, K. H. (2013). Insight into mycoviruses infecting *Fusarium* species. *Adv. Virus Res.* 86, 273–288. doi: 10.1016/B978-0-12-394315-6.00010-6

Crivelli, G., Ciuffo, M., Genre, A., Masenga, V., and Turina, M. (2011). Reverse genetic analysis of *Ourmiaviruses* reveals the nucleolar localization of the coat protein in *Nicotiana benthamiana* and unusual requirements for virion formation. *J. Virol.* 85, 5091–5104. doi: 10.1128/jvi.02565-10

Darissa, O., Adam, G., and Schäfer, W. (2012). A dsRNA mycovirus causes hypovirulence of *Fusarium graminearum* to wheat and maize. *Eur. J. Plant Pathol.* 134, 181–189. doi: 10.1007/s10658-012-9977-5

Di Pietro, A., Madrid, M. P., Caracuel, Z., Delgado-Jarana, J., and Roncero, M. I. G. (2003). *Fusarium oxysporum*: exploring the molecular arsenal of a vascular wilt fungus. *Mol. Plant Pathol.* 4, 315–325. doi: 10.1046/j.1364-3703.2003.00180.x

Donaire, L., Rozas, J., and Ayllón, M. A. (2016). Molecular characterization of *Botrytis* ourmia-like virus, a mycovirus close to the plant pathogenic genus *Ourmiavirus*. *Virology* 489, 158–164. doi: 10.1016/j.virol.2015.11.027

Ghabrial, S. A., Castón, J. R., Jiang, D., Nibert, M. L., and Suzuki, N. (2015). 50-plus years of fungal viruses. *Virology* 479–480, 356–368. doi: 10.1016/j.virol.2015.02.034

Ghabrial, S. A., and Suzuki, N. (2009). Viruses of plant pathogenic fungi. *Annu. Rev. Phytopathol.* 47, 353–384. doi: 10.1146/annurev-phyto-080508-081932

Guo, J., Zhu, J. Z., Zhou, X. Y., Zhong, J., Li, C. H., Zhang, Z. G., et al. (2019). A novel ourmia-like mycovirus isolated from the plant pathogenic fungus *Colletotrichum gloeosporioides*. *Arch. Virol.* 164, 2631–2635. doi: 10.1007/s00705-019-04346-2

Hillman, B. I., Shapira, R., and Nuss, D. L. (1990). Hypovirulence-associated suppression of host functions in *Cryphonectria parasitica* can be partially relieved by high light intensity. *Phytopathology* 80, 950–956. doi: 10.1094/phyto-80-950

Hrabáková, L., Koloniuk, I., and Petrzik, K. (2017). Phomopsis longicolla RNA virus 1 – novel virus at the edge of myco- and plant viruses. *Virology* 506, 14–18. doi: 10.1016/j.virol.2017.03.003

Illana, A., Marconi, M., Rodríguez-Romero, J., Xu, P., Dalmay, T., Wilkinson, M. D., et al. (2017). Molecular characterization of a novel ssRNA ourmia-like virus from the rice blast fungus *Magnaporthe oryzae*. *Arch. Virol.* 162, 891–895. doi: 10.1007/s00705-016-3144-9

Kanematsu, S., Arakawa, M., Oikawa, Y., Onoue, M., Osaki, H., Nakamura, H., et al. (2004). A reovirus causes hypovirulence of *Rosellinia necatrix*. *Phytopathology* 94, 561–568. doi: 10.1094/PHYTO.2004.94.6.561

Kanematsu, S., Sasaki, A., Onoue, M., Oikawa, Y., and Ito, T. (2010). Extending the fungal host range of a partitivirus and a mycoreovirus from *Rosellinia necatrix* by inoculation of protoplasts with virus particles. *Phytopathology* 100, 922–930. doi: 10.1094/PHYTO-100-9-0922

Kumar, S., Stecher, G., and Tamura, K. (2016). MEGA7: molecular evolutionary genetics analysis version 7.0 for bigger datasets. *Mol. Biol. Evol.* 33, 1870–1874. doi: 10.1093/molbev/msw054

Kwon, S.-J., Lim, W.-S., Park, S.-H., Park, M.-R., and Kim, K.-H. (2007). Molecular characterization of a dsRNA mycovirus, *Fusarium graminearum* virus-DK21, which is phylogenetically related to hypoviruses but has a genome organization and gene expression strategy resembling those of plant potex-like viruses. *Mol. Cells* 23, 304–315. doi: 10.1007/s10059-009-0112-1

Lee, K. M., Cho, W. K., Yu, J., Son, M., Choi, H., Min, K., et al. (2014). A comparison of transcriptional patterns and mycological phenotypes following infection of *Fusarium graminearum* by four mycoviruses. *PLoS One* 9:e100989. doi: 10.1371/journal.pone.0100989

Lemus-Minor, C. G., Cañizares, M. C., García-Pedrajas, M. D., and Pérez-Artés, E. (2015). Complete genome sequence of a novel dsRNA mycovirus isolated from the phytopathogenic fungus *Fusarium oxysporum* f. sp. dianthi. *Arch. Virol.* 160, 2375–2379. doi: 10.1007/s00705-015-2509-9

Li, C. X., Zhu, J. Z., Gao, B. D., Zhu, H. J., Zhou, Q., and Zhong, J. (2019). Characterization of a novel ourmia-like mycovirus infecting *Magnaporthe oryzae* and implications for viral diversity and evolution. *Viruses* 11:223. doi: 10.3390/v11030223

Li, H., Bian, R., Liu, Q., Yang, L., Pang, T., Salaipeth, L., et al. (2019). Identification of a novel hypovirulence-inducing hypovirus from *Alternaria alternata*. *Front. Microbiol.* 10:1076. doi: 10.3389/fmicb.2019.01076

Li, M., Gong, X., Zheng, J., Jiang, D., Fu, Y., and Hou, M. (2005). Transformation of *Coniothyrium minitans*, a parasite of *Sclerotinia sclerotiorum*, with *Agrobacterium tumefaciens*. *FEMS Microbiol. Lett.* 243, 323–329.

Li, P., Bhattacharjee, P., Wang, S., Zhang, L., Ahmed, I., and Guo, L. (2019). Mycoviruses in *Fusarium* species: an update. *Front. Cell. Infect. Microbiol.* 9:257. doi: 10.3389/fcimb.2019.00257

Li, P., Zhang, H., Chen, X., Qiu, D., and Guo, L. (2015). Molecular characterization of a novel hypovirus from the plant pathogenic fungus *Fusarium graminearum*. *Virology* 481, 151–160. doi: 10.1016/j.virol.2015.02.047

Lisa, V., Milne, R. G., Accotto, G. P., Boccardo, G., Caciagli, P., and Parvizy, R. (1988). Ourmia melon virus, a virus from Iran with novel properties. *Ann. Appl. Biol.* 112, 291–302. doi: 10.1111/j.1744-7348.1988.tb02065.x

Marzano, S.-Y. L., Nelson, B. D., Ajayi-Oyetunde, O., Bradley, C. A., Hughes, T. J., Hartman, G. L., et al. (2016). Identification of diverse mycoviruses through metatranscriptomics characterization of the viromes of five major fungal plant pathogens. *J. Virol.* 90, 6846–6863. doi: 10.1128/jvi.00357-16

Mullins, E. D., Chen, X., Romaine, P., Raina, R., Geiser, D. M., and Kang, S. (2001). Agrobacterium-mediated transformation of *Fusarium oxysporum*: an efficient tool for insertional mutagenesis and gene transfer. *Phytopathology* 91, 173–180. doi: 10.1094/PHYTO.2001.91.2.173

Nuss, D. L. (2005). Hypovirulence: mycoviruses at the fungal–plant interface. *Nat. Rev. Microbiol.* 3, 632–642. doi: 10.1038/nrmicro1206

Ohkita, S., Lee, Y., Nguyen, Q., Ikeda, K., Suzuki, N., and Nakayashiki, H. (2019). Three ourmia-like viruses and their associated RNAs in *Pyricularia oryzae*. *Virology* 534, 25–35. doi: 10.1016/j.virol.2019.05.015

Potgieter, A. C., Page, N. A., Liebenberg, J., Wright, I. M., Landt, O., and van Dijk, A. A. (2009). Improved strategies for sequence-independent amplification and sequencing of viral double-stranded RNA genomes. *J. Gen. Virol.* 90(Pt 6), 1423–1432. doi: 10.1099/vir.0.009381-0

Sasaki, A., Kanematsu, S., Onoue, M., Oikawa, Y., Nakamura, H., and Yoshida, K. (2007). Artificial infection of *Rosellinia necatrix* with purified viral particles of a member of the genus *Mycoreovirus* reveals its uneven distribution in single colonies. *Phytopathology* 97, 278–286. doi: 10.1094/PHYTO-97-3-0278

Sharzei, B., Banihashemi, Z. A. D., and Afsharifar, A. R. (2007). Detection and characterization of a double-stranded RNA mycovirus in *Fusarium oxysporum* f. sp. melonis. *Iran J. Plant Pathol.* 43, 9–26.

Shi, M., Lin, X. D., Tian, J. H., Chen, L. J., Chen, X., Li, C. X., et al. (2016). Redefining the invertebrate RNA virosphere. *Nature* 540, 539–543. doi: 10.1038/nature20167

Suzuki, N., Ghabrial, S. A., Kim, K. H., Pearson, M., Marzano, S. Y. L., Yaegashi, H., et al. (2018). ICTV virus taxonomy profile: hypoviridae. *J. Gen. Virol.* 9, 615–616. doi: 10.1099/jgv.0.001055

Torres-Trenas, A., and Pérez-Artés, E. (2020). Characterization and incidence of the first member of the genus *Mitovirus* identified in the phytopathogenic species *Fusarium oxysporum*. *Viruses* 12:279. doi: 10.3390/v12030279

Turina, M., Hillman, B. I., Izadpanah, K., Rastgou, M., and Rosa, C. (2017). ICTV virus taxonomy profile: *Ourmiavirus*. *J. Gen. Virol.* 9, 129–130. doi: 10.1099/jgv.0.000725

van Dam, P., de Sain, M., ter Horst, A., van der Gragt, M., and Rep, M. (2018). Use of comparative genomics-based markers for discrimination of host specificity in *Fusarium oxysporum*. *Appl. Environ. Microb.* 84:e01868-17.

van Diepeningen, A. D., Debets, A. J. M., and Hoekstra, R. F. (1998). Intra- and interspecies virus transfer in Aspergilli via protoplast fusion. *Fungal Genet. Biol.* 25, 171–180. doi: 10.1006/fgbi.1998.1096

Wang, Q., Mu, F., Xie, J., Cheng, J., Fu, Y., and Jiang, D. (2020). A single ssRNA segment encoding RdRp is sufficient for replication, infection, and transmission of ourmia-like virus in fungi. *Front. Microbiol.* 11:379. doi: 10.3389/fmicb.2020.00379

Xie, J., and Jiang, D. (2014). New insights into mycoviruses and exploration for the biological control of crop fungal diseases. *Annu. Rev. Phytopathol.* 52, 45–68. doi: 10.1146/annurev-phyto-102313-050222

Xie, J., Wei, D., Jiang, D., Fu, Y., Li, G., Ghabrial, S., et al. (2006). Characterization of debilitation-associated mycovirus infecting the plant-pathogenic fungus *Sclerotina sclerotorium*. *J. Gen. Virol.* 87(Pt 1), 241–249. doi: 10.1099/vir.0.81522-0

Xie, J., Xiao, X., Fu, Y., Liu, H., Cheng, J., Ghabrial, S. A., et al. (2011). A novel mycovirus closely related to hypoviruses that infects the plant pathogenic fungus *Sclerotinia sclerotiorum*. *Virology* 418, 49–56. doi: 10.1016/j.virol.2011.07.008

Xu, Z., Wu, S., Liu, L., Cheng, J., Fu, Y., Jiang, D., et al. (2015). A *Mitovirus* related to plant mitochondrial gene confers hypovirulence on the phytopathogenic fungus *Sclerotinia sclerotiorum*. *Virus Res.* 197, 127–136. doi: 10.1016/j.virusres.2014.12.023

Yu, X., Li, B., Fu, Y., Jiang, D., Ghabrial, S. A., Li, G., et al. (2010). A geminivirus-related DNA mycovirus that confers hypovirulence to a plant pathogenic fungus. *Proc. Natl. Acad. Sci. U.S.A.* 107, 8387–8392. doi: 10.1073/pnas.0913535107

Yu, X., Li, B., Fu, Y., Xie, J., Cheng, J., Ghabrial, S. A., et al. (2013). Extracellular transmission of a DNA mycovirus and its use as a natural fungicide. *Proc. Natl. Acad. Sci. U.S.A.* 110, 1452–1457. doi: 10.1073/pnas.1213755110

Zheng, L., Shu, C., Zhang, M., Yang, M., and Zhou, E. (2019). Molecular characterization of a novel endornavirus conferring hypovirulence in rice sheath blight fungus *Rhizoctonia solani* AG-1 IA strain GD-2. *Viruses* 11:178. doi: 10.3390/v11020178

Zhou, J., Wang, Y., Liang, X., Xie, C., Liu, W., Miao, W., et al. (2020). Molecular characterization of a novel ourmia-like virus infecting *Phoma matteucciicola*. *Viruses* 12:231. doi: 10.3390/v12020231

Zuker, M. (2003). Mfold web server for nucleic acid folding and hybridization prediction. *Nucleic Acids Res.* 31, 3406–3415. doi: 10.1093/nar/gkg595

Conflict of Interest: The authors declare that the research was conducted in the absence of any commercial or financial relationships that could be construed as a potential conflict of interest.

frontiers in Microbiology

ORIGINAL RESEARCH
published: 11 December 2020
doi: 10.3389/fmicb.2020.607795

Phenotypic and Molecular Biological Analysis of Polymycovirus AfuPmV-1M From *Aspergillus fumigatus*: Reduced Fungal Virulence in a Mouse Infection Model

Azusa Takahashi-Nakaguchi[1], Erika Shishido[1], Misa Yahara[1], Syun-ichi Urayama[2,3], Akihiro Ninomiya[2], Yuto Chiba[2], Kanae Sakai[1,4], Daisuke Hagiwara[1,2,3], Hiroji Chibana[1], Hiromitsu Moriyama[5] and Tohru Gonoi[1]*

[1] *Medical Mycology Research Center, Chiba University, Chiba, Japan,* [2] *Faculty of Life and Environmental Sciences, University of Tsukuba, Tsukuba, Japan,* [3] *Microbiology Research Center for Sustainability, University of Tsukuba, Tsukuba, Japan,* [4] *Graduate School of Science, Technology and Innovation, Kobe University, Kobe, Japan,* [5] *Department of Applied Biological Sciences, Tokyo University of Agriculture and Technology, Fuchu, Japan*

OPEN ACCESS

Edited by:
Nobuhiro Suzuki, Okayama University, Japan

Reviewed by:
Robert Henry Arnold Coutts, University of Hertfordshire, United Kingdom
Daohong Jiang, Huazhong Agricultural University, China

***Correspondence:**
Azusa Takahashi-Nakaguchi
azusan_takahashi@faculty.chiba-u.jp

Specialty section:
This article was submitted to Virology, a section of the journal Frontiers in Microbiology

Received: *18 September 2020*
Accepted: *24 November 2020*
Published: *11 December 2020*

Citation:
Takahashi-Nakaguchi A, Shishido E, Yahara M, Urayama S, Ninomiya A, Chiba Y, Sakai K, Hagiwara D, Chibana H, Moriyama H and Gonoi T (2020) Phenotypic and Molecular Biological Analysis of Polymycovirus AfuPmV-1M From Aspergillus fumigatus: Reduced Fungal Virulence in a Mouse Infection Model. Front. Microbiol. 11:607795. doi: 10.3389/fmicb.2020.607795

The filamentous fungal pathogen *Aspergillus fumigatus* is one of the most common causal agents of invasive fungal infection in humans; the infection is associated with an alarmingly high mortality rate. In this study, we investigated whether a mycovirus, named AfuPmV-1M, can reduce the virulence of *A. fumigatus* in a mouse infection model. AfuPmV-1M has high sequence similarity to AfuPmV-1, one of the polymycovirus that is a capsidless four-segment double-stranded RNA (dsRNA) virus, previously isolated from the genome reference strain of *A. fumigatus*, Af293. However, we found the isolate had an additional fifth dsRNA segment, referred to as open reading frame 5 (ORF5), which has not been reported in AfuPmV-1. We then established isogenic lines of virus-infected and virus-free *A. fumigatus* strains. Mycovirus infection had apparent influences on fungal phenotypes, with the virus-infected strain producing a reduced mycelial mass and reduced conidial number in comparison with these features of the virus-free strain. Also, resting conidia of the infected strain showed reduced adherence to pulmonary epithelial cells and reduced tolerance to macrophage phagocytosis. In an immunosuppressed mouse infection model, the virus-infected strain showed reduced mortality in comparison with mortality due to the virus-free strain. RNA sequencing and high-performance liquid chromatography (HPLC) analysis showed that the virus suppressed the expression of genes for gliotoxin synthesis and its production at the mycelial stage. Conversely, the virus enhanced gene expression and biosynthesis of fumagillin. Viral RNA expression was enhanced during conidial maturation, conidial germination, and the mycelial stage. We presume that the RNA or translation products of the virus affected fungal phenotypes, including spore formation and toxin synthesis. To identify the mycovirus genes responsible for attenuation of fungal virulence, each viral ORF was ectopically expressed in the virus-free KU strain. We found that the

expression of ORF2 and ORF5 reduced fungal virulence in the mouse model. In addition, ORF3 affected the stress tolerance of host *A. fumigatus* in culture. We hypothesize that the respective viral genes work cooperatively to suppress the pathogenicity of the fungal host.

Keywords: *Aspergillus fumigatus*, dsRNA, mycovirus, hypovirulence, mouse

INTRODUCTION

Aspergillus fumigatus is a ubiquitous environmental fungus that is currently the most commonly encountered mold pathogen in severely immunocompromised patients. The emergence of drug-resistant fungi and the toxic side effects of antifungal drugs are two major problems associated with the treatment of fungal infections. Therefore, the development of new therapeutic strategies is urgently required. This may include the discovery of new chemotherapeutic drugs based on the identification of novel fungal targets and finding novel therapeutic methods for alleviating the pathogenic effects of fungi. One such hypothetical therapeutic strategy may include the use of mycoviruses, which can selectively infect pathogenic fungi.

Mycoviruses are viruses that selectively infect fungi and are widespread among all major taxa of fungi (Ghabrial and Suzuki, 2009; Ghabrial et al., 2015). The majority of characterized mycoviruses of plant-pathogenic fungi have double-stranded RNA (dsRNA) genomes. Mycoviruses with dsRNA genomes have been classified into eight families (the families *Totiviridae*, *Partitiviridae*, *Chrysoviridae*, *Amalgaviridae*, *Curvulaviridae*, *Reoviridae*, *Megavirnaviridae*, and *Polymycoviridae*; Several unsigned viruses including AfuPmV-1 have recently been established as a new family *Polymycoviridae* (Zhai et al., 2016; Jia et al., 2017; Kotta-Loizou and Coutts, 2017b; Niu et al., 2018; Zoll et al., 2018; Mahillon et al., 2019; Sato et al., 2020) (International Committee on Taxonomy of Viruses (ICTV)[1]. Although many mycoviruses do not appear to cause symptoms in their hosts, some affect mycelial growth, sporulation, and pigmentation, while in some botanical pathogenic fungi, mycoviruses have been shown to reduce their virulence in plant hosts (Pearson et al., 2009). However, our knowledge of mycoviruses in fungal pathogens infecting animals and humans remains limited (van de Sande et al., 2010; van de Sande and Vonk, 2019).

Screening of clinical and environmental *A. fumigatus* isolates for mycoviruses has revealed chrysovirus (AfuCV), partitivirus-1 (AfuPV-1), narnavirus-2 (AfuNV-1 and AfuNV-2), mitovirus-1 (AfuMV-1), and polymycovirus-1 (AfuPmV-1) in *A. fumigatus* strains (Bhatti et al., 2012; Kanhayuwa et al., 2015; Kotta-Loizou and Coutts, 2017a; Zoll et al., 2018). However, previous studies have reported that the introduction of AfuCV (Jamal et al., 2010) or AfuPV-1 virus (Bhatti et al., 2011) to host fungi provoked no significant alterations of pathogenicity in murine infection models. Two exceptions are: (1) infection with AfuPmV-1 virus showed slight potentiation in pathogenicity in an insect infection model (Kanhayuwa et al., 2015), and (2) our previous report of chrysovirus, a different viridae from the present work, showed reduced fungal virulence in a mouse model (Takahashi-Nakaguchi et al., 2020). Therefore, further mycoviruses that reduce *A. fumigatus* pathogenicity in a murine infection model remain to be detected (Özkan and Coutts, 2015).

The genome reference strain of *A. fumigatus*, Af293, contains a dsRNA mycovirus (Bhatti et al., 2012; Kanhayuwa et al., 2015). In this study, we report molecular biological and phenotypic analyses of a mycovirus that we detected in the Af293 strain. This virus exhibits high genome sequence similarity to the AfuPmV-1 virus (GenBank accession nos. HG975302–HG975305) but has a fifth dsRNA segment, which has not previously been described. Using a mouse infection model, we showed that the mycovirus-infected *A. fumigatus* strain possesses reduced virulence compared with that of the virus-free strain. We also discuss the roles played by each gene product in the attenuation of fungal pathogenicity, based on the findings of a gene expression experiment.

MATERIALS AND METHODS

Isolates of *A. fumigatus* and Culture Methods

A. fumigatus strain Af293 was obtained from the American Type Culture Collection (ATCC), strain KU was obtained from the Fungal Genetics Stock Center (FGSC), and they were stored at Medical Mycology Research Center (MMRC), Chiba University. Fungi were grown on potato dextrose agar (PDA, Difco) at 37°C for 7 days until conidia were fully mature. To obtain mycelia for dsRNA extraction or virus purification, conidia were cultured in potato dextrose broth (PDB, Difco) at 37°C for 14 days with shaking at 180 rpm.

Detection of dsRNA From Mycelia

Total nucleic acid was extracted from mycelia, and dsRNAs were purified by chromatography on CF-11 cellulose (Whatman) (Morris, 1979; Okada et al., 2013); any DNA or ssRNA segments were eliminated by treatment with DNase 1 (Takara Bio) and S1 nuclease (Takara Bio), respectively. The extracted dsRNAs were subjected to electrophoresis on 1% agarose gel in TAE buffer.

cDNA Cloning and Phylogenetic Analysis

Five dsRNA segments and small fragments isolated from Af293 mycelia were fractionated by 5% (w/v) polyacrylamide gel electrophoresis and excised for further analysis. Double-stranded cDNA was synthesized from the dsRNAs using a cDNA Synthesis Kit (Roche). The cDNAs were then converted into an Illumina sequencing library, according to the manufacturer's protocol

[1]https://talk.ictvonline.org/taxonomy/

(TruSeq RNA Sample Preparation Kit v2 -Set A, Illumina). Libraries were sequenced on an MiSeq (Illumina) as 250-bp paired-end reads. CLC Genomics Workbench (CLC bio.) was used to analyze the sequencing results. Sequences similar to those encoded by the dsRNA open reading frames (ORFs) were identified from the NCBI database using the BLASTn and BLASTp programs. Molecular phylogenetic analyses using the deduced amino acid sequences of the putative RdRp gene of AfuPmV-1M dsRNA1 were carried out using the CLUSTAL_X (Thompson et al., 1997) and MEGA 5 programs (Tamura et al., 2011). A bootstrap test was conducted with 1,000 resamplings for the neighbor-joining tree. Genome sequences of the five dsRNA segments isolated from Af293 were confirmed by Northern blot hybridization and RT-PCR. To obtain PCR clones that corresponded to the terminal region of each dsRNA, 5′RACE was used (5′Full RACE Core set; Takara Bio). Genome sequences for AfuPmV-1M were deposited in DDBJ/GenBank/EMBL, under the accession numbers LC517041–LC517045.

Northern Blot Analysis

Samples of dsRNA (2-μg) were electrophoresed on 1% agarose–2.2 M formaldehyde gels and blotted onto Nylon Transfer Membrane (GE Healthcare). The hybridization probes used in this study were generated by PCR using the primers listed in **Supplementary Table S3**. Probes were labeled with AlkPhos Direct (GE Healthcare) and visualized using an LAS-1000 mini (Fujifilm co.).

Relative Quantification of Viral RNA Expression Levels

For the synchronized induction of asexual development, conidia (10^5 conidia/mL) were cultivated at 37°C in 20 mL PDB medium for 7 days, and conidia-free mycelia were harvested using Miracloth (Merck, Germany), washed with distilled water, and transferred onto PDA plates. The plates were then incubated at 37°C for specified times. The start of this plate incubation was referred to as 0 h, and mycelia were harvested at the time points of 0, 6, 12, 24, and 48 h.

Total RNA was isolated from *A. fumigatus* mycelium or conidia using an RNeasy Mini kit (Qiagen). Synthesis of cDNA from the total RNA was conducted with ReverTraAce using random primers (Toyobo, Japan). Subsequently, real-time PCR was conducted in 96-well plates with 20 μL reaction volumes containing THUNDERBIRD SYBR qPCR Mix (Toyobo). The samples were subjected to denaturation at 95°C for 30 s, followed by 40 cycles of amplification (95°C for 15 s, 60°C for 30 s) using a LightCycler 96 (Roche). Expression levels of viral RNA were normalized to the level of the constitutively expressed *A. fumigatus tef-1* gene, which served as an internal control (Gravelat et al., 2008). Primer sets are shown in **Supplementary Table S4**.

Growth, Conidiation, and Germination Tests

To prepare fresh conidial suspensions, well-segregated conidia were inoculated onto a PDA slant and incubated at 37°C for 7 days. An appropriate volume of phosphate-buffered saline supplemented with 0.1% Tween 20 (PBST) was added and vortexed gently to obtain conidial suspensions. To test for colony growth, 10^5 conidia of each strain were point-inoculated onto PDA plates, which were incubated at 37°C for 48 h. The numbers of conidia were counted using a hemocytometer. Counts were made in triplicate, and the mean values with standard deviations (SD) were reported. For analysis of germination, approximately 10^4 conidia were incubated at 37°C in PDB. Germination was scored microscopically at 6 h.

Scanning Electron Microscopy

For ultrastructural analysis of Af293 strains, conidia were cultured on PDA medium for 72 h, then fixed using the osmium vapor technique. Following fixation, samples were dried in a desiccator and deposited with platinum. All specimens were mounted on specimen stubs, sputter coated, and viewed under an S-3400N scanning electron microscope (HITACHI, Tokyo, Japan).

Mycelial Dry-Weight Measurement

After culturing conidia of each strain in PDB at 37°C with rotation at 200 rpm for 24 h, the fungal communities were collected by filtration through a Miracloth (Merck Biosciences, United States). Following lyophilization, the dry weight of the cells was measured. The experiment was performed in triplicate.

RNA-Seq

Total RNA was extracted from fungal cells using an RNeasy Mini Kit (Qiagen) and treated with DNase I (TaKaRa, Japan). Polyadenylated mRNA was then extracted from the total RNA and fragmented using a TruSeq RNA Sample Preparation Kit v2 – Set A (Illumina). A 200- to 300-nucleotide size selection was performed, and the RNA was then converted into an Illumina sequencing library according to the manufacturer's protocol. Libraries were sequenced on a MiSeq sequencer (Illumina) as 50-bp single-end reads. The CLC Genomics Workbench ver. 12 (Filgen) was used to analyze the sequence results. Transcripts were categorized using FungiFun 2.2.8[2]. The sequence data have been deposited in the DDBJ/EMBL/GenBank database under the GEO accession number PRJDB9242.

Detection of Gliotoxin and Fumagillin by HPLC

Conidia of AfuPmV-1M virus-infected and virus-free *A. fumigatus* (2.0×10^7) were inoculated in 20 mL PDB and cultured for 6 days at 37°C with agitation at 120 rpm. Five independent culture experiments were performed for each strain. The culture supernatant was extracted using an equivalent volume of ethyl acetate. The mycelia were freeze-dried and extracted with 3 mL acetone. The extracts of the supernatant (5 mL) and the mycelia (1.5 mL) were dried *in vacuo* and dissolved in methanol. The solution was applied to an octadecylsilane column (Cosmosil 140C18-OPN, Nacalai Tesque,

[2]https://elbe.hki-jena.de/fungifun/

Inc., Kyoto, Japan) and eluted with methanol. The methanol fraction was dried *in vacuo* and dissolved in 100 μL DMSO. The DMSO solution was analyzed using a 1260 Infinity LC system (Agilent Technologies, Inc., Santa Clara, CA, United States) with a Poroshell 120 ECC18 column (ϕ3.0 mm × 100 mm, particle size 2.7 μm; Agilent). The LC analytical condition was a gradient elution of 5–100% acetonitrile containing 0.5% acetic acid for 18 min. Gliotoxin in the supernatant and fumagillin in mycelia were detected by absorbance at wavelengths of 254 and 330 nm, respectively.

Virulence Assays in Mice

Six-week-old ICR male mice were supplied by Takasugi Experimental Animals Supply Company (Saitama, Japan). Mice were immunosuppressed with cyclophosphamide (Shionogi Pharmaceutics Co. Ltd., Osaka, Japan) at a dose of 25 mg kg^{-1} injected subcutaneously on days −2, 0, and 2 of conidial inoculation. The mice were housed in sterile cages with sterile bedding and provided with sterile feed and drinking water containing 300 mg/L tetracycline hydrochloride to prevent bacterial infection. The mice were intratracheally inoculated with 5×10^7 conidia in 20 μL PBST on days 0 and 1. Mortality was monitored for 14 days, and statistical significance was assessed using the Kaplan–Meier log rank test.

The mice were euthanized, and their lungs were dissected at day 3 to determine fungal burdens by colony count and to facilitate histopathological examination (three mice per fungal strain). To count viable fungal cells, the lungs were weighed and homogenized using a Polytron homogenizer (PT1200E, KINEMATICA, Switzerland). The homogenate was spread over 9-cm PDA plates containing 0.05 mg/mL chloramphenicol. The plates were incubated at 37°C for 24 h and any colonies that formed were counted.

For the histopathological analysis, infected animals were euthanized on day 3 post-inoculation. The lungs were removed, fixed with formalin, and paraffin-embedded sections were stained with hematoxylin and eosin, as well as with Grocott's methenamine silver. To compare the disease progress in the lungs of live mice, we used a third generation CT scanner, LaTheta LCT-200 (Hitachi-Aloka, Tokyo, Japan), on day 14. Prior to CT scanning, animals were anesthetized by inhalation of isoflurane (DS Pharma Animal Health Co., Ltd., Osaka, Japan) and maintained under isoflurane narcose during CT scanning.

Adherence Assay

Cells of the type II human pneumocyte cell line A549 were obtained from ATCC and maintained in RPMI 1640 medium containing 10% fetal bovine serum (FBS, Gibco), 100 mg/L streptomycin, and 16 mg/L penicillin (both from Sigma). Cells were maintained at 37°C in a humidified 5% CO_2 incubator. A549 cells were plated at 10^5 cells/well in 6-well culture plates (BM Equipment Co., Ltd., Tokyo, Japan) and grown to confluence. The wells were overlaid with RPMI 1640 medium containing 100 conidia per well and incubated at 37°C under 5% CO_2. After incubation for 2 h, wells were washed three times with PBS, overlaid with Sabouraud dextrose agar (SDA), and incubated at 37°C. After 24 h, conidia adhering to the wells were counted. In text, conidia adherence levels are expressed as the percentage ± SD of the number of adhering conidia divided by the original conidial number, based on three independent experiments.

Cytotoxicity of *A. fumigatus* Against Cultured Cells

To measure the viability of mammalian cells in culture with the *A. fumigatus* strains, lactate dehydrogenase (LDH) levels were determined using the Cytotoxicity Detection KitPLUS (Roche). Samples were incubated with LDH substrate at 37°C for 5 min, then the absorbance was read on a microplate reader at 490 nm. Data were expressed as the percentage (±SD) of control cells without fungi, based on three independent experiments.

Phagocytosis Assay

Murine macrophage-like cells (J774.1) were grown at a concentration of 10^5 cells per well in RPMI 1640 medium supplemented with 10% (v/v) FBS and 100 mg/L streptomycin and 16 mg/L penicillin (both from Sigma) in 6-well plates overnight at 37°C under 5% (v/v) CO_2. The cells were then co-incubated with 1×10^2 *A. fumigatus* conidia for 2 h at 37°C under 5% CO_2. To eliminate conidia not adhering to cells, the wells were washed with PBS and incubated for a further 5 h. The wells were overlaid with SDA and incubated at 37°C. Colony numbers were counted after 24 h incubation and were taken to represent the number of surviving conidia in the wells. In text, conidia survival rates are expressed as the percentage of the adhered conidial number divided by the overlaid conidial number.

Measurement of Stress Responses

For assessing oxidative stress tolerance, 1×10^2 conidia/mL were incubated with 32.6 mM H_2O_2 in PDB medium. After incubation for 1 h at 37°C, 100 μL samples of the suspensions were immediately plated onto SDA on 9-cm Petri dishes. After incubation for 24 h at 37°C, the number of visible colonies was counted. The growth ratio under oxidative stress was calculated by comparing the colony numbers on SDA for cells plated with and without H_2O_2. This procedure was based on a previously described method (Paris et al., 2003). To measure fungal growth under osmotic stress conditions, 10^6 conidia of each strain were point-inoculated on yeast–glucose minimal medium (0.1% yeast extract–1% glucose, YGM), containing 0.8 M NaCl. After incubation for 72 h at 37°C, colony diameters were measured. The data are presented as the mean ± SD of three independent experiments.

RESULTS

Nucleotide Sequences of dsRNAs

dsRNA extracted from Af293 cells was resolved into four bands by agarose gel electrophoresis, or five bands by polyacrylamide gel electrophoresis (**Figure 1A**, labeled segments 1 through 5). Sequences of the five dsRNAs were read and confirmed using a genome sequencer. Four of the five sequences had high sequence

similarity to those of the previously reported AfuPmV-1 segments 1–4 (97.0, 96.8, 95.0, and 98.4% identity, respectively) (Özkan and Coutts, 2015; Kanhayuwa et al., 2015). We named the virus AfuPmV-1M as it was stocked at the Medical Mycology Research Center, Chiba, Japan. The new fifth dsRNA segment was then named AfuPmV-1M dsRNA 5. It should be noted that the AfuPmV-1M dsRNA 5 was slightly larger than dsRNA 4 of AfuPmV-1 and AfuPmV-1M (**Figure 1B**).

Northern hybridization analysis using DIG-labeled cDNA probes specific for each of the five dsRNA segments further confirmed that each segment had a unique sequence (**Figure 1C**). Sequence analysis of full-length cDNAs of segments 1–5 revealed they were 2,403, 2,330, 1,971, 1,158, (dsRNA 5), and 1,140 (dsRNA 4) bps (slightly different from those reported by Kanhayuwa et al., 2015 for AfuPmV-1) and that each segment contained a single open reading frame (ORF) (**Figure 1B**).

The 5′ and 3′ termini sequences in the five dsRNAs are shown in **Supplementary Figure S1** and indicate high sequence conservation among these sequences. RNA sequencing of the Af293 strain was performed, and mapped to the genome of AfPmV1-M. The reads were mapped except for 1 to 2 bases at the very tip, which are difficult to map, indicating that the genome sequencing was correct. We also confirmed the results by viral RNA sequencing using fragmented and primer ligated dsRNA sequencing (FLDS; Urayama et al., 2016, 2018). This sequence conservation supports the idea that the five different segments belong to the same virus.

An examination of the deduced amino acid sequence of the AfuPmV-1M dsRNA 1 ORF revealed conserved motifs characteristic of RNA-dependent RNA polymerases (RdRp) of dsRNA viruses found in simple eukaryotes (Bruenn, 1993). A BLASTp search of the deduced amino acid sequence showed that it had high sequence similarity to RdRp encoded by Aspergillus fumigatus tetramycovirus-1 (AfuPmV-1, GenBank accession no. CDP74618.1; 98.4% identity), Botryosphaeria dothidea virus 1 (BdV-1, GenBank accession no. AKE49495.1; 54.4% identity), and Cladosporium cladosporioides virus 1 (CcV-1, GenBank accession no. YP_009052470.1; 46.0% identity). A phylogenetic tree based on RdRp sequences of AfuPmV-1M and 34 other selected RNA viruses was generated using the neighbor-joining (NJ) method (Saitou and Nei, 1987) and MEGA X (Tamura et al., 2011), indicating AfuPmV-1M belongs to the polymycoviridae dsRNA group (**Supplementary Figure S2** and **Supplementary Table S1**).

A BLASTp search of the deduced amino acid sequence of AfuPmV-1M dsRNA 2 showed it had 99.6% identity with AfuPmV-1 dsRNA 2. It also showed sequence similarity to dsRNAs of BdV-1 (46.7% identity) and CcV-1 (32.3% identity). The functions of these proteins are unknown.

A MOTIF search[3] of the deduced amino acid sequence of the AfuPmV-1M dsRNA 3 ORF revealed the presence of the conserved motif for methyltransferase from nucleotide positions 140 to 255, as seen in AfuPmV-1 from amino acids 110 to 250 (Kanhayuwa et al., 2015). A BLASTp search of the deduced amino acid sequence showed that it had sequence similarity to dsRNA 3 of AfuPmV-1 (97.9% identity) and the hypothetical proteins encoded by BdV-1 (42.8% identity) and CcV-1 (26.7% identity).

A BLASTp search of the deduced amino acid sequence of the AfuPmV-1M dsRNA 4 ORF showed that it had sequence similarity to dsRNA 4 of the PAS (proline/alanine/serine)-rich protein encoded by AfuPmV-1 (99.6% identity) and the hypothetical proteins encoded by BdV-1 (53.1% identity) and CcV-1 (39.8% identity).

Sequence analysis of AfuPmV-1M dsRNA 5 showed that it contained a single open reading frame (AfuPmV-1M dsRNA 5 ORF) from nucleotide positions 87 to 980. The dsRNA 5 ORF encodes a protein of 280 amino acid residues with a predicted molecular mass of 31 kDa (**Figure 1B**). A BLASTp search of the deduced amino acid sequence of dsRNA 5 revealed no significant sequence similarity with any virus proteins, while a BLASTn search revealed the nucleotide sequence from position 206 to 234 of dsRNA 5 had similarity to a conserved sequences of 29 nt in herpesviruses [CGTCGAGGACCCGTGGGCCCTGCCCGCGG (90% identity, GenBank accession number KP098534.1)].

During a series of experiments, bands of molecular weight lower than dsRNA 4 occasionally appeared following polyacrylamide gel electrophoresis (**Figure 1A**). Sequence analysis and Northern blotting (**Figure 1C**) revealed that one of these bands contained dsRNA 3 of AfuPmV-1M, as shown in **Figures 1A,C**, which lacked nucleotides from position 438 to 844 (resulting in a fragment that was 735 bp). Similar bands of less than 800 bp were occasionally observed during polyacrylamide gel analysis (data not shown). Sequence analysis revealed they contained 3′- and 5′-end parts of fragments 1 or 4 with missing central part similarly for the case of dsRNA 3, but they were not analyzed further in the present work.

Expression Pattern of AfuPmV-1M Genes

Relative expression levels of AfuPmV-1M genes in *A. fumigatus* were examined using real-time quantitative reverse transcription-PCR (qRT-PCR). Our results revealed that mycoviral RNA levels changed during the progression of fungal development. For all five AfuPmV-1M genes (dsRNAs 1–5), transcript levels were high at 6 h and 3–6 days after incubation in liquid medium; these time points corresponded to the germination stage of mycelial development and when mycelia were fully extended, respectively (**Figure 2A**). On the other hand, during sporulation (**Figure 2B**), transcript levels of the five ORFs were highest at a timepoint corresponding to the conidial maturation stage (24 h). ORF4 showed the highest expression level among the five ORFs (**Figure 2**).

Effect of AfuPmV-1M Infection on *A. fumigatus* Colony Morphology and Mycelial Growth

To investigate whether the mycovirus was responsible for growth and virulence of *A. fumigatus*, we eliminated the mycovirus from the host using a single-spore isolation method. Elimination of the dsRNAs from the fungal hyphae was confirmed by dsRNA extraction, followed by agarose gel

[3]https://www.genome.jp/tools/motif/

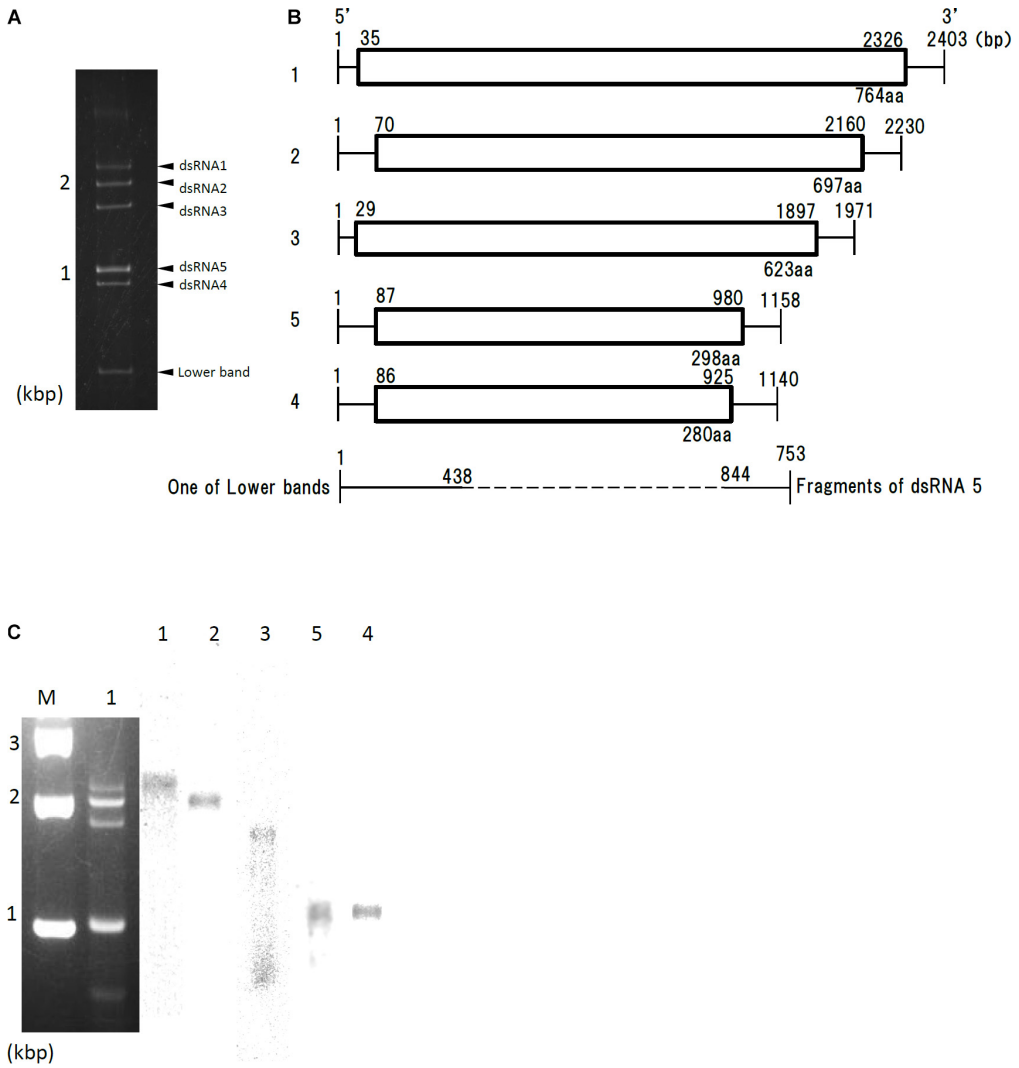

FIGURE 1 | Genome organization of AfuPmV-1M. **(A)** dsRNA was extracted and electrophoresed on a 5% (w/v) polyacrylamide gel. **(B)** Schematic drawing of the genomic organization of AfuPmV-1M. "1"–"5" on the left indicates contigs. The horizontal lines and boxes indicate full dsRNA lengths and ORFs, respectively. The ORF sense orientations are from left to right for all contigs. Numbers on the lines and boxes indicate nucleotide numbers. Numbers under the boxes indicate amino acid (aa) lengths. **(C)** Left: Agarose gel electrophoresis of dsRNAs purified from the *A. fumigatus* strain infected with AfuPmV-1M (lane 1). Lane M, molecular weight marker. Right: Northern blot detection of dsRNA segments using digoxigenin-labeled DNA probes against dsRNA segments 1–5. dsRNA samples were electrophoresed on five different lanes of a single agarose gel and blotted. The five blotted lanes were separated and hybridized with the probes for each dsRNA. Lanes 1–5 of panel C were then reconstituted from the hybridized strips.

electrophoresis and ethidium bromide staining and RNA sequencing (**Supplementary Figure S3**).

Two days after spotting conidia on potato dextrose agar (PDA) plates, the virus-free strain formed a colony of a homogeneous green color but the virus-infected strain formed a colony with stripes of green and white (**Figure 3A**). The difference in colony color had almost disappeared by day 3, when both colonies showed a homogenous green color. The virus-infected strain showed a reduced colony growth rate (**Figure 3B**), reduced numbers of conidiophores, and reduced conidia formation in comparison with the results of the virus-free strain (**Figures 3C,D**). During the *in vitro* experiments, conidia from the virus-infected strain showed delayed swelling and germination in comparison with these events in the virus-free strain (**Figures 4A,B**). Under liquid culture conditions in potato dextrose broth (PDB) medium, the mycelial mass of the virus-infected strain was also reduced (**Figure 4C**).

Influence of AfuPmV-1M on *A. fumigatus* Gene Expression

To characterize how *A. fumigatus* responds to AfuPmV-1M infection, we performed RNA-seq analysis to compare gene expression between virus-infected and virus-free strains at two distinct time points: just before the start of swelling (4 h after the start of incubation, a stage referred to here as the 4-h swelling

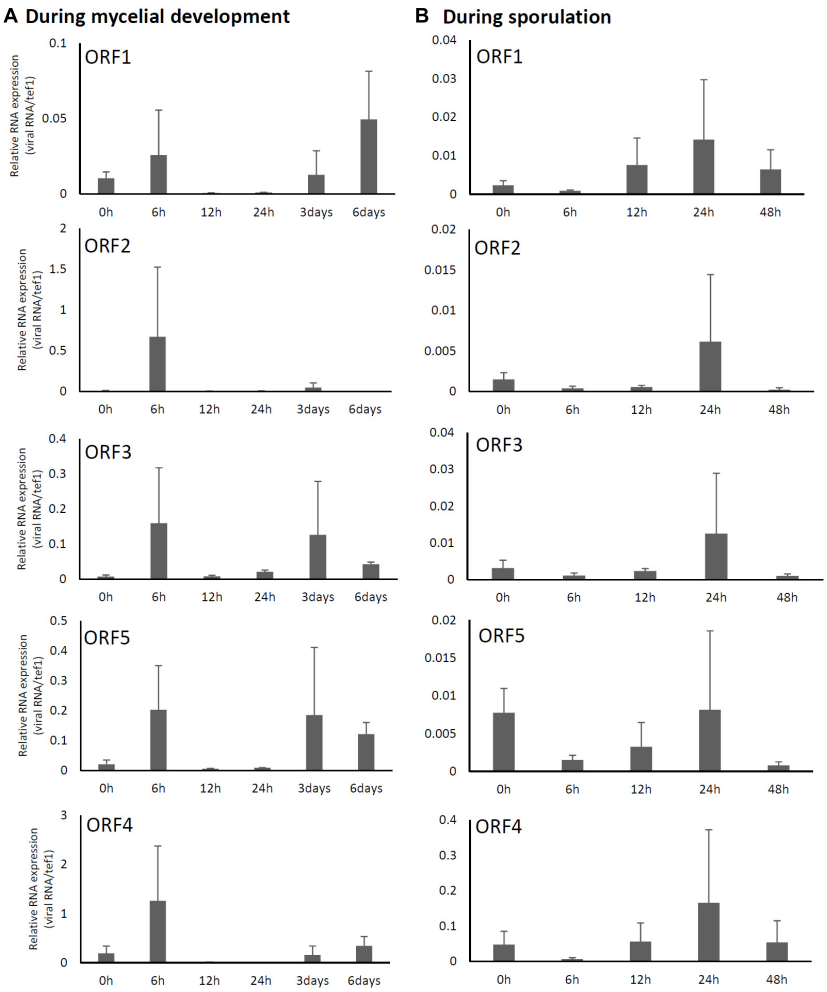

FIGURE 2 | Changes in viral ORF transcript levels at different stages of growth in the AfuPmV-1M-infected strain. **(A)** RNA levels were analyzed by real-time PCR during the fungal life-cycle, with time points following exposure to liquid medium as follows: 0 h (conidia), 6 h (germination), and later stages of mycelial development (12 h, 24 h, and days 3 and 6). **(B)** RNA levels were analyzed using real-time PCR during sporulation, with time points as follows: 0 h (day 7, mycelia), 6 h (vesicle formation), 12 h (phialide formation), and 24 h and 48 h (conidial formation). Data values were normalized to that of the internal control, the *A. fumigatus* tef-1 gene, and presented as means ± SD of three independent experiments.

stage) and at the hyphal stage (day 6). At the 6-day hyphal stage, the pattern of host fungal gene expression differed more dramatically between the infected and the virus-free strains in comparison with gene expression at the 4-h swelling stage (4 h: $r = 1.00$, 6 days: $r = 0.86$, where "r" is the correlation coefficient) (**Supplementary Figures S4A–C**).

For gene expression assessed on day 6 after the start of incubation, 67 genes were down-regulated, and 198 genes were up-regulated, more than fivefold (**Supplementary Table S2**). There were some particular differences in virus-infected strains compared with the virus-free strains (**Supplementary Figure S5** and **Supplementary Table S2**). In virus-infected strains, a series of genes in the fumagillin-related cluster increased (AFUA_8G00370 polyketide synthase, putative, AFUA_8G00380 DltD N-terminal domain protein, AFUA_8G00390 O-methyltransferase, putative, AFUA_8G00400 uncharacterized protein, AFUA_8G00430 uncharacterized protein, AFUA_8G00440 steroid monooxygenase, putative, AFUA_8G00480 phytanoyl-CoA dioxygenase family protein, AFUA_8G00500 acetate-CoA ligase, putative, AFUA_8G00510 cytochrome P450 oxidoreductase OrdA-like, putative, AFUA_8G00520 fumagillin beta-trans-bergamotene synthase, AFUA_8G00540 non-ribosomal peptide synthetase 14). Conversely, a series of genes in the gliotoxin-related cluster decreased (AFUA_6G09630 C6 finger domain protein GliZ, AFUA_6G09640 aminotransferase GliI, AFUA_6G09680 O-methyltransferase GliM, AFUA_6G09690 glutathione S-transferase GliG, AFUA_6G09700 gliotoxin biosynthesis protein GliK, AFUA_6G09710 MFS gliotoxin efflux transporter GliA, AFUA_6G09720 methyltransferase GliN, AFUA_6G09730 cytochrome P450 oxidoreductase GliF, AFUA_6G09740 thioredoxin reductase GliT, AFUA_6G09660 non-ribosomal

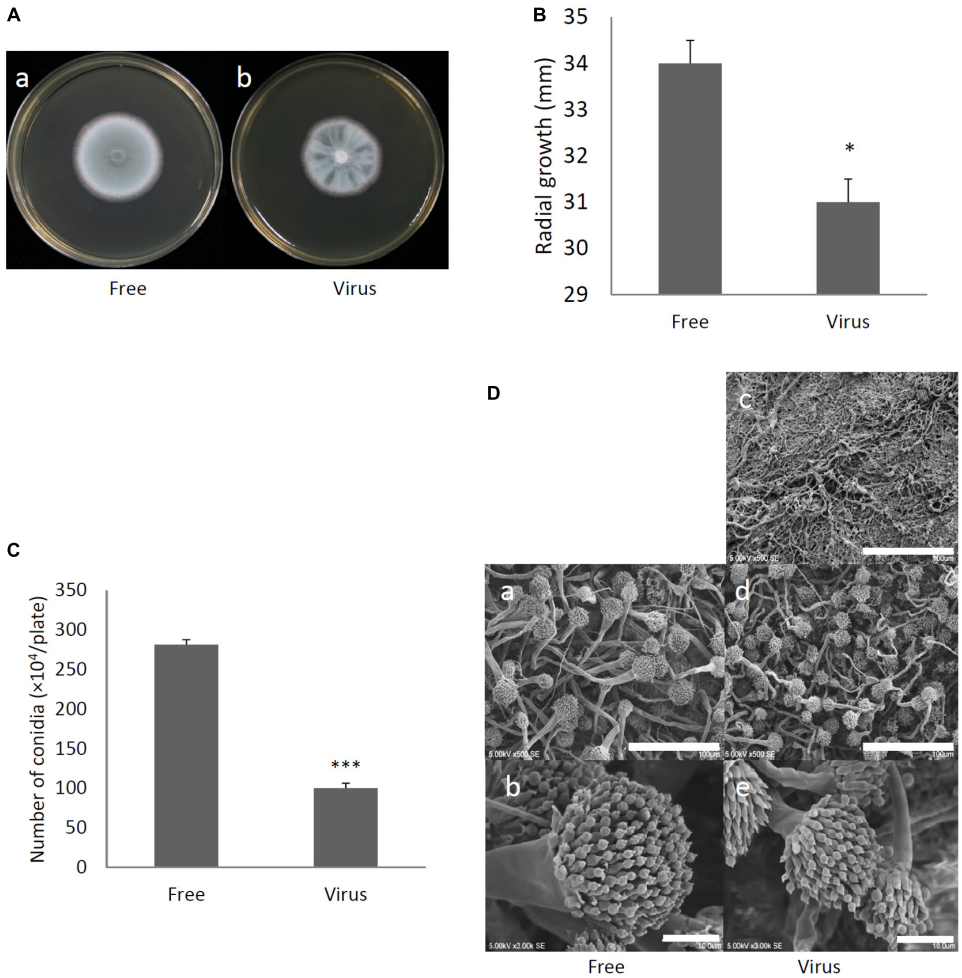

FIGURE 3 | Comparisons of colony morphology and conidial formation of virus-free (Free) and virus-infected (Virus) strains. **(A)** Colony morphology of AfuPmV-1M virus-free **(a)** and virus-infected **(b)** *A. fumigatus* strains (cultured for 2 days). **(B)** Radial growth of colonies formed by virus-free and AfuPmV-1M virus-infected *A. fumigatus* strains. Statistically significance was determined using a two-tailed Student's *t*-test, $*p < 0.05$. **(C)** Numbers of conidia formed by the strains at 24 h post-inoculation. Statistically significance, $***p < 0.001$. **(D)** Conidiophore formation in virus-free and virus-infected *A. fumigatus* strains. SEM images. **(a,b)** Virus-free. **(c–e)** Virus infected strain. **(a,d)** Green areas of the colonies. **(c)** White area of the colony. **(b,e)** Conidiophores. The scale bars indicate 100 μm for **(a,c,d)** and 10 μm for **(b,e)**.

peptide synthetase 10, gliotoxin synthesis protein). The quantities of fumagillin and gliotoxin in fungal cultures were measured by high-performance liquid chromatography (HPLC) and the results of this also supported the RNA-seq results. The amount of gliotoxin in supernatants was decreased, whereas the amount of fumagillin in mycelia was increased in virus-infected strains compared with the quantities in virus-free strains. In addition, gene ontology (GO) analysis showed that some RNA polymerase-related genes were down-regulated at both 4 h and 6 days (**Supplementary Table S2**).

Hypovirulence of the dsRNA Virus-Infected *A. fumigatus* Strain in a Mouse Infection Model

To determine the effects of dsRNA virus infection on the virulence of *A. fumigatus*, virus-infected and virus-free strains were intratracheally administrated to ICR mice immunosuppressed with hydrocortisone acetate. As shown in **Figure 5A**, the survival rate was significantly higher in mice infected with the virus-infected *A. fumigatus* strain compared with the survival of those mice infected with the virus-free strain ($p < 0.05$, Kaplan–Meier log rank test). Computed tomography (CT) imaging was performed in mice infected with the virus-infected and virus-free strains on day 14 following infection. Mice infected with the virus-free *A. fumigatus* strain showed a dense consolidation of the lung, consistent with pneumonia, while mice infected with the virus-containing *A. fumigatus* showed no radiographic or pathologic evidence of pneumonia (**Figure 5B**). The pulmonary fungal burden at 72 h after fungal infection was significantly lower in mice infected with the virus-infected fungal strain than in mice infected with the virus-free strain (**Figure 5C**). The results of Grocott's methenamine silver (GMS) staining of the lungs at 72 h after infection revealed that

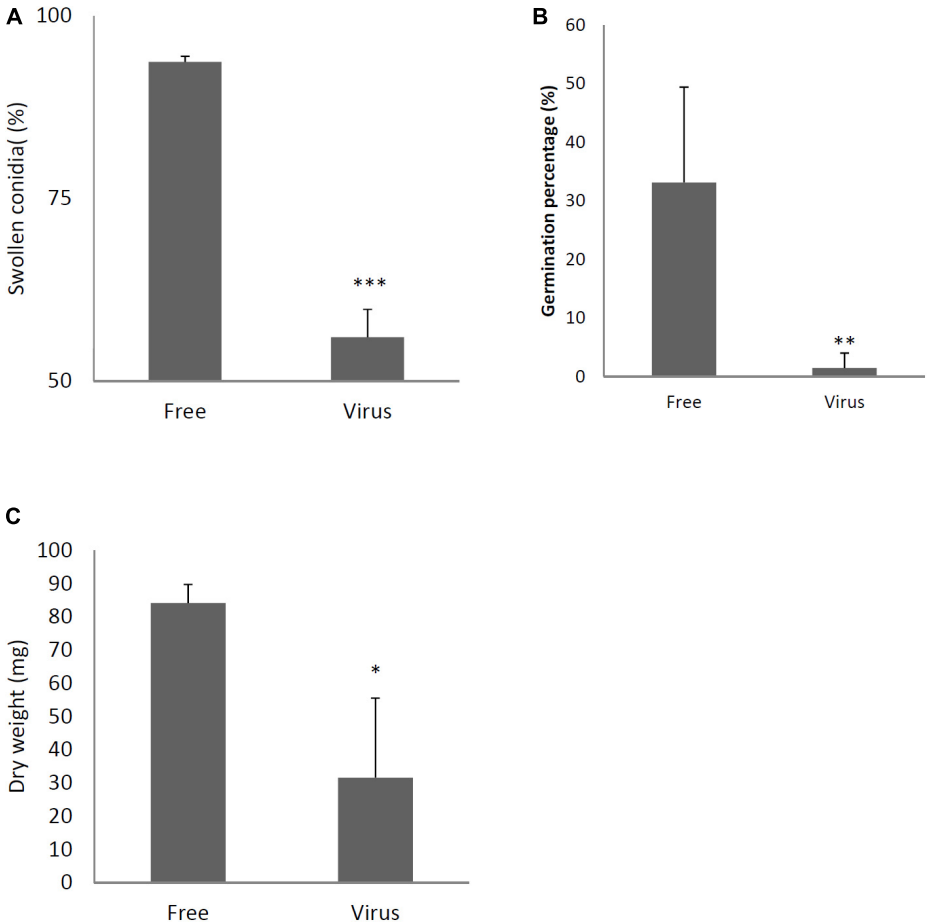

FIGURE 4 | Comparisons of conidial swelling and germination rates and mycelial dry weight between the virus-free (Free) and virus-infected (Virus) strains. Percentage of swollen conidia at 6 h after plating **(A)** and percentage of germinating conidia at 8 h after plating conidia **(B)** are shown. **(C)** Mycelial growth. Growth was quantified by measuring dry weights of mycelia at 24 h after the incubation of conidia began. Data are presented as means ± SD of three independent experiments. *$p < 0.05$, **$p < 0.01$, ***$p < 0.001$, by two-tailed Student's *t*-test.

hyphae were observed in mice lungs infected with the virus-free *A. fumigatus* strain, but no hyphal growth was observed from conidia of the virus-infected strain (**Figure 5D**).

We considered it possible that the reduction of virulence in the mycovirus-infected strain may be due to decreased adherence of the conidia to host epithelial cells or, alternatively, reduced survival rate of fungi after phagocytosis by macrophages in the lungs of mice. We therefore, studied the impact of the mycovirus on the conidial adherence of *A. fumigatus* to lung epithelial cells and on the survival rate of conidia of virus-infected or virus-free strains after *in vitro* culturing with macrophages. As shown in **Figure 6A**, conidia of the virus-infected strain showed reduced adherence to cells of the type II human pneumocyte cell line A549 in comparison with the adherence of the virus-free strain. Also, conidia from the virus-infected strain showed a reduced survival rate after co-culturing with mouse macrophage J774 cells compared with the survival rate of the virus-free strain (**Figure 6B**).

Previous reports have claimed that reactive oxygen species are manufactured in macrophages for the purpose of killing invading microorganisms (Weiss and Schaible, 2015). Our experiment showed the conidia of the virus-infected strain were more sensitive to oxidative stress caused by H_2O_2 in comparison with the virus-free strains (**Figure 6C**). Tolerance to osmotic stress was also decreased in the virus-infected strain (**Figure 6D**). An LDH (lactate dehydrogenase) assay was used to quantitatively assess epithelial cell lysis upon infection. No significant difference in epithelial damage was observed between the virus-infected and virus-free strains (**Figure 6E**).

Phenotypic Analysis of Fungal Strains Expressing Individual ORF

We attempted to identify which gene products of AfuPmV-1M are involved in hypovirulence by establishing *A. fumigatus* strains which express the individual viral ORFs. Each of the AfuPmV-1M ORFs was expressed in an originally virus-free strain (KU) using a pCB1004 plasmid vector. Viral gene expression in each transformants during sporulation were confirmed by qRT-PCR (**Supplementary Figure S7**). Compared

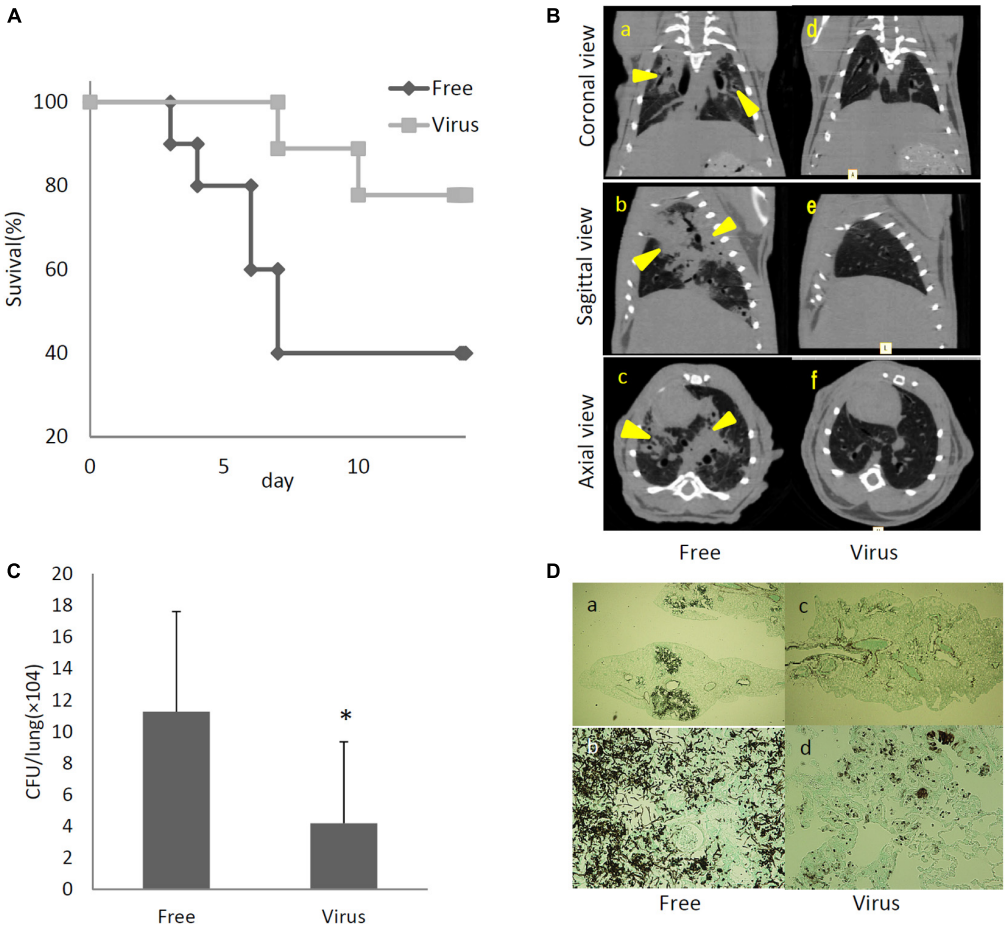

FIGURE 5 | Comparisons of virulence in mice of virus-free (Free) and virus-infected (Virus) strains. **(A)** Survival rates of mice infected with the AfuPmV-1M virus-infected and virus-free strains. *$p < 0.05$ by the Kaplan–Meier log rank test. **(B)** CT scans of mouse chests at 14 days post-infection. **(a–c)** Virus-free fungal strain, **(d–f)** AfuPmV-1M virus-infected fungal strain. Shadows can be seen in the lungs of virus-free *A. fumigatus*-infected mice (arrowheads in **a–c**). **(C)** Fungal growth from the lungs of infected mice. Fungal burdens were estimated as CFUs per gram of lung. Data are presented as means ± SD of three independent experiments. *$p < 0.05$ by two-tailed Student's *t*-test. **(D)** Lung histology of mice at 3 days post-infection (Gomori's methenamine silver-staining-Grocott's variation). **(a,b)** virus-free strains; **(c,d)** virus-infected strains.

with the KU strain or a strain transformed with the empty vector, ORF2- and ORF3-expressing strains showed significant changes in colony morphology, with radial growth being largely suppressed (**Figures 7A,B**). Expression of ORF2 also reduced the number of conidia formed after 3 days in culture (**Figure 7C**). Microscopic examination revealed that the numbers of swollen conidia were reduced in transformants expressing ORF1 and ORF3 (**Figure 7D**), while mycelial growth in liquid culture was not significantly changed by the expression of any of the ORFs (**Figure 7E**).

The virulence of *A. fumigatus* KU strain expressing each ORF or only the empty vector was then assessed in immunosuppressed ICR mice. As shown in **Figure 8A**, we observed that the expression of ORF2 and ORF5 decreased the fungal burden in the lungs (CFU/g), as observed 3 days after infection and compared with the empty vector control. *In vitro* assays revealed that conidia of ORF1- and ORF2-expressing strains showed reduced adherence to A549 cells in comparison with the adherence of the KU strain transformed with the empty vector (**Figure 8B**). Damage to epithelial cells was increased in the ORF4- and ORF5-expressing strains (**Figure 8C**). The survival rate of the fungi in co-culture with J774A.1 mouse macrophages decreased in the ORF3-expressing strain (**Figure 8D**). Tolerance to oxidative stress was decrease in the ORF2- and ORF3-expressing strains (**Figure 8E**), while tolerance to osmotic stress was decreased in the ORF3- and ORF5-expressing strains (**Figure 8F**).

DISCUSSION

It is possible that the study of mycoviruses could provide clinically useful information because the virus might cause hypovirulence in its fungal hosts. Although several mycoviruses are known to be associated with latent infections in human pathogenic fungi, few reports have described their effects on fungal pathogenicity against hosts. The present study revealed the

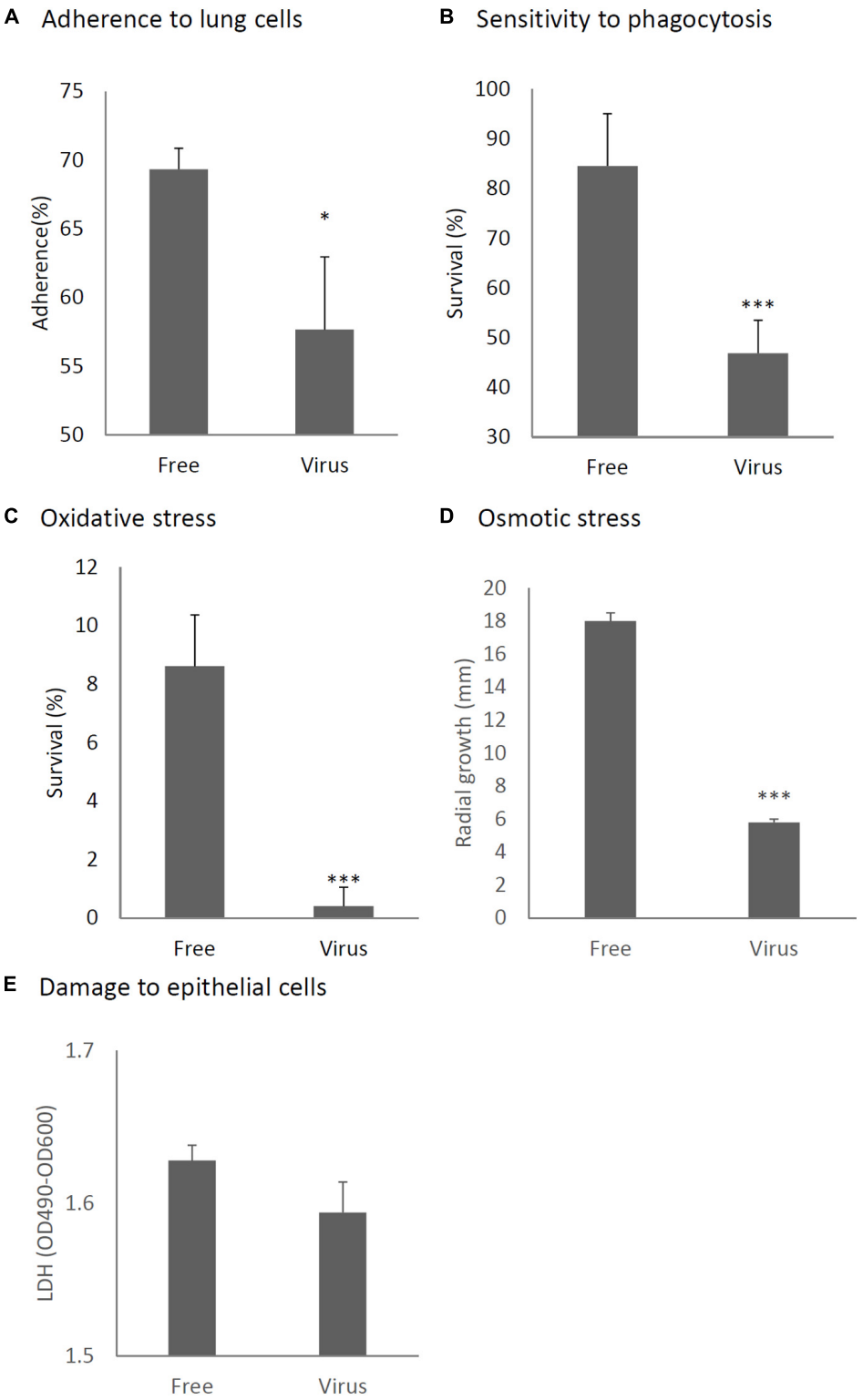

FIGURE 6 | Comparison of phenotypes and tolerance to stresses between virus-free (Free) and virus-infected (Virus) strains. **(A)** Adherence of conidia to A549 human pneumocyte cells. **(B)** Sensitivity of the *A. fumigatus* strains to phagocytosis by J774A.1, a murine macrophage cell line. **(C)** Germination rates of the virus-free and virus-infected strains under oxidative stress (germination following 24-h exposure to 32.6 nM H_2O_2). **(D)** Growth of the virus-free and virus-infected *A. fumigatus* strains under osmotic stress conditions (conidial growth in the presence of 0.8 M NaCl). **(E)** Mammalian epithelial cell (A549) lysis after co-incubation with conidia. From **(A)** to **(E)**, all experiments were independently repeated three times. Mean ± SD. $*p < 0.05$, $***p < 0.001$, by two-tailed Student's *t*-test.

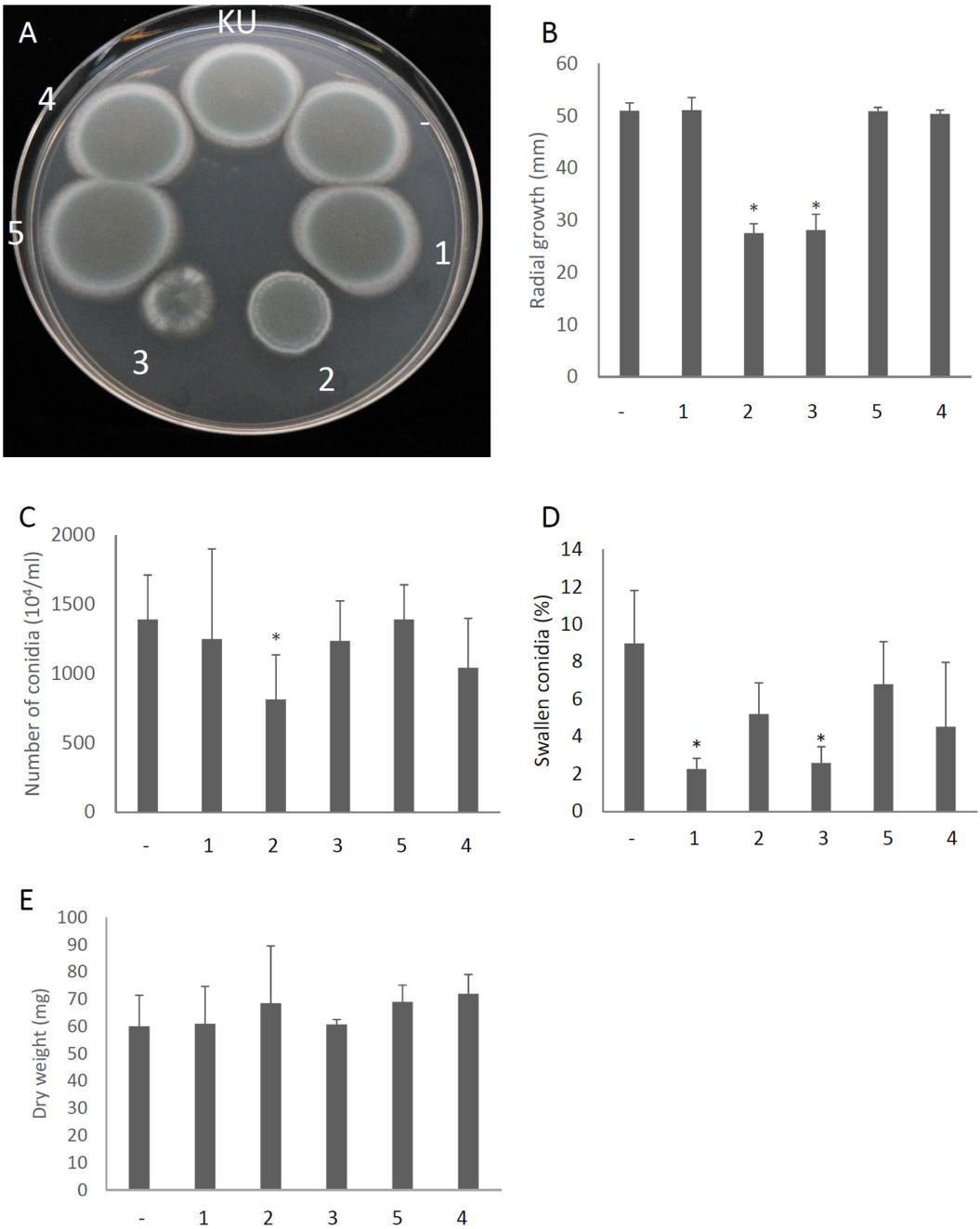

FIGURE 7 | Morphological comparisons of AfuPmV-1M ORF expressing and non-expressing KU strains. **(A)** Colonies formed by native KU strain (KU), empty-vector expressing (–), and each AfuPmV-1M ORF-expressing KU strain (1–5). **(B)** Radial growth of colonies by ORF expressing (1–5) and non-expressing (–) KU strains. **(C)** Number of conidia formed by the strains at 3 days post- inoculation. **(D)** Percentages of swelling conidia at 6 h after the start of incubation. **(E)** Dry weight of mycelia. Mycelial growth was quantified by measuring their dry weight at 24 h after starting the incubation of conidia. Data are presented as means ± SD of three independent experiments. *$p < 0.05$, by one-way ANOVA, Dunnett's test.

AfuPmV-1M dsRNA mycovirus, carried by *A. fumigatus* strain Af293, causes hypovirulence in its host human pathogenic fungi. To the best of our knowledge, this is only the second report after one about AfuCV41362 (Takahashi-Nakaguchi et al., 2020) of a mycovirus causing hypovirulence of invasive fungal infection in mammals. It should be noted that AfuCV41362 is classified in the *Chrysoviridae*, while AfuPmV-1M, described here, is classified in the *Polymycoviridae*.

In previous studies, four separate viral dsRNA bands from the Af293 strain were visible by agarose gel electrophoresis (Kanhayuwa et al., 2015; Morley, 2017). However, in the present study we found a fifth dsRNA (dsRNA segment 5) and additional

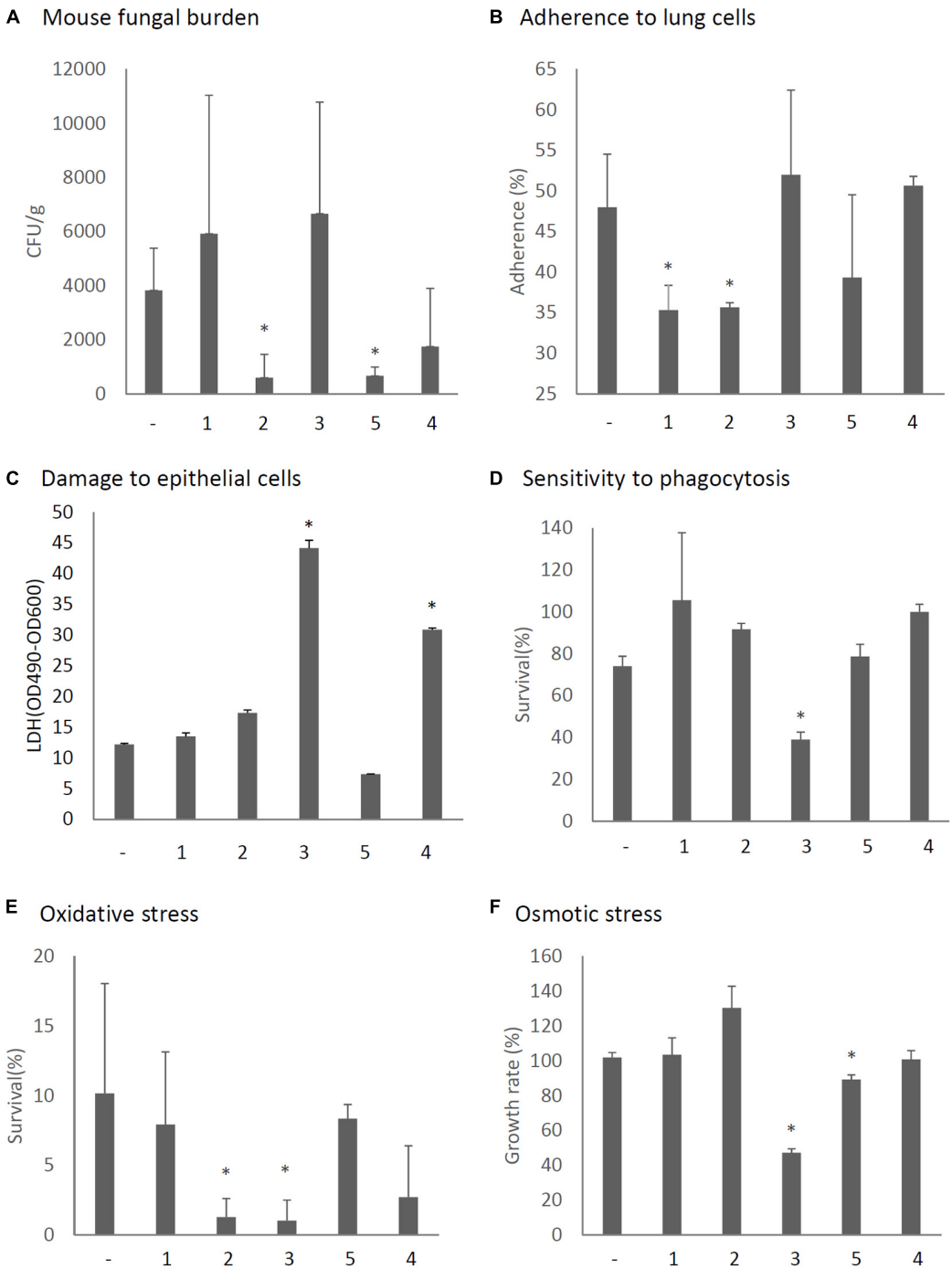

FIGURE 8 | Phenotypic comparisons of each AfuPmV-1M ORF (1–5)-expressing and non-expressing (–) KU strain. **(A)** Fungal burden in mouse lungs. Fungal cell numbers in mouse lungs were estimated as CFU of lung tissues 3 days after infection with each fungal strain. **(B)** Adherence of conidia from each strain to A549 human pneumocyte cells. **(C)** Cellular cytotoxicity of each ORF expressing (1–5) and non-expressing (–) strain assayed by LDH activity. A549 cells were incubated with each strain for 24 h for the LDH assay. **(D)** Sensitivity of each strain to phagocytosis by J774A.1, a murine macrophage cell line. **(E)** Effect of hydrogen peroxide on the growth of each strain. **(F)** Growth of each strain under osmotic stress conditions. $*p < 0.05$, by one-way ANOVA, Dunnett's test.

small bands were found by PAGE. Our sequence results indicated dsRNA 5 had a unique sequence, which has not previously been reported in the Af293 strain. We speculate AfuPmV-1 and AfuPmV-1M might share the same phylogenetic origin, but the fifth element has been lost in some branches of Af293 during passaging.

Since it was reported that some *A. fumigatus* strains, including the genome reference strain Af293, are infected with mycovirus,

no studies have been performed to elucidate whether the mycovirus provokes hypovirulence of the host fungi in a mouse model (Bhatti et al., 2011; Kanhayuwa et al., 2015). For example, AfuPmV-1 had no statistically significant virulent effect (Kanhayuwa et al., 2015), while A78, a species related to AfuPmV-1, had a hypervirulence effect in an insect model (Özkan and Coutts, 2015).

Among the five AfuPmV-1M dsRNAs, the 5′ and 3′ untranslated regions (UTRs) have conserved nucleotide sequences, as is commonly found in RNA viruses with multipartite and multi-component genomes. This suggests that AfuPmV-1M does indeed possess five genomic dsRNA segments which replicate separately as a multipartite dsRNA mycovirus (Mertens and Sangar, 1985; Attoui et al., 1997). In the present study, the complete nucleotide sequences of the fifth dsRNA were newly determined as well as the sequences of the other four dsRNA sequences, which showed high similarity to the ones reported by Kanhayuwa et al. (2015). Each of the five dsRNAs was found to have a single ORF.

At present, the functions of the proteins encoded by the dsRNAs of segments 2–5 are unknown, except that the protein encoded by dsRNA 3 has the conserved motifs characteristic of a domain of S-adenosyl-L-methionine-dependent methyltransferases (AdoMet_MTases). AdoMet_MTases catalyze the transfer of methyl groups from the ubiquitous cofactor S-adenosyl-L-methionine to a multitude of biological targets with high specificity, including DNA, RNA, protein, polysaccharides, lipids, and a range of small molecules in fungal cells (Polevoda and Sherman, 2007). It is well-known that viral methyltransferases cause various diseases in host cells (Kharbanda et al., 2013); therefore, dsRNA 3 of AfuPmV-1M may play a role in reducing the virulence of its pathogenic host *A. fumigatus* in animal infections.

Through a series of experiments, we found additional dsRNA bands smaller than dsRNA 4. Sequence analysis revealed these are fragments of conjugated 5′- and 3′-sequences but they lack the middle parts of sequences in dsRNAs 1, 3, and 4. AfuPmV-1 has been reported to produce virus-derived small interfering RNA (vsiRNA) (Özkan et al., 2017). Inferring from this previous report, the smaller bands which occasionally appeared in the gel analysis of AfuPmV-1M may be remaining RNA fragments produced through such vsiRNA processing. Experiments are underway to elucidate the origin of these smaller sequences.

We have previously reported a double-stranded mycovirus, AfuCV41362, isolated from a different origin, of *A. fumigatus* strain IMF 41362 (Takahashi-Nakaguchi et al., 2020). AfuCV41362 consists of four dsRNA fragments and belongs to the *Chrysoviridae*. In that report we examined expression levels of viral RNA in host filamentous fungi at each developmental stage (to the best of our knowledge for the first time). The time course of AfuPmV-1M dsRNA expression was different from that of AfuCV41362 dsRNAs during host fungal development, as examined by real-time PCR (Takahashi-Nakaguchi et al., 2020). Similarly to AfuCV41362 dsRNAs, the expression levels of AfuPmV-1M dsRNAs increased as germination of the host fungus *A. fumigatus* proceeded. However, unlike AfuCV41362, expression levels of AfuPmV-1M viral RNAs were seen to increase at the time when the hyphae were completely extended. Also, the level of AfuPmV-1M RNAs increased at the time of spore maturation, whereas AfuCV41362 RNA increased only during the early stage of sporulation. This difference may be related to the fact that AfuCV41362 produces virus particles while AfuPmV-1M presumably does not (Kanhayuwa et al., 2015).

The present *in vivo* and *in vitro* experiments indicated that AfuPmV-1M virus-infected fungal strains have reduced pathogenicity in comparison with the pathogenicity of virus-free strains, based on the following results (summarized in **Supplementary Table S3**). (1) Mice infected with virus-infected fungi showed reduced mortality in comparison with the mortality of mice infected with virus-free fungi. (2) Lung tissues isolated from mice infected with the virus-infected strain showed fewer CFUs and less damage on a CT scan and histological images in comparison with the virus-free fungal strain. (3) Conidia of the dsRNA virus-infected strains showed reduced adherence to lung cells, reduced tolerance to macrophage phagocytosis, and reduced tolerance to oxidative and osmotic stresses. Furthermore (4), the growth of fungal hyphae and formation of conidia were retarded in the virus-infected strains in comparison with the virus-free strain during *in vitro* experiments. Incidentally, effects of AfuPmV-1M mycovirus infection on *A. fumigatus* were re-confirmed by introducing the mycovirus into the originally virus-free KU strain (AfS35, FGSC A1159, akuA:loxP) via the protoplast fusion method (Kanematsu et al., 2004; Lee et al., 2011; Takahashi-Nakaguchi et al., 2020). Tolerance to oxidative and osmotic stresses was decreased even in the whole virus-introduced strain (**Supplementary Figure S8**). On the other hand, in insect infection experiments AfuPmV-1 is reported to exhibit no pathogen-suppressing effect (Kanhayuwa et al., 2015). This may be due to differences between insects and mice or the action of the fifth ORF, ORF5.

The difference between the effects of AfuPmV-1M and AfuCV41362 was also observed in the RNA-seq results. With AfuCV41362 infection, mRNA expression in the host *A. fumigatus* was more severely affected at the time of germination (4 h swelling stage) than in the hyphal stage, but with AfuPmV-1M infection, mRNA expression of the host *A. fumigatus* was more severely affected at the hyphal stage, when viral RNA was highly expressed. Adhesion to host cells was reduced in virus-infected strain (**Figure 6A**). We previously revealed 23 genes expressed during sporulation that are important for adherence to host cells (Takahashi-Nakaguchi et al., 2017). Although the stages examined were different from the conidial maturation stage, the expression levels of three of the genes (*AFUA_1G13670,* conserved hypothetical protein; *AFUA_4G02805,* Asp hemolysin-like protein; and *AFUA_5G00590*, hypothetical protein) were reduced during germination, and the expression levels of four genes (*AFUA_4G09310,* conserved hypothetical protein; *AFUA_1G04100*, conserved hypothetical protein; *AFUA_4G01030*, conserved hypothetical protein; and *AFUA_8G07060,* hydrophobin, putative) were reduced at the mycelial stage in virus-infected strains. Host macrophages and neutrophils also produce high levels of reactive oxygen species (ROS), which are harmful to *A. fumigatus* (Brown et al.,

2009). Multiple genes involved in the defense of *A. fumigatus* against ROS have been characterized, and the expression levels of several genes were reduced in the mycelium due to viral infection. These genes included *TcsC*, a sensor of oxidative stress (Chapeland-Leclerc et al., 2015), the stress response pathway gene *Pbs2*, and the gene encoding transcription factor AFUA_4G08120. In addition, the expression levels of osmotic stress sensor genes (*Msb1*, *Sho1*), which share oxidative stress and stress response pathways, were also down-regulated. Furthermore, the expression levels of 10 other stress response genes were also down-regulated by the virus in the mycelium (**Supplementary Table S2**). In particular, the expression of gliotoxin-related genes and gliotoxin production decreased and that of fumagillin-related genes and fumagillin production increased at the hyphal stage, a phenomenon not observed in the AfuCV41362 infected host (Takahashi-Nakaguchi et al., 2020). Gliotoxins have toxic and immunosuppressive properties against host immune effector cells, and has been implicated in virulence (Stanzani et al., 2005; Orciuolo et al., 2007; Sugui et al., 2007; Wang et al., 2014). It is presumed that the reduced production of gliotoxin caused by mycovirus is another factor that reduces the pathogenicity of the virus-infected fungus. In contrast to gliotoxin, gene expression levels and production of fumagillin, which is another toxin produced by *A. fumigatus*, were enhanced by the virus infection. Fumagillin is used as an antimicrobial agent and can block mammal blood vessel formation by binding to the enzyme methionine aminopeptidase 2; it is also toxic to erythrocytes at high doses (Guruceaga et al., 2019). At present, the effect of fumagillin in the pathogenicity of the fungal hosts remains unknown (Guruceaga et al., 2018).

To elucidate the role of each viral RNA, we expressed individual viral ORFs in the virus-free KU strain. The expression of ORF2 and ORF5 reduced the fungal burden in the lungs of host mice. In the whole AfuPmV-1M virus-infected strain a large amount of ORF2 was expressed during mycelial development and the sporulation stages, while colony growth and sporulation were severely defective in the ORF2-expressing strain. In addition, our data suggest that ORF2 suppresses fungal virulence by suppressing conidial adherence to lung cells and by reducing oxidative stress resistance. Although ORF5 suppressed osmotic tolerance, unlike ORF2, no other prominent virulence-suppressing effect was found in relation to ORF5. It should be noted that ORF5 is not present in AfuPmV-1, a closely related species that has previously been reported to have a low effect on suppressing fungal virulence in insects. The expression of ORF1, which contains RdRp, delayed the germination of host conidia. The expression of ORF3, which has a methyltransferase motif, resulted in abnormal colony morphology, delayed germination, enhanced phagocytosis by macrophages, and decreased oxidative stress and osmotic resistance, but did not affect the degree of fungal burden in mice. Although the expression level of ORF4 was high during the germination stages in whole-virus infected fungi, no significant effect on the fungal phenotypes was observed. Future analysis of each viral gene, under appropriate experimental conditions with controlled expression levels, should reveal the detailed roles of these viral components.

We conclude that the AfuPmV-1M mycovirus possess the ability to reduce fungal pathogenicity in a mouse infection model and suggest mycoviruses may provide novel information in the quest for novel therapeutic strategies for the treatment of aspergillosis. Further research aimed at the identification of mycovirus genes associated with reduced virulence of *A. fumigatus* is necessary to understand the underlying mechanisms and physiological roles of these genes. Such research may result in novel therapeutic biological agents for use against fungal infections.

DATA AVAILABILITY STATEMENT

The datasets generated for this study can be found in the online repositories. The names of the repository/repositories and accession number(s) can be found below: https://www.ncbi.nlm.nih.gov/genbank/, LC517041–LC517045; https://www.ncbi.nlm.nih.gov/genbank/, PRJDB9242.

ETHICS STATEMENT

The animal study was reviewed and approved by the Institutional Animal Care and Use Committee of Chiba University.

AUTHOR CONTRIBUTIONS

AT-N and HM designed the experiments. AT-N, ES, MY, SU, KS, HC, AN, YC, and DH performed the experiments. AT-N, ES, and TG analyzed the data. AT-N and TG wrote the manuscript. All authors contributed to the article and approved the submitted version.

FUNDING

This study was supported by the Hamaguchi Foundation for the Advancement of Biochemistry (Grant No. H30 to AT-N), KAKENHI 25860314 (to AT-N) and a Grant-in-Aid for Scientific Research (to AT-N and to TG) from the Ministry of Education, Science, Sports and Culture, and partly by a Cooperative Research Grant of NEKKEN (2010–2012), a Cooperative Research Program of the Medical Mycology Research Center, Chiba University (12-2) and the MEXT Special Budget for Research Projects: the Project on Controlling Aspergillosis and the Related Emerging Mycoses. This work was supported in part by the National BioResource Project-Pathogenic Microbes funded by the Ministry of Education, Culture, Sports, Science and Technology, Japan (http://www.nbrp.jp/).

SUPPLEMENTARY MATERIAL

The Supplementary Material for this article can be found online at: https://www.frontiersin.org/articles/10.3389/fmicb.2020.607795/full#supplementary-material

REFERENCES

Attoui, H., De Micco, P., and de Lamballerie, X. (1997). Complete nucleotide sequence of Colorado tick fever virus segments M6. S1 and S2. *J. Gen. Virol.* 78(Pt 11), 2895–2899. doi: 10.1099/0022-1317-78-11-2895

Bhatti, M. F., Bignell, E. M., and Coutts, R. H. A. (2011). Complete nucleotide sequences of two dsRNAs associated with a new partitivirus infecting *Aspergillus fumigatus*. *Arch. Virol.* 156, 1677–1680. doi: 10.1007/s00705-011-1045-1045

Bhatti, M. F., Jamal, A., Bignell, E. M., Petrou, M. A., and Coutts, R. H. A. (2012). Incidence of dsRNA mycoviruses in a collection of *Aspergillus fumigatus* isolates. *Mycopathologia* 174, 323–326. doi: 10.1007/s11046-012-9556-9555

Brown, A. J., Haynes, K., and Quinn, J. (2009). Nitrosative and oxidative stress responses in fungal pathogenicity. *Curr. Opin. Microbiol.* 12, 384–391. doi: 10.1016/j.mib.2009.06.007

Bruenn, J. A. (1993). A closely related group of RNA-dependent RNA polymerases from double-stranded RNA viruses. *Nucleic Acids Res.* 21, 5667–5669. doi: 10.1093/nar/21.24.5667

Chapeland-Leclerc, F., Dilmaghani, A., Ez-Zaki, L., Boisnard, S., Da Silva, B., Gaslonde, T., et al. (2015). Systematic gene deletion and functional characterization of histidine kinase phosphorelay receptors (HKRs) in the human pathogenic fungus *Aspergillus fumigatus*. *Fungal Genet. Biol.* 84, 1–11. doi: 10.1016/j.fgb.2015.09.005

Ghabrial, S. A., and Suzuki, N. (2009). Viruses of plant pathogenic fungi. *Annu. Rev. Phytopathol.* 47, 353–384. doi: 10.1146/annurev-phyto-080508-081932

Ghabrial, S. A., Castón, J. R., Jiang, D., Nibert, M. L., and Suzuki, N. (2015). 50-plus years of fungal viruses. *Virology* 47, 356–368. doi: 10.1016/j.virol.2015.02.034

Gravelat, F. N., Doedt, T., Chiang, L. Y., Liu, H., Filler, S. G., Patterson, T. F., et al. (2008). In vivo analysis of *Aspergillus fumigatus* developmental gene expression determined by real-time reverse transcription-PCR. *Infect. Immun.* 76, 3632–3639. doi: 10.1128/IAI.01483-07

Guruceaga, X., Ezpeleta, G., Mayayo, E., Sueiro-Olivares, M., Abad-Diaz-De-Cerio, A., Aguirre Urízar, J. M., et al. (2018). A possible role for fumagillin in cellular damage during host infection by *Aspergillus fumigatus*. *Virulence* 9, 1548–1561. doi: 10.1080/21505594.2018.1526528

Guruceaga, X., Perez-Cuesta, U., Abad-Diaz, de Cerio, A., Gonzalez, O., Alonso, R. M., et al. (2019). Fumagillin, a mycotoxin of *Aspergillus fumigatus*: biosynthesis. biological activities, detection, and applications. *Toxins* 12:7. doi: 10.3390/toxins12010007

Jamal, A., Bignell, E. M., and Coutts, R. H. A. (2010). Complete nucleotide sequences of four dsRNAs associated with a new chrysovirus infecting *Aspergillus fumigatus*. *Virus Res.* 153, 64–70. doi: 10.1016/j.virusres.2010.07.008

Jia, H., Dong, K., Zhou, L., Wang, G., Hong, N., Jiang, D., et al. (2017). A dsRNA virus with filamentous viral particles. *Nat. Commun.* 8:168. doi: 10.1038/s41467-017-00237-239

Kanematsu, S., Arakawa, M., Oikawa, Y., Onoue, M., Osaki, H., Nakamura, H., et al. (2004). A reovirus causes hypovirulence of rosellinia necatrix. *Phytopathology* 94, 561–568. doi: 10.1094/PHYTO.2004.94.6.561

Kanhayuwa, L., Kotta-Loizou, I., Özkan, S., Gunning, A. P., and Coutts, R. H. A. (2015). A novel mycovirus from *Aspergillus fumigatus* contains four unique dsRNAs as its genome and is infectious as dsRNA. *Proc. Natl. Acad. Sci.* 112, 9100–9105. doi: 10.1073/pnas.1419225112

Kharbanda, K. K., Bardag-Gorce, F., Barve, S., Molina, P. E., and Osna, N. A. (2013). Impact of altered methylation in cytokine signaling and proteasome function in alcohol and viral-mediated diseases. *Alcohol. Clin. Exp. Res.* 37, 1–7. doi: 10.1111/j.1530-0277.2012.01840.x

Kotta-Loizou, I., and Coutts, R. H. A. (2017a). Mycoviruses in aspergilli: a comprehensive review. *Front. Microbiol.* 8:1699. doi: 10.3389/fmicb.2017.01699

Kotta-Loizou, I., and Coutts, R. H. A. (2017b). Studies on the virome of the entomopathogenic fungus beauveria bassiana reveal novel dsrna elements and mild hypervirulence. *PLoS Pathog.* 13:e1006183. doi: 10.1371/journal.ppat.1006183

Lee, K.-M., Yu, J., Son, M., Lee, Y.-W., and Kim, K.-H. (2011). Transmission of fusarium boothii mycovirus via protoplast fusion causes hypovirulence in other phytopathogenic fungi. *PLoS One* 6:e21629. doi: 10.1371/journal.pone.0021629

Mahillon, M., Decroës, A., Liénard, C., Bragard, C., and Legrève, A. (2019). Full genome sequence of a new polymycovirus infecting *Fusarium redolens*. *Arch. Virol.* 164, 2215–2219. doi: 10.1007/s00705-019-04301-4301

Mertens, P. P., and Sangar, D. V. (1985). Analysis of the terminal sequences of the genome segments of four orbiviruses. *Prog. Clin. Biol. Res.* 178, 371–387.

Morley, J. P. (2017). *Studies of Clinical and Environmental Isolates of Aspergillus fumigatus*. Available online at: https://leicester.figshare.com/articles/thesis/Studies_of_clinical_and_environmental_isolates_of_Aspergillus_fumigatus/10228280/1 (accessed November 9, 2020).

Morris, T. J. (1979). Isolation and analysis of double-stranded RNA from virus-infected plant and fungal tissue. *Phytopathology* 69:854. doi: 10.1094/Phyto-69-854

Niu, Y., Yuan, Y., Mao, J., Yang, Z., Cao, Q., Zhang, T., et al. (2018). Characterization of two novel mycoviruses from Penicillium digitatum and the related fungicide resistance analysis. *Sci. Rep.* 8:5513. doi: 10.1038/s41598-018-23807-23803

Okada, R., Yong, C. K., Valverde, R. A., Sabanadzovic, S., Aoki, N., Hotate, S., et al. (2013). Molecular characterization of two evolutionarily distinct endornaviruses co-infecting common bean (*Phaseolus vulgaris*). *J. Gen. Virol.* 94, 220–229. doi: 10.1099/vir.0.044487-0

Orciuolo, E., Stanzani, M., Canestraro, M., Galimberti, S., Carulli, G., Lewis, R., et al. (2007). Effects of Aspergillus fumigatus gliotoxin and methylprednisolone on human neutrophils: implications for the pathogenesis of invasive aspergillosis. *J. Leukoc. Biol.* 82, 839–848. doi: 10.1189/jlb.0207090

Özkan, S., and Coutts, R. H. A. (2015). *Aspergillus fumigatus* mycovirus causes mild hypervirulent effect on pathogenicity when tested on Galleria mellonella. *Fungal Genet. Biol.* 76, 20–26. doi: 10.1016/j.fgb.2015.01.003

Özkan, S., Mohorianu, I., Xu, P., Dalmay, T., and Coutts, R. H. A. (2017). Profile and functional analysis of small RNAs derived from *Aspergillus fumigatus* infected with double-stranded RNA mycoviruses. *BMC Genomics* 18:416. doi: 10.1186/s12864-017-3773-3778

Paris, S., Wysong, D., Debeaupuis, J.-P., Shibuya, K., Philippe, B., Diamond, R. D., et al. (2003). Catalases of *Aspergillus fumigatus*. *Infect. Immun.* 71, 3551–3562. doi: 10.1128/iai.71.6.3551-3562.2003

Pearson, M. N., Beever, R. E., Boine, B., and Arthur, K. (2009). Mycoviruses of filamentous fungi and their relevance to plant pathology. *Mol. Plant Pathol.* 10, 115–128. doi: 10.1111/j.1364-3703.2008.00503.x

Polevoda, B., and Sherman, F. (2007). Methylation of proteins involved in translation. *Mol. Microbiol.* 65, 590–606. doi: 10.1111/j.1365-2958.2007.05831.x

Saitou, N., and Nei, M. (1987). The neighbor-joining method: a new method for reconstructing phylogenetic trees. *Mol. Biol. Evol.* 4, 406–425.

Sato, Y., Jamal, A., Kondo, H., and Suzuki, N. (2020). Molecular characterization of a novel polymycovirus from penicillium janthinellum with a focus on its genome-associated PASrp. *Front. Microbiol.* 11:592789. doi: 10.3389/fmicb.2020.592789

Stanzani, M., Orciuolo, E., Lewis, R., Kontoyiannis, D. P., Martins, S. L. R., St John, L. S., et al. (2005). *Aspergillus fumigatus* suppresses the human cellular immune response via gliotoxin-mediated apoptosis of monocytes. *Blood* 105, 2258–2265. doi: 10.1182/blood-2004-09-3421

Sugui, J. A., Pardo, J., Chang, Y. C., Zarember, K. A., Nardone, G., Galvez, E. M., et al. (2007). Gliotoxin is a virulence factor of *Aspergillus fumigatus*: gliP deletion attenuates virulence in mice immunosuppressed with hydrocortisone. *Eukaryot. Cell* 6, 1562–1569. doi: 10.1128/EC.00141-147

Takahashi-Nakaguchi, A., Sakai, K., Takahashi, H., Hagiwara, D., Toyotome, T., Chibana, H., et al. (2017). *Aspergillus fumigatus* adhesion factors in dormant conidia revealed through comparative phenotypic and transcriptomic analyses. *Cell. Microbiol.* 20:e12802. doi: 10.1111/cmi.12802

Takahashi-Nakaguchi, A., Shishido, E., Yahara, M., Urayama, S., Sakai, K., Chibana, H., et al. (2020). Analysis of an intrinsic mycovirus associated with reduced virulence of the human pathogenic fungus *Aspergillus fumigatus*. *Front. Microbiol.* 10:3045. doi: 10.3389/fmicb.2019.03045

Tamura, K., Peterson, D., Peterson, N., Stecher, G., Nei, M., and Kumar, S. (2011). MEGA5: molecular evolutionary genetics analysis using maximum likelihood, evolutionary distance, and maximum parsimony methods. *Mol. Biol. Evol.* 28, 2731–2739. doi: 10.1093/molbev/msr121

Thompson, J. D., Gibson, T. J., Plewniak, F., Jeanmougin, F., and Higgins, D. G. (1997). The CLUSTAL_X windows interface: flexible strategies for multiple sequence alignment aided by quality analysis tools. *Nucleic Acids Res.* 25, 4876–4882. doi: 10.1093/nar/25.24.4876

Urayama, S.-I., Takaki, Y., and Nunoura, T. (2016). FLDS: a comprehensive dsRNA sequencing method for intracellular RNA virus surveillance. *Microbes Environ.* 31, 33–40. doi: 10.1264/jsme2.ME15171

Urayama, S.-I., Takaki, Y., Nishi, S., Yoshida-Takashima, Y., Deguchi, S., Takai, K., et al. (2018). Unveiling the RNA virosphere associated with marine microorganisms. *Mol. Ecol. Resour.* 18, 1444–1455. doi: 10.1111/1755-0998.12936

van de Sande, W. W. J., and Vonk, A. G. (2019). Mycovirus therapy for invasive pulmonary aspergillosis? *Med. Mycol.* 57, S179–S188. doi: 10.1093/mmy/myy073

van de Sande, W. W. J., Lo-Ten-Foe, J. R., van Belkum, A., Netea, M. G., Kullberg, B. J., and Vonk, A. G. (2010). Mycoviruses: future therapeutic agents of invasive fungal infections in humans? *Eur. J. Clin. Microbiol. Infect. Dis.* 29, 755–763. doi: 10.1007/s10096-010-0946-947

Wang, D.-N., Toyotome, T., Muraosa, Y., Watanabe, A., Wuren, T., Bunsupa, S., et al. (2014). GliA in *Aspergillus fumigatus* is required for its tolerance to gliotoxin and affects the amount of extracellular and intracellular gliotoxin. *Med. Mycol.* 52, 506–518. doi: 10.1093/mmy/myu007

Weiss, G., and Schaible, U. E. (2015). Macrophage defense mechanisms against intracellular bacteria. *Immunol. Rev.* 264, 182–203. doi: 10.1111/imr.12266

Zhai, L., Xiang, J., Zhang, M., Fu, M., Yang, Z., Hong, N., et al. (2016). Characterization of a novel double-stranded RNA mycovirus conferring hypovirulence from the phytopathogenic fungus Botryosphaeria dothidea. *Virology* 493, 75–85. doi: 10.1016/j.virol.2016.03.012

Zoll, J., Verweij, P. E., and Melchers, W. J. G. (2018). Discovery and characterization of novel *Aspergillus fumigatus* mycoviruses. *PLoS One* 13:e0200511. doi: 10.1371/journal.pone.0200511

Conflict of Interest: The authors declare that the research was conducted in the absence of any commercial or financial relationships that could be construed as a potential conflict of interest.

frontiers in Microbiology

ORIGINAL RESEARCH
published: 20 January 2021
doi: 10.3389/fmicb.2020.620623

Late Male-Killing Viruses in *Homona magnanima* Identified as Osugoroshi Viruses, Novel Members of *Partitiviridae*

Ryosuke Fujita[1,2†], Maki N. Inoue[3†], Takumi Takamatsu[3], Hiroshi Arai[3], Mayu Nishino[3], Nobuhiko Abe[3], Kentaro Itokawa[4], Madoka Nakai[3], Syun-ichi Urayama[5], Yuto Chiba[5], Michael Amoa-Bosompem[1] and Yasuhisa Kunimi[3]*

[1] Laboratory of Sanitary Entomology, Faculty of Agriculture, Kyushu University, Fukuoka, Japan, [2] Department of Medical Entomology, National Institute of Infectious Diseases, Tokyo, Japan, [3] Department of Applied Biological Science, Tokyo University of Agriculture and Technology, Fuchu, Japan, [4] Pathogen Genomics Center, Natinal Institute of Infectious Diseases, Tokyo, Japan, [5] Department of Life and Environmental Sciences, University of Tsukuba, Tsukuba, Japan

OPEN ACCESS

Edited by:
Ioly Kotta-Loizou, Imperial College London, United Kingdom

Reviewed by:
Massimo Turina, National Research Council (CNR), Italy
Daohong Jiang, Huazhong Agricultural University, China

***Correspondence:**
Ryosuke Fujita
r-fujita@agr.kyushu-u.ac.jp

[†]These authors have contributed equally to this work

Specialty section:
This article was submitted to Virology, a section of the journal Frontiers in Microbiology

Received: *23 October 2020*
Accepted: *21 December 2020*
Published: *20 January 2021*

Citation:
Fujita R, Inoue MN, Takamatsu T, Arai H, Nishino M, Abe N, Itokawa K, Nakai M, Urayama S-i, Chiba Y, Amoa-Bosompem M and Kunimi Y (2021) Late Male-Killing Viruses in Homona magnanima Identified as Osugoroshi Viruses, Novel Members of Partitiviridae. Front. Microbiol. 11:620623. doi: 10.3389/fmicb.2020.620623

Late male-killing, a male-specific death after hatching, is a unique phenotype found in *Homona magnanima*, oriental tea tortrix. The male-killing agent was suspected to be an RNA virus, but details were unknown. We herein successfully isolated and identified the putative male-killing virus as Osugoroshi viruses (OGVs). The three RNA-dependent RNA polymerase genes detected were phylogenetically related to Partitiviridae, a group of segmented double-stranded RNA viruses. Purified dsRNA from a late male-killing strain of *H. magnanima* revealed 24 segments, in addition to the RdRps, with consensus terminal sequences. These segments included the previously found male-killing agents MK1068 (herein OGV-related RNA16) and MK1241 (OGV-related RNA7) RNAs. Ultramicroscopic observation of purified virions, which induced late male-killing in the progeny of injected moths, showed sizes typical of Partitiviridae. Mathematical modeling showed the importance of late male-killing in facilitating horizontal transmission of OGVs in an *H. magnanima* population. This study is the first report on the isolation of partiti-like virus from insects, and one thought to be associated with late male-killing, although the viral genomic contents and combinations in each virus are still unknown.

Keywords: male killing, *Homona magnanima*, *Partitiviridae*, horizontal transmission, insect virus

INTRODUCTION

Maternally inherited female-biased sex ratio is caused by a variety of mechanisms, including male-killing. The phenomenon of male-killing can be categorized into two types: early (male-specific death in the embryonic stage) or late (male-specific death in the larval or pupal stage), both of which result in female-biased sex ratios (Hurst, 1991, 1993; Dunn and Smith, 2001). Male killing in insects has been reported to be induced by infection with bacteria (e.g., with *Wolbachia*, *Rickettsia*, *Spiroplasma*, *Flavobacteria*, or *Arsenophonus*) or microsporidia (Skinner, 1985; Hurst et al., 1999; Huigens et al., 2000; Fukatsu et al., 2001; Morimoto et al., 2001; Agnew et al., 2002; Perlman et al., 2006; Gruwell et al., 2007; Hedges et al., 2008; Werren et al., 2008; Arai et al., 2020). *Homona magnanima*, oriental tea tortrix, is known as a pest for tea plants in East Asia. It also feeds on a variety of plant leaves, including apple trees and citrus. Previously, we identified a male-killing

agent, suspected to be an RNA virus, in *H. magnanima* (Nakanishi et al., 2008). The cause of the male-killing was identified as RNA fragments (MK1068 and MK1241); however, the details were not understood.

Viruses in insects are transmitted via two ways, horizontal transmission and vertical transmission. Most insecticidal viruses such as baculovirus spread their progeny by killing host insects and infecting other hosts (horizontal transmission) (Rohrmann, 2019). In this process, insecticidal functions facilitate virus escape from infected host cells and an efficient progeny virus spread. Dengue virus, a member of Flavivirus, is a mosquito-borne virus that infects host mosquitoes via blood-sucking. Dengue virus is also maintained in its lifecycle via vertical transmission (Lequime and Lambrechts, 2014). Dengue virus can be transferred to an egg in an infected female, which enables viral survival regardless of blood-feeding to virus-permissive animals. Thus, the insect viruses choose one of or both transmission methods to survive in the ecological system.

In this study, we identified the previously suggested late male-killing virus as Osugoroshi viruses (OGVs), considered as *Partitiviridae*-related viruses. We also discuss the role of the late male-killing function of OGVs with consideration for their survival strategy.

MATERIALS AND METHODS

Insects

H. magnanima (egg masses, larvae, or pupae) were collected at tea plantations in TYO (Tokyo Metropolitan), TKR (Saitama Pref.), AMI (Ibaraki Pref.), KWM (Miyazaki Pref.), KBY (Miyazaki Pref.), UJI (Kyoto Pref.), SMD (Shizuoka Pref.), YMK (Kanagawa Pref.), SZK (Shizuoka Pref.), NNB (Yamanashi Pref.), and MNM (Kagoshima Pref.) in Japan (**Supplementary Figure 1**). The collected *H. magnanima* populations were individually maintained in the lab (25°C, 16L8D) on a SilkMate 2S artificial diet (Nosan Co., Japan). The larvae of SMD and TYO strains were fed with SilkMate 2S containing 0.1% tetracycline to eliminate bacteria that may have influenced sex ratio [NSR-SMD strain (Tsugeno et al., 2017) and NSR-TYO strain (Arai et al., 2019), respectively]. After the establishment of NSR strains, larvae were fed with SilkMate 2S without tetracycline. The late male-killing strain established from the SMD population was maintained by mating with NSR-SMD males.

Nucleic Acid Extraction, PCR, and RT-PCR

DNA was isolated from *H. magnanima* pupae or adults as follows. *H. magnanima* was homogenized in lysis buffer (10 mM Tris-HCl pH 8.0, 100 mM EDTA, 1% SDS), then treated with Proteinase K at 50°C for 5 h. The lysates were further incubated with RNase A, and then proteins were removed by using Protein Precipitation Solution (Qiagen). DNA was precipitated with isopropanol and resuspended in distilled water.

RNA in *H. magnanima* was isolated from lysates using Isogen (Nippon Gene) according to the manufacturer's instructions. The extracted RNA was further treated with DNase I to remove DNA contaminants. Complementary DNA was synthesized using AMV Reverse Transcriptase XL (Takara) according to the manufacturer's instructions.

The DNA or cDNA was used as a template for PCR, which was carried out with *Ex*Taq (Takara) using specific primer sets, listed in **Supplementary Table 3**. Products were separated by agarose gel electrophoresis.

The dsRNA purification was carried out using CF11-cellulose. Briefly, total RNA was extracted as described above, then mixed with CF-11 cellulose in binding buffer (50 mM Tris-HCl pH 6.8, 130 mM NaCl, 1 mM EDTA, 16% ethanol, 5% β-mercaptoethanol). Unbound nucleic acids were washed out twice with binding buffer. The resin was incubated in elution buffer (50 mM Tris-HCl pH 6.8, 130 mM NaCl, 1 mM EDTA) to release dsRNAs. The dsRNAs were recovered by ethanol precipitation and resolved in RNase-free water. The purified dsRNAs were analyzed by 1.5% agarose gel electrophoresis.

Next-Generation Sequencing Analysis and RACE Sequencing

H. magnanima female adults of the male-killing strain (hereinafter referred to as the late strain) were homogenized in PBS as above and passed through a 0.45 μm filter. The filtrates were treated with RNase A and DNase I as described previously (Fujita et al., 2016); then RNA was extracted using Isogen II (Nippon Gene). Construction of a cDNA library and sequencing analysis was carried out according to the method described in Fujita et al. (2016). Reads were analyzed with CLC Genomic Workbench software (CLC bio) or the SPAdes algorithm (Bankevich et al., 2012). Complete OGV genomic sequences were determined by the FLDS sequencing method as described previously (Urayama et al., 2016). Complete OGV nucleotide sequences were submitted to the DDBJ/GenBank/EMBL database under accession numbers LC383810-LC383814 and LC597875-LC597896.

Sequence Analysis

Phylogenetic analysis using partitivirus RdRp amino acid sequences was carried out as follows. The RdRp sequences were first aligned using ClustalW (*http://clustalw.ddbj.nig.ac.jp/*), then the aligned matrix data were confirmed manually. The NCBI accession numbers of the sequences used in this analysis are listed in **Supplementary Table 4**. The amino acid sequences completely conserved among viruses were analyzed in MEGA7 (Kumar et al., 2016) using the maximum likelihood method with the JTT matrix model. The statistical significance of the resulting tree was evaluated using a bootstrap test with 1,000 replications.

Virion Purification and Electron Microscopy

H. magnanima late strain adult females were homogenized in PBS, and large debris was removed by centrifugation. Virions in the homogenates were separated by ultracentrifugation (100,000 × g, 3 h, 4°C) with 20 and 50% sucrose cushions. The virion-containing layer was recovered and further separated in a 20–50% sucrose gradient solution (100,000 × g, 16 h, 4°C). The recovered

virions were dialyzed using 10 mM Tris-HCl buffer (pH 7.4) and then observed by electron microscopy.

The purified virions were loaded on membrane-coated transmission electron microscopy grids and stained with 2% phosphotungstic acid solution (pH 7.0). The samples were observed using a JEM-2100 transmission electron microscope (Jeol).

RESULTS

We previously identified two RNA fragments as the components of the late male-killing agent for *H. magnanima*. Because those two RNAs did not show any specific similarity with known cellular genes, we speculated that the male-killing agent is an RNA virus. To isolate and identify the virus, we first collected 18 *H. magnanima* populations from 10 regions (**Supplementary Figure 1**) and examined the sex ratio of their progeny. RT-PCR targeting MK1241 RNA showed that 12 of the 18 populations (97/636 tested individuals in total) carried the putative late male-killing virus, although most of the tested populations showed typical sex ratios (**Table 1**). Then, we cultured the collected *H. magnanima* SMD strain (see Methods and **Supplementary Figure 1**) under laboratory condition. *Wolbachia* was eliminated from an SMD strain by feeding with an artificial diet containing tetracycline. The resultant *H. magnanima* strain exhibiting late male-killing was designated as the late strain. This late strain carried MK1241 RNA but was free from *Wolbachia* and *Spiroplasma* infection (**Supplementary Figure 2**). We also established a strain from the SMD *H. magnanima* population, which was infected with neither MK1241 RNA, *Spiroplasma,* nor *Wolbachia* (**Supplementary Figure 2**). The progeny of this strain showed a normal sex ratio and is hereinafter referred to as the non-biased sex ratio (NSR-SMD) strain. Because all late strain males died before the adult stage, the late strain was maintained by mating with NSR-SMD males. We also determined hatchability and mortality for each strain. The hatchability of the late strain was almost the same as that of the NSR-SMD strain, but 68% of late strain hatchlings died before adult emergence (**Supplementary Figure 2**).

To identify the virus in the late strain, we carried out next-generation sequencing (NGS) analysis. For the extraction of viral RNA, late strain female moths were homogenized and centrifuged at low speed. The supernatant was treated with DNase and RNase to concentrate viral RNAs (Fujita et al., 2016). Total RNA was isolated from the nuclease-treated homogenates and used as a template for cDNA library construction. In the NGS analysis, we obtained 27 contigs (**Supplementary Table 1**), and as expected, sequences consistent with MK1241 and MK1068 sequences were included in the contigs (MK-3 and MK-14, respectively). We successfully identified two contigs encoding RNA-dependent RNA polymerases (RdRp) related to *Partitiviridae* viruses (MK-11 and MK-25). Another assembler algorithm, SPADes (Bankevich et al., 2012), detected one more partitiviral RdRp gene (MKsp30) (**Supplementary Table 2**). Thus, late strain female moths carried at least three novel partiti-like RdRp sequences.

The putative partitiviral RdRp sequences (MK-11, MK-25, and MKsp30) were significantly different from each other, but all contained conserved motifs (**Supplementary Figure 3**) (Vásquez-Del Carpio et al., 2006), suggesting that these RdRps are active RNA polymerases. Blast analysis revealed MK-11, MK-25, and MKsp30 to be novel, unclassified *Partitiviridae* species (King et al., 2011). We designated these three partitiviruses Osugoroshi virus as (OGV) 1, 2, and 3, respectively (**Figure 1**). In the phylogenetic tree, OGV2 and OGV3 were located in the same clade and showed similarity to Hubei coleoptera virus 5 and Hubei coleoptera virus 4, respectively (Shi et al., 2016). Because all viral-like sequences in this clade were found from Coleoptera or Araneae, these viruses (or viral-like sequences) are thought to be invertebrate-specific. OGV1 was located in a different clade and showed similarity to Hubei partiti-like virus 33, which also appeared in Coleoptera. Based on this data, OGVs and other related viruses were considered a group of invertebrate partitiviruses.

From this data, we assumed that OGVs are partiti-like viruses with a segmented dsRNA genome. Therefore, we purified dsRNA from the *H. magnanima* late strain for detailed analysis. The purified dsRNAs was about 1.3 kb in size (**Figure 2A**). In the primary NGS virome analysis, we found 20 other contigs uniquely appearing in the late strain, some of which were suspected to be components of OGVs (**Supplementary Table 2** and **Supplementary Figure 4**). To verify this, we carried out complete sequencing of the purified dsRNAs with the FLDS method. We successfully determined the sequences of 27 contigs, which included OGV1–3 RNA1, MK1068, and MK1241 (**Table 2** and **Figure 2B**). The length of the 27 RNAs ranged between 1,200 and 1,497 bp, corresponding to the agarose gel electrophoresis data (**Table 2** and **Figure 2A**). Interestingly, they all had consensus in their 5′- and 3′-terminal sequences (GGUAAUU on 5′-terminus and ANG/UCCC on 3′-terminus, in sense strands). OGV1 RNA1 had complete consensus in the first seven nucleotide sequences with OGV-related RNA2–25, with the exception of RNA16. OGV2 RNA1 had different sequences on its 5′-termini (GGAAACA) and 3′-termini (ACCCGT), and they were almost the same as OGV-related RNA16 (5′: GGAAAUA, 3′: ACCCGT). The 5′-terminal sequence of OGV3 RNA1, GGAAUAG, was partly similar to the 5′-terminal sequence of OGV1 RNA1. On the other hand, the 3′-terminal sequence was somewhat similar to OGV2 RNA1 and OGV-related RNA16. Considering the nucleotide sequence structures and the lack of poly-A tails, we concluded that these dsRNAs were components of the newly identified partiti-like viruses, OGVs.

We then tried to purify the OGV virions from homogenates of *H. magnanima* late strain. The fractionation of virions in sucrose gradient ultracentrifugation led to the successful isolation of viral particles with an estimated size of 30 nm (**Figure 2D**). SDS-PAGE analysis of the purified fraction revealed a relatively major band around the 29 kDa molecular size mark; however, the crude composition of proteins in the sample made it difficult to identify structural proteins (**Supplementary Figure 5**). All the dsRNAs carried at least one open reading frame with estimated product

TABLE 1 | The sex ratios and prevalence of MK1241 RNA in natural populations of *Homona magnanima* collected from tea fields in Japan.

Year	Month	Population[a]	No. of collected samples at each stage							No. of pupae examined		Pupal sex ratio (% male)	No. of adults examined		Adult sex ratio (% male)	% adult prevalence rate of MK1241 RNA (No. of tested sample)
			Egg	Larvae					Pupa	Female	Male		Female	Male		
				1st	2nd	3rd	4th	5th								
2007	Mar	TKR	0	0	0	2	2	19	0	11	8	0.42	6	8	0.57	30.0 (10)
	Mar	AMI	0	0	0	33	30	30	0	31	17	0.35	28	16	0.36	41.9 (31)
	May	KWM	0	0	0	0	3	82	9	47	30	0.39	37	24	0.39	14.9 (47)
	May	KBY	0	0	0	0	6	44	1	22	24	0.52	20	24	0.55	0.0 (23)
	Jun	TKR	0	2	1	4	24	14	0	14	19	0.58	12	15	0.56	15.4 (13)
	Jun	AMI	0	0	0	8	41	46	0	33	16	0.33	23	9	0.28	37.5 (32)
	Jun	UJI	0	0	1	9	7	0	0	7	8	0.53	6	8	0.57	0.0 (7)
	Sep	SMD	98	0	0	0	0	0	0	1239	1072	0.46	1041	1000	0.49	7.1 (42)
2008	Apr	TKR	0	0	0	11	46	122	0	78	67	0.46	61	56	0.48	25.7 (74)
	Jun	TKR	0	0	0	1	46	44	0	41	26	0.39	35	22	0.39	21.1 (38)
	Jun	YMK	0	0	0	0	27	47	0	33	25	0.43	22	19	0.46	23.5 (34)
	Jul	TKR	0	2	11	31	67	94	2	74	69	0.48	58	59	0.50	18.3 (71)
	Jul	SMD	0	0	0	2	23	43	0	32	27	0.46	27	26	0.49	0.0 (28)
	Aug	SZK	0	0	0	7	17	35	0	22	18	0.45	12	15	0.56	0.0 (21)
	Aug	NNB	0	0	0	0	7	28	0	16	13	0.45	13	8	0.38	0.0 (16)
	Sep	TKR	0	0	0	8	40	48	0	31	26	0.46	26	26	0.50	0.0 (30)
	Nov	MNM	7	0	0	0	0	55	86	56	51	0.48	28	33	0.54	6.2 (65)
	Dec	TKR	4	6	53	25	52	25	0	52	66	0.56	39	55	0.59	9.3 (54)

[a] *For the abbreviations, see* ***Supplementary Figure 1****.*

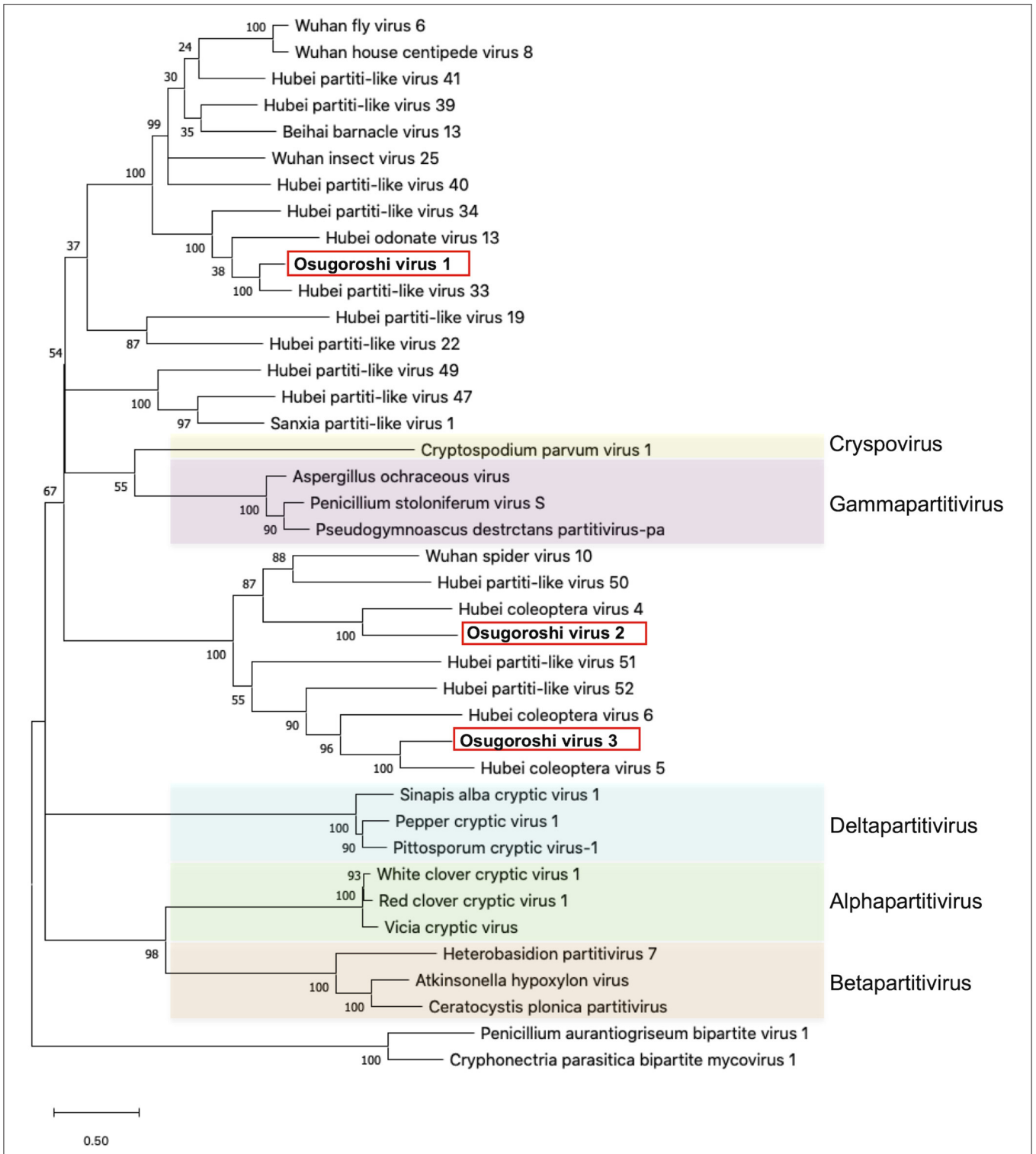

FIGURE 1 | Identification of partitiviruses in the *Homona magnanima* late strain. Phylogenetic analysis of the amino acid sequences of partitivirus RdRp was represented. The top 10 hits from BLAST analysis of Osugoroshi virus (OGV) 1, OGV2 (MK-25), and OGV3-encoded RdRp and 13 viruses categorized in previously defined genera (colored) were used in the alignment of two outgroup viruses (see also **Supplementary Table 4**).

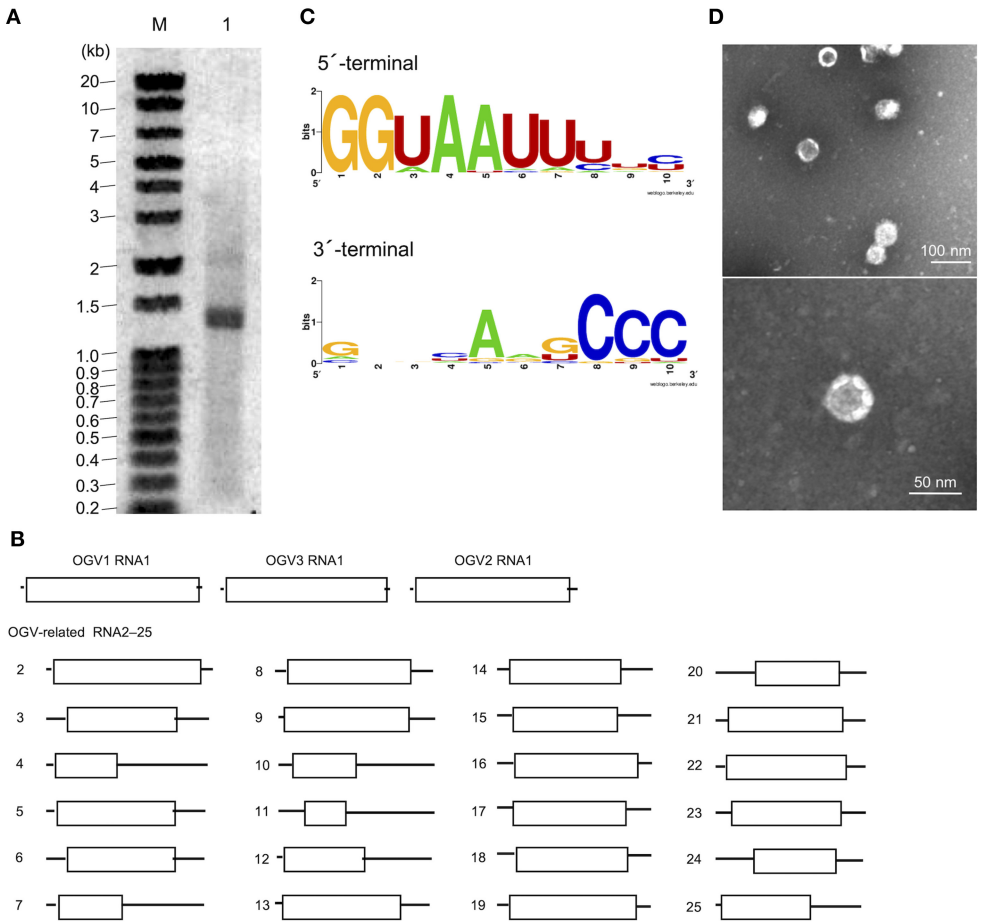

FIGURE 2 | Identification of Osugoroshi viruses (OGVs) in the *Homona magnanima* late strain. **(A)** dsRNA was isolated from the *H. magnanima* adult females of the late strain (lane 1) and separated by 1.5% agarose gel electrophoresis. The DNA marker was also shown (lane M). **(B)** The schematics of the identified OGVs' RNA1 and other OGV-related RNAs. Boxes indicated the position of open reading frames (ORFs). **(C)** The consensus sequences of the first and the last ten nucleotides among the 27 identified OGV's RNAs (in sense strands). **(D)** Electron microscopic image of viral particles purified from the adult female's homogenate of the late strain. The particles were negatively stained, and the scale was indicated in each panel.

sizes between 12.6–54.4 kDa; however, the lack of significant similarity to known genes prevented accurate prediction of their function(s) (**Figure 2B** and **Table 2**). Alignment with reported partitiviral capsid proteins (CPs) and phylogenetic analysis did not show a clear cluster, and failed to identify OGVs' CP genes. This observation may be due to the low similarity between the sequences and genomic reassortment between partitiviruses, facilitated by the encapsidation of partitivirus genomic RNA (RNA 1 and 2) in separate capsids (Nibert et al., 2013).

To determine whether OGVs are responsible for late male-killing, we inoculated purified viral particles (**Figure 2C**) into 17 NSR-TYO 4th-instar larvae and traced OGVs' RNA1 and OGV-related RNA7 (MK1241) and 16 (MK1068), the previously identified markers for male-killing agents (Nakanishi et al., 2008). Ten adult female moths (samples 2, 6, 7, 9, 12, 14, 15, 16, 17, and 19 in **Figure 3**) were obtained in G_0 and mated with NSR-TYO males. OGV infection status was examined by RT-PCR using RNA extracted from adult females after oviposition. OGV3 RNA1 and OGV-related RNA7 appeared in most G_0 individuals (**Figure 3**). On the other hand, OGV1 RNA1, OGV2 RNA1, and OGV-related RNA16 were found only in five, four, and eight individuals, respectively. From these moths, two lineages were obtained (lineage 7 and 16) in the next generation (G_1), both of which exhibited a female-biased sex ratio due to late male-killing (Numbers of male and female moths are, respectively, 0 and 31 in lineage 7, and 0 and 3 in lineage 16). An adult female was selected from each lineage and checked for OGV infection. Moths in lineage 7 possessed all the five tested RNAs. In the G_1 adult female lineage 16, all but OGV1 RNA1 were detected, although it had appeared in the maternal moth. Despite the absence of OGV1 RNA1, G_1 of lineage 16 exhibited complete late male-killing, suggesting that OGV1 RNA1 may not be necessary for late male-killing in *H. magnanima*. In the control group, phosphate-buffered saline (PBS) was injected into 68 NSR-TYO 4th-instar larvae, and 13 female moths oviposited. The percentage of females in G_1 (sample c4 in **Figure 3**) was 42.9%, and no OGV RNAs were detected in this group. Based on these results, we

TABLE 2 | Contigs determined in FLDS analysis using purified ds RNA of *Homona magnanima* late strain.

Contig name	Read counts (FLDS)	Length (nts)	Product	Encoded protein (kDa)	*Corresponds to the contig	The first 10 nucleotides	The last 10 nucleotides
OGV1 RNA1	3,099	1,497	RdRp	54.4	MK11	GGTAATTTAT-	-GGTTAGTCCC
OGV3 RNA1	5,718	1,393	RdRp	49.9	MKsp30	GGAATAGTTC-	-GCACCCCGTA
OGV2 RNA1	1,774	1,382	RdRp	48.6	MK25	GGAAACATTT-	-GGTGACCCGT
OGV-related RNA 2	11,670	1,364	unknown	44.6	MK16	GGTAATTTCG-	-GAGCAAGCCC
OGV-related RNA 3	19,084	1,337	unknown	34.4	MK15	GGTAATTTAC-	-GATTAGGCCC
OGV-related RNA 4	18,356	1,321	unknown	19.6	MK9	GGTAATTTTC-	-CCAAGTTCCC
OGV-related RNA 5	2,847	1,315	unknown	36.7	MK27	GGTAATTTGT-	-GTGCAAGCCC
OGV-related RNA 6	33,872	1,304	unknown	34.3	MK4	GGTAATTTAA-	-GGTTAGGCCC
OGV-related RNA 7	12,147	1,294	unknown	20.8	MK3	GGTAATTTTC-	-CCCAAAGCCC
OGV-related RNA 8	10,020	1,292	unknown	38.0	MK22	GGTAATTTGT-	-GTACAAGCCC
OGV-related RNA 9	15,191	1,291	unknown	38.7	MK10	GGTAATTCGT-	-GTGCAAGCCC
OGV-related RNA 10	14,245	1,290	unknown	20.1	MK5	GGTAATTTCG-	-ACCCAGTCCC
OGV-related RNA 11	2,575	1,283	unknown	12.6	MK20	GGTAATTTTC-	-TGCAGGTCCC
OGV-related RNA 12	5,385	1,282	unknown	25.1	MK13	GGTAATTCGT-	-GAGCAAGCCC
OGV-related RNA 13	13,580	1,279	unknown	36.1	–	GGTAATTTTC-	-GTGCATGCCC
OGV-related RNA 14	338,949	1,277	unknown	34.6	MKsp11	GGTAATTATC-	-GATTAAGCCC
OGV-related RNA 15	8,245	1,271	unknown	32.6	MK17	GGTAATTTTC-	-GGTTAGGCCC
OGV-related RNA 16	7,770	1,269	unknown	37.8	MK14	GGAAATACAT-	-ATGAACCCGT
OGV-related RNA 17	9,601	1,267	unknown	34.6	MK1	GGTAATTTTC-	-ACGCAAGCCC
OGV-related RNA 18	8,235	1,265	unknown	35.1	MK18	GGTAATTATC-	-GGTTAAGCCC
OGV-related RNA 19	3,764	1,261	unknown	39.4	MK19	GGTAATTTTC-	-ACGCAAGCCC
OGV-related RNA 20	12,372	1,239	unknown	26.0	MK23	GGTAATTCGT-	-CACAAGTCCC
OGV-related RNA 21	3,527	1,235	unknown	35.4	MK2	GGTAATTTTC-	-GTGCAAGCCC
OGV-related RNA 22	27,072	1,233	unknown	37.1	MKsp26	GGTAATTCGT-	-GTGCAGTCCC
OGV-related RNA 23	5,817	1,230	unknown	34.9	MK26	GGTAATTTTC-	-GGTTAGGCCC
OGV-related RNA 24	12,872	1,220	unknown	25.7	MK24	GGTAATTCGT-	-CCATAGTCCC
OGV-related RNA 25	4,246	1,200	unknown	26.9	MK12	GGTAATTTTC-	-GTGCAAGCCC

*See ***Supplementary Tables 1, 2***.

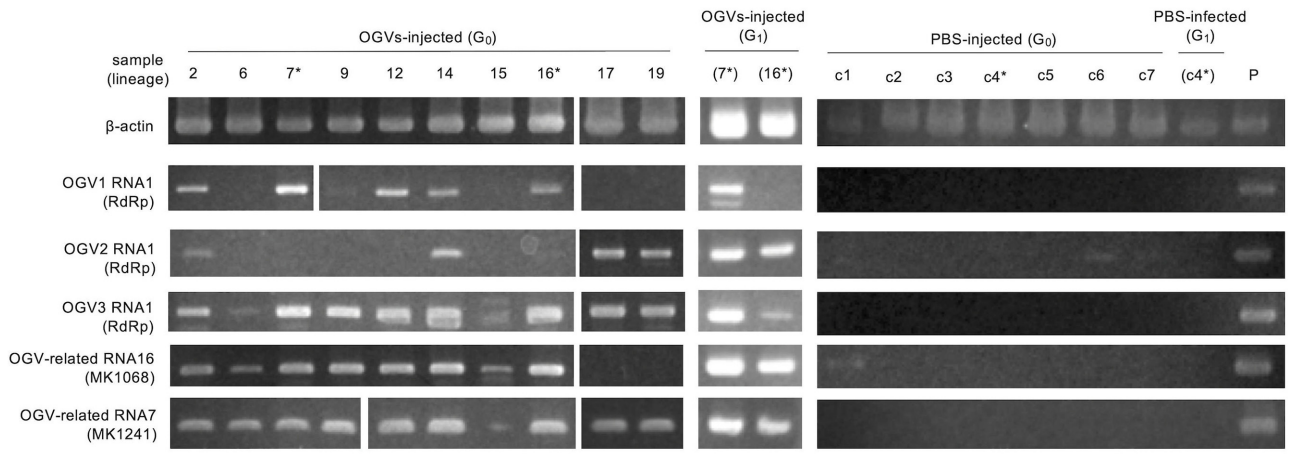

FIGURE 3 | Injection of purified Osugoroshi virus (OGV) virions into the *Homona magnanima* non-biased sex ratio (NSR) strain. RT-PCR confirmed OGV infection. Fourth instar larvae of *H. magnanima* NSR-TYO strain were injected with purified OGVs or phosphate-buffered saline (PBS), and total RNA was extracted from 10 adult female moths (G_0). G_1 adult females were generated from the G_0 females (asterisks) by mating with NSR males. The total RNA from adult females of the laboratory-maintained late strain was used as a positive control (P). *shows the linage relationships.

conclude that OGV was responsible for inducing late male-killing in *H. magnanima*.

OGVs were thought to be mainly maintained in female *H. magnanima* through vertical transmission, which implies that the OGV RNAs behave as a maternal genetic factor. If the infection of OGVs does not contribute to the fitness of infected females, the infection rate of OGVs in the population will decrease through generations without the contribution of genetic drift. Indeed, the larval development time of OGV-infected females was prolonged, with a decreased pupal body weight (Takamatsu et al., 2020). Therefore, a propagation strategy other than vertical transmission seems to be required to maintain an OGV population. In the late male-killing, OGVs also multiply in males at least until the larval stage, and then they are spread around the dead males. The progenies of OGVs from the dead males would infect other larvae through horizontal transmission [possibly oral infection, observed in experimental condition (Takamatsu et al., 2020)]. Here we hypothesized that the late male-killing phenotype increases the infection rate of OGVs by horizontal transmission. We built a mathematical model for viral infection rates and host moth numbers through generations (**Figure 4A**). The model started from 5 populations with 20 adult individuals in each population, where an OGV-infected female was introduced into one of these populations. Larvae and adults interact among the populations according to the distance between each population (D) and the wandering of larvae (W_L) and adults (W_A) (**Figure 4B**). This model included the oviposition numbers (E) and survival rates to the larval stage (S_1), to the pupal stage (S_2), and to the adult stage (S_3). The given parameters led to constant moth populations without virus infection. We also put a mating success rate (r_m) because male and female numbers would be varied due to male-killing (male-killing rate $= r_k$). In field observation, OGV-infected male larvae died in leaf-rolls, and sometimes leaf-rolls were reused by larvae in the next generations. Therefore, we considered that the horizontal transmission would occur in the leaf-roll (**Figure 4B**, blocked arrows). The parameter for vertical transmission rate (r_V) was constant here (=0.9). When we put the parameter of the horizontal transmission rate (r_H) as 0.03 (**Figure 4C**, left), the viral infection rate increased in the first four generations (to 10.2%), then decreased and became constant as 5.4%. If the horizontal transmission triggered by late male-killing did not appear ($r_k = 0$), the infection rate was always constant, like the vertical transmission only model (**Figure 4C** center and right). Note that the good contribution of the horizontal transmission for viral survival was achieved with a combination of certain population size and horizontal

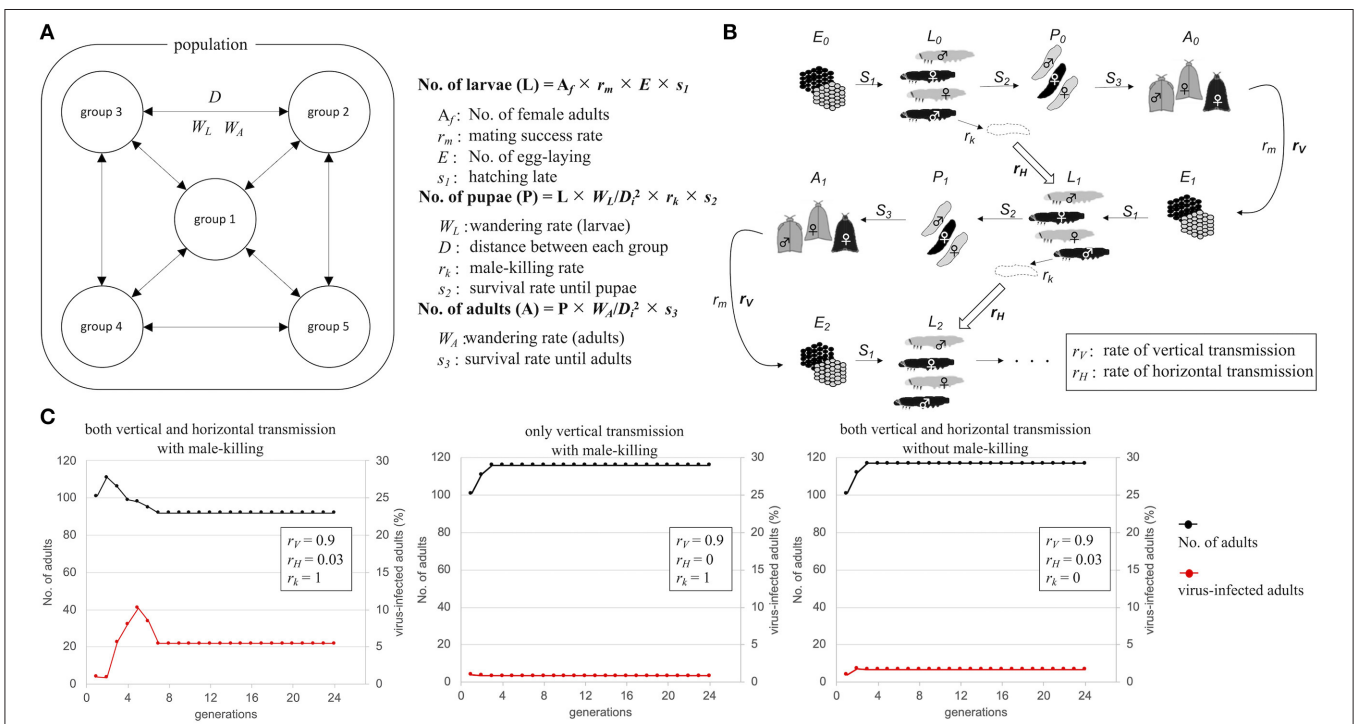

FIGURE 4 | Schematic model of Osugoroshi virus (OGV) infection in a *Homona magnanima* population. **(A)** Population setting for mathematical modeling. An *H. magnanima* population is composed of five separated groups. Some parts of larvae (W_L) and adult (W_A) moths wander across each group according to the relative distance to another group (D). **(B)** Infection model of OGV and through *H. magnanima* populations. During the stages, OGV-infected male larvae (black) go to die (r_k) and spread virus progenies, and the larvae in the next generation uptake viruses with a certain probability (r_H). OGVs are also transmitted to the next generation from virus-infected females (r_V). **(C)** Population simulation of *H. magnanima* after OGV-contamination with various situations. The populations start with 100 naïve individuals and 1 OGV-infected female (black lines). OGV-infected moths (red lines) are maintained throught generations by vertical and/or horizontal transfer.

transmission rate. For example, when the model started with twice the population size, the number of virus-infected moths rapidly increased, and the moth population was disrupted by eliminating all-male moths (**Supplementary Figure 7**, left). The lower r_H gave a moderate increase of viruses in populations without disruption of the moth population even with a higher number of individuals (**Supplementary Figure 7**, right). Thus, the horizontal transmission via late male-killing could facilitate OGV's spread in *H. magnanima* populations without disrupting the host ecosystem.

DISCUSSION

The present study is the first report of the isolation of partitivirus from insects, in which we identified the late male-killing virus, OGV. However, two critical issues have yet to be addressed. The first is the actual genomic composition of the late male-killing virus. As described above, we identified 27 partiti-like viral segments, including three segments encoding RdRp. Unfortunately, we are yet to confirm whether all of these segments were coordinated in virus replication and late male-killing in *H. magnanima*. The extracted virion-inoculation experiment showed that late male-killing occured without OGV1 RNA1 (G_1 strain 16 in **Figure 3**). This would imply that if the RdRp encoded in OGV1 RNA1 is responsible for the replication of the 23 OGV-related RNAs (Exception being RNA 16; **Table 2**), then all 23 RNAs will have no role in male killing. In this scenario, OGV2 RNA1, OGV3 RNA1, or OGV-related RNA16 is responsible for the late male-killing phenotype, and OGV2 RNA1-encoded RdRp transcribes OGV-related RNA16 because they share terminal sequences. However, the detection of OGV-related RNA7 in G1 in the absence of OGV1 RNA1, makes this scenario unlikely. It suggests that the recognition of OGV-related RNA segments is not restricted to one RdRp or the other, but shared. Moreover, the fact that partitiviral virions encapsidate each segment singularly makes it difficult to define the actual genomic composition of OGVs (Nibert et al., 2013). To address this issue, some experiments, e.g., a reconstruction of OGV with infectious clone RNA, will be required.

The second issue, regarding the mechanisms of late male-killing by OGVs, is related to the first. OGV infection did not affect hatchability but did induce male-specific toxicity, especially in the larval stage (**Supplementary Figure 2**). Although the mechanism of late-male killing remains largely unknown, one possibility is a putative toxic gene in OGVs, which functions only in *H. magnanima* males after hatching.

What is the role of male-killing for OGVs? One possible effect is inbreeding inhibition of host *H. magnanima*. Late male-killing results in eliminating males in an egg mass, which would prevent inbreeding among the females. Our field investigation demonstrated that OGVs were widely distributed in Japan and are frequently found in tea fields (**Table 1**). This observation implies that OGV infection in *H. magnanima* possibly leads to a higher genetic diversity of *H. magnanima* populations.

Viruses require host cells for their replications. Therefore, the good survival of the infected host is crucial for viruses. On the other hand, the viruses' pathogenicity helps virion escape from their host through the disruption of host cells. OGVs kill male *H. magnanima* after hatching. Unlike embryonic male-killing, the late male-killing phenotype would facilitate efficient viral replication according to the increase of host biomass. We hypothesized that late male-killing facilitates the horizontal transmission of OGVs in the *H. magnanima* population, and our mathematical model shows a positive effect on the OGVs population by late male-killing (horizontal transfer) without disruption of host populations and resulted in an equilibrium of infection (**Figure 4**). The observed percentages of OGV-related RNA7-positive moth in the field study varied between 0 and 41.9% (the average was 13.9%) (**Table 1**). Our simple model showed the equilibrium infection rate of 5.8%, which was almost consistent with the field observation.

Interestingly, the ratio of virus-infected moth in the "non-male killing virus" is lower than the male-killing model. It indicates the importance of horizontal transfer for OGVs survival. Our model also showed that the rapid propagation of viruses could lead to the disruption of colonies due to the elimination of males (**Supplementary Figure 7**). The individually packaged virions of partitiviridae RNA segments however reduce the horizontal transmission efficiency of OGV, preventing fatal propagation of OGVs in *H. magnanima* populations.

As we assumed in the mathematical model, the effect of male-killing (elimination of males) in the field would be masked by transmigration of moths, resulting in the observed typical sex ratio (**Table 1**). This is likely because if there was no masking effect on male-killing, the population would be lost.

Partitiviridae has been known as a group of fungal viruses. In this study, we successfully identified and isolated OGVs as *Partitiviridae*-related viruses. As found in **Figure 1**, the recent metagenomic analysis demonstrated that many invertebrates possess virus-like sequences related to OGVs, suggesting various unidentified potential male-killing viruses in insects.

DATA AVAILABILITY STATEMENT

The datasets presented in this study can be found in online repositories. The names of the repository/repositories and accession number(s) can be found in the article/**Supplementary Material**.

AUTHOR CONTRIBUTIONS

RF identified OGVs, purified virions, carried out TEM analysis, analyzed viral sequences, wrote the manuscript, and supervised the study. MI planned the experiments, carried out the field

surveys and the RACE sequencing, and supervised the study. TT carried the PCR in the diagnosis of bacterial infections. HA and MNi carried out the inoculation experiments. NA examined rates of hatching and fatality of the colony strains. KI supported NGS analysis. MNa carried out the field surveys and supervised the study. SU and YC carried out the FLDS analysis. MA-B supported manuscript preparation with English proofreading. YK conceived the original idea and supervised the study. All authors contributed to the article and approved the submitted version.

ACKNOWLEDGMENTS

We would like to thank Enago (www.enago.jp) for the English language review.

SUPPLEMENTARY MATERIAL

The Supplementary Material for this article can be found online at: https://www.frontiersin.org/articles/10.3389/fmicb.2020.620623/full#supplementary-material

REFERENCES

Agnew, P., Becnel, J., Ebert, D., and Michalakis, Y. (2002). "Symbiosis of microsporidia and insects," in *Insect Symbiosis*, eds. K. Bourtzis and T. A. Miller (Boca Raton, FL: CRC Press), 145–163. Available online at: https://www.mivegec.ird.fr/images/stories/PDF_files/0129.pdf (accessed January 6, 2020).

Arai, H., Hirano, T., Akizuki, N., Abe, A., Nakai, M., Kunimi, Y., et al. (2019). Multiple infection and reproductive manipulations of *Wolbachia* in *Homona magnanima* (Lepidoptera: Tortricidae). *Microb. Ecol.* 77, 257–266. doi: 10.1007/s00248-018-1210-4

Arai, H., Lin, S. R., Nakai, M., Kunimi, Y., and Inoue, M. N. (2020). Closely related male-killing and nonmale-killing *Wolbachia* strains in the oriental tea tortrix *Homona magnanima*. *Microb. Ecol.* 79, 1011–1020. doi: 10.1007/s00248-019-01469-6

Bankevich, A., Nurk, S., Antipov, D., Gurevich, A. A., Dvorkin, M., Kulikov, A. S., et al. (2012). SPAdes: A new genome assembly algorithm and its applications to single-cell sequencing. *J. Comput. Biol.* 19, 455–477. doi: 10.1089/cmb.2012.0021

Dunn, A. M., and Smith, J. E. (2001). Microsporidian life cycles and diversity: the relationship between virulence and transmission. *Microbes Infect.* 3, 381–388. doi: 10.1016/S1286-4579(01)01394-6

Fujita, R., Kuwata, R., Kobayashi, D., Bertuso, A. G., Isawa, H., and Sawabe, K. (2016). Bustos virus, a new member of the negevirus group isolated from a Mansonia mosquito in the Philippines. *Arch. Virol.* 162, 1–10. doi: 10.1007/s00705-016-3068-4

Fukatsu, T., Tsuchida, T., Nikoh, N., and Koga, R. (2001). *Spiroplasma* symbiont of the pea aphid, *Acyrthosiphon pisum* (Insecta: Homoptera). *Appl. Environ. Microbiol.* 67, 1284–1291. doi: 10.1128/AEM.67.3.1284-1291.2001

Gruwell, M. E., Morse, G. E., and Normark, B. B. (2007). Phylogenetic congruence of armored scale insects (Hemiptera: Diaspididae) and their primary endosymbionts from the phylum Bacteroidetes. *Mol. Phylogenet. Evol.* 44, 267–280. doi: 10.1016/j.ympev.2007.01.014

Hedges, L. M., Brownlie, J. C., O'Neill, S. L., and Johnson, K. N. (2008). *Wolbachia* and virus protection in insects. *Science* 322:702. doi: 10.1126/science.1162418

Huigens, M. E., Luck, R. F., Klaassen, R. H. G., Maas, M. F. P. M., Timmermans, M. J. T. N., and Stouthamer, R. (2000). Infectious parthenogenesis. *Nature* 405, 178–179. doi: 10.1038/35012066

Hurst, G. D., Graf von der Schulenburg, J. H., Majerus, T. M., Bertrand, D., Zakharov, I. A., Baungaard, J., et al. (1999). Invasion of one insect species, *Adalia bipunctata*, by two different male-killing bacteria. *Insect Mol. Biol.* 8, 133–139. doi: 10.1046/j.1365-2583.1999.810133.x

Hurst, L. D. (1991). The evolution of cytoplasmic incompatibility or when spite can be successful. *J. Theor. Biol.* 148, 269–277. doi: 10.1016/S0022-5193(05)80344-3

Hurst, L. D. (1993). The incidences, mechanisms and evolution of cytoplasmic sex ratio distorters in animals. *Biol. Rev. Camb. Philos. Soc.* 68, 121–194. doi: 10.1111/j.1469-185X.1993.tb00733.x

King, A. M. Q., Lefkowitz, E., Adams, M. J., and Carstens, E. B. (2011). *Ninth Report of the International Committee on Taxonomy of Viruses*. Amsterdam: Academic Press.

Kumar, S., Stecher, G., and Tamura, K. (2016). MEGA7: Molecular evolutionary genetics analysis version 7.0 for bigger datasets. *Mol. Biol. Evol.* 33, 1870–1874. doi: 10.1093/molbev/msw054

Lequime, S., and Lambrechts, L. (2014). Vertical transmission of arboviruses in mosquitoes: a historical perspective. *Infect. Genet. Evol.* 28, 681–690. doi: 10.1016/j.meegid.2014.07.025

Morimoto, S., Nakai, M., Ono, A., and Kunimi, Y. (2001). Late male-killing phenomenon found in a Japanese population of the oriental tea tortrix, *Homona magnanima* (Lepidoptera: Tortricidae). *Heredity.* 87, 435–440. doi: 10.1046/j.1365-2540.2001.00924.x

Nakanishi, K., Hoshino, M., Nakai, M., and Kunimi, Y. (2008). Novel RNA sequences associated with late male killing in *Homona magnanima*. *Proc. Biol. Sci.* 275, 1249–1254. doi: 10.1098/rspb.2008.0013

Nibert, M. L., Tang, J., Xie, J., Collier, A. M., Ghabrial, S. A., Baker, T. S., et al. (2013). 3D structures of fungal Partitiviruses. *Adv. Virus Res.* 86, 59–85. doi: 10.1016/B978-0-12-394315-6.00003-9

Perlman, S. J., Hunter, M. S., and Zchori-Fein, E. (2006). The emerging diversity of *Rickettsia*. *Proc. R. Soc. B Biol. Sci.* 273, 2097–2106. doi: 10.1098/rspb.2006.3541

Rohrmann, G. F. (2019). *Baculovirus Molecular Biology, 4th Edn*. Bethesda, MD: National Center for Biotechnology Information.

Shi, M., Lin, X.-D., Tian, J.-H., Chen, L.-J., Chen, X., Li, C.-X., et al. (2016). Redefining the invertebrate RNA virosphere. *Nature* 540, 1–12. doi: 10.1038/nature20167

Skinner, S. W. (1985). Son-killer: a third extrachromosomal factor affecting the sex ratio in the parasitoid wasp, *Nasonia* (=*Mormoniella*) *vitripennis*. *Genetics* 109, 745–759.

Takamatsu, T., Arai, H., Abe, N., Nakai, M., and Inoue, M. N. (2020). Coexistence of two male-killers and their impact on the development of oriental tea tortrix *Homona magnanima*. *Invertebr. Microbiol.* doi: 10.1007/s00248-020-01566-x. [Epub ahead of print].

Tsugeno, Y., Koyama, H., Takamatsu, T., Nakai, M., Kunimi, Y., and Inoue, M. N. (2017). Identification of an early male-killing agent in the oriental tea tortrix, Homona magnanima. *J. Hered.* 108, 553–560. doi: 10.1093/jhered/esx049

Urayama, S. I., Takaki, Y., and Nunoura, T. (2016). FLDS: a comprehensive DSRNA sequencing method for intracellular RNA virus surveillance. *Microbes Environ.* 31, 33–40. doi: 10.1264/jsme2.ME15171

Vásquez-Del Carpio, R., Morales, J. L., Barro, M., Ricardo, A., and Spencer, E. (2006). Bioinformatic prediction of polymerase elements in the rotavirus VP1 protein. *Biol. Res.* 39, 649–659. doi: 10.4067/S0716-97602006000500008

Werren, J. H., Baldo, L., and Clark, M. E. (2008). *Wolbachia*: master manipulators of invertebrate biology. *Nat. Rev. Microbiol.* 6, 741–751. doi: 10.1038/nrmicro1969

Conflict of Interest: The authors declare that the research was conducted in the absence of any commercial or financial relationships that could be construed as a potential conflict of interest.

frontiers in Microbiology

ORIGINAL RESEARCH
published: 02 February 2021
doi: 10.3389/fmicb.2021.606366

The Polymycovirus-Mediated Growth Enhancement of the Entomopathogenic Fungus *Beauveria bassiana* Is Dependent on Carbon and Nitrogen Metabolism

*Charalampos Filippou[1,2], Rebecca M. Diss[1], John O. Daudu[2], Robert H. A. Coutts[2] and Ioly Kotta-Loizou[1]**

[1] Department of Life Sciences, Imperial College London, London, United Kingdom, [2] Department of Clinical, Pharmaceutical and Biological Science, University of Hertfordshire, Hatfield, United Kingdom

Polymycoviridae is a growing family of mycoviruses whose members typically have non-conventional capsids and multi-segmented, double-stranded (ds) RNA genomes. *Beauveria bassiana* polymycovirus (BbPmV) 1 is known to enhance the growth and virulence of its fungal host, the entomopathogenic ascomycete and popular biological control agent *B. bassiana*. Here we report the complete sequence of BbPmV-3, which has six genomic dsRNA segments. Phylogenetic analysis of RNA-dependent RNA polymerase (RdRp) protein sequences revealed that BbPmV-3 is closely related to the partially sequenced BbPmV-2 but not BbPmV-1. Nevertheless, both BbPmV-3 and BbPmV-1 have similar effects on their respective host isolates ATHUM 4946 and EABb 92/11-Dm, affecting pigmentation, sporulation, and radial growth. Production of conidia and radial growth are significantly enhanced in virus-infected isolates as compared to virus-free isogenic lines on Czapek-Dox complete and minimal media that contain sucrose and sodium nitrate. However, this polymycovirus-mediated effect on growth is dependent on the carbon and nitrogen sources available to the host fungus. Both BbPmV-3 and BbPmV-1 increase growth of ATHUM 4946 and EABb 92/11-Dm when sucrose is replaced by lactose, trehalose, glucose, or glycerol, while the effect is reversed on maltose and fructose. Similarly, both BbPmV-3 and BbPmV-1 decrease growth of ATHUM 4946 and EABb 92/11-Dm when sodium nitrate is replaced by sodium nitrite, potassium nitrate, or ammonium nitrate. In conclusion, the effects of polymycoviruses on *B. bassiana* are at least partially mediated *via* its metabolic pathways.

Keywords: fungal growth, fungal sporulation, *Beauveria bassiana*, *Polymycoviridae*, mycovirus

OPEN ACCESS

Edited by:
Nobuhiro Suzuki, Okayama University, Japan

Reviewed by:
Mingde Wu, Huazhong Agricultural University, China
Wenxing Xu, Huazhong Agricultural University, China

***Correspondence:**
Ioly Kotta-Loizou
i.kotta-loizou13@imperial.ac.uk

Specialty section:
This article was submitted to Virology, a section of the journal Frontiers in Microbiology

Received: *14 September 2020*
Accepted: *04 January 2021*
Published: *02 February 2021*

Citation:
Filippou C, Diss RM, Daudu JO, Coutts RHA and Kotta-Loizou I (2021) The Polymycovirus-Mediated Growth Enhancement of the Entomopathogenic Fungus Beauveria bassiana Is Dependent on Carbon and Nitrogen Metabolism. Front. Microbiol. 12:606366. doi: 10.3389/fmicb.2021.606366

INTRODUCTION

Polymycoviridae is a recently established family exclusively accommodating viruses infecting fungi in its sole genus *Polymycovirus*. The first member of the family, *Aspergillus fumigatus* tetramycovirus 1, was reported in 2015 (Kanhayuwa et al., 2015) and since then over 20 related mycoviruses have been fully or partially sequenced (**Supplementary Table S1**). Polymycoviruses

have a variable number of double-stranded (ds) RNA genomic segments, ranging from three (Mu et al., 2018) to eight (Jia et al., 2017; Mahillon et al., 2019), while a closely related, single-stranded (ss) RNA virus with 11 genomic segments named Hadaka virus was recently discovered (Sato et al., 2020). Polymycoviruses are the first dsRNA viruses found to be infectious not only as purified entities but also as naked dsRNA (Kanhayuwa et al., 2015; Jia et al., 2017; Niu et al., 2018); the majority are non-conventionally encapsidated.

Beauveria bassiana is an ascomycete belonging to the family *Cordycipitaceae*, order Hypocreales. *B. bassiana* has a widespread geographical distribution and can be found in soil (Garrido-Jurado et al., 2015) and in plants as an endophyte (McKinnon et al., 2017); importantly, *B. bassiana* is an arthropod pathogen with a wide host range and serves as the active ingredient of many popular biopesticides (de Faria and Wraight, 2007). Mycoviruses in general (Herrero et al., 2012; Kotta-Loizou et al., 2015; Koloniuk et al., 2015; Gilbert et al., 2019) and polymycoviruses in particular (Kotta-Loizou and Coutts, 2017; Filippou et al., 2018) have been found to infect *B. bassiana* isolates, in some cases increasing their growth and virulence (Kotta-Loizou and Coutts, 2017) and illustrating potential in biological control applications.

Here we report the complete sequence of *B. bassiana* polymycovirus (BbPmV) 3 and its phylogenetic relationships with members of the *Polymycoviridae* family. Both BbPmV-3 and the previously characterized BbPmV-1 have similar effects on the morphology, sporulation, and growth of their respective host isolates. Polymycovirus-mediated phenotypes are dependent on the constituents of the growth medium, suggesting that polymycoviruses may interfere with carbon and nitrogen metabolism of their host fungus.

MATERIALS AND METHODS

Fungal Isolates and Growth Media

Beauveria bassiana isolates EABb 92/11-Dm and ATHUM 4946 originate from Spain and Greece, respectively. The isolates were grown at 25°C, on Potato Dextrose Agar (PDA; Sigma–Aldrich) or Czapek-Dox minimal medium (MM; Sigma–Aldrich) or Czapek-Dox complete medium (CM; MM in addition to 1.5 g/L malt extract, peptone, and yeast extract). For growth assays, the sucrose and sodium nitrate in Czapek-Dox MM were substituted with different carbon and nitrogen sources (**Supplementary Table S2**; Cai et al., 2018). A cocktail of antibiotics (ampicillin, kanamycin, and streptomycin, each at a final concentration of 100 μg/mL) was used to prevent bacterial contamination. For curing experiments, the protein synthesis inhibitor cycloheximide was added at concentrations up to 1000 μg/mL.

Growth and Sporulation Assays

Fungal spores from agar plates were collected in phosphate buffered saline (PBS), filtered through Miracloth, and counted using the FastRead counting slides (Immune Systems). The concentration of the fungal spore suspension was adjusted, and 1000 fungal spores were spotted centrally on solid Czapek-Dox CM and growth was monitored for up to 18 days. All experiments were performed in triplicate using three independent stocks for each fungal isolate and statistical analysis was performed using GraphPad Prism 6. Differences in growth were considered to be statistically significant if measurements for at least five consecutive late time points were shown to be statistically significant (p-value < 0.05; ANOVA) between virus-infected and virus-free isogenic lines.

Nucleic Acid Extraction

BbPmV-1 and BbPmV-3 genomic dsRNAs were purified using a small-scale dsRNA extraction procedure. Briefly, total nucleic acids were treated with phenol/chloroform, DNase I (Promega), and S1 nuclease (Promega), and the remaining dsRNA was precipitated with sodium acetate and ethanol. Total fungal RNA and DNA were purified using the RNeasy and DNeasy Plant Mini Kits (Qiagen), respectively, according to the manufacturer's instructions.

Reverse Transcription (RT), Polymerase Chain Reaction (PCR), and Molecular Cloning

Random reverse transcription (RT)-polymerase chain reaction (PCR) and RNA ligase mediated rapid amplification of cDNA ends (RLM-RACE) were performed as described by Froussard (1992) and Coutts and Livieratos (2003), respectively. Sequence specific oligonucleotide primers used for RT-PCR include those amplifying the BbPmV-3 RdRp sequence (5′-CCT CAT CTC GCT CAT GTC CC-3′ and 5′-GCA GGC GTA TAG GTC CCT TC-3′) and the universal ITS1F primers (5′-CTT GGT CAT TTA GAG GAA GTA A-3′; Gardes and Bruns, 1993) and ITS4 (5′-TCC TCC GCT TAT TGA TAT GC-3′; White et al., 1990) amplifying the internal transcribed spacer (ITS) sequence. All PCR amplicons were cloned into the pGEM-T Easy vector (Promega) and transformed into *Escherichia coli* XL-10 Gold competent cells (Agilent). Recombinant plasmid DNA was purified using the QIAprep Spin Miniprep Kit (Qiagen). At least three clones for each PCR amplicon were sequenced by Genewiz.

Computational Analyses

BLASTx analysis (Altschul et al., 1990) using the non-redundant protein database updated on August 2020 was performed to identify sequence similarities. The Pfam database (El-Gebali et al., 2019) was used to identify protein family domains. Sequence logos were generated using WebLogo (Crooks et al., 2004). Intrinsic disorder was predicted using PONDR-FIT (Xue et al., 2010). Maximum-likelihood (ML) phylogenetic analysis was performed using MEGA 6 (Tamura et al., 2013). The sequences were aligned with MUSCLE as implemented by MEGA 6, and all positions with less than 30% site coverage were eliminated. The LG + G + I + F substitution model was used for the RdRP, the putative scaffold protein, and the methyl transferase; the WAG + G substitution model was used for the PASrp. Homologous proteins from the closely related Hadaka virus 1 (Sato et al., 2020) were used as outgroups for the RdRP,

the putative scaffold protein, and the methyl transferase; the PASrp from *B. bassiana* non-segmented virus 1 (BbNV-1; Kotta-Loizou et al., 2015) was used as outgroup for the polymycovirus PASrp. The Protein Homology/analogY Recognition Engine v2.0 (Phyre2; Kelley et al., 2015) was used for protein structure predictions. Molecular graphics images were produced using the UCSF Chimera package from the Computer Graphics Laboratory, University of California, San Francisco (supported by NIH P41 RR-01081; Pettersen et al., 2004).

RESULTS AND DISCUSSION

Sequence Analysis of BbPmV-3

BbPmV-3 has the typical genomic organization of other members of the *Polymycoviridae* family (**Table 1**). The genome of BbPmV-3 comprises six dsRNAs, ranging from 2.5 to 0.9 kbp in length, each one carrying an open reading frame (ORF) flanked by 5′ and 3′ untranslated regions (UTRs; **Figure 1A**). Both the 5′ and 3′ UTR termini are conserved (**Figure 1B**), supporting the notion that all six dsRNAs comprise the genome of one single virus. The BbPmV-3 full genomic sequences were submitted to the European Nucleotide Archive (primary accession number PRJEB42287; secondary accession number ERP126123). It should be noted that BbPmV-3 partial sequences corresponding to less than 10% of its genome have been reported previously (Kotta-Loizou and Coutts, 2017) for dsRNAs 1-3 (accession numbers LN896318-LN896320). The first polymycovirus discovered, *Aspergillus fumigatus* tetramycovirus 1, has four genomic segments (Kanhayuwa et al., 2015). Subsequently, related viruses with five (Botryosphaeria dothidea RNA virus 1; Zhai et al., 2016), six (BbPmV 3; Kotta-Loizou and Coutts, 2017), seven (BbPmV 2; Kotta-Loizou and Coutts, 2017), and eight (*Colletotrichum camelliae* filamentous virus 1; Jia et al., 2017; *Fusarium redolens* polymycovirus 1; Mahillon et al., 2019) genomic segments were found. The variability in the number of genomic segments is not a unique feature of the *Polymycoviridae* family; the *Chrysoviridae* family, whose original members also possessed four genomic segments, now accommodates viruses with three to seven genomic segments (Kotta-Loizou et al., 2020).

The largest genomic component, dsRNA1, encodes the RNA-dependent RNA polymerase (RdRP) responsible for the replication of the virus. The BbPmV-3 RdRP sequence is most closely related to BbPmV-2 RdRP (identity: 85.53%; E-value: 0.0).

TABLE 1 | Properties of BbPmV-3.

Segment	Length (bp)	ORF size			UTR length (bp)		Putative function
		(nt)	(aa)	(kDa)	5′-UTR	3′-UTR	
dsRNA 1	2401	2304	767	83	26	71	RdRP
dsRNA 2	2240	2094	697	74	70	90	Scaffold protein
dsRNA 3	1989	1848	615	66	51	90	Methyl-transferase
dsRNA 4	1131	807	268	29	110	214	PASrp
dsRNA 5	937	513	170	18	101	323	Unknown
dsRNA 6	865	618	205	22	104	143	Unknown

Similarly to its homologs in all known polymycoviruses, BbPmV-3 RdRP belongs to the protein family RdRP_1 (PF00680) and has three conserved motifs (**Supplementary Figure S1**). The GDNQ motif, typically found in negative-sense ssRNA viruses of the order *Monogenavirales*, is conserved in all members of the family *Polymycoviridae*, replacing the GDD motif found in most dsRNA and positive-sense ssRNA viruses (**Supplementary Figure S1**).

The second largest component, dsRNA2, encodes a protein of unknown function, hypothesized to act as a scaffold protein (Kotta-Loizou and Coutts, 2017). This protein, similarly to all its homologs, contains a conserved N-terminus and a cysteine-rich, zinc finger-like motif (**Supplementary Figure S2**), and is rich in arginine repeats (R-R, R-X-R), associated with endoplasmic reticulum (ER) retention signals.

The third largest component, dsRNA3, encodes a methyl transferase, responsible for adding a capping structure at the 5′-termini of the positive-sense strands of the viral dsRNAs (Kanhayuwa et al., 2015; Kotta-Loizou and Coutts, 2017). Similarly to other redox enzymes from all kingdoms of life, the polymycovirus methyl transferases are two-domain proteins (**Supplementary Figure S3**), containing a methyltransferase catalytic motif and an N-terminal Rossmann-fold domain belonging to the protein family methyltransf_25 (PF13649) and the protein clan FAD/NAD(P)-binding Rossmann fold (NADP_Rossmann; CL0063).

The fourth largest component, dsRNA4, encodes a proline-alanine-serine-rich protein (PASrp). BbPmV-3 PASrp is the least enriched in these residues as compared to its homologs, whose PAS content can be up to 32%; however, its PAS content, approximately 22%, is still higher than the UniprotKB average of 20% (**Supplementary Figure S4A**). The predicted intrinsic disorder in polymycovirus PASrp ranges from 15% for *Magnaporthe oryzae* polymycovirus 1–50% for *Aspergillus spelaeus* tetramycovirus 1, while BbPmV-3 PASrp is 22% disordered (**Supplementary Figure S4B**). All PASrp have high a pI (**Supplementary Figure S4C**); with the exception of the *Cladosporium cladosporioides* virus 1 PASrp that has a pI of 7.75, the rest range from 8.37 for *F. redolens* polymycovirus 1 to 9.61 for *A. spelaeus* tetramycovirus 1, while BbPmV-3 PASrp has a pI of 8.94. PASrp is believed to coat the viral RNA genome *in lieu* of a capsid (Kanhayuwa et al., 2015; Zhai et al., 2016; Kotta-Loizou and Coutts, 2017; Niu et al., 2018) and its amino acid composition, intrinsic disorder, and high pI are characteristics that would facilitate protein–RNA interactions. It should be noted that conventional, filamentous particles have been reported for the *C. camelliae* filamentous virus 1 (Jia et al., 2017), which is one of the two known polymycoviruses with eight segments; it is possible that the viral proteins encoded by the additional segments play a role in virion formation.

The two smallest BbPmV-3 dsRNAs, dsRNA5 and dsRNA6, respectively, encode proteins homologous to BbPmV-2 dsRNA6 (identity: 71.76%; E-value: 7e-88) and dsRNA7 (identity: 82.93%; E-value: 6e-111). No other proteins with significant similarity were found in public databases, including those produced by other polymycoviruses or related viruses such as the Hadaka virus (Sato et al., 2020). Typically, polymycovirus proteins produced by RNAs other than the largest four (or in some cases three)

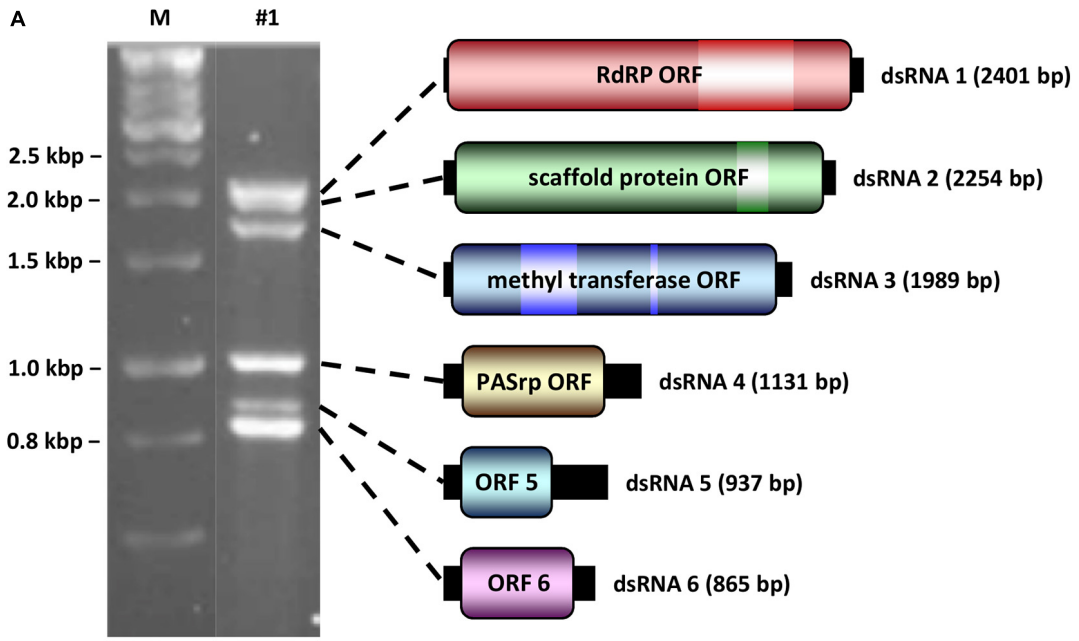

B

```
BbPmV-3 5′-UTRs

dsRNA1      CGAACTAAAGAGTTTTTCTACACAAG----
dsRNA2      CGAACTCAAGAGTTTTTCTACACAAGCACT
dsRNA3      CGAACTCAAGAGTTTTTCTACACAAGCACT
dsRNA4      CGAACTCAAGAGTTTTTCTACACAAGCACG
dsRNA5      CGAACTCAAGCGTTTTTCTTCACAAGCCGG
dsRNA6      CGAAATCAAGAGTTCTTCTACGCAAGCACT
            **** * *** ***.**** *.****

BbPmV-3 3′-UTRs

dsRNA1      CGCGTGGCCCCTACTCGAGATGGAATTTT-
dsRNA2      CCACGGGGACCCCCCGAGTCGGGAATTTTT
dsRNA3      GCTTCAGTCTACCTTCGAGAGGAACTTTT-
dsRNA4      CCTTCAGTCCCCCGTCGAGAGGAACTTTT-
dsRNA5      AATTTTGTTCCCCCCCCGTCCATGACTTTT
dsRNA6      TCTTAGTTCCCCTTTCCAGTTGGAATTTT-
                     . . .  .  . . .***
```

FIGURE 1 | (A) Agarose gel electrophoresis (left) and schematic representation (right) of the BbPmV-3 dsRNA genome. The ORFs (dark colored boxes) are flanked by 5′- and 3′-UTRs (black boxes). The light colored box represents known motifs. M indicates DNA marker HyperLadder 1kb (Bioline). **(B)** Alignment of the 5′- and 3′-UTRs of BbPmV-3 dsRNAs 1–6. Asterisks signify identical nucleotides, and dots signify conserved purines or pyrimidines.

do not have any sequence homology or common biochemical properties (Kotta-Loizou and Coutts, 2017); therefore, the clear homology between the smallest dsRNAs of BbPmV-3 and BbPmV-2 indicates that these two viruses are very closely related.

It should be noted that a couple of errors in the sequence of BbPmV-2 dsRNA6 were detected, an additional C at position 487 within the ORF and an additional G at position 738 within the 3′ UTR, where long stretches of, respectively, C and G are located. The correct sequence was confirmed by sequencing three independent clones and the alterations resulted in a predicted protein foreshortened at the C-terminus. Both BbPmV-2 dsRNA6 and BbPmV-3 dsRNA5 possess remarkably long 3′ UTRs, 391 and 323 nt, respectively. BbPmV-2 dsRNA6 encodes a protein 172 aa in length and 18.8 kDa in mass; similarly, BbPmV-3 dsRNA5 encodes a homologous protein 170 aa in length and 18.5 kDa in mass.

Phylogenetic Analysis of BbPmV-3

Phylogenetic analysis was performed for all proteins known to be conserved in members of the family *Polymycoviridae*,

the RdRp, the scaffold protein, the methyl transferase, and the PASrp. As expected based on the sequence analysis, the BbPmV-3 RdRp is the closest taxon to the BbPmV-2 RdRp, while the BbPmV-1 RdRp appears to be phylogenetically distant (**Figure 2**). The distance between BbPmV-3 and BbPmV-1 is supported by the phylogenetic analysis of the scaffold protein (**Supplementary Figure S5A**), the methyl transferase (**Supplementary Figure S5B**), and the PASrp (**Supplementary Figure S5C**). Geographically, ATHUM 4946 harboring BbPmV-3 originated from Athens, Greece; BbPmV-2 has been reported in Syria, Russia, and Uzbekistan (Kotta-Loizou and Coutts, 2017); BbPmV-1 has been found predominantly in Spanish populations (Kotta-Loizou and Coutts, 2017; Filippou et al., 2018).

With the exception of the three polymycoviruses infecting *Aspergillus* spp., there appears to be no correlation between the evolutionary relationships of polymycoviruses and the organism they were isolated from, either in terms of taxonomy, geography, or preferred host. For instance, the five polymycoviruses associated with the oomycete *Plasmopara viticola* do not form a distinct group, but often appear to be more closely related to polymycoviruses infecting ascomycetes than to each other. The majority of polymycoviruses originate from Europe and Asia, with a couple found in Australia and South America (**Supplementary Table S1**). Most polymycoviruses were isolated from plant pathogens, with *Aspergillus* spp. and *C. cladosporioides* being human pathogens and *B. bassiana* the only arthropod pathogen. Nevertheless, these microorganisms do not have a sole habitat, so contact between them is not unlikely; however, how inter-species transmission of mycoviruses in achieved remains to be elucidated.

Generation of BbPmV-3-Infected and -Free Isogenic Lines

Beauveria bassiana isolate ATHUM 4946 was cured from BbPmV-3 using the protein synthesis inhibitor cycloheximide

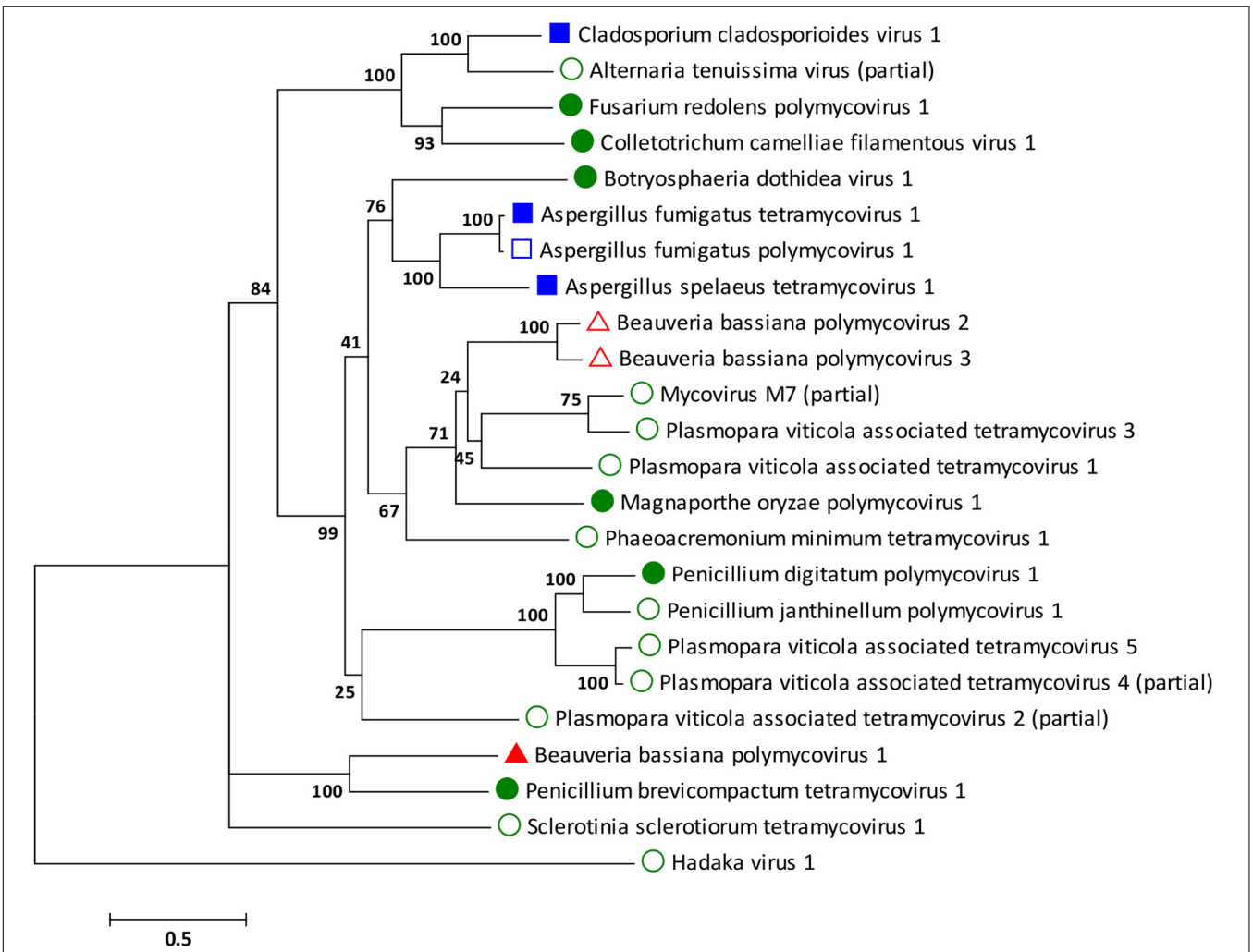

FIGURE 2 | ML phylogenetic tree created based on the RdRP sequences of polymycoviruses. At the end of the branches, established members of the family Polymycoviridae have shapes filled with dark color; other polymycoviruses and related viruses have shape outlines. Blue squares indicate that the virus infects human pathogens; green circles indicate that the virus infects plant pathogens; and red triangles indicate that the virus infects arthropod pathogens.

in combination with single conidia isolation (**Supplementary Figure S6A**). Elimination of BbPmV-3 was confirmed by RT-PCR using sequence specific oligonucleotide primers designed to generate amplicons 699 bp in length representing a fragment of the coding region of the BbPmV-3 RdRP gene (**Supplementary Figure S6B**). The identity of the BbPmV-3-infected and -free isolates was confirmed by extracting total DNA and amplifying, cloning, and sequencing the fungal ITS region with ITS specific oligonucleotide primers. Generating virus-free and virus-infected isogenic lines is essential for further phenotypic comparisons, ensuring that observed differences are due to the virus and not the genetic background of the host.

Effects of Polymycovirus Infection on Fungal Morphology and Sporulation

The morphology of BbPmV-3-infected and BbPmV-3-free isogenic lines was compared after growth on PDA at 25°C for 15 days, showing significant differences in pigmentation (**Figure 3A**). A less dramatic reduction in pigmentation had been observed previously in BbPmV-1-free *B. bassiana* isolate EABb 92/11-Dm as compared to its respective, virus-infected isogenic line (Kotta-Loizou and Coutts, 2017). Polymycovirus infection has been associated with various morphological alterations, including changes in pigmentation (Kanhayuwa et al., 2015; Kotta-Loizou and Coutts, 2017) and sectoring (Kanhayuwa et al., 2015; Zhai et al., 2016; Kotta-Loizou and Coutts, 2017).

The effects on BbPmV-1 and BbPmV-3 on the sporulation of *B. bassiana* isolates EABb 92/11-Dm and ATHUM 4946, respectively, were assessed. Both virus-infected strains produced approximately twofold more spores as compared to their virus-free isogenic lines, and in both cases, this difference was statistically significant (**Figures 3B,C**). Increased sporulation, in this case production of asexual conidia, enhances the potential of the fungus and therefore of the polymycovirus to disperse. The effects of polymycovirus infection on sporulation have not been investigated previously; however, other viruses such as *Sclerotinia sclerotiorum* partitivirus 1 (Xiao et al., 2014), *Pseudogymnoascus destructans* partitivirus-pa (Thapa et al., 2016), and uncharacterized dsRNA elements in *Nectria radicicola* (Ahn and Lee, 2001) have been reported to increase sporulation of their fungal hosts. Conversely, Cryphonectria hypovirus 1 (Kazmierczak et al., 1996; Robin et al., 2010), Diaporthe RNA Virus (Moleleki et al., 2003), *Colletotrichum acutatum* partitivirus 1 (Zhong et al., 2014), and two viruses in

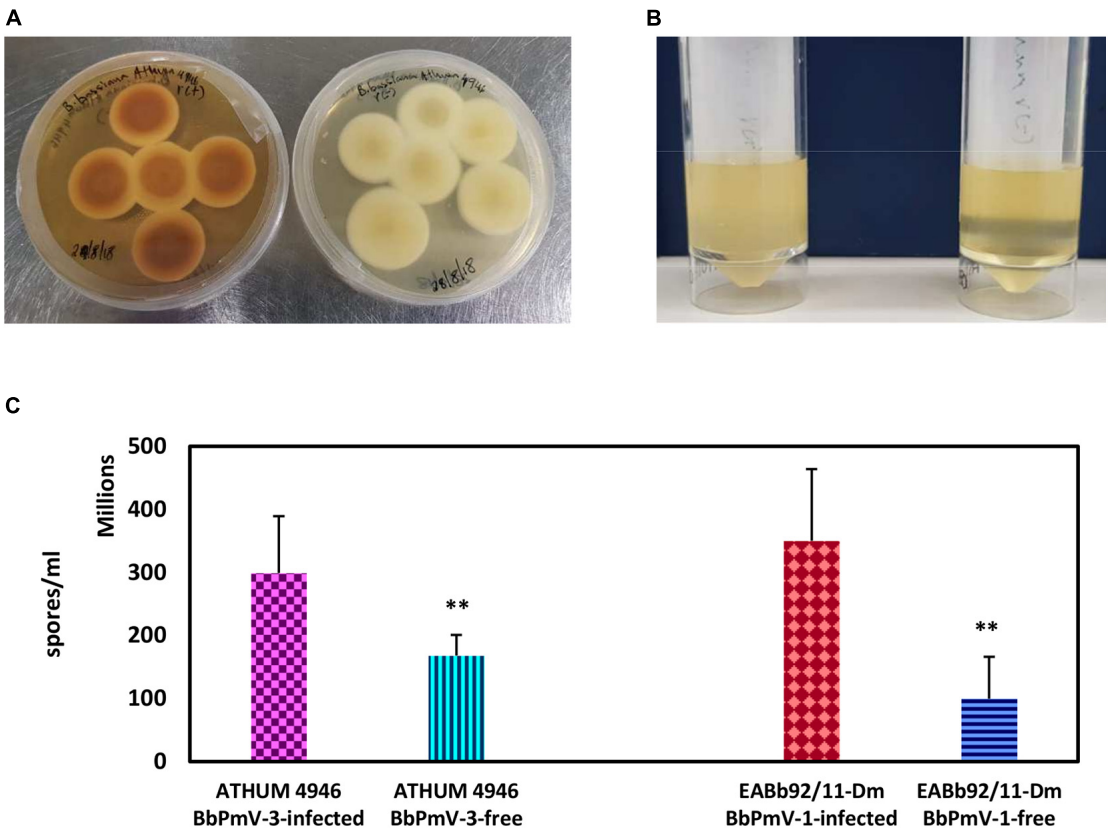

FIGURE 3 | (A) Cultures of BbPmV-3-infected (left) and BbPmV-3-free (right) isogenic lines of ATHUM 4649 grown on PDA at 25°C for 2 weeks, showing significant differences in pigmentation. **(B)** Spore suspensions from BbPmV-3-infected (left) and BbPmV-3-free (right) isogenic lines of ATHUM 4649, demonstrating increased sporulation in the BbPmV-3-infected isogenic line as compared to the BbPmV-3-free line. **(C)** Difference in sporulation between virus-infected and virus-free isogenic lines. Student's *t*-test: ** indicates *p*-value < 0.01.

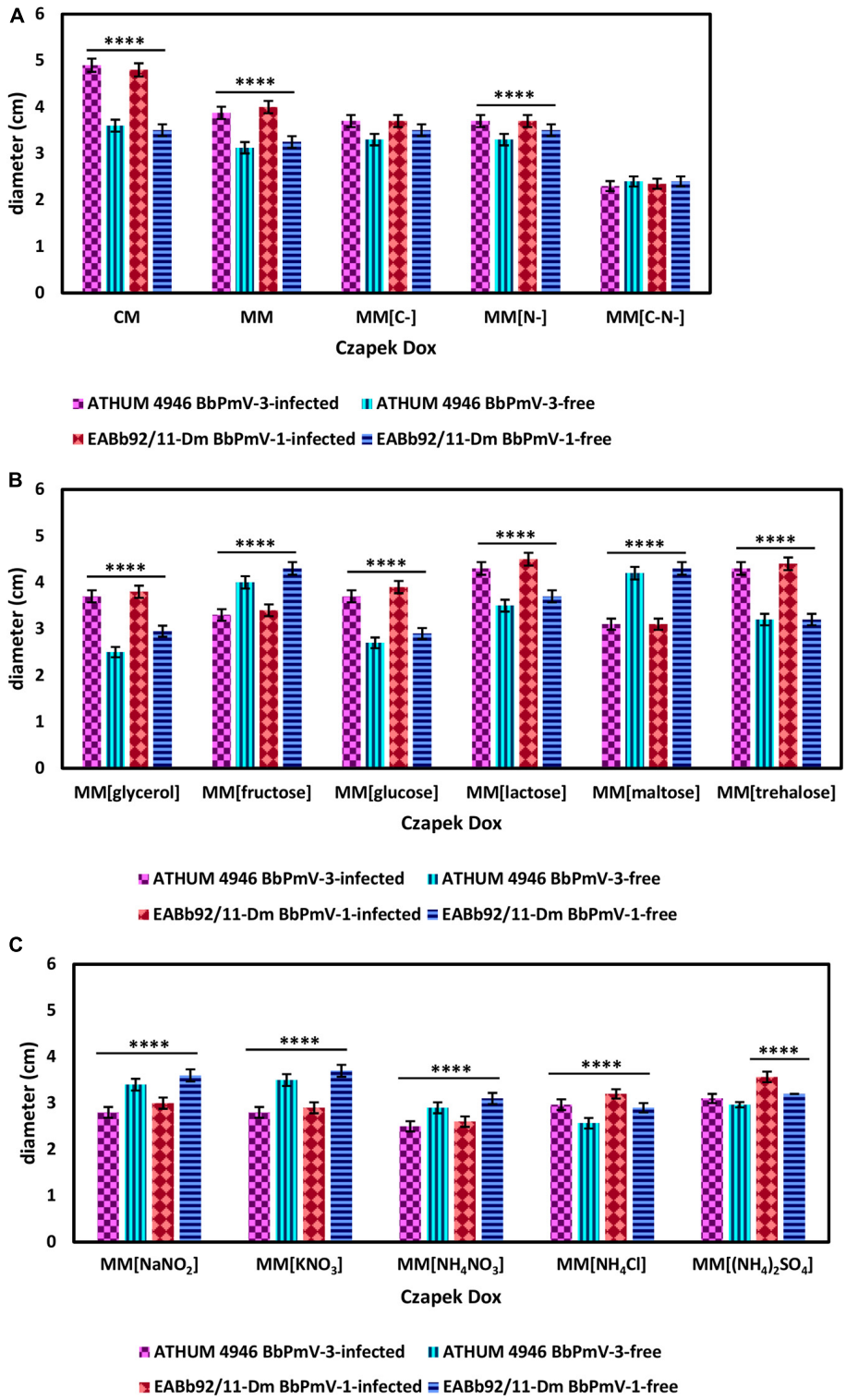

FIGURE 4 | Growth of ATHUM 4946 BbPmV-3-infected and -free (left) and EABb 92/11-Dm BbPmV-1-infected and -free (right) after 18 days on **(A)** Czapek-Dox CM; Czapek-Dox MM; Czapek-Dox MM lacking a carbon source; Czapek-Dox MM lacking a nitrogen source; Czapek-Dox MM lacking both a carbon and a nitrogen source; **(B)** Czapek-Dox MM containing lactose as a carbon source; Czapek-Dox MM containing maltose as a carbon source; Czapek-Dox MM containing trehalose as a carbon source; Czapek-Dox MM containing fructose as a carbon source; Czapek-Dox MM containing glucose as a carbon source; Czapek-Dox MM containing glycerol as a carbon source; **(C)** Czapek-Dox MM containing sodium nitrite as a nitrogen source; Czapek-Dox MM containing potassium nitrate as a nitrogen source; Czapek-Dox MM containing ammonium nitrate as a nitrogen source; Czapek-Dox MM containing ammonium chloride as a nitrogen source; Czapek-Dox MM containing ammonium sulfate as a nitrogen source. Two-way ANOVA; **** indicates p-value < 0.0001.

Botrytis cinerea (Potgieter et al., 2013) decrease sporulation of their fungal hosts.

Effects of Polymycovirus Infection on Fungal Growth

The effects on BbPmV-1 and BbPmV-3 on the growth of *B. bassiana* isolates EABb 92/11-Dm and ATHUM 4946, respectively, were investigated on different carbon and nitrogen sources. The disaccharide sucrose, which serves as the carbon source in Czapek-Dox MM, was replaced by the disaccharides lactose, maltose and trehalose, the monosaccharides fructose and glucose, glycerol, or omitted altogether. Sodium nitrate ($NaNO_3$), which serves as the nitrogen source in Czapek-Dox MM, was replaced by sodium nitrite ($NaNO_2$), potassium nitrate (KNO_3), ammonium nitrate (NH_4NO_3), ammonium chloride (NH_4Cl), ammonium sulfate [$(NH_4)_2SO_4$)], or omitted altogether.

BbPmV-3-infected ATHUM 4946 and BbPmV-1-infected EABb 92/11-Dm demonstrated significantly (p-value < 0.05) increased radial growth as compared to their virus-free isogenic lines on Czapek-Dox CM and MM (**Figure 4A** and **Supplementary Figures S7, S8A,B**), confirming previous observations on EABb 92/11-Dm (Kotta-Loizou and Coutts, 2017). When both a carbon and a nitrogen source were absent, all strains grew very slowly producing very thin mycelium (**Supplementary Figure S7**) and no significant differences between the virus-infected and the virus-free isogenic lines could be detected (**Figure 4A** and **Supplementary Figure S9C**).

When sucrose was replaced by other carbon sources, the virus-mediated increase in growth was maintained in the presence of the disaccharides lactose (**Figure 4B** and **Supplementary Figures S10, S11A**) and trehalose (**Figure 4B** and **Supplementary Figures S10, S11C**), the monosaccharide glucose (**Figure 4B** and **Supplementary Figures S11, S12B**), and glycerol (**Figure 4B** and **Supplementary Figures S10, S12C**). Conversely, the BbPmV-3-infected ATHUM 4946 and BbPmV-1-infected EABb 92/11-Dm grew significantly (p-value < 0.05) slower as compared to their virus-free isogenic lines in the presence of the disaccharide maltose (**Figure 4B** and **Supplementary Figures S10, S11B**) and the monosaccharide fructose (**Figure 4B** and **Supplementary Figures S10, S12A**). The virus-mediated effect on growth disappeared when a carbon source was absent (**Figure 4A** and **Supplementary Figures S7, S9A**). Since glucose is a direct substrate for glycolysis, the first step of respiration, and all other sugars need to be catabolized and/or modified to be utilized, it is possible that the polymycoviruses affect a metabolic process downstream of glycolysis.

It should be noted that trehalose in particular is the major carbohydrate in the insect hemolymph (Thompson, 2003), and is considered a growth-promoting factor in the case of entomopathogenic fungi such as *B. bassiana* (Pendland et al., 1993). The BbPmV-1-infected EABb 92/11-Dm strain grows significantly (p-value < 0.0001) faster on trehalose as compared to sucrose (**Table 2**). Fungi have evolved two mechanisms for trehalose utilization: (1) secretion of trehalases that hydrolyze extracellular trehalose into glucose, followed by uptake and assimilation of the resultant glucose, and (2) direct uptake of trehalose *via* active transport and subsequent intracellular catabolism. *B. bassiana* encodes homologs of AGT1, a glucoside transporter found in *Saccharomyces cerevisiae*, which is implicated in germination, vegetative growth, and conidial yield on various carbohydrate carbon sources (Wang et al., 2013).

The opposite phenotype in the case of maltose and fructose is due to both a significant (p-value < 0.0001) growth increase of the virus-free strains and a significant (p-value < 0.001) growth decrease of their virus-infected isogenic lines (**Table 2**). This may be attributed to potential effects of polymycoviruses on the metabolic pathway prior to the conversion of these sugars to glucose, such as the alpha/beta-glycosidase encoded by the *agdC* gene that cleaves the alpha(1,4)glycosidic bond of maltose to yield molecules of glucose.

TABLE 2 | Comparison of growth on different carbon sources.

	MM[lactose] *vs* MM	MM[maltose] *vs* MM	MM[trehalose] *vs* MM	MM[fructose] *vs* MM	MM[glucose] *vs* MM	MM[glycerol] *vs* MM
BbPmV-3-infected ATHUM 4946	NS	↓↓↓↓	NS	↓↓↓↓	↑	NS
BbPmV-3-free ATHUM 4946	NS	↑↑↑↑	NS	↑↑↑↑	NS	↓↓↓↓
BbPmV-1-infected EABb 92/11-Dm	↑↑↑↑	↓↓↓	↑↑↑↑	↓↓↓	↑↑↑↑	NS
BbPmV-1-free EABb 92/11-Dm	↑↑↑↑	↑↑↑↑	NS	↑↑↑↑	↑↑	NS

Two-way ANOVA; | *p-value < 0.05;* | | *p-value < 0.01;* | | | *p-value < 0.001;* | | | | *p-value < 0.0001.*

TABLE 3 | Comparison of growth on different nitrogen sources.

	MM[$NaNO_2$] *vs* MM	MM[KNO_3] *vs* MM	MM[NH_4NO_3] *vs* MM	MM[NH_4Cl] *vs* MM	MM[$(NH_4)_2SO_4$] *vs* MM
BbPmV-3-infected ATHUM 4946	↓↓↓↓	↓↓↓↓	↓↓↓↓	↓↓↓↓	↓↓↓↓
BbPmV-3-free ATHUM 4946	NS	NS	NS	↓↓↓↓	NS
BbPmV-1-infected EABb 92/11-Dm	↓↓↓↓	↓↓↓↓	↓↓↓↓	↓↓↓↓	NS
BbPmV-1-free EABb 92/11-Dm	↑↑	↑↑↑↑	NS	NS	NS

Two-way ANOVA; | *p-value < 0.05;* | | *p-value < 0.01;* | | | *p-value < 0.001;* | | | | *p-value < 0.0001.*

The BbPmV-3-infected ATHUM 4946 and BbPmV-1-infected EABb 92/11-Dm grew significantly (p-value < 0.05) slower as compared to their virus-free isogenic lines when sodium nitrate was replaced by other nitrogen sources (**Figure 4C** and **Supplementary Figure S13**), such as sodium nitrite (**Supplementary Figure S14A**), potassium nitrate (**Supplementary Figure S14B**), ammonium nitrate (**Supplementary Figure S14C**), ammonium chloride (**Supplementary Figure S15A**), ammonium sulfate (**Supplementary Figure S15B**), or omitted altogether (**Figure 4A** and **Supplementary Figures S7, S9B**). In most cases, the growth of virus-free ATHUM 4946 and EABb 92/11-Dm is the same on alternative nitrogen sources (**Table 3**). Conversely, the majority of virus-infected isogenic lines grow consistently slower (p-value < 0.0001) on any other nitrogen source as compared to sodium nitrate (**Table 3**). Moreover, it is evident (**Figure 4** and **Supplementary Figures S14, S15**) that any virus-mediated effects, either positive or negative, on fungal growth are more striking in the presence of nitrate and nitrite salts; the presence of ammonium salts lessens these effects that may even become non-significant (e.g., **Supplementary Figure S15B**). Nitrate is converted to nitrite and then to ammonia/ammonium, which can be used for amino acid biosynthesis. Therefore, it is likely that polymycoviruses specifically affect the uptake and/or the assimilation of nitrate salts. Remarkably, the opposing effects on fungal growth in the presence of two different nitrate salts, sodium nitrate (**Supplementary Figure S8B**) and potassium nitrate (**Supplementary Figure S14B**), indicate that the polymycovirus-mediated phenotypes may be pleiotropic and that effects may be exerted at different control points of metabolic pathways.

The growth trends illustrated by ATHUM 4946 and EABb 92/11-Dm on the various media are similar but not identical, suggesting that the fungal isolates themselves differ in their genetic background. ATHUM 4946 and EABb 92/11-Dm are infected with different polymycoviruses BbPmV-3 and BbPmV-1, respectively, which have the ability to modulate host metabolic pathways in a similar but not identical way. The observed variation may be attributed to the fungal hosts, the polymycoviruses, the specific host–virus pairs under study, the presence of a second virus BbNV-1 in EABb 92/11-Dm (Kotta-Loizou et al., 2015), and/or a combination of these factors.

The number of mycoviruses that enhance fungal growth and/or virulence is increasing in the literature (Ahn and Lee, 2001; Özkan and Coutts, 2015; Thapa et al., 2016; Kotta-Loizou and Coutts, 2017; Aihara et al., 2018; Okada et al., 2018; Shah et al., 2018, 2020); however, the majority of mycoviruses are known to cause no obvious phenotypic changes or a debilitating effect on their host fungus. In plant pathogenic fungi in particular, such as Cryphonectria parasitica, mycovirus-mediated hypovirulence has been successfully utilized in biological control applications (Rigling and Prospero, 2018). There is accumulating evidence that the ability of the mycoviruses to confer a specific phenotype to their fungal host is conditional and this has been clearly illustrated in the case of two betachrysoviruses: Alternaria alternata chrysovirus 1 downregulates growth in vitro and increases virulence in planta (Okada et al., 2018), while M. oryzae chrysovirus 1 strain A modulates pathogenicity depending on the rice variety (Aihara et al., 2018). Our present work on polymycoviruses further supports this notion, indicating that BbPmV-1 and -3 interfere with basic *B. bassiana* metabolic pathways.

DATA AVAILABILITY STATEMENT

The original contributions presented in the study are publicly available. These data can be found here: https://www.ncbi.nlm.nih.gov/PRJEB42287.

AUTHOR CONTRIBUTIONS

IK-L and RC conceived the project. IK-L designed the experiments. CF, RD, and JD performed the experiments. IK-L analyzed the data and wrote the manuscript. RC edited the manuscript. All authors contributed to the article and approved the submitted version.

FUNDING

This project was supported by funding from the Steel Charitable Trust, the Elizabeth Creak Charitable Trust, the Morley Trust Foundation, the Whitaker Charitable Trust, and the University of Hertfordshire Diamond Fund. CF was financially supported by a University of Hertfordshire Ph.D. research studentship.

ACKNOWLEDGMENTS

The authors wish to thank Chuan Xu and Aurélien Guy for technical assistance.

SUPPLEMENTARY MATERIAL

The Supplementary Material for this article can be found online at: https://www.frontiersin.org/articles/10.3389/fmicb.2021.606366/full#supplementary-material

REFERENCES

Ahn, I. P., and Lee, Y. H. (2001). A viral double-stranded RNA up regulates the fungal virulence of *Nectria radicicola*. *Mol. Plant Microbe Interact.* 14, 496–507. doi: 10.1094/mpmi.2001.14.4.496

Aihara, M., Urayama, S., Le, M. T., Katoh, Y., Higashiura, T., Fukuhara, T., et al. (2018). Infection by *Magnaporthe oryzae* chrysovirus 1 strain A triggers reduced virulence and pathogenic race conversion of its host fungus, *Magnaporthe oryzae*. *J. Gen. Plant Pathol.* 84, 92–103. doi: 10.1007/s10327-018-0766-7

Altschul, S. F., Gish, W., Miller, W., Myers, E. W., and Lipman, D. J. (1990). Basic local alignment search tool. *J. Mol. Biol.* 215, 403–410.

Cai, Q., Wang, J. J., Fu, B., Ying, S. H., and Feng, M. G. (2018). Gcn5-dependent histone H3 acetylation and gene activity is required for the asexual development and virulence of *Beauveria bassiana*. *Environ. Microbiol.* 20, 1484–1497. doi: 10.1111/1462-2920.14066

Coutts, R. H. A., and Livieratos, I. C. (2003). A rapid method for sequencing the 5′- and 3′-termini of double-stranded RNA viral templates using RLM-RACE. *J. Phytopathol.* 151, 525–527. doi: 10.1046/j.1439-0434.2003.00755.x

Crooks, G. E., Hon, G., Chandonia, J. M., and Brenner, S. E. (2004). WebLogo: a sequence logo generator. *Genome Res.* 14, 1188–1190. doi: 10.1101/gr.849004

de Faria, M. R., and Wraight, S. P. (2007). Mycoinsecticides and mycoacaricides: a comprehensive list with worldwide coverage and international classification of formulation types. *Biol. Control* 43, 237–256. doi: 10.1016/j.biocontrol.2007.08.001

El-Gebali, S., Mistry, J., Bateman, A., Eddy, S. R., Luciani, A., Potter, S. C., et al. (2019). The Pfam protein families database in 2019. *Nucleic Acids Res.* 47, D427–D432.

Filippou, C., Garrido-Jurado, I., Meyling, N. V., Quesada-Moraga, E., Coutts, R. H. A., and Kotta-Loizou, I. (2018). Mycoviral population dynamics in Spanish isolates of the entomopathogenic fungus *Beauveria bassiana*. *Viruses* 10:665. doi: 10.3390/v10120665

Froussard, P. (1992). A random-PCR method (rPCR) to construct whole cDNA library from low amounts of RNA. *Nucleic Acids Res.* 20:2900. doi: 10.1093/nar/20.11.2900

Gardes, M., and Bruns, T. D. (1993). ITS primers with enhanced specificity for basidiomycetes–application to the identification of mycorrhizae and rusts. *Mol. Ecol.* 2, 113–118. doi: 10.1111/j.1365-294x.1993.tb00005.x

Garrido-Jurado, I., Fernández-Bravo, M., Campos, C., and Quesada-Moraga, E. (2015). Diversity of entomopathogenic Hypocreales in soil and phylloplanes of five Mediterranean cropping systems. *J. Invertebr. Pathol.* 130, 97–106. doi: 10.1016/j.jip.2015.06.001

Gilbert, K. B., Holcomb, E. E., Allscheid, R. L., and Carrington, J. C. (2019). Hiding in plain sight: new virus genomes discovered via a systematic analysis of fungal public transcriptomes. *PLoS One* 14:e0219207. doi: 10.1371/journal.pone.0219207

Herrero, N., Dueñas, E., Quesada-Moraga, E., and Zabalgogeazcoa, I. (2012). Prevalence and diversity of viruses in the entomopathogenic fungus *Beauveria bassiana*. *Appl. Environ. Microbiol.* 78, 8523–8530. doi: 10.1128/aem.01954-12

Jia, H., Dong, K., Zhou, L., Wang, G., Hong, N., Jiang, D., et al. (2017). A dsRNA virus with filamentous viral particles. *Nat. Commun.* 8:168.

Kanhayuwa, L., Kotta-Loizou, I., Özkan, S., Gunning, A. P., and Coutts, R. H. A. (2015). A novel mycovirus from *Aspergillus fumigatus* contains four unique dsRNAs as its genome and is infectious as dsRNA. *Proc. Natl. Acad. Sci. U.S.A.* 112, 9100–9105. doi: 10.1073/pnas.1419225112

Kazmierczak, P., Pfeiffer, P., Zhang, L., and Van Alfen, N. K. (1996). Transcriptional repression of specific host genes by the mycovirus *Cryphonectria hypovirus* 1. *J. Virol.* 70, 1137–1142. doi: 10.1128/jvi.70.2.1137-1142.1996

Kelley, L. A., Mezulis, S., Yates, C. M., Wass, M. N., and Sternberg, M. J. (2015). The Phyre2 web portal for protein modeling, prediction and analysis. *Nat. Protoc.* 10, 845–858. doi: 10.1038/nprot.2015.053

Koloniuk, I., Hrabáková, L., and Petrzik, K. (2015). Molecular characterization of a novel amalgavirus from the entomopathogenic fungus *Beauveria bassiana*. *Arch. Virol.* 160, 1585–1588. doi: 10.1007/s00705-015-2416-0

Kotta-Loizou, I., Sipkova, J., and Coutts, R. H. A. (2015). Identification and sequence determination of a novel double-stranded RNA mycovirus from the entomopathogenic fungus *Beauveria bassiana*. *Arch. Virol.* 160, 873–875. doi: 10.1007/s00705-014-2332-8

Kotta-Loizou, I., and Coutts, R. H. A. (2017). Studies on the virome of the entomopathogenic fungus *Beauveria bassiana* reveal novel dsRNA elements and mild hypervirulence. *PLoS Pathog.* 13:e1006183. doi: 10.1371/journal.ppat.1006183

Kotta-Loizou, I., Castón, J. R., Coutts, R. H. A., Hillman, B. I., Jiang, D., Kim, D. H., Moriyama, H., Suzuki, N., and ICTV Report Consortium (2020). ICTV Virus Taxonomy Profile: Chrysoviridae. *J. Gen. Virol.* 101, 143–144. doi: 10.1099/jgv.0.001383

Mahillon, M., Decroës, A., Liénard, C., Bragard, C., and Legrève, A. (2019). Full genome sequence of a new polymycovirus infecting *Fusarium redolens*. *Arch. Virol.* 164, 2215–2219. doi: 10.1007/s00705-019-04301-1

McKinnon, A. C., Saari, S., Moran-Diez, M. E., Meyling, N. V., Raad, M., and Glare, T. R. (2017). *Beauveria bassiana* as an endophyte: a critical review on associated methodology and biocontrol potential. *BioControl* 62, 1–17. doi: 10.1007/s10526-016-9769-5

Moleleki, N., van Heerden, S. W., Wingfield, M. J., Wingfield, B. D., and Preisig, O. (2003). Transfection of *Diaporthe perjuncta* with *Diaporthe* RNA virus. *Appl. Environ. Microbiol.* 69, 3952–3956. doi: 10.1128/aem.69.7.3952-3956.2003

Mu, F., Xie, J., Cheng, S., You, M. P., Barbetti, M. J., Jia, J., et al. (2018). Virome characterization of a collection of *S. sclerotiorum* from Australia. *Front. Microbiol.* 8:2540. doi: 10.3389/fmicb.2017.02540 eCollection 2017

Niu, Y., Yuan, Y., Mao, J., Yang, Z., Cao, Q., Zhang, T., et al. (2018). Characterization of two novel mycoviruses from *Penicillium digitatum* and the related fungicide resistance analysis. *Sci. Rep.* 8:5513.

Okada, R., Ichinose, S., Takeshita, K., Urayama, S. I., Fukuhara, T., Komatsu, K., et al. (2018). Molecular characterization of a novel mycovirus in Alternaria alternata manifesting two-sided effects: down-regulation of host growth and up-regulation of host plant pathogenicity. *Virology* 519, 23–32. doi: 10.1016/j.virol.2018.03.027

Özkan, S., and Coutts, R. H. A. (2015). *Aspergillus fumigatus* mycovirus causes mild hypervirulent effect on pathogenicity when tested on *Galleria mellonella*. *Fungal Genet. Biol.* 76, 20–26. doi: 10.1016/j.fgb.2015.01.003

Pendland, J. C., Hung, S. Y., and Boucias, D. (1993). Evasion of host defense by in vivo-produced protoplast-like cells of the insect mycopathogen *Beauveria bassiana*. *J. Bacteriol.* 175, 5962–5969. doi: 10.1128/jb.175.18.5962-5969.1993

Pettersen, E. F., Goddard, T. D., Huang, C. C., Couch, G. S., Greenblatt, D. M., Meng, E. C., et al. (2004). UCSF Chimera–a visualization system for exploratory research and analysis. *J. Comput. Chem.* 25, 1605–1612. doi: 10.1002/jcc.20084

Potgieter, C. A., Castillo, A., Castro, M., Cottet, L., and Morales, A. (2013). A wild-type *Botrytis cinerea* strain co-infected by double-stranded RNA mycoviruses presents hypovirulence-associated traits. *Virol. J.* 10:220. doi: 10.1186/1743-422x-10-220

Rigling, D., and Prospero, S. (2018). *Cryphonectria parasitica*, the causal agent of chestnut blight: invasion history, population biology and disease control. *Mol. Plant Pathol.* 19, 7–20. doi: 10.1111/mpp.12542

Robin, C., Lanz, S., Soutrenon, A., and Rigling, D. (2010). Dominance of natural over released biological control agents of the chestnut blight fungus *Cryphonectria parasitica* in south-eastern France is associated with fitness-related traits. *Biol. Control* 53, 55–61. doi: 10.1016/j.biocontrol.2009.10.013

Sato, Y., Shamsi, W., Jamal, A., Bhatti, M. F., Kondo, H., and Suzuki, N. (2020). Hadaka virus 1: a capsidless eleven-segmented positive-sense single-stranded RNA virus from a phytopathogenic fungus, *Fusarium oxysporum*. *mBio* 11:e00450-20.

Shah, U. A., Kotta-Loizou, I., Fitt, B. D. L., and Coutts, R. H. A. (2018). Identification, molecular characterization, and biology of a novel quadrivirus infecting the phytopathogenic fungus *Leptosphaeria biglobosa*. *Viruses* 11:9. doi: 10.3390/v11010009

Shah, U. A., Kotta-Loizou, I., Fitt, B. D. L., and Coutts, R. H. A. (2020). Mycovirus-induced hypervirulence of *Leptosphaeria biglobosa* enhances systemic acquired resistance to *Leptosphaeria maculans* in *Brassica napus*. *Mol. Plant Microbe Interact.* 33, 98–107. doi: 10.1094/mpmi-09-19-0254-r

Tamura, K., Stecher, G., Peterson, D., Filipski, A., and Kumar, S. (2013). MEGA6: molecular evolutionary genetics analysis version 6.0. *Mol. Biol. Evol.* 30, 2725–2729. doi: 10.1093/molbev/mst197

Thapa, V., Turner, G. G., Hafenstein, S., Overton, B. E., Vanderwolf, K. J., and Roossinck, M. J. (2016). Using a novel partitivirus in *Pseudogymnoascus destructans* to understand the epidemiology of white-nose syndrome. *PLoS Pathog.* 12:e1006076. doi: 10.1371/journal.ppat.1006076

Thompson, S. N. (2003). Trehalose – the insect 'blood' sugar. *Adv. In Insect Phys.* 31, 205–285. doi: 10.1016/s0065-2806(03)31004-5

Wang, X. X., Ji, X. P., Li, J. X., Keyhani, N. O., Feng, M. G., and Ying, S. H. (2013). A putative α-glucoside transporter gene BbAGT1 contributes to carbohydrate utilization, growth, conidiation and virulence of filamentous entomopathogenic fungus *Beauveria bassiana*. *Res. Microbiol.* 164, 480–489. doi: 10.1016/j.resmic.2013.02.008

White, T. J., Bruns, T. D., Lee, S. B., and Taylor, J. W. (1990). "Amplification and direct sequencing of fungal ribosomal RNA genes for phylogenetics," in *PCR Protocols: a Guide to Methods and Applications*, eds M. A. Innis, D. H. Gelfand, J. J. Sninsky, and T. J. White (London: Academic Press), 315–322. doi: 10.1016/b978-0-12-372180-8.50042-1

Xiao, X., Cheng, J., Tang, J., Fu, Y., Jiang, D., Baker, T. S., et al. (2014). A novel partitivirus that confers hypovirulence on plant pathogenic fungi. *J. Virol.* 88, 10120–10133. doi: 10.1128/jvi.01036-14

Xue, B., Dunbrack, R. L., Williams, R. W., Dunker, A. K., and Uversky, V. N. (2010). PONDR-FIT: a meta-predictor of intrinsically disordered amino acids. *Biochim. Biophys. Acta* 1804, 996–1010. doi: 10.1016/j.bbapap.2010.01.011

Zhai, L., Xiang, J., Zhang, M., Fu, M., Yang, Z., Hong, N., et al. (2016). Characterization of a novel double-stranded RNA mycovirus conferring hypovirulence from the phytopathogenic fungus *Botryosphaeria dothidea*. *Virology* 493, 75–85. doi: 10.1016/j.virol.2016.03.012

Zhong, J., Chen, D., Lei, X. H., Zhu, H. J., Zhu, J. Z., and Da Gao, B. (2014). Detection and characterization of a novel gammapartitivirus in the phytopathogenic fungus *Colletotrichum acutatum* strain HNZJ001. *Virus Res.* 190, 104–109. doi: 10.1016/j.virusres.2014.05.028

Conflict of Interest: The authors declare that the research was conducted in the absence of any commercial or financial relationships that could be construed as a potential conflict of interest.

frontiers in Microbiology

ORIGINAL RESEARCH
published: 03 February 2021
doi: 10.3389/fmicb.2021.633502

Two Novel Endornaviruses Co-infecting a *Phytophthora* Pathogen of *Asparagus officinalis* Modulate the Developmental Stages and Fungicide Sensitivities of the Host Oomycete

*Keiko Uchida[1], Kohei Sakuta[1], Aori Ito[1], Yumi Takahashi[1], Yukie Katayama[2], Tsutomu Omatsu[2], Tetsuya Mizutani[2], Tsutomu Arie[3], Ken Komatsu[3], Toshiyuki Fukuhara[1], Seiji Uematsu[1], Ryo Okada[1] and Hiromitsu Moriyama[1]**

[1] Laboratory of Molecular and Cellular Biology, Graduate School of Agriculture, Tokyo University of Agriculture and Technology, Fuchu, Japan, [2] Research and Education Center for Prevention of Global Infectious Diseases of Animals, Tokyo University of Agriculture and Technology, Fuchu, Japan, [3] Laboratory of Plant Pathology, Graduate School of Agriculture, Tokyo University of Agriculture and Technology, Fuchu, Japan

OPEN ACCESS

Edited by:
Nobuhiro Suzuki, Okayama University, Japan

Reviewed by:
Tomofumi Mochizuki, Osaka Prefecture University, Japan
Sotaro Chiba, Nagoya University, Japan

***Correspondence:**
Hiromitsu Moriyama
hmori714@cc.tuat.ac.jp

Specialty section:
This article was submitted to Virology, a section of the journal Frontiers in Microbiology

Received: *25 November 2020*
Accepted: *14 January 2021*
Published: *03 February 2021*

Citation:
Uchida K, Sakuta K, Ito A, Takahashi Y, Katayama Y, Omatsu T, Mizutani T, Arie T, Komatsu K, Fukuhara T, Uematsu S, Okada R and Moriyama H (2021) Two Novel Endornaviruses Co-infecting a Phytophthora Pathogen of Asparagus officinalis Modulate the Developmental Stages and Fungicide Sensitivities of the Host Oomycete. Front. Microbiol. 12:633502. doi: 10.3389/fmicb.2021.633502

Two novel endornaviruses, Phytophthora endornavirus 2 (PEV2) and Phytophthora endornavirus 3 (PEV3) were found in isolates of a *Phytophthora* pathogen of asparagus collected in Japan. A molecular phylogenetic analysis indicated that PEV2 and PEV3 belong to the genus *Alphaendornavirus*. The PEV2 and PEV3 genomes consist of 14,345 and 13,810 bp, and they contain single open reading frames of 4,640 and 4,603 codons, respectively. Their polyproteins contain the conserved domains of an RNA helicase, a UDP-glycosyltransferase, and an RNA-dependent RNA polymerase, which are conserved in other alphaendornaviruses. PEV2 is closely related to Brown algae endornavirus 2, whereas PEV3 is closely related to Phytophthora endornavirus 1 (PEV1), which infects a *Phytophthora* sp. specific to Douglas fir. PEV2 and PEV3 were detected at high titers in two original *Phytophthora* sp. isolates, and we found a sub-isolate with low titers of the viruses during subculture. We used the high- and low-titer isolates to evaluate the effects of the viruses on the growth, development, and fungicide sensitivities of the *Phytophthora* sp. host. The high-titer isolates produced smaller mycelial colonies and much higher numbers of zoosporangia than the low-titer isolate. These results suggest that PEV2 and PEV3 inhibited hyphal growth and stimulated zoosporangium formation. The high-titer isolates were more sensitive than the low-titer isolate to the fungicides benthiavalicarb-isopropyl, famoxadone, and chlorothalonil. In contrast, the high-titer isolates displayed lower sensitivity to the fungicide metalaxyl (an inhibitor of RNA polymerase I) when compared with the low-titer isolate. These results indicate that persistent infection with PEV2 and PEV3 may potentially affect the fungicide sensitivities of the host oomycete.

Keywords: asparagus phytophthora rot fungus, endornavirus, attenuation, fungicide sensitivity, zoosporangium formation, zoospore transmission

INTRODUCTION

Mycoviruses are widespread in all major fungal taxa in nature, and increasing numbers of mycoviruses are currently being identified through metatranscriptomics (Ghabrial and Suzuki, 2009; Pearson et al., 2009; Xie and Jiang, 2014; Ghabrial et al., 2015; Marzano et al., 2016). Mycoviruses are transmitted vertically via spores and, in most cases, horizontally via hyphal anastomosis (Ikeda et al., 2003; Tuomivirta et al., 2009; Ong et al., 2016). Most mycoviruses do not cause any visible abnormal symptoms in the fungal hosts. However, some mycoviruses cause phenotypic changes such as reduced pathogenicity and/or reduced growth rates (Nuss, 2005; Ghabrial et al., 2015). Such infections might be exploited in the biological control of fungal diseases.

The *Endornaviridae* family includes viruses with linear RNA genomes that range from 9.8 to 17.6 kb. Their genomes contain single open reading frames (ORFs) that encode polyproteins ranging from 3,217 to 5,825 amino acids (Valverde et al., 2019). Currently, this family is classified into two genera, *Alphaendornavirus* and *Betaendornavirus*, based on genome size, host type, and unique domains (Adams et al., 2017). Alphaendornaviruses infect plants, fungi, and oomycetes, while betaendornaviruses infect ascomycete fungi (Fukuhara et al., 2006; Valverde et al., 2019).

Most endornaviruses do not cause any apparent symptoms in their hosts. Indeed, endornaviruses have been widely detected in plant crops including broad bean (*Vicia faba*) (Grill and Garger, 1981; Pfeiffer, 1998), common bean (*Phaseolus vulgaris*) (Wakarchuk and Hamilton, 1985, 1990; Mackenzie et al., 1988; Okada et al., 2013), pepper (Valverde and Gutierrez, 2007), rice (Moriyama et al., 1995), and melon (*Cucumis melo*) (Coutts, 2005), and in most cases there were no obvious disease symptoms. There are also few reports on the effects of endornavirus infection on host growth in oomycetes and filamentous fungi (Hacker et al., 2005; Yang et al., 2018). However, some studies have revealed less obvious symptoms of endornavirus infection. For example, Vicia faba endornavirus causes cytoplasmic male sterility in *V. faba* (Grill and Garger, 1981; Turpen et al., 1988; Lefebvre et al., 1990; Pfeiffer et al., 1993), and Helicobasidium mompa endornavirus 1–670 decreases the virulence of the violet root rot fungus *Helicobasidium mompa* (Osaki et al., 2006). The first endornavirus detected in the genus *Phytophthora* was Phytophthora endornavirus 1 (PEV1), found in a *Phytophthora* sp. isolated from Douglas fir (Hacker et al., 2005). This endornavirus also has no noticeable impact on its host.

Phytophthora is a genus of plant pathogenic oomycetes that can infect a wide range of hosts including field crops, vegetable crops, fruit trees, ornamental plants, and tree plants all over the world. Many *Phytophthora* species are polyphagous and are important pathogens in agriculture and forestry. In 2014, 123 valid species were reported, and the numbers are still increasing. *Phytophthora* species can be divided into at least 10 clades based on the sequences of their rDNA ITS regions (Cooke et al., 2000; Blair et al., 2008). These oomycetes belong to the superphylum Stramenopiles, and are phylogenetically related to brown algae and diatoms (Cavalier-Smith and Chao, 2006; Webster and Weber, 2007).

Phytophthora rot of asparagus was first reported in California (Ark and Barret, 1938), and the pathogen was subsequently identified as *Phytophthora sojae* (Falloon, 1982). Asparagus has also been infected by *Phytophthora nicotianae* in Peru (Aragon-Caballero et al., 2008) and by *Phytophthora asparagi* in Michigan (Saude et al., 2008; Crous et al., 2012). In Japan, *P. nicotianae* infections of asparagus have been detected in Ehime and Saga prefectures, and a *Phytophthora* sp. has also been reported to infect asparagus in Toyama, Fukushima, and Hokkaido prefectures (Kodama et al., 2015). Control of these oomycete diseases relies mainly on fungicides from 16 different chemical groups including phenylamides, quinone outside inhibitors, carboxylic acid amides, and multisite inhibitors. However, the frequent use of fungicides can lead to fungicide-resistant oomycetes that are difficult to control chemically.

To date, there have been few reports on mycoviral infections of *Phytophthora* species. *Phytophthora infestans,* which is the causal agent of potato late blight, has been shown to host four unclassified double stranded RNA (dsRNA) viruses named Phytophthora infestans RNA viruses 1–4 (PiRV1–4) (Cai et al., 2009, 2012, 2013, 2019). The alphaendornavirus PEV1 was found in a *Phytophthora* isolate from Douglas fir in the United States (Hacker et al., 2005), and similar virus strains have since been found in *Phytophthora ramorum* isolates from various host plants including *Rhododendron* and *Viburnum* species in both the United States and Europe (Kozlakidis et al., 2010).

Previous studies of endornaviruses have mainly focused on their isolation, sequencing, and genome structures. Therefore, little is known about the effects of infection by endornaviruses on their hosts. In this study, we analyzed the genome organization and phylogeny of two novel endornaviruses (Phytophthora endornavirus 2, PEV2 and Phytophthora endornavirus 3, PEV3), which were discovered in a *Phytophthora* rot pathogen of asparagus. We identified *Phytophthora* host isolates with both high and low titers of the viruses, and used these to analyze the effects of PEV2 and PEV3 infection on the host phenotype and its sensitivity to several oomycete fungicides.

MATERIALS AND METHODS

Pathogen Isolates and Culture Methods

We screened 68 *Phytophthora* and 2 *Pythium* isolates for infection with mycoviruses, by looking for the presence of dsRNA molecules in mycelial cells. Sixty-one of these isolates represented 7 *Phytophthora* species found in a variety of plants from multiple locations in Japan (**Supplementary Table 1**). The remaining 7 *Phytophthora* sp. isolates were collected from asparagus (*A. officinalis*) in Toyama, Hokkaido, Akita, and Fukushima prefectures (**Table 1** and **Supplementary Table 1**). Among these, isolates CH98ASP060, CH98ASP059, and Ku-1 were collected from asparagus storage roots while isolates Ak-6-1 and Fk-3 were collected from rhizomes. The isolates were cultured on PDA (potato dextrose medium with 2% agar) at 25°C in the dark for 14 days, and then stored at 15°C on slants of

TABLE 1 | Sources of the *Phytophthora* isolates used in the study, and presence of endornaviruses in each isolate.

Isolate	Location	Infecting endornaviruses	
		dsRNA[a]	Contents[b]
CH98ASP060	Toyama	PEV2&PEV3	+++
CH98ASP060-a	Toyama	PEV2&PEV3#	++
CH98ASP051	Toyama	PEV2&PEV3	+++
CH98ASP059	Toyama	PEV2&PEV3	+++
CH98ASP059-L	Toyama	PEV2#&PEV3#	+
CH98ASP066	Toyama	PEV2&PEV3	+++
Ku-1	Hokkaido	14-kb dsRNAs	+++++
Ak-6-1	Akita	PEV2&PEV3	++
Fk-3	Fukushima	PEV2&PEV3	+++

[a]*# Invisible by EtBr staining (0.5 mg/ml) but detected by RT-PCR. PEV2; 14.3 kb, PEV3;13.8 kb.* [b]*dsRNA contents were estimated as described in the Section "Materials and Methods."*

modified Weitzman-Silva-Hunter agar (WSH; 10 g oatmeal, 1 g NaH_2PO_4, 1 g $MgSO_4{\cdot}7H_2O$, 1 g KNO_3, 20 g agar, 1,000 ml distilled water). For all experiments involving growth of the isolates, mycelia were precultured on PDA medium at 25°C in the dark for 7 days.

Extraction and Analysis of dsRNAs by Electrophoresis and RT-PCR

Mycelial discs (4 mm diameter) were removed from fungal mats grown on PDA using a cork borer. The disks were used to inoculate 1/3 YG liquid medium (0.17% yeast extract, 0.67% glucose), with 3 disks in 25 ml cultures or 20 disks in I L cultures. The cultures were incubated at 26°C for 2 weeks in the dark on a reciprocal shaker with 60 oscillation per min, then filtered through gauze. The mycelia were dried in a commercial dryer (SIS Co., Ltd., Japan) at 65°C for 10 min, and then stored at −80°C until used for dsRNA extraction. The mycelial yields were about 0.2 g from the 25 ml cultures and about 1 g from the 1 L cultures.

We used micro-spin columns with Cellulose D (Advantec, Japan) to extract total nucleic acids and then purify dsRNAs as described by Okada et al. (2015). Fungal mycelium (0.1 g dry weight) was pulverized in 500 μl extraction buffer [100 mM NaCl, 10 mM Tris-HCl pH 8.0, 1 mM EDTA, 1% SDS, and 0.1% (v/v) β-mercaptoethanol) and then extracted twice with equal volumes of phenol-chloroform-isoamyl alcohol (25:24:1). The aqueous phase was mixed with ethanol (final concentration 16%), and the dsRNA was purified using a spin column as described by Okada et al. (2015). Finally, the dsRNAs were concentrated by ethanol precipitation and stored at −30°C.

The purified dsRNAs were visualized by electrophoresis in 0.8% or 0.6% agarose gels stained with ethidium bromide. The level of dsRNA in each isolate was estimated using a gel imaging system (Ez-Capture MG ATTO, Japan). These estimates are indicated by + signs in **Table 1**.

Reverse transcription (RT)-PCR with virus-specific primers was also used to detect the PEV2 and PEV3 dsRNAs. We used the primers shown in **Supplementary Table 2** and set up the reactions using the SuperScript III One-Step RT-PCR System with Platinum Taq, following the manufacturer's protocol (Life Technologies, Carlsbad, CA, United States). The thermal cycling conditions were as described previously, with 40 cycles of amplification and an annealing temperature of 55°C (Komatsu et al., 2016).

Cloning and Sequence Analyses

Double-stranded RNAs extracted from the original isolate CH98ASP060 were used as templates for cDNA synthesis, and a series of overlapping cDNA clones were obtained as described by Aoki et al. (2009). These cDNA clones were sequenced using an Applied Biosystems 3130xl Genetic Analyzer. In addition, dsRNA purified from isolate CH98ASP060 was sequenced by next-generation sequencing using the Miseq system (Illumina Co., Ltd.; Miseq System Catalog No. MS-J-001). We obtained 2,270,543 raw reads that were assembled into 2,255 contigs, of which 28 contigs had coverage of more than 100. The 5′- and 3′-terminal sequences of each dsRNA segment were determined using the SMARTer® RACE cDNA Amplification Kit (Clontech Laboratories, Inc., Mountain View, CA, United States) (Frohman et al., 1988). We followed the manufacturer's protocol, and used the primers shown in **Supplementary Table 2**.

The nucleotide sequences were analyzed for ORFs, and the ORFs were translated into amino acid sequences using GENETYX version 9 software (GENETYX, Japan). We also used GENETYX to perform protein similarity searches. Multiple alignments based on the putative amino acid sequences were obtained by performing a series of pairwise alignments using CLUSTAL_X version 2.0 (Thompson et al., 1997; Larkin et al., 2007) and MEGA6 software (Tamura et al., 2013). Phylogenetic analysis under the maximum likelihood framework was performed using the optimal model of amino acid substitutions selected by ProtTest 2.4 and PhyML3.1 (Guindon et al., 2010). The bootstrap test was performed with 1,000 re-samplings.

Measurement of Hyphal Growth, Induction of Zoosporangium Formation, and Assessment of Virus Transmission via Monozoospores

To measure hyphal growth, mycelial disks (4 mm diameter) were cut from the margins of precultured colonies, transferred to fresh PDA plates, and incubated at 25°C in the dark for 7 days. For each isolate, average values for colony diameter were determined by measuring three independent colonies.

To induce zoosporangium formation, sterilized 1 cm × 1 cm filter paper pieces (Whatman 3MM) were placed on fresh PDA medium supplemented with 25 μg/ml β-sitosterol (MP Biomedicals, LLC, United States), and two precultured mycelial disks were placed adjacent to each piece of paper. These were incubated at 25°C in the dark for 14 days (Hendrix, 1970). Three pieces of filter paper covered with mycelia were then transferred to 50 ml of sterile rainwater in a flask, and cultured at 18°C under full-light conditions for 40 h with gentle shaking. The formation of zoosporangia and release of zoospores were confirmed under an optical microscope (Olympus IX71; Tokyo, Japan), and the

zoospore density was measured using a hemocytometer (Thoma). For each isolate, the average rate of zoosporangium formation was determined by counting the numbers of zoosporangia formed at the edges of 9 filter paper pieces ($n = 9$).

To assess virus transmission in the monozoospores, the zoospore concentrations were adjusted to 1×10^4 zoospores/ml, and 200 μl of each zoospore suspension was spread on PDA medium and cultured at 25°C in the dark for 2 days. Germinating hyphae from the monozoospores were transferred to flasks containing 50 ml of PD broth and incubated at 25°C in the dark for 14 days with gentle shaking. The dsRNAs were extracted from the resulting mycelia and visualized by gel electrophoresis as described above. RT-PCR was also performed using specific primers to detect PEV2 and PEV3.

Cystospore Formation and Determination of Cystospore Germination Rates

After zoosporangium formation was induced as described above, cystospore formation was induced using the vibration method with some modifications (Tokunaga and Bartnicki-Garcia, 1971; Kliejunas and Ko, 1974; Ko and Chan, 1974). The filter paper pieces with zoosporangia were moved from 18 to 25°C and incubated for 0.5 to 1 h to promote indirect germination of the zoospores (i.e., release of motile zoospores from the zoosporangia). We confirmed that the efficiency of indirect germination was more than 50%, which is the accepted diagnostic check for biologically functional zoosporangia. To induce encystment of the zoospores, 0.5 ml of the zoospore suspension was transferred to a 1.5 ml microtube and subjected to vibration at 1,800 rpm for 1–2 min (Deep Wellmaximizen, Bio shaker M., BR-022up, TITEC, Japan). The concentration of cystospores was determined using a hemocytometer and then adjusted to about 1×10^4 cystospores/ml. An aliquot (200 μl) of the suspension was spread on a PDA plate and incubated for 2 days at 25°C. The visible hyphal colonies were counted under a stereomicroscope, and the rates of cystospore hyphal germination were calculated.

Fungicide Sensitivity Tests

We used the following four fungicides in the sensitivity tests: benthiavalicarb-isopropyl (98.0%; FUJIFILM Wako Pure Chemical Corp.), famoxadone (98.8%; FUJIFILM Wako Pure Chemical Corp.), metalaxyl (98%; Toronto Research Chemicals, Inc.), and chlorothalonil (99.9%; FUJIFILM Wako Pure Chemical Corp.). Each chemical was dissolved in acetone (10 mg ml^{-1}) and stored at 5°C in the dark until used. n-Propyl gallate (PG; MP Biomedicals, Inc.) was used with the quinone outside inhibitor fungicide famoxadone to inhibit the activity of cyanide-insensitive alternative oxidase (AOX) (Hollomon et al., 2005; Ishii et al., 2009). The PG was dissolved in dimethyl sulfoxide to prepare a stock solution (1 M).

Mycelial disks (4 mm diameter) were cut from the margins of precultured colonies and transferred to fresh PDA media containing various concentrations of each fungicide. The final concentrations of the fungicides were as follows: 0, 0.003, 0.03, 0.3, 3, 30, and 150 μg ml^{-1} for benthiavalicarb-isopropyl; 0, 0.0015, 0.015, 0.15, 1.5, 15, 150, and 300 μg ml^{-1} for famoxadone; 0, 0.001, 0.01, 0.1, 1, 10, 100, and 500 μg ml^{-1} for metalaxyl; and 0, 0.004, 0.04, 0.4, 4, 40, 400, and 800 μg ml^{-1} for chlorothalonil. The media containing famoxadone, including the 0 μg ml^{-1} famoxadone plates, also contained 1 mM PG. Each fungicide was added aseptically to the molten PDA medium after sterilization at 120°C for 15 min. Colony diameters were measured after incubating for 14 days at 25°C. The rates of inhibition of mycelial growth were calculated as follows.

$$Inhibition\ (\%) = \frac{1 - (colony\ diameter\ on\ fungicide - amended\ PDA\ -\ 4\ mm)}{Colony\ diameter\ on\ unamended\ PDA\ -\ 4\ mm} \times 100 \quad (1)$$

The mean rates were based on measurements of 3 colonies for each fungicide concentration. The minimum inhibitory concentration (MIC) for each fungicide was determined as the minimum concentration that would result in 100% inhibition of hyphal growth.

RESULTS

Screening for Viral dsRNAs in Asparagus Phytophthora Rot

We screened 68 *Phytophthora* isolates and 2 *Pythium* isolates for the presence of viral dsRNAs. Sixty-one of the *Phytophthora* isolates represented 7 known species (*P. nicotianae*, *Phytophthora cactorum*, *Phytophthora citrophthora*, *Phytophthora cryptogea*, *Phytophthora palmivora*, *Phytophthora citricola*, and *Phytophthora cinnamomi*) that were found in a variety of plants including fruit trees, ornamentals, and vegetable crops, collected from multiple locations in Japan (**Supplementary Table 1**). The remaining 7 *Phytophthora* sp. isolates have not yet been classified. They were collected from asparagus (*A. officinalis*) displaying phytophthora rot disease (**Table 1** and **Supplementary Table 1**). We did not detect dsRNAs in any isolate except the 7 *Phytophthora* sp. isolates from asparagus. Each of these contained high molecular weight dsRNAs of approximately 14 kb, which were visually detected by ethidium bromide staining (**Table 1** and **Figure 1A**). Four of these dsRNA-infected isolates, CH98ASP051, CH98ASP059, CH98ASP060, and CH98ASP066 (**Figure 1A**, lanes 1, 3, 4, and 6), were collected in Toyama prefecture in central Japan near the Sea of Japan coast. The other three isolates, Ku-1, Ak-6-1, and Fk-3 (**Figure 1A**, lanes 7, 8, and 9) were collected in Hokkaido, Akita, and Fukushima prefectures, respectively.

During the subculture of isolate CH98ASP060 on PDA medium, we noticed several sectors of mycelium with an altered phenotype. We subcultured the two phenotypes separately to create the sub-isolate CH98ASP060-a. The original isolate, CH98ASP060, displayed severely impaired hyphal growth, while CH98ASP060-a showed partially recovered hyphal

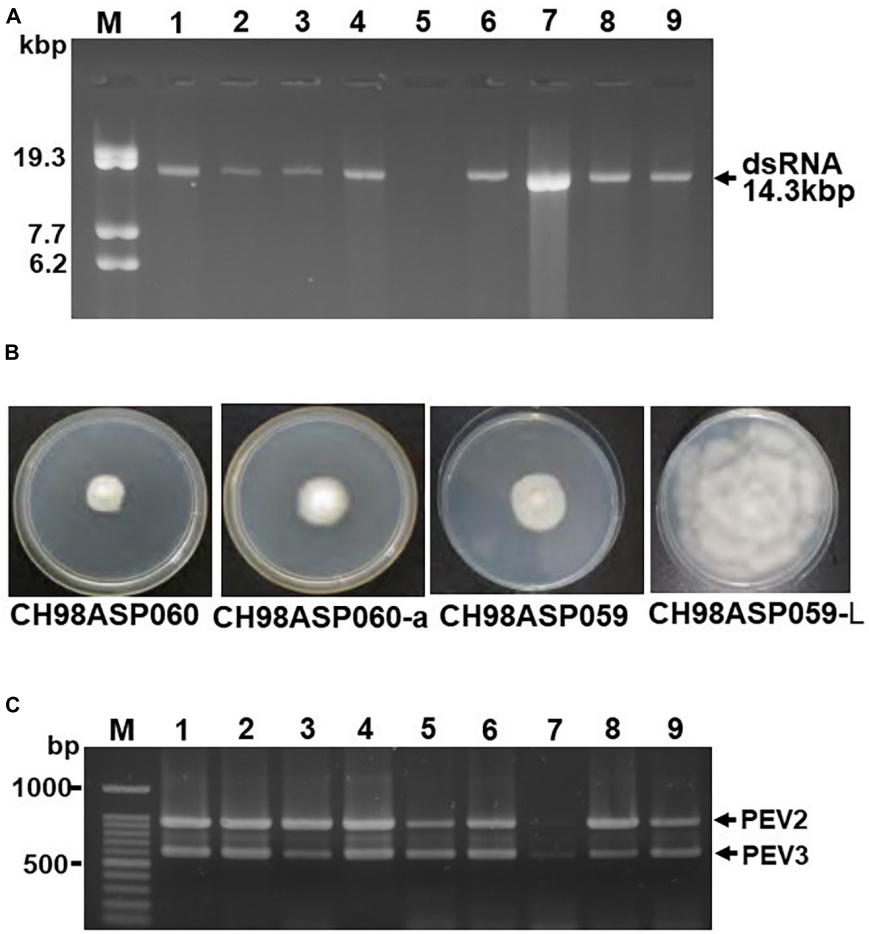

FIGURE 1 | Detection of the dsRNA genomes of PEV2 and PEV3 in *Phytophthora* sp. isolates. **(A)** Agarose gel electrophoresis of dsRNAs purified from each of the isolates. Lane designation: M, DNA marker (250 ng of λ DNA digested with EcoT14I); 1, CH98ASP060; 2, CH98ASP060-a; 3, CH98ASP051; 4, CH98ASP059; 5, CH98ASP059-L; 6, CH98ASP066; 7, Ku-1; 8, Ak-6-1; and 9, Fk-3. The dsRNAs derived from each of the isolates (0.1 g dry weight) were electrophoresed on a 0.8% agarose gel for 18 h at 20 V and stained with ethidium bromide (0.5 μg/ml). Arrows indicate the positions of the 14.3 kb dsRNAs. **(B)** Hyphal morphologies of four isolates. The original isolate CH98ASP060 and its derivative, CH98ASP060-a, the original isolate CH98ASP059 and its derivative CH98ASP059-L were grown on PDA plates at 25°C for 14 days. **(C)** Results of one-step duplex RT-PCR amplification using PEV2 and PEV3-specific primers (**Supplementary Table 2**). Lane designation: M, DNA size markers; 1, CH98ASP060; 2, CH98ASP060-a; 3, CH98ASP051; 4, CH98ASP059; 5, CH98ASP059-L; 6, CH98ASP066; 7, Ku-1; 8, Ak-6-1; and 9, Fk-3.

growth (**Figure 1B**). The 14 kb dsRNA was also detected in CH98ASP060-a (**Figure 1A**, lane 2). After electrophoresis for an extended period in a 0.6% agarose gel, we realized that the original CH98ASP060 had two closely sized dsRNAs of approximately 13.8 and 14.3 kb (**Supplementary Figure 1**). In sub-isolate CH98ASP060-a, the 14.3 kb dsRNA band was clearly visible whereas the 13.8 kb band was only faintly visible (**Supplementary Figure 1**).

As described in more detail below, we designated the 14.3 kb dsRNA as PEV2 and the 13.8 kb dsRNA as PEV3, and created PCR primers specific for each of these dsRNAs (**Supplementary Table 2**). We performed duplex RT-PCR using both sets of primers and found that all but one of the *Phytophthora* sp. isolates from asparagus carried easily-detected levels of both the PEV2 and PEV3 dsRNAs (**Table 1** and **Figure 1C**). These included the sub-isolate CH98ASP060-a (**Figure 1C**, lane 2). The isolate Ku-1 showed only faint amplification products (**Figure 1C**, lane 7), suggesting that this isolate may carry viral sequences that are similar, but not identical, to PEV2 and PEV3.

We also observed mycelium sectoring in the isolate CH98ASP059, and separated the sectors to create the sub-isolate CH98ASP059-L. The original isolate (CH98ASP059) showed impaired hyphal growth while the sub-isolate (CH98ASP059-L) displayed vigorous hyphal growth (**Figure 1B**). The dsRNA bands of approximately 14 kb were not detectable by gel electrophoresis of RNA isolated from CH98ASP059-L (**Figure 1A**, lane 5). However, when we performed duplex RT-PCR using the primers specific for PEV2 and PEV3, both dsRNAs were detected in CH98ASP059-L (**Table 1** and **Figure 1C**, lane 5). Thus, we found that isolates containing high titers of the 14 kb dsRNAs showed attenuated growth (CH98ASP060, CH98ASP060-a, and CH98ASP059; **Figure 1B**) while the low-titer isolate

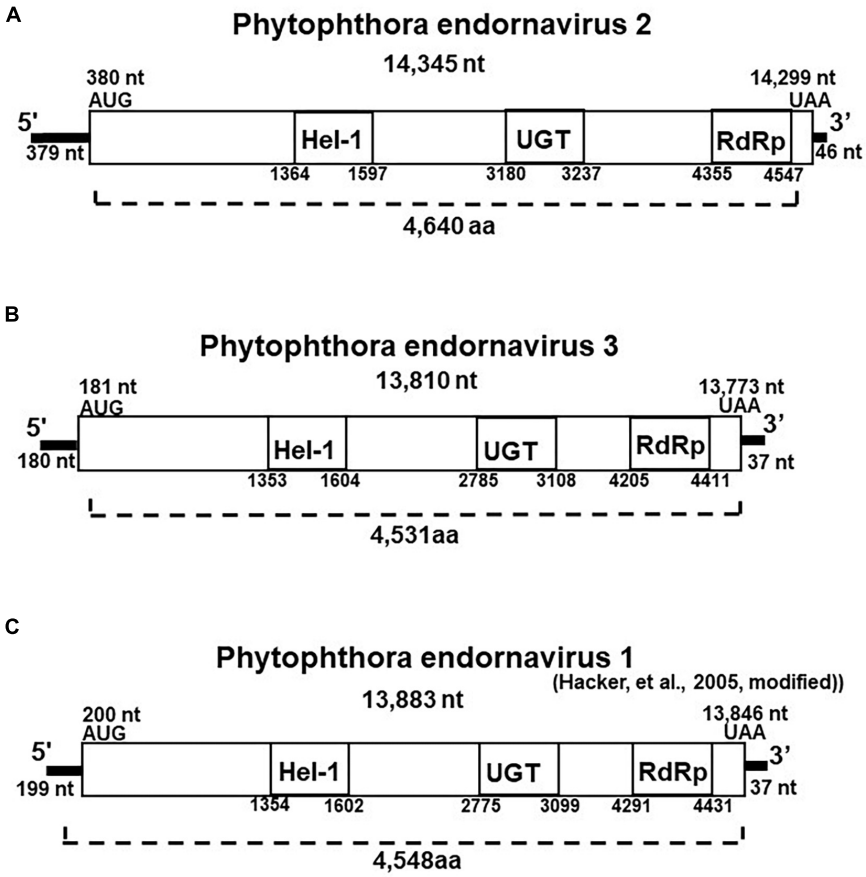

FIGURE 2 | Properties of the Phytophthora endornavirus (PEV) genomes. The total nucleotide length of each dsRNA genomes is shown below the virus name. The predicted amino acid numbers are shown. The boxes represent the large ORFs, whereas lines depict UTRs. Hel-1, viral helicase 1; UGT, UDP-glycosyltransferase; RdRp, viral RNA dependent RNA polymerase. **(A)** Genome organization of PEV2. The viral genome is 14,345 nt in length. **(B)** Genome organization of PEV3. The viral genome is 13,810 nt in length. **(C)** Genome organization of PEV1. The viral genome is 13,883 nt in length.

(CH98ASP059-L) showed vigorous hyphal growth. This suggested that the attenuated growth may be caused by high levels of the PEV2 and PEV3 viruses in the hyphal cells.

Nucleotide Sequence Analysis of PEV2 and PEV3

We created cDNA clones and sequenced the 14.3 and 13.8 kb viral dsRNAs from isolate CH98ASP060. Based on their genome size, genome organization, and similarity to other endornaviruses, we tentatively designated the 14.3 kb dsRNA as Phytophthora endornavirus 2 (PEV2) and the 13.8 kb dsRNA as Phytophthora endornavirus 3 (PEV3). The complete sequences were deposited in the Genbank (NCBI) database with accession numbers LC586217 (PEV2; 14,345 nt) and LC586218 (PEV3, 13,810 nt). The genome organizations of PEV2, PEV3, and PEV1 (Hacker et al., 2005) are illustrated in **Figure 2**. The PEV2 genome consists of a 379 bp 5′ untranslated region (UTR), a single ORF of 4,640 codons, and a 46 bp 3′ UTR, ending with 8 cytosine residues. The PEV3 genome has a 181 bp 5′ UTR, an ORF with 4,591 codons, and a 37 bp 3′ UTR, which also ends with 8 cytosine residues. These structures are very similar to that of PEV1. PEV1, and PEV3 are each also characterized by the lack of a stop codon in the 5′ UTR (**Figures 2B,C**).

The polyproteins encoded by the ORFs of PEV2 and PEV3 contain conserved protein domains, which we identified by searching the NCBI Conserved Domain Database (CDD; Marchler-Bauer et al., 2017). These conserved domains in the polyproteins of both viruses include a viral helicase (Superfamily 1; CDD accession pfam01443), a UDP:flavonoid glycosyltransferase (YjiC, YdhE family; CDD accession COG1819), a UDP glycosyltransferase (GT1_Gtf-like; CDD accession cd03784), and an RNA-dependent RNA polymerase 2 (RdRp 2; CDD accession pfam00978). The positions of the helicase (Hel-1), the UDP glycosyltransferase (UGT), and the RdRp in PEV1, PEV2, and PEV3 are shown in **Figure 2**. The conserved UDP:flavonoid glycosyltransferase domains were located at amino acid position 3,100–3,260 in PEV2 and position 2,991–3,108 in PEV3. The *E*-values indicating similarity to the conserved domains in the database were as follows: Hel-1, 1.97E-05 for PEV2 and 1.24E-08 for PEV3; UGT, 3.91E-04 for PEV2 and 1.73E-04 for PEV3; RdRp,

5.78 E-20 for PEV2 and 2.66E-14 for PEV3; and for the UDP:flavonoid glycosyltransferase, 1.14E-06 for PEV2 and 3.17E-06 for PEV3.

We found low levels of identity (11.2%) and similarity (51.8%) between the complete amino acid sequences of the polyproteins encoded by PEV2 and PEV3. The polyprotein of PEV3 shares 40% amino acid identity with that of PEV1, which infects *Phytophthora* taxon douglasfir (Genbank accession YP_241110.1; Hacker et al., 2005). The identities between the Hel-1, UGT, and RdRp 2 domains of PEV2 and PEV3 are 42, 21, and 53%, respectively. The RdRp and Hel-1 regions of PEV2 and PEV3 show 25–75% identity with the RdRp and Hel-1 domains of other endornaviruses from plants, fungi, and oomycetes (**Supplementary Tables 3**, **4**). On the other hand, we found no similarity between the UGT regions of PEV2 and PEV3 and those of other previously reported endornaviruses. Their UGT regions show 20–40% similarity with the reported UGT regions of bacteria and fungi (data not shown).

Phylogenetic Analysis of the Putative RdRps Encoded by the PEV2 and PEV3 dsRNAs

We constructed a maximum likelihood-based phylogenic tree using the putative RdRp regions of PEV2, PEV3, and 36 related endornaviruses, with Grapevine leafroll-associated virus 1 as the outgroup. The Genbank accession numbers of the viral-encoded sequences used in the analysis are listed in **Supplementary Table 5**. The tree was constructed using MEGA v. 6.0 (Tamura et al., 2013) and the bootstrap test was performed with 1,000

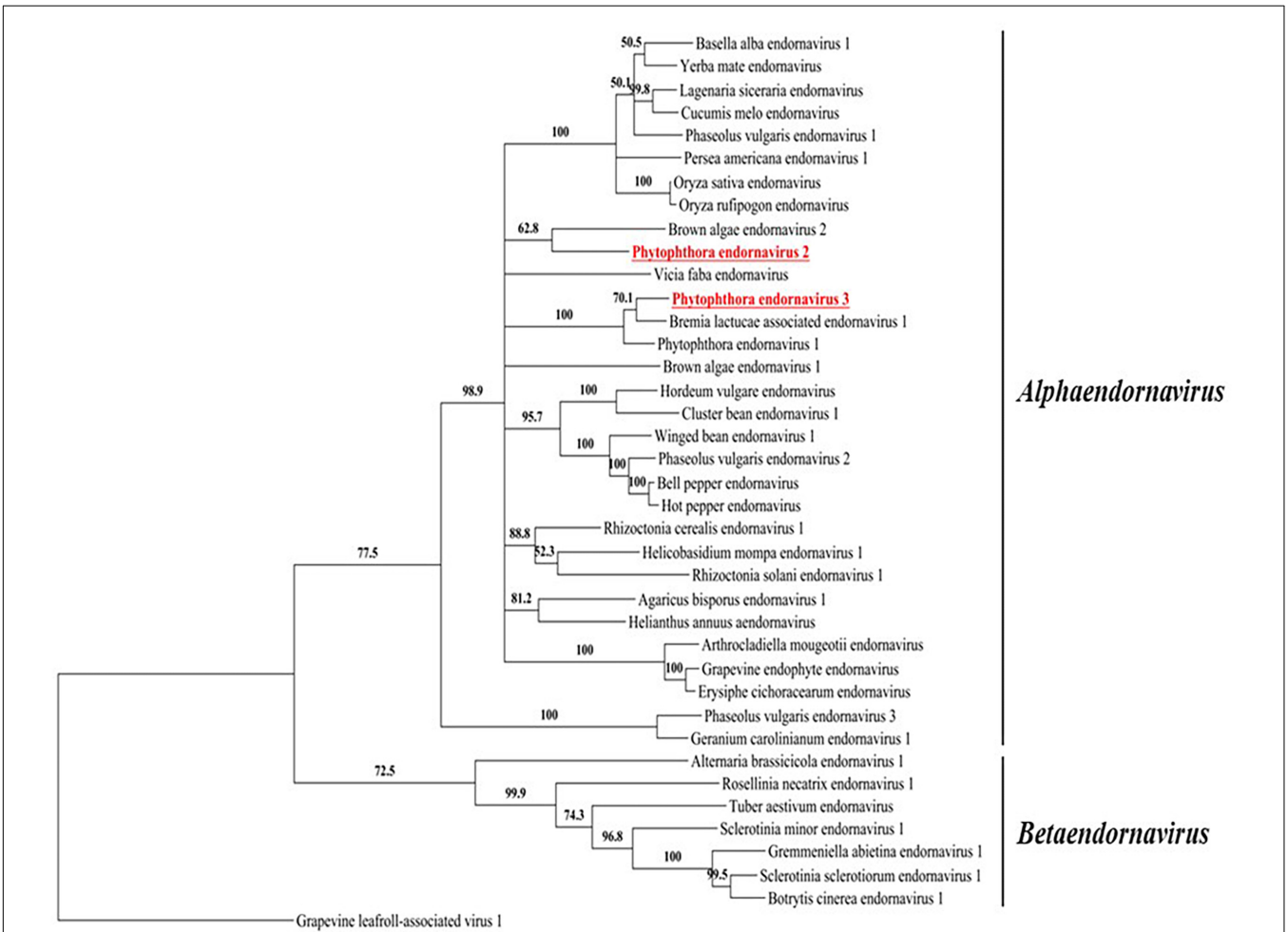

FIGURE 3 | A phylogenic tree based on the putative RdRp regions of PEV2, PEV3, and related endornaviruses. The evolutionary history was inferred by using the Maximum Likelihood method based on the Le_Gascuel_2008 model (Le and Gascuel, 2008). A discrete Gamma distribution was used to model evolutionary rate differences among sites [5 categories (+*G*, parameter = 1.2113)]. The rate variation model allowed for some sites to be evolutionarily invariable ([+*I*], 4.0463% sites). Evolutionary analyses were conducted in MEGA6 (Tamura et al., 2013). Support for nodes was assessed by a reliability percentage after 1,000 bootstrap iterations. Branches with less than 50% bootstrap values were collapsed with TreeGraph 2 ver. 2.14.0-771 beta (Stöver and Müller, 2010). The GenBank accession numbers of the analyzed genes are provided in **Supplementary Table 5**. Grapevine leafroll-associated virus 1 is an ampelovirus in the family *Closteroviridae* and was used as an outgroup. Undefined virus names are shown in italics.

resamplings (**Figure 3**). The tree indicated that the endornaviruses could be divided in two clades representing the genera *Alphaendornavirus* and *Betaendornavirus*. PEV2 and PEV3 (along with PEV1) fell within the genus *Alphaendornavirus*. PEV1, PEV2, and PEV3 belong to different virus species. Thus, the phylogenetic analysis supported the classification of PEV2 and PEV3 as new members of the family *Endornaviridae*.

Transmission of PEV2 and PEV3 via Monozoospores

To investigate the transmission efficiency of PEV2 and PEV3 via monozoospores, zoosporangia were induced to form on the edges of inoculated filter paper pieces that were incubated on PDA medium containing a low concentration of β-sitosterol (25 μg/ml). Release of the monozoospores was induced by incubating the paper pieces at 18°C in rainwater with gentle shaking. The zoospore suspensions were spread on fresh PDA medium, and after germination, individual germinating hyphae were transferred to flasks, and the mycelia were grown for dsRNA extraction. We cultivated mycelia from 102, 68, and 20 monozoospores derived from isolates CH98ASP060, CH98ASP060-a, and CH98ASP059, respectively. We then used both gel electrophoresis and RT-PCR with specific primers to tested for the presence of the PEV2 and PEV3 dsRNAs in each mycelial clone. All of the mycelial clones contained both the PEV2 and PEV3 dsRNAs. The results indicated that the two dsRNAs were stably transmissible via monozoospores at nearly 100% efficiency, and that no virus-free clones were formed during either zoosporangium formation or zoospore germination. Representative data are shown in **Figure 4**.

Effects of the Presence of PEV2 and PEV3 in the Host Vegetative Growth and Developmental Stages

Five of the original *Phytophthora* sp. isolates from asparagus, along with the sub-isolates CH98ASP060-a and CH98ASP059-L, were grown on PDA medium to compare their hyphal growth, zoosporangium formation, and cystospore germination rates (**Table 2**). Among the isolates examined, CH98ASP059-L exhibited extremely low titers of PEV2 and PEV3 (**Figure 1A**) and produced larger mycelial colonies when compared with CH98ASP060, CH98ASP060-a, CH98ASP059, Ku-1, Ak-6-1, and Fk-3 (**Table 2** and **Figure 1B**). Aside from the hyphal growth rates, the most profound differences between these seven isolates were observed in the zoosporangium numbers. Isolate CH98ASP059, which exhibited high titers of PEV2 and PEV3, produced abundant zoosporangia whereas the low-titer isolate CH98ASP059-L formed no zoosporangia (**Table 2** and **Figure 5**). The cystospore germination rates were not significantly different among the six isolates that produced zoosporangia. These results imply that accumulation of high PEV2 and PEV3 levels contributes to reduced hyphal growth and elevated zoosporangium formation in *Phytophthora* sp. infecting asparagus.

PEV2 and PEV3 Modulated the Fungicide Sensitivities of the Host Oomycetes

We investigated the potential effects of PEV2 and PEV3 infection on the fungicide sensitivities of the asparagus Phytophthora rot pathogens. We used the following four commercially available fungicides: benthiavalicarb-isopropyl (an inhibitor of cellulose synthase), famoxadone (a quinone outside inhibitor that inhibits cytochrome bc1 by binding the quinone binding site), metalaxyl (an inhibitor of RNA polymerase I), and chlorothalonil (an inhibitor of multi-site contact activity). We used serial dilutions of the fungicides in PDA plates and determined the levels of growth inhibition of isolates CH98ASP060, CH98ASP060-a, CH98ASP059, and CH98ASP059-L when compared with their growth on plates containing no fungicide (**Tables 3–6**). The data were used to determine the minimum inhibitory concentration (MIC) values for each isolate with each fungicide (**Supplementary Table 6**). **Figures 6–9** show hyphal colonies from each isolate, grown on plates containing each fungicide at the MIC for the high-titer isolates, CH98ASP060, CH98ASP060-a, and CH98ASP059.

The high-titer isolates (CH98ASP060, CH98ASP060-a, and CH98ASP059) were highly sensitive to benthiavalicarb-isopropyl and exhibited almost 100% growth inhibition at the concentration of 0.03 μg ml^{-1} (**Figure 6** and **Table 3**). On the other hand, the MIC value for the low-titer isolate (CH98ASP059-L) was 0.3 μg ml^{-1} (**Table 3** and **Supplementary Table 6**). A similar trend was observed with famoxadone: the high-titer isolates had MIC values of 1.5 μg ml^{-1} while the MIC for CH98ASP059-L was more than 150 μg ml^{-1} (**Figure 7**, **Table 4**, and **Supplementary Table 6**). Therefore, the high-titer isolates CH98ASP060, CH98ASP060-a, and CH98ASP059 showed higher susceptibility to both benthiavalicarb-isopropyl and famoxadone, suggesting that the presence of high levels of PEV2 and PEV3 in the host oomycetes increased their sensitivity to these fungicides. The data for chlorothalonil showed a similar, though less dramatic trend. At the recommended concentration for commercial use (400 μg ml^{-1}), the high-titer isolates CH98ASP060, CH98ASP060-a, and CH98ASP059 showed growth inhibition rates of 90.7, 90.2, and 81.1%, respectively (**Table 6**, **Figure 9**, and **Supplementary Table 6**). The growth inhibition for CH98ASP059-L was about half of these rates, at 47.1% (**Table 6** and **Figure 9**). Therefore, the presence of high amounts of PEV2 and PEV3 may also increase the sensitivity of these oomycetes to chlorothalonil.

In contrast, the low-titer isolate CH98ASP059-L was more sensitive to metalaxyl than the three high-titer isolates. At the recommended concentration for commercial use (100 μg ml^{-1}), the high-titer isolates CH98ASP060, CH98ASP060-a, and CH98ASP059 showed growth inhibition rates of 26.4, 20.7, and 68.0%, respectively (**Figure 8** and **Table 5**). On the other hand, the MIC for CH98ASP059-L was only 10 μg ml^{-1} metalaxyl

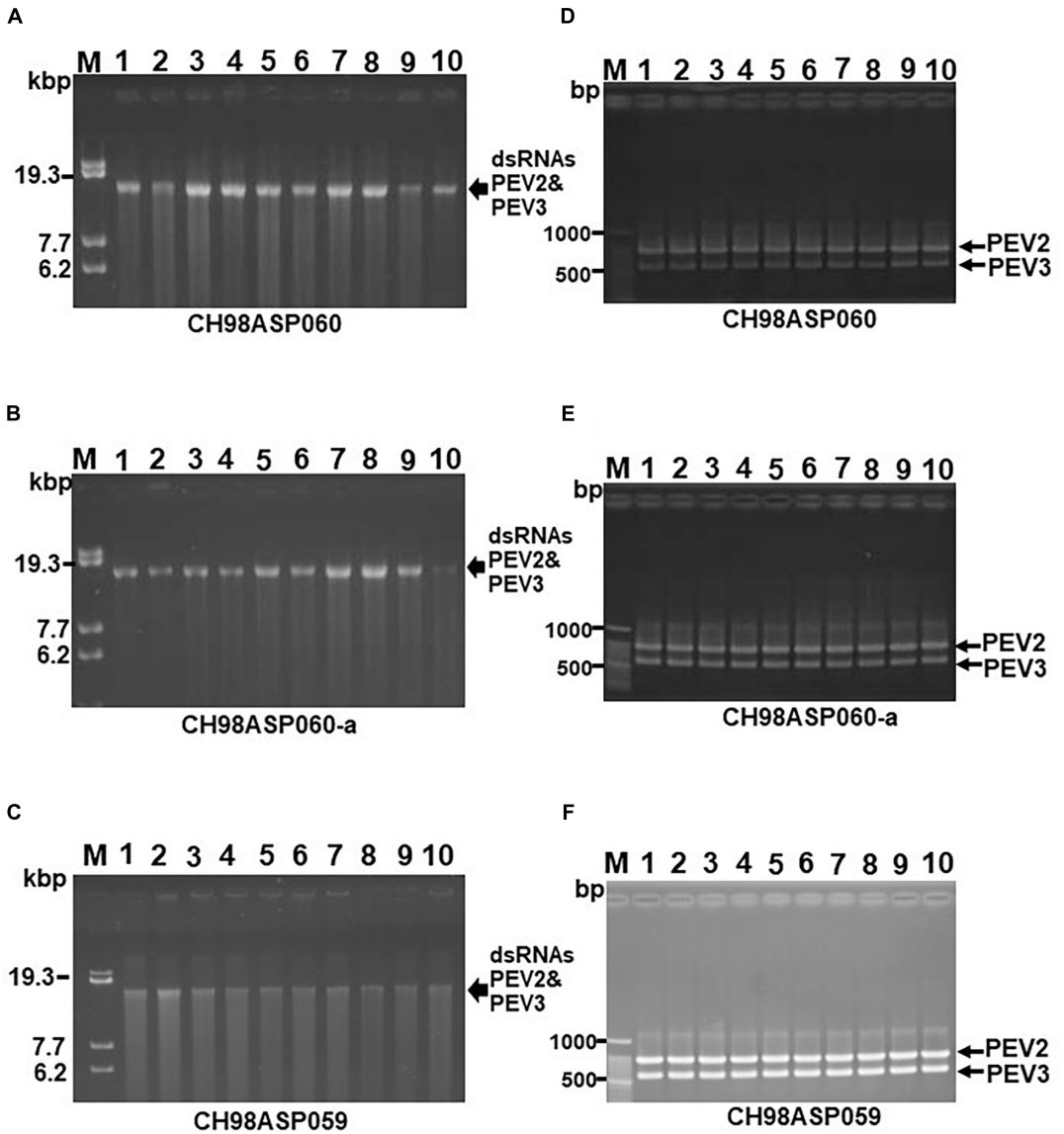

FIGURE 4 | Detection of the PEV2, PEV3 dsRNAs in monozoospore isolates. **(A–C)** Agarose gel electrophoresis of the dsRNA genomes of PEV2 and PEV3 in CH98ASP060 **(A)**, CH98ASP060-a **(B)**, and CH98ASP059 **(C)**. The dsRNAs derived from 0.1 g dry weight of each isolate were electrophoresed in 0.8% agarose gels for 16 h at 20 V and stained with ethidium bromide (0.5 μg/ml). Arrows indicate the positions of the PEV2 and PEV3 dsRNAs. **(D–F)** RT-PCR detection of the PEV2 and PEV3 dsRNA genomes in CH98ASP060 **(D)**, CH98APS060-a **(E)**, and CH98ASP059 **(F)**. RT-PCR was performed using specific primers to amplify the PEV2 and PEV3 dsRNA genomes. The amplified DNA fragments were subjected to electrophoresis in 1% agarose gels for 0.5 h at 100 V. Lane M, 100 bp DNA ladder. Lanes 1–10, individual monozoospore isolates designated numbers 1–10.

(**Figure 8**, **Table 5**, and **Supplementary Table 6**). Therefore, the higher amounts of PEV2 and PEV3 in the host oomycetes appear to have reduced their sensitivity to metalaxyl, which is an inhibitor of RNA polymerase I.

DsRNA Contents of PEV2 and PEV3 in the Host Oomycete Exposed to Metalaxyl

The continuous use of one fungicide or a group of fungicides with similar chemical properties can result in reduced sensitivity in the target organisms. In our fungicide sensitivity tests, the high-titer isolates showed reduced sensitivity to metalaxyl when compared with the low-titer isolate. We conducted an experiment to investigate whether the levels of PEV2 and PEV3 changed in the presence of metalaxyl (**Supplementary Figure 2**). The three high-titer isolates CH98ASP060, CH98ASP060-a, and CH98ASP059 were sub-cultured five times on PDA plates supplemented with either 0 or 100 μg ml^{-1} metalaxyl. We then grew the mycelia in liquid culture, isolated the dsRNAs, and examined them by gel electrophoresis and RT-PCR. A semiquantitative image system (Ez-Capture MG ATTO, Japan) was used to estimate the amounts of dsRNA in the agarose gels (see the **Supplementary Figure 2** legend). The

TABLE 2 | Biological effects of PEV2 and PEV3 on vegetative and developmental growths of *Phytophthora* sp.

isolate (dsRNA)	Hyphal growth (mm)[a]	Zoosporangium formation[b]	Cystospore suspension	hyphal germination from cystospore (%)[c]
CH98ASP060 (PEV2&PEV3)	14.8	21.7 ± 7.6	1×10^4	75.0
CH98ASP060-a (PEV2&PEV3#)[d]	21.5	193.0 ± 32.5**	2×10^4	76.0
CH98ASP059 (PEV2&PEV3)	21.9	193.0 ± 37.6**	1×10^4	100.0
CH98ASP059-L (PEV2#&PEV3#)[d]	33.0	0.0	–	–
Ku-1 (14 kb-dsRNAs)	20.3	214.0 ± 103.0**	2×10^4	93.0
Ak-6-1 (PEV2&PEV3)	22.2	23.7 ± 7.5	1×10^4	80.0
Fk-3 (PEV2&PEV3)	19.0	134.0 ± 28.1*	2×10^4	83.0

*[a] The diameter was measured after 7 days of culture on PDA medium (n = 3). [b] The number of zoosporangia occurring around the four edges of a filter paper (1 cm × 1 cm) after 40 h of incubation in rainwater at 18°C. Data are means ± SD from nine filter papers (n = 9). [c] Suspension including 1 × 10^4 cystospores was spread on PDA medium and grown at 25°C for 5 days. [d] # Invisible by EtBr staining (0.5 mg/ml) but detected by RT-PCR. PEV2; 14.3 kb, PEV3;13.8 kb. * and ** indicate p-values of <0.05 and 0.01, respectively (the Tukey–Kramer range test).*

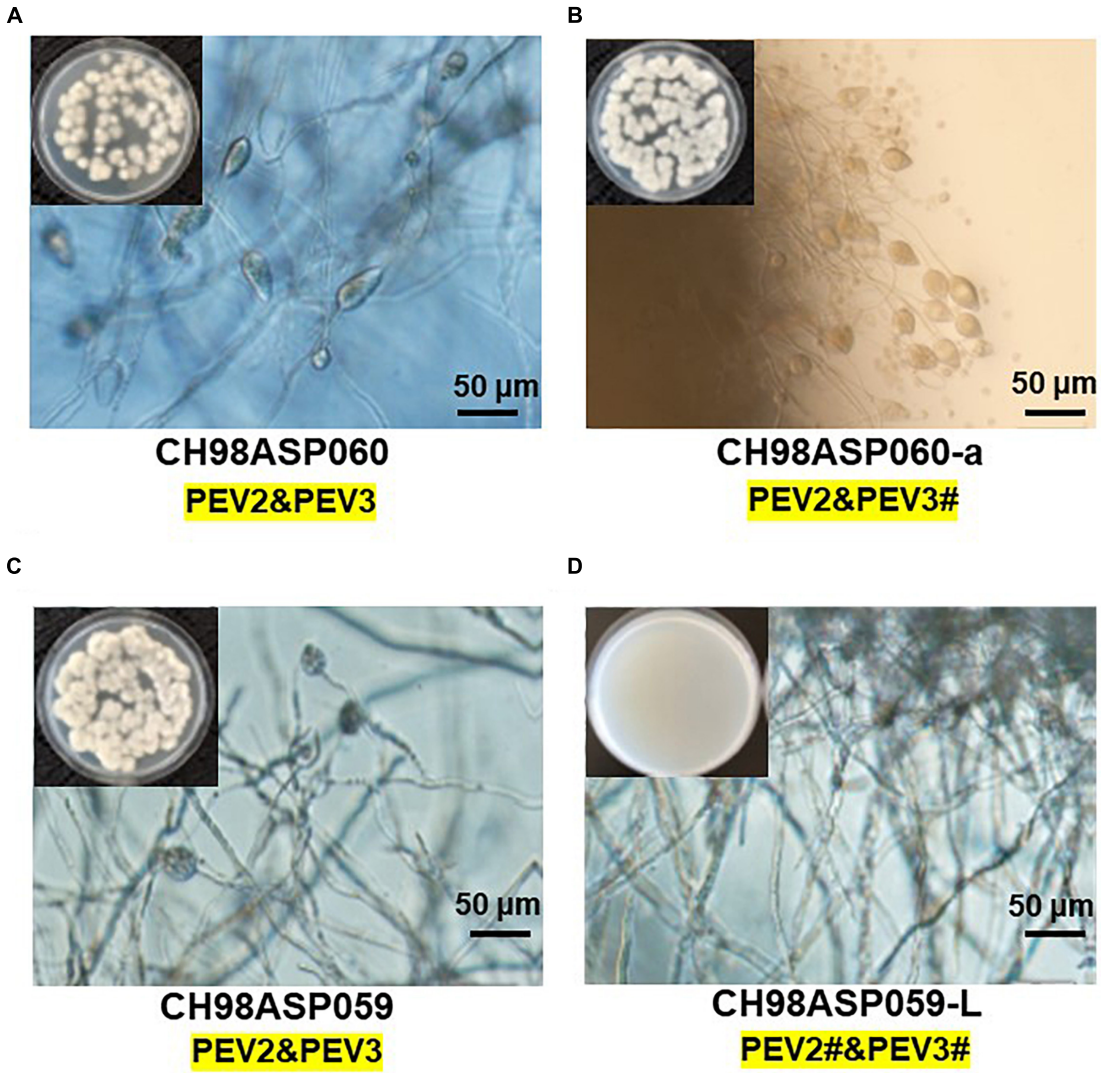

FIGURE 5 | The presence of PEV2 and PEV3 stimulates sporangium production in *Phytophthora* sp. Images show zoosporangium formation by the high-titer isolates CH98ASP060 **(A)**, CH98ASP060-a **(B)**, and CH98ASP059 **(C)** and the low-titer isolate CH98ASP059-L **(D)**. Inserts show hyphal growth on PDA after incubation at 25°C for 7 days. Bars show 50 µm. The # in the dsRNA label under the isolate name is not visible by EtBr staining (0.5 mg/ml) but is detected by RT-PCR. PEV2; 14.3 kb, PEV3; 13.8 kb. This is used in the same mean for the subsequent **Figures 6**–**9**.

TABLE 3 | Sensitivity of *Phytophthora* sp. isolates to benthiavalicarb-isopropyl.

Isolate	Endornaviruses	Mycelial growth inhibition (%) at					
		Benthiavalicarb-isopropyl (μg ml^{-1})					
		0.003	0.03	0.3	3	30[a]	150[b]
CH98APS060	PEV2&PEV3	34.8	100.0	100.0	100.0	100.0	100.0
CH98APS060-a	PEV2&PEV3#[c]	8.8	100.0	100.0	100.0	100.0	100.0
CH98ASP059	PEV2&PEV3	0.0	95.4	100.0	100.0	100.0	100.0
CH98ASP059-L	PEV2#&PEV3#[c]	3.8	81.8*	100.0	100.0	100.0	100.0

[a] *The recommended concentration for commercial use.* [b] *Five times the recommended concentration for commercial use.* [c] *# Invisible by EtBr staining (0.5 mg/ml) but detected by RT-PCR. PEV2; 14.3 kb, PEV3;13.8 kb * indicate groups that differ significantly ($p < 0.05$) according to the Tukey–Kramer range test.*

TABLE 4 | Sensitivity of *Phytophthora* sp. isolates to famoxadone.

Isolate	Endornaviruses	Mycelial growth inhibition (%) at						
		Famoxadone (μg ml^{-1}) + 1 mM PG						
		0.0015	0.015	0.15	1.5	15	150[a]	300[b]
CH98APS060	PEV2&PEV3	23.5	18.5	18.5	100.0	100.0	100.0	100.0
CH98APS060-a	PEV2&PEV3#[c]	0.0	15.8	12.6	100.0	100.0	100.0	100.0
CH98ASP059	PEV2&PEV3	0.0	0.0	2.1	100.0	100.0	100.0	100.0
CH98ASP059-L	PEV2#&PEV3#[c]	0.0	0.0	0.0	14.1*	21.5	32.3*	27.9*

[a] *The recommended concentration for commercial use.* [b] *Two times the recommended concentration for commercial use.* [c] *# Invisible by EtBr staining (0.5 mg/ml) but detected by RT-PCR. PEV2; 14.3 kb, PEV3;13.8 kb. * indicate groups that differ significantly ($p < 0.05$) according to the Tukey–Kramer range test.*

TABLE 5 | Sensitivity of *Phytophthora* sp. isolates to metalaxyl.

Isolate	Endornaviruses	Mycelial growth inhibition (%) at						
		Metalaxyl (μg ml^{-1})						
		0.001	0.01	0.1	1	10	100[a]	500[b]
CH98APS060	PEV2&PEV3	0.0	9.4	6.6	17.9	23.6*	26.4	92.1
CH98APS060-a	PEV2&PEV3#	0.0	8.0	8.0	11.5	19.5*	20.7	97.7*
CH98ASP059	PEV2&PEV3	0.0	21.0	24.0	43.0	28.9*	68.0*	93.2
CH98ASP059-L	PEV2#&PEV3#	0.0	11.1	62.1	92.2	100.0*	100.0*	100.0*

[a] *The recommended concentration for commercial use.* [b] *Five times the recommended concentration for commercial use. * indicate groups that differ significantly ($p < 0.05$) according to the Tukey–Kramer range test.*

TABLE 6 | Sensitivity of *Phytophthora* sp. isolates to chlorothalonil.

Isolate	Endornaviruses	Mycelial growth inhibition (%) at						
		Chlorothalonil (μg ml^{-1})						
		0.004	0.04	0.4	4	40	400[a]	800[b]
CH98APS060	PEV2&PEV3	0.0	1.2	27.9	48.2	82.6	90.7	92.7
CH98APS060-a	PEV2&PEV3#	0.0	0.0	25.2	74.4	68.3	90.2	93.5
CH98ASP059	PEV2&PEV3	0.0	0.0	20.5	50.8	73.8	81.1	82.8
CH98ASP059-L	PEV2#&PEV3#	2.2	1.4	0.8	10.6	28.6*	47.1*	64.4*

[a] *The recommended concentration for commercial use.* [b] *Two times the recommended concentration for commercial use. * indicate groups that differ significantly ($p < 0.05$) according to the Tukey–Kramer range test.*

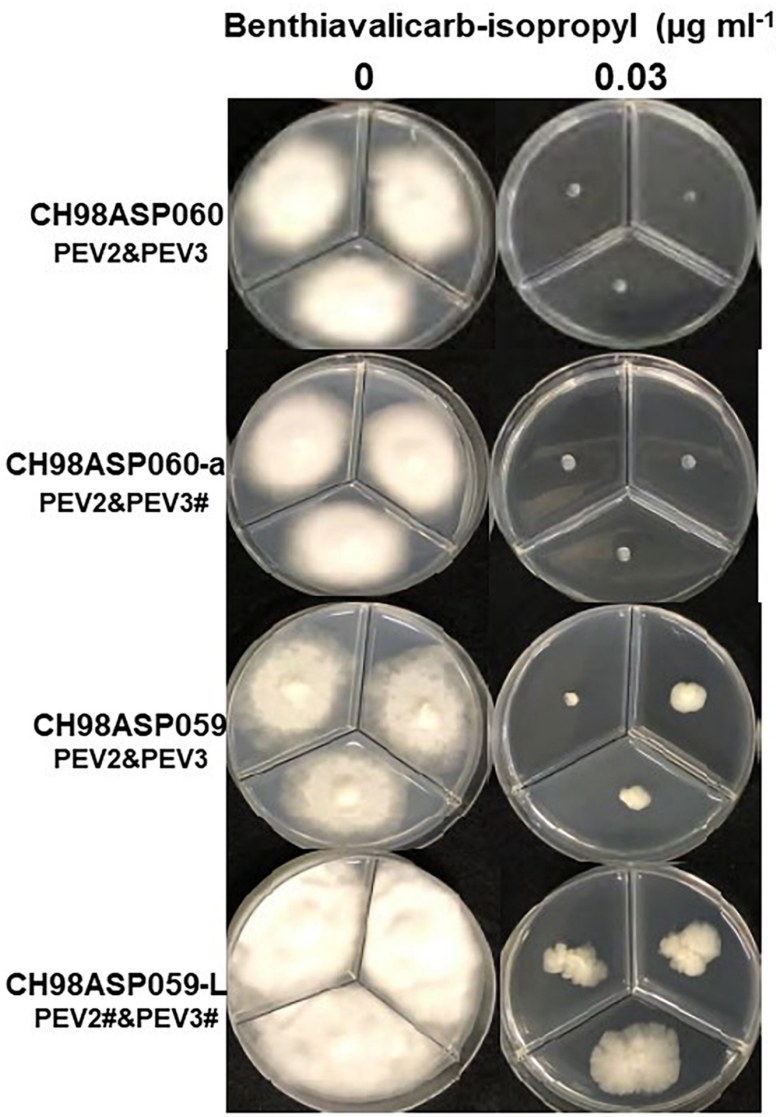

FIGURE 6 | Hyphal growth in on media containing benthiavalicarb-isopropyl (0.03 μg ml^{-1}). CH98ASP060, CH98ASP060-a, CH98ASP059, and CH98ASP059-L were grown in the presence **(right)** or absence **(left)** of the fungicide. The minimum inhibitory concentration (MIC) for the high-titer isolates (CH98ASP060, CH98ASP060-a, and CH98ASP059) was used.

results indicated that under the recommended concentration of 100 μg ml^{-1} metalaxyl, the levels of dsRNA were not significantly different between mycelia sub-cultured in the presence or absence of metalaxyl (**Supplementary Figure 2A**). The RT-PCR results showed that PEV2 and PEV3 were retained during culture in the presence and absence of metalaxyl (**Supplementary Figure 2B**).

Effects of PEV2 and PEV3 on Mycelial Growth in the Presence of *n*-Propyl Gallate

Generally, *n*-propyl gallate (PG) is used in fungicide sensitivity tests with quinone outside inhibitors such as famoxadone, to inhibit the activity of cyanide-insensitive alternative oxidase (AOX) (Hollomon et al., 2005; Ishii et al., 2009). In our sensitivity tests with famoxadone, we included 1 mM PG in all media, including the control medium containing 0 μg ml^{-1} famoxadone. We found that the high-titer isolates appeared to show some growth inhibition in presence of PG when compared with growth in non-supplemented media (compare **Figure 7** with **Figures, 6**, **8**, **9**). Therefore, we performed sensitivity tests with famoxadone in the absence of PG to determine the effect of famoxadone alone. Interestingly, in these tests the low-titer isolate showed no growth inhibition, even at the maximum concentration of 300 μg ml^{-1} famoxadone. The high-titer isolates showed some growth inhibition, but the inhibition was lower than when PG was included in the

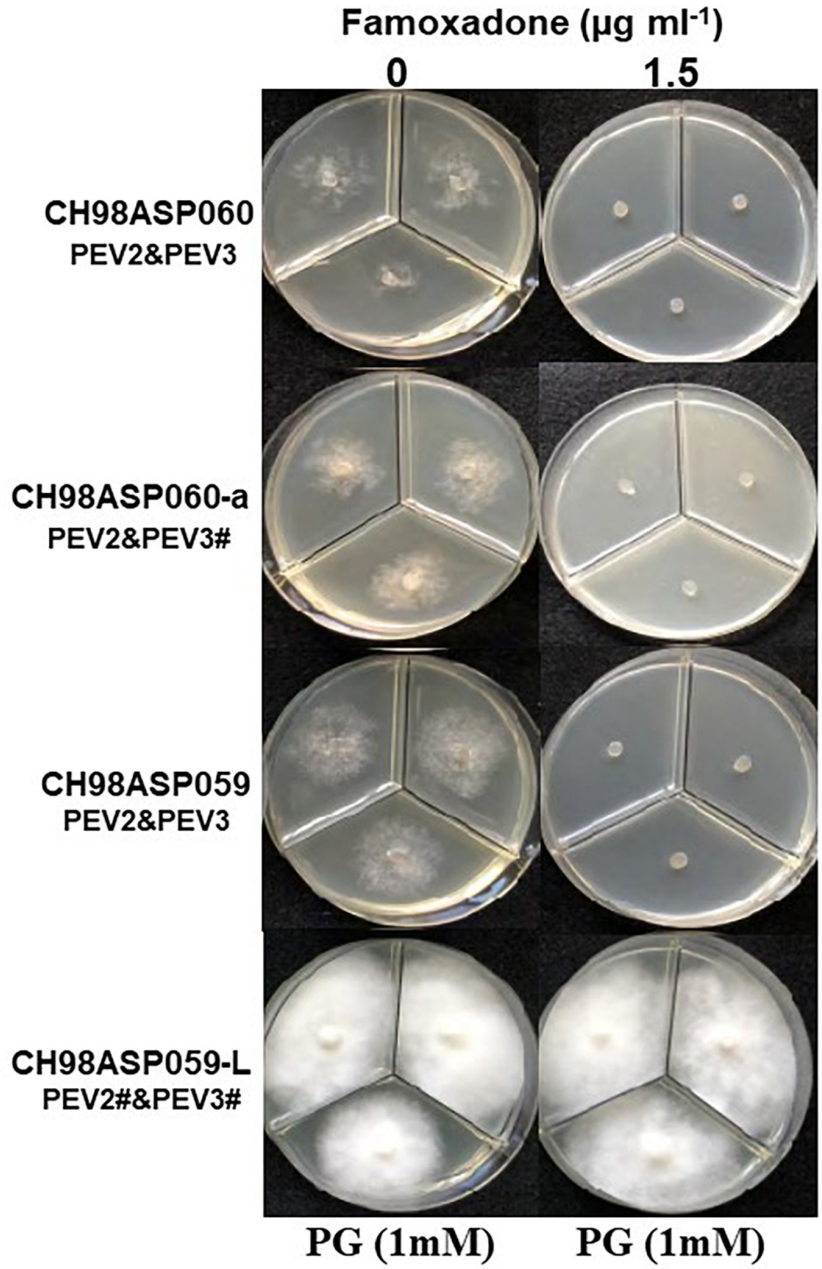

FIGURE 7 | Hyphal growth on media containing famoxadone (1.5 μg ml^{-1}). CH98ASP060, CH98ASP060-a, CH98ASP059, and CH98ASP059-L were grown in the presence **(right)** or absence **(left)** of the fungicide. The MIC for the high-titer isolates was used. PG (1 mM) was included in all media.

media (compare **Table 4** with **Supplementary Table 7**). We then determined the effect of PG alone on hyphal growth. In the presence of 1 mM PG, the high-titer isolates CH98ASP060, CH98ASP060-a, and CH98ASP059 showed growth inhibition rates of 59.5, 77.1, and 57.6%, respectively, compared with their growth on non-supplemented medium. The low-titer isolate showed a lower rate of growth inhibition (25.0%; **Supplementary Table 8**). Therefore, the presence of PEV2 and PEV3 at relatively high levels appears to confer increased sensitivity to PG.

DISCUSSION

In this study, we screened *Phytophthora* sp. collected in Japan for infection by mycoviruses, by looking for dsRNA molecules in their mycelia. We found two novel endornaviruses, Phytophthora endornavirus 2 (PEV2, 14,345 nt) and Phytophthora endornavirus 3 (PEV3, 13,810 nt). Phylogenetic analysis of these and other endornaviruses, based on their encoded RdRp sequences, showed that PEV2 and PEV3 are closely related to Phytophthora endornavirus 1 (PEV1) from *Phytophthora* sp.

FIGURE 8 | Hyphal growth on media containing metalaxyl (10 μg ml^{-1}). CH98ASP060, CH98ASP060-a, CH98ASP059, and CH98ASP059-L were grown in the presence **(right)** or absence **(left)** of the fungicide. The MIC for the low-titer isolate (CH98ASP059-L) was used.

isolates found in Douglas fir (Hacker et al., 2005) (**Figure 3**). A case in which three different endornaviruses were found in host organisms belonging to the same genus has also been reported in common bean, *P. vulgaris* (Okada et al., 2013, 2018). RT-PCR analysis of the dsRNA from isolate Ku-1, using PEV2- and PEV3-specific primers, resulted in only faint amplification products (**Figure 1C**). This suggested that the Ku-1 endornaviruses may have sequences that are similar to, but not identical to those of PEV2 and PEV3. This may indicate that the *Phytophthora* endornaviruses have other similar sister viruses. Interestingly, the phylogenetic analysis revealed that PEV2 and PEV3 are evolutionarily close to *Vicia faba* endornavirus (VfEV) (**Figure 3**, Pfeiffer, 1998). VfEV is the only plant endornavirus that causes significant damage to the host plant (Grill and Garger, 1981). When VfEV was present at a high titer, the anther of the broad bean

FIGURE 9 | Hyphal growth on media containing chlorothalonil (400 μg ml^{-1}). CH98ASP060, CH98ASP060-a, CH98ASP059, and CH98ASP059-L were grown in the presence **(right)** or absence **(left)** of the fungicide. All four isolates had MIC values >400 μg ml^{-1}.

V. faba exhibited an abnormal shape and was male sterile (Turpen et al., 1988).

When we compared hyphal growth rates between the high-titer isolate CH98ASP059 and its low-titer derivative CH98ASP059-L, we found that the high-titer isolate showed a lower growth rate and reduced hyphal density (**Figure 1B** and **Table 2**). Similarly, Plasmopara halstedii virus (PhV), which infects downy mildew, inhibited the growth of host hyphae (Grasse et al., 2013). It is possible that the suppression of vegetative hyphal growth by viruses may prevent the spread of oomycete pathogens in the field.

Interestingly, the high-titer isolate CH98ASP059 produced abundant zoosporangia, while the low-titer isolate CH98ASP059-L showed vigorous hyphal growth but produced extraordinarily few zoosporangia. These results suggest that the high accumulation of PEV2 and PEV3 in the host stimulated

zoosporangium production (**Figure 5** and **Table 2**). Similarly, Phytophthora infestans RNA virus 2 (PiRV-2) has been reported to stimulate zoosporangium formation (Cai et al., 2019). Zoosporangium formation requires plant sterols such as β-sitosterol. Sterols taken up into oomycete cells are transported from the Golgi apparatus via blastocoel spores, and are thought to play essential roles as materials for constructing zoospore cell membranes (Hendrix, 1970). The high levels of PEV2 and PEV3 in the host oomycetes may contribute to sterol uptake by the host oomycetes.

Phytophthora species are mainly transmitted in the soil, so fungicide management is not easy. Furthermore, the period from infection to spread is very short, and fungicide use has become more frequent over time, leading to reduced efficacy of the fungicides. Therefore, we investigated the sensitivities of our high- and low-titer isolates to four different fungicides. The high titers of PEV2 and PEV3 resulted in high sensitivity to the carboxylic acid amide fungicide, benthiavalicarb-isopropyl (an inhibitor of cellulose synthase). It is known that benthiavalicarb-isopropyl strongly suppresses hyphal growth, direct sporangia germination, cyst germination, and zoosporangium formation (Gisi and Sierotzki, 2015). Assuming that the biosynthesis of the cell wall of the host oomycete is weakened by infection with PEV2 and PEV3, it is possible that the fungicide sensitivity was increased due to increased uptake of the fungicide from the media.

In contrast, high titers of PEV2 and PEV3 resulted in lower sensitivity to metalaxyl (**Figure 8**, **Table 5**, and **Supplementary Table 6**). Metalaxyl is an acylalanine fungicide that functions systemically. It inhibits RNA polymerase I, the uptake of uridine into RNA, and the synthesis of RNA, DNA, and lipids. It affects all developmental stages of the host oomycete including hyphal growth, haustorium formation, and zoosporangium formation (Gisi and Sierotzki, 2015). A possible explanation for the decreased sensitivity to metalaxyl in the high-titer isolates is that the RdRp activities of PEV2 and PEV3 complemented the RNA polymerase I activity of the host during metalaxyl treatment. Suppression of ribosomal RNA synthesis in the host oomycete may make it easier for these endornaviruses to use the RNA substrates. Alternatively, it is also possible that these endornaviruses may autolyze to supply substrates for RNA synthesis by the host oomycete.

It is rare to find such contrasting effects of different fungicides, and it will be interesting to unveil the mechanisms that explain the differences in our results between metalaxyl and the other three fungicides used in this study. To date, few studies have investigated the effects of mycoviruses on host sensitivity to fungicides. It was reported that when Penicillium digitatum polymycovirus 1 (PdPmV1) and Penicillium digitatum Narna-like virus 1 (PdNLV1) co-infected *Penicillium digitatum*, the host showed increased sensitivity to prochloraz (Niu et al., 2018). It may be necessary to consider the presence of viruses in host organisms when examining fungicide sensitivities.

Similar to the case with benthiavalicarb-isopropyl, the high titers of PEV2 and PEV3 resulted in higher sensitivity to famoxadone, an inhibitor of mitochondrial respiration (**Figure 7** and **Table 4**). In this experiment, PG, an inhibitor of cyanide-insensitive alternative oxidase (AOX), was added to the media (Hollomon et al., 2005; Ishii et al., 2009). We found that the high-titer infection of PEV2 and PEV3 conferred increased sensitivity to PG alone (**Figure 7** left panels and **Supplementary Table 8**). AOX is a ubiquinol oxidase that exists on the matrix side of the inner mitochondrial membrane. It is generally present in plants and has also been found broadly in fungi, protozoa, and other lower eukaryotes (Moore et al., 2013). In the future, we would like to investigate the potential mechanisms by which endornaviruses affect the PG sensitivity of AOX in host oomycetes.

In this study, we compared high- and low-titer isolates to evaluate the effects of PEV2 and PEV3 infection on the growth, development, and fungicide sensitivities of the *Phytophthora* sp. isolates from asparagus. Ideally, an isolate with no virus present would have been a better control than the low-titer isolate, however, complete curing of PEV2 and PEV3 appears to be difficult. In addition to the monozoospore isolations described here, we attempted to obtain endornavirus-free clones derived from the low-titer isolate CH98ASP059-L by using the hyphal breakage method (Kim et al., 2012). We assessed 102 single zoospore isolates and 30 colony isolates but found no virus-free clones (data not shown). We also investigated about 30 colony isolates after protoplastization but again, endornaviruses-free hyphae were not obtained (data not shown). The highly efficient vertical transmission of PEV2 and PEV3 via zoospores is reminiscent of the high efficiency of seed transmission of the plant endornaviruses. For example, Oryza sativa endornavirus (OsEV) is mostly localized in the cytoplasm, but seed transmission rates through eggs or pollen were almost 100% (Moriyama et al., 1996). The highly efficient transmission of the endornaviruses during vegetative growth seems to be related to the intracellular localization of the endornaviruses. In interspecific hybrids between OsEV-infected *Oryza sativa* and *Oryza rufipogon*, or in hybrids between the *japonica* and *indica* varieties of *O. sativa*, some F2 individuals were OsEV-free, and this was inherited in a non-Mendelian fashion (Moriyama et al., 1999a,b; Horiuchi et al., 2003). Given these findings with plant endornaviruses, it may be possible to isolate virus-free variants of the *Phytophthora* sp. isolates from asparagus by creating interspecific hybrid cells. This may be achieved by hyphal or protoplast fusion.

DATA AVAILABILITY STATEMENT

The datasets generated for this study can be found in online repositories. The names of the repository/repositories and accession number(s) can be found in the article/ **Supplementary Material**.

AUTHOR CONTRIBUTIONS

SU collected the materials. KU, KS, and AI performed the experiments with academic and technical assistance from KK,

TA, TF, and SU. RO, YT, YK, TO, and TM contributed to the DNA sequencing experiments and phylogenetical analyses. KU and HM analyzed the data and wrote the first draft of the manuscript. All authors critically reviewed the manuscript and approved the final submission.

FUNDING

This work was supported by a Grant-in-Aid for Challenging Exploratory Research from the Japan Society for the Promotion of Science (19K05946 and 18H02245 to HM).

ACKNOWLEDGMENTS

We would like to express our gratitude to emeritus Professor Tohru Teraoka, Tokyo University of Agriculture and Technology, for giving us helpful advice.

SUPPLEMENTARY MATERIAL

The Supplementary Material for this article can be found online at: https://www.frontiersin.org/articles/10.3389/fmicb.2021.633502/full#supplementary-material

REFERENCES

Adams, M. J., Lefkowitz, E. J., King, A. M. Q., Harrach, B., Harrison, R. L., Knowles, N. J., et al. (2017). Changes to taxonomy and the international code of virus classification and nomenclature ratified by the international committee on taxonomy of viruses. *Arch. Virol.* 162, 2505–2538. doi: 10.1007/s00705-017-3358-5

Aoki, N., Moriyama, H., Kodama, M., Arie, T., Teraoka, T., and Fukuhara, T. (2009). A novel mycovirus associated with four double-stranded RNAs affects host fungal growth in *Alternaria alternate*. *Virus Res.* 140, 179–187. doi: 10.1016/j.virusres.2008.12.003

Aragon-Caballero, L. M., Hurtado-Gonzales, O. P., Flores-Torres, J. G., Apaza-Tapia, W., and Lamour, K. H. (2008). First report of *Phytophthora nicotianae* causing asparagus spear and root rot in peru. *Plant Dis.* 92, 982.2–982.2. doi: 10.1094/PDIS-92-6-0982B

Ark, P. A., and Barret, J. T. (1938). Phytophthora rot of asparagus in California. *Phytopathology* 28, 754–756.

Blair, J. E., Coffey, M. D., Park, S.-Y., Geiser, D. M., and Kang, S. (2008). A multi-locus phylogeny for *Phytophthora* utilizing markers derived from complete genome sequences. *Fungal Genet. Biol.* 45, 266–277. doi: 10.1016/j.fgb.2007.10.010

Cai, G., Krychiw, J. F., Myers, K., Fry, W. E., and Hillman, B. I. (2013). A new virus from the plant pathogenic oomycete *Phytophthora infestans* with an 8 kb dsRNA genome: the sixth member of a proposed new virusgenus. *Virology* 435, 341–349. doi: 10.1016/j.virol.2012.10.012

Cai, G., Myers, K., Fry, W. E., and Hillman, B. I. (2012). A member of the virus family Narnaviridae from the plant pathogenic oomycete *Phytophthora infestans*. *Arch. Virol.* 157, 165–169. doi: 10.1007/s00705-011-1126-5

Cai, G., Myers, K., Fry, W. E., and Hillman, B. I. (2019). Phytophthora infestans RNA virus 2, a novel RNA virus from *Phytophthora infestans*, does not belong to any known virus group. *Arch. Virol.* 164, 567–572. doi: 10.1007/s00705-018-4050-0

Cai, G., Myers, K., Hillman, B. I., and Fry, W. E. (2009). A novel virus of the late bligt pathogen, *Phytophthora infestans*, with two RNA segments and a supergroup 1 RNA-dependent RNA polymerase. *Virology* 392, 52–61. doi: 10.1016/j.virol.2009.06.040

Cavalier-Smith, T., and Chao, E. E.-Y. (2006). Phylogeny and megasystematics of phagotrophic heterokonts (kingdom Chromista). *J. Mol. Evol.* 62, 388–420. doi: 10.1007/s00239-004-0353-8

Cooke, D. E., Drenth, A., Duncan, J. M., Wagels, G., and Brasier, C. M. (2000). A molecular phylogeny of phytophthora and related oomycetes. *Fungal Genet. Biol.* 30, 17–32. doi: 10.1006/fgbi.2000.1202

Coutts, R. H. A. (2005). First report of an endornavirus in the Cucurbitaceae. *Virus Genes*. 31, 361–362. doi: 10.1007/s11262-005-3255-y

Crous, P. W., Summerell, B. A., Shivas, R. G., Burgess, T. I., Decock, C. A., Dreyer, L. L., et al. (2012). Fungal planet description sheets: 107-127. *Persoonia* 28, 138–182. doi: 10.3767/003158512X652633

Falloon, P. G. (1982). Baiting, pathogenicity and distribution of *Phytophthora megasperma* var. *sojae* in New Zealand asparagus soils. *N. Z. J. Agric. Res.* 25, 425–429. doi: 10.1080/00288233.1982.10417907

Frohman, M. A., Dush, M. K., and Martin, G. R. (1988). Rapid production of full-length cDNAs from rare transcripts: amplification using a single gene-specific oligonucleotide primer. *Proc. Natl. Acad. Sci. U.S.A.* 85, 8998–9002. doi: 10.1073/pnas.85.23.8998

Fukuhara, T., Koga, R., Aoki, N., Yuki, C., Yamamoto, N., Oyama, N., et al. (2006). The wide distribution of endornaviruses, large double-stranded RNA replicons with plasmid-like properties. *Arch. Virol.* 151, 995–1002. doi: 10.1007/s00705-005-0688-5

Ghabrial, S. A., Castón, J. R., Jiang, D., Nibert, M. L., and Suzuki, N. (2015). 50-plus years of fungal viruses. *Virology* 356, 479–480. doi: 10.1016/j.virol.2015.02.034

Ghabrial, S. A., and Suzuki, N. (2009). Viruses of plant pathogenic fungi. *Annu. Rev. Phytopathol.* 47, 353–384. doi: 10.1146/annurev-phyto-080508-081932

Gisi, U., and Sierotzki, H. (2015). "Oomycete fungicides: phenylamides, quinone outside inhibitors, and carboxylic acid amides," in *Fungicide Resistance in Plant Pathogens*, eds H. Ishii and D. Hollomon (Tokyo: Springer), 145–174. doi: 10.1007/978-4-431-55642-8_10

Grasse, W., Zipper, R., Totska, M., and Spring, O. (2013). *Plasmopara halstedii* virus causes hypovirulence in *Plasmopara halstedii*, the downy mildew pathogen of the sunflower. *Fungal Genet. Biol.* 57, 42–47. doi: 10.1016/j.fgb.2013.05.009

Grill, L. K., and Garger, S. J. (1981). Identification and characterization of double-stranded RNA associated with cytoplasmic male sterility in *Vicia faba*. *Proc. Natl. Acad. Sci. U.S.A.* 78, 7043–7046. doi: 10.1073/pnas.78.11.7043

Guindon, S., Dufayard, J.-F., Lefort, V., Anisimova, M., Hordijk, W., and Gascuel, O. (2010). New algorithms and methods to estimate maximum-likelihood phylogenies: assessing the performance of PhyML 3.0. *Syst. Biol.* 3, 307–321. doi: 10.1093/sysbio/syq010

Hacker, C. V., Brasier, C. M., and Buck, K. W. (2005). A double-stranded RNA from a *Phytophthora* species is related to the plant endornaviruses and contains a putative UDP glycosyltransferase gene. *J. Gen. Virol.* 86, 1561–1570. doi: 10.1099/vir.0.80808-0

Hendrix, J. W. (1970). Sterols in growth and reproduction of fungi. *Annu. Rev. Phytopathol.* 8, 111–130. doi: 10.1146/annurev.py.08.090170.000551

Hollomon, D. W., Wood, P. M., Reeve, C., and Miguez, M. (2005). "Alternative oxidase and its impact on the activity of Qo and Qi site inhibitors," in *Modern Fungicides and Antifungal Compounds IV*, eds H. W. Dehne, U. Gisi, K. H. Kuck, P. E. Russell, and H. Lyr (Alton: BCPC), 31–34.

Horiuchi, H., Moriyama, H., and Fukuhara, T. (2003). Inheritance of *Oryza sativa* endornavirus in F1 and F2 hybrids between japonica and indica rice. *Genes Genet. Syst.* 78, 229–234. doi: 10.1266/ggs.78.229

Ikeda, K. I., Nakamura, H., and Matsumoto, N. (2003). Hypovirulent strain of the violet root rot fungus *Helicobasidium mompa*. *J. Gen. Plant Pathol.* 69, 385–390. doi: 10.1007/s10327-003-0076-5

Ishii, H., Fountaine, J., Chung, W.-H., Kansako, M., Nishimura, K., Takahashi, K., et al. (2009). Characterisation of QoI-resistant field isolates of *Botrytis cinerea* from citrus and strawberry. *Pest Manag. Sci.* 65, 916–922. doi: 10.1002/ps.1773

Kim, J.-X., Jung, J.-E., Park, J.-A., Park, S.-M., Cha, B.-J., and Dae-Hyuk Kim, D.-H. (2012). Biological function of a novel chrysovirus, CnV1-BS122, in the Korean Cryphonectria nitschkei BS122 strain. *J. Biosci. Bioeng.* 115, 1–3. doi: 10.1016/j.jbiosc.2012.08.007

Kliejunas, J. T., and Ko, W. H. (1974). Effect of motility of *Phytophthora palmivora* zoospores on disease severity in Papaya seedlings and substrate colonization in soil. *Phytopathology* 64, 426–428. doi: 10.1094/phyto-64-426

Ko, W. H., and Chan, M. J. (1974). Infection and colonization potential of sporangia, zoospores, and chlamydospores of phytophthora palmivora in soil. *Phytopathology* 64, 1307–1309. doi: 10.1094/Phyto-64-1307

Kodama, F., Sonoda, T., Kawamura, T., Okada, T., Fujii, N., Nara, C., et al. (2015). First report of blight disease of asparagus by *Phytophthora* sp. in clade 6 in Japan. *Plant Dis.* 99:1857. doi: 10.1094/PDIS-02-15-0210-PDN

Komatsu, K., Katayama, Y., Omatsu, T., Mizutani, T., Fukuhara, T., Kodama, M., et al. (2016). Genome sequence of a novel mitovirus identified in the phytopathogenic fungus Alternaria arborescens. *Arch Virol*. 161, 2627–2631. doi: 10.1007/s00705-016-2953-1

Kozlakidis, Z., Brown, N. A., Jamal, A., Phoon, X., and Coutts, R. H. A. (2010). Incidence of endornaviruses in *Phytophthora* taxon douglasfir and *Phytophthora ramorum*. *Virus Genes* 40, 130–134. doi: 10.1007/s11262-009-0421-7

Larkin, M. A., Blackshields, G., Brown, N. P., Chenna, R., McGettigan, P. A., McWilliam, H., et al. (2007). Clustal W and Clustal X version 2.0. *Bioinformatics* 23, 2947–2948. doi: 10.1093/bioinformatics/btm404

Le, S. Q., and Gascuel, O. (2008). An improved general amino acid replacement matrix. *Mol. Biol. Evol.* 25, 1307–1320. doi: 10.1093/molbev/msn067

Lefebvre, A., Scalla, R., and Pfeiffer, P. (1990). The double-stranded RNA associated with the '447' cytoplasmic male sterility in *Vicia faba* is packaged together with its replicase in cytoplasmic membranous vesicles. *Plant Mol. Biol*. 14, 477–490. doi: 10.1007/BF00027494

Mackenzie, S. A., Pring, D. R., and Bassett, M. J. (1988). Large doublestranded RNA molecules in *Phaseolus vulgaris* L. are not associated with cytoplasmic male sterility. *Theor. Appl. Genet*. 76, 59–63. doi: 10.1007/BF00288832

Marchler-Bauer, A., Bo, Y., Han, L., He, J., Lanczycki, C. J., Lu, S., et al. (2017). CDD/SPARCLE: functional classification of proteins via subfamily domain architectures. *Nucleic Acids Res.* 45, D200–D203. doi: 10.1093/nar/gkw1129

Marzano, S. L., Nelson, B. D., Ajayi-Oyetunde, O., Bradley, C. A., Hughes, T. J., Hartman, G. L., et al. (2016). Identification of diverse mycoviruses through metatranscriptomics characterization of the viromes of five major fungal plant pathogens. *J. Virol*. 90, 6846–6863. doi: 10.1128/JVI.00357-16

Moore, A. L., Shiba, T., Young, L., Harada, S., Kita, K., and Ito, K. (2013). Unraveling the heater: new insights into the structure of the alternative oxidase. *Annu. Rev. Plant Biol*. 64, 637–663. doi: 10.1146/annurev-arplant-042811-105432

Moriyama, H., Horiuchi, H., Koga, R., and Fukuhara, T. (1999a). Molecular characterization of two endogenous double-stranded RNAs in rice and their inheritance by interspecific hybrids. *J. Biol. Chem.* 274, 6882–6888. doi: 10.1074/jbc.274.11.6882

Moriyama, H., Horiuchi, H., Nitta, T., and Fukuhara, T. (1999b). Unusual inheritance of evolutionarily-related double-stranded RNAs in interspecific hybrid between rice plants *Oryza sativa* and *Oryza rufipogon*. *Plant Mol. Biol.* 39, 1127–1136. doi: 10.1023/a:1006118304093

Moriyama, H., Kanaya, K., Wang, J. Z., Nitta, T., and Fukuhara, T. (1996). Stringently and developmentally regulated levels of a cytoplasmic double-stranded RNA and its high-efficiency transmission via egg and pollen in rice. *Plant Mol. Biol*. 31, 713–719. doi: 10.1007/BF00019459

Moriyama, H., Nitta, T., and Fukuhara, T. (1995). Double-stranded RNA in rice: a novel RNA replicon in plants. *Mol. Gen. Genet.* 248, 364–369. doi: 10.1007/BF02191603

Niu, Y., Yuan, Y., Mao, J., Yang, Z., Cao, Q., Zhang, T., et al. (2018). Characterization of two novel mycoviruses from *Penicillium digitatum* and the related fungicide resistance analysis. *Sci. Rep*. 8:5513. doi: 10.1038/s41598-018-23807-3

Nuss, D. L. (2005). Hypovirulence: mycoviruses at the fungal-plant interface. *Nat. Rev. Microbiol*. 3, 632–642. doi: 10.1038/nrmicro1206

Okada, R., Alcalá-Briseño, I. R., Escalante, C., Sabanadzovic, S., Rodrigo, A., and Valverde, R. A. (2018). Genomic sequence of a novel endornavirus from *Phaseolus vulgaris* and occurrence in mixed infections with two other endornaviruses. *Virus Res.* 257, 63–67. doi: 10.1016/j.virusres.2018.09.005

Okada, R., Kiyota, E., Moriyama, H., Fukuhara, T., and Natsuaki, T. (2015). A simple and rapid method to purify viral dsRNA from plant and fungal tissue. *J. Gen. Plant Pathol.* 81, 103–107. doi: 10.1007/s10327-014-0575-6

Okada, R., Yong, C. K., Valverde, R. A., Sabanadzovic, S., Aoki, N., Hotate, S., et al. (2013). Molecular characterization of two evolutionarily distinct endornaviruses co-infecting common bean (*Phaseolus vulgaris*). *J. Gen. Virol.* 94, 220–229. doi: 10.1099/vir.0.044487-0

Ong, J. W. L., Li, H., Sivasithamparam, K., Dixon, K. W., Jones, M. G. K., and Wylie, S. J. (2016). Novel endorna-like viruses, including three with two open reading frames, challenge the membership criteria and taxonomy of the Endornaviridae. *Virology* 499, 203–211. doi: 10.1016/j.virol.2016.08.019

Osaki, H., Nakamura, H., Sasaki, A., Matsumoto, N., and Yoshida, K. (2006). An endornavirus from a hypovirulent strain of the violet root rot fungus, *Helicobasidium mompa*. *Virus Res*. 118, 143–149. doi: 10.1016/j.virusres.2005.12.004

Pearson, M. N., Beever, R. E., Boine, B., and Arthur, K. (2009). Mycoviruses of filamentous fungi and their relevance to plant pathology. *Mol. Plant Pathol*. 10, 115–128. doi: 10.1111/j.1364-3703.2008.00503.x

Pfeiffer, P. (1998). Nucleotide sequence, genetic organization and expression strategy of the double-stranded RNA associated with the '447'cytoplasmic male sterility in *Vicia faba*. *J. Gen. Virol*. 79, 2349–2358. doi: 10.1099/0022-1317-79-10-2349

Pfeiffer, P., Jung, J. L., Heitzler, J., and Keith, G. (1993). Unusual structure of the double-stranded RNA associated with the '447'cytoplasmic male sterility in *Vicia faba*. *J. Gen. Virol*. 74, 1167–1173. doi: 10.1099/0022-1317-74-6-1167

Saude, C., Hurtado-Gonzales, O. P., Lamour, K. H., and Hausbeck, M. K. (2008). Occurrence and characterization of a *Phytophthora* sp. pathogenic to asparagus (*Asparagus officinalis*) in Michigan. *Phytopathology* 98, 1075–1083. doi: 10.1094/PHYTO-98-10-1075

Stöver, B. C., and Müller, K. F. (2010). TreeGraph 2: combining and visualizing evidence from different phylogenetic analyses. *BMC Bioinformatics* 5:7. doi: 10.1186/1471-2105-11-7

Tamura, K., Stecher, G., Peterson, D., Filipski, A., and Kumar, S. (2013). MEGA6: molecular evolutionary genetics analysis version 6.0. *Mol. Biol. Evol*. 30, 2725–2729. doi: 10.1093/molbev/mst197

Thompson, J. D., Gibson, T. J., Plewniak, F., Jeanmougin, F., and Higgins, D. G. (1997). The CLUSTAL_X windows interface: flexible strategies for multiple sequence alignment aided by quality analysis tools. *Nucleic Acids Res*. 25, 4876–4882. doi: 10.1093/nar/25.24.4876

Tokunaga, T., and Bartnicki-Garcia, S. (1971). Cyst wall formation and endogenous carbohy drate utilization during synchronous encystment of *Phytophthora palmivora* zoospores. *Arch. Mikrobiol*. 79, 283–292. doi: 10.1007/BF00424905

Tuomivirta, T. T., Kaitera, J., and Hantula, J. (2009). A novel putative virus of *Gremmeniella abietina* type B (Ascomycota: helotiaceae) has a composite genome with endornavirus affinities. *J. Gen. Virol*. 90, 2299–2305. doi: 10.1099/vir.0.011973-0

Turpen, T., Garger, S. J., and Grill, L. K. (1988). On the mechanism of cytoplasmic male sterility in the 447 line of Vicia faba. *Plant Mol. Biol*. 10, 489–497. doi: 10.1007/BF00033604

Valverde, R. A., and Gutierrez, D. L. (2007). Transmission of a dsRNA in bell pepper and evidence that it consists of the genome of an endornavirus. *Virus Genes* 35, 399–403. doi: 10.1007/s11262-007-0092-1

Valverde, R. A., Khalifa, M. E., Okada, R., Fukuhara, T., and Sabanadzovic, S. (2019). ICTV virus taxonomy profile: *Endornaviridae*. *J. Gen. Virol*. 100, 1204–1205. doi: 10.1099/jgv.0.001277

Wakarchuk, D. A., and Hamilton, R. I. (1985). Cellular double-stranded RNA in *Phaseolus vulgaris*. *Plant Mol. Biol*. 5, 55–63. doi: 10.1007/BF00017873

Wakarchuk, D. A., and Hamilton, R. I. (1990). Partial nucleotide sequence from enigmatic dsRNAs in *Phaseolus vulgaris*. *Plant Mol. Biol*. 14, 637–639. doi: 10.1007/BF00027512

Webster, J., and Weber, R. W. S. (2007). *Introduction to Fungi*. Cambridge: Cambridge University Press, 841.

Xie, J., and Jiang, D. (2014). New insights into mycoviruses and exploration for the biological control of crop fungal diseases. *Annu. Rev. Phytopathol*. 52, 45–68. doi: 10.1146/annurev-phyto-102313-050222

Yang, D., Wu, M., Zhang, J., Chen, W., Li, G., and Yang, L. (2018). Sclerotinia minor endornavirus 1, a novel pathogenicity debilitation-associated mycovirus with a wide spectrum of horizontal transmissibility. *Viruses* 27:589. doi: 10.3390/v10110589

Conflict of Interest: The authors declare that the research was conducted in the absence of any commercial or financial relationships that could be construed as a potential conflict of interest.

frontiers in Microbiology

ORIGINAL RESEARCH
published: 11 February 2021
doi: 10.3389/fmicb.2021.622261

A Phenome-Wide Association Study of the Effects of *Fusarium graminearum* Transcription Factors on Fusarium Graminearum Virus 1 Infection

Jisuk Yu[1] *and Kook-Hyung Kim*[1,2,3]*

[1] *Plant Genomics and Breeding Institute, Seoul National University, Seoul, South Korea,* [2] *Department of Agricultural Biotechnology, College of Agriculture and Life Sciences, Seoul, South Korea,* [3] *Research Institute of Agriculture and Life Sciences, Seoul National University, Seoul, South Korea*

OPEN ACCESS

Edited by:
Eeva Johanna Vainio, Natural Resources Institute Finland (Luke), Finland

Reviewed by:
Hideki Kondo, Okayama University, Japan
Shin-Yi Lee Marzano, Agricultural Research Service, United States Department of Agriculture, United States

***Correspondence:**
Kook-Hyung Kim
kookkim@snu.ac.kr

Specialty section:
This article was submitted to Microbe and Virus Interactions with Plants, a section of the journal Frontiers in Microbiology

Received: *29 October 2020*
Accepted: *07 January 2021*
Published: *11 February 2021*

Citation:
Yu J and Kim K-H (2021) A Phenome-Wide Association Study of the Effects of Fusarium graminearum Transcription Factors on Fusarium Graminearum Virus 1 Infection. Front. Microbiol. 12:622261. doi: 10.3389/fmicb.2021.622261

The Fusarium graminearum virus 1 (FgV1) causes noticeable phenotypic changes such as reduced mycelial growth, increase pigmentation, and reduced pathogenicity in its host fungi, *Fusarium graminearum*. Previous study showed that the numerous *F. graminearum* genes including regulatory factors were differentially expressed upon FgV1 infection, however, we have limited knowledge on the effect(s) of specific transcription factor (TF) during FgV1 infection in host fungus. Using gene-deletion mutant library of 657 putative TFs in *F. graminearum*, we transferred FgV1 by hyphal anastomosis to screen transcription factors that might be associated with viral replication or symptom induction. FgV1-infected TF deletion mutants were divided into three groups according to the mycelial growth phenotype compare to the FgV1-infected wild-type strain (WT-VI). The FgV1-infected TF deletion mutants in Group 1 exhibited slow or weak mycelial growth compare to that of WT-VI on complete medium at 5 dpi. In contrast, Group 3 consists of virus-infected TF deletion mutants showing faster mycelial growth and mild symptom compared to that of WT-VI. The hyphal growth of FgV1-infected TF deletion mutants in Group 2 was not significantly different from that of WT-VI. We speculated that differences of mycelial growth among the FgV1-infected TF deletion mutant groups might be related with the level of FgV1 RNA accumulations in infected host fungi. By conducting real-time quantitative reverse transcription polymerase chain reaction, we observed close association between FgV1 RNA accumulation and phenotypic differences of FgV1-infected TF deletion mutants in each group, i.e., increased and decreased dsRNA accumulation in Group 1 and Group 3, respectively. Taken together, our analysis provides an opportunity to identify host's regulator(s) of FgV1-triggered signaling and antiviral responses and helps to understand complex regulatory networks between FgV1 and *F. graminearum* interaction.

Keywords: *Fusarium graminearum*, transcription factor, mycovirus, FgV1, phenome

INTRODUCTION

Virus divert many cellular resources to produce virus-specific components and counteract to host defense responses during virus infection (Carrera and Elena, 2012). This virus-host interaction often leads to the expression of disease symptoms in the host by triggering physiological alteration and modifying cytoskeleton or membrane structures (Osterbaan and Fuchs, 2019).

Transcription factors (TFs) are DNA-binding proteins responsible for modulating gene regulatory systems by cooperating with a range of proteins, including other upstream or downstream TFs, transcription initiation complex, and epigenetic regulators (Spitz and Furlong, 2012; Shelest, 2017; Mitsis et al., 2020). During virus-host interaction, TFs are directly or indirectly regulate defense response by activation or repression of downstream signaling pathways (Alves et al., 2014). In plant, members of TF families belonging to WRKY family, myeloblastosis related proteins (MYB), basic leucine zipper (bZIP), APETELA2/Ethylene-Responsive Factor (AP2/ERF) family, and NAC transcription factors have been shown to be associated with defense response against plant viruses as well as abiotic stress responses (Alves et al., 2014; Ng et al., 2018).

A filamentous fungus *Fusarium graminearum* causes Fusarium head blight of major cereal crops, such as wheat, barley, and rice (Dweba et al., 2017). *Fusarium* species also produce mycotoxins such as deoxynivalenol (DON), nivalenol, and zearalenone that are considered threat to the animals and human health (Ferrigo et al., 2016). Since the report of the complete genome sequence of *F. graminearum*, many researchers have attempt to characterize function(s) of TFs and their target genes in gene regulatory network using diverse computational and experimental approaches (Son et al., 2011; Liu et al., 2019; Guo et al., 2020). Systematic loss-of function studies and transcriptomic studies under comparable condition provide new insights into the role of TFs in complex regulatory networks for mycotoxin biosynthesis, sexual development, and virulence in *F. graminearum* (Son et al., 2011; Kim et al., 2015; Kazan and Gardiner, 2018; Chen Y. et al., 2019; Guo et al., 2020). Their interconnection and specific roles on signaling pathways, however, are largely unknown. In previous study, to determine the functions and interconnectedness of individual TFs, the gene-disruption library of 657 potential TF genes in *F. graminearum* was constructed and analyzed (Son et al., 2011). Each of TF deletion mutant was categorized by phenotypic characteristics, such as mycelial growth, sexual and asexual developments, virulence, toxin production, and stress responses (Son et al., 2011).

Fusarium graminearum virus 1 (FgV1) is a single-stranded RNA (ssRNA) virus and closely related to the proposed family "*Fusariviridae*" (Kwon et al., 2007; Honda et al., 2020). FgV1 infection causes remarkable phenotypic change such as reduced growth rate, increased pigmentation, reduced mycotoxin synthesis, reduced pathogenicity, and defects in sexual development in *F. graminearum* (Chu et al., 2002; Lee et al., 2014). Previous literature review provides a summary of fungal host proteins that might be associated with FgV1 accumulation, mycovirus transmission, and symptom development in *F. graminearum* (Yu and Kim, 2020). FgHex1 that functions in the maintenance of cellular integrity enhances the FgV1 RNA synthesis by binding to the FgV1 genomic RNA (Son et al., 2016b). FgHal2 is required for the vegetative growth and methionine biosynthesis of *F. graminearum* and *FgHal2* gene deletion reduces FgV1 RNA accumulation and vertical transmission of virus (Yu et al., 2015; Yun et al., 2015). Transcriptional reduction of *FgSWI6*, encoding possible transcription cofactor in *F. gramimearum*, following FgV1 infection might be related to the changes of fungal host colony morphology caused by FgV1 infection (Son et al., 2016c). However, these studies focused on biological functions of individual components, and specific biological processes and pathways remains elusive. Using transcriptomic analysis, we previously demonstrated that numerous *F. graminearum* genes including transcription factors were differentially expressed upon FgV1 infection (Lee et al., 2014). Recent study reported that FgV1 protein pORF2 could inhibit transcriptional induction of *FgDICER* and *FgAGO* genes to counteract host's antiviral RNA silencing response (Yu et al., 2020). This previous study proposed that FgV1 might be able to affect gene regulatory networks directly or indirectly, which lead to pleiotropic phenotypes on the presence of significant amount of viral RNA in fungal host.

Here, to gain new insights on the role(s) of host transcription factors that might be associated with viral RNA replication or symptom development following FgV1 infection, we transferred FgV1 to gene-deletion mutant library of 657 putative TFs in *F. graminearum*. Based on this library, we analyzed phenotype of virus-infected mutants and the relationship between FgV1 RNA accumulation and phenotypic differences of FgV1-infected TF deletion mutants. To our knowledge, this is the first description of phenome-based association study in characterizing effects of *Fusarium graminearum* transcription factors on FgV1 infection.

MATERIALS AND METHODS

Fungal Strains and Growth Condition

Fusarium graminearum GZ03639 WT strain and 657 TF deletion mutant library were provided by the Center for Fungal Genetic Resources (Seoul, South Korea). All fungal isolates were stored in 20% (v/v) glycerol at −80°C and TF deletion mutants were reactivated at 25°C on potato dextrose agar (PDA) with geneticin (50 μg/ml). TF deletion mutants were subcultured on complete medium (CM) agar containing geneticin for further experiment. Fungal colonies incubated on CM agar at 25°C for 120 h were photographed. Fungal cultures used for extraction of RNA were prepared as previously described (Lee et al., 2014). Briefly, freshly grown mycelia was inoculated into CM broth, and the cultures were incubated at 25°C for 120 h. Hyphae were collected by filtering through 3 MM paper followed by washing with distilled water, dried by blotting mycelia between paper towels, and frozen at −80°C.

Virus Transmission

FgV1-infected *F. graminearum* GZ03639 (WT-VI) was generated by using protoplast fusion method (Lee et al., 2011). We confirmed FgV1 infection by total RNA extraction and reverse transcription polymerase chain reaction (RT-PCR) using virus specific primer pair and selected WT-VI as positive control for further experiments. FgV1 was introduced into TF deletion mutant by hyphal anastomosis between WT-VI and TF deletion mutant library. An agar block of WT-VI and individual TF deletion mutant strain was placed on CM agar media and incubated at 25°C for 4 days. Overlapped region of two fungal strains were isolated, transferred to CM agar contained geneticin (50 μg/ml), and subcultured twice to eliminate unstable virus-infected colony. Multiple replicates of all virus-infected mutant strains have obtained. After virus transmission has failed during at least three times repetition, we determined these TF deletion mutant strains as non-transmissible *via* hyphal anastomosis.

Measurement of Mycelial Growth

For phenotype analysis, virus-infected TF deletion mutants were photographed after 5 days of cultivation (**Supplementary Figure 1**). Radial growth of mycelia from the inoculum was measured using ImageJ software (Schneider et al., 2012). The TF deletion mutants that showed reduced mycelial growth after gene deletion was also assessed (**Supplementary Table 1**).

Preparation of Total RNA Samples and cDNA Synthesis

For nucleic acid extraction, frozen mycelia were pulverized using liquid nitrogen and a mortar and pestle. Total RNAs were extracted with RNAiso Plus reagent (Takara Bio, Shiga, Japan) followed by treatment with *DNase*I (Takara Bio) to remove genomic DNA according to the manufacturer's instructions. As described previously, 4 M LiCl was added to total RNA extract to a final concentration of 2 M to isolate ssRNA fraction (Yu et al., 2018). Samples were then incubated at −20°C for 2 h, ssRNA pellets were washed in 75% ethanol and suspended in RNase-free water. Next, 3 μg of ssRNA of each sample was used to synthesize first-strand cDNA with an oligo $(dT)_{18}$ primer and GoScript™ reverse transcriptase (Promega, Madison, WI, United States) according to the manufacturer's protocols. All synthesized cDNAs were diluted to 20 ng of mixture with nuclease-free water.

Real-Time RT-PCR Analysis

Real-time quantitative RT-PCR (qRT-PCR) was performed with a Bio-Rad CFX384™ Real-time PCR system using gene-specific internal primers as described previously with slight modification (Yu et al., 2018). Each reaction mix (10 μl) consisted of 20 ng of cDNA, 5 μl of 2 X iQ™SYBR® Green Supermix (Bio-Rad, Hercules, CA, United States), and 10 pmoles of each primer. The thermal profile was as follows: 3 min at 95°C and 40 cycles of 10 s at 95°C, 30 s at 59°C, and melting curve data obtained by increasing the temperature from 55 to 95°C. Two endogenous reference genes, i.e., ubiquitin C-terminal hydrolase (*UBH*, locus FGSG_01231) and elongation factor 1α (*EF1α*, locus FGSG_08811), were used as internal controls to normalize qRT-PCR results. Data were analyzed using the Bio-Rad CFX Manager V1.6.541.1028 software (Bio-Rad). RNA samples were extracted from at least two independent, biologically replicated experiments, and each PCR product was evaluated in at least three independent experiments, including three technical replicates. All primer sets used in this study are listed in **Supplementary Table 2**.

Viral dsRNA Confirmation and Semi-Quantification

Three micrograms of *DNase*I-treated total RNAs from all virus-infected TF deletion mutants were treated by 30 units of S1 Nuclease (Takara Bio). Samples were loaded into 1% agarose gel for analysis of viral double-stranded (dsRNA) accumulation. After separation on agarose gel, dsRNA was visualized in a UV transilluminator. To measure relative accumulation of FgV1 viral dsRNA in TF deletion mutants, 3 μg of total RNA from all virus-infected mutants were loaded and separated on 1% agarose gel. Ethidium bromide-stained gels were visualized in a UV transilluminator. Band intensity were measured using ImageJ software (Schneider et al., 2012). The relative amount of viral genomic dsRNA was estimated by measuring the amount of FgV1 RNA relative to 18S rRNA.

RESULTS

Phenotype Analysis of FgV1-Infected TF Gene-Deletion Mutants

To investigate the effect of TF genes on FgV1 infection in *F. graminearum*, we transferred FgV1 to putative 657 TF gene deletion mutants. Among 709 TF genes, 657 TF genes were successfully disrupted and other 52 TF genes were excluded due to lethality or technical problem of generation of homologous recombination construct (Son et al., 2011). FgV1 could effectively transmitted by hyphal anastomosis between FgV1-infected strain GZ03639 (WT-VI) strain and virus-free TF deletion mutant strains. Among total of 657 TF deletion mutants, we could not transmit FgV1 onto a 17 TF deletion mutants despite repeated trials (**Table 1** and **Supplementary Table 1**). Representative image of colony morphologies for each FgV1-infected TF deletion mutants (total 640) were shown in **Supplementary Figure 1**. Typically, colony morphology of WT-VI (a FgV1-infected strain) includes irregular colony shape, no aerial mycelium, and dense mycelia with deep red or brown color. Most of FgV1-infected TF deletion mutants showed similar colony morphologies compared to that of WT-VI, but several virus infected fungal colonies showed abnormal colony morphology (e.g., slower or faster mycelial growth, low density and scarce hyphal growth, curly mycelia, aerial mycelia development, and change of pigment production).

FgV1-infected TF deletion mutants were classified into three groups according to the mycelial growth phenotype compared to that of WT-VI or virus-free TF deletion mutant (**Figure 1** and **Table 1**). For this, the mycelial length of WT-VF was set

TABLE 1 | Analysis of FgV1-infected transcription factor deletion mutants.

TF Classification	TF	ΔTF	TF-FgV1	Group[a]		
				1	2	3
bHLH	16	15	15	0	11	4
bZIP	22	22	22	0	21	1
C2H2 zinc finger	98	94	94	5	84	5
Heteromeric CCAAT factors	8	8	8	3	5	0
HMG	37	34	34	3	30	1
Homeodomain-like	14	7	7	1	6	0
Nucleic acid-binding, OB-fold	47	40	40	4	35	1
Winged helix repressor DNA-binding	27	26	26	0	23	3
Helix-turn-helix, AraC type	8	7	7	0	6	1
GATA type zinc finger	8	7	7	0	7	0
Zinc finger, CCHC-type	12	12	12	0	12	0
Zn2Cys6 zinc finger	316	296	286[b]	16	254	16
Myb	19	17	17	1	13	3
Others	77	72	65[b]	2	52	11
Total	709	657	640	35	559	46

[a]*Groups 1–3 were determined by mycelial growth on complete media (CM). Average radial growth on CM of FgV1-infected TF deletion mutants compared to virus-free strain or wild-type (WT) strain (set to a value of 100) was divided as groups (Group 1, less than 33; Group 2, 33–62.9; Group 3, 63–100 of WT strain.*
[b]*Some of TF deletion mutants did not obtain FgV1 through hyphal anastomosis.*

to a value of 100 (±11). Mycelial length of WT-VI decreased to 40–55 (average 47.5 ± 7) compared to that of WT-VF. In case of TF deletion mutant showing growth retardation, this virus-free TF deletion mutant was used as standard to compare FgV1-infected TF mutant. Comparing with each virus-free TF deletion strain or wild-type (WT) strain, we classified Group 1 and 3 of FgV1-infected TF deletion mutants determined by growth under 33 (0–32.9) or over 63 (63–100), respectively. The FgV1-infected TF deletion mutants in Group 1 indicated slow or weak mycelial growth compared to that of WT-VI. Among FgV1-infected TF deletion mutants in Group 2 (mycelial growth, 33–62.9), we could divide them into two subgroups. One showed similar colony morphology of WT-VI while the other subgroup did not follow typical phenotype WT-VI and showed fluffy but low density of mycelia phenotype. In contrast, Group 3 consists of virus-infected TF deletion mutants showing mild symptoms, such as faster mycelial growth and partially restored aerial mycelia formation.

Approximately 88% of FgV1-infected TF deletion mutants (Group 2) showed similar phenotype and mycelial growth regardless of phenotype of virus-free TF gene deletion mutants. Among FgV1-infected TF deletion mutants in Group 3, which growth reduction rate was lower than 10%, colony morphology of most mutants in this group showed recovery phenotype and viral accumulation level was as low as 10% of WT-VI although FgV1 infection might still affect colony morphology. In this regard, comparisons of colony morphology including mycelial growth of TF deletion mutants following hypovirulence-associated FgV1 infection help screening host gene(s) that might attribute or affect development of virus-derived symptom and FgV1 replication. We observed that *F. graminearum* TF candidates belong to the groups of bHLH (basic–helix–loop–helix) motif and heteromeric CCAAT-binding factor showed relatively high phenotypic variation following FgV1 infection compared to that of other TF families (**Table 1**).

TF Factors That Might Be Involved in FgV1-Derived Host Symptom

Previous study analyzed phenotypes of putative 657 TF deletion mutants and divided them based upon their major phenotypic categories such as mycelial growth, sexual development, conidia production, toxin production, and stress responses (Son et al., 2011). This phenome-based analysis demonstrated that fungal virulence, growth, and DON production were highly correlated with sexual development (Son et al., 2011). Because FgV1 infection causes multiple phenotypic alterations, this simultaneous and multiple FgV1-derived symptom might also be consequences of interaction between virus and host factor that have pivotal roles in gene regulatory network. In this regard, we selected 35 TF deletion mutants that exhibit multiple defects in mycelial growth, virulence, sexual development, and toxin production (**Figure 2** and **Supplementary Table 3**; Son et al., 2011). Ten out of 35 selected TF deletion mutants that were not related with environmental stress responses or DNA damages were shown in **Figure 2A**, except *FgNHP6A* (FGSG_00385) deletion mutant that showed pH 4-resistance. Among these 35 TF deletion mutants, most of gene deletion mutants showed decreased mycelial growth compared to WT. Colony morphology of virus-free deletion mutants including *FgSWI6* (FGSG_04220), *FgNOT3* (FGSG_13746), *GzC2H090* (FGSG_10517), *GzWing019* (FGSG_08572), and *FgCrz1A* (FGSG_13711) showed similar phenotypes to those of WT-VI such as reduced aerial mycelia, reduced mycelial growth, and increased pigmentation (**Figure 2A** and **Supplementary Table 1**, compare to WT-VI in **Figure 1**). When we confirmed gene expression level of these five TFs after FgV1 infection by qRT-PCR, those of all five TFs showed decreased level compared to WT-VF (**Supplementary Table 4**). Comparing phenotype changes upon FgV1 infection in Group 1, *GzC2H003* (FGSG_00477) and *FgNHP6A* (FGSG_00385) TF deletion mutants showed slow mycelial growth after FgV1 infection compared to WT-VI (**Figure 2A**, compare to WT-VI in **Figure 1**). On the contrary, mycelial growth in virus-infected TF deletion mutants in Group 3, *FgCrz1A* (FGSG_13711), *GzZC108* (FGSG_08769), *GzMADS003* (FGSG_09339), and *FgStuA* (FGSG_10129) showed little reduction of mycelial growth compared to WT-VI. Six out of those 35 TF deletion mutants including *GzAPSES004* (FGSG_10384) and *FgFSR1* (FGSG_01665) mutants were not able to uptake FgV1 *via* hyphal anastomosis method, this result might be explained as growth defect in those deletion mutants (**Supplementary Figure 1**).

Comparison of Phenotypes Produced in Response to Deletion and FgV1 Infection of the TFs Associated With Environmental Stress Response

TF phenome analysis described phenotypic change under diverse abiotic stresses, including osmotic stress, reactive oxygen species

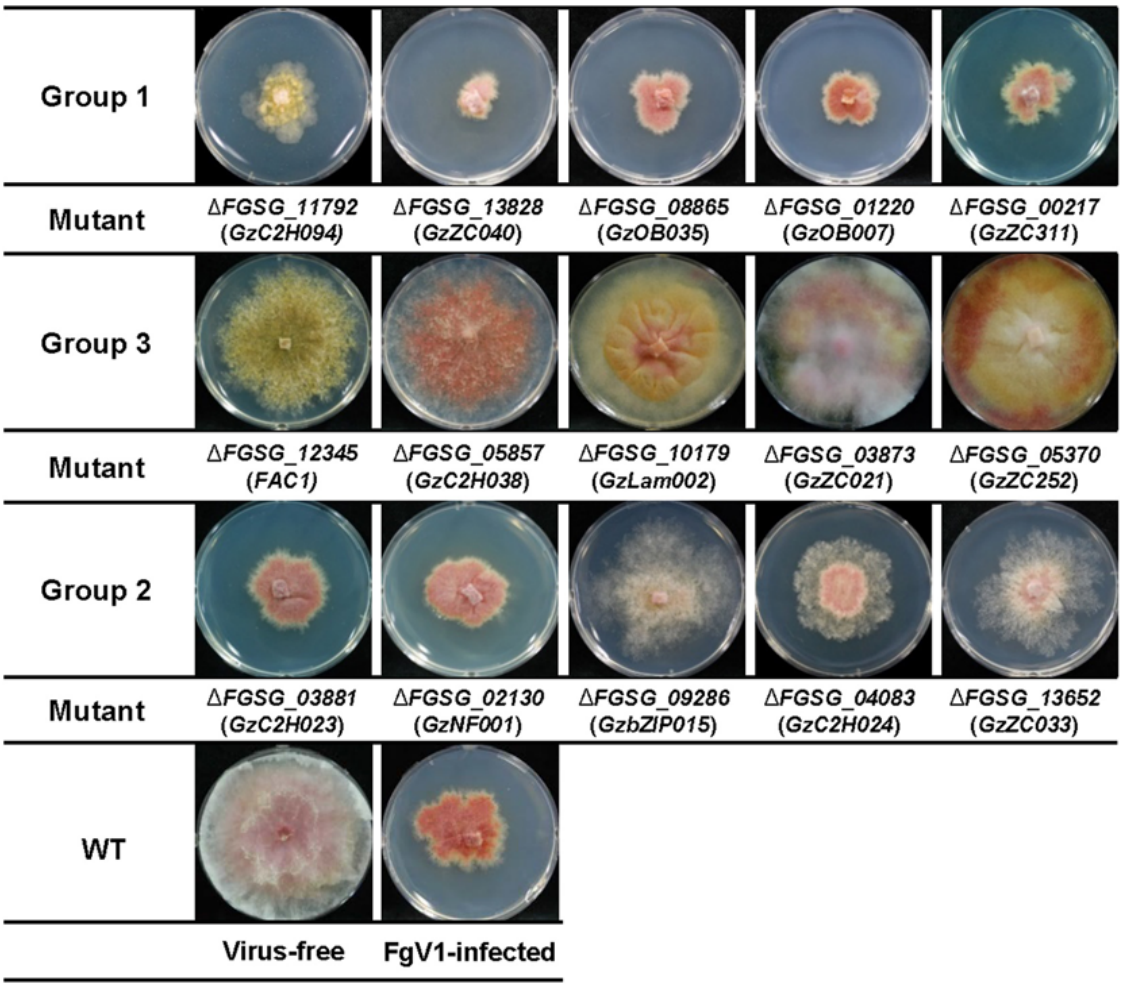

FIGURE 1 | Representative FgV1-infected colony morphology according to mycelial growth. Representative examples of colony morphology of FgV1-infected TF deletion mutants are shown. All cultures were photographed after incubating 5 days on complete media (CM). WT, *Fusarium graminearum* wild-type (WT) strain GZ03639. The virus-free TF deletion mutants that correspond to FgV1-infected TF deletion mutants in this figure did not changed mycelial growth compared to virus-free WT.

(ROS) stress, fungicide, cell wall stress, and acidic (pH = 4) or basic (pH = 11) conditions (Son et al., 2011). We compared TF phenotypes in response to those stress factors, considering FgV1 infection as biotic stress in *F. graminearum*, whether TF gene disruptions that showed different response to abiotic stress might also relate to response against to the FgV1 infection (**Figure 2B**). In results, among pH 11-sensitive or pH 11-resistant TF deletion mutants, *GzbHLH001* (FGSG_00545), *GzC2H048* (FGSG_07075), and *ZIF1* (FGSG_01555) deletion mutants showed more damaged virus-infected phenotype compared to WT-VI though they were belong to the Group 2. The other pH 11 responsive gene *FgPac1* (FGSG_12970) deletion mutant showed similar phenotype to WT-VI. Δ*GzC2H048* and Δ*ZIF1* also showed osmotic stress response. Between two pH 4-resistance TF deletion mutants, Δ*GzC2H005* (FGSG_00653) and Δ*GzMyb008* (FGSG_02719), they showed different phenotype. FgV1-infected Δ*GzC2H005* deletion mutant showed very weak and low density of colony morphology. In contrast, FgV1-infected Δ*GzMyb008* (Group 3) showed much faster mycelial growth and formed rhombus-shape of red line at the outside region of colony. In case of *GzDHHC003* (FGSG_06542) and *GzZC086* (FGSG_8924), related with oxidative stress response, showed normal growth but with relatively reduced mycelia growth compared to WT-VI. *FgFlbA* (FGSG_06228) showed increased transcript level following FgV1 infection and deletion mutant showed resistance phenotype in all stress factors except for pH 11 stress response. The virus-infected Δ*FgFlbA* (Group 2) colony grow normally but contain clustering region around fungal colony. In contrast, while Δ*GzWing020* (FGSG_08719, Group 3) showed sensitive responses to all stress responsive factors in phenome data, FgV1-infected colony showed increased aerial mycelia production and hyphal growth compared to WT-VI. Obtained results indicated that some of *F. graminearum* TF candidates that showed sensitive response in pH, fungicide or ROS stress alone also involved in response to FgV1 infection as well as TF candidates that response in broad range of environmental stress factors.

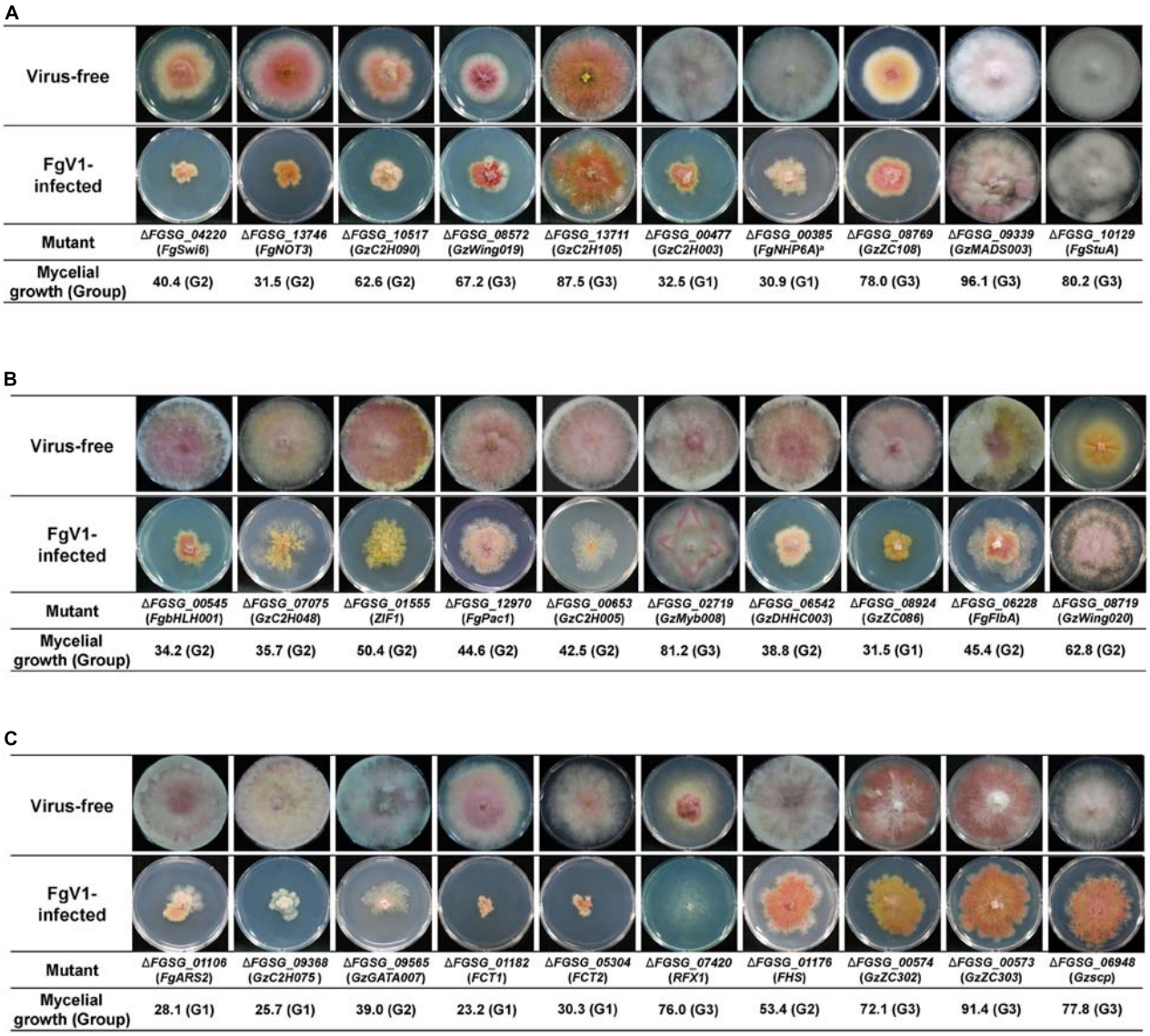

FIGURE 2 | Selected colony morphology of FgV1-infected TF deletion mutants. Colony morphology of virus-free and of FgV1-infected TF gene-deletion mutant strains. **(A)** TF gene-deletion mutants that showed multiple defect phenotypes after single gene deletion. **(B)** TF gene-deletion mutants that related to sensitive response against abiotic stress factor. **(C)** TF gene-deletion mutants that related to DNA damage response. All cultures were photographed after 5-day incubation on CM.

The Relationship Between FgV1 Infection and TFs Involved in DNA Damage Response

Previous study identified 16 putative TFs involved in DNA damage responses (DDRs) (Son et al., 2016a). In this study, we found that these DDR TF gene deletion group included relatively high portion of FgV1-infected TF deletion mutants that belong to Groups 1 and 3. Among 13 FgV1-infected TF, four FgV1-infected TF deletion mutants including *FgARS2* (FGSG_01106), *GzC2H075* (FGSG_09368), *FCT1* (FGSG_01182), and *FCT2* (FGSG_05304) were divided in Group 1. FgV1-infected Δ*GzGATA007* (FGSG_09565) belong to Group 2, however, showed retarded growth compared to WT-VI or to the typical colony morphologies of FgV1-infected TF deletion mutants belonging to Group 2 (**Figure 2C**, compare to WT-VI in **Figure 1**). *GzC2H075* (FGSG_09368) and *GzGATA007* (FGSG_09565) deletion mutants, which showed apparent reduction in mycelial growth following FgV1 infection, exhibited sensitive response only to DNA damage reaction in phenome data. Individual mycelial growth value of *RFX1* (FGSG_07420; Group 3) deletion mutant was slightly higher than that of WT-VI, however, virus-infected mutant showed strong inhibition of mycelial growth phenotype so we are unable to process further experiment. *FHS* (FGSG_01176; Group 2) deletion mutant that showed oxidative stress and ROS response along with

DDR did not show significant change of colony morphology following FgV1 infection. The colony morphology of *GzZC302* (FGSG_00574; Group 3) and *GzZC303* (FGSG_00573; Group 3) deletion mutants showed similar reduced aerial mycelia, increased pigmentation, and responded to multiple stress factors include oxidative, ROS and pH, however, their virus-infected phenotypes were not significantly different compared to WT-VI. Δ*Gzscp* (FGSG_06948; Group 3), which exhibit multiple defects along with DDR, showed little reduction of mycelial growth compared to WT-VI.

Although all DDR-related putative TF genes exhibited different sensitivity to DNA damaging agent include methyl methanesulfonate, hydroxyurea, bleomycin, and camptothecin (Son et al., 2016a), we could not correlate a common DNA damaging agent that links to displayed phenotype among FgV1-infected TF deletion mutants belong to Group 1.

Comparisons With RNA-Seq Data and Phenome Data

Previous study demonstrated that 24 TF genes were up- or down-regulated following FgV1 infection using transcriptomics-based analysis (Lee et al., 2014). We validated these RNA-Seq data with selected TF genes in this study (**Supplementary Table 5**). Among those 24 TF genes, only two TF genes including *GzZC252* (FGSG_05370) and *GzZC311* (FGSG_00217) were grouped into 1 and 3, respectively, following FgV1 infection (**Figure 1**). Interestingly, expression of both *GzZC252* (FGSG_05370) and *GzZC311* (FGSG_00217) genes were up-regulated upon FgV1 infection (Lee et al., 2014; **Supplementary Table 5**). Δ*GzZC311* did not show significant phenotypic change in mycelial growth compared to WT. Phenotype of FgV1-infected Δ*GzZC311* showed slow growth of mycelia compared to that of WT-VI. In contrast, Δ*GzZC252*-VF showed flat colony morphology with scarce growth of aerial mycelia but regular growth of mycelial growth in length. FgV1-infected Δ*GzZC252* did not decrease mycelial growth but caused color change from pale yellow to dark yellow in overall area of culture plate. The other 21 TF gene deletion mutants showed similar colony morphology compared to WT-VI. Although RNA-Seq analysis also identified *GzbHLH006* (FGSG_02516), *GzbHLH007* (FGSG_02814) *GzC2H006* (FGSG_00764), *TRI15* (FGSG_03881), and *GzGATA003* (FGSG_04626) that showed significant changes of gene expression levels upon FgV1, Fusarium graminearum virus 2 (FgV2; a Chrysovirus), FgV3 (a Fusagravirus), and Fusarium graminearum hypovirus 1 infections (Lee et al., 2014; Wang et al., 2016), those deletion mutants did not show significant change of colony morphology following FgV1 infection. In addition, we selected several TF genes in Groups 1 and 3 for confirmation of change of gene expressions following FgV1 infection (**Supplementary Table 4**). In Group 1, *FGSG_08865* and *FGSG_13828* genes showed significantly increased expression levels following FgV1 infection among 5 genes. In Group 3, expression levels of *FGSG_09339, FGSG_08455*, and *FGSG_03873* genes were decreased while expression level of FGSG_12742 was increased compared to that of WT-VI. These results showed FgV1 infection affects the expression levels of some putative TF genes, however, all of these changes might not be directly related with FgV1 accumulation or FgV1-mediated colony morphology in *F. graminearum*.

TFs That Might Be Involved in FgV1 RNA Accumulation

To isolate TFs that might be associated with viral replication, we confirmed dsRNA and viral ssRNA accumulation levels in FgV1-infected TF deletion mutants (**Table 2**). We selected several FgV1-infected TF deletion mutants belong to Groups 1, 2, and 3. Selected isolates include FgV1-infected mutants with phenotypic changes such as defect in sexual development, TF genes responsive to stress or DNA damage, and significantly up- or down-regulated TF genes upon FgV1 infection from RNA-Seq analysis. In results, increased viral ssRNA accumulation level was observed in *FgNHP6A* (FGSG_00385), *GzZC040* (FGSG_13828), *GzZC086* (FGSG_8924), *TRI15* (FGSG_03881), *FgFlbB* (FGSG_03597), *GzDHHC003* (FGSG_06542), and *GzZC267* (FGSG_01669) deletion mutants. Among them, dsRNA accumulation level was also significantly increased in FgV1-infected *GzZC086* deletion mutants. Δ*GzZC021* (FGSG_03873), *GzZC252* (FGSG_05370), and Δ*GzZC303* (FGSG_00573) in Group 3 showed significant decrease in viral dsRNA accumulation level. FgV1-infected Δ*GzZC252* showed significant reduction in dsRNA accumulation but not in viral ssRNA accumulation level compared to that of WT-VI. In addition, we observed dsRNA patterns of these TF deletion mutants (**Figure 3**). TF deletion mutants classified into Group 3 including Δ*GzZC021* (FGSG_03873), Δ*GzZC252* (FGSG_05370), and Δ*GzZC197* (FGSG_03892) showed decreased dsRNA accumulation compared to those of WT-VI and other mutants classified into Groups 1 and 2 (**Figure 3A**). Defective RNAs (D-RNAs, approximately 2–3 kbp long) were often observed in TF gene deletion mutants that showed multiple phenotypic changes and related with stress or DNA damage responses (**Figure 3B**). Among TF deletion mutants in Group 2, FgV1-infected mutants including Δ*GzbZIP015* (FGSG_09286), Δ*GzC2H024* (FGSG_04083), and Δ*GzZC033* (FGSG_13652) produced fluffy but low density of aerial mycelia (**Figure 1**) and also accumulated D-RNAs during FgV1 replication (**Figure 3C**, right panel). These results indicated that deletion of single TF gene affects FgV1 replication at different step(s) and generation of D-RNAs. In **Figure 1**, we simplify FgV1-infected TF deletion mutants by grouping based upon mycelial growth rate as the first step. We postulated that mycelial growth and viral RNA accumulation might inversely correlated in FgV1-infected fungal strains if mycelial growth of mutant did not changed by target gene deletion. To examine relationship between mycelial growth and viral RNA accumulation, we plot dsRNA or ssRNA accumulation (y) against mycelial length (x) using selected FgV1-infected TF deletion mutants (**Figure 4**). In general, FgV1-infected TF deletion mutants that grew slower than WT-VI accumulated higher level of viral dsRNA compared to WT-VI. In contrast, FgV1-infected TF deletion mutants that grow faster than WT-VI accumulated lower level of viral dsRNA compared

to WT-VI. Altogether, this result indicates that the relative levels of viral dsRNA accumulation in fungal colonies negatively correlate with mycelial growth of FgV1-infected TF mutant.

DISCUSSION

Identifying host factors involved in FgV1-derived symptom induction and viral RNA accumulation is a key aspect of understanding the molecular mechanism during *F. graminearum*-FgV1 interactions. Previous studies suggested that viral components interfere with host cell signaling pathways and progressively cause alteration in physiological and developmental processes, which culminate in visible virus-induced symptoms (Urbanowski et al., 2008; Pesti et al., 2019). In this respect, we used genome-wide TF deletion mutant library for *F. graminearum* to find host transcription factors and host-cell signaling pathways that might be associated with pleiotropic effects of FgV1 infection on fungal host and to identify novel host factor which might be involved in FgV1 RNA accumulation in host cell.

We observed different phenotype change in fungal colony color which turns yellow after virus infection without greater reduction of mycelial growth in some TF deletion mutants. Those genes were not listed in phenome data as pH sensitive responsive mutants that showed reduced mycelial growth at pH 4 or pH 11 (Son et al., 2011). However, it is worth noting that pH also impacts on pigment production and mycelium color. For example, the red pigment of *F. graminearum* is pH sensitive and changes color from red to yellow as the pH drop (Leslie and Summerell, 2008). Because pH affects wide range of fungal physiological processes and gene expression in fungal cells (Bousset et al., 2019), change of colony morphology of those TFs deletion mutants might be related with pH stability following virus infection. In addition, dsRNA accumulation was decreased in Δ*GzZC197* (FGSG_03892) as shown in **Figure 3**, pH stability might also affect replication of viral RNA. Since whether pH impacts virus-host interactions is not clear in *F. graminearum,* further studies are needed.

In TF deletion mutant library, we were interested in TF deletion mutants showing pleiotropic phenotype similar with FgV1-infection derived phenotype in *F. graminearum*. We expected it would provide information for identifying host factor(s) or characterizing signaling pathway that related with hypovirulence-associated traits of FgV1 regardless of phenotype observation of FgV1-infected TF deletion mutant. As mentioned above, several TF deletion mutants showed WT-VI like colony morphology. Some of these TFs might play central roles in reprogramming transcriptional network or function as an important downstream regulator, which results in pleiotropic effects by gene deletion. For example, *FgSWI6* and *GzAPSES004* were suggested as hub regulators of virulence, mycotoxin synthesis, and sexual reproduction-associated networks (Guo et al., 2020). Previous study reported that decreased expression level of *FgSWI6* following FgV1 infection seems to be related with FgV1-derived phenotypic alteration (Son et al., 2016c). Because constitutive overexpression *FgSWI6* moderately attenuate symptom expression by FgV1 infection although it contained increased FgV1 accumulation level compared to WT (Son et al., 2016c). *FgCrz1A* is reported as a possible

TABLE 2 | Comparisons of relative ratio of mycelial growth, dsRNA accumulation, and ssRNA accumulation of FgV1-infected TF deletion mutants.

	Mycelial length[a]	dsRNA[b]	ssRNA[c]	Note[d]
WT-VI	47.5	1.04 ± 0.1	0.98 ± 0.1	
Group 1				
Δ*FGSG_00477*	32.5	0.98 ± 0.2	3.01 ± 0.9	MD
Δ*FGSG_01106*	28.1	1.46 ± 0.7	0.62 ± 0.02	MD, DDR
Δ*FGSG_09368*	25.7	0.96 ± 0.2	0.45 ± 0.1	DDR
Δ*FGSG_00385*	30.9	1.32 ± 0.1	4.41 ± 1.4*	MD, pH4(R)
Δ*FGSG_08865*	30.4	1.54 ± 0.3	2.19 ± 0.7	N
Δ*FGSG_13828*	19.4	1.47 ± 0.8	3.98 ± 1.8*	N
Δ*FGSG_08924*	31.5	1.91 ± 0.6*	6.68 ± 3.0*	Fung, virus response
Δ*FGSG_00217*	32.2	1.41 ± 0.4	5.34 ± 2.5*	Virus response
Δ*FGSG_00324*	32.6	2.05 ± 1.3	1.79 ± 1.0	MD, os
Group 2				
Δ*FGSG_09286*	46.3	1.20 ± 0.2	5.09 ± 2.4	Virus response
Δ*FGSG_03881*	41.7	1.28 ± 0.3	3.62 ± 1.7*	Virus response
Δ*FGSG_04083*	47.3	1.33 ± 0.1	0.78 ± 0.2	Virus response
ΔFGSG_08617	42.2	0.86 ± 0.3	2.32 ± 0.4	Virus response
Δ*FGSG_08893*	37.2	1.26 ± 0.1	8.44 ± 0.7*	N
Δ*FGSG_06110*	45.5	1.32 ± 0.01	2.61 ± 0.6*	Virus response
ΔFGSG_02615	33.4	1.41 ± 0.2	2.05 ± 0.5	Virus response
Δ*FGSG_03597*	45.3	0.98 ± 0.1	3.94 ± 1.1*	N
Δ*FGSG_06542*	38.8	1.14 ± 0.5	8.81 ± 5.2*	MD, ROS
Δ*FGSG_11686*	38.0	1.00 ± 0.1	1.43 ± 0.2	N
Δ*FGSG_01669*	45.3	0.89 ± 0.3	5.31 ± 0.5*	Virus response
Group 3				
Δ*FGSG_03873*	88.9	0.17 ± 0.2**	0.31 ± 0.1**	N
Δ*FGSG_13625*	73.3	0.54 ± 0.2	0.29 ± 0.1**	N
Δ*FGSG_05370*	95.3	0.15 ± 0.1**	2.71 ± 0.2*	Virus response
Δ*FGSG_00574*	72.1	0.89 ± 0.1	3.10 ± 0.5*	MD, DDR, Os,ROS,Fung,pH11
Δ*FGSG_00573*	91.4	0.20 ± 0.1**	0.87 ± 0.3	DDR, Os,ROS,Fung,pH11

[a]*Radial growth was measured after a 5-day incubation on CM. Average radial growth on CM of FgV1-infected TF deletion mutants compared to virus-free strain or WT strain (set to a value of 100) was divided as groups (Group 1, less than 33; Group 2, 33–62.9; Group 3, 63–100 of WT strain).*

[b]*Relative accumulation of FgV1 viral dsRNA in TF deletion mutants was measured using 3 μg total RNA samples at 120 h post-inoculation (hpi). Values were normalized to the FgV1 RNA in WT-VI (set to a value of 1), with the standard deviation based on at least two independent RNA preparations. Different number of asterisks indicate data are significantly differed ($P < 0.05$) from each other and mean for FgV1-infected GZ03639 WT strain based on LSD test.*

[c]*Quantification of FgV1 viral ssRNA at 120 hpi using real-time RT-PCR. cDNAs were generated from ssRNA samples obtained after 120 h of incubation. EF1α and UBH gene transcripts were used as internal controls. Values are means (+ SD) of two biological replicates with at least two experimental replication.Different number of asterisks indicate data are significantly differed ($P < 0.05$) from each other and mean for FgV1-infected GZ03639 WT strain based on LSD test.*

[d]*MD, multiple defects after TF gene deletion; DDR, TF deletion mutant related with DNA damage responses; os, sensitive in osmotic stress; ROS, sensitive in ROS stress; Fung, sensitive in fungicide response; pH4(R), resistance response against pH 4 stress; N, TF deletion mutant not showing any significant change; virus response, level of gene expression was changed after virus infection.*

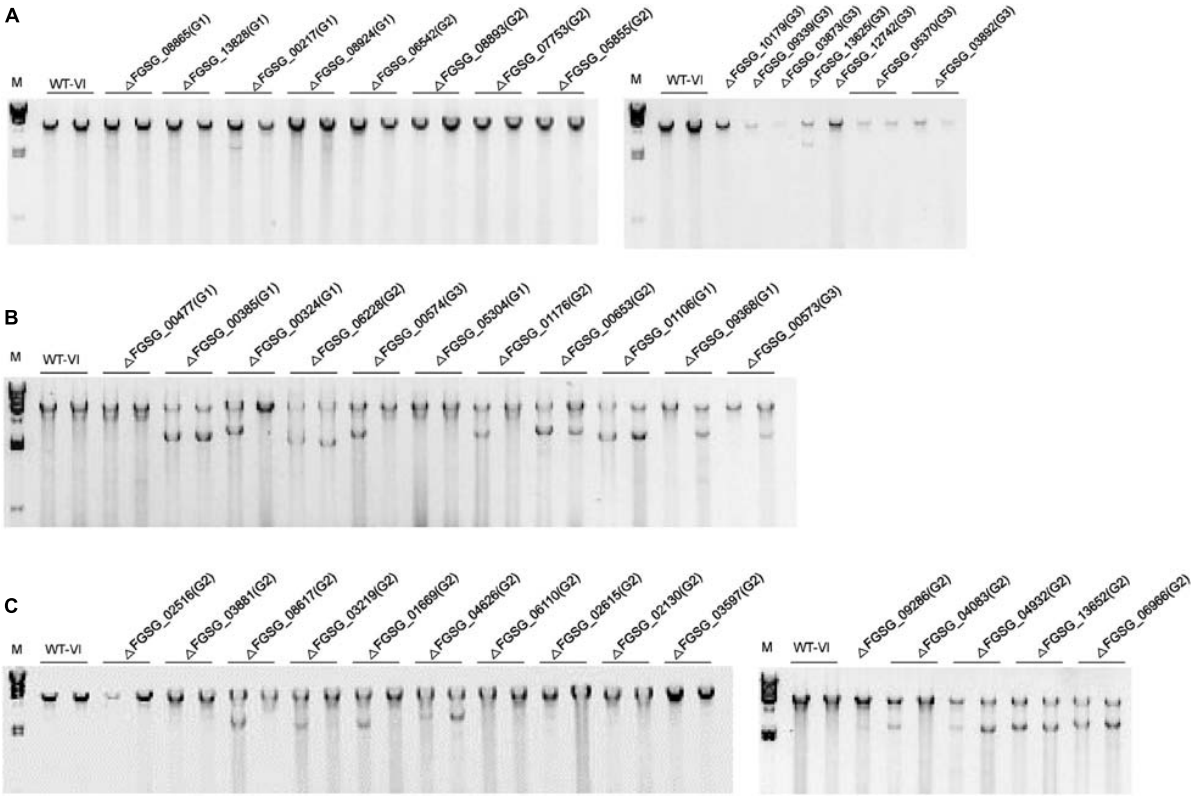

FIGURE 3 | Accumulation of FgV1 viral double-stranded RNA in virus-infected TF deletion mutant strains of *F. graminearum*. **(A)** dsRNA accumulation of TF gene-deletion mutants that belong to Groups 1 to 3. **(B)** TF gene-deletion mutants that showed multiple defect phenotypes after single gene deletion, TF gene-deletion mutants related to sensitive response against abiotic stress factor and DNA damage response. **(C)** TF gene-deletion mutants showing significant changes of gene expression levels upon FgV1 (left) and TF gene-deletion mutants showing abnormal colony morphology in Group 2 (right). Number in parenthesis represents group of each sample. A 3 μg quantity of total RNAs per sample was treated with *DNase*I and S1 Nuclease and separated in 1% agarose gel. The largest band in the each sample represents the full-length FgV1 dsRNA (6.6 kb); smaller bands indicate internally deleted forms of viral dsRNA. The lane marked M correspond to lambda DNA digested with *Hin*dIII. WT-VI, FgV1-infected WT GZ03639 strain.

ortholog of *Saccharomyces cerevisiae Crz1* that has crucial role in regulating calcineurin- and Ca^{2+}/calmodulin-dependent signaling (Chen L. et al., 2019). Δ*FgCrz1A* displayed multiple abnormalities in phenotypes including increased sensitivity to metal cations Ca^{2+}, Mg^{2+}, Mn^{2+}, and Li^{+} (Chen L. et al., 2019). We observed small decrease in mycelial growth in FgV1-infected Δ*FgCrz1A* compared to WT-VI. However, including *FgCrz1A,* we are not sure whether these TF function in facilitating FgV1 replication or in regulating defense pathways of fungal host. The attempts to establish relationships between FgV1 and phenotype-associated cellular signaling pathways are required in further study.

Recent study demonstrated that *FgARS2* physically interacts with the cap-binding complex to form a stable tertiary complex (Bui et al., 2019), however, key components and regulation processes of DDR in *F. graminearum* are largely unknown. In this study, we found FgV1 infection significantly impacts on mycelial growth of several DDR-related TF deletion mutants, i.e., Δ*FgARS2* (FGSG_01106; Bui et al., 2019), Δ*FCT1* (FGSG_01182; Kim et al., 2020), Δ*FCT2* (FGSG_05304; Kim et al., 2020), Δ*GzC2H075* (FGSG_09368), Δ*GzZC303* (FGSG_00573), and Δ*GzZC302* (FGSG_00574; **Figure 2**). However, ss and dsRNA accumulations of those mutants were similar or slightly decreased compared to WT-VI (**Table 2**). These results indicated DNA damage might be induced by FgV1 infection and those DDR-related gene deletion caused significant change in mycelial growth even they contain relatively low or similar amount of viral RNA compared to WT-VI. Accordingly, genetic instability plays a considerable role in pathogenicity of FgV1 and is likely to be a key factor of FgV1-associated symptom development. In addition, we often found FgV1 infection resulted in significant accumulation of DI RNAs as were in case of Δ*FgARS2*, Δ*GzC2H075*, Δ*GzZC303*, and Δ*GzZC302* mutants. It might suggest possible role of DDR in supporting virus replication. Like other DNA viruses, some RNA viruses also have ability to trigger DDR signaling to assist host cellular conditions that are beneficial for viral replication (Ryan et al., 2016). Although it has not been determined whether FgV1 replication and symptom development are closely related with DDR in present study, this phenotype-based analysis would lead to investigate the interactions between FgV1 and the DDR in *F. graminearum* in further.

Previous transcriptome study described that 24 TF genes were differentially expressed upon FgV1 infection, however, 114 of 709 TF genes were not detected (Lee et al., 2014). Because expression levels of many TF genes vary through different phase of fungal development and environmental condition, it might has limitation in finding crucial TF genes that play crucial role(s) during FgV1 infection from transcriptome profiles obtained at a particular time-point measurement under a certain condition. Several studies analyzed transcription profiles of *F. graminearum* in response to different mycovirus infections (Lee et al., 2014; Wang et al., 2016; Bormann et al., 2018). In addition, other transcription profiles has revealed subsets of transcriptionally regulated genes using mutant strains that involved in mycotoxin synthesis, asexual or sexual development, RNAi process, abiotic stress response, and post-translational modification (Brauer et al., 2020). For examples, *GzZC196* (FGSG_03912; Group 1) and *GzZC197* (FGSG_03892; Group 3) showed reduced gene expression level in *FgDICER*s or *FgAGO*s double knockout mutant strains compared to WT (Son et al., 2017; **Supplementary Table 1**). *GzbHLH011* (FGSG_06262) and *GzHOMEL018* (FGSG_07243) showed reduced gene expression level in both Δ*FgGCN5* and Δ*FgSAS3* that are putative histone acetyltransferase (HATs) in *F. graminearum* (Kong et al., 2018). Both Δ*GzbHLH011* and Δ*GzHOMEL018* belong to Group 3 (**Supplementary Table 1**). In case of *GzZC086* (FGSG_08924), involved in oxidative stress in *F. graminearum* (Lee et al., 2018), FgV1-infected Δ*GzZC086* (Group 1) showed significantly increased viral RNA accumulation level (**Table 2**). Therefore, combined phenome data from this study and transcriptome data obtained from diverse conditions will help in understanding common and unique roles of TFs and signaling pathways that might be associated with host response against virus infection.

In this study, among FgV1-infected TF deletion mutants that belonged to Groups 1 and 3, we found overlapped result with transcriptome analysis. *GzZC311* (FGSG_00217) and *GzZC252* (FGSG_05370) that were grouped into 1 and 3, respectively, showed increased gene expression level following FgV1 infection but result of FgV1 transmission into each gene deletion mutant showed different colony morphology. *GzZC311* and *GzZC252* encoded hypothetical protein contain fungal-specific regulatory protein domain, however, their cellular functions have not been identified yet. Δ*GzZC252* negatively affects FgV1 dsRNA accumulation but not for ssRNA accumulation. Further investigation with complementation or overexpression mutant is required to confirm whether this gene is required for FgV1 RNA accumulation. Among Group 2, FgV1 infections in Δ*GzbZIP015* (FGSG_09286) and Δ*GzZC050* (FGSG_12597) mutants showed similar colony morphology like WT-VI (**Figure 1**). *GzbZIP015* encoded protein which has similarity with cross-pathway control protein 1, the ortholog of GCN4 in the yeast *S. cerevisiae*, is a main regulator of protein synthesis and might have role in longevity and stress response in *Neurospora crassa* (Hinnebusch, 2005). Given that increased expression of *GzbZIP015* gene upon FgV1 infection (Lee et al., 2014) and increased accumulation of FgV1 ssRNA in FgV1-infected Δ*GzbZIP015* mutant, *GzbZIP015* might serve as an antiviral host factor following virus infection (**Table 2**).

We confirmed ss and dsRNA accumulation using several TF genes deletion mutants belong to Group 2 but it showed differential gene expression upon FgV1 infection (**Table 2**). FgV1 ssRNA accumulation levels were increased compared to WT-VI, however, gene deletion did not seem to directly affect dsRNA accumulation. This result suggested that dsRNA accumulation level could determine FgV1-derived symptom rather than ssRNA accumulation (**Figure 4**).

Viruses need host factors not only to assist their replication but also to face the host antiviral defense response. Mycovirus infection in host cell boosts host antiviral response such as RNA interference (RNAi). Interestingly, Cryphonectria hypovirus 1 (CHV1) and FgV1 exhibit suppression activity against host antiviral response through suppression of RNAi component-related gene transcription (Sun et al., 2009;

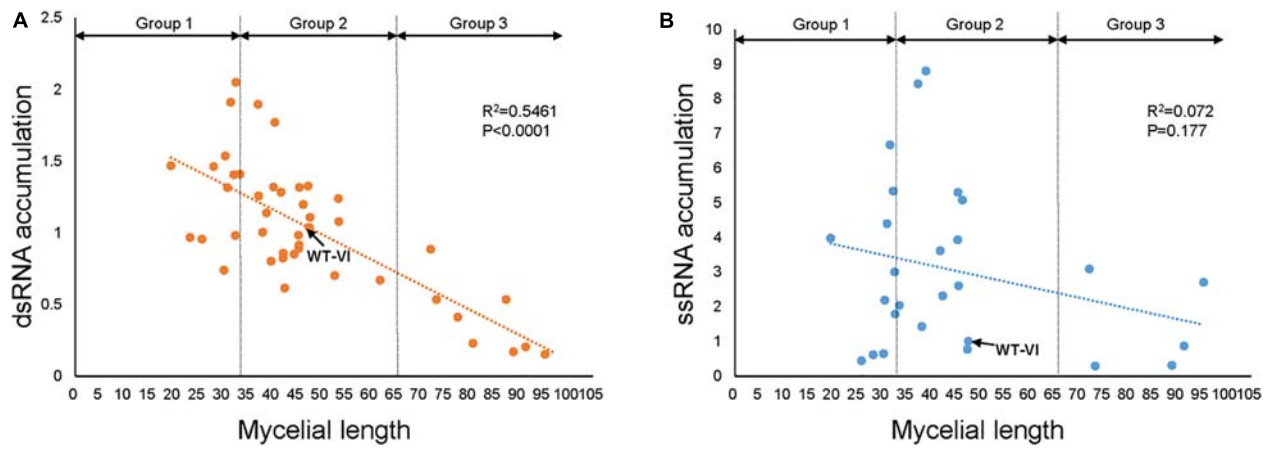

FIGURE 4 | Relationship between mycelial growth and the viral RNA accumulation in TF deletion mutants. Relationship between radial growth of mycelia and FgV1 RNA replication was estimated by calculating the viral dsRNA **(A)** and ssRNA **(B)** accumulations in FgV1-infected TF deletion mutants. Dotted and dashed lines indicate the linear regression between the mycelial growth and viral RNA accumulation.

Yu et al., 2020). Previous studies demonstrated that the Spt–Ada–Gcn5 acetyltransferase (SAGA) transcriptional activator regulates the induction of the essential antiviral RNA-silencing components, dicer-like 2 (*dcl2*) and argonaute-like 2 (*agl2*) in *Cryphonectria parasitica* (Andika et al., 2017). We attempted to identify TFs that involved in transcriptional regulation of *FgDICER*s or *FgAGO*s genes using TF deletion mutant library, however, FgV1 was not suitable for screening candidate genes because of the presence of pORF2, suppressor of RNAi (Yu et al., 2020). Further investigations are in progress to identify TFs that play roles in regulating gene expressions of *FgDICER*s or *FgAGO*s combined with present research and other FgV-infected TF deletion mutants.

As mentioned earlier, we had failed to transmit FgV1 *via* hyphal anastomosis into several TF deletion mutants including Δ*GzZC030* (FGSG_06380), Δ*GzZC032* (FGSG_00153), Δ*GzZC044* (FGSG_12094), Δ*GzZC060* (FGSG_08808), Δ*GzZC232* (FGSG_07067), Δ*FgArt1* (FGSG_02083), Δ*GzZC301* (FGSG_00404), and Δ*GzZC316* (FGSG_00125). Most of those gene deletion mutants did not show specific alteration in mycelial growth. Among them, we confirmed gene expression levels of 9 TFs by qRT-PCR (**Supplementary Table 4**). Seven out of nine genes showed significant changes of gene expression levels following FgV1 infection. Some of these genes might be involved in cell-to-cell interaction regulation that has been proposed as a defense mechanism of host fungi to limit the transmission of mycoviruses (Nuss, 2011). For example, *GzZC232* encoded protein shares 59% sequence identity with *Epichloë festucae* ProA, which is similar to *N. crassa* ADV-1 and *Sordaria macrospora* Pro1 (Tanaka et al., 2013). ProA deletion mutant is defective in hyphal fusion under nutrient limitation condition (Tanaka et al., 2013). In case of *FgArt1*, it is associated with biosynthesis of trichothecene and fumonisin by regulating genes involved in starch hydrolysis, however, it remains unclear if *FgArt1* plays a role in cell fusion or related biological processes (Oh et al., 2016). Many genes and molecular signaling networks are involved during hyphal fusion in *N. crassa* including MAPKinase cascades, a STRIPAK complex, transcription factors, a NADPH-oxidases complex, ROS systems, and Ca^{2+}-binding regulators (Fischer and Glass, 2019). Further detailed study is required to explain this inability of hyphal fusion in some TF deletion mutants in *F. graminearum*.

Kinases and phosphatases also contribute to the regulation of gene expression by interacting with transcription factors (Ariño et al., 2019; González-Rubio et al., 2019). Both phosphatidylinositol-3-kinase (PI3K) and Akt signaling pathways promote viral replication and activate antiviral response (Dunn and Connor, 2012). Since systematic characterization of the kinome and phosphatome has been reported in *F. graminearum* previously (Wang et al., 2011; Yun et al., 2015), applying FgV1 into kinome and phosphatome in *F. graminearum* will provide a valuable resource to understand fungal host cell signaling pathway involved in antiviral or proviral functions. Although the TF phenome data illustrated characteristics of phenotype of all TF deletion mutants in previous research, it has limitation in expecting possible functions of TF genes that do not show distinct phenotypic change. In this regard, FgV1-infected TF deletion mutant library obtained in present study would provide chance to better characterize function(s) of novel TF genes that showed distinguishable phenotypes following FgV1-infection. Further study will explore the roles of these TF genes and their putative target genes during FgV1 infection.

DATA AVAILABILITY STATEMENT

The raw data supporting the conclusions of this article will be made available by the authors, without undue reservation.

AUTHOR CONTRIBUTIONS

JY and K-HK designed the experiments, analyzed the data, and wrote the manuscript. JY performed the experimental work. Both authors contributed to the article and approved the submitted version.

FUNDING

This research was supported in part by grants from the National Research Foundation of Korea funded by the Ministry of Science and ICT (NRF-2020R1C1C1011779) and Agenda Program (No. PJ01488703), the Rural Development Administration (RDA), South Korea.

SUPPLEMENTARY MATERIAL

The Supplementary Material for this article can be found online at: https://www.frontiersin.org/articles/10.3389/fmicb.2021.622261/full#supplementary-material

REFERENCES

Alves, M. S., Dadalto, S. P., Gonçalves, A. B., De Souza, G. B., Barros, V. A., and Fietto, L. G. (2014). Transcription factor functional protein-protein interactions in plant defense responses. *Proteomes* 2, 85–106. doi: 10.3390/proteomes2010085

Andika, I. B., Jamal, A., Kondo, H., and Suzuki, N. (2017). SAGA complex mediates the transcriptional up-regulation of antiviral RNA silencing. *Proc. Natl. Acad. Sci. U.S.A.* 114, E3499–E3506.

Ariño, J., Velázquez, D., and Casamayor, A. (2019). Ser/Thr protein phosphatases in fungi: structure, regulation and function. *Microb. Cell* 6, 217–256. doi: 10.15698/mic2019.05.677

Bormann, J., Heinze, C., Blum, C., Mentges, M., Brockmann, A., Alder, A., et al. (2018). Expression of a structural protein of the mycovirus FgV-ch9 negatively affects the transcript level of a novel symptom alleviation factor and causes virus infection-like symptoms in *Fusarium graminearum*. *J. Virol.* 92, e00326-18.

Bousset, L., Ermel, M., Soglonou, B., and Husson, O. (2019). A method to measure redox potential (Eh) and pH in agar media and plants shows that fungal growth

is affected by and affects pH and Eh. *Fungal Biol.* 123, 117–124. doi: 10.1016/j.funbio.2018.11.008

Brauer, E. K., Subramaniam, R., and Harris, L. J. (2020). Regulation and dynamics of gene expression during the life cycle of *Fusarium graminearum*. *Phytopathology* 110, 1368–1374. doi: 10.1094/phyto-03-20-0080-ia

Bui, D.-C., Kim, J.-E., Shin, J., Lim, J. Y., Choi, G. J., Lee, Y.-W., et al. (2019). ARS2 plays diverse roles in DNA damage response, fungal development, and pathogenesis in the plant pathogenic fungus *Fusarium graminearum*. *Front. Microbiol.* 10:2326. doi: 10.3389/fmicb.2019.02326

Carrera, J., and Elena, S. F. (2012). Computational design of host transcription-factors sets whose misregulation mimics the transcriptomic effect of viral infections. *Sci. Rep.* 2:1006.

Chen, L., Tong, Q., Zhang, C., and Ding, K. (2019). The transcription factor FgCrz1A is essential for fungal development, virulence, deoxynivalenol biosynthesis and stress responses in *Fusarium graminearum*. *Curr. Genet.* 65, 153–166. doi: 10.1007/s00294-018-0853-5

Chen, Y., Kistler, H. C., and Ma, Z. (2019). *Fusarium graminearum* trichothecene mycotoxins: biosynthesis, regulation, and management. *Annu. Rev. Phytopathol.* 57, 15–39.

Chu, Y.-M., Jeon, J.-J., Yea, S.-J., Kim, Y.-H., Yun, S.-H., Lee, Y.-W., et al. (2002). Double-stranded RNA mycovirus from *Fusarium graminearum*. *Appl. Environ. Microbiol.* 68, 2529–2534. doi: 10.1128/aem.68.5.2529-2534.2002

Dunn, E. F., and Connor, J. H. (2012). HijAkt: the PI3K/Akt pathway in virus replication and pathogenesis. *Prog. Mol. Biol. Transl. Sci.* 106, 223–250.

Dweba, C., Figlan, S., Shimelis, H., Motaung, T., Sydenham, S., Mwadzingeni, L., et al. (2017). *Fusarium* head blight of wheat: pathogenesis and control strategies. *J. Crop Prot.* 91, 114–122. doi: 10.1016/j.cropro.2016.10.002

Ferrigo, D., Raiola, A., and Causin, R. (2016). *Fusarium* toxins in cereals: occurrence, legislation, factors promoting the appearance and their management. *Molecules* 21:627. doi: 10.3390/molecules21050627

Fischer, M. S., and Glass, N. L. (2019). Communicate and fuse: how filamentous fungi establish and maintain an interconnected mycelial network. *Front. Microbiol.* 10:619. doi: 10.3389/fmicb.2019.00619

González-Rubio, G., Fernández-Acero, T., Martín, H., and Molina, M. (2019). Mitogen-activated protein kinase phosphatases (MKPs) in fungal signaling: conservation, function, and regulation. *Int. J. Mol. Sci.* 20:1709. doi: 10.3390/ijms20071709

Guo, L., Ji, M., and Ye, K. (2020). Dynamic network inference and association computation discover gene modules regulating virulence, mycotoxin and sexual reproduction in *Fusarium graminearum*. *BMC Genomics* 21:179. doi: 10.1186/s12864-020-6596-y

Hinnebusch, A. G. (2005). Translational regulation of GCN4 and the general amino acid control of yeast. *Annu. Rev. Microbiol.* 59, 407–450. doi: 10.1146/annurev.micro.59.031805.133833

Honda, S., Eusebio-Cope, A., Miyashita, S., Yokoyama, A., Aulia, A., Shahi, S., et al. (2020). Establishment of *Neurospora crassa* as a model organism for fungal virology. *Nat. Commun.* 11, 1–13.

Kazan, K., and Gardiner, D. M. (2018). Transcriptomics of cereal–*Fusarium graminearum* interactions: what we have learned so far. *Mol. Plant Pathol.* 19, 764–778. doi: 10.1111/mpp.12561

Kim, H.-K., Jo, S.-M., Kim, G.-Y., Kim, D.-W., Kim, Y.-K., and Yun, S.-H. (2015). A large-scale functional analysis of putative target genes of mating-type loci provides insight into the regulation of sexual development of the cereal pathogen *Fusarium graminearum*. *PLoS Genet.* 11:e1005486. doi: 10.1371/journal.pgen.1005486

Kim, J.-E., Nam, H., Park, J., Choi, G. J., Lee, Y.-W., and Son, H. (2020). Characterization of the ccAAt-binding transcription factor complex in the plant pathogenic fungus *Fusarium graminearum*. *Sci. Rep.* 10, 1–11.

Kong, X., van Diepeningen, A. D., van der Lee, T. A., Waalwijk, C., Xu, J., Xu, J., et al. (2018). The *Fusarium graminearum* histone acetyltransferases are important for morphogenesis. DON biosynthesis, and pathogenicity. *Front. Microbiol.* 9:654. doi: 10.3389/fmicb.2018.00654

Kwon, S.-J., Lim, W.-S., Park, S.-H., Park, M.-R., and Kim, K.-H. (2007).). Molecular characterization of a dsRNA mycovirus, Fusarium graminearum virus-DK21, which is phylogenetically related to hypoviruses but has a genome organization and gene expression strategy resembling those of plant potex-like viruses. *Mol. Cells* 23, 304–315.

Lee, K.-M., Cho, W. K., Yu, J., Son, M., Choi, H., Min, K., et al. (2014). A comparison of transcriptional patterns and mycological phenotypes following infection of *Fusarium graminearum* by four mycoviruses. *PLoS One* 9:e100989. doi: 10.1371/journal.pone.0100989

Lee, K.-M., Yu, J., Son, M., Lee, Y.-W., and Kim, K.-H. (2011). Transmission of *Fusarium boothii* mycovirus via protoplast fusion causes hypovirulence in other phytopathogenic fungi. *PLoS One* 6:e21629. doi: 10.1371/journal.pone.0021629

Lee, Y., Son, H., Shin, J. Y., Choi, G. J., and Lee, Y. W. (2018). Genome-wide functional characterization of putative peroxidases in the head blight fungus *Fusarium graminearum*. *Mol. Plant Pathol.* 19, 715–730. doi: 10.1111/mpp.12557

Leslie, J. F., and Summerell, B. A. (2008). The Fusarium Laboratory Manual. Hoboken, NJ: John Wiley & Sons.

Liu, Z., Jian, Y., Chen, Y., Kistler, H. C., He, P., Ma, Z., et al. (2019). A phosphorylated transcription factor regulates sterol biosynthesis in *Fusarium graminearum*. *Nat. Commun.* 10, 1–17.

Mitsis, T., Efthimiadou, A., Bacopoulou, F., Vlachakis, D., Chrousos, G. P., and Eliopoulos, E. (2020). Transcription factors and evolution: an integral part of gene expression. *World Acad. Sci.* 2, 3–8.

Ng, D. W., Abeysinghe, J. K., and Kamali, M. (2018). Regulating the regulators: the control of transcription factors in plant defense signaling. *Int. J. Mol. Sci.* 19:3737. doi: 10.3390/ijms19123737

Nuss, D. L. (2011). Mycoviruses, RNA silencing, and viral RNA recombination. *Adv. Virus Res.* 80, 25–48. doi: 10.1016/b978-0-12-385987-7.00002-6

Oh, M., Son, H., Choi, G. J., Lee, C., Kim, J. C., Kim, H., et al. (2016). Transcription factor ART 1 mediates starch hydrolysis and mycotoxin production in *Fusarium graminearum* and *F. verticillioides*. *Mol. Plant Pathol.* 17, 755–768. doi: 10.1111/mpp.12328

Osterbaan, L. J., and Fuchs, M. (2019). Dynamic interactions between plant viruses and their hosts for symptom development. *Plant Pathol. J.* 101, 885–895. doi: 10.1007/s42161-019-00323-5

Pesti, R., Kontra, L., Paul, K., Vass, I., Csorba, T., Havelda, Z., et al. (2019). Differential gene expression and physiological changes during acute or persistent plant virus interactions may contribute to viral symptom differences. *PLoS One* 14:e0216618. doi: 10.1371/journal.pone.0216618

Ryan, E. L., Hollingworth, R., and Grand, R. J. (2016). Activation of the DNA damage response by RNA viruses. *Biomolecules* 6:2. doi: 10.3390/biom6010002

Schneider, C. A., Rasband, W. S., and Eliceiri, K. W. (2012). NIH Image to ImageJ: 25 years of image analysis. *Nat. Methods* 9, 671–675. doi: 10.1038/nmeth.2089

Shelest, E. (2017). Transcription factors in fungi: TFome dynamics, three major families, and dual-specificity TFs. *Front. Genet.* 8:53. doi: 10.3389/fgene.2017.00053

Son, H., Fu, M., Lee, Y., Lim, J. Y., Min, K., Kim, J.-C., et al. (2016a). A novel transcription factor gene FHS1 is involved in the DNA damage response in *Fusarium graminearum*. *Sci. Rep.* 6, 1–12.

Son, M., Choi, H., and Kim, K.-H. (2016b). Specific binding of *Fusarium graminearum* Hex1 protein to untranslated regions of the genomic RNA of Fusarium graminearum virus 1 correlates with increased accumulation of both strands of viral RNA. *Virology* 489, 202–211. doi: 10.1016/j.virol.2015.12.013

Son, M., Lee, Y., and Kim, K.-H. (2016c). The transcription cofactor Swi6 of the *Fusarium graminearum* is involved in fusarium graminearum virus 1 infection-induced phenotypic alterations. *Plant Pathol. J.* 32, 281–289. doi: 10.5423/ppj.oa.12.2015.0267

Son, H., Park, A. R., Lim, J. Y., Shin, C., and Lee, Y.-W. (2017). Genome-wide exonic small interference RNA-mediated gene silencing regulates sexual reproduction in the homothallic fungus *Fusarium graminearum*. *PLoS Genet.* 13:e1006595. doi: 10.1371/journal.pgen.1006595

Son, H., Seo, Y.-S., Min, K., Park, A. R., Lee, J., Jin, J.-M., et al. (2011). A phenome-based functional analysis of transcription factors in the cereal head blight fungus. *Fusarium graminearum*. *PLoS Pathog.* 7:e1002310. doi: 10.1371/journal.ppat.1002310

Spitz, F., and Furlong, E. E. (2012). Transcription factors: from enhancer binding to developmental control. *Nat. Rev. Genet.* 13, 613–626. doi: 10.1038/nrg3207

Sun, Q., Choi, G. H., and Nuss, D. L. (2009). A single argonaute gene is required for induction of RNA silencing antiviral defense and promotes viral RNA recombination. *Proc. Natl. Acad. Sci. U.S.A.* 106, 17927–17932. doi: 10.1073/pnas.0907552106

Tanaka, A., Cartwright, G. M., Saikia, S., Kayano, Y., Takemoto, D., Kato, M., et al. (2013). ProA, a transcriptional regulator of fungal fruiting body development, regulates leaf hyphal network development in the *Epichloë festucae*–L olium perenne symbiosis. *Mol. Microbiol.* 90, 551–568. doi: 10.1111/mmi.12385

Urbanowski, M. D., Ilkow, C. S., and Hobman, T. C. (2008). Modulation of signaling pathways by RNA virus capsid proteins. *Cell. Signal.* 20, 1227–1236. doi: 10.1016/j.cellsig.2007.12.018

Wang, C., Zhang, S., Hou, R., Zhao, Z., Zheng, Q., Xu, Q., et al. (2011). Functional analysis of the kinome of the wheat scab fungus *Fusarium graminearum*. *PLoS Pathog.* 7:e1002460. doi: 10.1371/journal.ppat.1002460

Wang, S., Zhang, J., Li, P., Qiu, D., and Guo, L. (2016). Transcriptome-based discovery of *Fusarium graminearum* stress responses to FgHV1 infection. *Int. J. Mol. Sci.* 17:1922. doi: 10.3390/ijms17111922

Yu, J., and Kim, K.-H. (2020). Exploration of the interactions between mycoviruses and *Fusarium graminearum*. *Adv. Virus Res.* 106, 123–144. doi: 10.1016/bs.aivir.2020.01.004

Yu, J., Lee, K. M., Son, M., and Kim, K. H. (2015). Effects of the deletion and over-expression of Fusarium graminearum gene FgHal2 on host response to mycovirus Fusarium graminearum virus 1. *Mol. Plant Pathol.* 16, 641–652. doi: 10.1111/mpp.12221

Yu, J., Park, J. Y., Heo, J. I., and Kim, K. H. (2020). The ORF2 protein of Fusarium graminearum virus 1 suppresses the transcription of *FgDICER2* and *FgAGO1* to limit host antiviral defences. *Mol. Plant Pathol.* 21, 230–243. doi: 10.1111/mpp.12895

Yu, J., Lee, K.-M., Cho, W. K., Park, J. Y., and Kim, K.-H. (2018). Differential contribution of RNA interference components in response to distinct Fusarium graminearum virus infections. *J. Virol.* 92:e01756-17.

Yun, Y., Liu, Z., Yin, Y., Jiang, J., Chen, Y., Xu, J. R., et al. (2015). Functional analysis of the *Fusarium graminearum* phosphatome. *New Phytol.* 207, 119–134.

Conflict of Interest: The authors declare that the research was conducted in the absence of any commercial or financial relationships that could be construed as a potential conflict of interest.

frontiers in Microbiology

ORIGINAL RESEARCH
published: 25 May 2021
doi: 10.3389/fmicb.2021.659210

Infection of Two Heterologous Mycoviruses Reduces the Virulence of *Valsa mali*, a Fungal Agent of Apple Valsa Canker Disease

Shian Yang[1†], Ruoyin Dai[1†], Lakha Salaipeth[2†], Lili Huang[1], Jie Liu[3], Ida Bagus Andika[3] and Liying Sun[1*]*

[1] State Key Laboratory of Crop Stress Biology for Arid Areas, College of Plant Protection, Northwest A&F University, Xianyang, China, [2] School of Bioresources and Technology, King Mongkut's University of Technology Thonburi, Bangkok, Thailand, [3] College of Plant Health and Medicine, Qingdao Agricultural University, Qingdao, China

OPEN ACCESS

Edited by:
Hiromitsu Moriyama, Tokyo University of Agriculture and Technology, Japan

Reviewed by:
Syun-ichi Urayama, University of Tsukuba, Japan
Satoko Kanematsu, NARO Institute of Fruit Tree Science, Japan
Maria A. Ayllón, Polytechnic University of Madrid, Spain

***Correspondence:**
Ida Bagus Andika
idabagusyf@yahoo.com
Liying Sun
sunliying@nwafu.edu.cn;
sunly_de@126.com

† These authors have contributed equally to this work

Specialty section:
This article was submitted to Virology, a section of the journal Frontiers in Microbiology

Received: *27 January 2021*
Accepted: *13 April 2021*
Published: *25 May 2021*

Citation:
Yang S, Dai R, Salaipeth L, Huang L, Liu J, Andika IB and Sun L (2021) Infection of Two Heterologous Mycoviruses Reduces the Virulence of Valsa mali, a Fungal Agent of Apple Valsa Canker Disease. Front. Microbiol. 12:659210. doi: 10.3389/fmicb.2021.659210

Mycovirus infection has been widely shown to attenuate the virulence of phytopathogenic fungi. *Valsa mali* is an agriculturally important fungus that causes Valsa canker disease in apple trees. In this study, two unrelated mycoviruses [*Cryphonectria hypovirus* 1 (CHV1, genus *Hypovirus*, and single-stranded RNA) and Mycoreovirus 1 (MyRV1, genus *Mycoreovirus*, double-stranded RNA)] that originated from *Cryphonectria parasitica* (chestnut blight fungus) were singly or doubly introduced into *V. mali* via protoplast fusion. CHV1 and MyRV1 stably infected *V. mali* and caused a reduction in fungal vegetative growth and virulence. Co-infection of both viruses further reduced the virulence of *V. mali* but compromised the stability of CHV1 infection and horizontal transmission through hyphal anastomosis. Infections of MyRV1 and, to a lesser extent, CHV1 up-regulated the transcript expression of RNA silencing-related genes in *V. mali*. The accumulation of CHV1 (but not MyRV1) was elevated by the knockdown of *dcl2*, a key gene of the RNA silencing pathway. Similarly, the accumulation of CHV1 and the efficiency of the horizontal transmission of CHV1 during co-infection was restored by the knockdown of *dcl2*. Thus, CHV1 and MyRV1 are potential biological control agents for apple Valsa canker disease, but co-infection of both viruses has a negative effect on CHV1 infection in *V. mali* due to the activation of antiviral RNA silencing by MyRV1 infection.

Keywords: mycovirus, hypovirus, mycoreovirus, *Valsa mali*, hypovirulence, RNA silencing

INTRODUCTION

Apple Valsa canker disease is a destructive plant disease that affects apple trees particularly in East Asian countries (Lee et al., 2006; Abe et al., 2007). The elongated cankers occur on the branches and the trunk, leading to the death of the tree and failure of the entire orchard (Chen et al., 1987). This plant disease is widespread in many apple-producing regions in China and results in significant yield losses (Wang et al., 2011; Li et al., 2013). Apple Valsa canker is caused by the plant pathogenic ascomycete fungus, interchangeably referred to as *Valsa mali* or *Valsa ceratosperma* due to synonymization of *V. mali* that was initially identified as a new species for the causative pathogen of apple Valsa canker, to *V. ceratosperma*. Although *V. ceratosperma* was later found

to be a heterogeneous species complex, further analyses revealed that apple strains of *V. mali* and *V. ceratosperma* from East Asia represent the same fungal species (Wang et al., 2011, 2014, 2020). Apple Valsa canker is difficult to control using chemical treatments even though many types of fungicide have been tested (Wang et al., 2009). Currently, strategies for controlling the disease include strict cultivation management and scraping away of lesions before the application of fungicides. However, highly effective prevention and control measures for this disease are not available (Keqiang et al., 2009).

Research in the field of plant pathology has been aiming to the development of sustainable control methods for fungal diseases that have minimal negative effects on the environment and human health (Raymaekers et al., 2020). In this regard, the biological control method which utilizes mycoviruses (fungal viruses) as control agents (virocontrol) is a promising method for the protection of plants against phytopathogenic fungi (Xie and Jiang, 2014; García-Pedrajas et al., 2019). Mycoviruses are widespread among fungal groups (Ghabrial and Suzuki, 2009). Several species of mycoviruses can reduce the virulence of their host, however, most do not affect the host (Hillman et al., 2018). The mycovirus *Cryphonectria hypovirus* 1 (CHV1) has been successfully used in Europe as a biological control agent to manage chestnut blight caused by the plant pathogenic fungus *Cryphonectria parasitica* (Rigling and Prospero, 2018). CHV1 infection is associated with attenuated virulence, reduced pigmentation, suppressed asexual sporulation, and altered expression of certain genes of its host (Dawe and Nuss, 2001). CHV1 is a non-segmented, positive-sense, single-stranded RNA virus belonging to the genus *Hypovirus* of the family *Hypoviridae*. Its genome (12.7 kilobases) contains two open reading frames (ORFs), ORF A and ORF B. These ORFs encode multifunctional polyproteins such as the papain-like proteases, p29 and p48, which are responsible for proteolytic cleavage in the generation of functional viral proteins (Shapira et al., 1991b). The p29 encoded in CHV1 ORF A is a multifunctional protein which plays a role in the suppression of host pigmentation, sporulation, and RNA silencing (Craven et al., 1993; Sun et al., 2009; Chiba and Suzuki, 2015).

Besides CHV1, Mycoreovirus 1 (MyRV1), isolated from *C. parasitica* in the United States, is a potential biological control agent. MyRV1 is a member of the genus *Mycoreovirus* within the family *Reoviridae*. Its genome contains 11 segments of double-stranded RNA (dsRNA; S1 to S11) ranging from 4127 to 732 base pairs (bp) in length (Hillman et al., 2004). MyRV1 markedly reduces the virulence of its host, but it shows minimal effects on pigmentation and asexual sporulation (Hillman et al., 2004). Mixed infection of CHV1 and MyRV1 in *C. parasitica* presents a one-way synergism in which CHV1 enhances the replication and vertical transmission of MyRV1 through asexual spores (Sun et al., 2006).

A previous study showed that introduction of CHV1 into *V. ceratosperma* via biolistic delivery of infectious cDNA clone results in colony morphology changes and reduced virulence (Sasaki et al., 2002). Another study demonstrated that infection of Rosellinia necatrix Mycoreovirus 3, a mycoreovirus originated from the white root rot fungus *Rosellinia necatrix* in *V. ceratosperma* causes reduction in fungal virulence (Kanematsu et al., 2010). A more recent study identified a new hypovirus naturally infecting *V. ceratosperma*, but the infection of this virus is not associated with reduction of fungal virulence (Yaegashi et al., 2012).

RNA silencing is a sequence-specific gene downregulation that is also important as an antiviral defense mechanism in eukaryotes including fungi (Aliyari and Ding, 2009; Chang et al., 2012). In antiviral RNA silencing, viral-derived dsRNAs are cleaved by a Dicer-like protein (DCL) to generate small interfering RNAs that guide an Argonaute (AGO)-containing RNA silencing-induced complex for sequence-specific degradation of a viral RNA target (Ding, 2010). Ascomycete fungi are known to encode two DCLs and a varying number of AGOs, according to the species of fungus (Nakayashiki et al., 2006). The *V. mali* genome contains two *dcl* genes (*dcl1* and *dcl2*) and three Argonaute-like (*agl*) genes (*agl1*, *agl2,* and *agl3*; Feng et al., 2017a,b) but their roles in antiviral defense responses have not been demonstrated.

In this study, we examined the effects of single and double infection of CHV1 and MyRV1 on vegetative growth and the virulence of *V. mali*. Our results suggest that CHV1 and MyRV1 are potential biological control agents for *V. mali* but co-infection of both viruses compromised the stability of CHV1 infection. Furthermore, we examined the interaction of CHV1 and MyRV1 with antiviral RNA silencing in *V. mali* in the context of single and double infection.

MATERIALS AND METHODS

Fungal Strains and Viruses

The *C. parasitica* strains EP713 (Nuss et al., 2005) and 9B21 (Hillman et al., 2004), naturally infected with CHV1 and MyRV1, respectively, were provided by Dr. Nobuhiro Suzuki from Okayama University in Japan. The wild-type and *dcl2* knockout mutants of *V. mali* strains were described previously (Feng et al., 2017a).

All fungal strains were grown for 3 to 5 days on potato dextrose agar (PDA, Difco) under benchtop conditions at 24∼26°C for morphological observation or in potato dextrose broth (PDB, Difco) when mycelia were used for the preparation of protoplasts. For maintenance, fungal strains were cultured on regeneration plates (Churchill et al., 1990) and stored at 4°C until further use. To observe the formation of asexual fruiting bodies, the fungal strains were continually cultured on PDA for 4 to 5 additional weeks.

Protoplast Preparation

The protoplasts of all fungal strains were prepared individually using a method described previously (Eusebio-Cope et al., 2009) with a slight modification. The fungal strains grown on PDA medium were cut into small pieces, cultured in 20 ml PDB (50 ml flask) and incubated in the dark at 25°C for 3 days without shaking. The young mycelia were harvested, washed with 0.6 M $MgSO_4$ and suspended in an enzymatic solution containing 3∼6 mg lysine enzyme, 10∼15 mg β-glucuronidase and 6∼12 mg

bovine serum albumin in 10 ml of 1.2 M $MgSO_4$. This was followed by incubation at 27°C for 3∼4 h with gentle shaking. The protoplast suspensions were slowly poured into a new 50 ml plastic tube. A 1.25 volume of trapping buffer (0.4 M sorbitol in 100 mM Tris–HCl, pH 7.0) was overlaid onto the protoplast suspensions and centrifuged at 3,500 rpm for 20 min at 4°C to concentrate the protoplasts at the interface. The protoplasts were diluted in 2 volumes of 1 M sorbitol, centrifuged at 3,500 rpm for 20 min at 4°C and washed again with 10 ml of STC (1 M sorbitol, 100 mM $CaCl_2$, 100 mM Tris–HCl, and pH 8.0). Finally, the protoplasts were suspended in a small volume of STC to obtain approximately 1×10^7 protoplasts per ml. This suspension was immediately used or stored at –80°C until further use.

Protoplast Fusion

To introduce CHV1 and MyRV1 into *V. mali*, the protoplasts prepared from *C. parasitica* strains EP713 (infected with CHV1) or 9B21 (infected with MyRV1) were fused with *V. mali* protoplasts using polyethylene glycol (PEG). To obtain doubly infected strain, *V. mali* protoplasts were simultaneously fused with the protoplasts prepared from both *C. parasitica* strains EP713 and 9B21. *V. mali* protoplasts (100 μl 1×10^7 of protoplasts/ml) and *C. parasitica* protoplasts (100∼200 μl of 1×10^6 protoplasts/ml) were mixed gently and placed on ice for 30 min. After adding 500 μl of PTC solution (40% PEG 4000, 100 mM Tris–HCl pH 8.0, and 100 mM $CaCl_2$) to each protoplast suspension, the mixtures were combined gently and incubated at room temperature for 20 min. The protoplast mixtures were then centrifuged at 3,500 rpm for 5 min at 4°C, resuspended with 100 ml of 1 M sorbitol, divided into 10 aliquot parts and each placed in the center of a petri dish, and then 20∼25 ml of YCDA (0.1% yeast extract, 0.1% casein hydrolysate, 0.5% glucose, and 1.5% agar) was added. The Petri dishes were left on the benchtop for 5 to 7 days and a small piece of hypha from the edges of the colonies was subsequently transferred to new PDA plates and examined for the *V. mali* phenotype or prepared for dsRNA extraction. To ensure the homogeneity of *V. mali* isolates obtained from protoplast fusion, the fungal isolates were cultured on PDA plates from single hypha of fungal colonies that grew after regeneration of protoplasts. Basically, *V. mali* can be isolated due to the faster growth of *V. mali* on YCDA or PDA medium than that of *C. parasitica*. Furthermore, the purity of *V. mali* isolates obtained from the protoplast fusion is confirmed by observation of fungal colony morphology and sequencing of ribosomal-DNA intergenic spacer regions.

Horizontal Transmission of Viruses

The horizontal transmission of viruses through hyphal anastomosis was performed as described previously (Chiba et al., 2013). The virus-infected donor strain was cultured with a virus-free recipient strain at a distance of 1 cm on a PDA plate and incubated at 24∼26°C. After 5 or 7 days of hyphal contact, mycelial plugs were taken from three different positions (near, middle, and far) on the recipient side and cultured on PDA plates layered with cellophane for 4 days before RNA extraction for viral dsRNA analysis or RT-PCR detection.

Phenotypic and Virulence Assays

The growth of fungal colonies on a PDA plate (maintained on a benchtop at 24∼26°C for 4 days) was measured based on the colony area of three replicates. The morphology of the fungi was analyzed and photographed. Virulence has been measured in apples according to the area of the lesions induced by fungal growth (Hillman et al., 1990). Apples (cv. Gala) were purchased from a supermarket and 2-year-old apple twigs were obtained from apple trees planted at an experimental station at Northwest A&F University, China. The fruits and branches were washed with tap water, the surface was wiped with 75% ethanol and they were then rinsed several times with sterile distilled water. Small holes of 6 mm in diameter were created on the surface of the fruits and branches, after which an agar plug from the growing margin of a 4-day-old colony was placed directly on each hole and wrapped with parafilm. The apples were placed in a container with wet tissue paper, and the ends of each twig were covered with wet tissue paper. All samples were maintained at 25°C for 5 or 10 days. The parafilm wraps were removed 2 days after inoculation. After 5 or 10 days of inoculation, lesion sizes were measured as indicators of disease development. Each sample contained five inoculation points, and five apples, and five twigs were used for each strain. Virulence assays were repeated three times independently.

dsRNA Isolation

A rapid, small-scale extraction of dsRNA was performed. Fungal mycelia grown for 4 days were collected from PDA plates layered with cellophane or PDB cultures, then ground into a powder with liquid nitrogen and homogenized with 1 ml of EBA buffer (50 mM Tris–HCl pH 8.5, 50 mM EDTA, 3% SDS, 1% PVPP, and 1% DTT). The suspensions were centrifuged at 4°C for 15 min at 12,000 rpm. The supernatant (600 μl) was mixed with 600 μl of STE (10 mM Tris–HCl pH 8.0, 1 mM EDTA, and 150 mM NaCl), ethanol (up to 16% volume) and a small amount of CC41 cellulose in preparation for column chromatography analysis of dsRNAs. After 40∼60 min of continuous agitation at room temperature, each tube was washed three times with STE-EtOH (16% EtOH; v/v), with vortexing and centrifugation between washes. The dsRNAs were eluted from the dried CC41 by adding 700 μl of STE buffer and centrifuging at 12,000 rpm for 2 min. The eluate was collected and mixed with an equal volume of isopropanol, incubated for 10 min at room temperature and centrifuged at 4°C for 30 min at 12,000 rpm. The dsRNA pellet was washed with 70% ethanol, air-dried at room temperature and dissolved in 30∼50 μl of RNase-free water. Each sample was subjected to 1.4% agarose gel electrophoresis in 1X TBE buffer.

Total RNA Extraction and Viral dsRNA Quantification

Total RNA was prepared from *V. mali* mycelia cultured in PDA with cellophane for 3 days, as described previously (Sun et al., 2006). The RNA concentration was adjusted to 2 μg/μl using a Nano Photometer (N50 Touch) for use in agarose gel electrophoresis. Viral genomic dsRNA was quantified using densitometry, as described previously (Suzuki et al., 2003).

Total RNA samples were analyzed by electrophoresis using a 1.4% agarose gel in a 1X TAE (40 mM Tris/acetate pH 7.8, 1 mM EDTA) buffer system and stained with ethidium bromide. The RNA bands were visualized using a UV lamp under a transilluminator and were photographed digitally at various exposures. The RNA bands were analyzed and quantified using Image J Macro software. Relative amounts of MyRV1 genomic RNA were quantified by measuring the amount of S1, S2, and S3 RNA segments normalized to the amount of host fungal 18S rRNA. A similar method was used to quantify CHV1 genomic RNA accumulation.

RT-PCR and Quantitative PCR Analyses

The single stranded RNAs (ssRNAs) were extracted from fungal mycelia (3 days old) following the procedure described previously (Sun et al., 2006). First-strand cDNA was synthesized with ReverTra Ace reverse transcriptase (Toyobo) using 0.2 μg of ssRNAs as a template (according to the manufacturer's instructions) and then used for PCR amplification using 2-mixture DNA polymerase (Kangwei) and primers specific for CHV1 p29. Quantitative PCR was performed using a CRX96TM Real-Time PCR Detection System (Bio-Rad) via a Kapa SYBR Fast ABI Prism qPCR mix kit (Kapa Biosystems). The 18S RNA of *V. mali* was used as an internal control. Three biological replicates were used for each sample and the experiments were repeated three times independently. The primers used in this study are listed in **Supplementary Table 1**.

Statistic Analysis

One-way ANOVA analysis was performed in Microsoft Excel with *post hoc t*-tests.

RESULTS AND DISCUSSION

CHV1 and MyRV1 Can Infect *V. mali*

To investigate whether our *V. mali* strain can host mycoviruses and become hypovirulent, CHV1 and MyRV1 were introduced into *V. mali* via protoplast fusion using two protoplast fractions prepared from CHV1- or MyRV1-infected *C. parasitica* and virus-free *V. mali*. CHV1 and MyRV1 were also simultaneously introduced to *V. mali* through protoplast fusion using the mixture of protoplasts prepared from *C. parasitica* that were infected with CHV1 and MyRV1. After protoplast fusion, regeneration of *V. mali* protoplasts and transfer to new PDA plates, viral dsRNA accumulation in individual *V. mali* isolates was analyzed at 4 days after transference to a PDA plate. The results showed accumulations of 12.7-kilobase dsRNA of CHV1 or 11 dsRNA genome segments (4,127 to 732 bases) of MyRV1 in *V. mali* isolates regenerated after protoplast fusion, using corresponding CHV1- or MyRV1-infected *C. parasitica*. Moreover, simultaneous accumulation of CHV1 and MyRV1 dsRNAs was also detected in *V. mali* after protoplast fusion using the mixture of protoplasts prepared from *C. parasitica* that were infected with CHV1 and MyRV1 (**Figure 1A**). These results indicate that this *V. mali* strain is a compatible host for CHV1 and MyRV1. Notably, defective interfering RNAs (DI-RNAs) of the CHV1 genome were frequently observed in doubly infected fungi but not in singly infected fungi (**Figure 1A**). Infection of CHV1 in *C. parasitica* usually gives rise to DI-RNAs at a very high frequency (Shapira et al., 1991a) and DI-RNAs were also formed in *C. parasitica* doubly infected with CHV1 and MyRV1 (**Supplementary Figure 1**). Because *dcl2* gene is essential for production of DI-RNAs (Zhang and Nuss, 2008), it is thus possible that generation of CHV1 DI-RNAs during co-infection with MyRV1 in *V. mali* is due to the upregulation of *dcl2* gene expression (further supporting data and discussion are presented below).

CHV1 and MyRV1 Infection Reduced the Growth and Virulence of *V. mali*

To examine the effect of CHV1 and MyRV1 infection on *V. mali*, singly and doubly infected fungi, as well as virus-free fungi, were cultured under the same conditions, and the colony growth and morphology were analyzed. *V. mali* strains infected with either virus showed a reduction in colony size, although the fungus colony infected with CHV1 was much smaller than that infected with MyRV1 and showed an irregular margin and less dense mycelia (**Figures 1B,C**). Moreover, the MyRV1-infected fungal colony showed a slight increase in brown-colored pigments compared with the CHV1-infected and virus-free *V. mali* strains. Similarly, in previous studies, MyRV1 infection in *C. parasitica* resulted in reduced growth of aerial hyphae and enhanced the production of brown pigments (Sun et al., 2006; Tanaka et al., 2011). *V. mali* co-infected with both viruses exhibited a smaller colony size than when infected with CHV1 alone (**Figures 1B,C**). Next, the formation of asexual fruiting bodies (pycnidia) of *V. mali* cultured on a PDA plate was investigated at a later growth stage of the fungus (**Figure 1D**). CHV1 infection reduced pycnidia production, whereas MyRV1 infection increased pycnidia production (**Figure 1E**). The *V. mali* strain infected with both viruses produced a similar number of pycnidia as the virus-free strain (**Figure 1E**), suggesting that MyRV1 infection compromised the negative effects of CHV1 infection on pycnidia production in *V. mali*.

For the fungal virulence assay, virus-infected and virus-free *V. mali* strains (agar plugs) were inoculated in apples and the virulence levels were evaluated by measuring the area of lesions at 5 days after inoculation. The virus-free *V. mali* strain induced the largest lesions on apples, while the *V. mali* strains infected with either CHV1 or MyRV1 exhibited significantly smaller canker lesions although CHV1 infection induced a stronger effect than MyRV1 (**Figures 2A,C**). The doubly infected *V. mali* strain did not produce obvious lesions in apples (**Figures 2A,C**), suggesting that double infection strongly reduces the virulence of *V. mali*. A virulence assay was performed in parallel using apple twigs. In general, the effects of single and double infection on the virulence of *V. mali* using apple twigs observed at 5 and 10 days after inoculation were similar to those observed in apples (**Figures 2B,D** and **Supplementary Figure 2**). Our observations indicate that CHV1 and MyRV1 confer hypovirulence in *V. mali* and co-infection of these mycoviruses further reduces the virulence of the fungus. The differing levels of hypovirulence

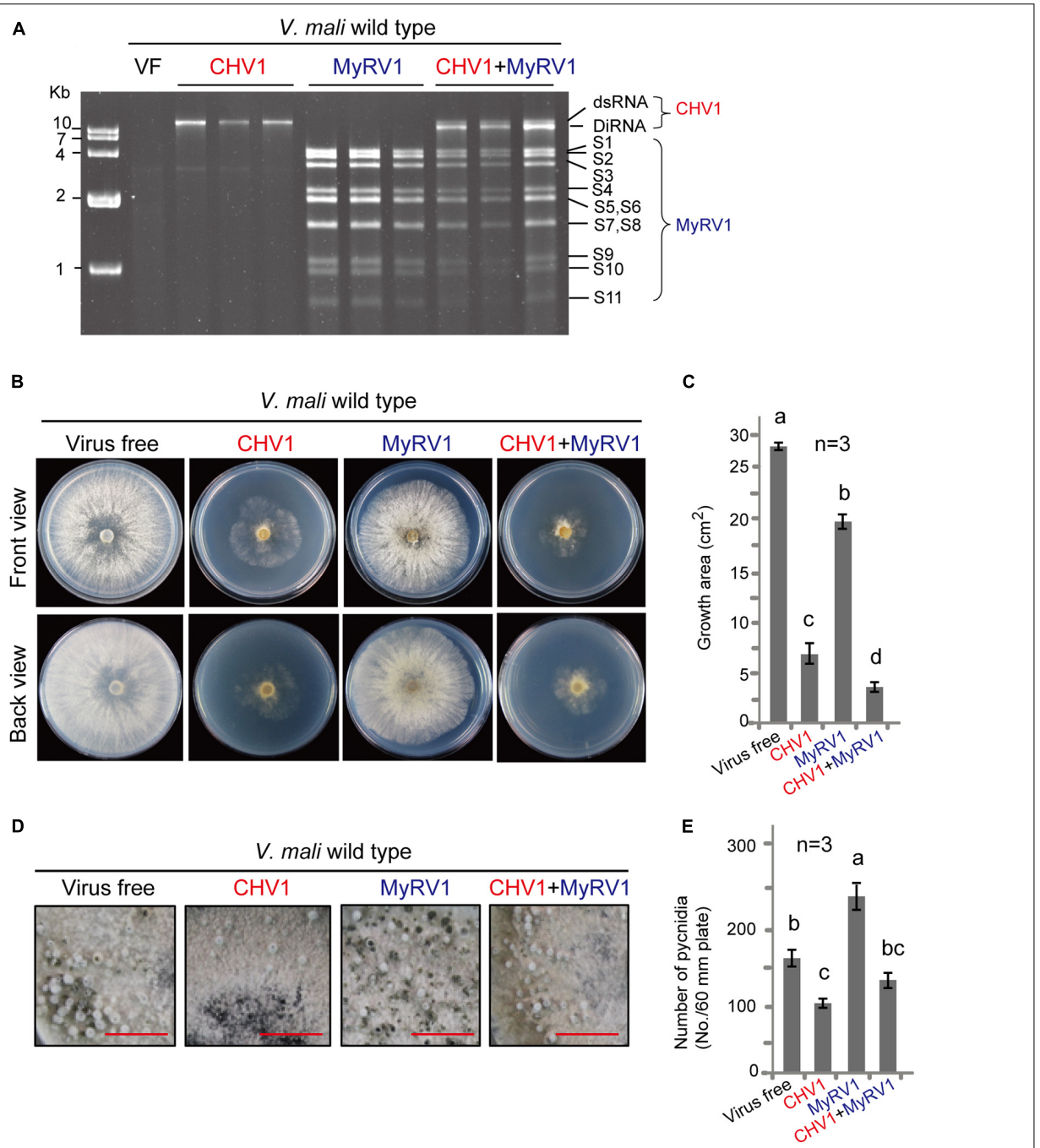

FIGURE 1 | Infection of CHV1 and MyRV1 in *V. mali*. **(A)** Agarose gel electrophoresis of dsRNAs extracted from *V. mali* strains singly or doubly infected with CHV1 and MyRV1. The dsRNA samples were analyzed via electrophoresis in an agarose gel stained with ethidium bromide. The CHV1 dsRNA bands that migrated slightly faster than the wild-type CHV1 are defective interference RNA (DI-RNA). **(B)** Phenotypic growth on PDA medium of representative *V. mali* strains singly or doubly infected with CHV1 and MyRV1. The colonies were grown on PDA for 4 days and then photographed. **(C)** The growth areas of fungal strains described in **(B)**. The data are the means ± SD ($n = 3$). The different letters indicate a significant difference at $p < 0.01$ (one-way ANOVA). **(D)** Representative images showing the formation of asexual fruiting bodies (pycnidia) of the fungal strains described in **(B)**. The fungi were cultured on PDA medium for 4–5 weeks until the pycnidia were produced. Bars equal 1 cm. **(E)** The number of pycnidia counted from the fungal strains described in **(D)**. The data are the means ± SD ($n = 3$). The different letters indicate a significant difference at $p < 0.01$ (one-way ANOVA).

observed in this study between CHV1 and MyRV1 in *V. mali* were opposite to that observed in *C. parasitica* where MyRV1 showed a stronger effect than CHV1 in attenuating fungal virulence (Sun et al., 2006). Moreover, CHV1 and MyRV1 co-infection in *C. parasitica* did not markedly reduce the virulence of the fungal host relative to that induced by single infection

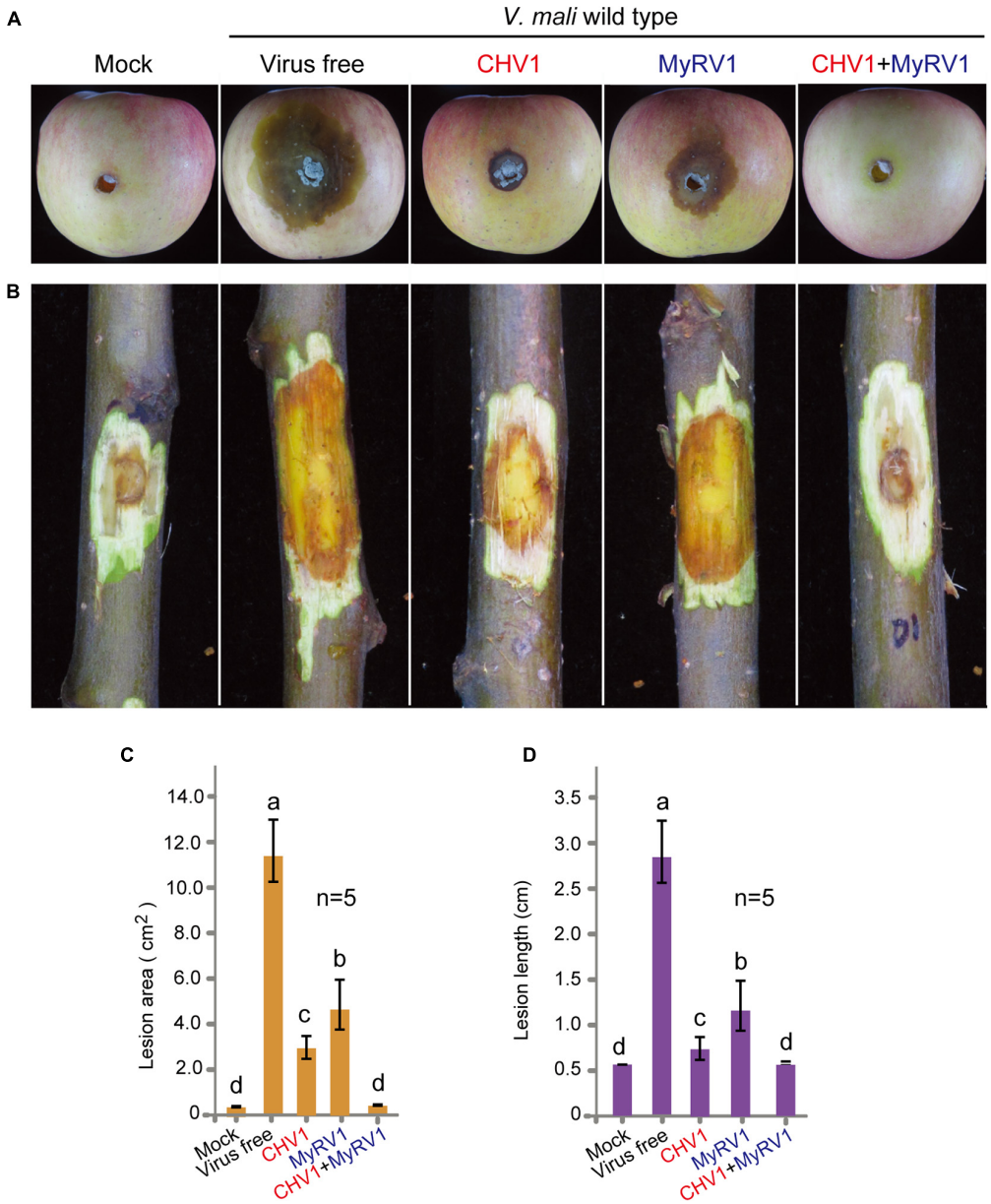

FIGURE 2 | The virulence levels of *V. mali* strains singly or doubly infected with CHV1 and MyRV1. **(A)** Representative images showing lesions on apples induced by *V. mali* strains. The cankers were photographed at 5 days post-inoculation. **(B)** Representative images showing lesions on apple twigs induced by *V. mali* strains. The lesions on twigs were photographed at 5 days post-inoculation. **(C)** Lesion areas on apples measured in the experiment described in **(A)**. The data are the means ± SD (n = 5). The different letters indicate a significant difference at $p < 0.01$ (one-way ANOVA). **(D)** Lesion lengths on apple twigs measured in the experiment described in **(B)**. The data are the means ± SD (n = 5). The different letters indicate a significant difference at $p < 0.01$ (one-way ANOVA).

(Sun et al., 2006). Thus, the molecular mechanisms underlying the hypovirulence caused by CHV1 and MyRV1 may differ between *V. mali* and *C. parasitica*.

Co-infection With MyRV1 Causes Unstable Infection of CHV1 in *V. mali*

Subsequent subculturing on PDA plates of *V. mali* strains that were co-infected with CHV1 and MyRV1 revealed that most fungal strains regained their vegetative growth rate, which contrasts with the small colony size initially exhibited by these strains (**Figure 3A**). dsRNA and RT-PCR analyses showed that CHV1 was undetectable or its accumulation decreased in the fungal strain that recovered to a higher growth rate, whereas MyRV1 stably accumulated in all strains after fungal subculture (**Figure 3B**). In the *V. mali* strains singly infected with CHV1 or MyRV1, stable virus accumulation was observed in subsequent fungal cultures (**Supplementary Figure 3**). These observations

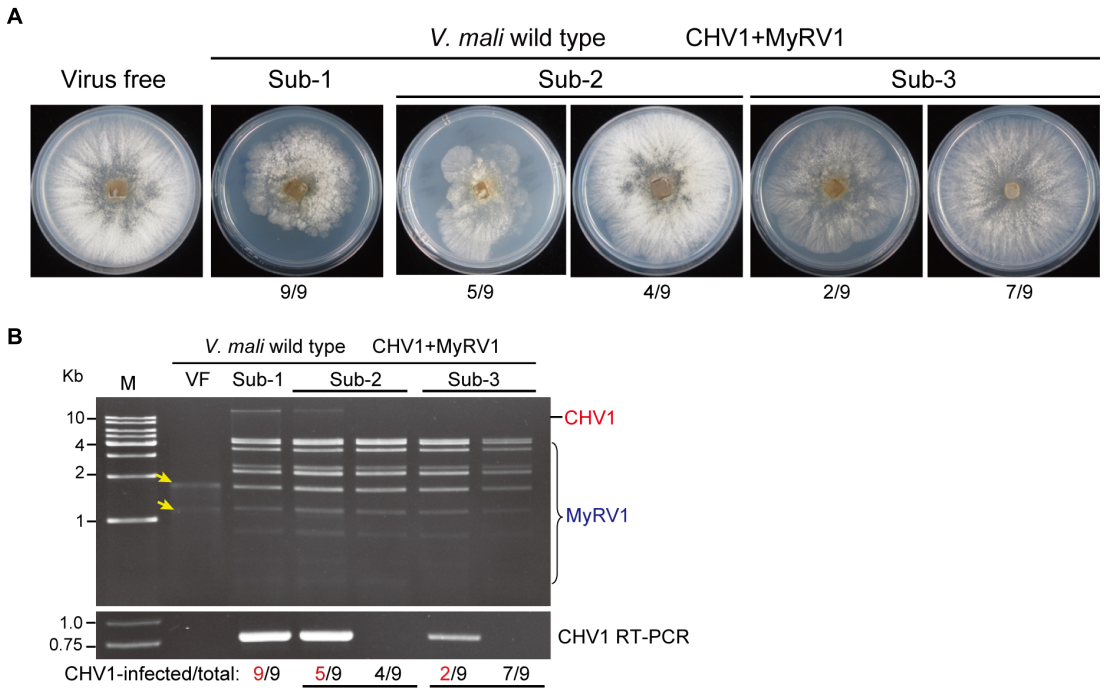

FIGURE 3 | The accumulation of CHV1 and MyRV1 in co-infected *V. mali* after subsequent subculturing. **(A)** The phenotypic growth on PDA medium of representative *V. mali* strains co-infected with CHV1 and MyRV1 in the first to third fungal subcultures (Sub-1 to Sub-3). The colonies were grown on PDA for 4 days and then photographed. The numbers below the images indicate the number of fungal colonies showing a similar phenotype as presented in the photo per total number of colonies shown. **(B)** Viral dsRNA and RT-PCR analyses of doubly infected *V. mali* strains described in **(A)**. The numbers below the lanes indicate the number of samples in which CHV1 was detected or undetected per total number of samples. Yellow-colored arrows mark the traces of ribosomal RNAs in virus-free (VF) sample incorporated during dsRNA isolation.

suggest that MyRV1 infection has an antagonistic effect on CHV1 accumulation in *V. mali*. The interactions between co-infecting viruses can be either synergistic/facilitative or antagonistic while in plant and fungi, RNA silencing mechanism has been shown to be the most common underlying mechanism of both types of virus-virus interactions (Sun et al., 2006; Syller, 2012; Chiba and Suzuki, 2015; Mascia and Gallitelli, 2016; Aulia et al., 2019; Bian et al., 2020).

Horizontal Transmission of CHV1 and MyRV1 in *V. mali*

To examine whether CHV1 and MyRV1 were horizontally transmitted in *V. mali* via hyphal anastomosis, a virus-infected strain (donor), and a virus-free strain (recipient) were co-cultured on a PDA plate and after 5 days of hyphal fusion, agar plugs taken from the recipient colony side were grown in PDB culture and subjected to dsRNA extraction. As no specific marker gene or antibiotic resistance is available in the recipient strains for selection, the mycelial plugs, which were taken from recipient side may include the donor cells. To discern such possibility, agar plugs were taken from three positions that are near, middle, and far distance from the hyphal fusion areas in the recipient colony. Following hyphal fusion on the PDA plate, the virus-free *V. mali* strain co-cultured with the CHV1-infected strain showed a CHV1-infected phenotype, while the virus-free strain co-cultured with the MyRV1-infected strain showed no obvious phenotypic change, due to a slightly altered phenotype of MyRV1-infected strain on the PDA plate (**Figure 4A**). dsRNA analysis showed the accumulation of CHV1 or MyRV1 dsRNAs in all fungal strains taken from the three different positions in the recipient colonies (**Figures 4B,C**). Intriguingly, in hyphal fusion with the CHV1 and MyRV1 co-infected strain, the virus-free strain did not showed altered phenotype as observed for hyphal fusion using the CHV1-infected strain (**Figure 4A**). Accordingly, the fungal strains taken from the recipient colonies co-cultured with the CHV1 and MyRV1 co-infected strain as a donor, all accumulated MyRV1 dsRNAs, however, several strains accumulated no or low levels of CHV1 dsRNA, in particular to a higher number when mycelial plugs were taken far from the hyphal fusion areas (**Figure 4D**). Although in this assay we cannot rule out the possibility of the presence of donor strains in some of fungal strains taken from the recipient colonies, the results of our co-culture assays using up to 12 PDA plates for each single and double infection suggest that co-infection with MyRV1 interferes with the efficient horizontal transmission of CHV1 in *V. mali*. To further examine whether the co-infection condition affects the horizontal transmission of CHV1 and MyRV1, CHV1- and MyRV1-infected strains were co-cultured on 13 PDA plates to allow for hyphal anastomosis (**Figure 4E**). dsRNA analysis showed that neither CHV1 nor MyRV1 were efficiently transmitted to the recipient

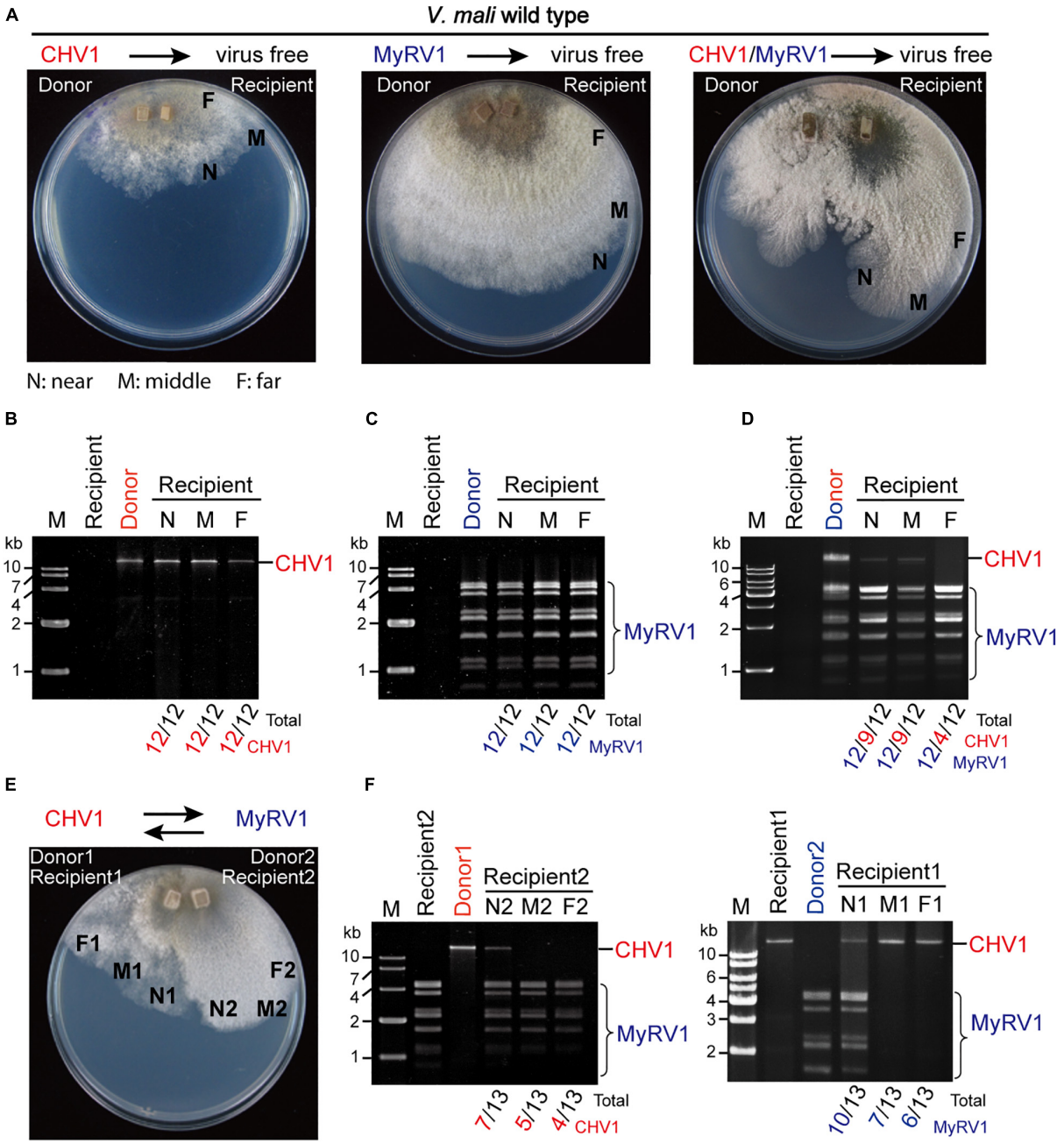

FIGURE 4 | The efficiency of CHV1 and MyRV1 horizontal transmission via hyphal anastomosis in *V. mali*. **(A)** Co-culture on PDA plates of the virus-free *V. mali* strain and the virus-infected *V. mali* strain as recipient and donor viruses, respectively. After 1 week of hyphal contact, mycelial plugs were removed from three locations (a near, middle, and far distance from the hyphal fusion areas) in the recipient side, transferred onto new PDA plates and cultured in PDB for dsRNA extraction. **(B–D)** Detection of viral dsRNAs in recipient strains co-cultured with CHV1-infected **(B)**, MyRV1-infected **(C)**, and CHV1 + MyRV1-infected strains **(D)**. The numbers below the lanes indicate the number of samples in which viral dsRNAs were detected per total number of samples. **(E)** Co-culture of CHV1-infected and MyRV1-infected *V. mali* strains on a PDA plate. After 1 week of hyphal contact, mycelial plugs were removed from three locations on both sides, transferred onto new PDA plates and cultured in PDB for dsRNA extraction. **(F)** Detection of viral dsRNAs in fungal strains obtained in the co-culture experiment described in **(E)**.

side of the fungus (**Figure 4F**), suggesting that CHV1 and MyRV1 have an antagonistic effect on each other concerning horizontal transmission.

Mycoviruses are transmitted vertically from the mycelium to spores or horizontally via hyphal anastomosis (Hillman et al., 2018). Therefore, transmission efficiency is an important factor when evaluating a mycovirus for its potential as a biological control agent. Under natural conditions, the spreading of mycoviruses is limited by vegetative incompatibility among fungal species and strains

in a fungal population (Choi et al., 2012), however, some studies on filamentous phytopathogenic fungi have demonstrated the occurrence of virus transmission between vegetatively incompatible fungal hosts (Brusini and Robin, 2013; Hamid et al., 2018). Sclerotinia sclerotiorum Mycoreovirus 4 (genus *Mycoreovirus* of the family Reoviridae), which originated from the phytopathogenic fungus *Sclerotinia sclerotiorum*, can suppress host non-self recognition and thus enable the horizontal transmission of heterologous viruses (Wu et al., 2017). Our research group recently proposed a model in which mycoviruses could spread across vegetatively incompatible fungal strains or to different fungal species through plant–fungal-mediated routes facilitated by plant viruses (Bian et al., 2020). Conversely, the present study showed that the efficiency of CHV1 and MyRV1 horizontal transmission is reduced under co-infection conditions. Further investigations should be conducted to assess whether such inhibitory effects on horizontal transmission between co-infected viruses commonly occurs among mycoviruses.

CHV1 and MyRV1 Infection Up-regulates the Transcript Expression of RNA Silencing-Related Genes in *V. mali*

CHV1 and MyRV1 infection in *C. parasitica* was shown to increase the transcript expression of *dcl2* and *agl2* genes, two key components of the antiviral RNA silencing pathway in *C. parasitica* (Sun et al., 2009; Chiba and Suzuki, 2015; Andika et al., 2017). To examine whether such effects of CHV1 and MyRV1 infection also occur in *V. mali*, transcript expression of *V. mali dcl1*, *dcl2*, *agl1*, *agl2,* and *agl3* genes were analyzed by quantitative RT-PCR following single and double virus infection. The analyses revealed that single infection and co-infection generally enhanced the transcript expression of all the genes, however, the highest increase in expression was observed for *dcl2* and *agl3*, particularly following MyRV1 infection (**Figure 5**). This suggests that RNA silencing is activated by CHV1 or MyRV1 infection in *V. mali*, however, CHV1 may suppress the activation of the RNA silencing response through the activity of the CHV1-encoded p29 silencing suppressor, as previously demonstrated in *C. parasitica* (Sun et al., 2009; Chiba and Suzuki, 2015). Moreover, much more increase of *dcl2* transcript levels following co-infection of CHV1 and MyRV1 than CHV1 single infection supports the notion that generation of CHV1 DI-RNAs during co-infection with MyRV1 (**Figure 1A**) is related to the high expression of *dcl2* gene.

The Inactivation of *dcl2* in *V. mali* Enhances the dsRNA Accumulation and Stability of CHV1

To investigate whether RNA silencing contributes to the inhibition of mycovirus multiplication in *V. mali*, CHV1 and MyRV1 were introduced to a *dcl2* knockout mutant (Δ*dcl2*) of *V. mali* by hyphal anastomosis. Single infection or co-infection of CHV1 and MyRV1 reduced Δ*dcl2* growth and produced a similar pattern as that observed in the *V. mali* wild-type

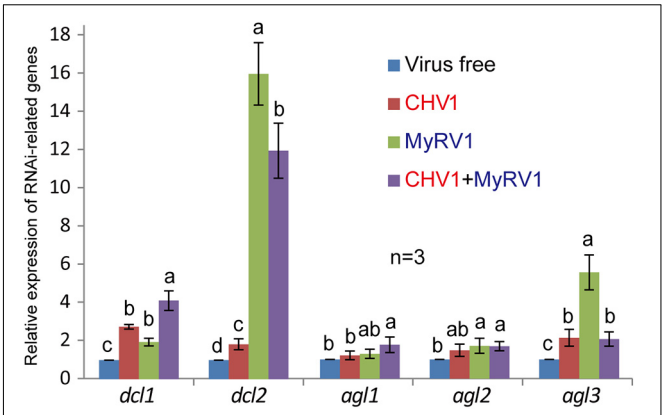

FIGURE 5 | The relative transcript expression of RNA silencing-related genes in *V. mali* strains singly or doubly infected with CHV1 and MyRV1. The transcript expression of *V. mali dcl1*, *dcl2*, *agl1*, *agl2,* and *agl3* genes following single and double virus infection were analyzed by quantitative RT-PCR. The data are the means ± SD (n = 3). The different letters indicate a significant difference at $p < 0.01$ (one-way ANOVA).

(**Figures 6A,B**). Next, the relative viral dsRNA accumulation levels in the wild-type and Δ*dcl2* mutant were compared by extracting the total RNA from the infected fungi. The accumulation of the viral dsRNAs was visualized through agarose gel electrophoresis. CHV1 dsRNA accumulation was enhanced in the Δ*dcl2* mutant in the case of single infection or co-infection with MyRV1, while MyRV1 dsRNA accumulation levels were similar in the wild-type and Δ*dcl2* mutant during single infection but were enhanced in the Δ*dcl2* mutant during co-infection with CHV1 (**Figures 6C,D**). This suggests that MyRV1 is less affected by antiviral RNA silencing responses in *V. mali* than CHV1. This is similar to an observation in *C. parasitica* where the inactivation of *dcl2* increased CHV1 RNA accumulation but had no effect on MyRV1 RNA accumulation (Chiba and Suzuki, 2015). It was also observed that co-infection reduced CHV1 dsRNA accumulation relative to that of single infection but had no effect on MyRV1 dsRNA accumulation (**Figures 6C,D**). The Δ*dcl2* mutant strains co-infected with CHV1 and MyRV1 maintained restrained vegetative growth in successive fungal subcultures (**Figure 6E**). Accordingly, CHV1 stably accumulated after successive fungal subculturing in the Δ*dcl2* mutant co-infected with these two viruses (**Figure 6F**), similar as the stability of CHV1 and MyRV1 single infection in the Δ*dcl2* mutant (**Supplementary Figure 3**). These results indicate that DCL2 is responsible for the suppression of CHV1 accumulation during co-infection with MyRV1. Notably, formation of CHV1 DI-RNAs was not observed in co-infected Δ*dcl2* mutant (**Figure 6F**), further supporting the view that a high expression of *dcl2* transcripts during co-infection with MyRV1 is responsible for generation of CHV1 DI-RNAs.

Previous studies have shown that DCL2 (but not DCL1) is critical for antiviral RNA silencing in *C. parasitica* and *Colletotrichum higginsianum* (Segers et al., 2007; Campo et al., 2016), while DCL2 and DCL1 are functionally

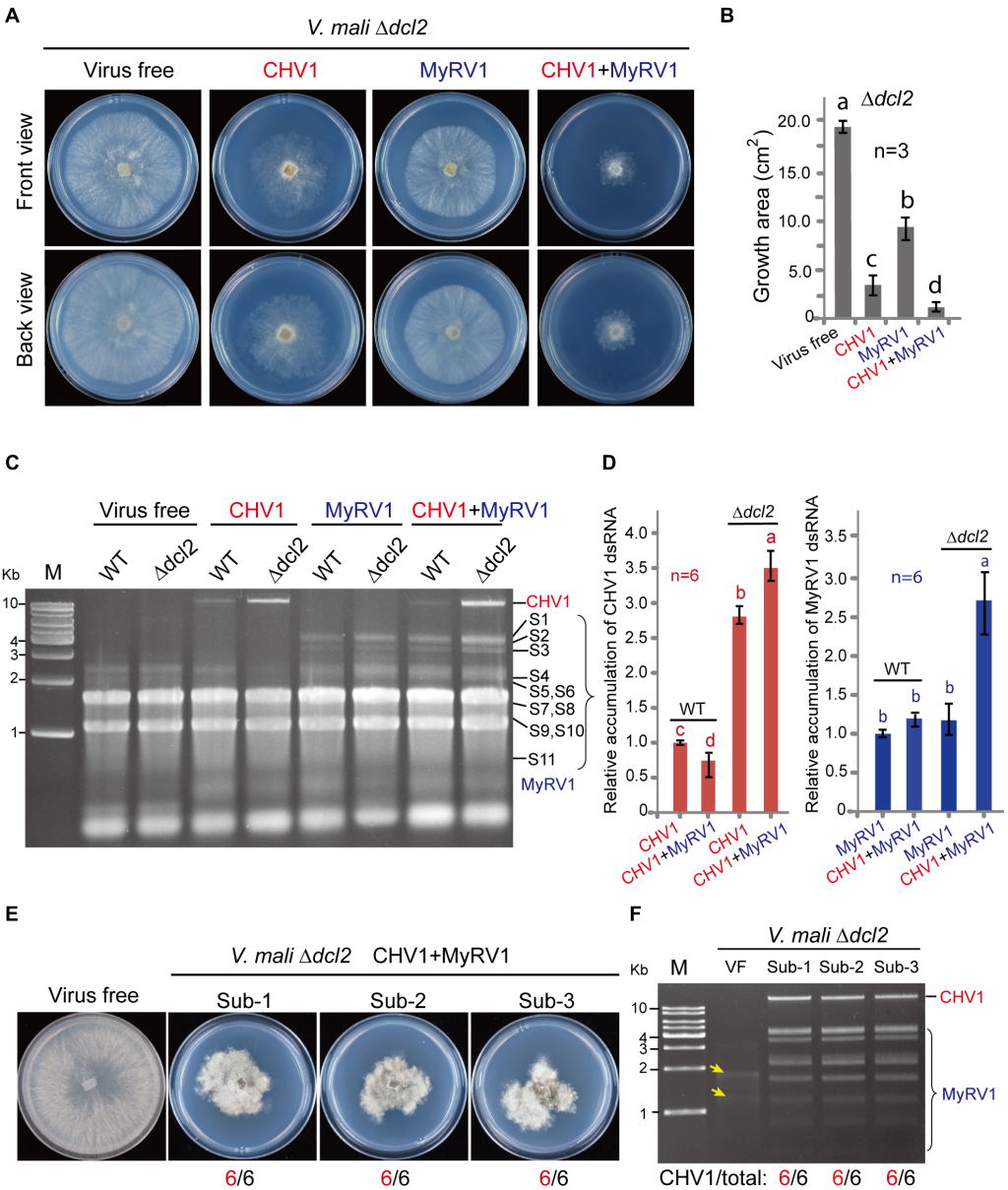

FIGURE 6 | The accumulation of CHV1 and MyRV1 in the *dcl2* knockout mutant of *V. mali*. **(A)** The phenotypic growth on PDA medium of the representative *V. mali* mutant strains singly or doubly infected with CHV1 and MyRV1. The colonies were grown on PDA for 4 days and then photographed. **(B)** The growth areas of the fungal strains described in **(A)**. The data are the means ± SD (n = 3). The different letters indicate a significant difference at $p < 0.01$ (one-way ANOVA). **(C)** Agarose gel electrophoresis of the total RNA samples extracted from the wild-type and *dcl2* knockout mutant of *V. mali* strains singly or doubly infected with CHV1 and MyRV1. The total RNA samples were analyzed via electrophoresis in agarose gel stained with ethidium bromide. **(D)** The relative dsRNA accumulation levels of CHV1 and MyRV1 in the wild-type and Δ*dcl2* knockout mutant. The dsRNA bands detected in the experiment described in **(C)** were quantified and analyzed using Image J Macro software. The data are the means ± SD (n = 6). The different letters indicate a significant difference at $p < 0.01$ (one-way ANOVA). **(E)** The phenotypic growth on PDA medium of the representative *V. mali* mutant strains co-infected with CHV1 and MyRV1 in the first to third fungal subcultures (Sub-1 to Sub-3). The colonies were grown on PDA for 6 days and then photographed. The numbers below the images indicate the number of fungal colonies showing a similar phenotype as that presented in the photo per total number of colonies. **(F)** Viral dsRNA analysis of the doubly infected *V. mali* mutant strains described in **(E)**. The numbers below the lanes indicate the number of samples in which CHV1 dsRNAs were detected per total number of samples. Yellow-colored arrows mark the traces of ribosomal RNAs in virus-free (VF) sample incorporated during dsRNA isolation.

redundant in antiviral RNA silencing in *Fusarium graminearum*, *S. sclerotiorum,* and *Neurospora crassa* (Yu et al., 2018; Neupane et al., 2019; Honda et al., 2020). To a lesser degree, CHV1 or MyRV1 infection also increased the expression of *dcl1* transcripts (**Figure 5**). Further research is required using single and double *dcl* mutants to assess whether DCL1 also contributes to antiviral RNA silencing in *V. mali*.

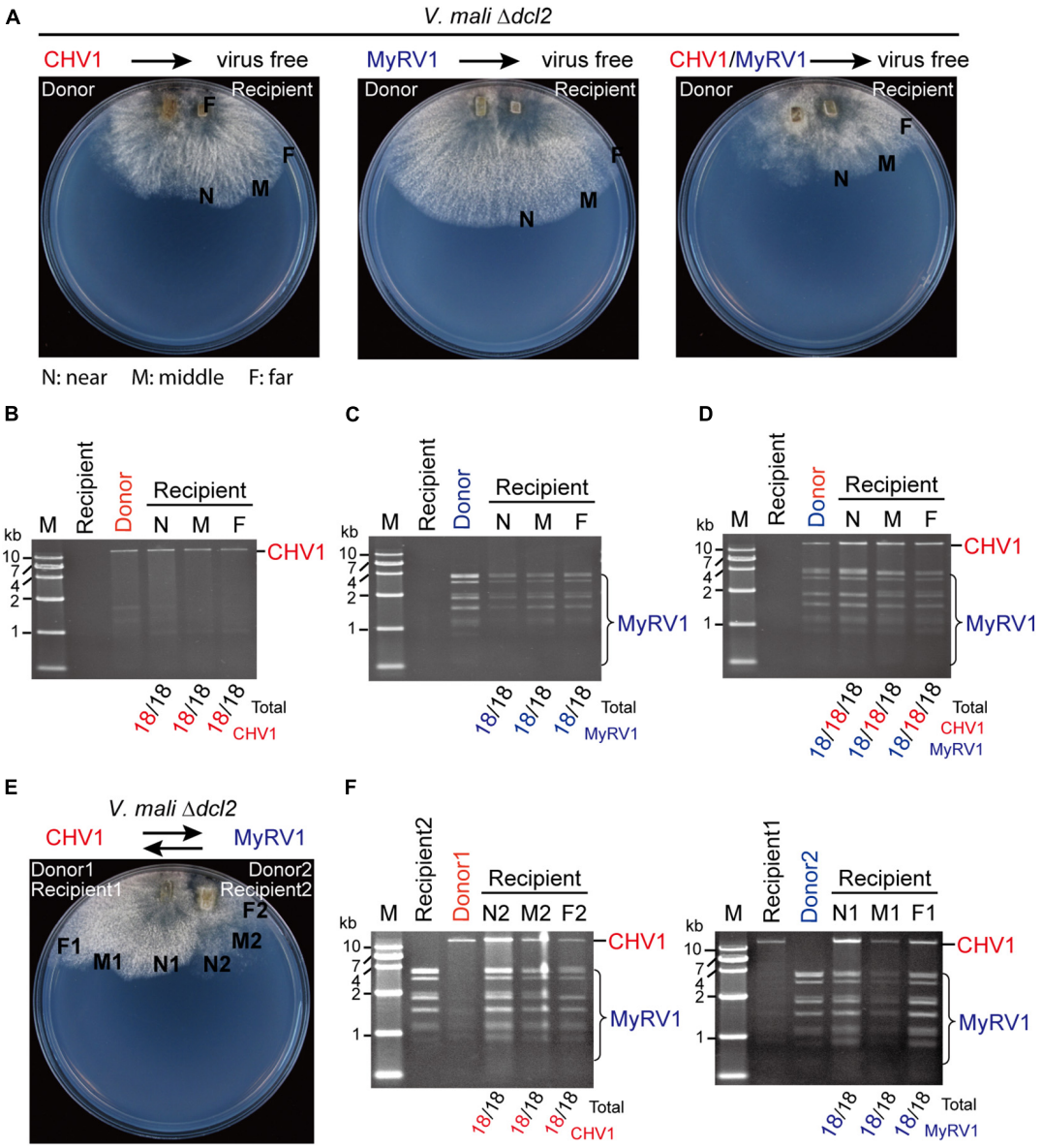

FIGURE 7 | The efficiency of CHV1 and MyRV1 horizontal transmission via hyphal anastomosis in the *dcl2* knockout mutant of *V. mali*. **(A)** Co-culture on PDA plates of the virus-free *V. mali* mutant strain and the virus-infected *V. mali* mutant strain as recipient and donor viruses, respectively. After 1 week of hyphal contact, mycelial plugs were taken from three locations (a near, middle, and far distance from the hyphal fusion areas) in the recipient side, transferred onto new PDA plates and cultured in PDB for dsRNA extraction. **(B–D)** Detection of viral dsRNAs in recipient strains co-cultured with CHV1-infected **(B)**, MyRV1-infected **(C)**, and CHV1 + MyRV1-infected strains **(D)**. The numbers below the lanes indicate the number of samples in which viral dsRNAs were detected per total number of samples. **(E)** Co-culture on a PDA plate of CHV1-infected and MyRV1-infected *V. mali* mutant strains. After 1 week of hyphal contact, mycelial plugs were removed from three locations on both sides, transferred onto new PDA plates and cultured in PDB for dsRNA extraction. **(F)** Detection of viral dsRNAs in fungal strains obtained in the co-culture experiment described in **(E)**.

The Inactivation of *dcl2* Restores the Horizontal Transmission Efficiency of CHV1 and MyRV1 During Co-infection

The effect of *dcl2* inactivation on the horizontal transmission of CHV1 and MyRV1 through hyphal fusion was also examined by co-culturing on 18 PDA plates for each donor and recipient combination. CHV1 and MyRV1 were efficiently transmitted to the virus-free Δ*dcl2* mutant under single or double infection conditions (**Figures 7A–D**). Moreover, when CHV1- and MyRV1-infected Δ*dcl2* mutants were co-cultured on a PDA plate, allowing for hyphal fusion (**Figure 7E**), both viruses were efficiently transmitted to the recipient side of the fungus (**Figure 7F**). These observations suggest that the efficiency of transmission of CHV1 is restored by the fact that its accumulation is increased in the Δ*dcl2* mutant and indirectly, the higher

concentration of CHV1 could also enhance the transference of MyRV1 transmission.

Multiple infections of mycoviruses in a single host are common in nature and, therefore, interplays between or among mycoviruses may occur (Thapa and Roossinck, 2019). Several studies on virus–virus interaction in *C. parasitica* demonstrated that an RNA silencing mechanism is implicated in either synergistic or antagonistic effects between viruses. In the case of a one-way interaction between CHV1 and MyRV1, CHV1 enhances MyRV1 replication and induces frequent generation of MyRV1 rearrangements (Sun et al., 2006; Sun and Suzuki, 2008). The p29 RNA silencing suppressor encoded by CHV1 plays an important role in synergism and MyRV1 rearrangement (Sun and Suzuki, 2008; Tanaka et al., 2011). A study on the interactions between two other members of genus *Hypovirus* and *Mycoreovirus* showed that Cryphonectria hypovirus 4 facilitates the stable infection and enhanced vertical transmission of Mycoreovirus 2, through suppressing the induction of *dcl2* transcripts (Aulia et al., 2019). Chiba and Suzuki (2015) demonstrated that the induction of *dcl2* transcripts by co-infection with MyRV1, or a mutant CHV1 lacking the p29 RNA silencing suppressor, leads to suppression of Rosellinia necatrix victorivirus 1 (genus *Totivirus* of family *Totiviridae*) multiplication, indicating an RNA silencing-mediated one-way interference between unrelated viruses. Similarly, the results of the present study demonstrated that co-infection with MyRV1 compromised the stability of infection and horizontal transmission of CHV1 in *V. mali* (**Figures 3**, **4**) and this was associated with highly up-regulated *dcl2* transcripts (**Figure 5**). Moreover, the inactivation of *dcl2* restored the stability and horizontal transmission efficiency of CHV1 in the presence of MyRV1 (**Figure 6**). This suggests that MyRV1 infection has inhibitory effects on CHV1 multiplication and horizontal transmission in *V. mali* through the activation of antiviral RNA silencing.

CONCLUSION

Valsa mali causes Valsa canker which penetrates deeply into the phloem and xylem of apple tree; therefore, the disease cannot be controlled effectively through chemical treatments. Research interest in mycoviruses has increased due to their potential use as a biological control agent for crop fungal diseases. Thus, expansion of the host range of hypovirulent mycoviruses and studies on virus-fungal host interactions could facilitate the development of biological control measures for fungal diseases. Hence, we introduced two hypovirulent mycoviruses (CHV1 and MyRV1) which originated from *C. parasitica* to *V. mali* using protoplast fusion. Overall, the results of this study revealed that infection with CHV1 and, to a lesser extent, MyRV1 markedly reduced the vegetative growth and virulence of *V. mali*. Therefore, these mycoviruses are potential biological control agents for Valsa canker disease. Moreover, the results demonstrated that co-infection of CHV1 and MyRV1 conferred stronger hypovirulent effects on *V. mali*. However, co-infection also suppressed the infection stability and horizontal transmission efficiency of CHV1, which is disadvantageous for its application as a biological control method. The results of this study provide a scientific base for future research on the development of the practical application of mycoviruses as a biological control agent for apple Valsa canker disease in the field.

DATA AVAILABILITY STATEMENT

The raw data supporting the conclusions of this article will be made available by the authors, without undue reservation.

AUTHOR CONTRIBUTIONS

LSu designed the experiments. SY, RD, LSa, LH, and JL performed the experimental work. IA and LSu analyzed the data and wrote the manuscript. All authors contributed to the article and approved the submitted version.

FUNDING

This work was supported in part by the National Natural Science Foundation of China (31970159), IA at the National Key Research and Development Program of China (2017YFD0201100), and LSu at the National Natural Science Foundation of China (30970163).

ACKNOWLEDGMENTS

We are most grateful to N. Suzuki for kindly providing research materials.

SUPPLEMENTARY MATERIAL

The Supplementary Material for this article can be found online at: https://www.frontiersin.org/articles/10.3389/fmicb.2021.659210/full#supplementary-material

Supplementary Figure 1 | Agarose gel electrophoresis of dsRNAs extracted from *C. parasitica* strains doubly infected with CHV1 and MyRV1.

Supplementary Figure 2 | (A) Representative images showing lesions on apple twigs induced by *V. mali* strains. The lesions on twigs were photographed at 10 days post-inoculation. **(B)** Lesion areas on apples measured in the experiment described in **(A)**. The data are the means ± SD ($n = 5$). The different letters indicate a significant difference at $p < 0.01$ (one-way ANOVA).

Supplementary Figure 3 | Agarose gel electrophoresis of dsRNAs extracted from wild-type and Δ*dcl2* mutant of *V. mali* strains singly infected with CHV1 or MyRV1. The numbers below the lanes indicate the number of samples in which viral dsRNAs were detected per total number of samples.

Supplementary Table 1 | List of primers used in this study.

REFERENCES

Abe, K., Kotoda, N., Kato, H., and Soejima, J. (2007). Resistance sources to valsa canker (*Valsa ceratosperma*) in a germplasm collection of diverse malus species. *Plant Breed.* 126, 449–453. doi: 10.1111/j.1439-0523.2007.01379.x

Aliyari, R., and Ding, S. W. (2009). RNA-based viral immunity initiated by the dicer family of host immune receptors. *Immunol. Rev.* 227, 176–188. doi: 10.1111/j.1600-065x.2008.00722.x

Andika, I. B., Jamal, A., Kondo, H., and Suzuki, N. (2017). SAGA complex mediates the transcriptional up-regulation of antiviral RNA silencing. *Proc. Natl. Acad. Sci. U.S.A.* 114, E3499–E3506.

Aulia, A., Andika, I. B., Kondo, H., Hillman, B. I., and Suzuki, N. (2019). A symptomless hypovirus, CHV4, facilitates stable infection of the chestnut blight fungus by a coinfecting reovirus likely through suppression of antiviral RNA silencing. *Virology* 533, 99–107. doi: 10.1016/j.virol.2019.05.004

Bian, R., Andika, I. B., Pang, T., Lian, Z., Wei, S., Niu, E., et al. (2020). Facilitative and synergistic interactions between fungal and plant viruses. *Proc. Natl. Acad. Sci. U.S.A.* 117, 3779–3788. doi: 10.1073/pnas.1915996117

Brusini, J., and Robin, C. (2013). Mycovirus transmission revisited by in situ pairings of vegetatively incompatible isolates of *Cryphonectria parasitica*. *J. Virol. Methods* 187, 435–442. doi: 10.1016/j.jviromet.2012.11.025

Campo, S., Gilbert, K. B., and Carrington, J. C. (2016). Small RNA-based antiviral defense in the phytopathogenic fungus *Colletotrichum higginsianum*. *PLoS Pathog.* 12:e1005640. doi: 10.1371/journal.ppat.1005640

Chang, S.-S., Zhang, Z., and Liu, Y. (2012). RNA interference pathways in fungi: mechanisms and functions. *Ann. Rev. Microbiol.* 66, 305–323. doi: 10.1146/annurev-micro-092611-150138

Chen, C., Li, M., Shi, X., and Wang, J. (1987). Studies on the infection period of *Valsa mali* miyabe et yamada, the causal agent of apple tree canker. *Acta Phytopathol. Sin.* 17, 65–68.

Chiba, S., Lin, Y.-H., Kondo, H., Kanematsu, S., and Suzuki, N. (2013). Effects of defective interfering RNA on symptom induction by, and replication of, a novel partitivirus from a phytopathogenic fungus, *Rosellinia necatrix*. *J. Virol.* 87, 2330–2341. doi: 10.1128/jvi.02835-12

Chiba, S., and Suzuki, N. (2015). Highly activated RNA silencing via strong induction of dicer by one virus can interfere with the replication of an unrelated virus. *Proc. Natl. Acad. Sci. U.S.A.* 112, E4911–E4918.

Choi, G. H., Dawe, A. L., Churbanov, A., Smith, M. L., Milgroom, M. G., and Nuss, D. L. (2012). Molecular characterization of vegetative incompatibility genes that restrict hypovirus transmission in the chestnut blight fungus *Cryphonectria parasitica*. *Genetics* 190, 113–127. doi: 10.1534/genetics.111.133983

Churchill, A., Ciuffetti, L., Hansen, D., Van Etten, H., and Van Alfen, N. (1990). Transformation of the fungal pathogen cryphonectria parasitica with a variety of heterologous plasmids. *Curr. Genet.* 17, 25–31. doi: 10.1007/bf00313245

Craven, M., Pawlyk, D., Choi, G., and Nuss, D. (1993). Papain-like protease p29 as a symptom determinant encoded by a hypovirulence-associated virus of the chestnut blight fungus. *J. Virol.* 67, 6513–6521. doi: 10.1128/jvi.67.11.6513-6521.1993

Dawe, A. L., and Nuss, D. L. (2001). Hypoviruses and chestnut blight: exploiting viruses to understand and modulate fungal pathogenesis. *Ann. Rev. Genet.* 35, 1–29. doi: 10.1146/annurev.genet.35.102401.085929

Ding, S.-W. (2010). RNA-based antiviral immunity. *Nat. Rev. Immunol.* 10, 632–644. doi: 10.1038/nri2824

Eusebio-Cope, A., Suzuki, N., Sadeghi-Garmaroodi, H., and Taga, M. (2009). Cytological and electrophoretic karyotyping of the chestnut blight fungus *Cryphonectria parasitica*. *Fungal Genet. Biol.* 46, 342–351. doi: 10.1016/j.fgb.2009.01.005

Feng, H., Xu, M., Liu, Y., Dong, R., Gao, X., and Huang, L. (2017a). Dicer-Like genes are required for H2O2 and KCl stress responses, pathogenicity and small RNA generation in *Valsa mali*. *Front. Microbiol.* 8:1166. doi: 10.3389/fmicb.2017.01166

Feng, H., Xu, M., Liu, Y., Gao, X., Yin, Z., Voegele, R., et al. (2017b). The distinct roles of argonaute protein 2 in the growth, stress responses and pathogenicity of the apple tree canker pathogen. *Forest Pathol.* 47:e12354. doi: 10.1111/efp.12354

García-Pedrajas, M. D., Cañizares-Nolasco, C., Sarmiento-Villamil, J. L., Jacquat, A. G., and Dambolena, J. S. (2019). Mycoviruses in biological control: from basic research to field implementation. *Phytopathology* 109, 1828–1839. doi: 10.1094/phyto-05-19-0166-rvw

Ghabrial, S. A., and Suzuki, N. (2009). Viruses of plant pathogenic fungi. *Ann. Rev. Phytopathol.* 47, 353–384. doi: 10.1146/annurev-phyto-080508-081932

Hamid, M., Xie, J., Wu, S., Maria, S., Zheng, D., Assane Hamidou, A., et al. (2018). A novel deltaflexivirus that infects the plant fungal pathogen, *Sclerotinia sclerotiorum*, can be transmitted among host vegetative incompatible strains. *Viruses* 10:295. doi: 10.3390/v10060295

Hillman, B. I., Annisa, A., and Suzuki, N. (2018). Viruses of plant-interacting fungi. *Adv. Virus Res.* 100, 99–116. doi: 10.1016/bs.aivir.2017.10.003

Hillman, B. I., Shapira, R., and Nuss, D. L. (1990). Hypovirulence-associated suppression of host functions in *Cryphonectria parasitica* can be partially relieved by high light intensity. *Phytopathol.* 80, 950–956. doi: 10.1094/phyto-80-950

Hillman, B. I., Supyani, S., Kondo, H., and Suzuki, N. (2004). A reovirus of the fungus *Cryphonectria parasitica* that is infectious as particles and related to the coltivirus genus of animal pathogens. *J. Virol.* 78, 892–898. doi: 10.1128/jvi.78.2.892-898.2004

Honda, S., Eusebio-Cope, A., Miyashita, S., Yokoyama, A., Aulia, A., Shahi, S., et al. (2020). Establishment of *Neurospora crassa* as a model organism for fungal virology. *Nat. Comm.* 11, 1–13.

Kanematsu, S., Sasaki, A., Onoue, M., Oikawa, Y., and Ito, T. (2010). Extending the fungal host range of a partitivirus and a mycoreovirus from *Rosellinia necatrix* by inoculation of protoplasts with virus particles. *Phytopathology* 100, 922–930. doi: 10.1094/phyto-100-9-0922

Keqiang, C., Liyun, G., and Baohua, L. (2009). Investigations on the occurrence and control of apple canker in china. *Plant Protec.* 35, 114–117.

Lee, D. H., Lee, S. W., Choi, K. H., Kim, D. A., and Uhm, J. Y. (2006). Survey on the occurrence of apple diseases in korea from 1992 to 2000. *Plant Pathol. J.* 22, 375–380. doi: 10.5423/ppj.2006.22.4.375

Li, Z., Gao, X., Du, Z., Hu, Y., Kang, Z., and Huang, L. (2013). Survey of apple valsa canker in weibei area of shaanxi province. *Acta Agri. Boreali-Occidentalis Sin.* 1:29.

Mascia, T., and Gallitelli, D. (2016). Synergies and antagonisms in virus interactions. *Plant Sci.* 252, 176–192. doi: 10.1016/j.plantsci.2016.07.015

Nakayashiki, H., Kadotani, N., and Mayama, S. (2006). Evolution and diversification of RNA silencing proteins in fungi. *J. Mol. Evol.* 63, 127–135. doi: 10.1007/s00239-005-0257-2

Neupane, A., Feng, C., Mochama, P. K., Saleem, H., and Marzano, S.-Y. L. (2019). Roles of argonautes and dicers on *Sclerotinia sclerotiorum* antiviral RNA silencing. *Front. Plant Sci.* 10:976. doi: 10.3389/fpls.2019.00976

Nuss, D., Hillman, B., Rigling, D., and Suzuki, N. (2005). *Family Hypoviridae. Virus Taxonomy: Eighth Report of the ICTV*. 597–601. **pub Loc&Name.

Raymaekers, K., Ponet, L., Holtappels, D., Berckmans, B., and Cammue, B. P. (2020). Screening for novel biocontrol agents applicable in plant disease management–a review. *Biol. Control* 144:104240. doi: 10.1016/j.biocontrol.2020.104240

Rigling, D., and Prospero, S. (2018). Cryphonectria parasitica, the causal agent of chestnut blight: invasion history, population biology and disease control. *Mol. Plant Pathol.* 19, 7–20. doi: 10.1111/mpp.12542

Sasaki, A., Onoue, M., Kanematsu, S., Suzaki, K., Miyanishi, M., Suzuki, N., et al. (2002). Extending chestnut blight hypovirus host range within diaporthales by biolistic delivery of viral cDNA. *Mol. Plant-Microbe Interact.* 15, 780–789. doi: 10.1094/mpmi.2002.15.8.780

Segers, G. C., Zhang, X., Deng, F., Sun, Q., and Nuss, D. L. (2007). Evidence that RNA silencing functions as an antiviral defense mechanism in fungi. *Proc. Natl. Acad. Sci. U.S.A.* 104, 12902–12906. doi: 10.1073/pnas.0702500104

Shapira, R., Choi, G., Hillman, B., and Nuss, D. (1991a). The contribution of defective RNAs to the complexity of viral-encoded double-stranded RNA populations present in hypovirulent strains of the chestnut blight fungus *Cryphonectria parasitica*. *EMBO J.* 10, 741–746. doi: 10.1002/j.1460-2075.1991.tb08005.x

Shapira, R., Choi, G. H., and Nuss, D. L. (1991b). Virus-like genetic organization and expression strategy for a double-stranded RNA genetic element associated with biological control of chestnut blight. *EMBO J.* 10, 731–739. doi: 10.1002/j.1460-2075.1991.tb08004.x

Sun, L., Nuss, D. L., and Suzuki, N. (2006). Synergism between a mycoreovirus and a hypovirus mediated by the papain-like protease p29 of the prototypic

hypovirus CHV1-EP713. *J. Gen. Virol.* 87, 3703–3714. doi: 10.1099/vir.0.82213-0

Sun, L., and Suzuki, N. (2008). Intragenic rearrangements of a mycoreovirus induced by the multifunctional protein p29 encoded by the prototypic hypovirus CHV1-EP713. *RNA* 14, 2557–2571. doi: 10.1261/rna.1125408

Sun, Q., Choi, G. H., and Nuss, D. L. (2009). A single argonaute gene is required for induction of RNA silencing antiviral defense and promotes viral RNA recombination. *Proc. Natl. Acad. Sci. U.S.A.* 106, 17927–17932. doi: 10.1073/pnas.0907552106

Suzuki, N., Maruyama, K., Moriyama, M., and Nuss, D. L. (2003). Hypovirus papain-like protease p29 functions in trans to enhance viral double-stranded RNA accumulation and vertical transmission. *J. Virol.* 77, 11697–11707. doi: 10.1128/jvi.77.21.11697-11707.2003

Syller, J. (2012). Facilitative and antagonistic interactions between plant viruses in mixed infections. *Mol. Plant Pathol.* 13, 204–216. doi: 10.1111/j.1364-3703.2011.00734.x

Tanaka, T., Sun, L., Tsutani, K., and Suzuki, N. (2011). Rearrangements of mycoreovirus 1 S1, S2 and S3 induced by the multifunctional protein p29 encoded by the prototypic hypovirus cryphonectria hypovirus 1 strain EP713. *J. Gen. Virol.* 92, 1949–1959. doi: 10.1099/vir.0.031138-0

Thapa, V., and Roossinck, M. J. (2019). Determinants of coinfection in the mycoviruses. *Front. Cell. Infect. Microbiol.* 9:169. doi: 10.3389/fcimb.2019.00169

Wang, L., Gao, Z., Huang, L., Wei, J., Zang, R., and Kang, Z. (2009). Screening fungicide for pathogen inhibition and disease control of apple tree valsa canker. *Acta Phytopathol. Sin.* 39, 549–554.

Wang, X., Shi, C.-M., Gleason, M. L., and Huang, L. (2020). Fungal species associated with apple valsa canker in east asia. *Phytopathol. Res.* 2, 1–14.

Wang, X., Wei, J., Huang, L., and Kang, Z. (2011). Re-evaluation of pathogens causing valsa canker on apple in china. *Mycologia* 103, 317–324. doi: 10.3852/09-165

Wang, X., Zang, R., Yin, Z., Kang, Z., and Huang, L. (2014). Delimiting cryptic pathogen species causing apple valsa canker with multilocus data. *Ecol. Evol.* 4, 1369–1380. doi: 10.1002/ece3.1030

Wu, S., Cheng, J., Fu, Y., Chen, T., Jiang, D., Ghabrial, S. A., et al. (2017). Virus-mediated suppression of host non-self recognition facilitates horizontal transmission of heterologous viruses. *PLoS Pathog.* 13:e1006234. doi: 10.1371/journal.ppat.1006234

Xie, J., and Jiang, D. (2014). New insights into mycoviruses and exploration for the biological control of crop fungal diseases. *Ann. Rev. Phytopathol.* 52, 45–68. doi: 10.1146/annurev-phyto-102313-050222

Yaegashi, H., Kanematsu, S., and Ito, T. (2012). Molecular characterization of a new hypovirus infecting a phytopathogenic fungus, *Valsa ceratosperma*. *Virus Res.* 165, 143–150. doi: 10.1016/j.virusres.2012.02.008

Yu, J., Lee, K.-M., Cho, W. K., Park, J. Y., and Kim, K.-H. (2018). Differential contribution of RNA interference components in response to distinct *Fusarium graminearum* virus infections. *J. Virol.* 92, e1717–e1756.

Zhang, X., and Nuss, D. L. (2008). A host dicer is required for defective viral RNA production and recombinant virus vector RNA instability for a positive sense RNA virus. *Proc. Natl. Acad. Sci. U.S.A.* 105, 16749–16754. doi: 10.1073/pnas.0807225105

Conflict of Interest: The authors declare that the research was conducted in the absence of any commercial or financial relationships that could be construed as a potential conflict of interest.

frontiers in Microbiology

ORIGINAL RESEARCH
published: 14 October 2021
doi: 10.3389/fmicb.2021.661554

Phenotypic Recovery of a *Heterobasidion* Isolate Infected by a Debilitation-Associated Virus Is Related to Altered Host Gene Expression and Reduced Virus Titer

Muhammad Kashif[1], Jaana Jurvansuu[2], Rafiqul Hyder[1], Eeva J. Vainio[1] and Jarkko Hantula[1]*

[1]Natural Resources Institute Finland, Helsinki, Finland, [2]Department of Biology, University of Oulu, Oulu, Finland

The fungal genus *Heterobasidion* includes forest pathogenic species hosting a diverse group of partitiviruses. They include the host debilitating Heterobasidion partitivirus 13 strain an1 (HetPV13-an1), which was originally observed in a slowly growing *H. annosum* strain 94233. In this study, a relatively fast-growing sector strain 94233-RC3 was isolated from a highly debilitated mycelial culture of 94233, and its gene expression and virus transcript quantities as well as the genomic sequence of HetPV13-an1 were examined. The sequence of HetPV13-an1 genome in 94233-RC3 was identical to that in the original 94233, and thus not the reason for the partial phenotypic recovery. According to RNA-seq analysis, the HetPV13-an1 infected 94233-RC3 transcribed eight genes differently from the partitivirus-free 94233-32D. Three of these genes were downregulated and five upregulated. The number of differentially expressed genes was considerably lower and the changes in their expression were small compared to those of the highly debilitated original strain 94233 with the exception of the most highly upregulated ones, and therefore viral effects on the host transcriptome correlated with the degree of the virus-caused debilitation. The amounts of RdRp and CP transcripts of HetPV13-an1 were considerably lower in 94233-RC3 and also in 94233 strain infected by a closely related mildly debilitating virus HetPV13-an2, suggesting that the virus titer would have a role in determining the effect of HetPV13 viruses on their hosts.

Keywords: mycovirus, coinfection, virus transmission, growth rate, conifer pathogen

OPEN ACCESS

Edited by:
Ioly Kotta-Loizou, Imperial College London, United Kingdom

Reviewed by:
Sotaro Chiba, Nagoya University, Japan
Dae-Hyuk Kim, Jeonbuk National University, South Korea

****Correspondence:***
Muhammad Kashif
muhammad.kashif@luke.fi

Specialty section:
This article was submitted to Virology, a section of the journal Frontiers in Microbiology

Received: *31 January 2021*
Accepted: *21 September 2021*
Published: *14 October 2021*

Citation:
Kashif M, Jurvansuu J, Hyder R, Vainio EJ and Hantula J (2021) Phenotypic Recovery of a Heterobasidion Isolate Infected by a Debilitation-Associated Virus Is Related to Altered Host Gene Expression and Reduced Virus Titer. Front. Microbiol. 12:661554. doi: 10.3389/fmicb.2021.661554

INTRODUCTION

Fungal viruses (mycoviruses) are found in a broad range of fungal taxa including Ascomycota and Basidiomycota as well as early diverging fungal lineages, such as Chytridiomycota, Blastocladiomycota, Neocallimastigomycota, Zoopagomycota, and Mucoromycota (Ghabrial and Suzuki, 2009; Pearson et al., 2009; Ghabrial et al., 2015; Sutela et al., 2019, 2020; Myers et al., 2020). Viruses are transmitted among fungal strains by cell to cell contacts (hyphal anastomosis) and sexual or asexual spores (Ghabrial and Suzuki, 2009; Vainio et al., 2015b; Kashif et al.,

2019). Mycoviruses usually cause asymptomatic infections. Hollings (1962) reported for the first time, debilitated growth of *Agaricus bisporus* mycelium caused by mycovirus infection on artificial agar media. Recently mycoviruses have also been reported to cause phenotypic alterations and hypovirulence (reduced virulence) in their hosts (Huang and Ghabrial, 1996; Preisig et al., 2000; Márquez et al., 2007; Yu et al., 2010; Hyder et al., 2013; Xiao et al., 2014; Vainio et al., 2018b). The hypovirulence responses have been well studied in *Cryphonectria parasitica* infected by Cryphonectria hypovirus 1 (Allen and Nuss, 2004; Deng et al., 2007; Dawe and Nuss, 2013; Eusebio-Cope et al., 2015). Genetically different fungal strains may also react differently to the same mycovirus strain (Hyder et al., 2013; Kim et al., 2015; Vainio et al., 2018b).

H. annosum s.lat. Species complex is considered as one of the most destructive groups of fungal pathogens of conifer forests in the Northern Hemisphere where these fungi cause root and butt rot diseases (Garbelotto and Gonthier, 2013). There are two geographical groups in this complex including three European species – *H. annosum*, *H. parviporum,* and *H. abietinum* – causing infections preferably on pine, spruce (*Picea abies* and others), and fir species, respectively (Niemelä and Korhonen, 1998; Dai and Korhonen, 1999), and two North American species – *H. irrugulare* and *H. occidentale* – infecting predominantly pines or overlapping host ranges of fir, spruce, and hemlock, respectively (Otrosina and Garbelotto, 2010; Garbelotto and Gonthier, 2013). For all these species, the primary infection is initiated by fungal spores landing and germinating on newly cut conifer stumps, or stem and root wounds, and continues as secondary infection *via* root contacts to neighboring trees (Stenlid and Redfern, 1998). They are also capable of both necrotic and saprotrophic growth. *H. irregulare* was the first *Heterobasidion* species to be characterized for complete genome sequence (Olson et al., 2012; Garbelotto and Gonthier, 2013), and thereafter also genomes of *H. annosum* (Sillo et al., 2015; Choi et al., 2017), *H. occidentale* (Liu et al., 2018), and *H. parviporum* (Zeng et al., 2018) have been characterized. There are different preventive control methods practiced against these root rot fungi, but truly curative methods are urgently needed. For this purpose, the use of mycoviruses has been suggested as a highly potential biocontrol option (Vainio and Hantula, 2016; Vainio et al., 2018b).

About 15% of *Heterobasidion* strains host dsRNA mycoviruses (Ihrmark, 2001; Vainio et al., 2015a; Vainio and Hantula, 2018) but the frequency of virus infections is considerably higher at forest sites with numerous *Heterobasidion* disease centers and thus ubiquitous mycelial contacts (Vainio et al., 2015b; Hyder et al., 2018). Up to 70% of Heterobasidion dsRNA virus infections are caused by Heterobasidion RNA virus 6 (HetRV6) (Vainio et al., 2012) belonging to the virus family *Curvulaviridae*, but also viruses belonging to genera *Alphapartitivirus, Betapartitivirus,* and family *Mitoviridae* have been observed (Vainio and Hantula, 2016; Vainio et al., 2018a,b), and actually partitiviruses form a major share of the viral species diversity in *Heterobasidion* spp. (Vainio et al., 2011, 2012; Kashif et al., 2015; Vainio et al., 2015a). The dsRNA genomes of partitiviruses are composed of two essential independently encapsidated segments coding for an RNA-dependent RNA polymerase (RdRp) and a coat protein (CP) (Nibert et al., 2014: Vainio et al., 2018a).

Although most *Heterobasidion* partitiviruses are cryptic, there are also strains causing variable and debilitating phenotypes on at least some of their hosts (Hyder et al., 2013; Jurvansuu et al., 2014). The best described of them is Heterobasidion partitivirus 13 strain an1 (HetPV13-an1) causing up to 90% reduction of its host's growth rate (Vainio et al., 2018b; Kashif et al., 2019). There is also a closely related virus, HetPV13-an2 (Kashif et al., 2015; Hyder et al., 2018), which does not seem to cause noticeable effects on its natural host *H. annosum* S45-8 (Hyder et al., 2018).

The mechanisms behind the debilitating effects by HetPV13-an1 are not clear, although transcriptome analysis revealed considerable changes in *Heterobasidion* gene expression (Vainio et al., 2018b). This study is based on our observation of a fast-growing sector isolate of the original host strain of HetPV13-an1, *H. annosum* 94233, that seemed to have recovered spontaneously although the virus was still present in its hyphae. We aimed to investigate how the host can recover from the virus-induced growth retardation and the relevance of this phenomenon to the potential use of the virus as a biocontrol agent by (1) sequencing of the virus genome to determine the possibility of viral mutations, (2) analyzing the sector isolate's gene expression to find changes that had occurred in the host, (3) quantifying viral genomes and transcripts in the recovered and debilitated isolates to determine whether changes had occurred in the virus quantity, and (4) analyzing the ratio of RdRp and CP transcripts of HetPV13-an1 among the isolates to test whether excess amount of viral polymerase transcripts correlates with a debilitated host phenotype as suggested earlier (Jurvansuu et al., 2014). A conspecific but apparently cryptic strain HetPV13-an2 was included in the phenotypical testing and analysis of viral transcript quantities to assess the effects of natural minor sequence variations to symptom severity.

MATERIALS AND METHODS

Fungi and Viruses

HetPV13-an1 (GenBank accession: KF963177-78) is naturally hosted by *H. annosum* 94233 (Kashif et al., 2015; Vainio et al., 2015a). 94233-RC3 is a fast-growing sector isolate from 94233 (**Figure 1**) which was detected and stored in 2013 and then refreshened and restored in 2017 and 2018 at +4°C. The originally stored strain of 94233-RC3 as well as the restored strain in 2017 had lost the virus during the storage by 2021. Fortunately, the recently stored sample 2018 had retained the virus and could be used for further analysis. However, also one of the replicates regrown from this vial was found to have lost HetPV13-an1 and was named as 94233-RC3-0. In addition, two other isolates designated as 94233-RC1 and 94233-RC2 appeared to have recovered but returned quickly to their original slow-growing phenotype and were not analyzed further. The recovered HetPV13-an1 infected sector isolate 94233-RC3 was studied for its growth rate and gene expression

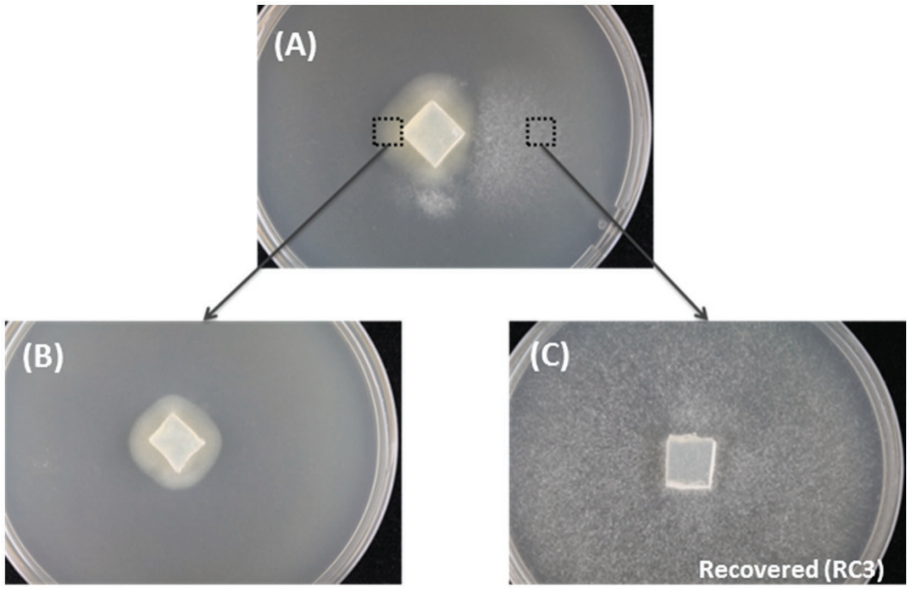

FIGURE 1 | The spontaneous recovery of HetPV13-an1 infected fungal isolate as shown by mycelial morphology. **(A)** The original mycelium with slow and fast growth on the left and right side of the dish, respectively. **(B)** Mycelia transferred from the left side of the original mycelium. **(C)** Recovered 94233-RC3 transferred from the right side of the original mycelium.

in 2013. The strain was then stored at 4°C and moved back to +20°C only recently, after which it was found to have been cured of HetPV13-an1 in two of the three vials available: Vials from 2013 to 2017 had lost the virus by 2021, whereas a vial from 2018 had retained the virus and was selected for further analysis. However, also one of the replicates regrown from this vial was found to have lost HetPV13-an1 and was named as 94233-RC3-0.

H. annosum S45-8 is naturally coinfected by HetPV13-an2 (KF963179-80) (Kashif et al., 2015) and HetPV7-an1-b (KY859975-76) (Hyder et al., 2018). S45-8-PV13-an2 is a derivative of S45-8 cured of HetPV7 by single hyphal tip isolation. 94233-32D and S45-8-0 are previously and newly created partitivirus-free derivatives of 94233 (Vainio et al., 2018b) and S45-8, respectively, from which partitiviruses have been removed by a thermal treatment. Strain 94233-PV13-an2 was created by a transmission of HetPV13-an2 to 94233-32D by hyphal anastomosis on artificial medium.

mRNA Sample Preparation and RNA-Sequencing

We analyzed the effects of virus infection on the gene expression of 94233-RC3 as compared to an isogenic partitivirus-free strain *H. annosum* 94233-32D. The fungal strains were grown on cellophane covered modified orange serum (MOS) plates (Müller et al., 1994) for 1 week. Mycelia were collected and homogenized in TRI-Reagent (Molecular Research Center Inc., United States) using the Fast-Prep FP120 homogenizer (JT Baker, Holland) with quartz sand grains as recommended by the manufactures. The sample was precipitated with isopropanol and total RNA was further purified with E.Z.N.A Fungal RNA Kit (Omega Bio-tek), and RNA was resuspended into DEPC-treated water (G. Biosciences, United States). RNA quantity and quality were checked with NanoVue (GE healthcare, United States) and bioanalyzer 2,100 (Agilent technologies, United States). Each analysis was performed with three biological replicates. For RNA-seq, the TruSeq RNA Library Prep kit v2 (Illumina Inc.) was used to prepare the samples. The process involved poly(A) selection with oligo(dT) beads without the depletion of rRNA. The sequencing was conducted with an Illumina HiSeq2500 instrument using paired-end sequencing chemistry with 50-bp read length (Bioinformatics Core of Turku Centre for Biotechnology, University of Turku and Åbo Akademi University).

dsRNA Extraction, RT-PCR, and Genome Sequence Determination

The dsRNA was extracted from 14 days old fungal mycelia cultivated on cellophane membrane-covered MOS agar plates. Isolation of dsRNA was conducted according to Jurvansuu et al. (2014). Briefly, mycelia were homogenized and thereafter, RNA was isolated by phenol–chloroform (1:1) and chloroform–isoamylalcohol (24:1) extractions followed by precipitation by adding ethanol and NaCl at final concentrations of 15% and 100 mm, respectively, and then adding cellulose fibers (medium) (Catalog no. C6288, Sigma-Aldrich, St. Louis, MO, United States). The precipitant was then moved to SigmaPrepTM spin columns (Sigma-Aldrich, United States) and washed. After eluting, the dsRNA was precipitated with ethanol. The dsRNA genome segments were excised from the gel and purified with RNAid Kit (MP Biomedicals, United States) and used in RT reaction.

T4RNA adapters were ligated and RT reactions set up using the RevertAid H minus M-MuLV reverse transcriptase (Thermo Scientific). The single primer amplification technique (Lambden et al., 1992) was used with previously described modifications (Tuomivirta and Hantula, 2003; Vainio et al., 2011; Kashif et al., 2015) to determine dsRNA sequences from isolate 94233-RC3. RT-PCR amplification was conducted using DyNAzyme DNA polymerase (Thermo Scientific) and specific primers (Kashif et al., 2015) as described before (Vainio et al., 2011). PCR products were sequenced at Macrogen Inc., South Korea[1] using an Applied Biosystems 96-capillary ABI 3730xl DNA analyzer.

Bioinformatics

The gene expression analysis based on RNA-seq (Illumina sequencing) was performed by the Bioinformatics Core of Turku Centre for Biotechnology, University of Turku and Åbo Akademi University as described in Vainio et al. (2018b). The resulting Illumina sequence reads were aligned against the reference genome of *H. irregulare*, named at the time as *H. annosum* v.2.0 at the Joint Genome Institute (JGI).[2] The read alignment was against the *H. annosum* v.2.0 reference genome using TopHat version 2.0.10 (Kim et al., 2013). Sequence annotations were based on known genes from *H. annosum* v.2.0 reference genome using HTSeq tool v.0.5.4p3 (Vainio et al., 2018b).

The data were normalized to make the values comparable across the sample set and the counts were normalized by the TMM normalization method of the edgeR R/Bioconductor package. Summary of the mapping statistics is provided in **Supplementary Table S1**. The expression level of each gene was analyzed by the number of sequenced reads mapped to the sequence of the reference gene, and differentially expressed genes (DEGs) were determined according to criteria used in Vainio et al. (2018b) based on their fold changes (FC) over a value of 4 and modified *t*-test value of p (=false-discovery-rate value of p) of 0.001 ($p < 0.001$).

Validation of Gene Expression Data Using RT-qPCR

In order to simultaneously validate the results of RNA-Seq and to make comparison to the results in previous study (Vainio et al., 2018b) on the gene expression differences caused by HetPV13-an1 to strain 94233, the same 28 DEGs encoding various cellular functions as in Vainio et al. (2018b) were subjected for the RT-qPCR analysis of 94233-RC3 (**Supplementary Table S2**). Three independent biological replicates of each fungal sample (*H. annosum* 94233/32D and 94233-RC3) were incubated for 1 week at 20°C and total RNA was extracted as described above for mRNA sequencing. The complementary DNA (cDNA) was diluted to a half-sample volume of water prior their use in RT-qPCR. The primers have been described in Vainio et al. (2018b), and three internal reference genes were used to normalize the results and primers as described by Raffaello and Asiegbu (2013) for RNA polymerase III transcription factor, Alfa tubulin, and Actin along with the 28 target genes.

RT-qPCR was carried out using EvaGreen® qPCR Mix Plus (Solis BioDyne, Estonia), 2 µl of cDNA and 1 µl (10 µm) of each primer in a total volume of 20 µl in the 36-well rotor of Rotor-GeneQ (Qiagen, United States) by following the manufacturer's instructions. Two replicates for each biological sample were prepared for each RT-qPCR reaction. Cycling conditions were as follows: pre-incubation at 95°C for 15 min, denaturation at 95°C for 15 s, using specific annealing temperatures for primers (Vainio et al., 2018b) for 20 s, and extension at 72°C for 20 s. Additionally, melting curve profile was analyzed to test the quality and specificity of the reactions. Relative gene expression (fold change) as expression ratios of samples to controls (normalized with three reference genes) were analyzed with relative expression software tool Rest2009[3] (Pfaffl et al., 2002) based on comparative quantitation analysis data. Relative expression (RT-qPCR) corresponds to $\log_2$ fold change of expression ratios measure by take-off values normalized with three reference genes.

Quantification of Viral Transcripts and Genome Segments

Total RNA Isolation and cDNA Synthesis

Total RNA was isolated from fungal mycelia after 1 week growth on MOS agar plates as described in Jurvansuu et al. (2014). In short, fungal mycelia were collected and total RNA was extracted by TRI-Reagent. The RNA pellet was eluted into DEPC-treated water and the concentration and purity of the isolated RNA were analyzed by NanoVue (GE healthcare, United States). cDNA was made from 2 µg of DNase I treated total RNA using RevertAid First Strand cDNA Synthesis Kit (Thermo Scientific, United States) and random hexamer primers (Thermo Scientific, United States).

RT-qPCR Quantification for Virus Transcripts

Diluted cDNAs to half volume were used before using them in quantitative-PCR (qPCR). EvaGreen® dye (Solis BioDyne, Estonia) was used in qPCR on Rotor-GeneQ (Qiagen, United States) as recommended by the manufacturer. PCR primers were used as follows: GAPDH as a reference gene and specific primers based on RdRp and CP genomic segments (proteins) of two virus strains including HetPV13-an1 and HetPV13-an2 (Vainio et al., 2015a) were used for virus transcripts. The purified plasmids of cloned genes of CP and RdRp of these viral strains (Jurvansuu et al., 2014; Kashif et al., 2019) were then used in absolute quantification as shown by Jurvansuu et al. (2014). The normalization of the viral transcript levels was done using the host GAPDH as a reference gene (Raffaello and Asiegbu, 2013) and the absolute quantities of RNA transcripts or virus copy number were calculated using a standard curve.

[1]http://www.macrogen.com
[2]http://genome.jgi.doe.gov/Hetan2/Hetan2.home.html
[3]http://rest.gene-quantification.info/

Phenotype Testing by Growth Rate Experiments

The effects of single viral infections by HetPV13-an1 or HetPV13-an2 were assessed by measuring the growth rate difference between pairs of isogenic HetPV13 infected and uninfected strains on 2% MEA plates at 20°C as described by Kashif et al. (2019). The growth rate effects of HetPV13-an1 were measured using derivatives of host strain 94233 and those of HetPV13-an2 using derivatives of host strains 94233 and S45-8. Each inoculum was a circular plug of 0.5 cm diameter, which was picked from a fresh mycelial culture (1–2 week old depending on the apparent growth rate), grown on 2% MEA plate and placed at the center of a 2% MEA plate. Twelve independent biological replicates were prepared for each isolate and fungal growth was measured every second day after mycelial growth was initiated 3 days post-inoculation and continued until the mycelium covered the plate. The fungal growth was measured with a digital planimeter (Planix 10S, Tamaya) and statistical analysis was done using *t*-test in Microsoft Excel 2010 (**Supplementary Table S3**).

RESULTS

Recovered Phenotype of Strain 94233

Three fast-growing sectors of *H. annosum* strain 94233 hosting HetPV13-an1 were initially observed in year 2013 and isolated as depicted in **Figure 1**. Two of the isolates returned quickly to their original slow-growing phenotype, but the third one, 94233-RC3, seemed to be stable in room temperature during several months. The presence of HetPV13-an1 in this fast-growing isolate was verified by RT-qPCR with specific primers 13an1RdRpF and 13an1RdRpRev as described earlier (Vainio et al., 2015a). The three mitoviruses previously shown to be hosted by *H. annosum* 94233 (Vainio et al., 2018b; Vainio, 2019) were also retained in 94233-RC3 as revealed by mapping of the RNA-Seq reads.

Sequencing of the Virus Genome to Determine the Possibility of Virulence Reducing Mutations

The genome sequence of HetPV13-an1 in the *H. annosum* 94233 sector isolate 94233-RC3 (accession numbers MW115956 and MW115957) was 100% identical with the previously determined sequence for HetPV13-an1 (KF963177-78). Therefore, the observed phenotypical change was not caused by mutations in the virus genome sequence. **Figure 2** shows a schematic presentation of the genome characterization scheme used. Each sequence site was covered by direct Sanger sequencing reactions including three PCR reactions each for CP and RdRp in two replicates, respectively.

Analysis of Host Gene Expression

The transcriptome analysis of the sector isolate 94233-RC3 was conducted simultaneously with that of the partitivirus-free strain *H. annosum* 94233/32D and the debilitated original isolate 94233 included in our earlier study (Vainio et al., 2018b). Here, we first compared the expression of the sector isolate to the primary results on the transcriptome of 94233-32D (cured of HetPV13-an1) and thereafter compared the degree of observed differences to the corresponding changes in 94233 (with HetPV13-an1). After those analyses, the sector isolate was stored at 4°C.

The RNA-seq analysis of 94233-RC3 involved three biological replicates each of which produced ~16–22 million reads (**Supplementary Table S1**). The raw sequencing reads are deposited in the NCBI GenBank SRA data archive under the submission number SAMN16435702 (BioProject PRJNA362289). The annotation of identified transcripts was made based on the reference genome *Heterobasidium annosum* (v2.0) and resulted in identifying putative functions for eight genes containing five upregulated and three downregulated transcripts based on the same criteria as in Vainio et al., 2018b on the expression ratio (fold change) between the compared sample groups and FDR-adjusted value of p for the comparison between the sample groups (**Table 1; Supplementary Table S4**).

The transcriptome of the sector isolate 94233-RC3 differed much less from that of the 94233-32D than the original virus-hosting strain 94233. Based on the number of reads related to each gene, only a total of eight transcripts were affected by HetPV13-an1 in 94233-RC3 (683 affected in 94233), of which five (276) were up- and three (414) downregulated (**Table 1**). All of the five genes upregulated in 94233-RC3 were upregulated also in 94233. In the case of the three downregulated genes, however, two of the genes were found to be almost five times less affected in 94233-RC3 than in 94233. Overall, the level of up- and downregulation of the host transcripts due to the HetPV13-an1 infection were considerably lower in 94233-RC3 than in 94233 (**Figure 3**).

The validation of 94233-RC3 gene expression by RT-qPCR mostly agreed with the RNA-seq data but there was also a significant exception: target gene (TG) 23 with clear down- and upregulation in RNA-seq and RT-qPCR, respectively (**Figure 3**). In addition, TGs 10, 24, 25, 26, and 28 for 94233-RC3 were found to be slightly downregulated based on RNA-seq but in RT-qPCR validation only negligible upregulation was observed (**Figure 3; Supplementary Table S2**). Target genes 17 and 21 did not amplify at all from *H. annosum* 94233 and therefore the fold change was not shown by RT-qPCR in **Figure 3** (Vainio et al., 2018b).

Qualitative Comparison of Gene Expressions of 94233-RC3 and 94233-32D in Relation to Biopathways

Probable gene functions affected by HetPV13-an1 in the sector isolate 94233-RC3 were assessed by comparing its transcript levels to the cured strain 94233-32D by RNA-Seq (**Supplementary Table S4**). The most prominent differences in the gene expression between HetPV13-an1 hosting sector isolate 94233-RC3 and the partitivirus-free strain 94233-32D were the three DEGs estExt_Genewise1Plus.C_080637, Hetan1.EuGene10000523, and e_gw1.12.503.1 that showed significant upregulation with FCs of 588, 387, and 180, respectively.

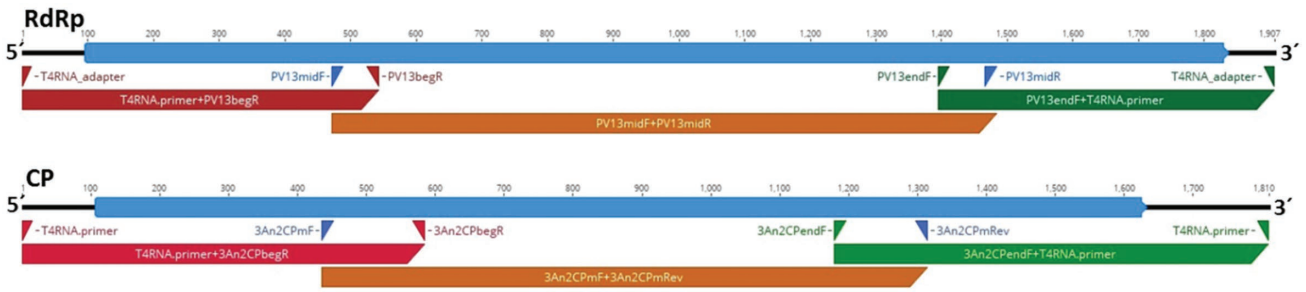

FIGURE 2 | Schematic presentation of the genome organization of HetPV13-an1 (94233-RC3) showing the predicted coding regions for the RNA-dependent RNA polymerase (RdRp) and CP (blue) and the location of primers and corresponding amplification products (red, brown, and green) used for genome sequence determination.

TABLE 1 | Summary of RNA-seq analysis of *H. annosum* 94233-RC3 and 94233 infected with HetPV13-an1 and 94233/32D, which is a partitivirus-free isogenic strain.

	FC[d]	PType[e]	*p*-value	MeanExprs[f]	Tot[g]	Up[h]	Down[i]
13an1[a] vs. ctr	4.000	FDR	0.001	0.125	683	276	414
RC3[b] vs. ctr[c]	4.000	FDR	0.001	0.125	8	5	3

Three biological replicates were used for each strain.
[a]*HetPV13-an1.*
[b]*94233-RC3.*
[c]*94233-32D.*
[d]*Expression ratio (fold change) between the compared sample groups, which is the lowest selection criteria or threshold limit of 4 and 2.5 to compare two groups (94233 and RC3-94233).*
[e]*FDR-adjusted value of p for the comparison between the sample groups.*
[f]*mean RPKM expression value.*
[g]*Total number of differentially expressed genes.*
[h]*Upregulated genes.*
[i]*Downregulated genes.*

These genes were related to putative Myosin class II heavy chain, Farnesyl cysteine-carboxyl methyltransferase (P450), and Sorbitol dehydrogenase proteins, corresponding to functions related to (1) fungal hyphal growth, septation, and conidial germination, (2) monooxygenase activity, and (3) secondary metabolites biosynthesis, transport, and catabolism, respectively. The functions of the two other upregulated genes are not known.

The difference in downregulated genes in the HetPV13-an1 infected 94233-RC3 was much smaller than in upregulated genes. DEG genesh1_kg.03__767__4245_1_CCOZ_CCPA_CCPB_CCPC_EXTA was downregulated 10-fold, but its function is not known. However, DEGs Hetan1.e_gw1.5.283.1 and Hetan1.estExt_fgenesh2_pg.C_100320 were downregulated less than 5-fold and code for putative L-fuculose-phosphate aldolase (fucA) and phenol 2-monooxygenase, respectively. The first of these functions is related to fructose and mannose metabolism, whereas the second one affects detoxification and aromatic compound metabolism.

RNAi-related genes are of a special interest because their functions are related to defense against mycoviruses. In 94233-RC3, none of these genes were up- or downregulated based on the RNA-Seq according to the criteria used here (and in Vainio et al., 2018b). However, in RT-qPCR analysis, two of the RNAi-related genes had significantly lower FC-values of −5.95 and −2.12, respectively. They code for a dicer (e_gw1.03.2068.1) and an argonaute gene (e_gw1.02.2254.1) (**Supplementary Table S2**). Thus, the effect of HetPV13-an1 on the viral RNAi-based defense of 94233-RC3 was quite low.

The Most Differentially Expressed Genes in 94233-RC3 Compared to 94233

The gene expression was in general significantly less affected by HetPV13-an1 in 94233-RC3 than in the original 94233 (Vainio et al., 2018b). However, the most differentially expressed genes in the sector isolate, estExt_Genewise1Plus.C_080637, Hetan1.EuGene10000523, and e_gw1.12.503.1, had FCs 588, 387 and 180 in 94233-RC3 and 871, 202 and 225 in 94233, respectively, suggesting that HetPV13-an1 was still able to modify considerably the most seriously affected genes in the sector isolate.

Analysis of the Ratio of HetPV13-an1 RdRp and CP Among the Isolates

The quantification of viral CP and RdRp mRNA transcripts using RT-qPCR revealed that the amounts of HetPV13-an1-encoded transcripts before storing 94233-RC3 were considerably lower in 94233-RC3 than in 94233 (**Figures 4A,B**) and differed between the two genes. The amounts of RdRp were 3.5 and 13.4 times of that of GAPDH RNA in 94233-RC3 and 94233,

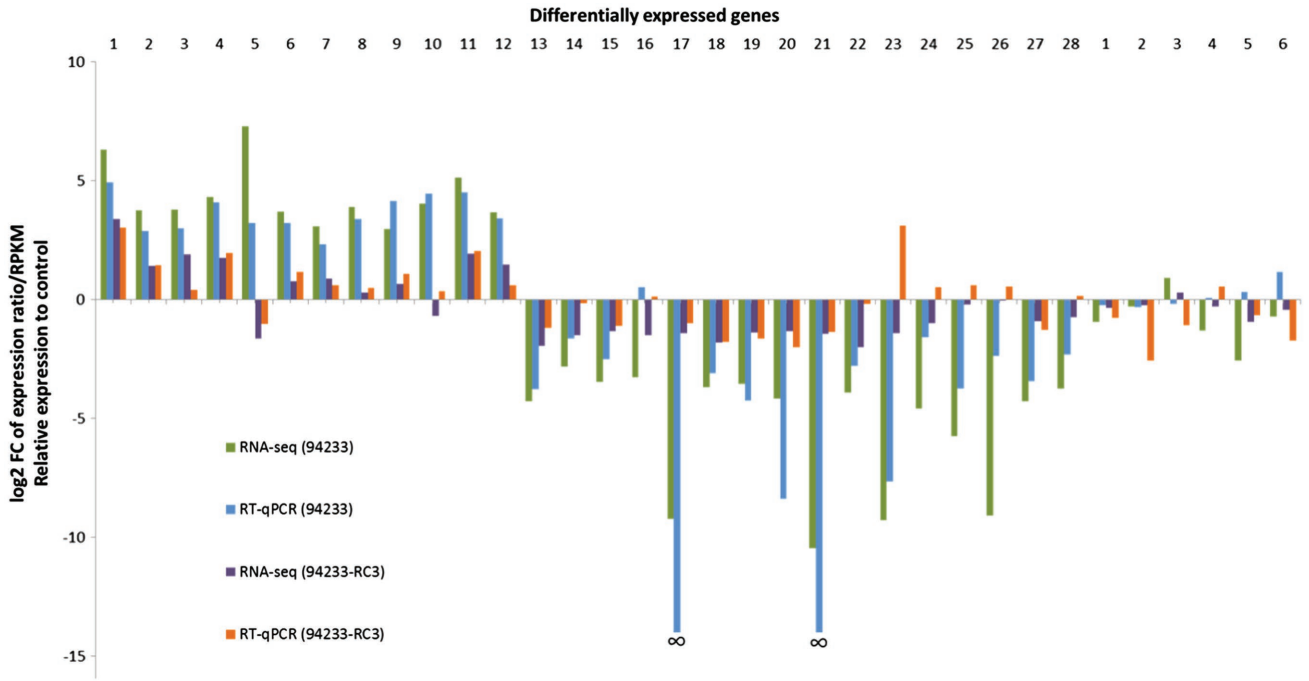

FIGURE 3 | 94233-RC3-transcriptome RNA-seq data and qPCR validation. The columns relate to fold changes in gene expression of HetPV13-an1 hosting *H. annosum* strains 94233 and 94233-RC3, each was compared to the HetPV13-an1-free control 94233-32D. Names and gene id numbers of the 28 and then 6 RNAi-related target genes are listed (**Supplementary Table S2**). The relative expression of RNA-Seq corresponds to $\log_2$ fold change of reads per kb of transcript per million mapped reads (RPKM). The data for HetRV3-an1 (94233) are taken from Vainio et al. (2018b).

and the corresponding values for CP were 0.45 and 1.5, respectively. However, the RdRp and CP amounts reduced to 0.71 and 0.14 times of that of GAPDH RNA after long storage (2013–2021) of 94233-RC3. Moreover, the quantities of transcripts for RdRp and CP in 94233-RC3 were only 26 and 32% in 2013, respectively, of that in 94233, which further reduced in 94233-RC3 to 5 and 9% after long storage, respectively (**Figures 4A,B**). Similarly, the transcript levels of HetPV13-an2 RdRp and CP were 32 and 36% of that observed for HetPV13-an1 in 94233. However, HetPV13-an2 in its native host S45-8 produced significantly lower titer of the virus-an2 and showed more equal amounts of both transcripts from its genome segments (**Figures 4C,D**).

The relative ratios of RdRp to CP were somewhat lower (7.7 and 5.2 before and after the long storage, respectively) in 94233-RC3 and 94233-PV13-an2 (7.7) compared to 94233 (8.7). Moreover, isolates 94233-RC1 and 94233-RC2 that recovered their growth rates temporarily had lowered levels of transcripts amounts (**Supplementary Figure 1**) and also had a significantly higher RdRp to CP ratios of 27 and 17, respectively (**Supplementary Figure 2**). In contrast, the ratio of RdRp and CP transcripts of HetPV13-an2 was about 90% lower in its original host S45-8 than in 94233 (**Figure 5**).

Growth Rates

Inoculums made from single 2% MEA plate in order to create 12 independent biological replicates of 94233-RC3 before and after storage 94233-RC3 appeared to be stable (**Supplementary Figure 3**) and had growth rates that were 45 and 62% of partitivirus-free 94233-32D and 12 and 16 times higher than the original HetPV13-an1 hosting 94233 (**Figure 6**). The 94233-RC3 strain that had lost HetPV13-an1 during the storage had a very similar growth rate as the virus-hosting strain 94233-RC3 before and after the storage.

94233-PV13-an2 showed a significant 64% growth reduction compared to 94233-32D, but S45-8-an2 had only 9.6% growth reduction compared to the cured S45-8-0 and thus grew at the same rate as 94233-32D. Originally HetPV13-an2 was found in coinfection with HetPV7-an1 in its original host S45-8 and showed similar growth rates as 94233-RC3, i.e., up to 45% slower growth compared to the partitivirus-free S45-8-0 (**Figure 6**).

DISCUSSION

This study was launched based on our observation that a *Heterobasidion* strain seriously debilitated due to a HetPV13-an1 infection had recovered spontaneously. That accords with some previous studies on other mycoviruses which have shown that coinfections of two fusarivirus strains of *F. graminearum* are linked with debilitating phenotypic alterations in their fungal hosts and that the effect of *Fusarium* mycoviruses in the fungal transcriptome is virus-specific (Darissa et al., 2012; Lee et al., 2014). In this study,

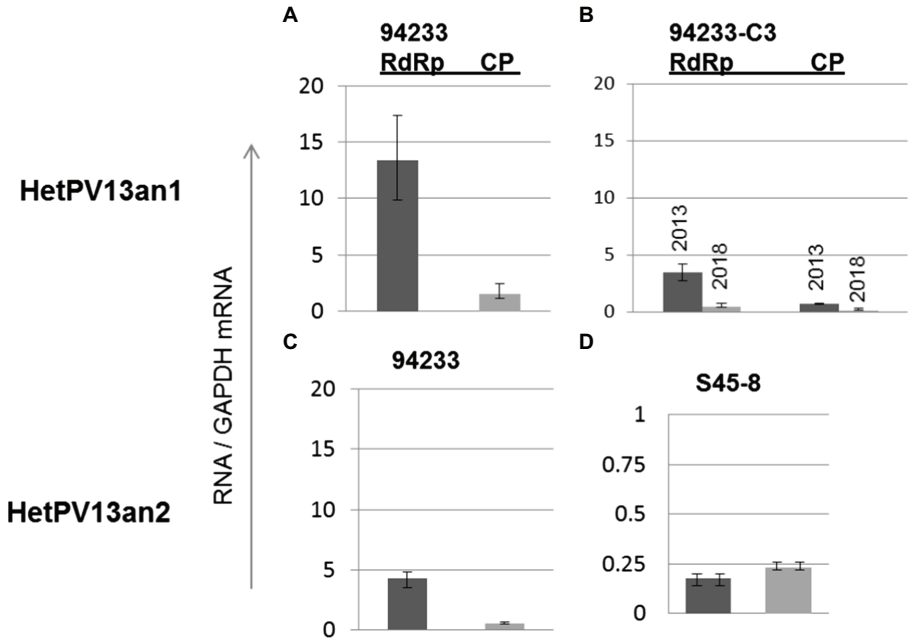

FIGURE 4 | The variation in viral CP and RdRp transcript levels in *H. annosum* strains infected by partitiviruses. **(A)** Strain 94233 with its natural viral infection HetPV13-an1, **(B)** fast-growing sector isolate 94233-RC3 with infection by HetPV13-an1 before (2013) and after storage (2018), and **(C,D)** the amounts of viral transcripts of HetPV13-an2 in 94233/32D and in its native host (S45-8). Note: The scale for mRNA transcript levels is different in D due to significantly lower levels of expression.

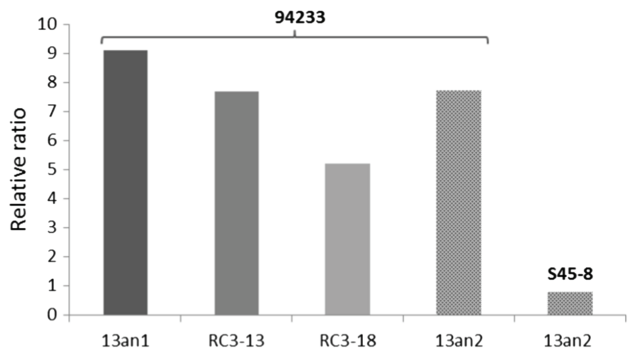

FIGURE 5 | Variation in the ratio of viral RdRp and CP in different host strains. Strains 94233 and 94233-RC3 hosted virus HetPV13-an1, and strains 94233-PV13-an2 and S45-8 hosted virus HetPV13-an2. 13an1 = HetPV13-an1 and RC3-13 = 94233-RC3 before storage; RC3-18 = 94233-RC3 after storage, 13an2 = HetPV13-an2.

we originally assumed that the fast-growing hyphal sector had been cured of the virus, but after examining the presence of the virus and its genome sequence, it was evident that there was no change in the virus itself. As mutation in the virus genome did not cause the altered phenotype of 94233-RC3, we conducted analyses of gene expression to investigate possible host-related reasons behind the recovery of our original fast-growing sector isolate. In a previously published study, the debilitating infection of HetPV13-an1 seriously affected many different biochemical pathways and the expression of some genes was even turned down completely (Vainio et al., 2018b). Similar analysis of the sector isolate 94233-RC3 revealed that the fungus had restored most of its gene regulation despite the presence of HetPV13-an1, including the two extremely downregulated (practically knocked out) genes in 94233. However, notably high changes were still observed in single genes related to the formation of fungal hypha, monooxygenase activity, and carbohydrate metabolism, although it remained unclear how and why the expression of these three genes was retained in the sector isolate 94233-RC3.

The recovery of most gene functions in 94233-RC3 was accompanied by a drastic drop in the quantities of viral transcripts, i.e., the viral titer: The amounts of RdRp and CP transcripts of HetPV13-an1 in 94233-RC3 were 74 and 68% lower, respectively, than in seriously debilitated 94233. In *F. oxysporum* and *Lentinula edodes*, the viral titer correlates with the degree of debilitation (Kim et al., 2015; Lemus-Minor et al., 2018; Yu and Kim, 2021), but there is also evidence that viral titers depend on host cell physiology (Schoffelen et al., 2013), culture conditions (Hillman et al., 1990), and environmental factors (Bryner and Rigling, 2011). Also RNA silencing could have a role in controlling the virus titers and associated phenotypic changes as, e.g., Mochama et al. (2018) showed that phenotypic alterations caused by virus infection are driven by RNA silencing mechanisms in *Sclerotium sclerotiorum* and antiviral RNA silencing responses led to phenotypic changes of fungal hosts in *Cryphonectria parasitica* (Segers et al., 2007) and *Colletotrichum higginsianum* (Campo

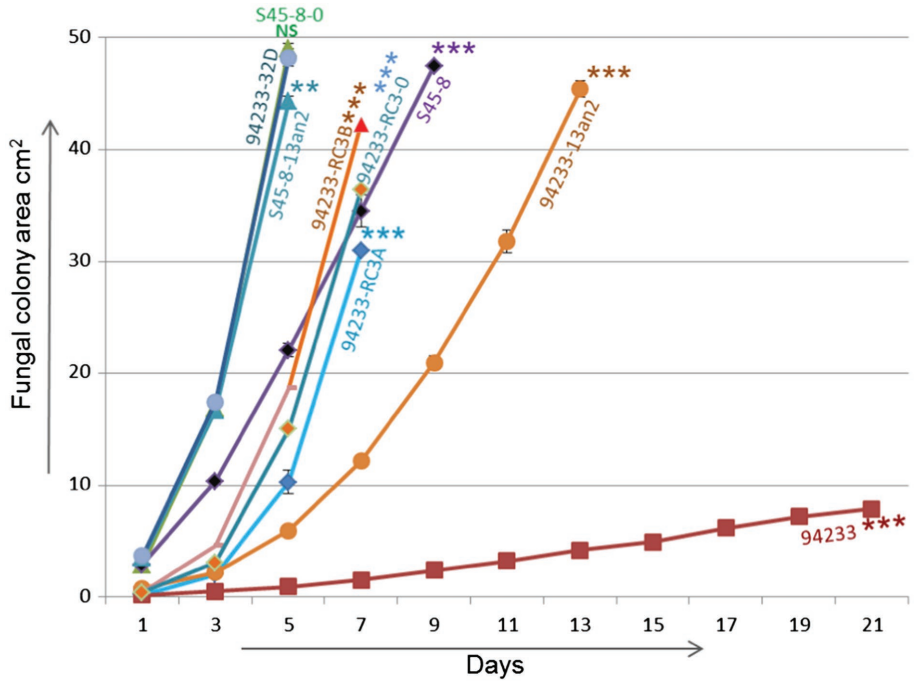

FIGURE 6 | Growth rate analysis. Growth rates of 94233-RC3 and its stored derivative 94233-RC3B infected with HetPV13-an1 including original 94233 with its consistent reduced phenotype and the partitivirus-free control 94233-32D (Kashif et al., 2019). 94233-RC3A = before storage; 94233-RC3B = after storage; 94233 (the original slow-growing strain hosting HetPV13-an1); S45-8-0 = virus-free control; S45-8-PV13an2 (single virus infection HetPV13-an2); S45-8 (the original strain with HetPV13-an2 and HetPV7-an1); and 94233-PV13an2 (HetPV13-an2 hosted by 94233 strain). The significance of the differences between the mean growth per day of the virus-free/cured and virus infected fungal isolates is shown by asterisks: $*p < 0.05$; $**p < 0.001$; and $***p < 0.0001$; # = single replicate; NS = Non-significant.

et al., 2016). The expression of genes for RNA silencing was only relatively slightly affected by the debilitating HetPV13-an1 infection of 94233 (Vainio et al., 2018b), and the sector isolate 94233-RC3 did not differ much from that. Therefore, our results support the view that RNA silencing is not much affected by an infection of HetPV13-an1.

Jurvansuu et al. (2014) suggested that the ratio of RdRp and CP transcripts of partitiviruses would be more important than their actual quantities in determining the phenotypic effects on the host. In this study, we observed slightly lower ratios of virus-encoded transcripts in 94233-RC3 and also in 94233-PV13-an2 hosting a closely related virus strain HetPV13-an2 causing only mild symptoms. Furthermore, the quantities of the two transcripts were almost equal in the original host S45-8 with a somewhat debilitating coinfection of HetPV13-an2 and HetPV7-an1, and highly similar to HetPV13-an1 in the recovered sector isolate 94233-RC3. These findings may be taken as support for the hypothesis by Jurvansuu et al. (2014), but also the direct transcript quantities correlate with the degree of symptoms. However, it has recently been described that RdRp transcripts in partitiviruses are often more abundant than CP transcripts although these infections seem to lack debilitating effects (Kashif et al., 2019; (Vainio et al., 2015a), which seems to contradict with the hypothesis of Jurvansuu et al. (2014).

94233-RC3 isolates before and after storage (2018) did not show significantly different growth rates. However, one of the replicates from the storage was free of HetPV13-an1, which might have been due to uneven distribution of viruses in the mycelium. The growth rate of this isolate 94233-RC3-0 was similar to 94233-RC3 strains that had retained the virus. This might suggest that the recovered phenotype of 94233-RC3 is due to a genetic or other change in the host mycelium that provides tolerance against the debilitating effects of HetV13-an1 but at the same time reduces the inherent growth rate of the mycelium. Non-uniform occurrence of virus particles within fungal mycelia has been reported by Ghabrial (1980), but in contrast to our observation, virus-like particles were observed more frequently in old than in actively growing hyphal tips by Border et al. (1972) and DeMarini et al. (1977).

A single infection of HetPV13-an2 was cryptic in its native host but caused considerable debilitation in a non-native host. This was in accordance to a previous study (Jurvansuu et al., 2014) where virus strains in exotic hosts seemed to have more significant phenotypic effects than in their native hosts. However, a coinfection with another virus strain HetPV7-an1 (S45-8) slowed down the growth by 45% after inoculation. This accords also with analyses by Kashif et al. (2019), who showed that different strains of HetPV11 affected differently the debilitating effects of HetPV13-an1. Interactions between viral double infections were also studied by Wu et al. (2010), who described suppression of replication of

Botrytis cinerea mitovirus 1 (BcMV1) by another related RNA virus (BcMV1-S). Also in *Rosellinia necatrix,* the phenotypic outcomes were different when the fungus was hosting single or coinfections of a megabirnavirus and a partitivirus (Sasaki et al., 2016). Moreover, phenotypic variations caused by interplay between partitiviruses (Telengech et al., 2020) and in a coinfection of a chrysovirus and a partitivirus in the human pathogen *A. fumigatus* caused unique phenotypic modifications (Bhatti et al., 2011).

The recovered HetPV13-an1 infected sector isolate 94233-RC3 was originally isolated and studied for its growth rate as well as for fungal and viral gene expressions almost a decade ago (but reported only here). In this study, we found that the virus infection in the sector isolate was low titer and susceptible/vulnerable to storage and culturing conditions. As HetPV13-an1 and other Heterobasidion partitiviruses have previously been stored in similar conditions for several years and even more than half a century (Kashif et al., 2015), this loss of a virus was surprising and suggests that the balance between the host and virus in 94233-RC3 was somewhat less stable than normally. However, loss of fungal viruses during a storage has previously been observed in other fungi, such as *C. parasitica* and *Fusarium circinatum* (Springer et al., 2013; Zamora-Ballesteros et al., 2021).

CONCLUSION

This study showed that *Heterobasidion* strains infected by a single partitivirus may show different phenotypes with considerably different fungal transcriptomes, viral titers, transcript ratios, and mycelial appearances.

DATA AVAILABILITY STATEMENT

The datasets presented in this study can be found in online repositories. The names of the repository/repositories and accession number(s) can be found in the article/**Supplementary Material**.

AUTHOR CONTRIBUTIONS

MK, EV, and JH conceived and designed the experiments. MK, JJ, and RH performed the experiments. MK, JJ, EV, and JH analyzed the data and wrote the paper. All authors contributed to the article and approved the submitted version.

FUNDING

This work was supported by the Academy of Finland (grant numbers 322001 and 309896).

ACKNOWLEDGMENTS

We are grateful to Juha Puranen, Tuija Hytönen, and Carita Karenius for technical assistance.

SUPPLEMENTARY MATERIAL

The Supplementary Material for this article can be found online at: https://www.frontiersin.org/articles/10.3389/fmicb.2021.661554/full#supplementary-material

REFERENCES

Allen, T. D., and Nuss, D. L. (2004). Specific and common alterations in host gene transcript accumulation following infection of the chestnut blight fungus by mild and severe hypoviruses. *J. Virol.* 78, 4145–4155. doi: 10.1128/JVI.78.8.4145-4155.2004

Bhatti, M. F., Jamal, A., Petrou, M. A., Cairns, T. C., Bignell, E. M., and Coutts, R. H. A. (2011). The effects of dsRNA mycoviruses on growth and murine virulence of *aspergillus fumigatus*. *Fungal Genet. Biol.* 48, 1071–1075. doi: 10.1016/j.fgb.2011.07.008

Border, D. J., Buck, K. W., Chain, E. B., Kempson-Jones, G. F., Lhoas, P., and Ratti, G. (1972). Viruses of Penicillium and aspergillus species. *Biochem. J.* 127, 4P–6P. doi: 10.1042/bj1270004P

Bryner, S. F., and Rigling, D. (2011). Temperature-dependent genotype-by-genotype interaction between a pathogenic fungus and its hyperparasitic virus. *Am. Nat.* 177, 65–74. doi: 10.1086/657620

Campo, S., Gilbert, K. B., and Carrington, J. C. (2016). Small RNA-based antiviral defense in the phytopathogenic fungus *Colletotrichum higginsianum*. *PLoS Pathog.* 12:e1005640. doi: 10.1371/journal.ppat.1005640

Choi, J., Lee, G. W., Kim, K. T., Jeon, J., Détry, N., Kuo, H. C., et al. (2017). Comparative analysis of genome sequences of the conifer tree pathogen, *Heterobasidion annosum*. *Genom. Data.* 14, 106–113. doi: 10.1016/j.gdata.2017.10.003

Dai, Y. C., and Korhonen, K. (1999). *Heterobasidion annosum* group S identified in northern-eastern China. *Eur. J. For. Pathol.* 29, 273–279. doi: 10.1046/j.1439-0329.1999.00153.x

Darissa, O., Adam, G., and Schafer, W. (2012). A dsRNA mycovirus causes hypovirulence of *Fusarium graminearum* to wheat and maize. *Eur. J. Plant Pathol.* 134, 181–189. doi: 10.1007/s10658-012-9977-5

Dawe, A. L., and Nuss, D. L. (2013). Hypovirus molecular biology: From koch's postulates to host self-recognition genes that restrict virus transmission. *Adv. Virus Res.* 86, 109–147. doi: 10.1016/B978-0-12-394315-6.00005-2

DeMarini, D. M., DeMarini, D. M., Kurtzman, C. P., and Fennell, D. I. (1977). Transmission of PsVF and PsV S mycoviruses during conidiogenesis of Penicillium stoloniferum. *J. Gen. Microbiol.* 100, 59–64. doi: 10.1099/00221287-100-1-59

Deng, F., Allen, T. D., Hillman, B. I., and Nuss, D. L. (2007). Comparative analysis of alterations in host phenotype and transcript accumulation following hypovirus and mycoreovirus infections of the chestnut blight fungus Cryphonectria parasitica Eukaryot. *Cell* 6, 1286–1298. doi: 10.1128/EC.00166-07

Eusebio-Cope, A., Sun, L., Tanaka, T., Chiba, S., Kasahara, S., and Suzuki, N. (2015). The chestnut blight fungus for studies on virus/host and virus/virus interactions: from a natural to a model host. *Virology* 477, 164–175. doi: 10.1016/j.virol.2014.09.024

Garbelotto, M., and Gonthier, P. (2013). Biology, epidemiology, and control of *Heterobasidion* species worldwide. *Annu. Rev. Phytopathol.* 51, 39–59. doi: 10.1146/annurev-phyto-082712-102225

Ghabrial, S. A. (1980). Effects of fungal viruses on their hosts. *Annu. Rev. Phytopathol.* 18, 441–461. doi: 10.1146/annurev.py.18.090180.002301

Ghabrial, S. A., Castón, J. R., Jiang, D., Nibert, M. L., and Suzuki, N. (2015). 50-plus years of fungal viruses. *Virology* 479, 356–368. doi: 10.1016/j.virol.2015.02.034

Ghabrial, S. A., and Suzuki, N. (2009). Viruses of plant pathogenic fungi. *Annu. Rev. Phytopathol.* 47, 353–384. doi: 10.1146/annurev-phyto-080508-081932

Hillman, B. I., Shapira, R., and Nuss, D. L. (1990). Hypovirulence-associated suppression of host functions in *Cryphonectria parasitica* can be partially relieved by high light intensity. *Phytopathology* 80, 950–956. doi: 10.1094/Phyto-80-950

Hollings, M. (1962). Viruses associated with a die-Back disease of cultivated mushroom. *Nature* 196, 962–965. doi: 10.1038/196962a0

Huang, S., and Ghabrial, S. A. (1996). Organization and expression of the double-stranded RNA genome of *Helminthosporium victoriae* 190S virus, a totivirus infecting a plant pathogenic filamentous fungus. *Proc. Natl. Acad. Sci. U. S. A.* 93, 12541–12546.

Hyder, R., Pennanen, T., Hamberg, L., Vainio, E. J., Piri, T., and Hantula, J. (2013). Two viruses of *Heterobasidion* confer beneficial, cryptic or detrimental effects to their hosts in different situations. *Fungal Ecol.* 6, 387–396. doi: 10.1016/j.funeco.2013.05.005

Hyder, R., Piri, T., Hantula, J., Nuorteva, H., and Vainio, E. J. (2018). Distribution of viruses inhabiting *Heterobasidion annosum* in a pine-dominated forest plot in southern Finland. *Microb. Ecol.* 75, 622–630. doi: 10.1007/s00248-017-1027-6

Ihrmark, K., (2001). *Double-Stranded RNA Elements in the Root Rot Fungus Heterobasidion Annosum*. Uppsala, Sweden: Dissertation. Swedish University of Agricultural Sciences.

Jurvansuu, J., Kashif, M., Vaario, L., Vainio, E., and Hantula, J. (2014). Partitiviruses of a fungal forest pathogen have species-specific quantities of genome segments and transcripts. *Virology* 462, 25–33. doi: 10.1016/j.virol.2014.05.021

Kashif, M., Hyder, R., De Vega Perez, D., Hantula, J., and Vainio, E. J. (2015). *Heterobasidion* wood decay fungi host diverse and globally distributed viruses related to Helicobasidium mompa partitivirus V70. *Virus Res.* 195, 119–123. doi: 10.1016/j.virusres.2014.09.002

Kashif, M., Jurvansuu, J., Vainio, E. J., and Hantula, J. (2019). Alphapartitiviruses of Heterobasidion wood decay fungi affect each other's transmission and host growth. *Front. Cell. Infect. Microbiol.* 9:64. doi: 10.3389/fcimb.2019.00064

Kim, D., Pertea, G., Trapnell, C., Pimentel, H., Kelley, R., and Salzberg, S. L. (2013). TopHat2: accurate alignment of transcriptomes in the presence of insertions, deletions and gene fusions. *Genome Biol.* 14:R36. doi: 10.1186/gb-2013-14-4-r36

Kim, J. M., Song, H. Y., Choi, H. J., Yun, S. H., So, K. K., Ko, H. K., et al. (2015). Changes in the mycovirus (LeV) titer and viral effect on the vegetative growth of the edible mushroom Lentinula edodes. *Virus Res.* 197, 8–12. doi: 10.1016/j.virusres.2014.11.016

Lambden, P. R., Cooke, S. J., Caul, E. O., and Clarke, I. N. (1992). Cloning of noncultivatable human rotavirus by single primer amplification. *J. Virol.* 66, 1817–1822. doi: 10.1128/jvi.66.3.1817-1822.1992

Lee, K. M., Cho, W. K., Yu, J., Son, M., Choi, H., Min, K., et al. (2014). A comparison of transcriptional patterns and mycological phenotypes following infection of *Fusarium graminearum* by four mycoviruses. *PLoS One* 9:e100989. doi: 10.1371/journal.pone.0100989

Lemus-Minor, C. G., Cañizares, M. C., García-Pedrajas, M. D., and Pérez-Artés, E. (2018). Fusarium oxysporum f. sp. dianthi virus 1 accumulation is correlated with changes in virulence and other phenotypic traits of its fungal host. *Phytopathology* 108, 957–963. doi: 10.1094/PHYTO-06-17-0200-R

Liu, J. J., Shamoun, S. F., Leal, I., Kowbel, R., Sumampong, G., and Zamany, A. (2018). Characterization of *Heterobasidion occidentale* transcriptomes reveals candidate genes and DNA polymorphisms for virulence variations. *Microb. Biotechnol.* 11, 537–550. doi: 10.1111/1751-7915.13259

Márquez, L. M., Redman, R. S., Rodriguez, R. J., and Roossinck, M. J. (2007). A virus in a fungus in a plant: three-way symbiosis required for thermal tolerance. *Science* 315, 513–515. doi: 10.1126/science.1136237

Mochama, P., Jadhav, P., Neupane, A., and Marzano, S.-Y. L. (2018). Mycoviruses as triggers and targets of RNA silencing in white mold fungus *Sclerotinia sclerotiorum*. *Viruses* 10:214. doi: 10.3390/v10040214

Müller, M. M., Kantola, R., and Kitunen, V. (1994). Combining sterol and fatty acid profiles for the characterization of fungi. *Mycol. Res.* 98, 593–603. doi: 10.1016/S0953-7562(09)80404-8

Myers, J. M., Bonds, A. E., Clemons, R. A., Thapa, N. A., Simmons, D. R., Carter-House, D., et al. (2020). Survey of early diverging lineages of fungi reveals abundant and diverse mycoviruses. MBio 11, e02027–e02020. doi: 10.1128/mBio.02027-20

Nibert, M. L., Ghabrial, S. A., Maiss, E., Lesker, T., Vainio, E., Jiang, D., et al. (2014). Taxonomic reorganization of family *Partitiviridae* and other recent progress in partitivirus research. *Virus Res.* 188, 128–141. doi: 10.1016/j.virusres.2014.04.007

Niemelä, T., and Korhonen, K. (1998). "Taxonomy of the genus Heterobasidion," in *Heterobasidion Annosum: Biology, Ecology*. eds. S. Woodward, J. Stenlid, R. Karjalainen and A. Hütterman (Impact and Control. C.A.B International), 27–33.

Olson, A., Aerts, A., Asiegbu, F., Belbahri, L., Bouzid, O., Broberg, A., et al. (2012). Insight into trade-off between wood decay and parasitism from the genome of a fungal forest pathogen. *New Phytol.* 194, 1001–1013. doi: 10.1111/j.1469-8137.2012.04128.x

Otrosina, W. J., and Garbelotto, M. (2010). *Heterobasidion occidentale* sp. nov. and *Heterobasidion irregulare* nom. nov.: a disposition of north American Heterobasidion biological species. *Fungal Biol.* 114, 16–25. doi: 10.1016/j.mycres.2009.09.001

Pearson, M. N., Beever, R. E., Boine, B., and Arthur, K. (2009). Mycoviruses of filamentous fungi and their relevance to plant pathology. *Mol. Plant Pathol.* 10, 115–128. doi: 10.1111/j.1364-3703.2008.00503.x

Pfaffl, M. W., Horgan, G. W., and Dempfle, L. (2002). Relative expression software tool (REST) for group-wise comparison and statistical analysis of relative expression results in real-time PCR. *Nucleic Acids Res.* 30:e36. doi: 10.1093/nar/30.9.e36

Preisig, O., Moleleki, N., Smit, W. A., Wingfield, B. D., and Wingfield, M. J. (2000). A novel RNA mycovirus in a hypovirulent isolate of the plant pathogen *Diaporthe ambigua*. *J. Gen. Virol.* 81, 3107–3114. doi: 10.1099/0022-1317-81-12-3107

Raffaello, T., and Asiegbu, F. (2013). Evaluation of potential reference genes for use in gene expression studies in the conifer pathogen (*Heterobasidion annosum*). *Mol. Biol. Rep.* 40, 4605–4611. doi: 10.1007/s11033-013-2553-z

Sasaki, A., Nakamura, H., Suzuki, N., and Kanematsu, S. (2016). Characterization of a new megabirnavirus that confers hypovirulence with the aid of a co-infecting partitivirus to the host fungus, *Rosellinia necatrix*. *Virus Res.* 219, 73–82. doi: 10.1016/j.virusres.2015.12.009

Schoffelen, A. F., Wensing, A. M., Tempelman, H. A., Geelen, S. P., Hoepelman, A. I., and Barth, R. E. (2013). Sustained virological response on second-line antiretroviraltherapy following virological failure in HIV-infected patients in rural SouthAfrica. *PLoS One* 8:e58526. doi: 10.1371/journal.pone.0058526

Segers, G. C., Zhang, X., Deng, F., Sun, Q., and Nuss, D. L. (2007). Evidence that RNA silencing functions as an antiviral defense mechanism in fungi. *Proc. Natl. Acad. Sci.* 104, 12902–12906. doi: 10.1073/pnas.0702500104

Sillo, F., Garbelotto, M., Friedman, M., and Gonthier, P. (2015). Comparative genomics of sibling fungal pathogenic taxa identifies adaptive evolution without divergence in pathogenicity genes or genomic structure. *Genome Biol. Evol.* 7, 3190–3206. doi: 10.1093/gbe/evv209

Springer, J. C., Davelos Baines, A. L., Chansler, M. T., and Jarosz, A. M. (2013). Evaluating the long-term storage of *Cryphonectria parasitica*. *Fungal. Genet. Rep.* 60, 11–15. doi: 10.4148/1941-4765.1007

Stenlid, J., and Redfern, D. B. (1998). "Spread within the tree and stand," in *Heterobasidion Annosum: Biology, Ecology, Impact and Control*. eds. S. Woodward, J. Stenlid, R. Karjalainen and A. Hütterman (Wallingford, UK: CAB International), 125–141.

Sutela, S., Forgia, M., Vainio, E. J., Chiapello, M., Daghino, S., Vallino, M., et al. (2020). The virome from a collection of endomycorrhizal fungi reveals new viral taxa with unprecedented genome organization. *Virus. Evol.* 6:veaa076. doi: 10.1093/ve/veaa076

Sutela, S., Poimala, A., and Vainio, E. J. (2019). Viruses of fungi and oomycetes in the soil environment. *FEMS Microbiol. Ecol.* 95:fiz119. doi: 10.1093/femsec/fiz119

Telengech, P., Hisano, S., Mugambi, C., Hyodo, K., Arjona-López, J. M., López-Herrera, C. J., et al. (2020). Diverse partitiviruses from the phytopathogenic fungus, *Rosellinia necatrix*. *Front. Microbiol.* 11:1064. doi: 10.3389/fmicb.2020.01064

Tuomivirta, T., and Hantula, J. (2003). Two unrelated double-stranded RNA molecule patterns in *Gremmeniella abietina* type A code for putative viruses of the families Totiviridae and Partitiviridae. *Arch. Virol.* 148, 2293–2305. doi: 10.1007/s00705-003-0194-6

Vainio, E. J. (2019). Mitoviruses in the conifer root rot pathogens *Heterobasidion annosum* and *H. parviporum*. *Virus Res.* 271:197681. doi: 10.1016/j.virusres.2019.197681

Vainio, E. J., Chiba, S., Ghabrial, S. A., Maiss, E., Roossinck, M., Sabanadzovic, S., et al. (2018a). ICTV virus taxonomy profile: *Partitiviridae*. *J. Gen. Virol.* 99, 17–18. doi: 10.1099/jgv.0.000985

Vainio, E. J., Hakanpää, J., Dai, Y., Hansen, E., Korhonen, K., and Hantula, J. (2011). Species of *Heterobasidion* host a diverse pool of partitiviruses with global distribution and interspecies transmission. *Fungal Biol.* 115, 1234–1243. doi: 10.1016/j.funbio.2011.08.008

Vainio, E. J., and Hantula, J. (2016). Taxonomy, biogeography and importance of *Heterobasidion* viruses. *Virus Res.* 219, 2–10. doi: 10.1016/j.virusres.2015.10.014

Vainio, E. J., and Hantula, J. (2018). "Fungal viruses," in *Viruses of Microorganisms*. eds. P. Hyman and S. T. Abedon (UK: Caister Academic Press), 193–209.

Vainio, E. J., Hyder, R., Aday, G., Hansen, E., Piri, T., and Dogmus-Lehtijarvi, T., T., Lehtijarvi, A., Korhonen, K., and Hantula, J. (2012). Population structure of a novel putative mycovirus infecting the conifer root-rot fungus *Heterobasidion annomm* sensu lato. *Virology* 422, 366–376. doi:10.1016/j.virol.2011.10.032.

Vainio, E. J., Jurvansuu, J., Hyder, R., Kashif, M., Piri, T., Tuomivirta, T., et al. (2018b). Heterobasidion partitivirus 13 mediates severe growth debilitation and major alterations in the gene expression of a fungal forest pathogen. *J. Virol.* 12, e01744–e01717. doi: 10.1128/JVI.01744-17

Vainio, E. J., Jurvansuu, J., Streng, J., Rajamäki, M., Hantula, J., and Valkonen, J. P. T. (2015a). Diagnosis and discovery of fungal viruses using deep sequencing of small RNAs. *J. Gen. Virol.* 96, 714–725. doi: 10.1099/jgv.0.000003

Vainio, E. J., Mueller, M. M., Korhonen, K., Piri, T., and Hantula, J. (2015b). Viruses accumulate in aging infection centers of a fungal forest pathogen. *ISME J.* 9, 497–507. doi: 10.1038/ismej.2014.145

Wu, M., Zhang, L., Li, G., Jiang, D., and Ghabrial, S. A. (2010). Genome characterization of a debilitation-associated mitovirus infecting the phytopathogenic fungus *Botrytis cinerea*. *Virology* 406, 117–126. doi: 10.1016/j.virol.2010.07.010

Xiao, X., Cheng, J., Tang, J., Fu, Y., Jiang, D., Baker, T. S., et al. (2014). A novel partitivirus that confers hypovirulence on plant pathogenic fungi. *J. Virol.* 88, 10120–10133. doi: 10.1128/JVI.01036-14

Yu, J., and Kim, K. (2021). A phenome-wide association study of the effects of *Fusarium graminearum* transcription factors on Fusarium graminearum virus 1 infection. *Front. Microbiol.* 12:622261. doi: 10.3389/fmicb.2021.622261

Yu, X., Li, B., Fu, Y., Jiang, D., Ghabrial, S. A., Li, G., et al. (2010). A geminivirus-related DNA mycovirus that confers hypovirulence to a plant pathogenic fungus. *Proc. Natl. Acad.* 107, 8387–8392. doi: 10.1073/pnas.0913535107

Zamora-Ballesteros, C., Wingfield, B. D., Wingfield, M. J., Martín-García, J., and Diez, J. J. (2021). Residual effects caused by a past Mycovirus infection in Fusarium circinatum. *Forests* 2:11. doi: 10.3390/f12010011

Zeng, Z., Sun, H., Vainio, E. J., Raffaello, T., Kovalchuk, A., Morin, E., et al. (2018). Intraspecific comparative genomics of isolates of the Norway spruce pathogen (*Heterobasidion parviporum*) and identification of its potential virulence factors. *BMC Genomics* 19:220. doi: 10.1186/s12864-018-4610-4

Conflict of Interest: The authors declare that the research was conducted in the absence of any commercial or financial relationships that could be construed as a potential conflict of interest.

Publisher's Note: All claims expressed in this article are solely those of the authors and do not necessarily represent those of their affiliated organizations, or those of the publisher, the editors and the reviewers. Any product that may be evaluated in this article, or claim that may be made by its manufacturer, is not guaranteed or endorsed by the publisher.

Advantages of publishing in Frontiers

OPEN ACCESS
Articles are free to read for greatest visibility and readership

FAST PUBLICATION
Around 90 days from submission to decision

HIGH QUALITY PEER-REVIEW
Rigorous, collaborative, and constructive peer-review

TRANSPARENT PEER-REVIEW
Editors and reviewers acknowledged by name on published articles

Frontiers
Avenue du Tribunal-Fédéral 34
1005 Lausanne | Switzerland

Visit us: www.frontiersin.org
Contact us: frontiersin.org/about/contact

REPRODUCIBILITY OF RESEARCH
Support open data and methods to enhance research reproducibility

DIGITAL PUBLISHING
Articles designed for optimal readership across devices

FOLLOW US
@frontiersin

IMPACT METRICS
Advanced article metrics track visibility across digital media

EXTENSIVE PROMOTION
Marketing and promotion of impactful research

LOOP RESEARCH NETWORK
Our network increases your article's readership